Using the yeast *Saccharomyces cerevisiae* to uncover regulatory mechanisms of cell surface membrane proteins

Katherine Mary Paine

Doctor of Philosophy

University of York
Biology

September 2022

Abstract

Membrane bound organelles define eukaryotic cells. Correct traffic of material between these organelles is crucial for proper cellular function. Arguably one of the most important membranes is the plasma membrane, separating the cell from its external environment. A cell must adapt and respond to its environment, which can change dramatically and rapidly. This is achieved through membrane trafficking mechanisms. The regulation of cell surface membrane proteins in their journey through trafficking pathways and within the plasma membrane itself is not fully understood. As many of these pathways and factors are conserved from yeast to humans, I used the yeast *Saccharomyces cerevisiae* as a model to uncover mechanistic details about how surface membrane proteins are regulated, with particular focus on cellular responses to nutrients. Following starvation, we detail how yeast cells upregulate endocytosis (Laidlaw et al., 2021) whilst simultaneously downregulating surface recycling (Amoiradaki et al., 2021; Laidlaw et al., 2022b) to drive degradation of surface membrane proteins. Curiously, not all nutrient transporters are degraded in response to starvation, with a small reserve pool being retained in special compartments of the plasma membrane termed eisosomes (Laidlaw et al., 2021). I went on to reveal that during starvation, eisosomes are regulated by dephosphorylation of its core structural subunit (Paine et al., 2022). Beyond this mechanistic work, I also set out to demystify trafficking pathways of surface proteins. I took advantage of the discovery that yeast cells grown in restricted uracil conditions rely on efficient trafficking of a uracil permease for efficient growth. This phenotype allowed me to perform a comprehensive genetic screen to identify and validate many known and novel candidate factors for surface protein trafficking (Paine et al., 2021). In combination, these discoveries represent a significant advance on our understanding of surface protein trafficking and will pave the way for many future studies, in both yeast and in cultured mammalian cell models.

Author's declaration

I, Katherine Mary Paine declare that this thesis is a presentation of original work and I am the sole author. This work has not previously been presented for an award at this, or any other, University. All sources are acknowledged as References.

Where the thesis is based on work done by myself jointly with others, I have made clear exactly what was done by others and what I have contributed myself.

The work in this thesis has either been published before submission or is under review and available online at bioRxiv.

Chapter II: Fur4 mediated uracil-scavenging to screen for surface protein regulators
Paine, K.M., Ecclestone, G., and MacDonald, C.
Fur4 mediated uracil-scavenging to screen for surface protein regulators.
Traffic.
Published: 23rd September 2021
DOI: 10.1111/tra.12815
PMID: 34498791

Chapter III: A glucose starvation response governs endocytic trafficking and eisosomal retention of surface cargoes
Laidlaw, K.M.E., Bisinski, D.D., Shashkova, S., Paine, K.M., Veillon, M.A., Leake, M.C., and MacDonald, C.
A glucose-starvation response governs endocytic trafficking and eisosomal retention of surface cargoes in budding yeast.
Journal of Cell Science.
Published: 25th January 2021
DOI: 10.1242/jcs.257733
PMID: 33443082

Chapter IV: The phosphatase Glc7 controls eisosomal response to starvation via posttranslational modification of Pil1
Paine, K.M., Evans, G.J.O., Laidlaw, K.M.E., and MacDonald, C.
The phosphatase Glc7 controls eisosomal response to starvation via posttranslational modification of Pil1.
Uploaded to bioRxiv: 11th August 2022
A revised version of this manuscript is under preparation following review at the Journal of Cell Science

Chapter V: Endosomal cargo recycling mediated by Gpa1 and Phosphatidylinositol-3-Kinase is inhibited by glucose starvation
Laidlaw, K.M.E., Paine, K.M., Bisinski, D.D., Calder, G., Hogg, K., Ahmed, S., James, S., O'Toole, P.J., and MacDonald, C.
Endosomal cargo recycling mediated by Gpa1 and phosphatidylinositol 3-kinase is inhibited by glucose starvation.
Molecular biology of the cell.
Published: 17th March 2022
DOI: 10.1091/mbc.E21-04-0163
PMID: 35080991

Acknowledgements

I would like to thank the Department of Biology for funding this PhD project, the wonderful staff at the technology facility who I have worked with over the years and for people in the lab who have trained and helped me. Thank you to my thesis advisory panel member Luke Mackinder for the helpful comments and suggestions.

A big thank you to Dr Chris MacDonald and Professor Nia Bryant. I never thought I was capable of embarking on PhD, and I cannot thank you enough for believing in me and giving me this opportunity. This PhD has given me space to grow both scientifically and in confidence. Your kindness over the years is something I will always remember. I cannot thank Chris enough for encouraging me to take every opportunity and being the most supportive supervisor. Special thank you to members of the MacDonald lab over the four years for making work so enjoyable: Kamilla, Savvas, Blythe, Sarah as well as those passing through. Whilst working in the J0 Cell Biology labs has involved many hours of pipetting and hard science there has also been lots of “lab shenanigans”, something that has eased the undulations of research and has contributed to making this experience so enjoyable. Thank you to Dimi for always keeping the J0 labs in order, I aspire to have a lab bench as tidy as yours! And to Lizzie and Hannah for being great lab and running friends.

When starting my PhD, I was worried it would be a quiet and lonely experience of which I am pleased to say I have been proven wrong! I have been lucky enough to have met some lovely, kind people both within my lab and in the wider Biology PhD community. Highlights include nights out in Flares during the first year, firepit and games nights through the pandemic, lab running club, many house parties and drinks by the river after work. I am very grateful and have made some friends for life. To Alex and Josh for the many “trash” movie nights, drinks and for getting through our PhDs together. Thank you to Evie for being a great housemate and friend. We have mastered the art of cocktail making, developed green fingers, and become experts in the BBQ and firepit realm – oh and managed to finish our PhDs! And of course, for my close friends outside of the department who have provided a support network and lots of fun visits and holidays: Jessamyn, Grace, Maria, Harriet, Paulina and Zara.

An important thank you to my family. My Mum and Dad for always being a phone call away, you have provided me with a consistent and unabating source of love. Thank you to my brother Joe, Grandma, Grandpa, Auntie Caroline, and Ella. My Grandma, Marion for always being interested in whatever I am doing and reading everything I write, you have provided me with such strength and love. My lovely Auntie Caroline for always being there for me and to Joe and Ella who I have grown up with, I am excited to see what you both do. I am feeling very grateful to have a support network both in the lab and outside of it. You have all softened the tough, challenging times (of which there have been a few over these four years!) and celebrated the lighter happier times and that is all I could ever hope for.

GRAPHICAL ABSTRACT

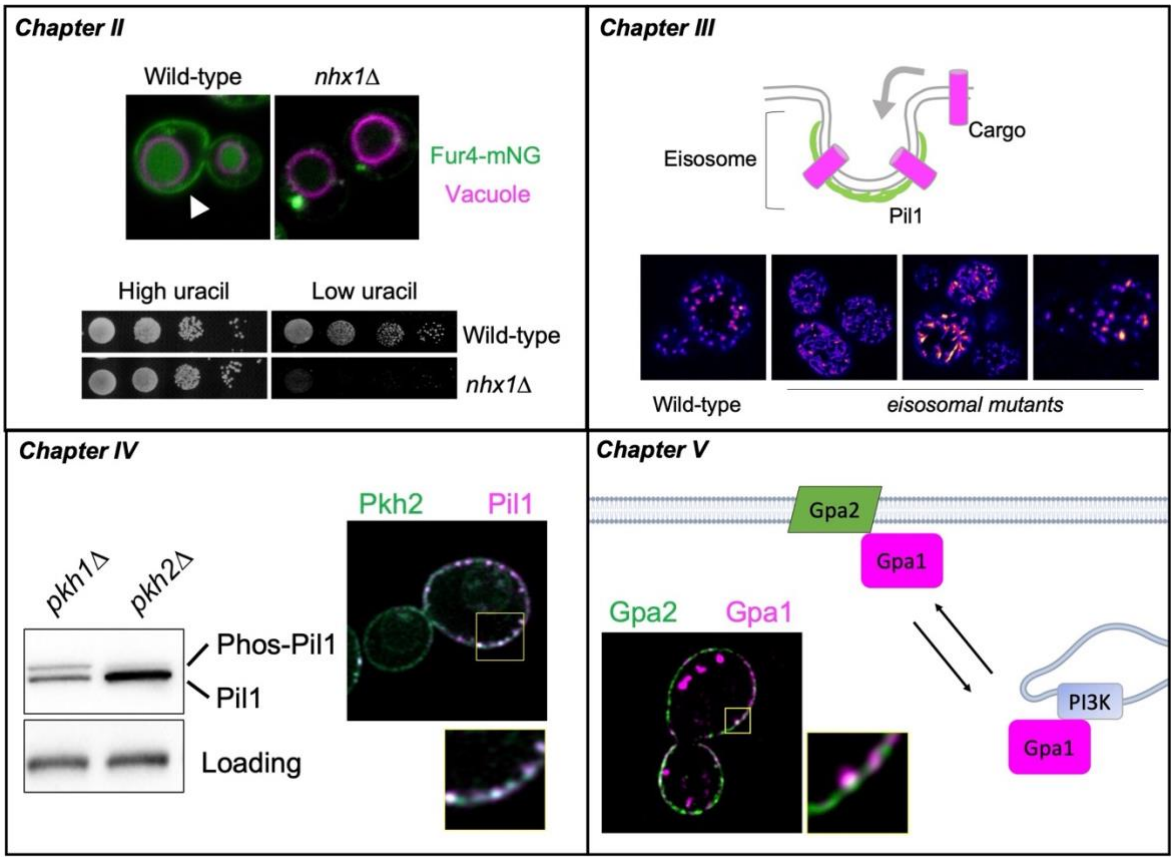

Table of Contents

Table of Figures

Table of Supplemental Figures

List of abbreviations

AP	Adaptor proteins
API	Aminopeptidase I
APC	Amino Acid-Polyamine-Organocation
ARF	ADP-ribosylation factor
ATP	Adenosine triphosphate
BAR	Bin/Amphiphysin/RVS
CHO	Chinese Hamster Ovary
cvt	cytoplasm to vacuole targeting
DHS	Dihydrosphingosine
ER	Endoplasmic reticulum
ESCRT	Endosomal Sorting Complexes Required for Transport
FRET	Förster resonance energy transfer
GFP	Green fluorescent protein
GPI	Glycosylphosphatidyl inositol
HEK	Human Embryonic Kidney
HeLa	Henrietta Lacks
IPC	Inositolphosphorylceramide
LCB	Long Chain Base
MCC	Membrane Compartment of Can1
MCP	Membrane Compartment Occupied by Pma1
MIPC	Mannose-inositol-phosphoceramide
$M(IP)_2C$	Mannose-(inositol-$P)_2$-ceramide
MVB	Multivesicular body
NEM	N-Ethylmaleimide
NSF	NEM sensitive factor
ORF	Open Reading Frame
PHS	Phytosphingosine
PI3K	Phosphatidylinositol 3-kinase
PI4P	Phosphatidylinositol-4-phosphate
$PI(4,5)P_2$	Phosphatidylinositol 4,5-bisphosphate
PtdIns3P	Phosphatidylinositol-3-phosphate
Rab	*ras* genes from rat brain
SNAP	Soluble NSF attachment protein
SNARE	SNAP receptor
SPT	Serine palmitoyltransferase
SR	SRP-receptor
SRP	Signal recognition particle
TGN	trans-Golgi network
TMS	Transmembrane spanning
UBD	Ubiquitin binding domains

Chapter I: Introduction

1.1. Cell biology: what is a eukaryotic cell?

Around 3.8 billion years ago simple life emerged (Cooper, 2000) and evolved into the complex cellular systems we know today. Living organisms were divided into two major groups by Edouard Chatton in 1938: prokaryotes, which include bacteria, and eukaryotes, which describe organisms with nucleated cells (Sapp, 2005). In 1990 it was proposed to organise life into the three broad categories of Prokaryotes, Eukaryotes and Archaea (Woese et al., 1990). Eukaryotic cells arose from prokaryotes through unknown mechanisms and are characterised by their membrane bound organelles, something not observed in prokaryotic cells (Lane and Martin, 2010; Martin et al., 2015; Pederson, 2011). From this a large variety of unicellular and multicellular eukaryotic organisms evolved (Sogin, 1991).

1.1.1. Organelles

Eukaryotic cells, like prokaryotic cells, are bound by a plasma membrane and contain ribosomes but additionally have other membrane bound organelles and a cytoskeleton (Cooper, 2000). The membrane bound organelles within eukaryotes are defined by their molecular composition, and communication between organelles is interconnected via a broad range of complex and distinct trafficking pathways. Proteins that function in these different organelles are synthesised and then must be trafficked to their destination (More et al., 2020). These trafficking pathways are highly conserved across eukaryotes (Schlacht et al., 2014). Disruption of these trafficking pathways leads to various pathologies (Yarwood et al., 2020), understanding the basic cellular biology of how they function is crucial to understanding health and disease. In this introduction I will mostly discuss membrane trafficking in the context of the eukaryotic budding yeast *Saccharomyces cerevisiae*, an overview of the pathways I will discuss is shown (**Figure 1.1**).

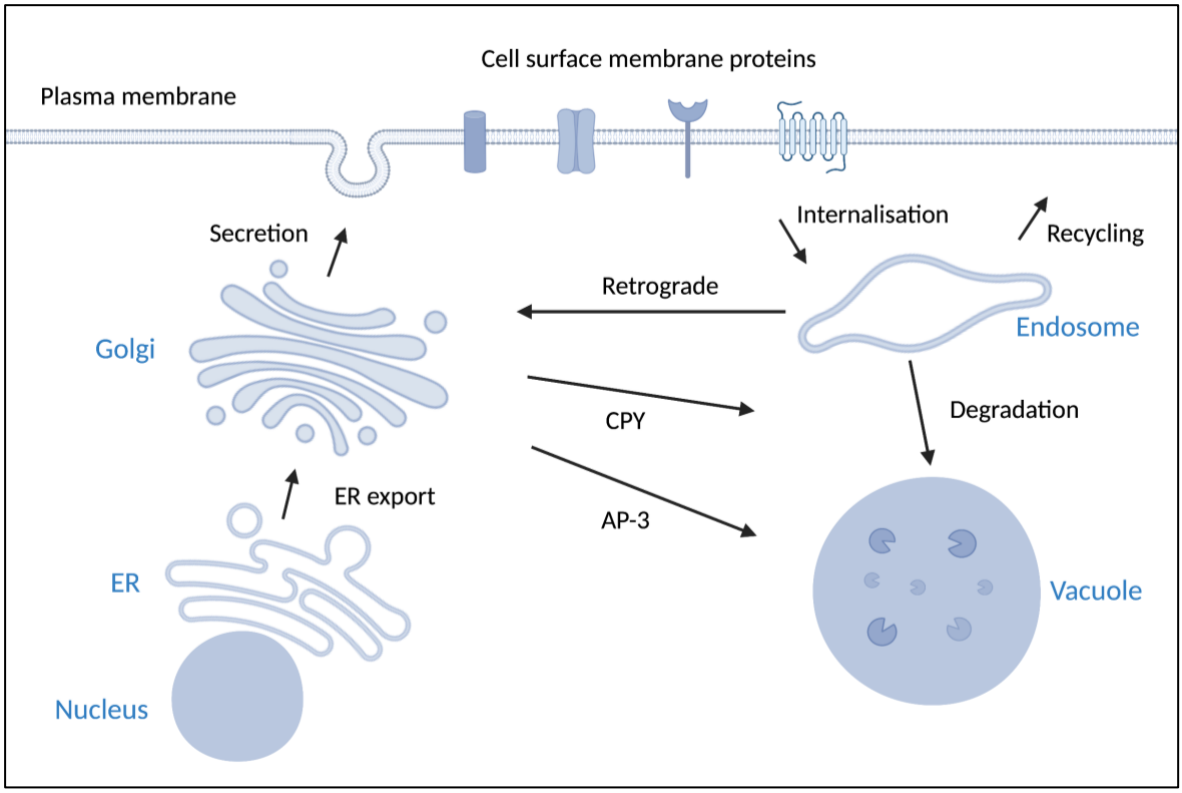

Figure 1. 1 Schematic showing overview of main trafficking pathways in *Saccharomyces cerevisiae.*

Schematic showing an overview of trafficking routes that proteins might take. Proteins are co-translationally imported to the endoplasmic reticulum (ER) and then transported by vesicular trafficking to the Golgi apparatus. Proteins destined to function at the plasma membrane or to be secreted from the cell can be directly trafficked to the plasma membrane. For proteins with other destinations, they can follow other pathways. For example, the CPY or AP-3 pathway to the late-endosomal or vacuolar system respectively. Surface proteins localised can be internalised to the endosomal system and either are trafficked back to the Golgi via the retrograde pathway, recycled back to the plasma membrane from endosomes directly, or traffic through the MVB pathway to the vacuole for degradation. These pathways are conserved across eukaryotes.

1.1.2. Trafficking pathways between organelles

1.1.2.1. Secretory pathway

Membrane trafficking begins with the synthesis of a polypeptide. The secretory pathway involves the traffic of nascent proteins through the endoplasmic reticulum (ER) and Golgi to the destination where they function. The first studies of the secretory pathway involved using autoradiography to track the movement of proteins in pancreatic exocrine cells (Caro and Palade, 1964; Palade, 1975). Work has exploited yeast genetics to identify key factors involved in these trafficking events. The *SEC* genes had been identified from yeast genetic screening approaches as encoding gene products involved with the secretory pathway (Novick et al., 1980). These gene products were then explored to understand the specific role they played in the pathway, later being attributed to specific roles or protein complexes in the secretory pathway such as the exocyst complex.

1.1.2.2. Traffic from the Golgi

From the Golgi, proteins can be trafficked to the plasma membrane. These vesicles fuse with the plasma membrane to either secrete soluble proteins into the extracellular space or deliver cell surface membrane proteins to their destination where they can fulfil their role. Exocytosis is the mechanism that promotes these trafficking events. The exocyst complex is required for the tethering of secretory vesicles to the plasma membrane to allow for SNARE-mediated membrane fusion (Luo et al., 2014). Alternatively, cargo not destined for the plasma membrane can be trafficked from the Golgi to its destination directly such as via the CPY and AP-3 pathways that deliver cargo to the late endosomal and vacuolar system (Hecht et al., 2014).

1.1.2.3. The endosomal system and multivesicular body (MVB) pathway

Proteins residing at the plasma membrane can be internalised in response to various extracellular and intracellular cues and enter the endosomal system. For receptor-mediated endocytosis, vesicles bud inward mediated by the formation of clathrin-coated pits and AP2 adaptors (Ahle et al., 1988). Like work done to understand the secretory pathway, genetic screens in yeast have uncovered various factors involved in these trafficking steps. Proteins are delivered to the lysosome for degradation through the multivesicular body (MVB) pathway. The “endosomal sorting complex required for transport” or ESCRT proteins are required for the regulation of MVB biogenesis. This machinery is conserved from yeast to humans (Katzmann et al., 2002; Leung et al., 2008).

1.2. Eukaryotic experimental systems

To understand how multicellular eukaryotic systems work, many experimental systems have been developed. Whilst *in vivo* animal models are used in research, they come with ethical considerations and it is encouraged where possible for them to be replaced with alternatives (Moran et al., 2016). There are a variety of different alternatives such as the use of cell culture or model organisms.

1.2.1. Cultured cells for biomedical research

The development of the first cultured cells *in vitro* in the late 19th and early 20th centuries has provided a tool that is now widely popular for research. It involved developing a way that cells could be cultured *in vitro* in physiologically relevant medium without infection from other organisms such as bacterium (Carrel, 1912; Carrel, 1923; Carrel and Burrows, 1911; Ringer, 1882). The ability to keep human and higher eukaryotic single cells alive outside of their multicellular organism was ground-breaking. Since then, many different types of cell lines have been developed such as the highly characterised HeLa (Henrietta Lacks) or Chinese Hamster Ovary (CHO) cell lines. HeLa cells have a controversial history. They came from Henrietta Lacks who was an African American woman suffering from cervical cancer. In the 1950s, whilst in hospital, a sample of her tissues was taken and without her permission by a researcher who was able to immortalise them (Scherer et al., 1953). Henrietta sadly succumbed to her cancer, but the cells taken from her were passed to whoever asked for them. Biotechnology companies used these cells and whilst they generated profit her descendants received nothing. Additionally, sequencing data from her cells was published which was a bioethical concern due to the potential information on her descendants health risks (Caulfield and McGuire, 2013). Her family have campaigned for the rightful justice and as a result of their work the US National Institutes of Health (NIH) has altered the regulations in publishing sequencing data (NIH, 2013). The Lacks family have also filed a lawsuit against Thermo Fisher seeking Intellectual property rights to her cells, which is currently ongoing (Summer 2022).

There is no doubt that HeLa cells have provided an invaluable tool for medical research and have been used to advance many areas of biomedical research, giving us many of the drugs we use today. Being from a human sample they are extremely relevant to biomedical research. They have provided researchers with the opportunity to understand how disease in human cells works (Aldhous, 1993; Martin-Serrano et al., 2001), for the development of new research tools such as microscopy (Chen et al., 2014) and understanding how certain drugs act on human cells (Brown and Henderson, 1983; Ito et al., 2010). Whilst they have provided many discoveries, HeLa cells also have their caveats. They have an abnormal karyotype and large genomic rearrangements with the potential to affect gene expression (Landry et al., 2013). Another popular cell line with aneuploidy is the Human Embryonic Kidney (HEK) 293 lineage (Lin et al., 2014). This cell line arose from the transformation of an adenovirus into human embryonic kidney cells in 1973 for work that aimed to explore how adenoviruses can cause cancer (Graham et al., 1977). As HEK 293 cells are human derived, they are popular option for generating biologics for humans and research has focussed on using them for gene therapies and the production of recombinant proteins (Abaandou et al., 2021). Another popular cell line is the Chinese Hamster Ovary (CHO) cell line which are widely used for the production of monoclonal antibodies for therapeutic use (Lalonde and Durocher, 2017).

Contamination of these cell cultures with viruses or mycoplasma can be a big problem experimentally. If your cells are infected with an organism such as mycoplasma, they are likely under some sort of stress and not behaving as expected. These infections affect individual cells in different ways (Drexler and Uphoff, 2002; Merten, 2002) meaning that this stress cannot be accounted for when interpreting results. Additionally, these cells have been taken from a multicellular organism and cultured outside of this organism and so the system is potentially not as physiologically relevant as other models such as *in vivo* mouse models depending on the research question being asked. To overcome this, 3D cell culture techniques are being developed with a focus on cell culture methods mimicking intracellular conditions as closely as possible (Costa et al., 2016; Jensen and Teng, 2020).

1.2.2. Caenorhabditis elegans and Drosophila melanogaster as model systems

An alternative for biomedical research is the use of eukaryotic model organisms that although not mammalian, have similarities genetically. They are without the same ethical concerns that come with *in vivo* mouse models. The nematode worm *Caenorhabditis elegans* (*C. elegans*) genome was fully sequenced and published online in 1998 (*C. elegans* sequencing consortium, 1998) and individual genes had begun to be identified and sequenced since the 1970s (Brenner, 1974). These worms have molecular similarities to mammalian systems and with their short lifespan (2 weeks) are a fast and simple way to study processes such as aging (Schaffitzel and Hertweck, 2006). They have also been used to study neurodegenerative diseases such as Alzheimer's disease (Alexander et al., 2014). The fruit fly *Drosophila melanogaster* (*D. melanogaster*) has been used as a model organism since the early 20th century, where in the early 1900s scientists developed methods of culturing and breeding to study inheritance (Davenport, 1941). Since then, the use of *D. melanogaster* in neuroscientific research has been widely used with many developmental pathways being first identified in fruit flies (Bellen et al., 2010). Being multicellular and sharing homology to mammalian systems, *D. melanogaster* and *C. elegans* have both allowed pathways such as the Notch signalling pathway to be delineated, where in unicellular model systems this wouldn't have been possible (Le Borgne, 2006).

1.2.3. Saccharomyces cerevisiae as a model organism

The yeast *S. cerevisiae* has been used extensively as a model system for eukaryotic cells. Yeast are unicellular and whilst they lack the complexity of a multicellular organism with different cell types they maintain the same fundamental cell biology seen in higher eukaryotes making them simple yet powerful tools (Botstein and Fink, 1988). The sequencing of the yeast genome was the first full eukaryotic genome to be sequenced and was published in 1996 (Goffeau et al., 1996), ahead of the human genome which was completed in 2001 (Lander et al., 2001). Replacing certain yeast genes with their human orthologues has proved that despite these two species having evolved separately, levels of functionality remain (Kachroo et al., 2015). Yeast cells have been used to understand many different processes such as aging (Fröhlich and Madeo, 2001), DNA repair (Kanaar et al., 1996), the secretory pathway (Novick et al., 1980) and the cell cycle (Hartwell et al., 1973) amongst many more.

Eukaryotic cells have four stages of their cell cycle: G_1, S, G_2 and M phase where the cells grow and prepare for cytokinesis (Cooper, 2000). The genes responsible for controlling this process were first identified in budding yeast. This began with the isolation of mutant yeast cells with growth arrested at points in the cell cycle (Hartwell et al., 1973). Nurse made the

link between cell growth and division and how disruption in this would lead to cells arising of abnormal sizes, from this a mutant that divided at half the time of wild-type cells was identified (Nurse, 1975). Following this, a set of 52 mutants termed "*wee"* mutants were linked to abnormal cell division (Nurse and Thuriaux, 1980). Finding the first human homologue to one of these genes the *CDC2* gene (Lee and Nurse, 1987) demonstrated that this process was conserved across species and allowed the work done in yeast to inform mammalian studies. Nurse and Hartwell were awarded a Nobel Prize in 2001 for this work (Murray, 2016). Another Nobel Prize winning discovery that used yeast as a model organism was understanding autophagy. Yoshinori Ohsumi developed an experimental system where he would mutate yeast cells and then trigger autophagy through starvation and observe the phenotype. Where cells with mutated autophagy genes would not display the characteristic autophagy phenotype (Takeshige et al., 1992).

Yeast are around 5µm in diameter and have an ellipsoid shape (Sherman, 2002). Upon visualising with differential interference contrast (DIC) microscopy the vacuole is visible and can be labelled using the lipid dye FM4-64 (**Figure 1.2**) (Vida and Emr, 1995). Other cellular organelles such as the endoplasmic reticulum can be visualised with fluorescently tagged proteins (**Figure 1.6**). Genetic manipulations are easier in yeast cells than in other systems such as mammalian cell culture, although advances like CRISPR/Cas9 have helped such efforts in the last decade (You et al., 2019). The homologous recombination machinery that allows DNA to be repaired (Krogh and Symington, 2004) can be used to allow the yeast genome to be moulded and manipulated for research. Genetic information can be integrated into the yeast genome or expressed via a plasmid (Orr-Weaver et al., 1981). Yeast strains engineered for research have been developed using auxotrophic markers for selection (Brachmann et al., 1998; Mortimer and Johnston, 1986; Winston et al., 1995) allowing fluorescently tagged or mutated proteins to be generated. Libraries for the deletion of non-essential mutants (Winzeler et al., 1999) or reduction in expression of essential genes (Breslow et al., 2008) are available allowing whole genome screens to be carried out over 96-well plates in both 384 and 1536 formation.

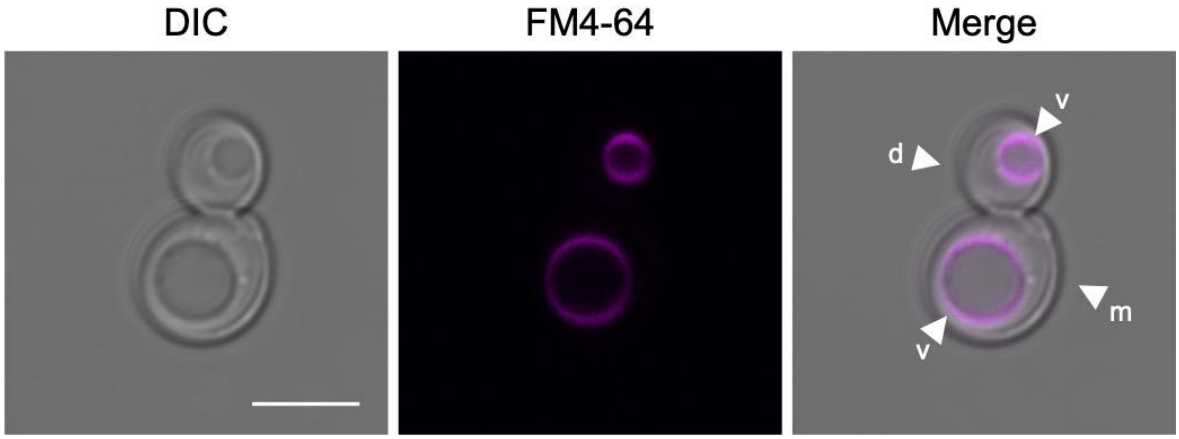

Figure 1. 2 Visualising yeast cells using microscopy.

Micrographs showing a mother (m) and daughter (d) cell using differential interference contrast (DIC) microscopy to visualise the cellular structure and the lipid dye to visualise the vacuoles (v: magenta). Images were taken using Zeiss 710. Scale bar = 5µm.

1.3. The composition of membranes

Polar lipids are the key component of membranes as it is their hydrophobic and hydrophilic regions that allow them to assemble into membrane-like structures (van Meer et al., 2008) underlying the ability of eukaryotic cells to be compartmentalised. Broadly lipids are composed of a hydrophilic head group and a hydrophobic "tail" composed of hydrocarbons (**Figure 1.3 Left**), these components can be modified and vary between types of lipids (Fahy et al., 2011). In aqueous environments lipids form micelles as the hydrophobic hydrocarbon chains of lipids are positioned inwards with the hydrophobic heads facing outwards (**Figure 1.3 Centre**). They can then form membranes, where two layers of lipids have their hydrophobic tails facing inwards (**Figure 1.3 Right**). It is various thermodynamic properties that govern the shape and size of structures that can form (Tanford, 1972; Tanford, 1978). Lipids form membranes but also can act as signalling molecules, in humans changes in these signalling lipids can underlie states such as inflammation (Wymann and Schneiter, 2008).

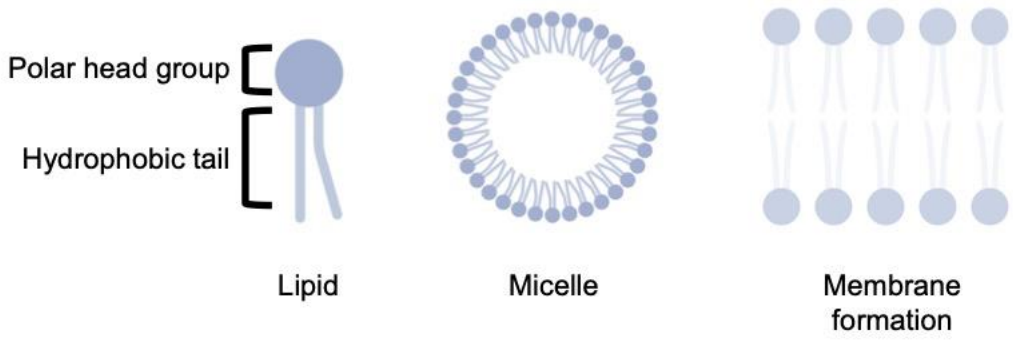

Figure 1. 3 The structure of lipid molecules.

Schematic showing the basic structure of the individual lipid molecule and then subsequent micelle and membrane formation.

1.3.1. Phosphatidylinositol

Phospholipids are the primary structural component of the plasma membrane in yeast (Daum et al., 1998). There are a variety of different phosphoinositides (PIs) that are generated to function in structural and regulatory roles. PI has five sites on its head group that can be phosphorylated to generate different species that can function as intermediates, directly interact with target proteins or alter membrane composition (Fruman et al., 1998). Phosphatidylinositol 4,5-bisphosphate [PI(4,5)P_2] is mainly generated through the phosphorylation of phosphatidylinositol (PI) by PI 4-kinases (PI4K or PI4K2) to generate phosphatidylinositol 4-phosphate (PI4P). PI4P can then be phosphorylated further to generate PI(4,5)P_2 (De Camilli et al., 1996). The cellular distribution of PI4P is wide and has been demonstrated to localise to pools at the Golgi, plasma membrane and Rab-7 positive endosomes (Hammond et al., 2014). Signalling through PIs is important in membrane trafficking such as through the Vps34/Vps15 PI3-kinase complex, which phosphorylates PIs at the Golgi and endosome to mediate trafficking between these organelles (Odorizzi et al., 2000). Various species of PIs can act as second messengers after a cell surface receptor tyrosine kinase has been activated by binding to its ligand (Backer et al., 1992; Soltoff et al., 1992). Phosphatidylinositol metabolism has been linked to membrane trafficking events,

such as work done in mammalian neuronal cells (Cremona et al., 1999). Fab1 is a PI(3)P 5-kinase that functions to generate PI species at the vacuole (Cooke et al., 1998).

1.3.2. Sphingolipids

Sphingolipids are lipids that have a variety of different roles throughout the cell, they are composed of a long chain base (LCB), a fatty acid and a polar head group. Sphingolipid metabolism is complex and the variety of different species generated have different roles in the cell (Hannun and Obeid, 2018). In yeast there are two types of LCB that make up spingolipids: dihydrosphingosine (DHS) and phytosphingosine (PHS) (Dickson and Lester, 2002). Sphingolipid biogenesis begins at the endoplasmic reticulum (ER) where serine palmitoyltransferase (SPT) catalyses the condensation of serine with fatty acyl-CoA, generating 3-ketodihydrosphingosine (ketosphinganine) (Hanada, 2003). 3-ketodihydrosphingosine is then reduced to DHS, catalysed by the reductase Tsc10 (Beeler et al., 1998). The DHS can then be modified to generate phytoceramide through either hydroxylation at C-4 by Sur2/Syr2 or hydroxylated by Sur2 to generate PHS which is then amide linked to a C_{26} fatty acid to generate the phytoceramide (Grilley et al., 1998; Haak et al., 1997). Then the fatty acids are elongated from C_{14} – C_{18} in the ER (Toke and Martin, 1996) to generate ceramides which are transported to the Golgi where inositolphosphorylceramide (IPC) is formed (Funato and Riezman, 2001). IPC contains inositol and so the inositol pathway feeds into sphingolipid synthesis in this way and therefore this feeds TORC2 signalling into this pathway (Tabuchi et al., 2006). IPC is mannosylated to generate mannose-inositol-phosphoceramide (MIPC) which then through the addition of another phosphoinositol group generates mannose-(inositol-P)$_2$-ceramide (M(IP)$_2$C) (Dickson and Lester, 1999). These pathways are similar between yeast and mammalian cells but at points different moieties are generated which is thought to alter regulation as seen in the different species (Dickson, 1998).

1.3.3. Ergosterol

Ergosterol is the primary membrane sterol of yeast and modulates the fluidity of these membranes. As ergosterol is essential for fungal cells it is a target for anti-fungal drugs (Zhang and Rao, 2010). The role ergosterol plays in membrane trafficking is well documented with it first being identified as being required for endocytosis (Heiniger et al., 1976). We now know it is also required to target nutrient transporters to the plasma membrane from the late secretory pathway (Umebayashi and Nakano, 2003). A subdomain of the plasma membrane termed eisosomes were identified to be rich in ergosterol, where ergosterol was found to disperse out of these eisosomes after membrane depolarization (Grossmann et al., 2007). The mammalian version of ergosterol, cholesterol can be uptaken and used by yeast cells but does not replace the role ergosterol plays completely (Ramgopal and Bloch, 1983; Rodriguez and Parks, 1983). Ergosterol is different from cholesterol as it contains unsaturated carbons at C-7,8, C-22 and C-24 (Daum et al., 1998). Highlighting a potentially difference in functionality between these species.

1.4. The principles of membrane fusion

I have discussed how membranes are made and organised in eukaryotic cells. A fundamental question that underlies membrane trafficking is how two opposing membranes fuse, something required for the exchange of material between compartments. There are two aspects to this question: how this happens on a biophysical level and the molecular machinery that facilitates this.

1.4.1. The biophysical properties of membrane fusion

There are a lot of biophysical barriers to overcome for membranes to fuse. The stalk hypothesis of membrane fusion involves clear steps and allows energetic barriers to be overcome to enable membrane fusion (Kozlov and Markin, 1983; Markin et al., 1984). To begin there is initial contact between membranes and electrostatic forces must be overcome to allow membranes into close proximity (Jahn et al., 2003). Opposing bilayers are observed to not just have flat surfaces but also curved surfaces as a result of electrostatic repulsion from internal bilayers (Rand et al., 1981). The energy required for overcoming the repulsion from opposing membranes is proportional to the area of close contact and so membrane bending reduces this energy requirement and enables the energy barrier to be overcome (Leikin et al., 1987). Once these electrostatic forces have been overcome, the hydration barrier prevents lipids of opposing membranes to interact. This barrier needs to be destabilised to allow for a stalk to form (Markin et al., 1984). After contact a hemifusion "stalk" forms which turns into a hemifusion "diaphragm" before a pore opens allowing contents to mix and at this point full fusion can occur (Chernomordik et al., 1987).

1.4.2. The SNARE hypothesis

SNARE proteins are the molecular machinery required for membrane fusion (Weber et al., 1998). Membranes contain opposite types of SNARE protein that are required to form a complex. It is the formation of the SNARE complex that brings two opposing membranes into close proximity (**Figure 1.4**) and allows the electrostatic forces of repulsion between membranes to be overcome and membrane fusion to occur (Chen and Scheller, 2001). Originally SNARE proteins on vesicles were denoted v-SNAREs and those on the target membrane denoted as t-SNAREs. This was not found to be accurate as it did not include homotypic fusion, so they were renamed as R-SNAREs and Q-SNAREs due to their contribution to the ionic layer of arginine or glutamine respectively (Fasshauer et al., 1998). This ionic layer in SNARE proteins is highly conserved and required for the dissociation of the complex (Scales et al., 2001). SNARE proteins themselves are highly conserved across eukaryotes demonstrating the conserved nature of this trafficking step (Kloepper et al., 2007).

Although they are the minimal machinery required for membrane fusion (Weber et al., 1998), SNARE proteins do not function alone and many other factors are involved such as N-ethylmaleimide-sensitive factor (NSF) and soluble NSF attachment proteins (SNAPs) (Söllner et al., 1993b). N-Ethylmaleimide (NEM) is a compound that inhibits protein trafficking through Golgi stacks in vitro. The use of NEM in a cell-free system allowed an ATPase required for membrane fusion, termed "NEM sensitive factor" or NSF to be identified, NSF is a tetramer made up of 76 kDa subunits (Block et al., 1988; Glick and Rothman, 1987; Tagaya et al., 1993). NSF uses ATP to rearrange SNARE proteins prior to fusion (Banerjee et al., 1996). After SNARE complex formation and membrane fusion,

SNAPs and NSF are required for SNARE protein disassembly (Söllner et al., 1993a). Both SNAPs and NSF are conserved across evolution from yeast to mammalian cells, with the yeast homolog of NSF being termed Sec18 (Clary et al., 1990; Wilson et al., 1989).

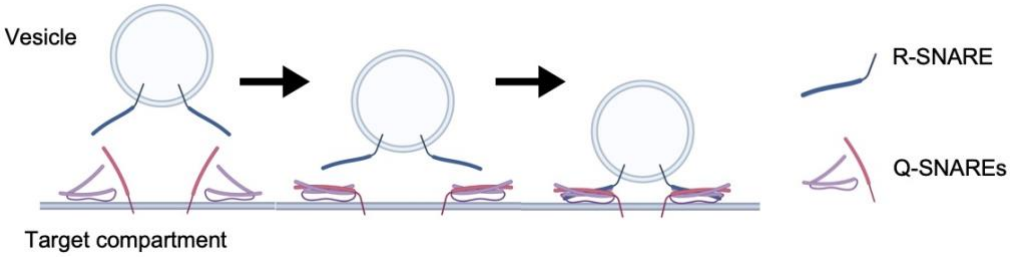

Figure 1. 4 SNARE proteins are required for membrane fusion.

Schematic showing the fusion of two membranes. Where there are three Q-SNAREs and one R-SNARE that bind to form a SNARE complex, thus bringing the membranes into close proximity and overcoming electrostatic forces of repulsion to enable membrane fusion.

1.4.2.1. Sec1/Munc18 proteins

SM proteins are a class of proteins first identified from rat brain homogenates to bind to the syntaxin family of Q-SNAREs (Hata et al., 1993) and are implicated in acting before the formation of the fusion pore (Jahn and Südhof, 1999). Syntaxins are a type of Q SNARE and were first identified in rat neuronal cells through biochemical and localisation studies (Bennett et al., 1992). They were demonstrated to provide membrane specificity after being observed to localise to different intracellular compartments (Bennett et al., 1993).

One example of an SM protein in yeast is Vps45 and its cognate Q-SNARE Tlg2 are required for delivery of vesicles from the cytoplasm to the vacuole (Abeliovich et al., 1999). Vps45 acts as a chaperone for Tlg2 and to activate the formation of its ternary SNARE complex (Bryant and James, 2001). Sec1 is another example of a SM protein in yeast, Sec1 was first identified from the *SEC* genetic screen in the 1980s (Novick et al., 1980). It was later implicated in functioning late in the secretory pathway in exocytosis (Carr et al., 1999), where it is now known to interact with the Sec6 subunit of the exocyst complex to facilitate membrane fusion (Morgera et al., 2012).

1.4.3. Rabs and coats assist the membrane fusion machinery

In addition to SNAPs, NSF and SM proteins, other molecular players are required to assist with membrane fusion. For instance, *ras* genes from rat brain (Rab) proteins are GTPases required for SNARE complex assembly and GTP cycle of Rab proteins dictates the frequency of membrane docking and fusion events (Kabcenell et al., 1990; Rybin et al., 1996; Søgaard et al., 1994).Rab proteins also offer a layer of specificity to membrane trafficking events which is partially conferred through their highly variable C-terminal domain that binds to membranes (Chavrier et al., 1991; Li et al., 2014). Different Rab proteins function at different points of membrane trafficking. For example, the mammalian Rab5 and its yeast homolog Vps21 function in the endocytic pathway (Rybin et al., 1996; Singer-Krüger et al., 1994; Stenmark et al., 1994). Or the Rab GTPase Sec4 that functions late in the secretory pathway to regulate trafficking from the Golgi to the plasma membrane (Goud et al., 1988)

Coat proteins function to allow specific molecules to be transported in vesicles and to be targeted to specific membranes (Bonifacino and Lippincott-Schwartz, 2003). Coated vesicles were first identified in the 1960's in mosquito oocytes where they were seen to form around vesicles that were uptaking protein into the oocyte (Roth and Porter, 1964) and later in guinea pig brain and liver fractionations (Kanaseki and Kadota, 1969). Clathrin was the first coat protein to be identified followed by COPI and COPII coats (Bonifacino and Glick, 2004)

1.4.4. Clathrin

Clathrin was identified first as a 180 kDa protein that forms a coat around vesicles (Kanaseki and Kadota, 1969; Pearse, 1975). Clathrin forms a triskelion shape comprised of three heavy chains and three noncovalently bound light chains (Kirchhausen and Harrison, 1981; Ungewickell and Branton, 1981). The assembly and disassembly of these clathrin triskelions drives the formation and release of vesicles. The formation of the clathrin coat structure is driven by adaptor proteins (AP) (Keen, 1987). Clathrin functions in different locations and so these APs give a layer of specificity. Clathrin was found to not be involved in the secretory pathway as yeast cells lacking clathrin were still observed to secrete proteins thus suggesting an alternative unknown at the time coat protein (Payne and Schekman, 1985). A study shortly after this also deleted the clathrin gene but these cells were inviable unless they contained a suppressor mutation at a specific locus (Lemmon and Jones, 1987). They later identified this locus encoded Pal2 which they implicated in functioning at an early stage of clathrin-mediated endocytosis (Moorthy et al., 2019) and explaining why their cells were viable.

1.4.5. COPI/coatomer coat

The COPI coat was first identified due to it looking different from the hexagonal shape seen in clathrin coated vesicles and was observed to be coating vesicles budding from the Golgi (Orci et al., 1993). COPI vesicles are derived from the Golgi and are coated with a complex termed coatomer (Kappler et al., 1991). Their formation requires ADP-ribosylation factor (ARF) proteins and GTP (Orci et al., 1993). COPI vesicles enable the retrieval of ER-resident proteins from the Golgi, coatomer recognises the KKXX motifs seen in ER-resident proteins (Cosson and Letourneur, 1994; Letourneur et al., 1994). One subunit of coatomer is Beta-COP, which is a 110kDa Golgi membrane protein (Duden et al., 1991).

1.4.6. COPII coat

Initially it was thought that proteins were trafficking from the ER to the Golgi in a bulk-flow mechanism (Wieland et al., 1987), we now know that this process is much more controlled and selective. Nascent polypeptides are targeted to the Golgi from the Endoplasmic reticulum through vesicles coated in COPII coats. Sec23 was identified to function in trafficking between the ER and Golgi and it was noted that it likely was part of a large complex (Hicke and Schekman, 1989). Which we now know to be the COPII coat complex. In yeast cells the COPII coat is comprised of: Sec23 complex, Sec13 complex and the GTPase Sar1 (Barlowe et al., 1994; Nakańo and Muramatsu, 1989). The interaction of these factors with the lipids that make up the ER membrane is what drives COPII formation (Matsuoka et al., 1998). Cargo selection is mediated by Sec24 (part of the Sec23 complex), which contains various domains to recognise sorting signals (Miller et al., 2003).

1.5. Components of the secretory pathway

1.5.1. The endoplasmic reticulum

The ER is made up of various interconnected structures such as sheets, tubules and a nuclear envelope that perform different functions (Schwarz and Blower, 2016). The ER is composed of cortical ER (cER) and perinuclear ER (pER) (Voeltz et al., 2002) (**Figure 1.6 left**). Contact sites to the plasma membrane (ER-PM contact sites) are required for the maintenance of correct ER function and involved in signalling and lipid metabolism (Manford et al., 2012; Zaman et al., 2020). Ribosomes localise to the cytosolic face of the ER through SRP-dependent or SRP-independent mechanisms to allow protein synthesis to begin (Costa et al., 2018). Nascent proteins are synthesised in the endoplasmic reticulum (ER) and traffic to the surface via the Golgi (Novick et al., 1981). The *SEC* genes which were first identified in *S. cerevisiae* encode proteins that orchestrate the traffic through these secretory pathways (Novick et al., 1980). Proteins are trafficked into the ER in yeast via the complex that is composed of Sec61, Sec62 and Sec63, in addition to other proteins: Sec70, Sec71 and Sec72 (Deshaies and Schekman, 1989; Feldheim et al., 1993; Green et al., 1992). Sec61 complex allows for signal recognition at the ER (Saraogi and Shan, 2011), where the signal sequence binds and directly contacts Sec61 and Sec62 (Plath et al., 2004). Shown below is a schematic of the Sec complex along with other mentioned ER proteins, where members of the Sec complex can be used as markers for the ER (**Figure 1.5**). Mammalian homologues of Sec61, Sec62 and Sec63 were found and shown to be involved in translocation of proteins into the ER (Meyer et al., 2000; Tyedmers et al., 2000).

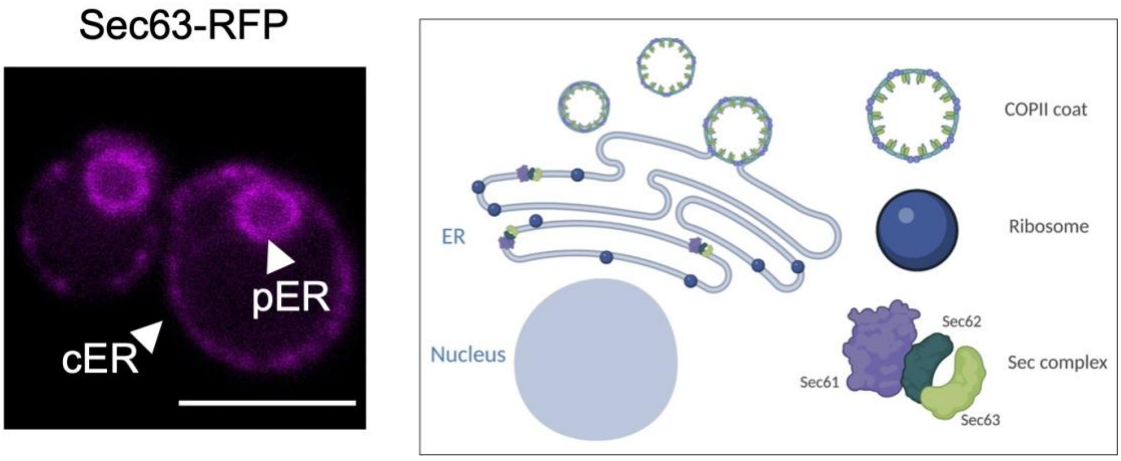

Figure 1. 5 Components of the Endoplasmic Reticulum

Micrograph of fluorescently tagged Sec63, a marker of perinuclear (pER) and cortical (cER), to visualise the ER in yeast cells. Imaged using Zeiss 710. Scale bar = 5µm. (**left**). Schematic showing some components of the endoplasmic reticulum (ER) such as the COPII coated vesicles, ribosomes and the Sec complex (**right**).

1.5.1.1. SRP dependent translocation

Nascent polypeptides can be imported into the ER through different mechanisms. One such way is by binding the signal recognition particle (SRP) (Walter and Blobel, 1981), which causes them to be targeted as ribosome-associated complexes to the ER via SRP-receptor (SR). This is a cotranslational translocation through a protein-conducting channel formed at the rough ER (Simon and Blobel, 1991). Then Sec61 complex (Sec61 alpha, beta and gamma) interacts with membrane-bound ribosomes and forms a translocon and allows the release of the polypeptide from the SRP-SR complex (Görlich et al., 1992). For the SRP-SR-polypeptide complex to dissociate GTP hydrolysis is required, the Sec61 complex facilitates this hydrolysis and forms a pore to allow the translocating polypeptide through (Connolly et al., 1991; Plath et al., 2004; Song et al., 2000). For this to occur Sec63 and Kar2 are required (Young et al., 2001). When exploring the SRP it was observed that yeast cells lacking the SRP were viable and that some protein translocation could occur. It also appeared that factors affected in *sec63* mutant strains (for example) were less affected in SRP disrupted strains and vice versa (Hann and Walter, 1991). Leading to the thought that there was an alternative SRP-independent translocation pathway.

1.5.1.2. SRP independent translocation

As hypothesised, there is an alternative translocation pathway, an SRP-independent translocation which involves Sec62 and Sec63 (Ng et al., 1996). Studies in yeast and mammalian cells began to uncover the two translocation pathways and the differences seen in these species (Rothe and Lehle, 1998). In yeast, the prepro-alpha factor was observed to translocate into the ER post translationally without the requirement of a membrane potential but requiring ATP instead (Waters and Blobel, 1986). So prepro-alpha factor was used to study the mechanism by which this works. This SRP-independent translocation was seen to require the Sec61 complex as well as four membrane proteins and the presence of Kar2 and ATP (Panzner et al., 1995). Kar2 was first identified as being a homolog for the mammalian BiP/GRP78 and is necessary for nuclear fusion (Polaina and Conde, 1982; Rose et al., 1989). Studies in yeast on the Kar2 protein implicated its role in translocation of proteins into the ER which illuminated the role that BiP plays in mammalian cells (Vogel et al., 1990). BiP was known to have a role in protein folding in the ER but upon using yeast

its role in translocation was uncovered (Nguyen et al., 1991). As mentioned above Kar2 and Sec63 are required for SRP dependent translocation (Young et al., 2001) where Sec62 is not (Ng et al., 1996) demonstrating the separate roles that these proteins play.

1.5.2. Golgi apparatus

In mammalian cells, the Golgi is organised into stacks of membrane-bound cisternae, where transport between cisternae occurs through vesicles (Rothman, 1981). The Golgi has polarity with regions on the vacuolar or secretory side being referred to as “trans” and the opposite side as “cis” (Ehrenreich et al., 1973). *S. cerevisiae’s* Golgi takes on a different structure, where its Golgi cisternae are scattered throughout the cytoplasm (Franzusoff et al., 1991; Preuss et al., 1992). Although structurally they differ, proteins in *S. cerevisiae* undergo the same processing steps in the Golgi as in mammalian cells. Where the *S. cerevisiae* Golgi contains the same distinct regions and resident enzymes as in mammalian cells (Duden and Schekman, 1997).

From the ER, these proteins are transported to the Golgi, a process driven by COPII coated vesicles (Barlowe et al., 1994). Nascent proteins are modified as they transit through the Golgi. At the Golgi, proteins can be post-translationally modified, such as by glycosylation, before being packaged into vesicles and targeted to the plasma membrane where they perform different functions (Stanley, 2011). When the coat protein clathrin is associated with AP1 adaptors it functions in the transport of proteins from the trans-Golgi network (TGN) to endosomes (Ahle et al., 1988).

For fusion with the plasma membrane, a GTPase, SNARE proteins and the exocyst complex are required (Novick et al., 1995). Exocyst acts as a tether for the vesicles and is comprised of eight proteins: Sec6, Sec8, Sec15, Sec3, Sec5, Sec10, Exo70 and Exo84. Some of these factors were identified in the *SEC* genetic screen for late acting secretory proteins (Guo et al., 1999; Novick et al., 1980; Terbush et al., 1996). Exocyst was discovered in yeast cells and later identified in mammalian cells. Studies in rats identified rSec6 and rSec8 to be homologous to yeast Sec6 and Sec8 respectively(Hsu et al., 1996; Ting et al., 1995). The Sec6 subunit plays an important role in this process by initially binding the membrane t-SNARE Sec9 to form an intermediate complex (Sivaram et al., 2005). Sec1 and exocyst act to regulate SNARE complex assembly. Upon release of Sec9, Sec6 forms a complex with the SM protein Sec1 (Morgera et al., 2012). For this process a GTPase is also required, the GTP bound GTPase Cdc42 binds to the exocyst subunit Sec3 to fulfil this role (Zhang et al., 2001). Sec3 also interacts with membrane lipids and its interactions with $PI(4,5)P_2$ and Cdc42 are both required for exocytosis (Zhang et al., 2008).

1.6. The eukaryotic plasma membrane

The eukaryotic plasma membrane is composed of proteins and lipids. Understanding how lipids might organise in a plasma membrane is experimentally challenging. Eukaryotic cells contain membrane bound organelles which are hard to separate out fully from the plasma membrane through methods such as centrifugation. Additionally, the plasma membrane contains inner and outer leaflets that have different lipid compositions (Feigenson, 2006). How these lipids then interact with proteins within the plasma membrane is a vast field.

1.6.1. Models for protein and lipid interactions

The “mattress model” uses thermodynamics to describe how lipids and proteins might interact. The concept is that there is a mismatch in lipid hydrophobic regions which alters the temperature range of lipid phases and therefore alters how peptides in the membrane can be organised (Mouritsen and Bloom, 1984). Hydrophobic interactions governing protein folding (Chothia, 1976) allow proteins to reside within the plasma membrane but alternatively proteins can be anchored to the plasma membrane through covalent attachments to the polypeptide with anchors such as Glycosylphosphatidyl inositol (GPI) (Low et al., 1986). GPI is a glycoprotein first characterised from *Trypanosoma brucei* (Ferguson et al., 1988; Fox et al., 1986). This attachment is added in the lumen of the ER and then subsequent modification of the attachment in the Golgi, precedes trafficking to the plasma membrane. The process of generating this GPI moiety is conserved across species (Ferguson et al., 2009). One difference is that in yeast cells GPI anchored proteins are separated from non-GPI anchored proteins when they traffic from the ER to the Golgi, something that doesn’t happen in mammalian cells until Golgi to plasma membrane traffic. This is due to the mechanisms by which each organism packages cargo into COPII vesicles, which in yeast is closely linked to sphingolipid synthesis and protein-lipid interactions (Rivier et al., 2010). A key part of the lipid raft hypothesis is the clustering of GPI-anchored proteins

1.6.2. The organisation of lipids within the plasma membrane

Early work on the composition of surface membranes suggested that lipids form separate domains within the plasma membrane (Klausner et al., 1980). Since then, there have been different theories as to how they are organised. The fluid mosaic model states that integral membrane proteins are arranged in an amphipathic structure with the nonpolar groups buried in the hydrophobic interior of the plasma membrane. These proteins are embedded in a matrix of phospholipids that is organised in a fluid bilayer (Singer and Nicolson, 1972). In this model, the lipids and proteins are able to diffuse freely within the bilayer but later evidence suggested against proteins diffusing freely and that lipids might be organised into domains and protein interactions with other components might dictate their location in the bilayer (Karnovsky et al., 1982). This gave way to the “lipid-raft model” of organisation. The lipid raft model describes how cholesterol and sphingolipids in the outer leaflet of the plasma membrane cluster into domains.

There was a lot of discussion surrounding the definition of lipid rafts that had been ongoing for years in this interdisciplinary field (Jacobson et al., 2007). At the 2006 Keystone Symposium on Lipid Rafts and Cell Function a general definition was agreed upon, where lipid rafts can be described as being “small (10 – 200 nm), heterogeneous, highly dynamic, sterol- and sphingolipid-enriched domains that compartmentalize cellular processes” (Pike,

2006). Inevitably, in such a complex area of research, even now there is still a lot of controversy surrounding defining lipid rafts (Levental et al., 2020). Biophysical studies have demonstrated the self-assembly of lipids to form bilayers and the clustering into “rafts” (Simons and Ikonen, 1997). A challenge has been demonstrating that lipid rafts occur *in vivo*. Lipid rafts are insoluble in Triton X-100 and so can be extracted. After the use of triton to collect the insoluble lipid fraction, chromatography can be used to determine the lipid composition (Brown and Rose, 1992). But to understand where these complexes originate from organelles must be isolated prior to Triton X-100 extraction and this does not report on the functionality of these lipids *in vivo*. Through this technique proteins with a wide range of functions have been identified in the insoluble fraction which suggested that potentially this protocol was not specifically isolating raft-associated proteins and rather broadly isolating various insoluble proteins (Kurzchalia et al., 1995).

1.6.3. The organisation of proteins within and at the plasma membrane

Proteins are segregated into non-homogenous patterns across the plasma membrane, which is influenced by the lipid composition of the plasma membrane. Cell surface membrane proteins fit into two broad categories: integral and peripheral. The organization of these proteins at and within the plasma membrane is tightly regulated. Transmembrane sequences (TMS) of surface proteins also influence these proteins lateral organisation at the plasma membrane (Spira et al., 2012). The plasma membrane is host to a wide range of proteins including receptors such as the family of G protein-coupled receptors (Weinberg and Puthenveedu, 2019), ion channels (Gustin et al., 1986) and nutrient transporters (Busto and Wedlich-Söldner, 2019). One such family of transporters is the Amino Acid-Polyamine-Organocation (APC) family of transporters that are specific for amino acids, polyamines and choline which are found across species from yeast to humans (Reizer et al., 1993). This superfamily of transporters has undergone phylogenetic analysis in order to understand the evolutionary relationship of these transporters across species, from eukaryotes to prokaryotes (Jack et al., 2000). The APC superfamily has been shown to have arisen from a two transmembrane spanning (TMS) hairpin structure (Wong et al., 2012).

1.6.4. The distinct domains of the plasma membrane

In yeast, studies have been conducted to understand the organisation of proteins and lipids within the plasma membrane. Through the tagging of surface proteins with Green Fluorescent Protein (GFP) and visualising over time where they localise (Malínská et al., 2003). Early studies noted that the arginine symporter Can1 (Ahmad and Bussey, 1986) and the plasma membrane ATPase Pma1 (Serrano et al., 1986) localised to distinct non-overlapping regions of the plasma membrane (Malínská et al., 2003). The region that Pma1 localised to was termed the “membrane compartment occupied by Pma1” or MCP (Grossmann et al., 2007). The region that Can1 was seen to localise to was called the “Membrane Compartment of Can1” or MCC (Malínská et al., 2003) which was later termed “eisosomes” (Walther et al., 2006). More recent work has used superresolution microscopy tools to understand the organisation of the plasma membrane (Spira et al., 2012). Pil1 is a core eisosomal component (Walther et al., 2006), fluorescently tagging Pil1 allows the punctate pattern of eisosomes across the plasma membrane to be visualised (**Figure 1.6**).When there is a lack of methionine, the methionine APC transporter Mup1 localises to these MCC domains where it is protected from endocytosis but in response to methionine is observed to localise to a different network-like domain across the plasma membrane where it is susceptible to endocytosis (Busto et al., 2018). The G alpha subunit Gpa2, that localises to the plasma membrane (Huh et al., 2003; Nakafuku et al., 1988), is seen to occupy a more network-like domain compared to the eisosomal core component Pil1 (**Figure 1.6**).

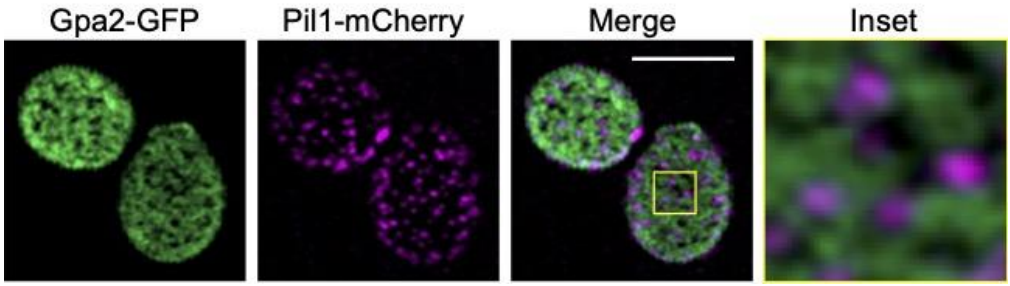

Figure 1. 6 The organisation of proteins within the plasma membrane.

Micrographs showing top focus of cells expressing Gpa2-GFP, which exhibits a meshwork network across the surface and Pil1-mCherry, which demark specific distinct compartments of defined protein and lipid composition. Cells were imaged using Zeiss 980 with an Airyscan 2 detector. Scale bar = 5µm.

1.6.5. Eisosomes as protective compartments

Eisosomes were first identified as distinct domains of the plasma membrane in the early 2000's (Malinska et al., 2004; Malínská et al., 2003). In 2006 these distinct domains were named "eisosomes". Thought to be sites of endocytosis, their name was derived from the Greek for portal '*eis*' and body '*soma*'. The belief that they were sites of endocytosis was based on their apparent co-localisation with actin patches and genetic interactions between eisosomal components and endocytic effectors (Walther et al., 2006). From the data presented and available at the time it was a fair conclusion to draw that eisosomes marked sites of endocytosis. It is now established that rather than marking sites of endocytosis they are regions where membrane proteins are not susceptible to the endocytic machinery (Brach et al., 2011; Grossmann et al., 2008). When in eisosomes, nutrient transporters are in an inactive state and changes in the proton gradient of the plasma membrane cause these sequestered inactive transporters to leave eisosomes (Moharir et al., 2018).

Pil1 assembly drives the formation of eisosomes. Eisosomes form de novo in the daughter cells of budding yeast which has allowed their formation to be studied temporally. Eisosome component Seg1 begins to localise before the assembly of Pil1/Lsp1 that drives eisosome formation (Moreira et al., 2012). The phosphorylated status of Pil1 is important for eisosome assembly. Where hyperphosphorylated Pil1 causes eisosomal disassembly (Walther et al., 2007)Nce102 is a tetraspan protein that regulates the formation of eisosomes through inhibition of the kinase responsible for Pil1 phosphorylation (Fröhlich et al., 2009). Amongst these factors that drive the formation of eisosomes, various other proteins have been found to localise to eisosomes. Future work will likely involve teasing out the roles that these proteins play in eisosome formation and function.

1.6.6. Core eisosomal components Pil1 and Lsp1 are BAR domain proteins

Core eisosomal components Pil1 and Lsp1 are Bin/amphiphysin/Rvs (BAR) domain proteins. The conserved BAR domain can bind negatively charged membranes and cause membrane curvature (Peter et al., 2004). The ability to bend a membrane is biophysically a challenge and so it is not surprising that eisosomes are composed of multiple types of BAR domain protein that can contribute to this membrane bending. Pil1 and Lsp1 are N-BAR domain proteins, whilst other eisosomal components Slm1/Slm2 are F-BAR domain

proteins (Olivera-Couto et al., 2011). F- and N-BAR domain protein dimers the positively charged concave face binds to the negatively charged membrane and this enables the membrane to be bent (Peter et al., 2004). Pil1 and its BAR domain are important for eisosome formation, with cells with mutated Pil1 BAR domains displaying defects in eisosome organisation and an increase in cytoplasmic Pil1 (Olivera-Couto et al., 2011).

1.7. Components of the endosomal system

Proteins at the plasma membrane can be internalised, one well characterised mechanism is clathrin-mediated endocytosis. The stages broadly involve the following steps: initiation, cargo selection, coat assembly, scission and uncoating (McMahon and Boucrot, 2011). Additional proteins were identified to bridge clathrin and the membrane proteins in the vesicle and were later broadly termed “adaptor proteins” (Robinson, 1987). Clathrin adaptors select the cargo to be internalized and allow the assembly of clathrin to begin (Maldonado-Báez and Wendland, 2006). These adaptor proteins such as the AP-2 complex bind lipids in the plasma membrane (PtdIns(4,5)P_2), in the case of AP-2 this region of binding is conserved across species (Gaidarov et al., 1996). The class of AP180 proteins found in mammalian cells (Morris et al., 1993) and also a homologous version found in yeast cells. The yeast AP180 proteins are found to localise to the plasma membrane and assist with clathrin coat assembly (Wendland and Emr, 1998). The formation of clathrin-coated pits then leads to the formation of clathrin-coated vesicles (**Figure 1.7**) which is mediated by adaptor proteins such as AP-2 or AP180s (Traub, 2003). For the internalisation of this vesicle, actin is required and this is observed in both yeast and mammalian cells (Kübler and Riezman, 1993).

There are clathrin-independent internalisation pathways, in mammalian cells various ones have been characterised such as those through caveolar or fluid-phase endocytosis (Kiss and Botos, 2009; Mayor and Pagano, 2007). In yeast cells there are also clathrin-independent internalisation pathways, such as one that relies on the GTPase Rho1 (**Figure 1.7**(Prosser et al., 2011)), similar to one seen in mammalian cells (Lamaze et al., 2001). In yeast it wasn’t clear which factors were involved in endocytosis but genetic screens using reporters such as attaching enzymes with a readout to the surface protein Snc1 to identify mutants defective in Snc1 internalisation (Burston et al., 2009). Snc1 is a R-SNARE that is functionally redundant with Snc2 in the fusion of secretory vesicles at the cell surface for bulk secretion (Protopopov et al., 1993; Shen et al., 2013). Snc1 also interacts with t-SNAREs Tlg1/Tlg2 to retrieve proteins from the plasma membrane (Gurunathan et al., 2000).

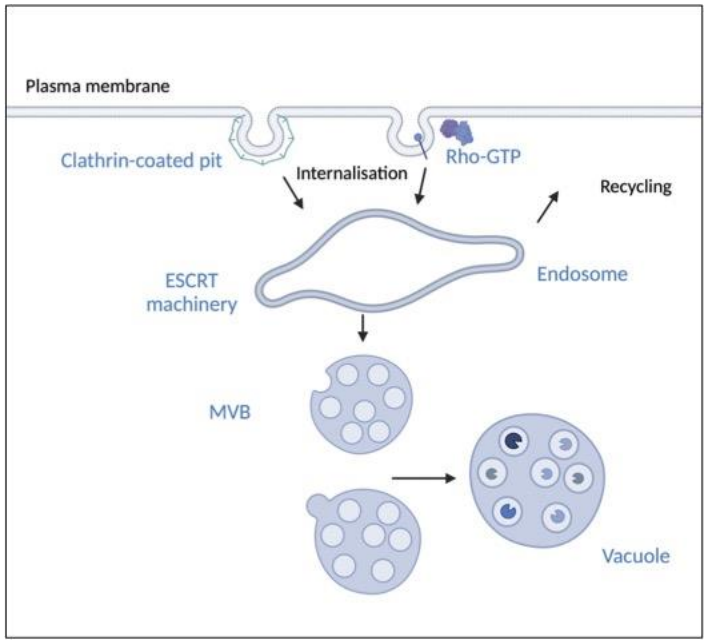

Figure 1. 7 The endosomal system

Schematic showing an overview of the endosomal system. Internalisation from the plasma membrane by clathrin mediated endocytosis (CME) and clathrin independent endocytosis (CIE) which requires the Rho-GTPase. Following internalisation, proteins can be recycled back to the plasma membrane or trafficked to the trans-Golgi network (TGN) through retrograde trafficking. A signal for degradation sends the internalised cargo through the multivesicular body (MVB) pathway, initiated by the ESCRT machinery. The cargo reaches the vacuole for degradation.

1.7.1 The process of ubiquitination

Ubiquitin is a 8.5 kDa protein (Goldstein et al., 1975) that is highly conserved at the sequence and structural level across eukaryotes (Burroughs et al., 2012), work done in the early 1980s found that its addition to polypeptides lead to the polypeptide being degraded (Hershko et al., 1980; Wilkinson et al., 1980). Ubiquitination is a crucial component of cellular function and highly conserved across living species. Proteins can be monoubiquitinated or a chain of ubiquitin molecules can be built, these different combinations allow a variety of different signalling to be activated (Komander and Rape, 2012). Addition of a ubiquitin molecule to substrates requires a cascade of signalling. This cascade involves three enzymes: E1 ubiquitin-activating enzymes, E2 ubiquitin conjugating enzymes and E3 ubiquitin ligases are required for the attachment of ubiquitin molecules to substrates. E1 ubiquitin-activating enzymes begin the cascade by forming an intermediate with a ubiquitin which can then be recognised by the E2 enzyme (Pickart, 2001; Schulman and Wade Harper, 2009). E3 ligases recognise targets and enable the transfer of ubiquitin from an E2 enzyme (**Figure 1.8**) (Deshaies and Joazeiro, 2009). The recognition of the ubiquitin attachment by various proteins dictates the fate of that protein. The lysine residue that ubiquitin is attached to is important for specificity. Whether this ubiquitin moiety is ubiquitinated to form a polyubiquitin chain or remains as a monoubiquitin moiety dictates the fate of the protein. For example, monoubiquitination signals for endocytosis whereas homotypic polyubiquitination on Lys48 signals for proteasomal degradation (Husnjak and Dikic, 2012).

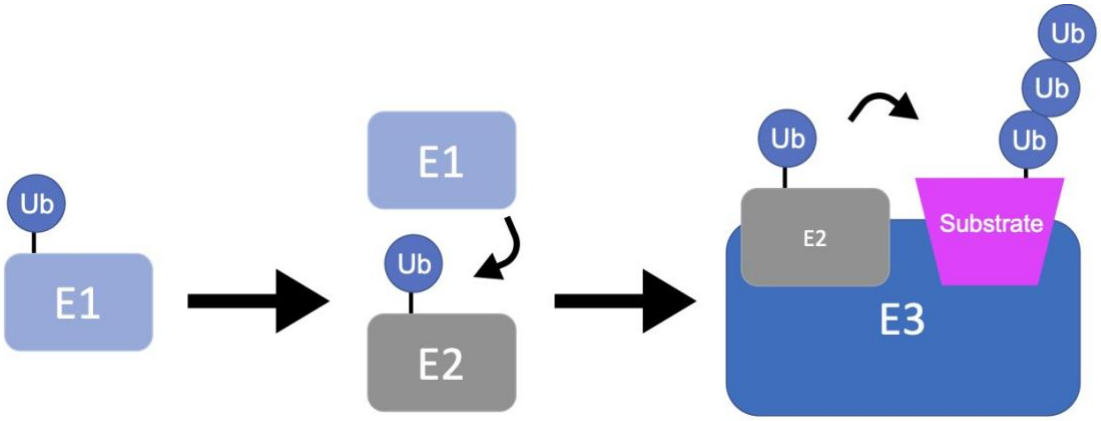

Figure 1. 8 The cascade of ubiquitination.

The E1 ubiquitin-activating enzyme (E1) covalently attaches to a ubiquitin (Ub) moiety. E1-Ub is recognised by the E2 conjugating enzyme (E2) where the Ub is transferred to the E2 enzyme. This E2-Ub moiety is then recognised by the E3 ubiquitin ligase (E3) where the Ub is transferred to the substrate.

1.7.1.1. Ubiquitination in membrane trafficking

Ubiquitin binding domains (UBD) in proteins allow them to non-covalently bind to monoubiquitin or ubiquitinated proteins (Hicke et al., 2005). Various ESCRT proteins contain UBDs, in particular subunits within the ESCRT-0 and ESCRT-I complexes (Katzmann et al., 2001). Not only are ESCRTs responsible for acting as receptors for ubiquitinated cargo destined for degradation but are also responsible for generating the intraluminal vesicles that bud in the MVB (Piper and Katzmann, 2007). To form vesicles, the limiting membrane of the endosome buds inwards in a process driven by ESCRT polymerisation that deforms the membrane (Babst, 2011). Rsp5 is a ubiquitin ligase (Huibregtse et al., 1997) that has a variety of different roles in membrane trafficking (Belgareh-Touzé et al., 2008). Such as its ubiquitination of the vast majority of cargoes that are destined for degradation (Ren et al., 2007; Stringer and Piper, 2011). Nutrient transporters such as the uracil permease Fur4 are ubiquitinated by Rsp5 at the plasma membrane, this signals their internalisation and subsequent degradation (Galan et al., 1996). This specificity is conferred by adaptor proteins that can recruit Rsp5 to specific targets, such as Sna3 recruitment of Rsp5 to the methionine transporter Mup1 (MacDonald et al., 2012c).

1.7.2. ESCRT machinery

The ESCRT machinery is a conserved set of protein complexes that facilitate the sorting of ubiquitinated cargo through the MVB pathway. ESCRT-0, which is composed of Vps27 and Hse1, initiates the MVB pathway and begins the cascade of events for MVB generation (**Figure 1.9.**). Vps27 recognises and interacts with a phosphatidylinositol 3- phosphate (PI3P) through its FYVE domain allowing the complex to interact with lipids directly (Misra and Hurley, 1999), directing the ESCRT-0 complex to endosomes (Katzmann et al., 2003). The ESCRT-0 complex recognises and binds to ubiquitinated cargo (Bilodeau et al., 2002) along with the Vps23 subunit of ESCRT-I which is recruited next to the endosomal membrane (Bilodeau et al., 2003). ESCRT-I is a 350kDa complex that is made up of Vps23, Vps28 and Vps37 and is conserved from yeast to mammalian cells (Katzmann et al., 2001). The Vps23 subunit of ESCRT-I interacts with Vps27 from ESCRT-0 (Bilodeau et al., 2003).

ESCRT-0, I and II are imported to the endosome as preformed complexes (Teis et al., 2008). The ESCRT-II complex (Vps22, Vps25 and Vps36) functions downstream of

ESCRT-I but immediately before ESCRT-III where its transient interaction with the endosomal membrane initiates the formation of ESCRT-III (Babst et al., 2002a). ESCRT-III (Vps2, Vps20, Vps24 and Snf7) assembles at endosomes after its subunits have been recruited from the cytoplasm (Babst et al., 2002b). The ESCRT-III complex is required for the final stages of MVB sorting where cargo is sequestered (Teis et al., 2008). ESCRT-III assembly causes the endosomal membrane to deform and bud inwards (Saksena et al., 2009). ESCRT-IV is required to disassemble ESCRT-III and therefore enable the recycling of its subunits (Babst et al., 2002b). ESCRT-IV or Vps4 is an AAA+ ATPase (Babst et al., 1997) and functions with ESCRT-III to deform and cause the scission of membranes to allow the vesicle to bud off (Babst et al., 1998). The ESCRT machinery also plays a role in processes other than cargo sorting through the MVB, such as in separation of cells in cytokinesis (Caballe and Martin-Serrano, 2011). Or in the context of mammalian cells, where a cell has been infected with a virus such as human immunodeficiency virus (HIV) the virus hijacks the cells ESCRT machinery and this allows the virus to be packaged and released (Von Schwedler et al., 2003; Votteler and Sundquist, 2013).

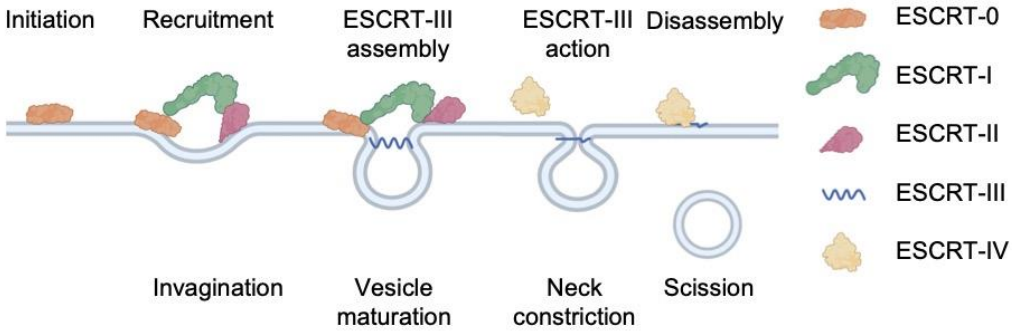

Figure 1. 9 Budding of vesicle mediated by the ESCRT machinery

Schematic showing an overview of ESCRT function in the generation of MVBs, where factors are recruited throughout the stages. Initiation of this process is started by ESCRT-0, upon ESCRT-1 and ESCRT-II recruitment membrane invagination begins. ESCRT-III allows the vesicle to mature and then its action causes constriction of the bud neck before ESCRT-IV (Vps4) allows for membrane scission.

1.7.3. The vacuole

In mammalian cells there are lysosomes which are the organelle responsible for the degradation in the endosomal system. Yeast have a similar organelle termed the vacuole (Li and Kane, 2009). The yeast vacuole, like the mammalian lysosome, is acidic and this acidity is generated and maintained by proton pumps (Li and Kane, 2009). Cargo is delivered to the vacuole both through selective and non-selective mechanisms. These pathways are regulated by different complements of proteins but there is some overlap between them (Bryant and Stevens, 1998). I have described the delivery of proteins to the vacuole through the MVB pathway, but vacuolar resident proteins are delivered directly to the vacuole through pathways such as the CPY and ALP pathways. Vacuolar proteases are delivered to the vacuole as zymogens that are cleaved to become activated preventing degradation occurring outside of the vacuole (Hecht et al., 2014; Hemmings et al., 1981; van den Hazel et al., 1992).

Autophagy is the process by which material in the cell is delivered to the lysosome/vacuole for degradation (Yorimitsu and Klionsky, 2005). This is a conserved process across eukaryotes (Reggiori and Klionsky, 2002). Autophagy is upregulated during periods of starvation in order to generate material for the cell (Takeshige et al., 1992). The cytoplasm-

to-vacuole (cvt) pathway delivers proteins to the vacuole. Aminopeptidase I (API) is a vacuolar hydrolase encoded by the APE1 gene that reaches its destination through this cvt pathway (Cueva et al., 1989; Klionsky et al., 1992; Scott et al., 1996). Specifically, API is a zinc metalloproteinase that acts to breakdown material by hydrolysing peptide bonds (Schu, 2008). Vps34 plays a role in retrograde traffic from the endosome to the Golgi but was first identified as being required for the sorting of proteins through the vacuolar system (Robinson et al., 1988; Schu et al., 1993). In both mammalian and yeast cells it has been found to play a role in autophagy (Jaber et al., 2012).

1.7.3.1. The CPY pathway

Carboxypeptidase Y (CPY) is a yeast vacuolar enzyme (Wiemken et al., 1979). Mutations in the signal sequence (N-terminal region) of CPY result in its failure to be trafficked to the vacuole and instead is secreted from the cell (Johnson et al., 1987; Valls et al., 1987) and defects in the trafficking pathway also result in its aberrant secretion (Rothman and Stevens, 1986). The studying of CPY trafficking in these mutants helped characterise this class of mutants now to be termed “vacuolar protein sorting” or *vps* mutants. These mutants were seen to cause CPY to be secreted, demonstrating their role in the sorting of proteins from the Golgi to the vacuole (Bankaitis et al., 1986; Rothman and Stevens, 1986). Additionally, the vacuolar morphology of some of these mutants was altered, this provided a basis of classification (Banta et al., 1988). The trafficking of other vacuolar proteins was studied in these mutants to help classify them further, at this point in the late 1980’s there were around 50 proteins that had been identified (Robinson et al., 1988). By the early 1990’s these mutants had been classified into six groups based on their vacuolar morphology (Raymond et al., 1992). A later screen for *vps* mutants published in 2002 identified many more potential gene products involved in the regulation of vacuolar protein sorting (Bonangelino et al., 2002).

1.7.3.2. ALP pathway (AP-3 pathway)

Alkaline phosphatase (ALP) is a vacuolar enzyme (Onishi et al., 1979). None of the known *vps* mutants at this time were observed to mislocalise ALP to the plasma membrane suggesting it followed an alternative pathway (Raymond et al., 1992). This alternative pathway was later identified (Piper et al., 1997) and ALP is directed through this alternative pathway through its N-terminal vacuolar sorting signal (Cowles et al., 1997; Klionsky and Emr, 1990). AP-3 was identified as a coat protein that functioned independently to clathrin in the traffic of proteins from the Golgi to the lysosome (Simpson et al., 1996; Simpson et al., 1997) and was later shown to be essential for the trafficking of ALP through this alternative pathway to the vacuole (Stepp et al., 1997).

1.7.4. Retrograde trafficking

Endosome to Golgi retrograde traffic is required to return Golgi-resident proteins and allow endocytosed proteins to be recycled back to the plasma membrane. This is facilitated by the coat complex termed retromer which is comprised of Vps5, Vps29, Vps35, Vps17 and Pep8 (Hettema et al., 2003; Seaman, 2004; Seaman et al., 1998). Vps5 which is part of the retromer complex is classified as a sorting nexin (Nothwehr and Hindes, 1997). Sorting nexins are proteins with phox homology (PX) domains and are found in both *S. cerevisiae* and mammalian cells (Haft et al., 1998; Ponting, 1996). PX domains bind to phosphatidylinositol-3-phosphate (PtdIns3P) and thus enable interactions with membranes (Kanai et al., 2001; Xu et al., 2001). Generation of phosphatidylinositol species are required for retromer to function. Vps34 is a phosphatidylinositol 3-kinase (PI3K) conserved in yeast and mammalian cells (Auger et al., 1989). Vps34 forms a complex that contains Vps15 and

generates PtdIns3P at the endosome to allow recruitment and activation of the retromer complex (Burda et al., 2002). The Golgi-associated retrograde protein (GARP) complex regulates sphingolipid homeostasis in endosome-to-Golgi retrograde traffic (Fröhlich et al., 2015). It is required for this retrograde traffic from early and late endosomes to the Golgi and is comprised of Vps51, Vps52, Vps53 and Vps54 (Conibear and Stevens, 2000). Vps51 is the subunit of the GARP complex that binds to Tlg1 to link the GARP tethering complex to the SNARE fusion machinery (Conibear et al., 2003; Reggiori et al., 2003).

1.7.5. Endocytic recycling

Internalised cargo isn't always degraded. I described earlier the retrograde traffic of cargo from the endosome to the Golgi. Internalised proteins can also be recycled back to the plasma membrane from the endosome/TGN either through deubiquitination or other mechanisms involving interactions with the COPI coat (Laidlaw and MacDonald, 2018). In the case of COPI, the coat protein can interact with polyubiquitin chains which facilitates recycling back to the TGN from endosomes (Xu et al., 2017). Cargo can be recycled back to the plasma membrane via the Golgi, this pathway involves sorting nexins and the retromer complex (Hettema et al., 2003). But a pathway in yeast where cargo can also be recycled back directly to the plasma membrane has been identified, thought to be mediated through the protein Rcy1 (MacDonald and Piper, 2017; Wiederkehr et al., 2000).

Recycling to the plasma membrane from the endosome can occur through the deubiquitination of cargo (MacDonald and Piper, 2016). A class of proteases termed deubiquitinating enzymes (DUbs) function to remove ubiquitin from proteins (Amerik et al., 2000a). Doa4 is a well characterised DUb in yeast that acts on ubiquitin-tagged cargo destined for the vacuole for degradation (Amerik et al., 2000a; Amerik et al., 2000b; Papa and Hochstrasser, 1993). Doa4 requires the protein Bro1 for its recruitment to the endosome (Luhtala and Odorizzi, 2004; Nickas and Yaffe, 1996). Bro1 has a mammalian orthologue called Alix that has a variety of different roles including at endosomes with the ESCRT machinery (Odorizzi, 2006). It was proposed that like Alix, Bro1 functions early in the endocytic pathway with ESCRT-0 and then its recruitment of Doa4 occurs later in MVB formation (Pashkova et al., 2013).

Eukaryotic cells are polarised, and this asymmetry is essential for various basic cellular functions. For example, in mammalian epithelial cells, cell polarity is important for cell-cell adhesion or in budding yeast cells cell polarity is required for defining the mother-daughter axis amongst other things (Nelson, 2003). Proteins at the plasma membrane can be distributed in a polarised fashion. In *S. cerevisiae* the exocytic SNARE Snc1 is observed to localise to regions of polarised growth at all stages of the cell cycle. This is maintained through its endocytosis and recycling back to the plasma membrane (Lewis et al., 2000; Valdez-Taubas and Pelham, 2003). The recycling back to the plasma membrane of internalised Snc1 occurs through a pathway that traffics from endosomes to the late Golgi (Hettema et al., 2003; Lewis et al., 2000). This pathway is distinct from the direct recycling of nutrient transporters such as Mup1 from the endosomal system back the plasma membrane (Laidlaw et al., 2022a). I think the differences in the recycling back to the plasma membrane seen in proteins like Snc1 which are polarised and nutrient transporters such as Mup1 are intriguing and must underlie the differences in function.

For a while the direct recycling of cargo from the early endosome to the plasma membrane was thought to not occur and it was proposed that all recycling occurred via the trans-Golgi network (TGN) (Day et al., 2018). In part this work used the recycling of FM4-64 to demonstrate their findings. FM4-64 does appear to recycle via the TGN but in their micrographs there appears to be non-TGN colocalised dots that are likely the early

endosome. Later work proposed that the deubiquitination of cargo allows recycling from the early endosome (Laidlaw et al., 2022a).

1.8. Summary

1.8.1. My research aims

My PhD project has broadly focussed on how cell surface proteins are regulated. I developed an assay based on the surface activity of a surface membrane nutrient transporter, and used this to perform a genome wide screen to identify novel trafficking factors (Paine et al., 2021). This assay was also the basis for a recovery assay that led to better understanding of nutrient transporter sequestration in eisosomes (Laidlaw et al., 2021). I have also been involved in more focussed projects aimed at understanding the molecular mechanisms of surface proteins regulators, including: Gpa1-PI3K mediated recycling (Laidlaw et al., 2022b); control at the transcriptional level (Amoiradaki et al., 2021); and the post translational control of a key eisosomal factor (Paine et al., 2022) .

1.8.1.1. Chapter II: Fur4-mediated uracil-scavenging to screen for surface protein regulators

Chapter II contains my work performing a genetic screen to identify novel trafficking factors (Paine et al., 2021). For this project I optimised a high-throughput screening protocol to carry out to test all non-essential deletion mutants. This allowed an exploratory approach to be taken and factors identified from this screen to be further investigated. Additionally, I used the experimental protocol that I had optimised to assist with another project in the lab involving the study of the recycling complex Rpd3 (Amoiradaki et al., 2021).

1.8.1.2. Chapter III: A glucose-starvation response governs endocytic trafficking and eisosomal retention of surface cargoes in budding yeast

This chapter contains work I became part of involved with understanding how proteins at the plasma membrane are regulated in response to glucose starvation. Where we show that this is mediated by an increase in expression of clathrin adaptors. My work on this project demonstrated that there is a physiological benefit for storing nutrient transporters in eisosomes in response to glucose starvation (Laidlaw et al., 2021).

1.8.1.3. Chapter IV: The phosphatase Glc7 controls eisosomal response to starvation via posttranslational modification of Pil1

From the work in **Chapter III**, it was noted that core eisosomal component Pil1 was dephosphorylated in response to glucose starvation. From this we wanted to understand the potential phosphatase responsible for this. I performed a screen of phosphatase mutants to identify those with a Pil1 phosphorylation phenotype and came across the essential phosphatase Glc7. We propose that Glc7 is likely the phosphatase that acts to dephosphorylate Pil1 in response to glucose starvation.

1.8.1.4. Chapter V: Endosomal cargo recycling mediated by Gpa1 and phosphatidylinositol 3-kinase is inhibited by glucose starvation

The work presented in this chapter aimed to uncover how the G alpha subunit Gpa1 acts to mediate recycling. We demonstrate the action of Gpa1 at endosomes with the yeast PI3K that is crucial for efficient recycling of cargo to the plasma membrane and that Gpa1 can be sequestered away from this role by Gpa2 at the plasma membrane.

2. Chapter II: Fur4 mediated uracil-scavenging to screen for surface protein regulators

Graphical abstract

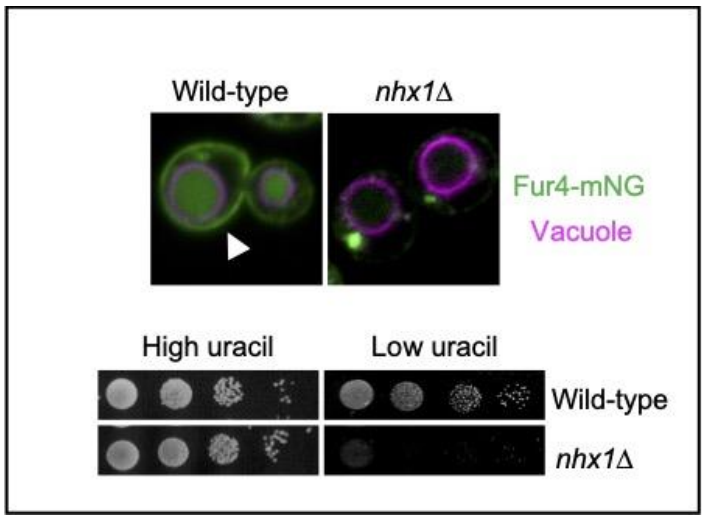

Wild type cells localise the uracil transporter Fur4 to the surface (arrow, left) in addition to the lumen of the vacuole (labelled in magenta). However, in trafficking mutants, like *nhx1*Δ cells lacking an endosomal ion channel, surface levels of Fur4 are greatly reduced. This does not impact growth in uracil replete media, however in restricted uracil conditions, the lack of surface Fur4 inhibits growth. This phenotype was the basis for a genetic screen to identify new machinery that is required to traffic Fur4 to the surface.

2.1. Introduction to project

Saccharomyces cerevisiae is a well characterised eukaryotic model organism. The generation of yeast deletion or mutant collections has provided a tool to allow for high-throughput genetic screens to be carried out. Full deletion collections of non-essential genes (Winzeler et al., 1999) or collections with reduced expression of essential genes (Breslow et al., 2008) are available. Additionally, collections with fluorescently tagged proteins have been generated (Huh et al., 2003; Weill et al., 2018; Yofe et al., 2016), allowing for the localisation of individual proteins to be identified. Collectively these libraries provide powerful tools for the whole yeast genome to be systematically tested. The work described in this chapter makes use of a non-essential gene deletion collection (representing all ~5200 non-essential *S. cerevisiae* genes) to perform a high-throughput genetic screen for novel trafficking factors. This screen was based on the observation that uracil auxotroph cells require efficient trafficking of Fur4 to the plasma membrane to allow for extracellular uracil acquisition and optimal growth, specifically when uracil levels are reduced.

Yeast cells uptake nutrients from their external environment and this uptake is facilitated by a variety of specific transporters that reside at the plasma membrane such as Gap1 (General amino acid permease 1) that senses and uptakes amino acids (Grenson et al., 1970), Mup1 that uptakes methionine (Isnard et al., 1996) and the uracil permease Fur4 (Jund and Lacroute, 1970). As described in the paper we assessed the ability of both Fur4 and Mup1 localisation to provide a readout for inhibited growth in low nutrient media, of which Mup1 and methionine acquisition did not (**Supplemental Figure S2.2**). We moved forward with uracil acquisition as it provided a clear indirect readout of cell surface localisation, which was validated in established surface trafficking mutants (**Figure 2.1**).

One reason uracil scavenging provided an excellent readout for efficient trafficking is that Fur4 is regulated through many of these pathways we wanted to explore. When cells experience excess uracil conditions, which can be toxic, uptake is no longer essential and *FUR4* transcription is reduced (Séron et al., 1999). In addition to regulation at the transcript level, Fur4 is also regulated post-translationally such as by phosphorylation (Volland et al., 1992) and ubiquitination. These modifications alter the localisation of Fur4, such as ubiquitination at its cytoplasmic N-terminus signalling for the endocytosis of Fur4 from the plasma membrane (Marchal et al., 1998). Conformational changes of Fur4 which renders the site of ubiquitination open to Rsp5 are caused by direct binding of uracil to Fur4 (Keener and Babst, 2013). Once ubiquitinated Fur4 is targeted to the vacuole for degradation. Fur4 can also be targeted for degradation at the Golgi, enabling for it to be sorted directly to the vacuole for degradation and therefore by passing the plasma membrane (Blondel et al., 2004).

This work was the project I started my PhD with. It began by optimising the uracil growth assay on a small scale and then optimising high throughput robotic approaches to upscale and screen a library on non-essential deletion strains. The ROTOR high density array robot by Singer proved useful to analyse growth of yeast from 96-well plates onto solid agar plates, however it was necessary to plate from liquid cultures that has been a) freshly grown and b) diluted to get unequivocal results. 16 replicas were spotted out per mutant, in each of the three conditions (replete and two restricted conditions), to avoid any technical errors

skewing results. Singer had a scanner that accompanied the ROTOR called a PhenoBooth that I used to scan the agar plates to obtain high resolution images for analysis. The PhenoBooth had colony counting software that we had hoped to use for our screen where we were looking for strains that grew normally on replete media but displayed a growth defect under low uracil concentrations. However, the PhenoBooth, even with customised help from their development team, was unable to reliably identify and quantify yeast growth under uracil limiting conditions, where contrast was reduced. I next set out to try write a code in R and trial various ImageJ Plugins, however, the issue persisted. It became clear to us that the differences in growth that we could clearly see by eye were too subtle for a computer to identify. We decided to qualitatively assess the growth phenotypes, using a low stringency double blind strategy. Any possible mutants, even with very subtle phenotypes, were then grown in optimal culturing conditions and used to create serial dilutions for traditional plate-based growth assays (**Figure 2.3.C**). Although a much more laborious process, this effort yielded highly reproducible, and even subtle mutants, to be identified, in addition we noticed that some mutants displayed a growth advantage under uracil limiting conditions.

Once we had our list of hits, we set about exploring them and noticed that we had a large number of transcriptional regulators. At this time, around July 2020, the pandemic meant all undergraduate projects were performed remotely. We therefore developed a project that used available bioinformatic data related to the transcriptional regulators identified in my screen to ascertain whether known trafficking factors or other hits from the screen were being regulated in this manner. I mentored Gabi Ecclestone throughout the year whilst she worked from home to complete her integrated Master's project. During my undergraduate degree, my final year project had been an exciting and enjoyable experience and is what confirmed to me that I wanted to do a PhD. I felt for the students who were working from home under these circumstances as I could appreciate how their learning experience had been hindered. For many reasons it was a rewarding experience mentoring Gabi throughout the year, but even more so that particular year given the challenges of finishing a degree under multiple lockdowns. She developed the bioinformatic side to the project and found some exciting hits. It was great to see her achieve the first-class degree she deserved and secure a PhD position. Furthermore, as I managed to validate these hits experimentally, we included these contributions in the manuscript.

We received positive reviews for this paper. Suggestions included incorporating the systematic names of screen hits as well as their standard names, which was an excellent suggestion as some proteins have multiple standard names. We also addressed queries about whether some of our fluorescently tagged markers were localising to the cortical ER or the plasma membrane, it was important for us to investigate this and provide microscopy with markers for both the cortical ER and the plasma membrane. This led to the development of a whole new figure (**Figure 2.7**), that explored various tools to study surface proteins and demonstrated the benefits of the growth assay we had developed.

2.1.1. Aims of chapter

This chapter describes the development and optimisation of a uracil- based growth assay that was then performed on 5132 non-essential deletion mutants. From this effort, 150 candidates were identified as displaying a defect in growth, potentially as a result of their failure to correctly traffic Fur4. The screen identified various molecular complexes and genes with associated function demonstrating its robustness.

2.1.2. Declaration of authorship

All experimental work presented in this chapter was carried out by K. M. Paine.
Bioinformatic analysis in the following figures was carried out by G. B. Ecclestone:
Figure 2.5.C and E
Figure 2.6.B and C
Supplemental Figure S2.3.
Supplemental Figure S2.4.
Supplemental Figure S2.5.

2.1.2.1. Author contributions

Conceptualization: C.M.; Methodology: **K.M.P**., G.B.E., C.M.; Validation: **K.M.P.**, C.M.; Formal analysis: **K.M.P.**, C.M.; Investigation: **K.M.P.**, G.B.E., C.M.; Resources: C.M.; Data curation: C.M.; Writing - original draft: **K.M.P.**, C.M.; Writing - review & editing: **K.M.P.**, C.M.; Visualization: **K.M.P.**,C.M.; Supervision: **K.M.P.**, C.M.; Project administration: C.M.; Funding acquisition: C.M

2.1.2.2. Manuscript history

Uploaded to bioRxiv: 27th May 2021
Submitted to Traffic: 28th May 2021
Published at Traffic: 23rd September 2021
DOI: 10.1111/tra.12815
PMID: 34498791

2.2. Fur4 mediated uracil-scavenging to screen for surface protein regulators

Katherine M. Paine, Gabrielle B. Ecclestone and Chris MacDonald*

York Biomedical Research Institute and Department of Biology, University of York, York, UK
***** *Correspondence: Email: chris.macdonald@york.ac.uk Tel: +44 (0) 1904 328 609*

ABSTRACT

Cell surface membrane proteins perform diverse and critical functions and are spatially and temporally regulated by membrane trafficking pathways. Although perturbations in these pathways underlies many pathologies, our understanding of these pathways at a mechanistic level remains incomplete. Using yeast as a model, we have developed an assay that reports on the surface activity of the Fur4 uracil permease in uracil auxotroph strains grown in the presence of limited uracil. This assay was used to screen a library of haploid deletion strains and identified mutants with both diminished and enhanced comparative growth in restricted uracil media. Factors identified, including various multi-subunit complexes, were enriched for membrane trafficking and transcriptional functions, in addition to various uncharacterised genes. Bioinformatic analysis of expression profiles from many strains lacking transcription factors required for efficient uracil-scavenging, validated particular hits from the screen, in addition to implicating essential genes not tested in the screen. Finally, we performed a secondary mating factor secretion screen to functionally categorise factors implicated in uracil-scavenging.

INTRODUCTION

Cell surface membrane proteins are regulated by a variety of overlapping and often co-regulated membrane trafficking pathways. Surface cargoes are co-translationally imported into the endoplasmic reticulum (ER) (Deshaies et al., 1991) before transiting the secretory pathway to the plasma membrane (PM) for function (Stalder and Gershlick, 2020). Surface proteins are internalised via clathrin mediated endocytosis, followed by recycling back to the PM or entering the lysosomal degradation pathway (Laidlaw and MacDonald, 2018). These pathways allow surface localisation and activity of a myriad of proteins to be precisely controlled to meet cellular demands, for example during the cell cycle or in response to reduced nutrient availability; however, these pathways remain incompletely characterised. The budding yeast system has been useful to discover and define membrane trafficking mechanisms. Yeast cells uptake nutrients from their external environment by a variety of transporters that localise to the PM, such as transporters for sugars, metal ions and vitamins (Lagunas, 1993; Nelson, 1999; Perli et al., 2020). Amino acids are also actively transported into yeast cells via permeases, for example Gap1 broadly uptakes amino acids (Grenson et al., 1970), Mup1 uptakes methionine (Isnard et al., 1996) and Fur4 uptakes uracil (Jund and Lacroute, 1970). Permease activity can be controlled by changes in transporter expression, the rate of turnover by ubiquitin mediated vacuolar degradation, in addition to spatiotemporal control between eisosomes and other regions of the PM (Babst, 2019; Bianchi et al., 2019; Ljungdahl and Daignan-Fornier, 2012; MacDonald et al., 2020; Sardana and Emr, 2021). To develop an assay that reports on amino acid uptake via surface transporters, we focussed on the uracil permease Fur4 (Jund and Lacroute, 1970), which is controlled by the above-described trafficking pathways and regulatory mechanisms. For example, the presence of uracil downregulates expression of *FUR4* (Blondel et al., 2004; Séron et al., 1999) whilst also triggering endocytosis and Rsp5-mediated ubiquitination and degradation of Fur4 (Hein et al., 1995; Keener and Babst, 2013). Furthermore, Fur4 activity is regulated in response to metabolic stress via storage in eisosomes(Appadurai et al., 2019; Laidlaw et al., 2021; Moharir et al., 2018). Beyond this, Fur4 mediated uptake of uracil might be considered particularly important for many lab strains that cannot synthesise uracil biosynthetically, due to disruption of the orotidine-5'-phosphate decarboxylase *URA3* gene, (e.g. *ura3-52* or *ura3*Δ), which causes the useful selection characteristics of auxotrophy and resistance to 5-Fluroorotic Acid (Boeke et al., 1984). Indeed, many genome-wide libraries (Arita et al., 2021a; Ghaemmaghami et al., 2003; Giaever et al., 2002; Huh et al., 2003; Weill et al., 2018; Winzeler et al., 1999; Yofe et al., 2016) have been created from parental *ura3*Δ strains (Brachmann et al., 1998). We therefore chose Fur4-mediated uptake to develop a simple and cost-effective growth assay that indirectly reports on the surface mediated uptake of uracil by the Fur4 transporter, which we have used to screen a haploid library of deletion mutants for factors that regulate Fur4 trafficking.

RESULTS & DISCUSSION

A Fur4-activity based growth assay

The uracil permease Fur4 is dispensable for growth in rich media but is critically required when uracil-auxotroph cells are grown in synthetic defined media containing replete (4 mg/L) uracil (**Figure 2.1.A - 1C**). Importantly, the robust Fur4-dependent growth of BY4742 cells, which harbour a *ura3*Δ mutation (Brachmann et al., 1998), herein referred to as wild-type, corresponds to the concentration of available uracil. There is a significantly reduced rate growth when wild-type cells are grown in media containing only 0.1 mg/L uracil, but Fur4 dependent uracil-scavenging supports growth (**Figure 2.1.B, 2.1.C**). Fur4 localisation has been previously shown to respond to extracellular uracil (Séron et al., 1999), and we confirm steady state surface localisation of Fur4 tagged with mNeonGreen (mNG) is redistributed to FM4-64 stained vacuoles following 1-hour of uracil addition to the media (**Figure 2.1.D**). Collectively these results show that the activity of the uracil sensitive permease Fur4 correlates with cellular growth in limited uracil conditions.

To test if low uracil-specific growth could be used to screen for membrane trafficking factors that influence Fur4 surface levels, we next compared Fur4-mNG localisation in wild-type cells and mutants that mis-localise Fur4 (**Figure 2.2.A**). As expected, a temperature sensitive *sec7-1* allele, which disrupts activity of the Sec7 Arf-exchange factor required for transit through the Golgi (Franzusoff et al., 1991; Novick et al., 1980), inhibits trafficking of Fur4 through the secretory pathway, with Fur4-mNG accumulating in intracellular puncta instead of the PM. Fur4-mNG localisation is also affected in *did4*Δ (*vps2*Δ) ESCRT mutants (Babst et al., 2002a), that do not permit vacuolar sorting and Fur4-mNG instead accumulates in endosomes. However, uracil-scavenging is likely efficient in *did4*Δ cells as significant Fur4-mNG recycling back to the PM is observed, unlike Mup1-GFP that is trapped by Snf7-oligomers (Teis et al., 2008). In contrast, surface levels of Fur4-mNG was greatly reduced in both *rcy1*Δ or *nhx1*Δ mutants, (**Figure 2.2.A**), which lack factors required for endosomal recycling (Brett et al., 2005; MacDonald and Piper, 2017; Wiederkehr et al., 2000). Therefore, we compared growth of *rcy1*Δ or *nhx1*Δ mutants with wild-type cells on plates of varying uracil concentrations. There was no statistically significant difference in growth between wild-type and trafficking mutant cells in the range of 1 mg/L - 32 mg/L uracil, but at lower uracil concentrations the *rcy1*Δ and *nhx1*Δ mutants, which have reduced surface Fur4, exhibit a low-uracil specific growth defect (**Figure 2.2.B, 2.2.C and S2.1.a**). Although significant defects were observed at 0.5 mg/L and 0.25 mg/L uracil, we selected 0.1 mg/L and 0.05 mg/L uracil for scavenging conditions, as wild-type cells grow efficiently but *rcy1*Δ or *nhx1*Δ both show dramatically reduced growth. Low-uracil specific growth defects were not observed in *vps2*Δ cells, demonstrating the PM levels observed by microscopy are sufficient to scavenge uracil, or *sec7-1* cells at permissive temperature, but lethality at 37^{o}C was confirmed (**Supplemental Figure S2.1.b**). We tested this concept with another surface-localised nutrient transporter, the methionine transporter Mup1 grown in methionine auxotroph (*met15*Δ) cells but no methionine concentration that supports growth could distinguish trafficking mutants (**Supplemental Figure S2.2.**). We assume differences in steady state surface levels, substrate affinity and uptake pathways (Isnard et al., 1996) account for this.

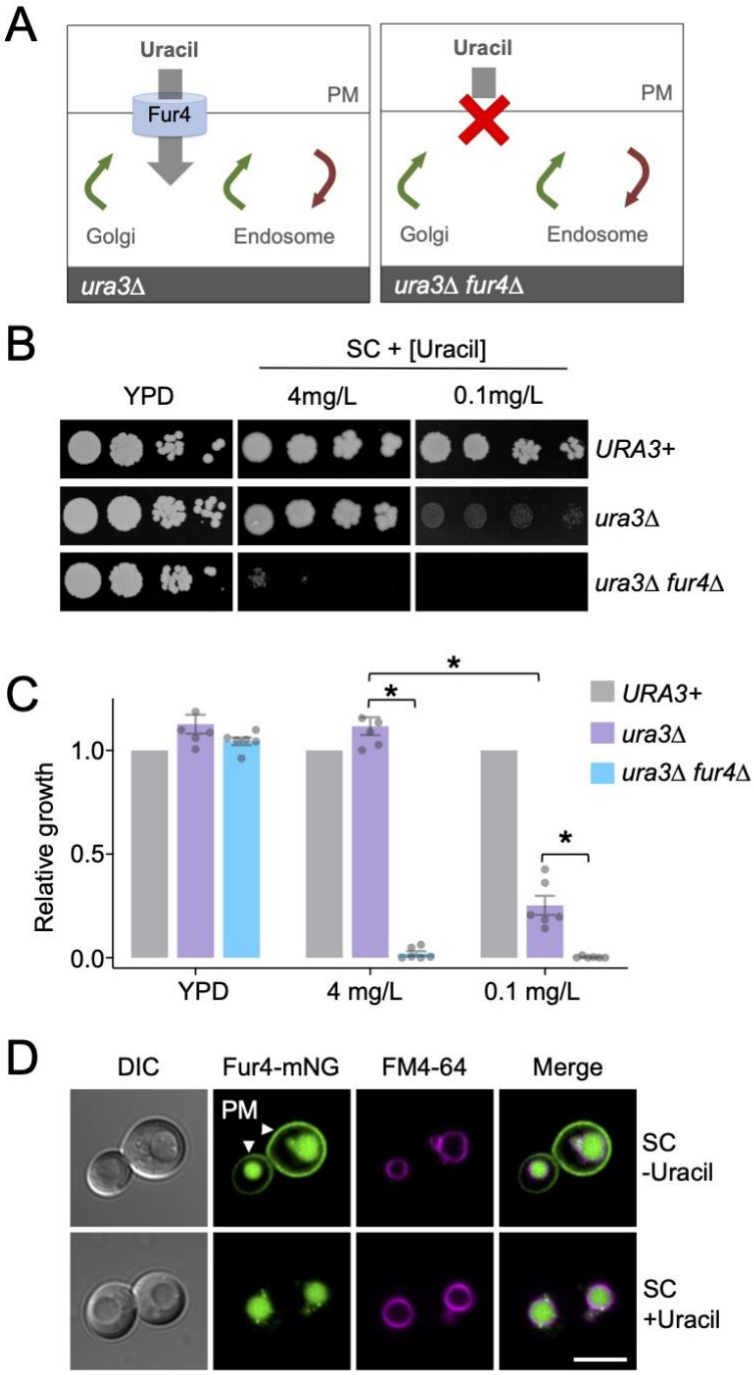

Figure 2. 1 Low uracil growth relies on the Fur4 transporter

A: Schematic illustration showing uracil-auxotroph cells (*ura3*Δ) with (left) and without (right) the uracil permease Fur4.
B: Indicated yeast strains were grown to mid-log phase before plating on rich (YPD) and synthetic complete (SC) media containing either 4 mg/L or 0.1 mg/L uracil.
C: Quantification of yeast growth from **B**, asterisks (*) indicate Student's *t*-test comparisons p = <0.001.
D: Wild-type cells expressing Fur4-mNeonGreen (Fur4-mNG) from its endogenous promoter were labeled with FM4-64 for 1-hour, grown to mid-log phase in SC-Ura media (upper) or in the presence of 40 µg/ml uracil for 1 hour (lower) prior to confocal microscopy. Arrows indicated plasma membrane (PM), scale bar = 5µm.

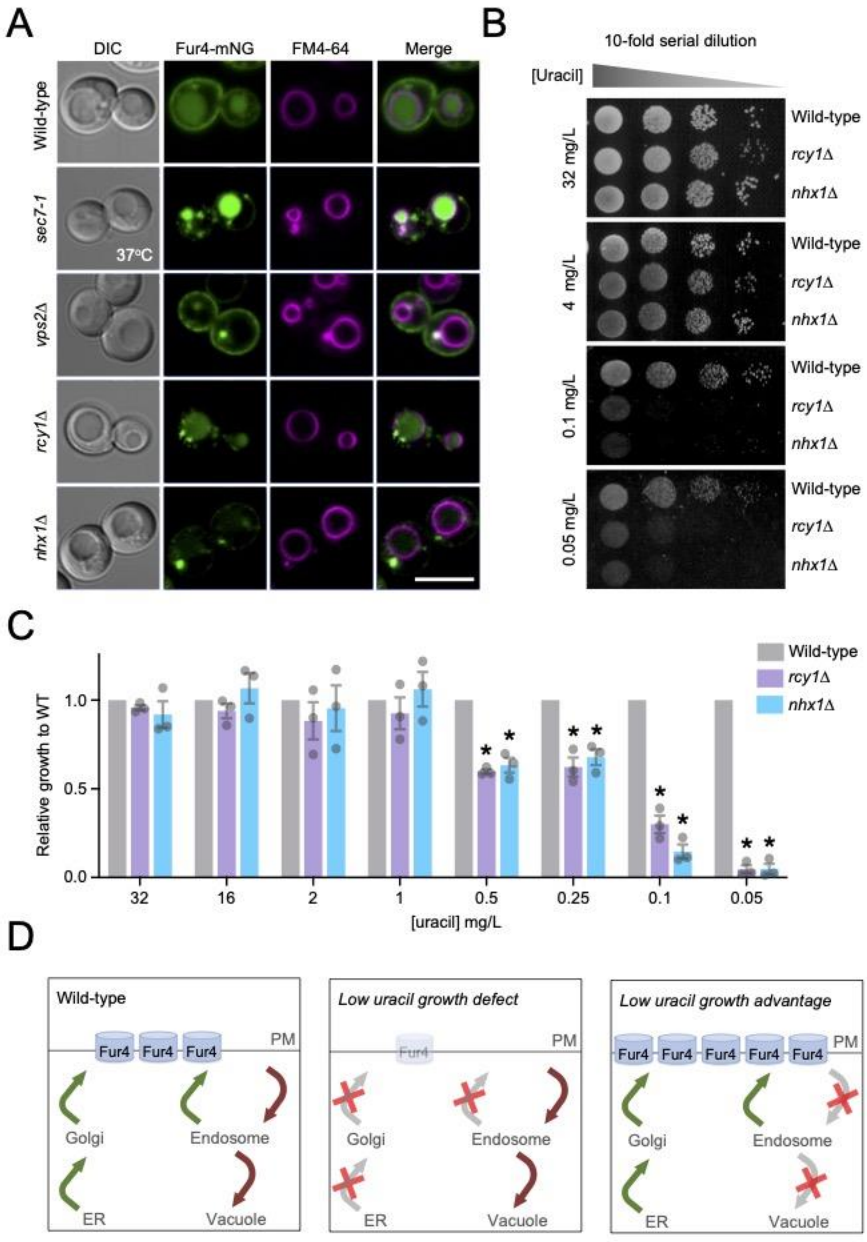

Figure 2. 2 Surface localization of Fur4 is required for growth in low-uracil

A: Vacuoles from indicated strains expressing Fur4-mNeonGreen (mNG) were labelled with FM4-64 prior to confocal imaging.
B: Wild-type, *rcy1*Δ and *nhx1*Δ cells grown to mid-log phase were then spotted in a 1 in 10 serial dilution onto plates titrated with indicated concentrations of uracil and grown at 30°C for 3 days.
C: Growth of strains from **B** were quantified, asterisks (*) indicate Student's *t*-test comparisons of mutants with wild-type cells, p = <0.005
D: Schematic diagrams showing the predicted effects on Fur4 following different trafficking pathway perturbations. Scale bar = 5 µm.

A genome-wide screen for uracil-scavenging mutants

We hypothesised that mutants with growth similar to wild-type in replete uracil but differences specifically at low uracil could be used to identify mutants from a non-essential haploid deletion library (Winzeler et al., 1999) with perturbed surface levels of Fur4 (**Figure 2.2.D**). Cultured yeast strains representing 5132 different mutants were diluted and spotted out (16 replicates of each) on to solid agar media containing replete (4 mg/L) and limited (0.1 mg/L and 0.05 mg/L) uracil concentrations (**Figure 2.3.A**). As expected, mutants with growth differences in uracil-replete media were observed, but the screen was specifically focused on differences in growth between high and low uracil concentrations. This is exemplified by the mutants used to calibrate the assay, *rcy1*∆ and *nhx1*∆, which both exhibit growth defects specifically in low-uracil when compared with neighboring mutants (**Figure 2.3.B**). A low stringency scoring system was used to identify 208 null mutants for follow up analysis. Candidates were grown to mid-log phase then serially diluted and spotted on 4 mg/L, 0.1 mg/L and 0.05 mg/L uracil media. Growth was quantified for the 208 mutant strains compared to a wild-type control from the same plate, and then values were used to compare growth across uracil concentrations (**Supplemental Table 1**). Statistical comparisons of mutants from these optimized growth assays revealed 58 mutants, such as *cla4*∆ (**Figure 2.3.C**), that did not show a significant difference in growth compared to wild-type. However, 126 mutants with significant growth defects specifically in uracil-scavenging conditions were identified (**Figure 2.3.D**), ranging from relatively subtle defects (e.g. *vps74*∆ at 0.1 mg/L = 0.78 ± 0.04) to extreme (e.g. *vps3*∆ at 0.1 mg/L = 0.004 ± 0.003). Furthermore, although the assay was calibrated for mutants with defective growth in low-uracil, the screen identified 24 mutants with enhanced growth compared to wild-type. We note many of these strains exhibit growth defects in uracil replete media, such as *ipk1*∆ (**Figure 2.3.C**), allowing for benefits to be observed at low uracil (**Supplemental Table 1**).

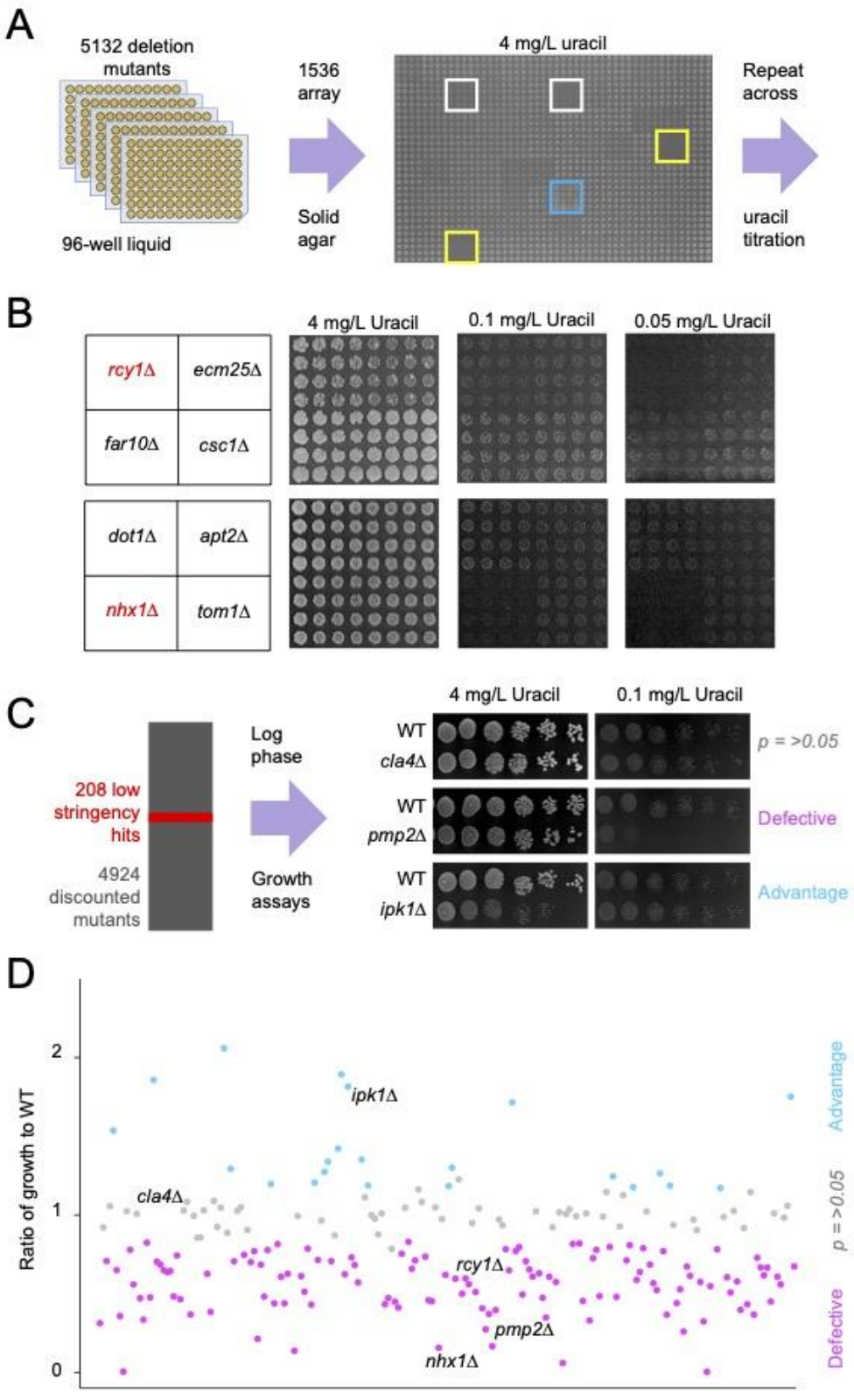
A
5132 deletion mutants
96-well liquid
1536 array
Solid agar
4 mg/L uracil
Repeat across
uracil titration
B
rcy1Δ
ecm25Δ
far10Δ
csc1Δ
dot1Δ
apt2Δ
nhx1Δ
tom1Δ
4 mg/L Uracil
0.1 mg/L Uracil
0.05 mg/L Uracil
C
208 low stringency hits
4924 discounted mutants
Log phase
Growth assays
4 mg/L Uracil
0.1 mg/L Uracil
WT
cla4Δ
p = >0.05
WT
pmp2Δ
Defective
WT
ipk1Δ
Advantage
D
Ratio of growth to WT
2
1
0
ipk1Δ
cla4Δ
rcy1Δ
pmp2Δ
nhx1Δ
Advantage
p = >0.05
Defective

Figure 2. 3 A genetic screen for mutants that affect uracil-scavenging

A: Yeast strains grown overnight in 96-well plates were diluted 20-fold in water then replicated 16 times onto solid agar plates containing varying uracil concentrations. An example 4 mg/L uracil plate shows identifier wells (yellow), alongside strains with defective (white) and accelerated (blue) growth.
B: Example of screen data showing indicated mutants grown on media containing 4 mg/L, 0.1 mg/L and 0.05 mg/L uracil, including known Fur4 trafficking mutants (red).
C: The screen identified 208 candidates that were subsequently grown to mid-log phase and spotted out over a 6-step, 10-fold serial dilution onto high (4 mg/L) and lower (0.1 mg/L and 0.05 mg/L) uracil containing media. Uracil-related cellular growth relative to wild-type was quantified and categorized as defective (e.g. *pmp2*Δ), advantageous (e.g. *ipk1*Δ) or not significantly altered (e.g. *cla4*Δ).
D. Ratio of relative growth between 4 mg/L and 0.1 mg/L uracil from **C** was plotted for all candidates.

Screen enriched for molecular complexes

A comparative orthologue search (Balakrishnan et al., 2012) of uracil-scavenging mutants identified 94 highly conserved genes, corresponding to 267 human orthologues associated with 87 distinct diseases (**Supplemental Table 2**). Gene Ontology (GO) Slim terms were obtained (Cherry et al., 2012) and revealed a number of cellular component enrichments of molecular complexes (**Supplemental Figure S2.3.**), including the GET complex and the prefoldin complex (**Figure 2.4.A**). The identification of multiple complex members suggests the screen was stringent and robust. For example, deletion of *GET1*, *GET2*, or *GET3* results in low-uracil growth defects (**Figure 2.4.B**). As the GET complex is required for sorting of tail-anchored single-pass membrane proteins (Schuldiner et al., 2008), many of which are essential factors in secretory pathway trafficking, such as SNARE proteins (Bulbarelli et al., 2002), we presume the role of the GET complex in efficient surface trafficking of Fur4 is via an indirect membrane trafficking mechanism. Various prefoldin complex members were also identified as having defective growth specifically on low uracil (**Figure 2.4.C**), implicating it as a potential regulator of Fur4 trafficking. This could be explained by prefoldin-mediated assembly of cytoskeleton proteins (Geissler et al., 1998; Vainberg et al., 1998). Indeed, actin filament structures observed in wild-type cells are absent in prefoldin mutant cells *pfd1*∆ and *pac10*∆ (**Figure 2.4.D**), indicating impaired cytoskeletal function that could adversely affect correct trafficking of Fur4 to the surface. However, the prefoldin complex is also involved in transcriptional elongation (Millán-Zambrano et al., 2013), so its role in uracil-scavenging could less direct.

Screen enriched for trafficking and transcriptional machinery

GO enrichments for biological process revealed almost a third (45/150) of annotations were for machinery associated with membrane trafficking and signalling (**Figure 2.5.A, Supplemental Table S3**), including the blind identification of *rcy1*∆ and *nhx1*∆ mutants that were used to calibrate the assay (**Figure 2.2.**). The other biological process significantly enriched was transcription, including 3 prefoldin subunits annotations (**Figure 2.5.A, Supplemental Table S3**). Physically interacting transcription factors were identified (**Supplemental Figure S2.3**), such as members of the COMPASS complex, Swd1, Swd3, and Sdc1 (Gerber and Shilatifard, 2003) alongside the Swi3/Snf5 pair (Zhou et al., 2020) amongst others that gave significant defects in low uracil (**Figure 2.5.B**). We reasoned transcriptional regulators could be indirectly involved in Fur4 membrane trafficking, controlling gene expression of either essential genes not tested in the primary screen or mutants identified from the screen itself. To explore transcription factors (TFs) implicated in uracil-scavenging, we assembled genome-wide expression datasets for wild-type cells versus 28 TF-null mutants from a large-scale microarray analyses (Kemmeren et al., 2014). A matrix of all mutants showed high correlation of associated factors, such as known complex members (**Supplemental Figure S2.4**). Cross-referencing expression data for 1183 genes that are essential for viability (**Supplemental Table 4**), followed by hierarchical clustering was used to generate a heat map of related gene expression changes (**Figure 2.5.C**). Strains, such as *ies2*∆, *bre1*∆ and *elf1*∆ created distinct expression signatures, but others were similar, such as each of the COMPASS complex mutants *swd1*∆*, swd3*∆, and *sdc1*∆. Particularly modulated clusters of genes were identified from this analysis (**Supplemental Table 5**), including genes associated with membrane trafficking that we chose for experimental testing (Pma1, Gpi8, Mrs6, Gpi12 and Sec62). To achieve this, we performed uracil-scavenging assays with strains containing Decreased Abundance by mRNA Perturbation (DAmP) cassettes at the 3' UTR of each candidate. This analysis revealed *sec62-DAmP* cells, which have very low protein levels of

Sec62 (Schuldiner et al., 2005), have specific growth defects in low uracil (**Figure 2.5.D**). *SEC62* expression was greatly reduced upon deletion of several TFs from the screen, for example *uba4*Δ and *met18*Δ mutants (**Figure 2.5.E**). The uracil-scavenging defects in *sec62-DAmP* cells can be explained in the context of reduced Fur4 trafficking to the surface, as shown by localization defects of Fur4-mNG, and an unrelated transporter Mup1-GFP (**Figure 2.5.F**). Collectively this example suggests that Uba4 and Met18 regulate expression of sufficient levels of Sec62, which are all required for proper trafficking of cargoes to the PM (**Figure 2.5.G**).

A

Cellular Component			
GO term_ID	Description	Corrected p-value	Annotations
GO:0016272	Prefoldin complex	4.66E-06	5
GO:0032991	Macromolecular complex	0.000211299	75
GO:0043234	Protein complex	0.000270865	48
GO:0005797	Golgi medial cisterna	0.001291189	4
GO:0043529	GET complex	0.001888469	3

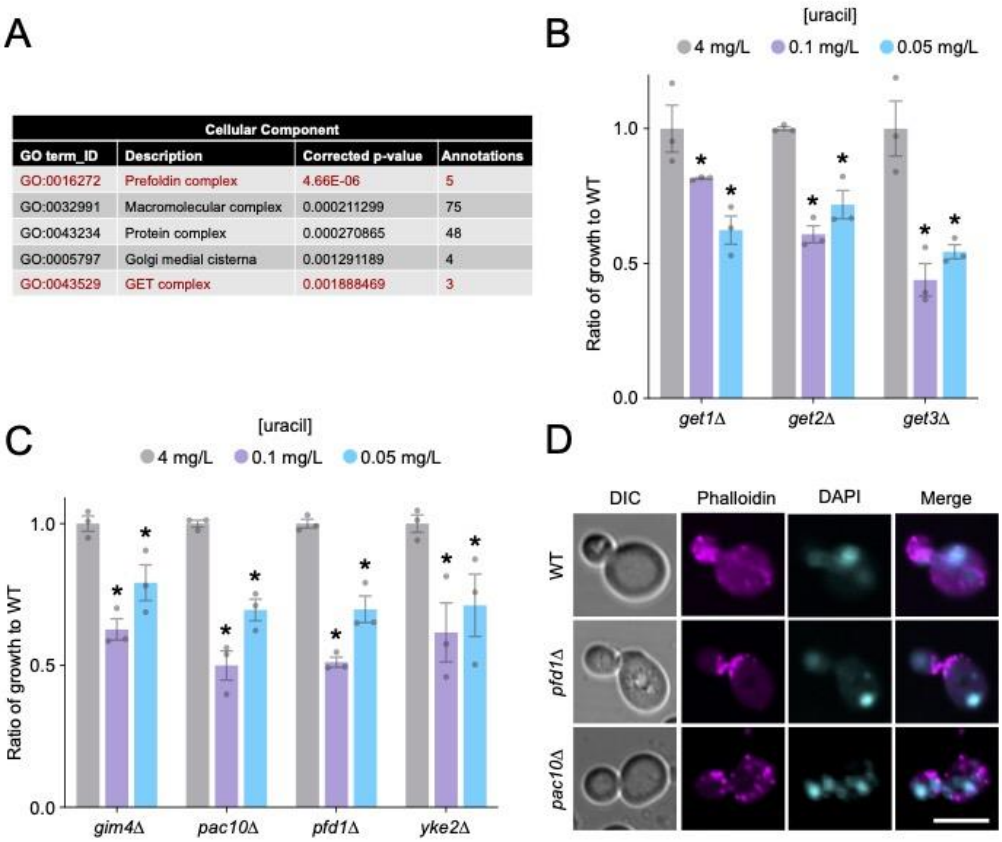

Figure 2. 4 Low-uracil screen identifies multi-subunit complexes

A: Gene Ontology enrichment analysis for cellular component of the 150 factors identified from the screen.
B: Ratio of growth compared to wild-type cells at 4 mg/L, 0.1 mg/L and 0.05 mg/L uracil for GET complex mutants: *get1*Δ, *get2*Δ and *get3*Δ. Asterisks (*) indicate Student's *t*-test comparisons p = <0.001.
C: Ratio of growth compared to wild-type cells at 4 mg/L, 0.1 mg/L and 0.05 mg/L uracil for indicated Prefoldin complex mutants: *gim4*Δ, *pac10*Δ, *pfd1*Δ and *yke2*Δ. Asterisks (*) indicate Student's *t*-test comparisons p = <0.01.
D: Confocal microscopy of wild-type (WT) and prefoldin mutants: *pfd1*Δ and *pac10*Δ stained with actin dye Phalloidin-594 and nuclear dye DAPI and fixed with 4% paraformaldehyde. Scale bar = 5µm.

A

Biological Process			
GO term_ID	Description	Corrected p-value	Annotations
GO:0007021	Tubulin complex assembly	0.000710553	5
GO:0016043	Cellular component organization	0.001154833	71
GO:0016192	Vesicle-mediated transport	0.003546653	25
GO:0007154	Cell communication	0.004875328	25
GO:0006355	Regulation of transcription, DNA-templated	0.007664094	30
GO:1903506	Regulation of nucleic acid-templated transcription	0.007664094	30
GO:2001141	Regulation of RNA biosynthetic process	0.007664094	30
GO:1901362	Organic cyclic compound biosynthetic process	0.009444717	43
GO:0070887	Cellular response to chemical stimulus	0.009594294	22

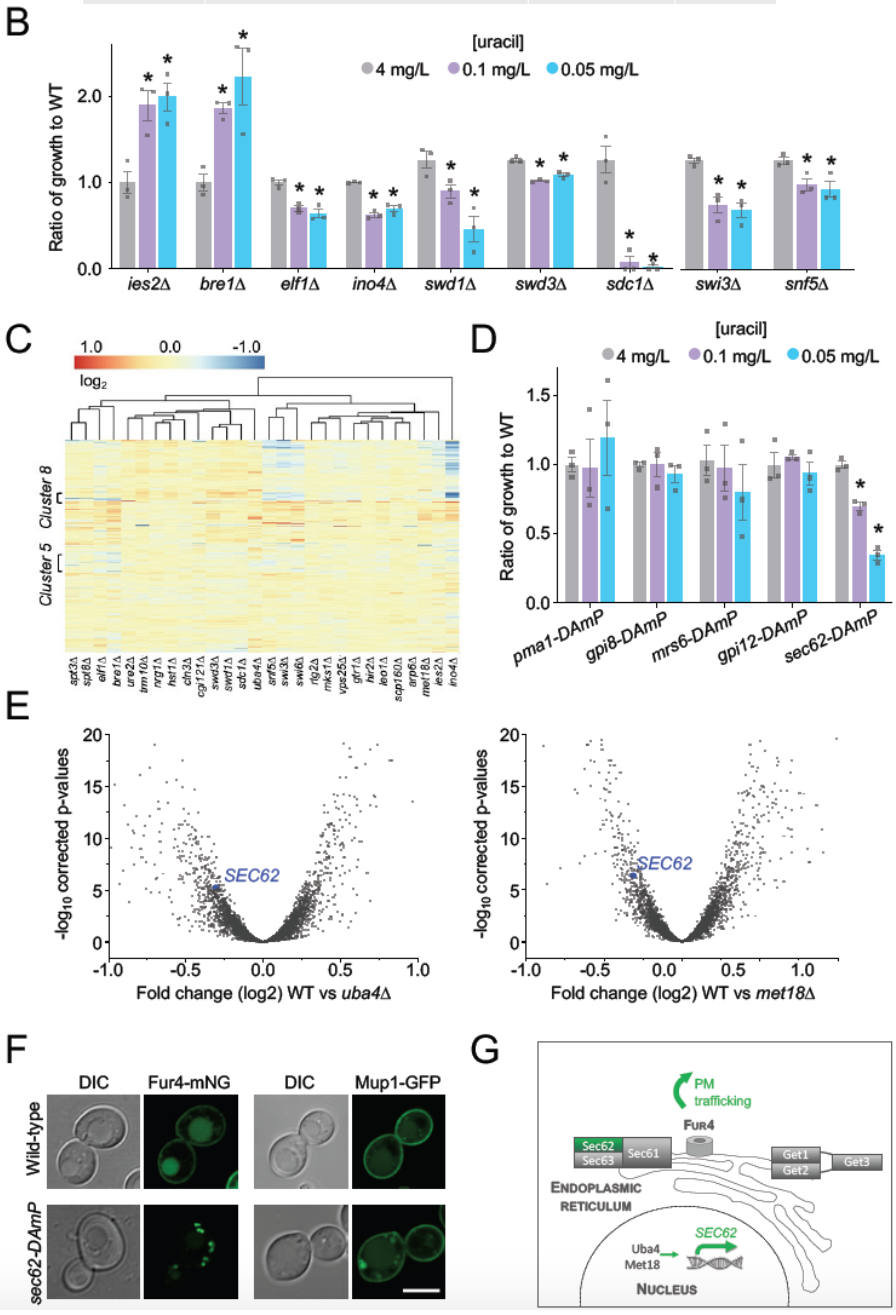

Figure 2. 5 Trafficking screen enriched for transcriptional regulation

(A) Details of enriched annotations for Gene Ontology terms related to for biological processes for the 150 candidates identified in the screen. **(B)** Ratio of growth for selected transcription factor mutants identified in the screen compared to wild-type cells at 4 mg/L, 0.1 mg/L and 0.05 mg/L uracil. Asterisks (*) indicate Student's *t*-test comparisons p = <0.05. **(C)** Hierarchical clustering and heat map of essential gene expression profiles in 28 different transcription factor null cells, coloured based on fold change.
D: Ratio of growth for indicated mutant strains compared to wild-type (WT) cells grown on media containing 4 mg/L, 0.1 mg/L and 0.05 mg/ uracil. Asterisks (*) indicate Student's *t*-test comparisons p = <0.0001.
E: Volcano plots were constructed for $\log_2$ fold changes and their corresponding $-\log^{10}$ corrected p-values for genes in microarray analyses comparing wild-type cells to indicated mutants, with *SEC62* labelled (blue).
F: Airyscan microscopy of Fur4-mNG or Mup1-GFP expressed from their respective endogenous promoters in wild-type and *sec62-DAmP* cells. Scale bar= 5 µm.
G: Schematic diagram highlighting transcriptional and ER-associated factors identified from the screen that contribute to efficient trafficking of Fur4 to the surface.

Uncharacterized factors are controlled at the transcriptional level

The uracil-scavenging screen identified ten uncharacterized candidates (**Figure 2.6.A**). In an effort to understand whether these were also regulated by the TFs from the screen, we used a similar approach to cross-reference gene expression profiles of the TF-deletion strains against the 150 genes identified in the screen. Again, hierarchical clustering revealed many gene profiles share signatures across different TF deletion experiments (**Figure 2.6.B**). We were particularly intrigued by *ydr222w*Δ mutants defective in growth from the screen (**Figure 2.6.A**) as *YDR222W* was greatly downregulated in many of the transcription factor null mutants, including the *swi3Δ*, *spt3*Δ and COMPASS complex mutants, but upregulated in other mutants not associated with low-uracil growth (**Figure 2.6.C, Supplemental Figure S2.5**). We find *ydr222w*Δ mutants are defective in general surface protein trafficking, as the distinct Mup1-GFP cargo exhibits mislocalisation phenotypes at mid-log phase and upon increased endocytosis via Sna3 (Macdonald et al., 2012b) and Cos proteins (MacDonald et al., 2015a; MacDonald et al., 2015b) at late-log phase (**Figure 2.6.D**). This approach helps prioritize factors, like the uncharacterized protein Ydr222w, for follow up testing and can be used for essentially any genetic screen, even retrospectively, that identifies transcriptional regulators. In an effort to help functionally categorise all the 150 mutants from the screen, and to begin unravelling where uncharacterised factors like Ydr222w might function, a secondary screen was performed based on the trafficking of Alpha factor through the secretory pathway to induce cell cycle arrest on a lawn of Mat A yeast, which are sensitised to arrest by virtue of a mutation in the gene that encodes the Bar1 mating factor protease (*bar1-1*). Alpha factor is synthesised and subjected to post-translational modifications through the secretory pathway before being secreted (Waters et al., 1988). We hypothesised that mutants with defects in the secretory pathway leading to reduced alpha factor secretion would result in a reduction in the growth arrest response seen when Mat**α** cells are spotted onto a lawn of MatA cells (**Figure 2.6.E**). Conversely, mutants with no halo phenotype could act downstream of the PM, or indirectly, to explain uracil-scavenging phenotypes. We observed mutants to have a reduction in halo size (eg. *bud16*Δ) or a halo comparable to WT cells (eg. *adk1*Δ). Mutants of proteins well characterized to act in the early stages of the secretory pathway such as GET-complex nulls (discussed above) and *apl2*Δ (Rad et al., 1995; Schuldiner et al., 2008) were seen to display a significantly reduced halo phenotype. Whilst mutants of factors acting downstream of the secretory pathway in the endosomal system such as *rcy1*Δ and *nhx1*Δ (Brett et al., 2005; Wiederkehr et al., 2000) were seen to display a halo phenotype not significantly different from WT (**Figure 2.6.F**). Interestingly, uncharacterized mutant *ydr222w*Δ gave a halo type not significantly different to WT cells. It might be the role of Ydr222w, which shares homology to the Svf1 protein implicated in survival pathways (Vander Heiden et al., 2002), functions at endosomes to regulate nutrient transporters in response to changes in extracellular nutrients.

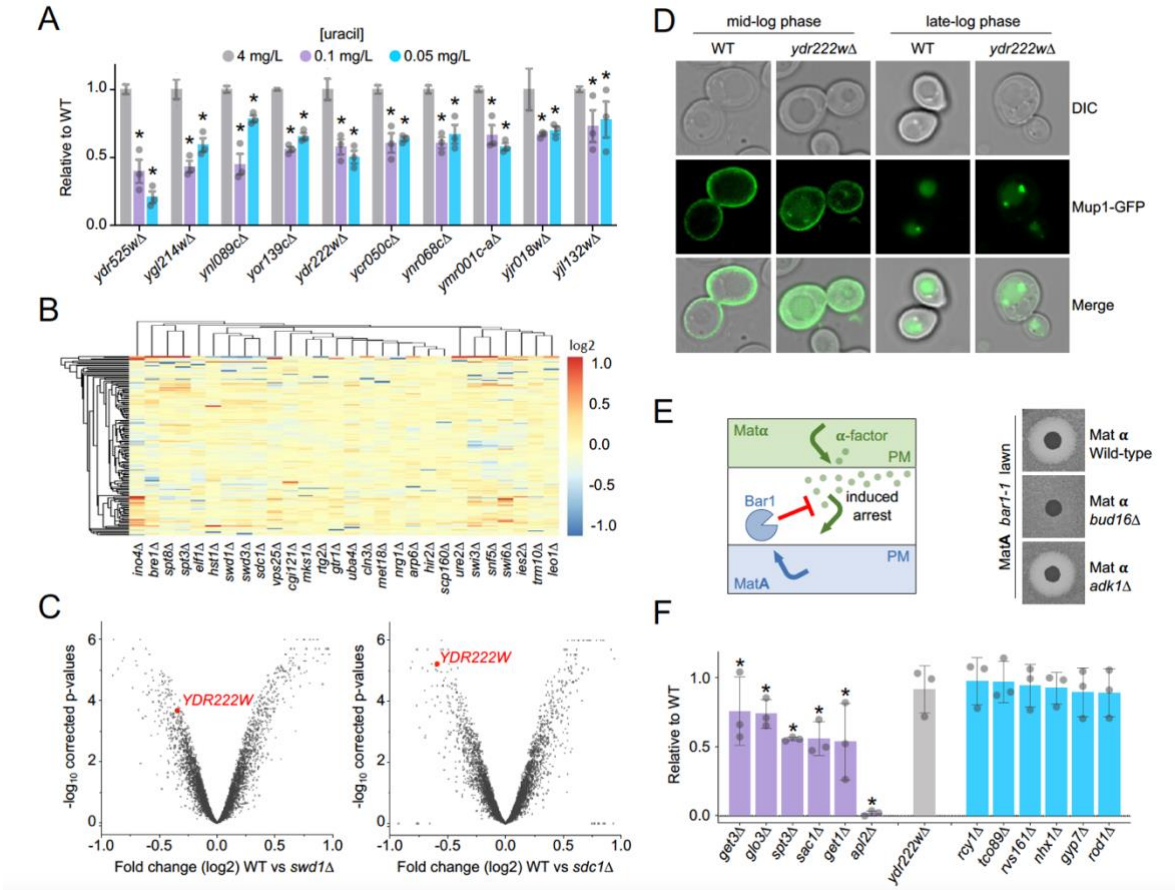

Figure 2. 6 Previously uncharacterised proteins implicated in membrane trafficking

A: Ratio of growth compared to wild-type cells at 4 mg/L, 0.1 mg/L and 0.05 mg/L uracil for indicated uncharacterised mutants identified in the screen. Asterisks (*) indicate Student's *t*-test comparisons p = <0.001.

B: Hierarchical clustering of genes identified from the screen, plotting expression profiles as a heat map based on fold changes following deletion of 28 different transcriptional regulators.

C: Volcano plots constructed for $\log_2$ fold changes and their corresponding p-values for genes in microarray analyses comparing wild-type cells to *swd1*∆ cells (left) and *sdc1*∆ cells (right). Value for *YDR222W* is shown in each plot (red).

D: WT and *ydr222w*∆ cells expressing Mup1-GFP were imaged at mid-log (OD_{600}=1.0) and late-log phase (OD_{600}>2). Scale bar = 5µm.

E: Schematic showing basis of **α**-factor induced inhibition of growth of mutants from the primary screen on a lawn of *bar1-1* Mat **A** mutants (left), with representative examples shown (right).

F: Quantification of growth inhibition surrounding spots of Mat**α** cells from screen described in **C**, shown relative to wild-type controls from same plate (n = 3). Asterisks (*) indicate Student's *t*-test comparisons p = <0.1.

Inducible tools to study surface proteins

In addition to fluorescently labelled Fur4-mNG for localisation experiments to validate trafficking mutants, we created GFP tagged versions of both full length Fur4, or a mutant lacking its N-terminal 60 residues under copper inducible *CUP1* promoter, to allow temporal control of trafficking (**Figure 2.7.A - 7D**). We reasoned Fur4$^{\Delta N}$-GFP would be a suitable reporter for secretory pathway mutants, as it cannot be endocytosed (Keener and Babst, 2013), however localisation in *get1*Δ, *get2*Δ and *get3*Δ was indistinguishable from wild-type cells (**Figure 2.7.E**). This might suggest the GET complex exhibits a distinct function in uracil-uptake. However, given the GET complex is known to be involved in secretory trafficking (Schuldiner et al., 2008) and not only were all 3 members identified form a blind screen for uracil-scavenging, but *get1*Δ *get2*Δ and *get3*Δ cells were all defective in secretion of mating factor (0.53 ± 0.28, 0.80 ± 0.15, and 0.76 ± 0.24 respectively), we favour the explanation that the uracil-scavenging assay is sensitive enough to reveal a phenotype that is not apparent from steady state localization experiments. We did observe small amounts of signal at the ER of the truncated Fur4$^{\Delta N}$-GFP. To confirm that the peripheral Fur4$^{\Delta N}$-GFP signal was indeed the PM, and not the cortical ER, we imaged the ER marker Sec63-RFP and GFP labelled versions of nicotinic acid permease Tna1, which traffics through the secretory pathway when tagged at the N-terminus (**Supplemental Figure S2.6**) but is retained in the ER when tagged at the C-terminus (Huh et al., 2003). Unlike these ER proteins, Fur4$^{\Delta N}$-GFP signal is contiguous at the surface and localises to eisosomes (**Figure 2.7.F**), as previously documented (Moharir et al., 2018). Furthermore, peri-nuclear signal of Fur4$^{\Delta N}$-GFP is very weak compared to the peripheral signal, unlike the ER protein that exhibit the opposite phenotype with an intense signal at the peri-nuclear ER compared with the cortical ER (**Figure 2.7.G**). Finally, clear distinction between Fur4$^{\Delta N}$-GFP at the PM and ER-PM contact sites (Zaman et al., 2020) indicated by Sec63-RFP (**Figure 2.7.H – 2.7.I**).

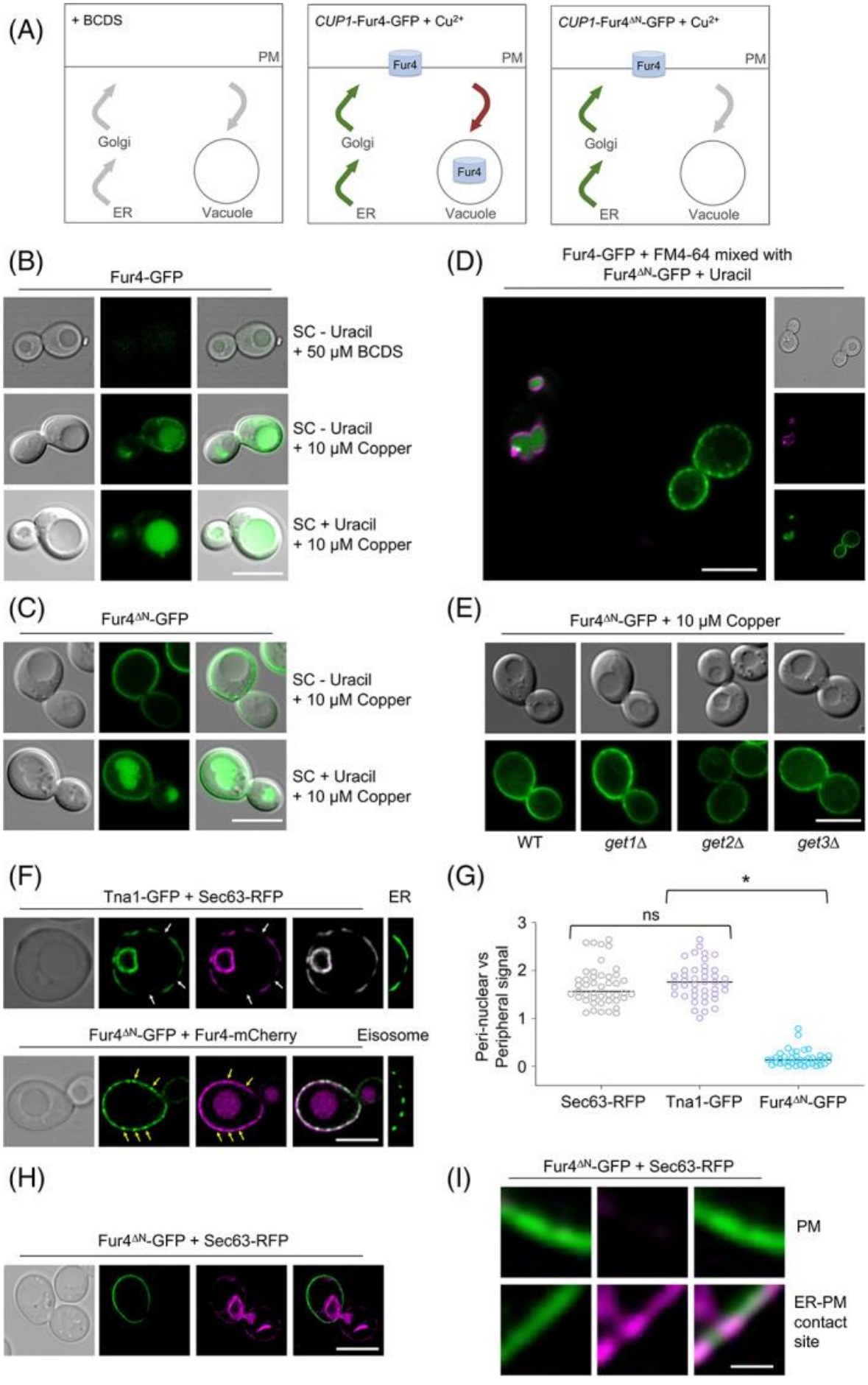
(A)
+ BCDS
PM
Golgi
ER
Vacuole
CUP1-Fur4-GFP + Cu2+
Fur4
PM
Golgi
ER
Fur4
Vacuole
CUP1-Fur4ΔN-GFP + Cu2+
Fur4
PM
Golgi
ER
Vacuole
(B)
Fur4-GFP
SC - Uracil
+ 50 µM BCDS
SC - Uracil
+ 10 µM Copper
SC + Uracil
+ 10 µM Copper
(C)
Fur4ΔN-GFP
SC - Uracil
+ 10 µM Copper
SC + Uracil
+ 10 µM Copper
(D)
Fur4-GFP + FM4-64 mixed with
Fur4ΔN-GFP + Uracil
(E)
Fur4ΔN-GFP + 10 µM Copper
WT
get1Δ
get2Δ
get3Δ
(F)
Tna1-GFP + Sec63-RFP
ER
Fur4ΔN-GFP + Fur4-mCherry
Eisosome
(G)
*
ns
Peri-nuclear vs
Peripheral signal
3
2
1
0
Sec63-RFP
Tna1-GFP
Fur4ΔN-GFP
(H)
Fur4ΔN-GFP + Sec63-RFP
(I)
Fur4ΔN-GFP + Sec63-RFP
PM
ER-PM
contact
site

Figure 2. 7 Inducible tools to study surface proteins

A: Schematic diagram showing repression of the *CUP1* promoter in the presence of BCDS (left), and the copper induced expression of Fur4-GFP, which localises to the PM and vacuole (middle) and Fur4$^{\Delta N}$-GFP that localises exclusively to the surface.
B-D: Wild-type cells transformed with *CUP1*-Fur4-GFP (B) and *CUP1*-Fur4$^{\Delta N}$-GFP plasmids were grown under indicated conditions prior to fluorescence microscopy. A mixture of these cells, with vacuoles of Fur4-GFP expressing cells first labelled with FM4-64, were also imaged simultaneously (**D**).
E: Indicated cells expressing Fur4$^{\Delta N}$-GFP were grown to log-phase followed by confocal microscopy.
F: Cells co-expressing Tna1-GFP and Sec63-RFP (upper) or Fur4$^{\Delta N}$-GFP and Fur4-mCherry (lower) were imaged by Airyscan microscopy. An example of Tna1-GFP localised to the cortical ER (upper) and Fur4$^{\Delta N}$-GFP localised to eisosomes is included on right panels. White arrows indicate regions of the cortical ER that are not closely associated with the PM, yellow arrows indicate eisosomes.
G: The fluorescence signal of peri-nuclear ER was compared with peripheral signal (either cortical ER or PM) for Sec63-RFP, Tna1-GFP and Fur4$^{\Delta N}$-GFP.
H: Wild-type cells expressing Fur4$^{\Delta N}$-GFP + Sec63-RFP were grown to mid-log phase and then imaged by Airyscan microcopy.
I: A zoomed in region of the periphery from (I) indicating Fur4$^{\Delta N}$-GFP localising exclusively to the PM (upper) and membrane contact sites with the ER (lower).

Summary

In conclusion, we report a simple growth assay that indirectly reports on surface protein trafficking via nutrient transporter activity of uracil auxotroph yeast strains. The assay relies on comparison of growth efficiency of yeast cells on relatively high and low uracil media to infer the capacity of the Fur4 transporter to scavenge uracil required for growth. It is therefore cheap, simple and easy to perform at high throughput, as demonstrated by testing a haploid deletion library of over 5000 yeast strains. This genetic screen identified many novel candidates as potential Fur4 regulators and was particularly enriched for membrane trafficking and transcriptional machinery. By cross-referencing essential genes and factors identified from the screen, with genome-wide expression pattens in the majority of these transcriptional regulators, we were able to identify connections between TFs and the genes they regulate, both of which relate to uracil-scavenging. As an example, our bioinformatics identified the essential gene *SEC62* and the uncharacterised gene *YDR222W*, as repressed in many of the TFs mutants identified from the screen. As proof of principle, we show experimentally that decreased expression of *SEC62* does, as expected, result in defects in surface protein trafficking. Similarly, we confirm a role for Ydr222w in surface protein trafficking, highlighting the discovery benefits in following transcriptional regulators identified for a given genetic screen. Indeed, we have recently identified an unexpected trafficking role for the Mig1 transcriptional regulator in endocytosis(Laidlaw et al., 2021) and endosomal recycling (Laidlaw et al., 2022b), suggesting the >20 candidates implicated in this study could also be explored functionally in the context of either global or cargo specific cargo trafficking mechanisms. Although we cannot exclude the possibility that mutants have indirect effects on uracil scavenging, for example via the biosynthetic or metabolic processes. However, as most genes were either enriched for membrane trafficking can be functionally explained in the context of gene expression of membrane trafficking machinery, this suggests the bulk of mutants reported likely affect trafficking pathways used by Fur4. Our data support the idea that mutants with even subtle decreases in Fur4 at the PM can reveal a uracil-scavenging phenotype. Therefore, we propose this uracil-scavenging assay, used in combination with fluorescently tagged cargoes (**Supplemental Figure S2.7**), the mating factor secretion assay and bioinformatic approaches all documented herein serve as useful tools to study surface protein trafficking. In addition, the mutants identified and characterized, many of which are novel and evolutionarily conserved, can inform future studies.

METHODS

Cell culture

Yeast cells were grown in rich yeast extract peptone dextrose (YPD) media (1% (w/v) yeast extract, 2% (w/v) peptone, 2% (w/v) D-glucose) or synthetic complete (SC) minimal media (0.675% (w/v) yeast nitrogen base without amino acids, 2% (w/v) D-glucose, plus the appropriate amino acid or base drop-outs for selection; (Formedium Norfolk, UK). Standard SC media contained 4 mg/L uracil and lower concentrations used, typically 0.1 mg/L and 0.05 mg/L for uracil stress conditions listed throughout. Cells were routinely cultured overnight to early/mid-log phase (OD_{600} <1.0) prior to experimental procedures. Yeast strains used in this study are listed in **Supplemental Table 7** and plasmids used are itemised in **Supplemental Table 8**.

Yeast growth assays

For the primary screen, 10µl culture of each mutant strain was grown in the well of a 96-well plate containing 150µl of YPD media with 250 µg/ml G418 overnight at 30°C in a humidified incubator. The bulk of YPD was then removed, followed by resuspension in water, and transfer of 10µl to a fresh 96-well plate containing 200µl sterile water. Dilutions were then mixed with a 96-pin replicator and pinned onto solid agar in 1,536 format using a ROTOR-HDA (Singer Instruments). Each mutant was pinned 16 times on solid media containing varying concentrations of uracil (4 mg/L or 0.1 mg/L or 0.05 mg/L) incubated at 30°C until sufficient growth was observed, followed by Phenobooth image capture (Singer Instruments) to record yeast growth. For follow up growth assays, the principle was the same, but cells were cultured in 5ml serial dilutions to capture mid-log phase cells, which were then harvested with equivalent volumes to other strains, including a wild-type control, to be plated together. 6-step serial dilutions (10-fold) of each strain was generated in sterile water, followed by plating on SC plates containing of 4 mg/L, 0.1 mg/L and 0.05 mg/L uracil. Plates were then incubated at 30°C for 3 days. Plates were imaged and the signal intensity of each spot was measured (ImageJ; NIH). Signal intensity of dilutions 3 – 5 were normalised to background and averaged and then values relative to WT were calculated.

Confocal microscopy

Yeast cells expressing GFP and/or mCherry tagged proteins were grown to mid-log phase and then viewed in kill-buffer (50mM Tris pH 8.0, 10mM NaN_3, 10mM NaF) or water (dH_2O) at room temperature on Zeiss laser scanning confocal instruments (LSM710 or LSM880 equipped with Airyscan) with a Plan-Apochromat 63x/1.4 Differential Interference Contrast (DIC) objective lens. Images were captured using Zen Black Imaging software and modified using Image J (NIH). Yeast vacuoles were labelled with 1.6µM FM4-64 (ThermoFisher) in YPD media, followed by 3x washes with SC media and further growth in SC media for 1-hour prior to imaging. Where stated cells were fixed for imaging by spinning down mid-log cultures and washing with 100 mM potassium phosphate buffer (pH 8) at 7000rpm. Cells were resuspended and incubated for 10 minutes at room temperature in 4% paraformaldehyde (950µl K-Phos, 50 µl PFA) before spinning at 7000rpm and resuspending in 1 x PBS. Fixed cells were stained with Rhodamine-phalloidin (Phalloidin-594) and DAPI.

α-factor induced arrest 'halo' assay

Wild-type and mutant Matα cells were grown to saturation overnight and then diluted back and grown for 4-6 hours in YPD media. Equivalent volumes of cells were harvested and spun down and brought up in 50 µl sterile water before spotting on low density lawns of MatA *bar1-1* cells created from mid-log phase cells on YPD plates. Plates were incubated

at 30 degrees overnight. Halos of growth inhibition for mutants relative to wild-type were determined using ImageJ (NIH).

Gene Ontology analyses

All GO enrichments were acquired using the GO Term Finder v0.86 (Cherry et al., 2012), using the default settings. The default background was used for all analyses except those for clusters derived from essential gene expression analysis, which instead used a background of essential genes listed in **Supplemental Table 4**.

Hierarchical clustering and gene expression analyses

Microarray data documenting changes in gene expression in mutant strains lacking transcriptional regulators compared to wild-type were assembled, representing 6123 genes. The data were read into R (v4.0.4; R Core Team, 2021) then processed using the dplyr v1.0.4 (Wickham et al., 2020) and janitor v2.0.1 (Firke, 2021) packages to include only 28 strains lacking transcription factors identified in the uracil-scavenging genetic screen. For downstream bioinformatic analyses, two gene reference subsets were generated: the first included all 147 verified candidates from the screen, and the second included 1183 genes denoted as essential for viability. For all analyses, hierarchical clustering was performed using the pheatmap package v1.0.12; (Kolde, 2019) using complete linkage. Elbow and silhouette analyses were performed using the factoextra package v1.0.7 (Alboukadel and Fabian, 2019) to determine the optimal number of clusters to guide further GO enrichment analyses. The Pearson correlation matrix of the whole genome expression data was produced with base R and visualised with the pheatmap package.

String analysis

Interactome analysis of physical interactions was carried out using STRING software (Szklarczyk et al., 2019).

Statistical analysis

Statistical significance for experimental conditions were calculated using a student's *t*-test/Bonferroni-Dunn method in GraphPad prism v8. Asterisks were used to denote significance on scatter plot histograms with p values documented in **Supplemental Tables 1 and 9**.

2.3. SUPPLEMENTAL MATERIAL

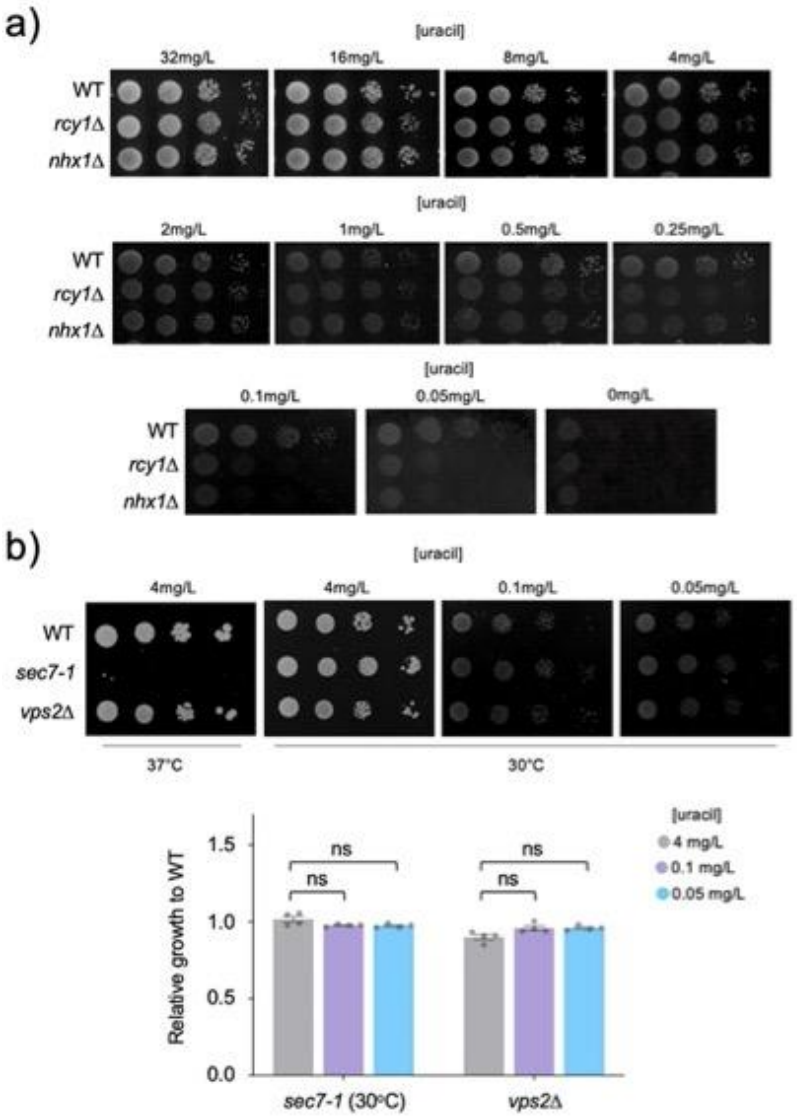

Supplemental Figure 2.1 Growth assay of known trafficking mutants

a) Wild-type, *rcy1*Δ and *nhx1*Δ cells grown to mid-log phase were spotted in a 1 in 10 serial dilution onto plates of 32, 16, 8, 4, 2, 1, 0.5, 0.25, 0.1, 0.05 and 0 mg/L uracil and incubated at 30°C for 3 days.

b) Wild-type, *sec7-1* and *vps2*Δ cells were spotted onto plates of 4, 0.1 and 0.05 mg/L and incubated at 37°C or 30°C for 3 days. A students t-test (was carried out to determine significance).

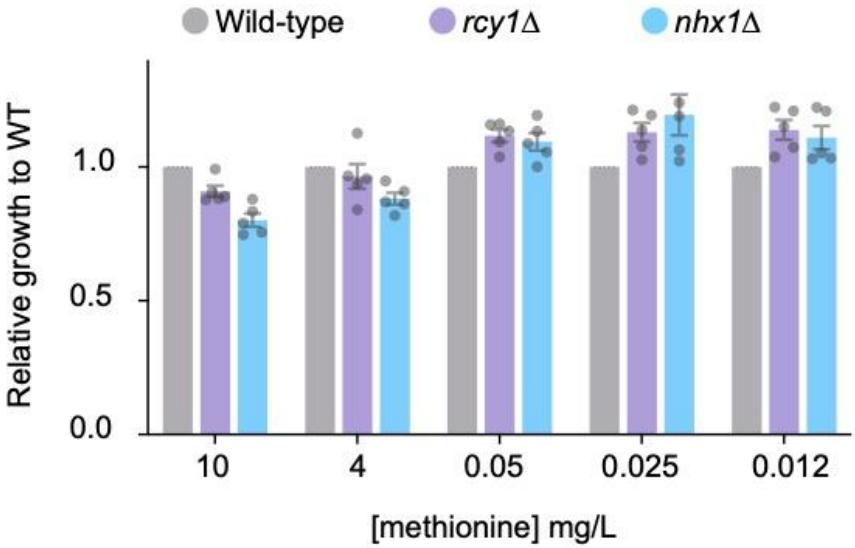

Supplemental Figure 2.2 Methionine auxotroph trafficking mutants grow efficiently in low methionine media

Wild-type BY4741 MatA cells harbouring the *met15*Δ mutation that confers methionine auxotrophy, and two additional strains in this background additionally harbouring *rcy1*Δ (purple) or *nhx1*Δ (blue) mutations, were grown on SC media plates containing various indicated concentrations of methionine. There was no concentration of methionine that supported growth whilst also resulting in any significant defect in the strains with defective trafficking to the surface.

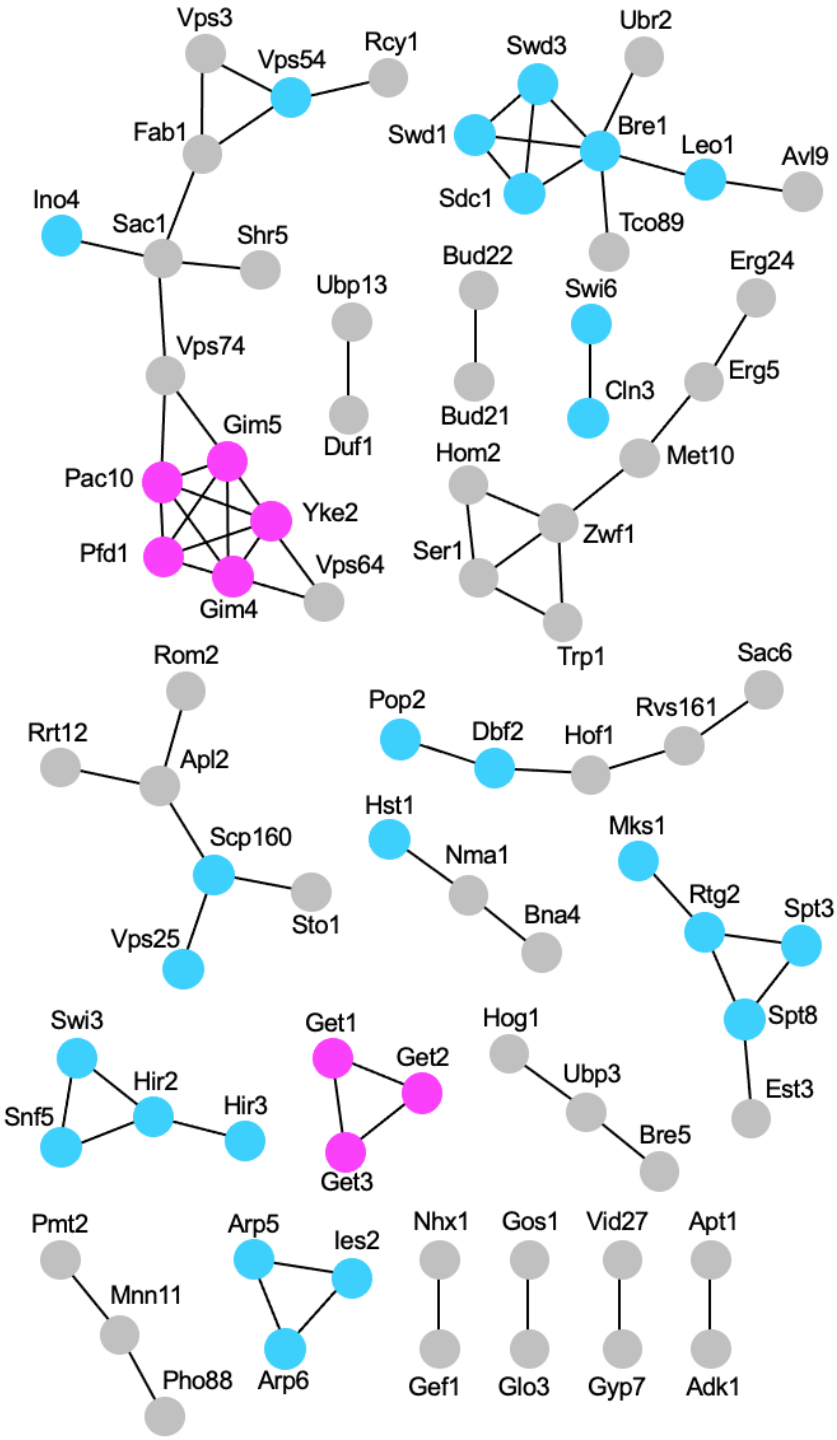

Supplemental Figure 2.3 Interactome analysis

STRING pathway analysis for factors with known physical interactions identified in the low uracil-specific growth screen. Factors enriched for GO terms associated with cellular component (pink) and those that are included in bioinformatic assessment of gene expression upon their deletion (blue) are indicated. Orphan candidates with no interactions have been removed.

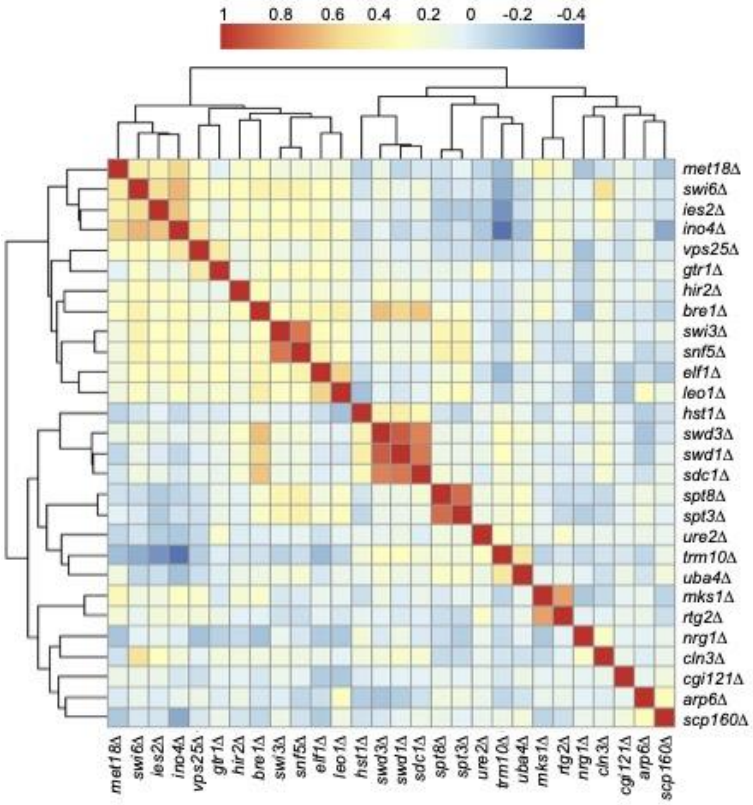

Supplemental Figure 2.4 Correlation matrix of responsive TF mutants of interest

Correlation matrix of responsive mutants of interest, where 1 is perfect correlation as found from comparing identical mutants. Mutants of known interacting partners, for example Swd1, Swd3, Sdc1, exhibit high levels of correlation.

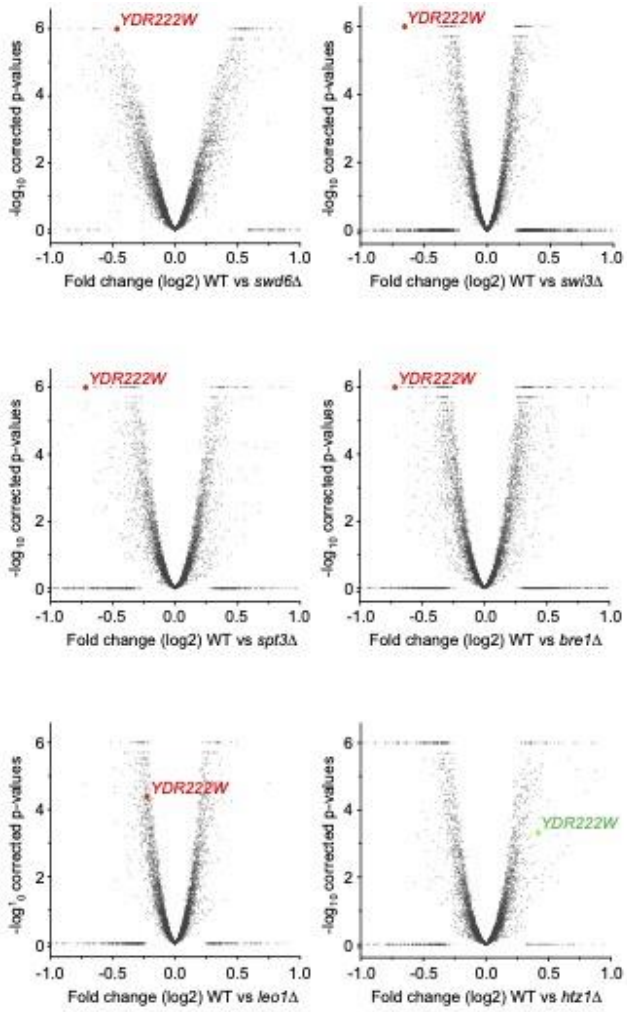

Supplemental Figure 2.5 Expression of YDR222W in transcriptional mutants

Volcano plots were constructed for $\log_2$ fold changes and their corresponding p-values for genes in microarray analyses comparing wild-type cells to indicated mutants. Value for YDR222W expression is shown in each plot from mutants identified fro mthe screen (red) and an independent analysis of *htz1*Δ mutants that were not identified as Fur4-related from the screen (green).

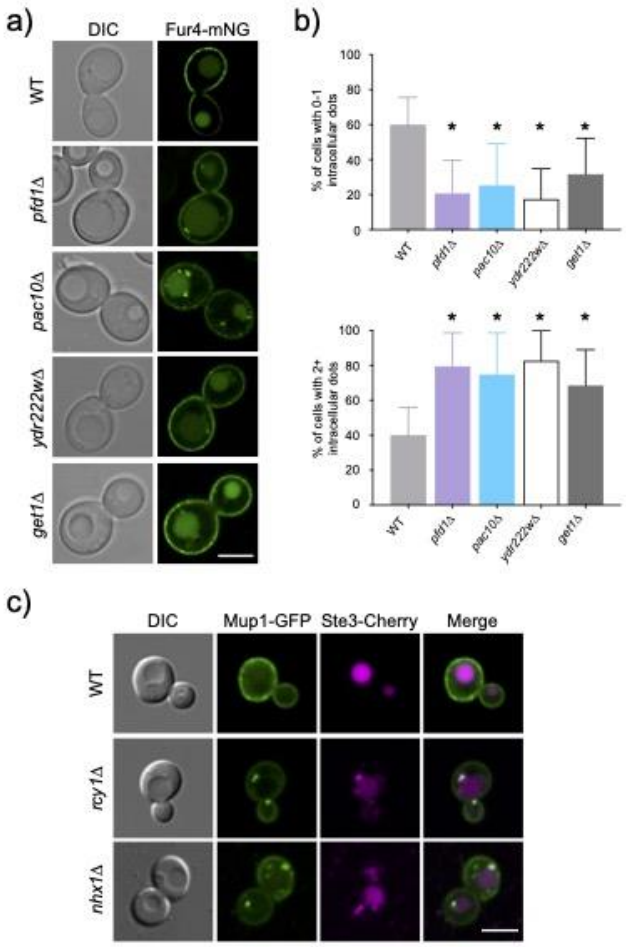

Supplemental Figure 2.6 Fluorescently labelled surface cargoes

a) Fur4-mNeonGreen localisation in indicated strains.
b) Percentage of cells with either 0-1 (upper) or 2+ (lower) intracellular puncta were quantified (n = >30).
c) Indicated cells were co-expressing Mup1-GFP and Ste3-mCherry under control of endogenous promoters were grown to mid-log phase and imaged by confocal microscopy.

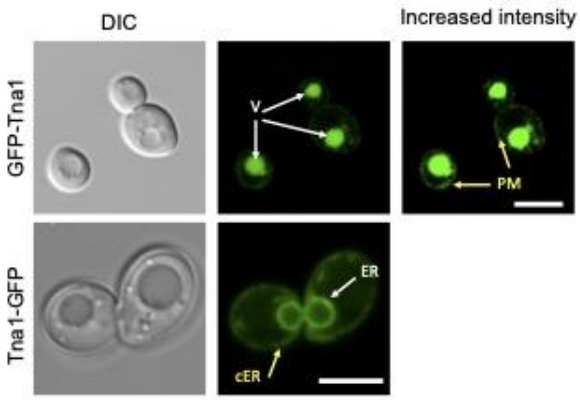

Supplemental Figure 2.7 Localisation effects of fluorescently tagging Tna1

Wild-type cells expressing either N-terminally (GFP-Tna1) or C-terminally (Tna1-GFP) GFP tagged Tna1 were imaged at log phase. PM = Plasma Membrane, cER = cortical Endoplasmic Reticulum and ER = Endoplasmic Reticulum. Scale bar = 5µm.

ACKNOWLEDGEMENTS

We would like to thank Luke Mackinder, Jared Cartwright and the Protein Production Laboratory at the York Bioscience Technology Facility (BTF) for access and assistance with the Rotor HDA robotics, and the Imaging and Cytometry Core of the York BTF for technical support with microscopy. Thanks to Daphne Ezer for assistance with bioinformatics, and to Maya Schuldiner (Weizmann Institute of Science, Israel) for providing DAmP-cassette integration yeast strains. We are grateful to Kamilla Laidlaw and other members of the lab for useful comments and assistance with the project. This research was supported by a Sir Henry Dale Research Fellowship from the Wellcome Trust and the Royal Society 204636/Z/16/Z (CM) and a York Biology PhD studentship (KP).

DECLARATION OF INTERESTS

The authors declare no competing interests.

2.4. The Rpd3-Complex Regulates Expression of Multiple Cell Surface Recycling Factors in Yeast

Konstantina Amoiradaki[1,2], Kate R Bunting[1,2], Katherine M Paine[2], Josephine E. Ayre[2], Karen Hogg[3], Kamilla ME Laidlaw[2], Chris MacDonald[2,4]

[1] *Equal contribution*
[2] *York Biomedical Research Institute and Department of Biology, University of York, York, UK*
[3] *Imaging and Cytometry Laboratory, Bioscience Technology Facility, Department of Biology, University of York, UK*
[4] *Correspondence: Email: chris.macdonald@york.ac.uk Tel: +44 (0) 1904 328 609*

Whilst the work described in Chapter 2 was being carried out, another project was ongoing in the lab. This project involved studying the histone deacetylase Rpd3-complex and its role in the regulation of the surface proteome. Previously, a recycling reporter had been used to identify recycling mutants and within those identified were Rpd3 complex members. This work set out to explore the role that these factors played in recycling. The assay I had developed for Chapter 2 was employed, but instead of using uracil and Fur4, the surface localisation of the tryptophan permease Tat2 and growth in limiting tryptophan conditions were used. This provided a quantitative readout for surface localisation. This work was published (DOI: 10.3390/ijms222212477) and below my work is shown (**Figure 2.8** (Figure 3 in paper)).

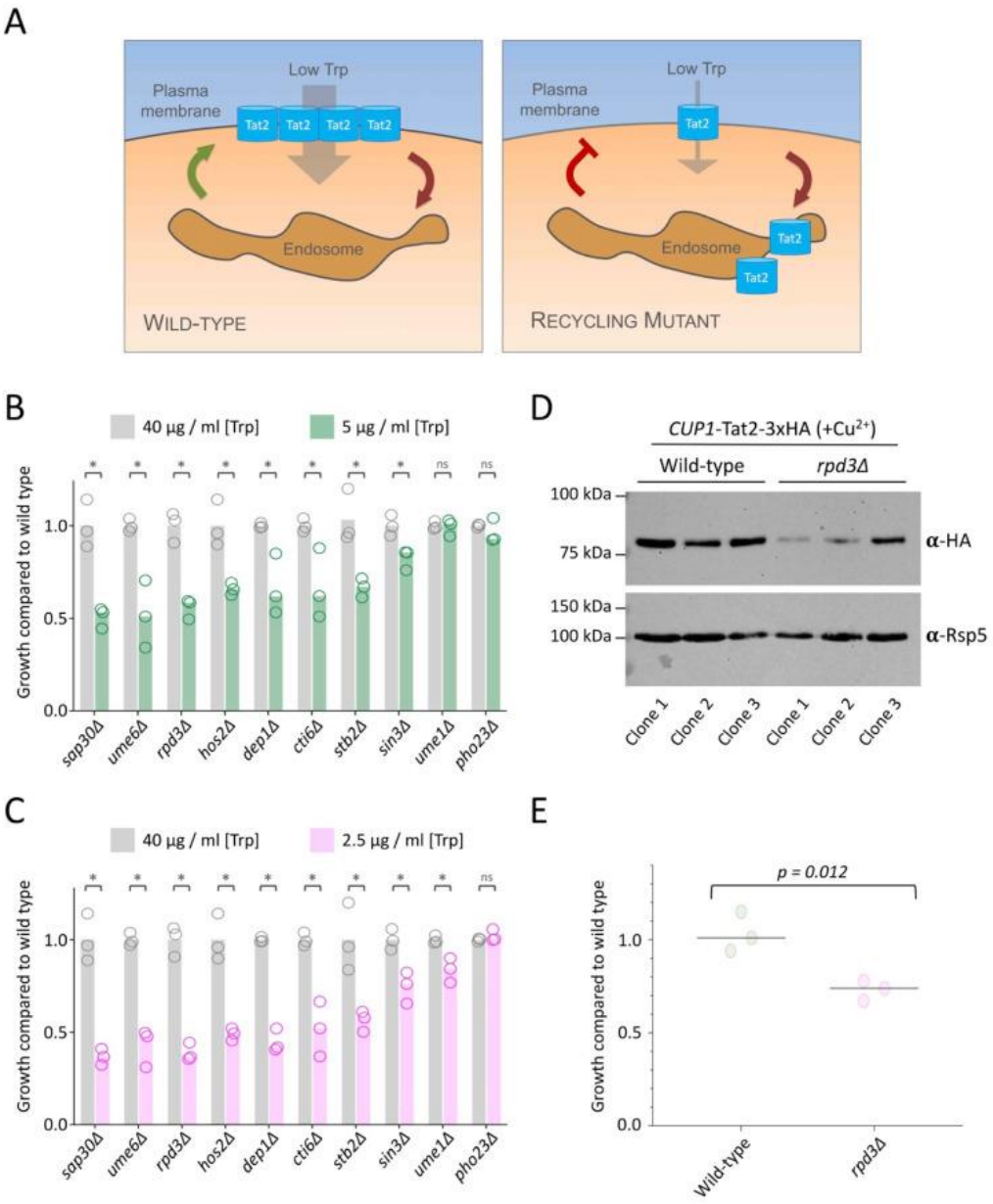

Figure 2. 8 The Rpd3-complex is required for Tat2 recycling.

(A) Schematic diagram showing the uptake of tryptophan via the high-affinity Tat2 permease. In tryptophan auxotroph cells grown on media containing low tryptophan concentrations, Tat2 uptake is required for efficient growth of wild-type cells (left) and Tat2 recycling defects inhibit growth (left). (B,C) Yeast were grown to mid-log phase and spotted out on media of replete (40 µg/mL) and limited, either 5 µg/mL in (B) and 2.5 µg/mL in (C) tryptophan concentration. Growth was measured across multiple serial dilutions and calculated as a ratio compared to wild-type cells from the same plate. Asterisks (*) used to indicate significant difference ($p < 0.03$) from t-test comparisons. (D) Cells transformed with a Tat2-3xHA plasmid containing a copper-inducible CUP1 promoter were grown in media containing 50 µM copper chloride to mid-log phase before lysates were generated for immunoblot analysis using α-HA and α-Rsp5 antibodies. (E) Densitometry was used to measure the signal intensity of Tat2-HA in different clones and strains from (D), normalized to loading control.

3. Chapter III: A glucose starvation response governs endocytic trafficking and eisosomal retention of surface cargoes

Graphical abstract

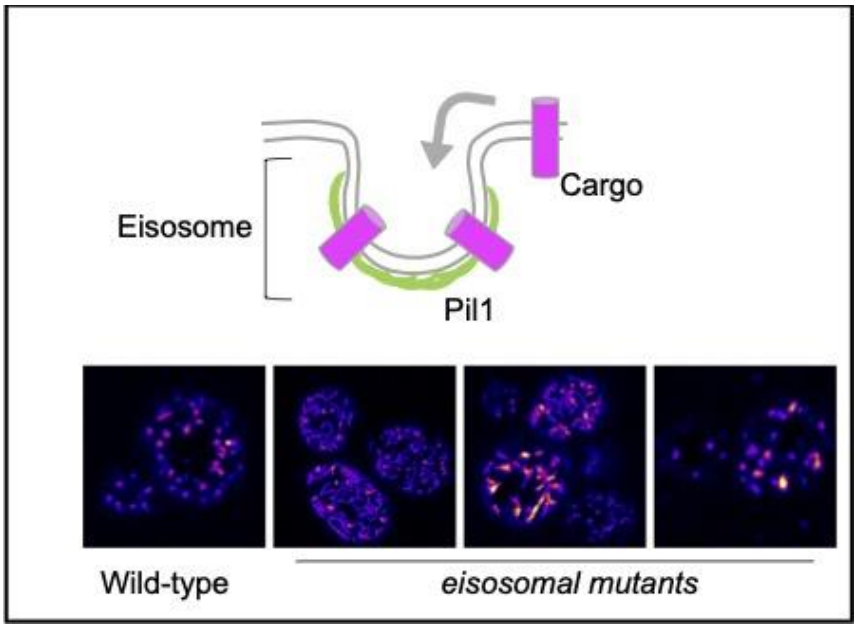

Nutrient transporter cargoes (magenta) can be sequestered in subdomains of the plasma membrane termed eisosomes in response to stress, shown with core eisosomal component Pil1 (upper). This pool of transporters can be deployed for nutrient uptake upon a return to replete conditions, providing a physiological benefit to cells recovering from starvation. Mutant strains lacking eisosomal components exhibit aberrant eisosome morphologies (lower), fail to properly retain transporters during starvation and are inefficient at recovering from starvation.

3.1. Introduction to project

The plasma membrane is divided into distinct regions, each defined by the composition of proteins and lipids resident within. The spatiotemporal dynamics of surface proteins within subdomains of the plasma membrane is known to regulate their activity. The work in this chapter focusses on the subdomains of the yeast plasma membrane termed eisosomes. The work for this paper was ongoing before I joined the project. Initial work from co-authors Dr. Kamilla Laidlaw and Daniel Bisinski had shown that surface membrane proteins were internalised and degraded in response to glucose starvation. This work was focussed on the transcriptional regulation of clathrin adaptors and the localisation of nutrient transporters to eisosomes in response to glucose starvation. It became clear that the principles of a growth assay I had developed for another project (**Chapter II**) could be used to test the hypothesis that retention of nutrient transporters in eisosomes in response to starvation provides a physiological benefit to cells.

Eisosomes, or previously termed MCC domains, were first identified as patched domains of the plasma membrane enriched with sterols (Grossmann et al., 2007; Young et al., 2002). Nutrient transporters such as Can1 and Fur4 were observed to localise to these regions (Malinska et al., 2004) and originally this was thought to mark sites of endocytosis (Walther et al., 2006). It is now established that rather than serving as sites of endocytosis, eisosomes act as protective compartments from the endocytic machinery (Kabeche et al., 2015). Nutrient transporters do not internalise from eisosomes, but instead move out of eisosomes in response to triggers which exposes them to the endocytic machinery (Gournas et al., 2018). BAR domain proteins Pil1 and Lsp1 assemble to form eisosomes which once formed are static structures (Moreira et al., 2009; Walther et al., 2006). Pil1 appears to be the core eisosomal component and eisosome biogenesis appears to be mediated by Pil1 phosphorylation (Luo et al., 2008; Walther et al., 2007).

Eisosomes are thought to play a role in the regulation of nutrient transporters at the plasma membrane and in stress response pathways (Appadurai et al., 2019). These two roles and the extent of their interplay is not yet fully understood. Surface proteins can localise to eisosomes which offers a protective mechanism from endocytosis and subsequent degradation (Grossmann et al., 2008). Eisosome clustering has been visualised to increase when cells are subjected to starvation conditions, a mechanism that requires Lsp1 (Gournas et al., 2018). There are many nutrient sensing signalling pathways that protect yeast from starvation conditions (Smets et al., 2010). Nutrient transporters have been demonstrated to be rapidly removed from eisosomes upon the addition of their substrate, thought to be through conformational changes to the transporter which allows its movement out of the eisosome compartment (Bianchi et al., 2018).

This work began by characterising the downregulation of surface proteins in response to glucose starvation before exploring the transcriptional response. The genes controlled by the transcriptional regulator Mig1 were investigated and it was discovered that clathrin adaptor genes *YAP1801* and *YAP1802* were upregulated in response to glucose starvation. Over-expression of these clathrin adaptors is sufficient to increase endocytosis. A surprising result was that although most nutrient transporters are degraded in response to glucose starvation, super resolution microscopy revealed that even in starved cells a small population of nutrient transporters like Mup1 were sequestered in eisosomes.

This work explored several aspects of glucose starvation and eisosomes but there was no demonstration of the physiological benefit to this. The work in **Chapter II** uses the surface localisation of the uracil permease Fur4 as a readout for trafficking defects. Fur4 localises to eisosomes (Malinska et al., 2004) and so this coupled with the cells dependence on the surface localisation on Fur4 for growth provided the basis for this recovery growth assay (**Figure 3.7.I – M** and **Supplemental Figure 3.8. F- I**).

I was familiar with this project through attending lab meetings. I had been working on my project using Fur4 and uracil acquisition to develop a growth assay (Paine et al., 2021). I trialled to see if the principles of my growth assay could be used in the context of glucose starvation. I was able to use Fur4 and uracil acquisition to study the ability of cells to store nutrient transporters in eisosomes. This was the first paper I worked on, giving me the opportunity to learn how a paper comes together and understand the process of submitting to a journal and receiving reviewers comments. Although the reviewers had a lot of comments, most of these were very constructive and I learned that backing up our model with additional and more quantitative approaches really strengthen the paper.

3.1.1. Aims of chapter

We propose a model for the role of eisosomes during glucose starvation conditions. Our published work demonstrates that specifically in response to glucose starvation, whilst most surface proteins are degraded, a reserve pool of nutrient transporters are sequestered in eisosomes. In eisosomes these nutrient transporters are protected from endocytosis and therefore degradation. We hypothesise this storage mechanism allows cells to respond rapidly upon a return to replete conditions. Where transporters can be quickly deployed into the plasma membrane from eisosomes to uptake nutrients.

3.1.2. Declaration of authorship

Experimental work presented in this chapter that was conducted by K. M. Paine:
Figure 7A - 7M: Eisosomes are required for efficient recovery following glucose starvation.
Supplemental Figure S7A – S7M: The role of eisosomes in cargo specific retention following starvation.

3.1.2.1. Author contributions

Conceptualization: C.M.; Methodology: M.C.L., C.M.; Validation: K.M.E.L., D.D.B.,S.S., **K.M.P.**, C.M.; Formal analysis: K.M.E.L., D.D.B., S.S., **K.M.P.**, C.M.; Investigation: K.M.E.L., D.D.B., S.S., **K.M.P.**, M.A.V., C.M.; Resources: M.C.L.; Data curation: C.M.; Writing - original draft: C.M.; Writing - review & editing: K.M.E.L., D.D.B., S.S., **K.M.P.**, M.C.L., C.M.; Visualization: K.M.E.L., D.D.B., S.S., **K.M.P.**,C.M.; Supervision: M.C.L., C.M.; Project administration: M.C.L., C.M.; Funding acquisition: M.C.L., C.M

3.1.2.2. History of manuscript

Uploaded to bioRxiv: 6th Feburary 2020
Submitted to Journal of Cell Science: 27th November 2020
Published at Journal of Cell Science: 25th January 2021
DOI: 10.1242/jcs.257733
PMID: 33443082

3.2. A glucose starvation response governs endocytic trafficking and eisosomal retention of surface cargoes

Kamilla M.E. Laidlaw[1], Daniel D. Bisinski[1,2], Sviatlana Shashkova[1,3,4], Katherine M. Paine[1], Malaury A. Veillon[1], Mark C. Leake[3,1], Chris MacDonald[1,5]

[1] York Biomedical Research Institute and Department of Biology, University of York, York, UK
[2] Present address: Department of Biology & Chemistry, University of Osnabrück, Osnabrück, Germany
[3] Department of Physics, University of York, York, UK
[4] Present address: Department of Microbiology & Immunology, University of Gothenburg, Gothenburg, Sweden
[5] Correspondence: Email: chris.macdonald@york.ac.uk Tel: +44 (0) 1904 328 609

ABSTRACT

Eukaryotic cells adapt their metabolism to the extracellular environment. Downregulation of surface cargo proteins in response to nutrient stress reduces the burden of anabolic processes whilst elevating catabolic production in the lysosome. We show that glucose starvation in yeast triggers a transcriptional response that increases internalisation from the plasma membrane. Nuclear export of the Mig1 transcriptional repressor in response to glucose starvation increases levels of the Yap1801 and Yap1802 clathrin adaptors, which is sufficient to increase cargo internalisation. Beyond this, we show that glucose starvation results in Mig1-independent transcriptional upregulation of various eisosomal factors. These factors serve to sequester a portion of nutrient transporters at existing eisosomes, through the presence of Ygr130c and biochemical and biophysical changes in Pil1, allowing cells to persist throughout the starvation period and maximise nutrient uptake upon return to replete conditions. This provides a physiological benefit for cells to rapidly recover from glucose starvation. Collectively, this remodelling of the surface protein landscape during glucose starvation calibrates metabolism to available nutrients.

INTRODUCTION

Cell surface membrane protein cargoes perform diverse roles, including initiating signal transduction pathways, uptaking nutrients and maintaining the ionic balance of the cell. Surface proteins are controlled by various complex and overlapping trafficking routes, many of which are conserved throughout evolution (Feyder et al., 2015). Endocytosis of surface proteins from the plasma membrane provides a layer of control, where cargoes can either be temporarily removed from the surface and recycled back or permanently removed via ubiquitin-mediated degradation in the lysosome(Laidlaw and MacDonald, 2018; MacDonald and Piper, 2016). In response to starvation, it is thought that many surface proteins are downregulated as a survival mechanism to reduce energy consumption via non-essential anabolic processes, whilst also increasing flux to the lytic lysosome for degradation and an increase in catabolic supply to the cell. How eukaryotic cells respond to changes in nutrients can be controlled at different levels, but mechanisms underlying many of these are not fully understood. Studies in yeast have revealed how large-scale surface protein degradation is mediated in response to restricted nutrients at late log phase (MacDonald et al., 2012c) or relatively severe starvation conditions lacking nitrogen or carbon (Lang et al., 2014; MacGurn et al., 2011; Müller et al., 2015). More specific nutrient starvation, such as depletion of vitamins or amino acids, trigger different trafficking responses to increase lysosomal degradation (Jones et al., 2012; MacDonald et al., 2015a; MacDonald et al., 2017).

Clathrin-mediated endocytosis is the best characterised mechanism to package cargo into endocytic vesicles and is governed by dozens of different factors. Although we are yet to fully understand how these factors cooperate, many aspects about the function (Kaksonen and Roux, 2018) and sequential coordination (Cocucci et al., 2012; Kaksonen et al., 2003; Mund et al., 2018) of these endocytic proteins has been revealed. The process is initiated by cytosolic adaptors, like assembly polypeptide 2 (AP2), which coordinates cargo recruitment at specific lipid interaction sites, in addition to binding clathrin (Kelly et al., 2014). Other adaptors, such as epsin, clathrin assembly lymphoid myeloid leukemia protein (CALM, also known as PICALM) or its neuronal counterpart assembly protein 180 kDa (AP180, also known as SNAP91), also interact with surface lipids through defined domains early in the endocytic process (Ford et al., 2001; Itoh et al., 2001; Miller et al., 2015b). Recruitment of clathrin and assembly of these components alongside actin polymerisation and membrane-bending Bin-Amphiphysin-Rvs (BAR) domain proteins serve to generate the burgeoning vesicle, followed by enzyme driven scission (Kaksonen and Roux, 2018). Internalised proteins that retain a ubiquitylation signal are recognised by the endosomal sorting complexes required for transport (ESCRT) apparatus and delivered through the multivesicular body (MVB) pathway for degradation in the lysosome/yeast vacuole (Piper and Katzmann, 2007). Although endosomal organisation and recycling mechanisms in yeast are less clear (Day et al., 2018; Ma and Burd, 2019), proteins that are not destined for degradation can recycle back to the surface via different mechanisms involving either ubiquitylation or deubiquitylation(MacDonald and Piper, 2017; MacDonald et al., 2017; Xu et al., 2017).

Surface cargoes are organised spatially within the PM, such as nutrient transporters in yeast that diffuse into plasma membrane invaginations termed eisosomes (Bianchi et al., 2018; Grossmann et al., 2008; Spira et al., 2012). Eisosomes have recently been shown to regulate both lipids and proteins at the surface in response to stress (Babst, 2019). Plasma membrane tension is sensed by the eisosomal osmotic stress sensors Slm1 and Slm2, which subsequently activate TORC2 to alter lipid

metabolism (Riggi et al., 2018). As to surface protein regulation, many nutrient transporters have been shown to localise to eisosomes, in particular during nutrient stress conditions when eisosomes maintain higher levels of these cargoes (Appadurai et al., 2019; Gournas et al., 2018; Grossmann et al., 2008; Moharir et al., 2018; Spira et al., 2012). Addition of transporter substrate results in a shift of transporters from eisosomes to other membrane compartments, where they can function to uptake nutrients before downregulation (Babst, 2019). It is not fully understood how eisosomes restrict access to endocytosis, but this affords cargo protection and preservation during mass downregulation.

Yeast has been a useful model to study physiological changes induced in response to changes in carbon source (Broach, 2012). Yeast preferentially uses glucose as a carbon source for fermentative growth, as with some rapidly growing mammalian cells (Diaz-Ruiz et al., 2011), but has also developed strategies to use various alternative carbon sources. During growth in replete glucose, genes from alternative carbon utilisation pathways, for example galactose (GAL), maltose (MAL) and sucrose (SUC) genes, are actively repressed (Gancedo, 1998). The glucose-sensitive transcriptional repressor Mig1, which binds consensus sequences in the promoter regions of these example genes, is responsible for this transcriptional repression (Griggs and Johnston, 1991; Hu et al., 1995; Nehlin and Ronne, 1990; Vallier and Carlson, 1994). Additionally, predicted Mig1 consensus binding sequences have been identified in promoters of other functionally diverse genes (Wollman et al., 2017). Gene expression profiles in mutant cells lacking MIG1 and/or the related repressor MIG2 also span various functional classes beyond sugar metabolism (Westholm et al., 2008). When glucose-starved cells are returned to glucose, alternative carbon transporters are endocytosed and rely on ubiquitylation for degradation, which is provided by spatially distinct, cognate arrestin-related trafficking adaptors (ARTs) at the surface and endolysosomal system (Becuwe and Léon, 2014; Becuwe et al., 2012; Hovsepian et al., 2018). Recent work has also shown how high-affinity glucose transporters, which are not required during glucose starvation, are specifically endocytosed and degraded via Rsp5 and the Csr2 ART adaptor, which is repressed by Mig1/Mig2 in glucose-rich conditions (Hovsepian et al., 2017). It is less clear whether such transcriptional and posttranslational regulatory mechanisms described for these sugar transporters during acute glucose starvation also control other surface membrane proteins.

In this study, we show that glucose privation alleviates Mig1-mediated repression of yeast clathrin AP180 adaptors, which increases endocytosis to more efficiently downregulate surface cargoes. We also find that eisosomal factors are transcriptionally upregulated during glucose starvation in a Mig1-independent manner. Specific eisosomes increase in size to sequester a small portion of nutrient transporters, which requires the presence of Ygr130c. We propose a model where this reserve pool of surface localised nutrient transporters provide a physiological benefit upon a return to nutrient-replete conditions, which outweighs the advantages of degrading an entire population of existing nutrient transporters.

RESULTS

Glucose depletion triggers cargo downregulation

We developed a microfluidic system to rapidly replace glucose with raffinose medium whilst monitoring the localisation of the methionine permease Mup1, a useful reporter for endocytosis (MacDonald et al., 2012c). We provided the trisaccharide raffinose, which undergoes slow enzymatic conversion outside the cell first (de la Fuente and Sols, 1962), to minimise changes in osmotic potential whilst inhibiting glucose-dependent signal transduction pathways. Extended incubations in glucose medium had little effect on the surface localisation of Mup1 (**Fig. 3.1.A; Movie 1**). However, glucose starvation triggered efficient Mup1–GFP endocytosis, with most signal internalised after ~45 min, following similar trafficking kinetics to substrate induced endocytosis (**Fig. S3.1.A**). Photobleaching during time-lapse microscopy did not affect endosomal GFP-tagged cargo but did reduce observable vacuolar signal in the confocal plane (**Fig. S3.1.B**). Therefore, Mup1 endocytosis and delivery to the vacuole for degradation was also assessed biochemically, with immunoblots of vacuolar processed GFP showing a large increase upon glucose starvation (**Fig. 3.1.B,C**). Raffinose exchange also induced downregulation of functionally and structurally distinct surface proteins, including the G-protein-coupled receptor Ste3 tagged with GFP, the uracil permease Fur4 tagged with mNeonGreen (mNG), and the arginine permease Can1 tagged with GFP (**Fig. 3.1.A; Fig. S3.1.C, Movie 2**). However, the ATP-binding cassette (ABC) transporter Yor1, which is downregulated in response to NAD+ starvation (MacDonald and Piper, 2015), showed no endocytosis, even at extended raffinose incubations (**Fig. S3.1.D**). Furthermore, although relatively long exposures to lactate medium triggers vacuolar delivery of high affinity hexose transporters tagged with GFP, we observed no sorting of Hxt6–GFP or Hxt7–GFP during raffinose treatment (**Fig. S3.1.E**). This suggests that glucose depletion simulates rapid downregulation of many, but not all, surface proteins, and demonstrates that raffinose provides a glucose-starvation condition without carbon source withdrawal. Raffinose treatment rapidly triggers relocalisation of Mup1–GFP to bright endosomal puncta at very short time points (e.g. 4 min), prior to sorting to the vacuolar lumen (**Fig. 3.1.D**). Additionally, endocytic uptake of FM4-64 at short time points was assessed in cells expressing a mutant of GFP–Snc1PM that is defective in endocytosis and therefore a surface marker (Lewis et al., 2000). Although raffinose-treated cells displayed lower levels of FM4-64 dye binding (**Fig. S3.1.F**), possibly due to changes in the lipid composition of the plasma membrane, we found efficient endocytosis in glucose depleted conditions, with significant FM4-64 internalised following 4 min uptake (**Fig. 3.1.E**). We conclude glucose starvation triggers large-scale endocytosis and downregulation of surface proteins.

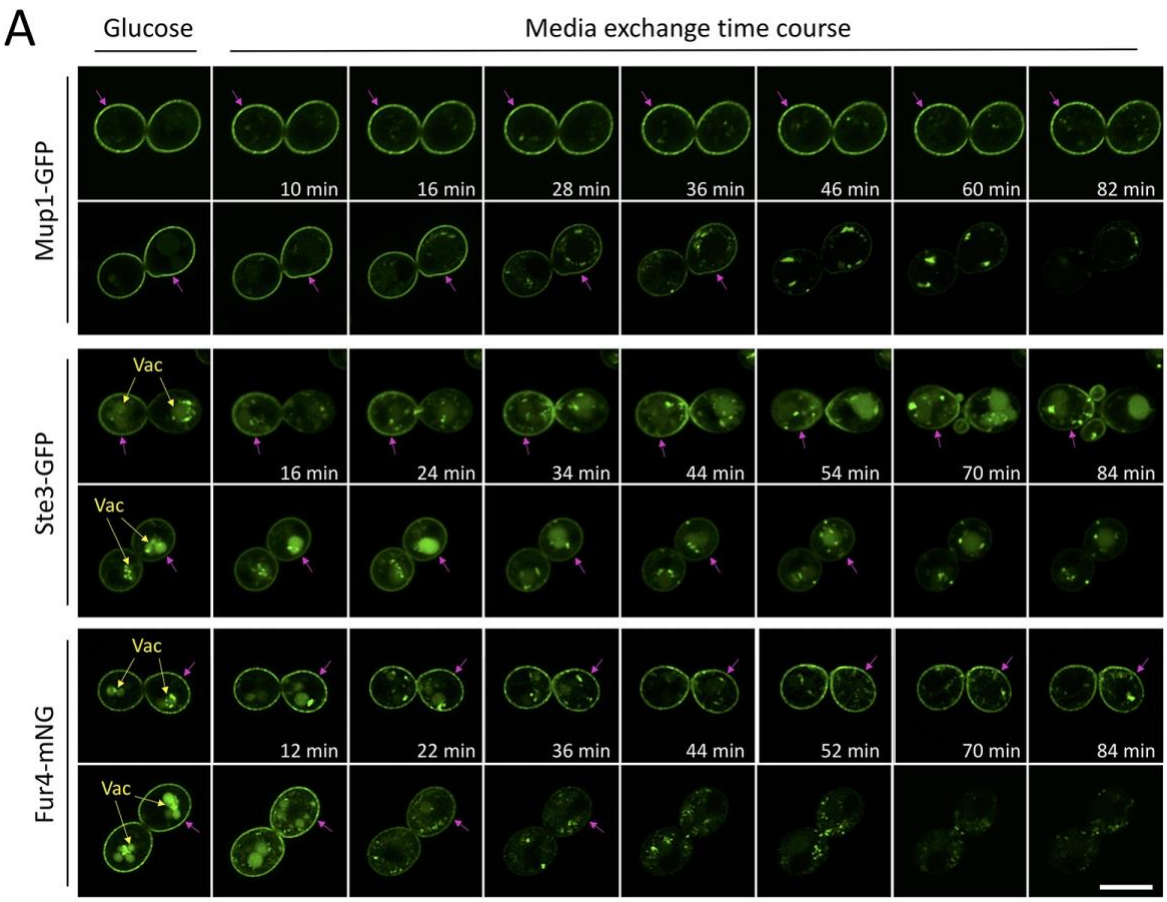
A
Glucose
Media exchange time course
Mup1-GFP
Ste3-GFP
Fur4-mNG
Vac
10 min
16 min
28 min
36 min
46 min
60 min
82 min
24 min
34 min
44 min
54 min
70 min
84 min
12 min
22 min
36 min
44 min
52 min
70 min
84 min
Glucose
Raffinose

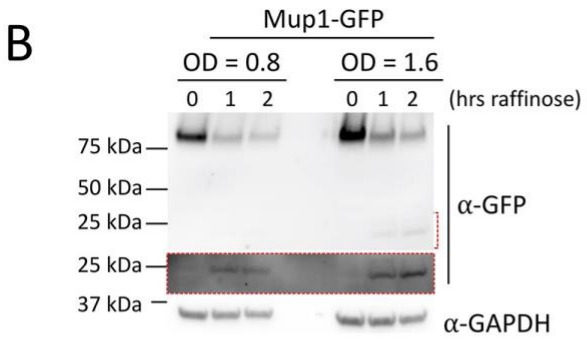
B
Mup1-GFP
OD = 0.8
OD = 1.6
0 1 2
0 1 2
(hrs raffinose)
75 kDa
50 kDa
25 kDa
25 kDa
37 kDa
α-GFP
α-GAPDH

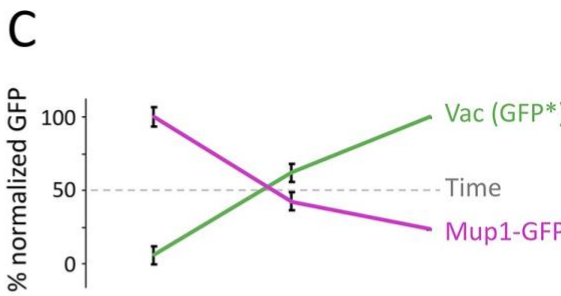
C
% normalized GFP
100
50
0
Vac (GFP*)
Time
Mup1-GFP

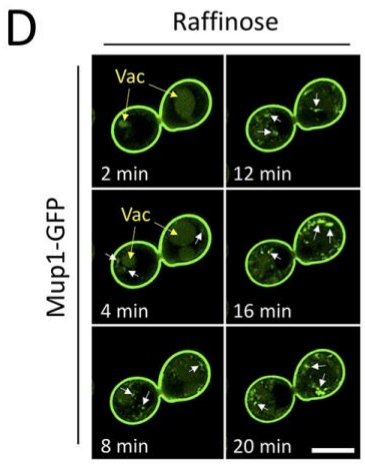
D
Raffinose
Mup1-GFP
Vac
2 min
12 min
4 min
16 min
8 min
20 min

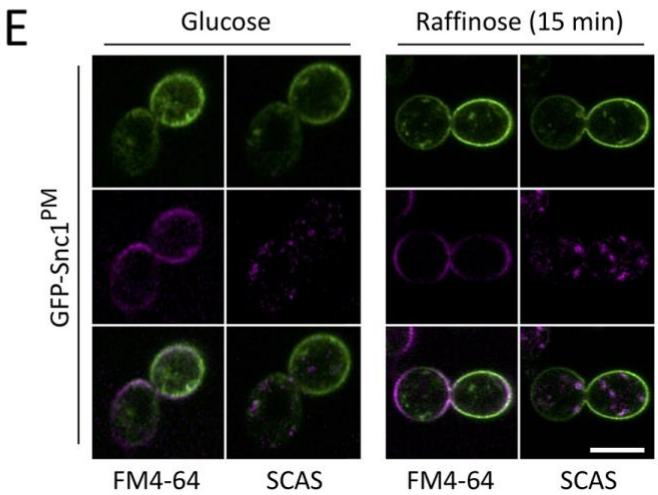
E
Glucose
Raffinose (15 min)
GFP-Snc1PM
FM4-64
SCAS
FM4-64
SCAS

Figure 3. 1 Glucose starvation results in downregulation of surface proteins:

A) Wild-type cells expressing labelled cargoes were grown to mid-log phase, processed for time-lapse microscopy and then imaged every 2-minutes in either glucose or raffinose media for indicated time course. Vacuoles are indicated with yellow arrows, and magenta arrows denote significant plasma membrane signal. **B)** Mup1-GFP levels in glucose and raffinose treated cells were assessed by immunoblot. Increased exposure (red box) shows levels of vacuolar processed GFP. Loading was assessed with anti-GAPDH antibodies. **C)** Graph depicts percentage full length Mup1-GFP versus vacuolar processed GFP following raffinose addition over time. Error bars show SD from three replicate experiments. **D)** Increased exposure of early time points from experiment **(A)** to show internalised Mup1-GFP (white arrows). **E)** Wild-type cells expressing GFP-Snc1^{PM} at log-phase were incubated with glucose or raffinose for 30 minutes prior to flushing with FM4-64 media for 5 minutes, then exchanging with media containing 2.4 µM SCAS (4-sulfonato calix[8]arene sodium salt) prior to imaging. Scale bar, 5 µm.

Mig1 regulates endocytic genes during starvation

We investigated a potential role for Mig1, which represses many genes in glucose-replete conditions (Nehlin et al., 1991; Nehlin and Ronne, 1990), in cargo endocytosis following glucose starvation. Mig1 repression in the nucleus is alleviated by its translocation to the cytoplasm upon medium exchange for alternative carbon sources (De Vit et al., 1997), including raffinose (**Fig. 3.2.A; Movie 3**). A consensus Mig1 binding sequence, containing motif (G/C)(C/T)GGGG, from validated promoters (Lundin et al., 1994) has been used to screen promoter regions (−500 bp of start codon) to identify 106 Mig1-target genes (Wollman et al., 2017). Potential Mig1 targets were clustered based on function, revealing many factors associated with protein downregulation (**Fig. 3.2.B**), including roles in ubiquitylation, autophagy and vacuolar degradation (**Table S1**). This list also included several endocytosis factors as potential Mig1 targets (**Fig. 3.2.C**), including genes encoding clathrin adaptors Yap1801, Yap1802, and Apl3 (Goode et al., 2015). We also noticed that other endocytic genes contained consensus Mig1 binding sequences in their open-reading frame (ORF) sequences, so included these in downstream transcriptomic analyses. Conditions f or qPCR were optimised for each potential Mig1 target gene (**Fig. S3.2.A–C**) to reveal that the yeast AP180 clathrin adaptors were upregulated in raffinose medium. Most prominently, *YAP1801* exhibited a robust ∼4-fold increase in expression levels 30 min after raffinose addition, which increased to ∼6 fold at 60 min (**Fig. 3.2.D**). *YAP1802* levels also increased significantly, with a sustained ∼2-fold increase following starvation incubations. Transcriptional upregulation of yeast AP180 adaptors was relatively acute, with transcript levels returning close to basal levels 90 min after raffinose (**Fig. 3.2.E**), a period sufficiently long to largely downregulate many cargoes (**Fig. 3.1.**). We found that *mig1Δmig2Δ* cells showed elevated levels of *YAP1801* and *YAP1802* transcript levels when compared to levels in wild-type cells (**Fig. 3.2.F**). There was no appreciable change in clathrin adaptor levels in *mig1Δ* cells, with it being necessary to also delete *MIG2*, which encodes a protein that has many of the same regulatory elements as Mig1 (Westholm et al., 2008) but is not translocated from the nucleus in responsive to glucose depletion (**Fig. S3.2.D**). We also found decreased *YAP1801* and *YAP1802* transcript levels in *msn2Δ* null cells (**Fig. 3.2.G**), which lack the Msn2 regulator that is known to activate many of the genes that Mig1 represses (Lin et al., 2015). This indirect evidence further supports a role of Mig1 in *YAP1801* and *YAP1802* expression, because expression of all other genes unaffected by raffinose treatment was unchanged in *msn2Δ* cells.

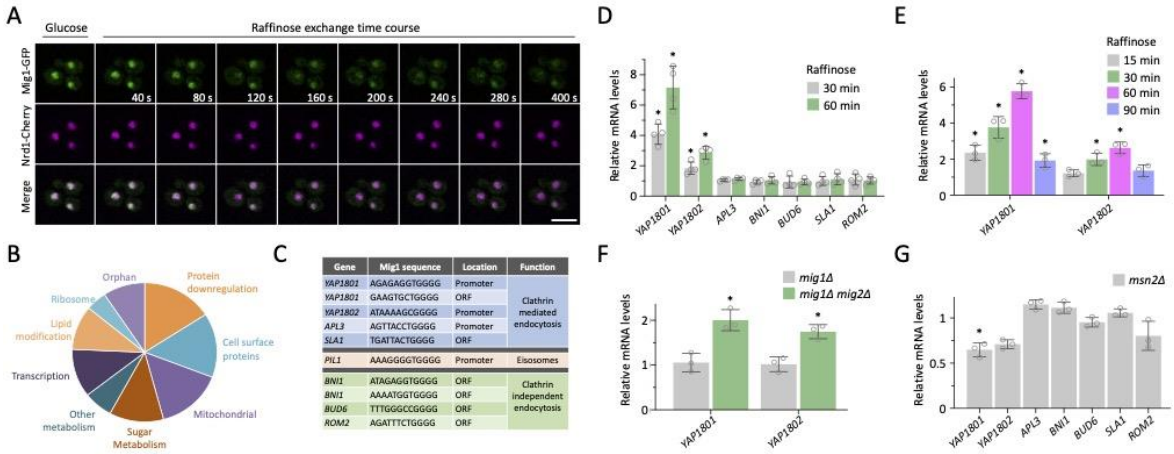

Figure 3. 2 Mig1 and glucose regulate expression of clathrin adaptor genes

A) Time-lapse microscopy of wild-type cells co-expressing Mig1–mGFP and Nrd1–mCherry grown in glucose medium prior to exchange with raffinose medium for the indicated times. **B)** Pie chart showing in silico categorisation of Mig1 binding targets in the yeast genome. **C)** Table of putative Mig1 target genes previously shown to function in endocytosis. **(D–G)** Total RNA was prepared and transcript levels measured by RT-qPCR of the indicated genes, using ACT1 and HEM2 genes as controls, from the indicated cells grown to mid-log phase in glucose medium. Comparing raffinose exchange for 30 and 60 min **(D)** or 15, 30, 60 and 90 min **(E)** with glucose controls or comparing *mig1Δ* and *mig1Δ mig2Δ* cells **(F)** and *msn2Δ* cells **(G)** with wild-type cells. Jitter plots show mean ± s.d. n=3–4 experiments, each with three technical replicates. *P<0.05 (unpaired Holm–Sidak t-test). Scale bar: 5 μm.

Glucose-sensitive AP180 adaptors trigger endocytosis

The AP180 proteins are conserved early acting endocytic factors that bind phosphatidylinositol 4,5-bisphosphate [PI(4,5)P2] at the plasma membrane, via their AP180 N-terminal homology (ANTH) domain, to recruit clathrin to endocytic sites (Ford et al., 2001; Wendland and Emr, 1998). We endogenously tagged the yeast AP180 adaptors with mGFP and confirmed that raffinose exchange resulted in a significant increase in Yap1801–mGFP, and a modest increase in Yap1802–mGFP levels (**Fig. 3.3.A,B**). Yeast AP180 proteins showed punctate surface localisation, with both distinct and overlapping localisations (**Fig. 3.3.C; Fig. S3.3.A**). These confocal experiments indicated an increase in fluorescence intensity following acute raffinose treatment (**Fig. S3.3.B–D**), but we sought a more accurate method to study endocytosis in living yeast cells. For this, we employed single-molecule Slimfield microscopy (**Fig.S3.3.E, Movie 4**), using a narrow field of laser excitation (Wollman and Leake, 2015), which enabled precise spatial resolution and millisecond-scale time sampling (Badrinarayanan et al., 2012; Reyes-Lamothe et al., 2010). This imaging system utilises spatially delimited illumination confined to the vicinity of a single cell and allows for detection of fluorescently labelled proteins directly in living yeast cells (Shashkova et al., 2021; Wollman et al., 2017). Based on the background and autofluorescence-corrected intensity of each cell, and the fluorescence intensity of a single mGFP and mCherry molecule, we were able to estimate the protein copy numbers within the cell. Levels of Yap1801 and Yap1802 were estimated to be ∼1000 and ∼400 molecules per cell, respectively, similar to previously reported estimates (Ho et al., 2018), with a significant increase in abundance for both Yap1801 and Yap1802 following glucose starvation (**Fig. 3.3.D**). Endogenously mCherry labelled versions of Yap1801 and Yap1802 were then used to monitor their localisation in relation to cargo in cells co-expressing Mup1–GFP. In replete conditions, Mup1 levels were dispersed across the plasma membrane, overlapping with spots of both Yap1801 and Yap1802 (**Fig. 3.3.E**). Most Mup1–GFP signal was internalised following raffinose treatment (**Fig. 3.1.**), but Airyscan confocal microscopy revealed that ∼2.0±1.3% (mean ± s.d.). Mup1–GFP localised to punctate surface structures after raffinose exchange (**Fig. S3.3.F**), including AP180-colocalised protein, presumably destined for internalisation, and cargo sequestered in eisosomes (discussed below).

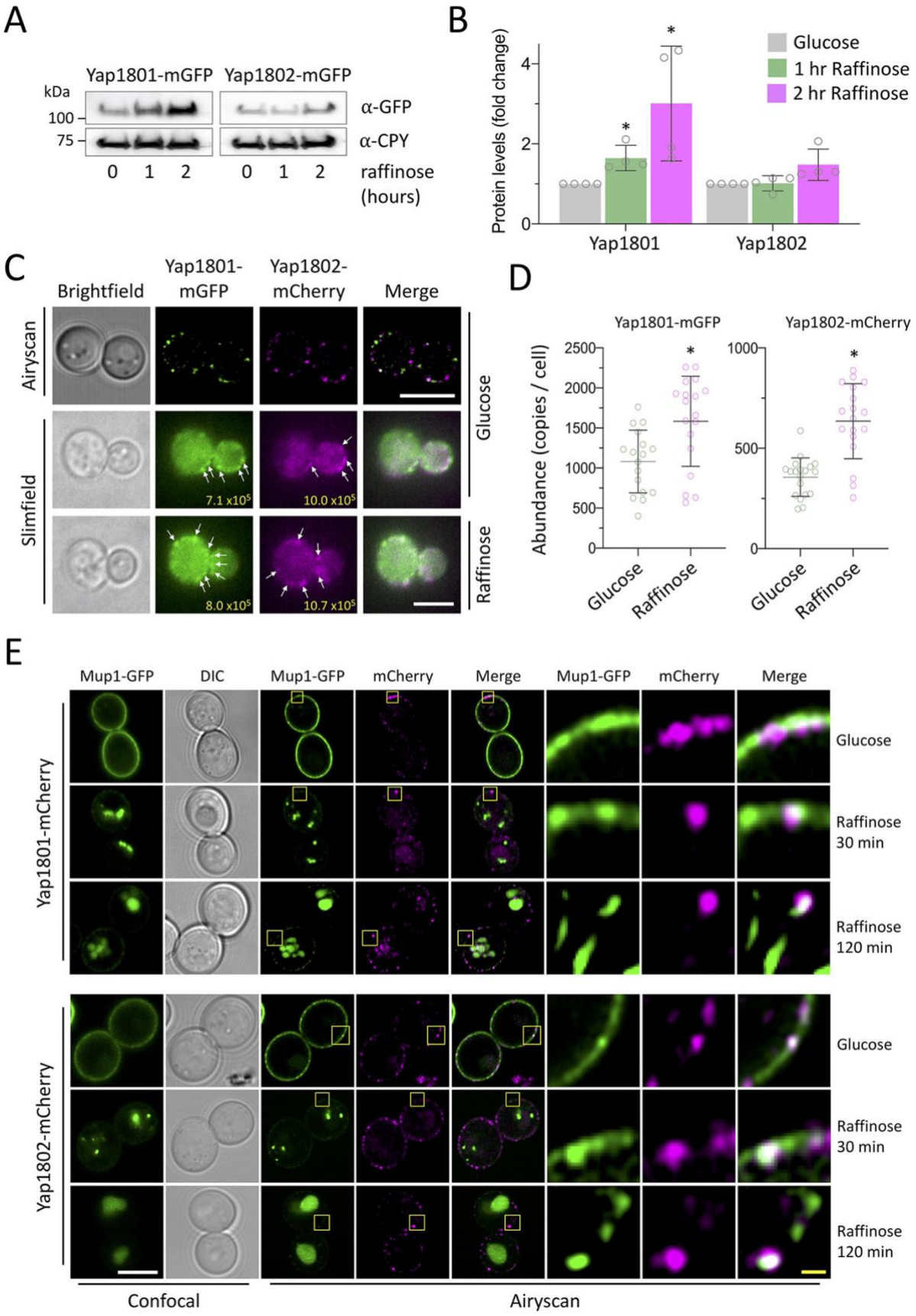
A
Yap1801-mGFP
Yap1802-mGFP
kDa
100
75
α-GFP
α-CPY
0 1 2 0 1 2
raffinose (hours)
B
Protein levels (fold change)
Glucose
1 hr Raffinose
2 hr Raffinose
Yap1801
Yap1802
C
Brightfield
Yap1801-mGFP
Yap1802-mCherry
Merge
Airyscan
Slimfield
Glucose
Raffinose
7.1 x10^5
10.0 x10^5
8.0 x10^5
10.7 x10^5
D
Yap1801-mGFP
Yap1802-mCherry
Abundance (copies / cell)
Glucose
Raffinose
E
Mup1-GFP
DIC
mCherry
Merge
Yap1801-mCherry
Yap1802-mCherry
Glucose
Raffinose 30 min
Raffinose 120 min
Confocal
Airyscan

Figure 3. 3 Yap1801 and Yap1802 proteins are upregulated during glucose starvation:

A) Immunoblot analysis of endogenously tagged Yap1801–mGFP and Yap1802–mGFP in wild-type cells grown in glucose and raffinose media. Anti-CPY antibody was used as a loading control. **B)** Histogram showing average Yap1801–mGFP and Yap1802–mGFP intensity, normalized to intensity in glucose medium. Mean ± s.d. of n=4. **C)** Wild-type cells expressing Yap1801–mGFP and Yap1802–mCherry at mid-log phase were imaged by Airyscan confocal and Slimfield microscopy. For Slimfield, bright foci are indicated with white arrows, and the integrated density for diving cells in each frame is shown in yellow. These data represent the first of 200 frames, acquired every 5 ms, with representative full datasets shown in Movie 3. **D)** Numbers of Yap1801 and Yap1802 molecules per cell (>20 cells) were estimated using autofluorescence- and background-corrected integrated density values obtained using ImageJ software. Mean ± s.d. is shown. **E)** Airyscan confocal colocalisation of Mup1–GFP with Yap1801–mCherry (upper panels) and Yap1802–mCherry (lower panels) in glucose and raffinose media. Yellow boxes denote zoomed-in regions shown in the panels to the right. *P<0.05 (unpaired Holm–Sidak t-test). Scale bars: 5 μm (white), 1 μm (yellow).

Our model predicts that elevated levels of Yap1801 and Yap1802 induced upon glucose starvation are sufficient to upregulate endocytosis. To test this, mCherry tagged AP180 adaptors were expressed from a plasmid under the control of the copper inducible CUP1 promoter. With no addition of copper, low levels of Yap1801–mCherry or Yap1802–mCherry, similar to endogenously tagged versions, had no effect on the surface localisation of co-expressed Mup1–GFP or Can1–GFP (**Fig. 3.4.A,B**). However, overexpression of mCherry tagged Yap1801 and Yap1802 was sufficient to trigger endocytosis. The yeast AP180 adaptors have been reported to have a range of localisation patterns (Burston et al., 2009; Carroll et al., 2012; Newpher et al., 2005; Yamamoto et al., 2018), but we did not find any particular localisations (**Fig. S3.4.A**) that correlated with specific endocytic events, only that elevated levels were sufficient to increase endocytosis. Furthermore, Mup1–GFP endocytosis was induced slightly in *mig1Δ* cells, and substantially more in *mig1Δmig2Δ* cells (**Fig. 3.4.C–E**), sorting of which is further accelerated when cells are grown to late log phase (MacDonald et al., 2015a; MacDonald et al., 2012c). Similarly, endocytosis of Can1–GFP, Ste3–GFP and Fur4–mNG was elevated in *mig1Δ mig2Δ* cells (**Fig. 3.4.F**), presumably through the increased levels of Yap1801 and Yap1802. As expected, endocytosis in *mig1Δ mig2Δ* cells was phenocopied in cells lacking the upstream Reg1 component, but not in cells lacking the low-glucose sensor Snf3 (**Fig. S3.4.B**). Efficiency of endocytosis upon raffinose exchange was attenuated in *yap1801Δ yap1802Δ* cells, shown by Mup1–GFP sorting to the vacuole (**Fig. 3.4.G**) and internalisation from the surface (**Fig. 3.4.H**) being reduced. Endocytosis of Mup1–GFP induced by growth to late log phase was also reduced (**Fig. S3.4.C**). Furthermore, as endocytosis of Mup1, Can1, Ste3 and Fur4 induced by deletion of *MIG1* and *MIG2* was ablated by the further deletion of *YAP1801* and *YAP1802* (**Fig. 3.4.I**), we conclude that Mig1 and/or Mig2 repress transcription of *YAP1801* and *YAP1802* in glucose-replete conditions, which is lifted in response to glucose starvation to trigger clathrin-mediated endocytosis of a broad range of cargoes.

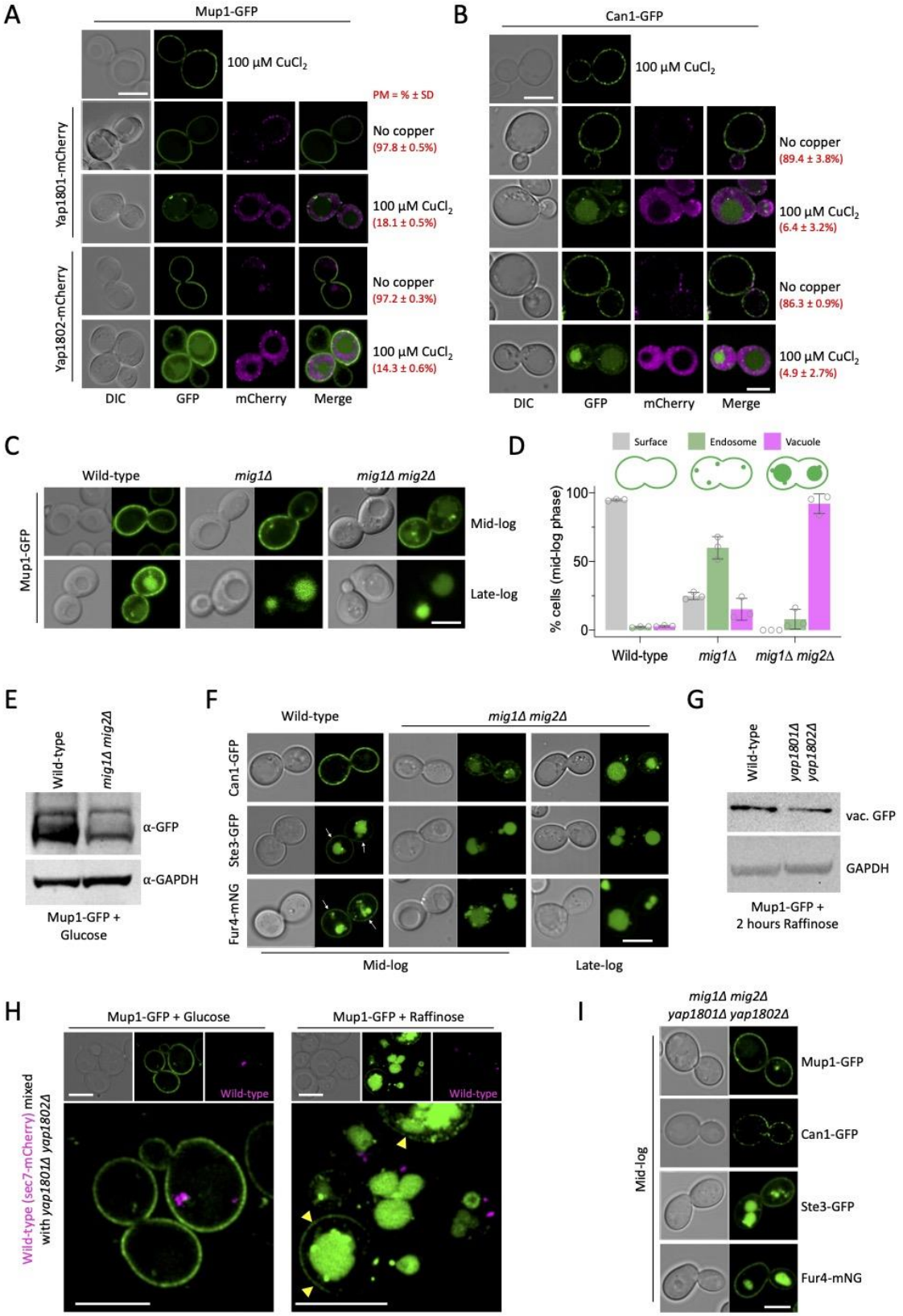
A
Mup1-GFP
100 µM CuCl2
PM = % ± SD
Yap1801-mCherry
No copper
(97.8 ± 0.5%)
100 µM CuCl2
(18.1 ± 0.5%)
Yap1802-mCherry
No copper
(97.2 ± 0.3%)
100 µM CuCl2
(14.3 ± 0.6%)
DIC
GFP
mCherry
Merge
B
Can1-GFP
100 µM CuCl2
No copper
(89.4 ± 3.8%)
100 µM CuCl2
(6.4 ± 3.2%)
No copper
(86.3 ± 0.9%)
100 µM CuCl2
(4.9 ± 2.7%)
DIC
GFP
mCherry
Merge
C
Wild-type
mig1Δ
mig1Δ mig2Δ
Mup1-GFP
Mid-log
Late-log
D
Surface
Endosome
Vacuole
% cells (mid-log phase)
100
50
0
Wild-type
mig1Δ
mig1Δ mig2Δ
E
Wild-type
mig1Δ mig2Δ
α-GFP
α-GAPDH
Mup1-GFP +
Glucose
F
Wild-type
mig1Δ mig2Δ
Can1-GFP
Ste3-GFP
Fur4-mNG
Mid-log
Late-log
G
Wild-type
yap1801Δ
yap1802Δ
vac. GFP
GAPDH
Mup1-GFP +
2 hours Raffinose
H
Mup1-GFP + Glucose
Mup1-GFP + Raffinose
Wild-type (sec7-mCherry) mixed
with yap1801Δ yap1802Δ
Wild-type
Wild-type
I
mig1Δ mig2Δ
yap1801Δ yap1802Δ
Mid-log
Mup1-GFP
Can1-GFP
Ste3-GFP
Fur4-mNG

Figure 3. 4 Increased Yap1801/Yap1802 increases rates of cargo endocytosis:

A-B) Airyscan confocal microscopy imaging of wild-type cells co-expressing Mup1–GFP (**A**) or Can1–GFP (**B**) and Yap1801–mCherry or Yap1802– mCherry, expressed under control of the copper-inducible CUP1 promoter. The mean±s.d. percentages of cells exhibiting exclusive plasma membrane localisation for each condition (>75 cells per conditions) are shown in red text. (**C**) Localisation of Mup1–GFP in wild-type, *mig1Δ*, and *mig1Δ mig2Δ* cells at mid- and late-log phase. (**D**) Quantification of the experiment shown in C, with 35–120 mid-log phase cells quantified from each condition. Mean ±s.d. n=3. (**E**) Immunoblot analysis of Mup1–GFP expressed in wild-type and *mig1Δ mig2Δ* cells. GAPDH was used as a loading control. (**F**) Wild-type and *mig1Δ mig2Δ* cells expressing Can1–GFP, Ste3–GFP and Fur4–mNG were imaged at mid- and late-log phase. Surface-localised signal is indicated with white arrows. (**G**) Immunoblot analysis of vacuolar GFP from lysates generated from wild-type and *yap1801Δ yap1802Δ* cells expressing Mup1-GFP. GAPDH was used as a loading control. (**H**) Mup1–GFP was expressed in wild-type cells labelled with Sec7–mCherry and in unlabelled *yap1801Δ yap1802Δ* cells, mixed in a 1:1 ratio and co-cultured for 2 h, followed by 90 additional minutes in glucose (left) or raffinose (right) media prior to fluorescence microscopy. Surface-localised signal is indicated with yellow arrowheads. (**I**) Quadruple-null *mig1Δ mig2Δ yap1801Δ yap1802Δ* cells expressing Mup1–GFP, Can1–GFP, Ste3–GFP or Fur4–mNG were imaged at mid-log phase. Scale bars: 5 µm.

Eisosomal reorganisation sequesters cargo during glucose starvation

Spatial mapping and functional analyses of surface cargoes have recently shown that lipid domains, termed eisosomes, harbour surface proteins and antagonise their endocytosis (Bianchi et al., 2018; Busto et al., 2018; Gournas et al., 2018; Moharir et al., 2018). Pil1 is required for proper formation of eisosomes (Walther et al., 2006) and PIL1 was implicated as a potential Mig1 target, we therefore examined its role in harbouring cargo in eisosomes. As expected, fluorescently tagged Pil1 failed to colocalise with sites of endocytosis marked by Yap1801 or Yap1802 (**Fig. 3.5.A**). Upregulation of eisosomes that contravene cargo endocytosis may seem contradictory in conditions that also upregulate endocytosis; however, cargo protection in eisosomes during starvation and osmotic shock has recently been documented (Appadurai et al., 2019; Gournas et al., 2018).We found that PIL1 was regulated at the transcriptional level in response to raffinose treatment, but we observed no difference in expression in *mig1Δ mig2Δ* cells (**Fig. 3.5.B; Fig. S3.5.A**), suggesting Pil1 protein levels are significantly increased during glucose starvation (**Fig. 3.5.C,D**) through a Mig1/2-independent mechanism. To test whether this transcriptional upregulation of eisosomes impacted cargo endocytosis we performed time-lapse microscopy of cells co-expressing Mup1–GFP cargo and Pil1–mCherry, to mark eisosomes. We optimised 4D confocal conditions to best observe eisosomes at the surface (**Fig.S3.5.B**) before initiating glucose starvation by flushing raffinose medium using microfluidics. Mup1–GFP colocalised with eisosomes in glucose-replete medium (**Fig. 3.5.E**), with the majority of Mup1–GFP being distributed at the plasma membrane. As shown, the bulk of Mup1–GFP is endocytosed following glucose starvation (**Fig. 3.1.**); however, we noticed concentration of Mup1–GFP within some, but not all, eisosomal structures (**Fig. 3.5.E**). This is in contrast to when the Mup1 substrate methionine was added, which triggers flux from eisosomes to distinct plasma membrane regions that allow internalisation (Busto et al., 2018), implying that this response is related to starvation of the cell and not a mechanism associated with typical transporter regulation. As Mup1–GFP was observed to diffuse out of eisosomes during initial starvation, eisosome targeting may be a stochastic process; it is curious that only certain eisosomes appear to accumulate Mup1–GFP, with no signal observed for other Pil1-marked compartments, suggesting a precise regulatory mechanism. In support of this idea, we captured dramatic reconfigurations of Pil1–mCherry in eisosomes retaining Mup1–GFP (Movie 5). We noted that Pil1-marked eisosomes increased in size and intensity over the course of time-lapse microscopy following raffinose exchange (**Fig. 3.5.F,G**), so we performed a series of steady-state experiments to fully quantify this phenotype which confirmed that the intensity of Mup1–GFP foci at eisosomes increased significantly following glucose starvation, with no change in intensity of Mup1–GFP molecules that were in other, non-eisosomal regions of the cell (**Fig. 3.5.H; Fig.S3.5.C**). Similarly, in raffinose grown cells, Pil1–mCherry intensity was unchanged in regions that lacked Mup1–GFP, but increased in eisosomes harbouring cargo (**Fig. 3.5.I**).

Although we observed an increase in Pil1 levels, at whole-cell level and at eisosomes, during raffinose exchange, we observed no change in eisosome number (**Fig. S3.5.D**), implying the increased levels of Pil1 localise to and regulate existing eisosomes to better sequester cargo, as shown by confocal microscopy (**Fig. 3.5.F,G**). Interestingly, we found that Pil1 was rapidly dephosphorylated upon raffinose treatment (**Fig. 3.5.C**); our optimised SDS-PAGE (MacDonald et al., 2020) revealed a marked shift from slower to faster migrating dephosphorylated bands that have been previously correlated with increased Pil1 assembly at eisosomes (Walther et al., 2007; Walther et al., 2006). Mup1–GFP- and Pil1–mCherry-expressing cells, in both glucose and raffinose media, were used for Slimfield imaging (**Fig. 3.5.J; Movie 6**), which allowed acquisition

of hundreds of images per field of view at 5 ms exposure times enabling a lateral localisation precision of ~40 nm until no fluorescence signal could be detected (Miller et al., 2015a). We then applied a bespoke MATLAB code for single-particle tracking to identify all fluorescent spots within one image and link them to those on the next image, so that trajectories of foci movements could be built for further diffusion and stoichiometry (number of molecules per bright spot) analysis (Leake et al., 2006; Shashkova and Leake, 2017). As fluorescent proteins photobleach in a stepwise manner, we applied previously optimised protocols for stoichiometry estimations by comparing intensity of each identified fluorescent spot with a single fluorophore intensity. Single-molecule analysis of plasma membrane-localised proteins showed that, although there were no physiological changes in Mup1–GFP (**Fig. S3.5.E,F**), there was an increase in the diffusion coefficient (**Fig. 3.5.K**) and molecular stoichiometry (**Fig. 3.5.L**) of Pil1–mCherry. It may be that increased Pil1 intensity represents an increase in eisosome size, or just more Pil1 molecules per eisosome. Either way, the molecular response to starvation serves to better sequester cargo. Also, although most Mup1–GFP molecules were no longer found within the surface region following starvation, the few spots retained showed that the stoichiometry of Pil1 in these regions increased (**Fig. 3.5.M**). Collectively, this helps rationalise how a relatively modest increase in PIL1 transcription and protein levels, alongside its rapid posttranslational modification, allow a subset of eisosomes to sequester Mup1–GFP during glucose starvation. Beside this, we also documented more dramatic raffinose-induced increases in expression of other eisosomal genes. Similar to *PIL1*, the levels of *PKH2* and *SEG1* were increased by ~2.5-fold, but others showed a larger increase, with mRNA levels of NCE102 and LSP1 increasing ~6-fold and SLM1 levels ~11-fold after 60 min raffinose (**Fig. 3.5.N**). We found that levels of Lsp1 increased significantly during raffinose exchange (**Fig. 3.5.O**), and the phenotype of Mup1–GFP localising to specific eisosomes was found with mCherry-labelled eisosome proteins Nce102, Lsp1 and Slm1 (**Fig. 3.5.P**). We therefore believe that eisosomes are relatively stable and that the transcriptional upregulation of factors triggers modulation of existing eisosomes to concentrate cargo during acute glucose starvation.

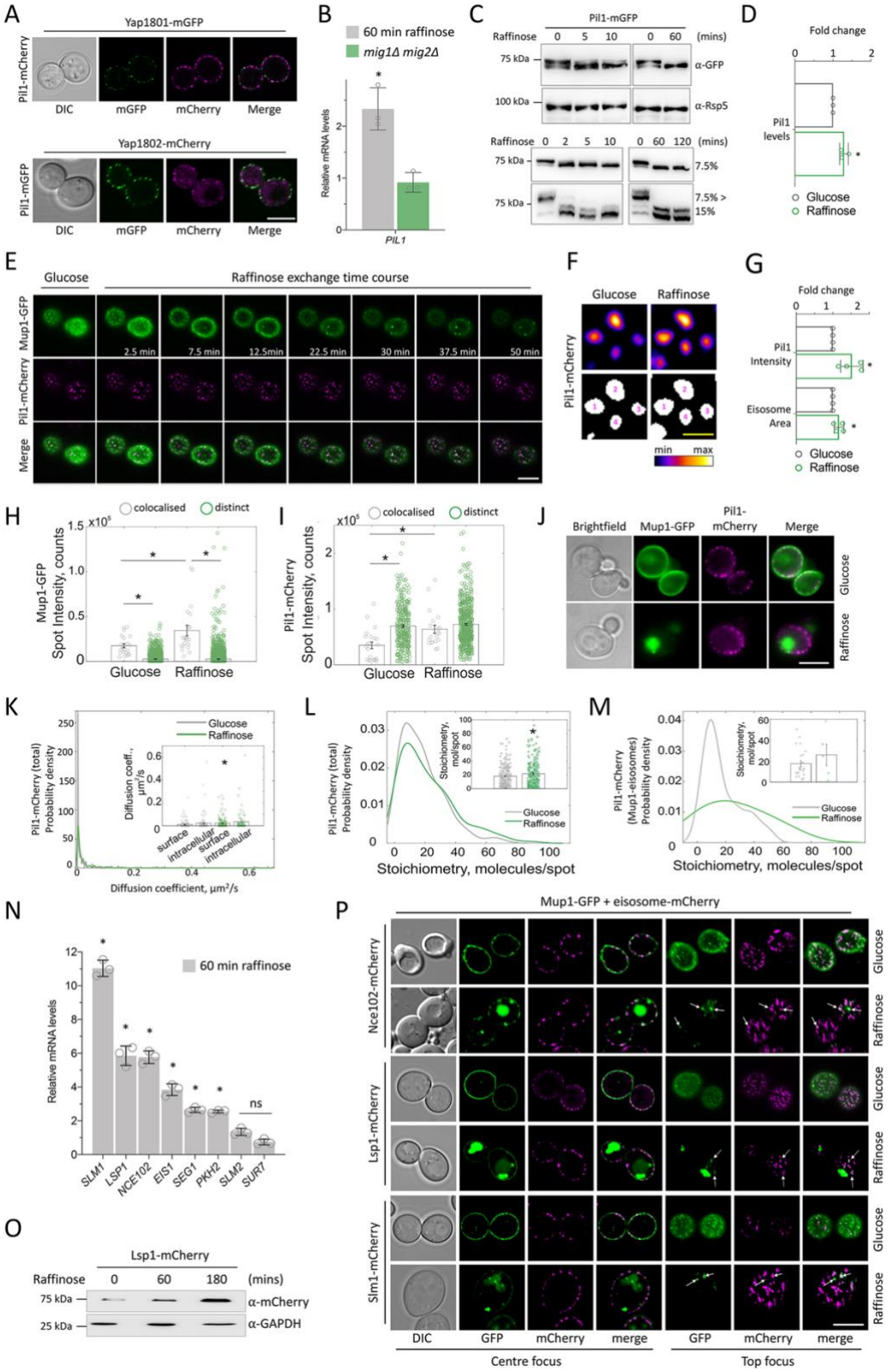
A
Yap1801-mGFP
Pil1-mCherry
DIC
mGFP
mCherry
Merge
Yap1802-mCherry
Pil1-mGFP
B
60 min raffinose
mig1Δ mig2Δ
Relative mRNA levels
PIL1
C
Pil1-mGFP
Raffinose 0 5 10 0 60 (mins)
75 kDa
α-GFP
100 kDa
α-Rsp5
Raffinose 0 2 5 10 0 60 120 (mins)
75 kDa
7.5%
75 kDa
7.5% > 15%
D
Fold change
Pil1 levels
Glucose
Raffinose
E
Glucose
Raffinose exchange time course
Mup1-GFP
Pil1-mCherry
Merge
2.5 min
7.5 min
12.5min
22.5 min
30 min
37.5 min
50 min
F
Glucose
Raffinose
Pil1-mCherry
min
max
G
Fold change
Pil1 Intensity
Eisosome Area
Glucose
Raffinose
H
colocalised
distinct
Mup1-GFP Spot Intensity, counts
Glucose
Raffinose
I
colocalised
distinct
Pil1-mCherry Spot Intensity, counts
Glucose
Raffinose
J
Brightfield
Mup1-GFP
Pil1-mCherry
Merge
Glucose
Raffinose
K
Glucose
Raffinose
Pil1-mCherry (total) Probability density
Diffusion coeff., μm²/s
surface
intracellular
surface
intracellular
Diffusion coefficient, μm²/s
L
Pil1-mCherry (total) Probability density
Stoichiometry, mol/spot
Glucose
Raffinose
Stoichiometry, molecules/spot
M
Pil1-mCherry (Mup1-eisosomes) Probability density
Stoichiometry, mol/spot
Glucose
Raffinose
Stoichiometry, molecules/spot
N
60 min raffinose
Relative mRNA levels
ns
SLM1
LSP1
NCE102
EIS1
SEG1
PKH2
SLM2
SUR7
O
Lsp1-mCherry
Raffinose 0 60 180 (mins)
75 kDa
α-mCherry
25 kDa
α-GAPDH
P
Mup1-GFP + eisosome-mCherry
Nce102-mCherry
Lsp1-mCherry
Slm1-mCherry
Glucose
Raffinose
DIC
GFP
mCherry
merge
GFP
mCherry
merge
Centre focus
Top focus

Figure 3. 5 Eisosomes sequester surface proteins in glucose-starvation conditions:

A) Fluorescence microscopy of cells expressing Yap1801– mGFP and Pil1–mCherry, or Yap1802–mCherry and Pil1–GFP. **B)** RT-qPCR of PIL1 was performed using RNA extracted from wild-type cells grown in glucose with or without 1 h in raffinose medium (grey) or from wild-type and *mig1Δ mig2Δ* cells grown in glucose (green). Mean±s.d. from n=3 biological replicates (each with n=3 technical replicates). **C)** Pil1–GFP levels in wild-type cells over a raffinose time course assessed by immunoblotting following resolution on standard (upper panels and lower panels, 7.5% acrylamide) and step-gradient (lower panels, 7.5%>15% acrylamide) resolving gels. Anti-Rsp5 was used as a loading control. **D)** Quantification of total Pil1–GFP levels from immunoblots (n=3) using cells grown in glucose or raffinose for 1 h. Mean±s.d. **E)** Average intensity projections of top-focussed Airyscan confocal images shown for a raffinose exchange timecourse of wild-type cells co- expressing Pil1–mCherry and Mup1–GFP. **F)** Pil1–mCherry intensity from time-lapse microscopy in glucose and raffinose compared with a gradient- based density look-up table (upper panels) and segmented using identical Li thresholding parameters (17/65,535) to create numbered eisosome regions of interest (ROIs; lower panels). **G)** ROIs generated in **F** were used to calculate average Pil1–mCherry intensities and eisosome areas. Mean±s.d. **(H,I)** Jitter plots of fluorescence intensities of Mup1–GFP **(H)** and Pil1–mCherry **(I)** spots measured for both colocalised (grey) and distinct (green) foci from cells grown to mid-log phase and either prepared directly for confocal microscopy (glucose) or first grown in raffinose media for 30 min. Mean ± s.e.m. **J)** Examples of the first frame of Slimfield acquisitions from cells co-expressing Mup1–GFP and Pil1–mCherry in glucose (upper panel) and raffinose solid media conditions (lower panel). **(K–M)** Kernel density plots of Pil1–mCherry foci diffusion coefficient distribution **(K)**, whole-cell Pil1–mCherry stoichiometry distribution **(L)** and Pil1–mCherry stoichiometry distribution from only foci that colocalise with Mup1–GFP **(M)** are shown from cells incubated in glucose (grey) or raffinose (green) media. Insets: jitter plots of diffusion coefficients and stoichiometries. Mean±s.d. **N)** RT-qPCR of the indicated genes was performed from RNA extracted from wild-type cells grown in glucose followed by 60 min raffinose exchange. Mean ± s.d from n=3 biological replicates (each averaged from three technical replicates). **O)** Levels of integrated Lsp1–mCherry was assessed using anti-mCherry immunoblotting of lysates generated from growth in raffinose medium for the indicated periods, with GAPDH blot as a loading control. **P)** Airyscan confocal microscopy of cells expressing the indicated mCherry-tagged eisosome proteins and co-expressing Mup1–GFP from a plasmid, after growth in glucose or 45 min in raffinose. Arrows indicate colocalisation of sequestered cargo with eisosome marker. *P<0.05; ns, not significant (Student's t-test). Scale bars: 5 μm (white); 1 μm (yellow).

Ygr130c is required for efficient cargo retention at eisosomes

As Mup1–GFP appears to target only a subset of eisosomes during glucose starvation, we performed bioinformatics analyses to identify possible eisosome factors that physically interact with the cargo Mup1 (**Tables S2,S3**) and might serve as eisosome anchors. Of ~70 known physical Mup1 interactions, three were eisosome factors: Lsp1, Slm1 and Ygr130c (**Fig. 3.6.A**). The functional roles of Lsp1 (Walther et al., 2006; Ziółkowska et al., 2011) and Slm1 (Audhya et al., 2004; Fadri et al., 2005) have been characterised, and we found that these proteins colocalise with all Pil1-marked eisosomes (**Fig. S3.5.G**) and behave as Pil1 during starvation-induced cargo retention (**Fig. 3.5.P**). Therefore, we focussed on the potential role of Ygr130c. Although identified as an eisosomal-resident protein from a visual screen (Grossmann et al., 2008), and shown to interact with the PI(4,5)P2 phosphatase Inp51, along with other eisosome factors (Fröhlich et al., 2014), the function of Ygr130c remains unknown; although it has been implicated in regulation of chronological lifespan through an unknown mechanism (Borklu Yucel and Ulgen, 2011). We tagged Ygr130c with mCherry and found that it colocalises with Pil1–GFP eisosomes (**Fig. 3.6.B**) and Mup1–GFP in both glucose and raffinose conditions (**Fig. 3.6.C**). To test the hypothesis that Ygr130c could act as a physical eisosomal anchor for Mup1, we expressed Mup1–GFP in mutant *ygr130cΔ* cells and found that its distribution across the plasma membrane was more dispersed than in wild-type cells, where Mup1–GFP was found to colocalise with distinct Pil1–mCherry-marked eisosomes (**Fig. 3.6.D**). We developed a method to calculate the size of Mup1–GFP signals at the plasma membrane (**Fig. S3.6.**), which showed a statistically significant increase in contiguous length of Mup1–GFP signals at the surface of *ygr130cΔ* cells, indicating reduced residency in eisosomes (**Fig. 3.6.E**). This was more evident following glucose starvation, where after 1 h raffinose exchange, surface-retained Mup1 was primarily colocalised with Pil1–mCherry puncta (**Fig. 3.6.F**). In contrast, Mup1–GFP signal was more diffuse at the surface of glucose-starved *ygr130cΔ* cells, and the most concentrated signal was observed in regions distinct from Pil1–mCherry. We propose the role of Ygr130c is to increase residency of Mup1 diffusing into eisosomes, which is particularly important to retain a reserve pool of Mup1 during glucose starvation. Beyond Mup1, other surface nutrient transporter proteins that physically interact with Ygr130c have been identified, including uridine (Fui1), inositol (Itr1) and polyamine (Tpo4) transporters (Table S2). Furthermore, Ygr130c interactors include nutrient transporters for iron (Ftr1), choline (Hnm1), and biotin (Vht1), and these cargoes have been previously shown to colocalise to some degree (coefficients of 0.09±0.01, 0.08±0.01, and 0.08±0.01, respectively) with the eisosome marker Sur7 (Spira et al., 2012). This retention mechanism therefore may extend to additional nutrient transporters and might explain why a relatively high number of known Mup1 interactors are also known to physically bind Ygr130c (**Fig. 3.6.G**).

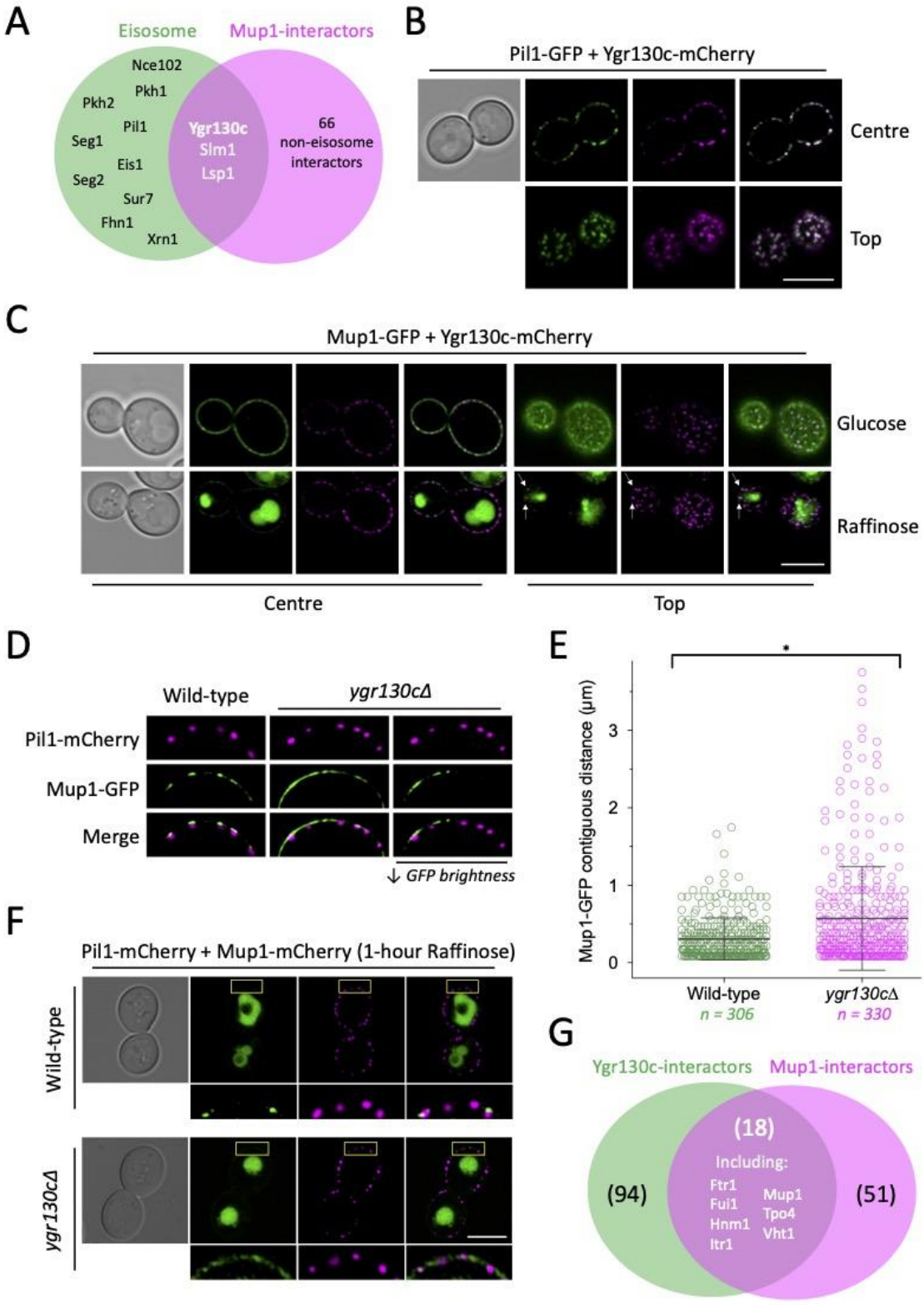
A
Eisosome
Mup1-interactors
Nce102
Pkh1
Pkh2
Pil1
Seg1
Ygr130c
Slm1
Lsp1
66
non-eisosome
interactors
Eis1
Seg2
Sur7
Fhn1
Xrn1
B
Pil1-GFP + Ygr130c-mCherry
Centre
Top
C
Mup1-GFP + Ygr130c-mCherry
Glucose
Raffinose
Centre
Top
D
Wild-type
ygr130cΔ
Pil1-mCherry
Mup1-GFP
Merge
↓ GFP brightness
E
*
Mup1-GFP contiguous distance (µm)
0
1
2
3
Wild-type
n = 306
ygr130cΔ
n = 330
F
Pil1-mCherry + Mup1-mCherry (1-hour Raffinose)
Wild-type
ygr130cΔ
G
Ygr130c-interactors
Mup1-interactors
(94)
(18)
Including:
Ftr1
Fui1
Hnm1
Itr1
Mup1
Tpo4
Vht1
(51)

Figure 3. 6 Ygr130c is required for efficient eisosomal cargo retention.

A) Venn diagram showing overlap between known eisosome proteins (green) and Mup1 physical interactors (magenta). **B)** Cells co-expressing Pil1–GFP (green) and Ygr130c–mCherry (magenta) were imaged at centre and top focus planes using confocal microscopy. Merge images are shown on the right. **C)** Cells expressing Ygr130c–mCherry (magenta) were transformed with a Mup1–GFP (green) plasmid and imaged in glucose or raffinose media by Airyscan confocal microscopy. Merge images are shown on the right for each condition. Arrows indicate spots of colocalisation. **D)** Colocalisation of Mup1–GFP- and Pil1–mCherry-marked eisosomes in wild-type and *ygr130cΔ* mutants was recorded by Airyscan confocal imaging. A panel of reduced GFP brightness is included to better show GFP distribution (right). **E)** Contiguous plasma membrane GFP signal (in µm) was measured in wild-type (green) and *ygr130cΔ* cells (magenta). Mean±s.d. **F)** Wild- type and *ygr130cΔ* cells co-expressing Pil1–mCherry (magenta) and Mup1–GFP (green) following 1 h of raffinose exchange were compared using Airyscan microscopy. Boxes indicate regions shown in enlarged images below. **G)** Venn diagram between physical interactors of Ygr130c (green) and Mup1 (magenta); 18 proteins are present in both sets. *P<0.05 (Student's t-test). Scale bars: 5 µm (white), 1 µm (yellow).

Eisosomes provide a recovery growth benefit following starvation

Not all surface cargoes localise to eisosome compartments, for example the receptor Ste3–GFP, and a version retained at the plasma membrane (Ste3–GFP-DUb) showed no colocalisation with Pil1–mCherry (**Fig. S3.7.A**). We propose that eisosomes increase in size or structure specifically to better harbour nutrient transporters, to persist through glucose-starvation periods and provide a physiological benefit upon a return to glucose-replete conditions. We reasoned that cells deficient in this eisosome function would exhibit growth deficiencies by virtue of their inability to maximise nutrient uptake. However, growth on rich and synthetic defined media, and estimated doubling times, showed no obvious difference between wild-type and null cells lacking various eisosome components (**Fig. 3.7.A; Fig. S3.7.B**). Despite this, we did observe that some mutants, including *pil1Δ*, *lsp1Δ* and *nce102Δ*, failed to reach the optical density of wild-type cells upon growth to saturation (**Fig.S3.7.C**), implying their nutrient uptake capacity might be compromised. The eisosomal-localised permease Fur4 (**Fig. 3.7.B**) is required for the uptake of uracil (Jund and Lacroute, 1970) and growth of *ura3Δ* auxotroph strains in minimal medium with low uracil concentrations (**Fig. 3.7.C**). We reasoned that Fur4-mediated uracil scavenging following glucose starvation would provide a recovery-based assay with a dynamic range to test the role of eisosomes. For this, we used *pkh2Δ* cells, which have reduced levels of unmodified and phosphorylated Pil1 (**Fig. 3.7.D**), and redistributed Pil1 localisation into reticular structures at the plasma membrane (**Fig. 3.7.E**) reminiscent of structures observed in *pkh2Δ* cells carrying a temperature-sensitive allele of *pkh1* (Walther et al., 2007).We also used *eis1Δ* and *nce102Δ* mutants, which are defective in eisosome assembly and cargo retention (Aguilar et al., 2010; Fröhlich et al., 2009; Loibl et al., 2010) (**Fig. 3.7.E; Fig. S3.7.D**). These eisosome mutants had a decreased amount of Fur4–mNG localised to eisosomes (**Fig. 3.7.F,G**) and showed higher rates of cargo endocytosis in both glucose and raffinose conditions (**Fig. 3.7.H;Fig. S3.7.E**), allowing us to test the hypothesis that cargo storage in eisosomes aids recovery from nutrient stress. Log-phase cells were exchanged with raffinose medium for 2 h before return to replete medium of varying concentrations of uracil, and growth was recorded over time (**Fig. 3.7.I**). The recovery rate of growth for wildtype cells was significantly better than that of all three null mutants with defective eisosomes, across all concentrations of uracil tested (**Fig. 3.7.J,K; Fig. S3.7.F,G**) or when cells were returned to medium with only 10% amino acid levels (**Fig. S3.7.H**). This benefit can be attributed in part to Fur4-mediated uracil uptake, as uracil-prototroph eisosome mutants recovered better from glucose starvation compared with their auxotrophic counterparts (**Fig. 3.7.L,M; Fig. S3.7.I**). However, there was still a statistically significant reduction in recovery of eisosome mutants prototrophic for uracil compared with recovery of the Ura+ wild type, so we conclude that, whilst Fur4 is an important cargo sequestered in eisosomes to facilitate recovery following starvation, it is not the only nutrient transporter required for this response.

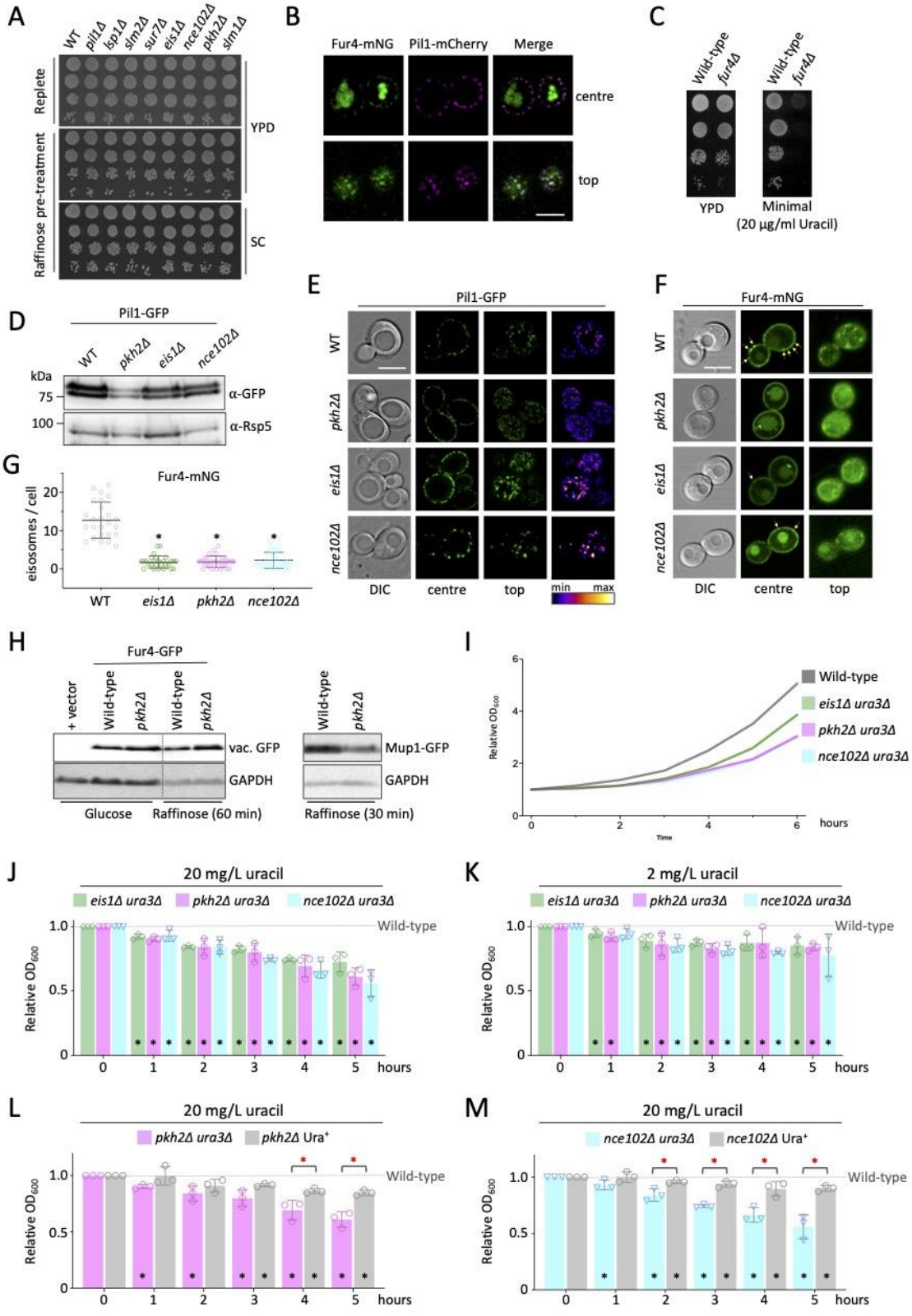
A
WT
pil1Δ
lsp1Δ
slm2Δ
sur7Δ
eis1Δ
nce102Δ
pkh2Δ
slm1Δ
Replete
Raffinose pre-treatment
YPD
SC
B
Fur4-mNG
Pil1-mCherry
Merge
centre
top
C
Wild-type
fur4Δ
YPD
Minimal
(20 µg/ml Uracil)
D
Pil1-GFP
WT
pkh2Δ
eis1Δ
nce102Δ
kDa
75
100
α-GFP
α-Rsp5
E
Pil1-GFP
DIC
centre
top
min
max
F
Fur4-mNG
G
Fur4-mNG
eisosomes / cell
H
Fur4-GFP
+ vector
vac. GFP
GAPDH
Glucose
Raffinose (60 min)
Mup1-GFP
Raffinose (30 min)
I
Relative OD600
Time
hours
Wild-type
eis1Δ ura3Δ
pkh2Δ ura3Δ
nce102Δ ura3Δ
J
20 mg/L uracil
K
2 mg/L uracil
L
pkh2Δ ura3Δ
pkh2Δ Ura+
M
nce102Δ ura3Δ
nce102Δ Ura+

Figure 3. 7 Eisosomes are required for efficient recovery following glucose starvation.

A) Mid-log cultures of the indicated yeast strains were incubated in glucose (replete) or raffinose media for 2 h, before plating on YPD or SC plates for two days at 30°C. **B)** Colocalisation of Pil1–mCherry and Fur4–mNG, by Airyscan confocal microscopy focussed at the centre and top, in cells grown to mid-log phase before imaging in minimal medium. **C)** Growth of wild- type and *fur4Δ* cells grown in rich medium prior to serial dilution and growth on YPD and SC (minimal) solid media for 2 days at 30°C. **D)** Levels of Pil1–GFP expressed from a plasmid in the indicated strains were assessed by immunoblot of lysates generated from mid-log phase cells using anti-GFP antibodies, with anti-Rsp5 antibodies used as a loading control. **E)** Pil1–GFP localisation of transformants from D grown to log phase was recorded by confocal microscopy at centre- and top-focussed planes. Images on the right show cells coloured using a lookup table of GFP intensity. **F)** The indicated strains were transformed with a plasmid expressing Fur4–mNG from its endogenous promoter and imaged by confocal microscopy. Yellow arrows on centre-focussed images indicate pronounced eisosomal concentrations. **G)** The numbers of eisosomally localised Fur4–mNG puncta per cell were quantified from the indicated yeast strains. Mean ± s.d. **H)** Levels of Fur4–GFP sorted to the vacuole (left) and full-length Mup1–GFP (right) were assessed from indicated strains and conditions by anti-GFP immunoblotting, using GAPDH as a loading control. **I)** Indicated strains were grown to mid-log phase in SC complete medium before harvesting and growth in raffinose medium for two hours, before average recovery growth was assessed by OD_{600} measurements from cells incubated in SC medium. **(J–M)** Average recovery from assay described in I was quantified relative to the wild-type control and plotted over time for the indicated mutants at either 20 mg/l uracil **(J,L,M)** or 2 mg/l uracil **(K)**. Mean ± s.d. from three biological replicates. Black asterisks indicate Student's t-test comparisons with wild-type samples, red asterisks indicate comparisons between strains; *P<0.05. Scale bars: 5 μm.

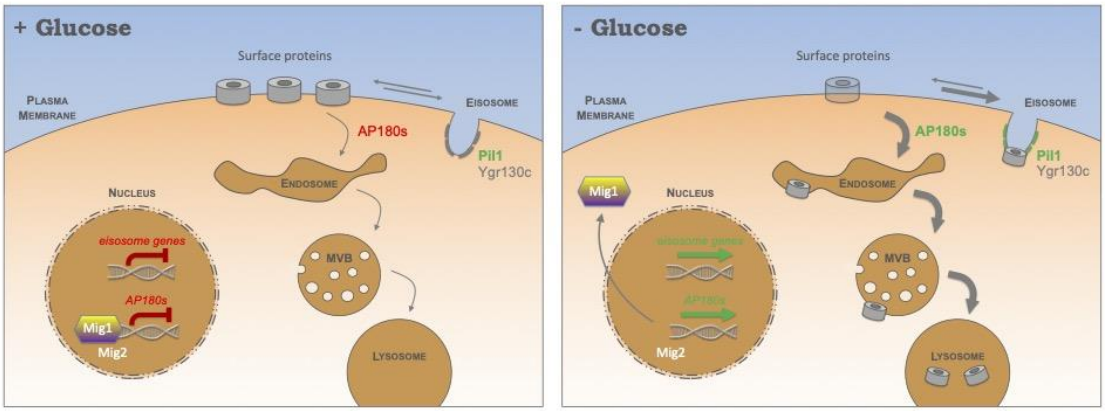

Figure 3. 8 Model for modes of surface protein regulation in response to glucose.

Schematic diagram shows the regulation of cell surface membrane protein cargoes in response to glucose starvation. When cells have access to glucose for maximal growth, internalisation occurs at a basal level through Mig1 (and Mig2) repression of endocytic adaptor genes YAP1801/YAP1802. Whilst resident at the surface, nutrient transporters diffuse in and out of eisosomes. The expression of many eisosome genes are repressed in glucose conditions (left). Following glucose starvation, Mig1 translocates from the nucleus, resulting in increased expression of YAP1801/YAP1802, which triggers increased cargo endocytosis and ubiquitin-mediated trafficking through the multivesicular body (MVB) pathway to the lysosome for degradation (right). Although most nutrient transporters are degraded following glucose starvation, a small reserve pool is sequestered in eisosomes, which are transcriptionally activated during starvation. Efficient cargo retention relies on Ygr130c, and eisosomes that specifically retain cargo during glucose starvation exhibit biochemical and biophysical changes in Pil1. This reserve pool of eisosomally retained nutrient transporters can be deployed upon a return to glucose-replete conditions for efficient recovery following the period of glucose starvation.

DISCUSSION

Yeast cells provided with appropriate carbon and ammonium can synthesise all amino acids for protein translation; however, amino acid biosynthesis and transporter-mediated uptake is coordinated with multiple metabolic programmes, including sugar utilisation (Ljungdahl and Daignan-Fornier, 2012).We find the replacement of glucose with raffinose, a suboptimal alternative carbon source, induces endocytosis and degradation of various surface proteins unrelated to sugar metabolism (e.g. amino acid transporters). We propose that a glucose-sensitive transcriptional response mediates surface cargo downregulation (**Fig. 3.8.**). In glucose-replete conditions, endocytosis is maintained at a basal level, in part through the transcriptional repression via Mig1 (and Mig2) of the clathrin adaptor genes *YAP1801* and *YAP1802*. When glucose is exchanged for raffinose, Mig1 translocates from the nucleus, resulting in elevated levels of cellular Yap1801 and Yap1802, which coincides with accelerated endocytosis (**Fig. 3.4**). Although AP180 adaptor null mutants exhibited only a modest effect in cargo endocytosis upon glucose depletion, their deletion in a *mig1Δmig2Δ* background supressed endocytosis. Our interpretation of this data is that AP180 adaptors are not essential for starvation-induced endocytosis, but their increased expression (by either glucose starvation, *MIG1 MIG2* deletion, or plasmid overexpression) triggers a cascade of events, likely involving much of the canonical endocytic machinery, that work collaboratively to package and internalise an array of surface proteins. In addition to lipid-binding domains, Yap1801 and Yap1802 associate with cortical clathrin (Newpher et al., 2005) and Pan1, which is required for endocytosis (Maldonado-Báez et al., 2008) and in turn activates Arp2/3-mediated actin assembly (Duncan et al., 2001; Wendland and Emr, 1998; Wendland et al., 1999). As the disordered domains of AP180 have been shown to amplify membrane curvature (Zeno et al., 2018), higher levels of these proteins are reasonable candidates for initiating a relatively broad downregulation of cargo following glucose replacement. This scenario best explains our observations that various cargoes are downregulated following increased levels of AP180 adaptors (in raffinose medium, in *mig1Δmig2Δ* cells and during plasmid-borne overexpression), as deletion of these adaptors, as with many other yeast endocytic factors, does not lead to a strong defect in endocytosis (Huang et al., 1999; Wendland and Emr, 1998) or only cargo-specific defects (Burston et al., 2009). We note that the increases in AP180 adaptor transcript levels in raffinose is relatively modest (up to 6-fold), which presumably can coordinate meaningful upregulation of clathrin-mediated endocytosis. This is in contrast to overexpression of AP180 (Ford et al., 2001) and its homologue CALM (Tebar et al., 1999) from plasmid-borne CMV promoter constructs in mammalian cells, which inhibits endocytosis; we presume this level of overexpression serves to sequester clathrin in a manner disruptive to multiple processes, including internalisation. The finding that FM4-64 internalises efficiently in raffinose (**Fig. 3.1.E**) but not in sugar-free medium (Lang et al., 2014) may be explained by (1) the lack of carbon source triggering shutdown of internalisation to protect ATP maintenance – a process not necessary in the presence of raffinose, which can be hydrolysed by invertase – or (2) changes in plasma membrane tension and/or osmotic pressure in medium lacking sugar triggering TORC2-mediated changes in lipid composition (Appadurai et al., 2019; Riggi et al., 2018) that affect FM4-64 binding. The finding that elevated endocytosis downregulates surface proteins conceptually aligns with a starvation model wherein existing resources are degraded to supply essential processes whilst non-essential processes are turned off. Increasing endosomal residency of surface proteins will enhance cargo ubiquitylation at late

endosomes, which is sufficient to trigger ESCRT recruitment, luminal vesicle formation and subsequent cargo sorting through the MVB pathway (MacDonald et al., 2012a). Endosomal cargo ubiquitylation is largely mediated by the E3 ubiquitin ligase Rsp5 in complex with cargo-specific adaptors, some of which are also regulated in response to glucose via adenosine monophosphate-activated protein kinase (AMPK) (O'Donnell and Schmidt, 2019). As certain Rsp5 adaptors, such as Rod1, Sna3 and Hua1, have been proposed to function later in the endocytic pathway, downstream of internalisation (Hovsepian et al., 2018; MacDonald et al., 2020; MacDonald et al., 2012c) these adaptors may be more important for downregulation when glucose is replaced with an alternative carbon source.

One initially contrary finding is that eisosomes, which antagonise endocytosis (Gournas et al., 2018; Grossmann et al., 2008; Moharir et al., 2018; Spira et al., 2012), contain many factors that are transcriptionally upregulated in raffinose (**Fig. 3.5.B,N**), suggesting that surface cargoes are controlled within subdomains of the plasma membrane. This finding can be rationalised by recent models that propose cargo protection in response to nutritional stress retains surface proteins for later use (Gournas et al., 2018; Moharir et al., 2018). Similarly, although our data shows that surface proteins are largely endocytosed and degraded in response to raffinose, there is a small population, for example Mup1–GFP (**Fig. 3.5.E**), that are retained and concentrated within eisosomes in these conditions. Increased Pil1 intensity following raffinose exchange, in addition to our 4D confocal microscopy capturing structural rearrangements of Pil1–mCherry at eisosomes that most significantly trap Mup1–GFP (Movie 5), suggests significant conformational changes occur in response to raffinose,with eisosomes increasing in size and possibly deepening to better sequester cargo. This also explains the initially confounding result that the diffusion coefficients from our single molecule analysis of Pil1–mCherry increased upon raffinose treatment (**Fig. S3.5.K**). Although the increase in Pil1 proteins levels was a modest ~29% increase, we note Pil1 is abundant, with different techniques providing estimates of 1.1×10^5–2.7×10^5 molecules per cell (Ghaemmaghami et al., 2003; Lahtvee et al., 2017; Tkach et al., 2012), suggesting that subtle changes could supply the cell with significant Pil1 at these cargo-capturing eisosomes. These subtle changes in Pil1 levels and molecular stoichiometry are accompanied by cellular Pil1 molecules undergoing rapid dephosphorylation during this period of starvation (**Fig. 3.5.C**), which in combination may modify eisosomes to better retain cargo following glucose starvation. Although single-cell stoichiometry estimates for Pil1showed an increase upon raffinose treatment, the single-eisosome analysis revealed that the most significant changes occurred at eisosomes that retain cargo. Notably, nitrogen starvation and the broad nutritional stress of incubating cells for 12 h after they reach stationary phase, following complete exhaustion of nutrients, results in an increase in eisosomal numbers (Gournas et al., 2018). Unlike this severe starvation condition, our study reveals that glucose starvation specifically triggers an acute response (<2 h) that modulates Pil1 at the transcriptional, biochemical and biophysical level to effect cargo retention during this initial starvation period. This suggests cargo retention is tuneable to nutrient availability and specific starvation conditions may trigger specific retention responses, for example a preference for specific cargoes. As removal of carbon source results in a decrease in Nce102 at eisosomes (Appadurai et al., 2019), we predict that raffinose treatment, which increases transcript levels of *NCE102* around 6-fold, triggers a distinct response to specifically upregulate eisosomes to retain nutrient transporters during the metabolic challenge of suboptimal sugars. A central finding of our study is that the sequestration of amino acid transporters provides a physiological benefit to cells during changes in sugar availability, by protecting a reservoir of nutrient

transporters during glucose limited conditions. Upon a return to more favourable nutritional conditions, wild-type cells grow better than mutants that fail to properly sequester cargo in eisosomes (**Fig. 3.7.**). In particular, Fur4-mediated uracil uptake is important for recovery, which might be explained by its apparent high affinity (**Fig. 3.7.C**) and the fact that strains used in this study, and in many lab settings, are uracil auxotrophs (Brachmann et al., 1998; Pronk, 2002). Our results imply that the cell senses acute starvation broadly or the transporters that diffuse within eisosomes are retained indiscriminately of their potential to uptake specific nutrients. We also assign a function for the Mup1-binding eisosomal protein Ygr130c for the first time (**Fig. 3.6.**), as an eisosomal anchor for Mup1 and possibly other nutrient transporters thought to diffuse within eisosomes (Babst, 2019). Although *ygr130cΔ* cells do not exhibit an obvious increase in nutrient transporter endocytosis, their diffusion within eisosomes is greatly reduced. It would be intriguing if future work assessed potential structural changes of eisosomes in these mutants. Our bioinformatics analysis suggests that many other nutrient transporters may also use Ygr130c to efficiently sequester in eisosomes (**Fig. 3.6.G**) and may function with Fur4 to achieve full recovery from starvation (**Fig. 3.7.**). The finding that *YAP1801* and *YAP1802* are regulated in response to glucose via Mig1 and Mig2 shows that membrane trafficking factors are modulated to adapt to changes in sugar availability. We did note that the levels of *YAP1801* and *YAP1802* were elevated more when cells were acutely shifted to raffinose than when wildtype cells were compared with *mig1Δ mig2Δ* mutants. This might be explained by additional transcriptional regulators contributing to the glucose starvation response, or by *mig1Δ mig2Δ* mutants having acquired additional mutations to compensate for the systemic loss of Mig1 and Mig2. As gene deletions are often associated with secondary mutations, many of which affect stress responses (Teng et al., 2013), this latter idea is reasonable for *mig1Δ* cells, which are defective in various processes (Santangelo, 2006). The reduced effect in *mig1Δ mig2Δ* cells compared with raffinose (2.8±1.0-fold, mean±s.d. calculated from the three examples we have uncovered) might explain an undetectable response (theoretical=0.8±0.1; experimental =0.9±0.2) in *PIL1* transcript levels in *mig1Δ mig2Δ* cells (**Fig. 3.5.B**). Alternatively, as glucose starvation induces expression of many eisosomal factors (**Fig. 3.5.N**), such as *NCE102*, *PKH2, SLM1, LSP1, EIS1* and *SEG1,* that were not predicted to be transcriptionally repressed by Mig1/Mig2, *PIL1* may also be a Mig1-independent gene target regulated in response to glucose levels. This transcriptional response, alongside the induction of the AP180 clathrin adaptors described above, allows for acute metabolic control in response to fluctuating nutrient conditions. Many elements of this control involve proteins conserved throughout evolution, so we propose that similar regulation of these pathways and membrane subdomains in other eukaryotes could maintain metabolism in response to changes in extracellular nutrients.

METHODS

Reagents

Yeast strains and plasmids are listed in Table S4 and Table S5, respectively. The *mig1Δ mig2Δ* and *mig1Δ mig2Δ mig3Δ* yeast strains were a generous gift from Hans Ronne. Fluorescently labelled Vps4 strains were a gift from David Teis. Polyclonal antibodies raised against GFP (Urbanowski and Piper, 1999) and Rsp5 (Stamenova et al., 2004), and monoclonal glyceraldehyde 3-phosphate dehydrogenase (GAPDH; clone 6C5; Ambion) and carboxypeptidase Y (CPY; clone 10A5-B5; Molecular Probes) antibodies, were used for immunoblot analysis. These antibodies were routinely used at 1:1000 dilution.

Cell culture

Yeast were grown in rich yeast extract peptone dextrose (YPD) medium (2% glucose, 2% peptone, 1% yeast extract) or synthetic complete (SC) minimal medium (2% glucose, yeast nitrogen base supplemented with appropriate amino acid and base dropout mixtures; Formedium, Norfolk, UK) for maintaining of plasmids. Cells were routinely grown overnight to early/midlog phase (OD600≤1.0) prior to experimental procedures, unless otherwise stated. To minimise nutritional challenges prior to starvation experiments, very low density cultures (OD600=0.1) were adhered to concavalin A-treated coverslips for time-lapse microscopy. For glucose-starvation experiments, rich and minimal media were supplemented with 2% raffinose instead of glucose, but were otherwise identical. Geneticin (Formedium), used at a concentration of 250 µg/ml in rich media, and methotrexate (Alfa Aesar), used at a working concentration of 20 mM, were prepared in SC minimal medium as described previously (MacDonald et al., 2015a). Expression of proteins from the CUP1 promoter was achieved by addition of 50–100 µM CuCl2 to the medium for at least 1 h prior to downstream analysis.

Confocal microscopy

Cells were grown to mid-log phase and prepared for fluorescence microscopy experiments by concentration in minimal medium before imaging or from a slide or glass-bottom dish using laser scanning confocal microscopes (LSM710 or LSM880 equipped with an Airyscan module; Zeiss) with a 63x Differential Interference Contrast (DIC) objective with a 1.4 numerical aperture. Argon laser excitation, 488 nm with emission filter set to 495 – 550 nm (for GFP, mGFP and mNeonGreen) and 561 nm with 570 – 620 nm emission filter (for mCherry and FM4-64) was used.

Microfluidics and time lapse microscopy

Cells were grown to early log phase (approximately OD_{600} = 0.2) overnight and then adhered to 35 mm concavalin A coated glass bottom dishes (Ibidi GmbH, Germany) prior to live cell imaging at room temperature. Plates were prepared by adding 1 mg/mL concavalin A in water to a coverslip for 5 minutes prior to several wash steps; plates were routinely stored at 4^{o}C. Sterile media exchanges were performed using syringes through tubing fused to the lid of 35 mm dishes. Live cells were labelled with 0.8 µM FM4-64 using microfluidics for 2 - 5 minutes before flushing with medium containing 2.4 µM 4-sulfonato calix[8]arene, sodium salt, SCAS (Biotium, Hayward, CA) for 30 seconds at room temperature to quench extracellular dye before further imaging.

Image analysis

Micrographs were processed usZeiss Zen and Fiji software. For time lapse movies bleach correction was carried out using a histogram matching method (https://imagej.net/Bleach_Correction). For images of the top section of a yeast cell, five slices with 0.18µm spacing were combined using the average intensity of the maximum intensity z-projection. Movies were made using time lapse image, of varying frame time points, as indicated in the movies. Numbers of eisosomes were identified using tracking software written in MATLAB and reported previously (Miller et al., 2015b; Wollman and Leake, 2015; Wollman et al., 2017).

Slimfield microscopy and fluorescent foci analysis

Slimfield excitation was implemented via co-aligned 488 nm and 561 nm wavelength 50 mW lasers (OBIS, Coherent) de-expanded to direct a beam onto the sample full width at half maximum of ~30µm. For visualisation of both fluorophores we employed rapid Alternating Laser Excitation (ALEX) with 5 ms exposure time per image frame for each laser (Syeda et al., 2019). Fluorescence emission was captured by a 1.49 NA oil immersion objective lens (Nikon), and subsequently split into separate green and red detection channels using a dual-pass green/red dichroic mirror centred at long-pass wavelength 560nm combined with 25 nm bandwidth emission filters (Chroma) centred on 525 nm and 594 nm wavelengths. Each channel was imaged separately at 5 ms exposure time by an EMCCD camera Prime 95B^{TM} Scientific CMOS, Teledyne Photometrics) using 50 nm/pixel magnification. The focal plane was set to mid-cell height using the bright field appearance of cells. As photobleaching of mGFP and mCherry proceeded during Slimfield excitation distinct fluorescent foci could be observed of width 250-300 nm, consistent with the diffraction-limited point spread function of our microscope system, which were tracked and characterized in terms of their stoichiometry and apparent microscopic diffusion coefficient. Distinct fluorescent foci that were detected within the microscope's depth of field could be tracked for up to several hundred ms, to a super-resolution lateral precision σ = 40 nm using a bespoke single particle tracking algorithm. The molecular stoichiometry for each track was determined by dividing the summed pixel intensity values associated with the initial unbleached brightness of each foci by the brightness corresponding to that calculated for a single fluorescent protein molecule (either mGFP for 488 nm wavelength excitation or mCherry for 561 nm wavelength excitation) measured using a step-wise photobleaching technique described previously (Shashkova et al., 2018; Wollman et al., 2017). The apparent microscopic diffusion coefficient, D was determined for each track by calculating the initial gradient of the relationship between the mean square displacement with respect to tracking time interval using the first five time intervals values while constraining the linear fit to pass through $4\sigma^2$ on the vertical axis corresponding to a time interval value of zero***.*** Cell body and membrane boundaries were detected based on the mCherry fluorescence images, considering the membrane width as 7nm.

Gene expression (qPCR) analysis

Yeast cultures (10 ml) were grown overnight to mid-log phase in YPD or exchanged with YPR (YPD containing 2% raffinose in place of glucose) for the indicated times prior to spheroplasting in yeast lysis buffer (1 M sorbitol 100 mM EDTA, 0.1% β-mercaptoethanol) with 5µl zymolase added for 2 minutes at room temperature. For reverse transcription-qPCR (RT-qPCR), extraction of total RNA media was performed using an RNeasy kit (QIAGEN) protocol with an additional DNaseI treatment, followed by a second DNaseI digestion with the TURBO DNA-free kit (Invirogen). Extracted mRNA was then used for cDNA synthesis with the SuperScript IV reverse transcriptase

(Invitrogen). 50ng/µl random hexamers, and 10mM dNTPs were added to 5µg RNA. Samples were incubated at 65°C for 5 minutes before addition of 100mM DTT, ribonuclease inhibitor and the Superscript IV reverse transcriptase to initiate the reaction (10 min at 23°C; 10 min at 55°C; 10 min at 80°C), and then was used immediately for the qPCR reaction. For qPCR optimisation, two sets of primers targeting amplicons 70–170 bp in length were designed for each gene of interest, and the best performing were chosen for use in quantitation (Tables S6,S7). Single product amplification was confirmed through PCR using genomic DNA, and near-100% amplification efficiencies were confirmed through qPCR on a standard curve of known input quantity, all performed in duplicate reactions (examples shown in Fig. S2). All qPCR reactions were performed on 20 ng cDNA, or relevant negative controls, in 20 µl reactions containing 350 nM forward and reverse primers and 10 µl Fast SYBR Green mastermix (Thermo Fisher Scientific). Reactions were carried out using the QuantStudio 3 system (Thermofisher) under the following conditions: 40 cycles of 95°C for 1 s and 60°C for 20 s before a continuous ramp from 60°C to 95°C at a rate of 0.1°C/s for melt-curve analysis. Gene expression levels were quantified using the comparative Ct (ΔΔCt) method, relative to the expression of the housekeeping gene (*ACT1* or *HEM2*) and were normalised to the control sample (i.e. wild type when testing mutant strains;glucose when assessing effects of raffinose timecourse). To avoid bias caused by averaging data that had been transformed through the equation 2^{-Ct} to give fold changes in gene expression, all statistics were performed on Ct values.

Immunoblotting

Equivalent amounts of cells were harvested from early and late log phase (OD_{600} = 0.5 and 2.0, respectively) yeast cultures. Lysates were generated by alkali treatment with 0.2 M NaOH for 3 minutes prior to resuspension in lysis buffer (8 M Urea, 10% glycerol, 50mM Tris.HCl pH 6.8, 5% SDS, 0.1% bromophenol blue and 10% 2-Mercaptoethanol). Proteins were resolved by SDS-PAGE prior to transfer to a nitrocellulose membrane using the iBlot 2 dry transfer system (ThermoFisher Scientific). Membrane was probed with appropriate antibodies and visualised using enhanced chemiluminescence (ECL) super signal Pico Plus (ThermoFisher Scientific), with intensity digitally captured using a ChemiDoc Imager (BioRad).

Flow cytometry

Intensity from GFP expressing (excitation laser 488 nm, emission filter (525 / 40 nm) and FM4-64 labelled (561 nm excitation laser, 710 / 50 nm emission filter) labelled live cells at room temperature was recorded using a CytoFLEX flow cytometer (Beckman Coulter) and intensity measurements from gated cells measured with FCS Express v6.0 (DeNovo software). Typically, 100,000 cells, gated for fluorescence positive yeast cells (using forward/side scatter), were flowed at ~600 V to maintain a rate of approximately 500 – 1000 cells measured per second. Unlabelled / non-expressing cells were used for background calibration. Channel recordings from other detectors (e.g. 530 / 50 nm) were also recorded to measure background autofluorescence. Intensity measurements are plotted. The co-efficient of variation (CV) equal to the population standard deviation divided by the population mean is expressed as a percentage.

Yeast growth and recovery assays

Yeast cultures were grown overnight in glucose containing YPD or SC media diluted to OD_{600} = 0.4 and used to create a 10-fold serial dilutions in a sterile 96-well plate, which were then plated on the indicated media and grown for 2 days at 30°C before growth

was recorded using a Phenobooth Imager (Singer Instruments). For recovery-based assays, cells were exchanged to raffinose media for 2 hours prior to equivalent cell numbers being harvested and either plated on the indicated solid media or brought up in glucose containing minimal media containing various concentrations of uracil and OD_{600} measurements were recorded every 60 minutes using a MultiSkanGo plate reader and SkanIt software (ThermoFisher Scientific).

Statistical analyses

The statistical significance for each experimental condition (e.g. raffinose media, mutant yeast strains) in comparison to control conditions (e.g. glucose media, wild-type cells) was calculated using unpaired t-test / Holm-Sidak method in GraphPad Prism v8.3.1. An asterisk (*) is used in graphs to denote p-values of <0.05 or less, as indicated in figure legends, in graphs and all generated p-values for each experiment are included in Supplemental Table S5.

ACKNOWLEDGMENTS

We are grateful to the York Bioscience Technology Facility, including Peter O'Toole and the imaging team for technical assistance, Karen Hogg for help with flow cytometry, and Sally James for guidance with gene expression analysis. We would like to thank Hans Ronne for the generous gift of *mig1*Δ *mig2*Δ and *mig1*Δ *mig2*Δ *mig3*Δ yeast strains, which were used for initial work and to David Teis for fluorescently labelled Vps4 strains. We are grateful to Chris Burd for suggestions based on an earlier version of this story and Nia Bryant for helpful comments on the manuscript. This research was supported by a Sir Henry Dale Research Fellowship from the Wellcome Trust and the Royal Society 204636/Z/16/Z (CM), and EPSRC EP/T002166/1 (ML), BBSRC BB/R001235/1 (ML), Marie Curie EU FP7 ITN Ref 764591 (ML), and the Leverhulme Trust RPG-2019-156/ RPG-2017-340 (ML).

Funding

This research was supported by a Sir Henry Dale Research Fellowship from the Wellcome Trust and the Royal Society 204636/Z/16/Z (C.M.), and by the Engineering and Physical Sciences Research Council (EP/T002166/1 to M.L.), Biotechnology and Biological Sciences Research Council (BB/R001235/1 to M.L.), FP7 People: Marie-Curie Actions (ITN Ref. 764591 to M.L.) and Leverhulme Trust (RPG-2019-156/RPG-2017-340 to M.L.). Open access funding provided by the University of York. Deposited in PMC for immediate release.

DECLARATION OF INTERESTS

The authors declare no competing interests.

3.3. Supplemental material

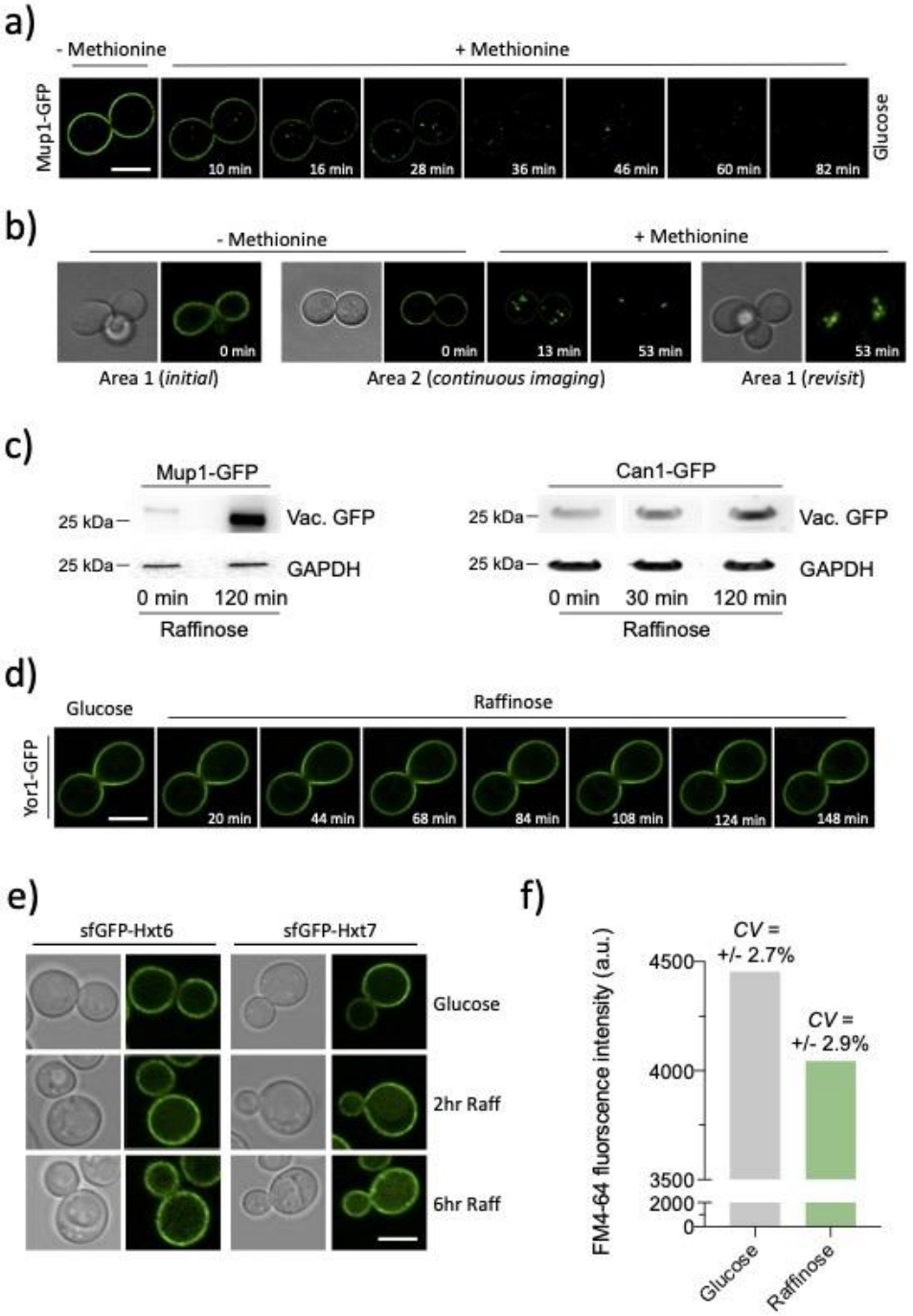

Supplemental Figure 3.1 Differential cargo trafficking effects following glucose starvation.

a) Wild-type cells expressing Mup1-GFP were grown to mid-log phase in SC media lacking methionine, processed for time-lapse microscopy and then imaged every 2 minutes following addition of 20 µg/ml methionine. **b)** Vacuolar GFP bleaching in wild-type cells expressing Mup1-GFP grown to mid-log phase in SC media lacking methionine and processed for time-lapse microscopy. Area 1 was imaged before addition of methionine, before moving to a distinct region of the same plate (Area 2) for continuous imagining from 0 – 53 minutes of methionine addition. Following this period, Area1 was re-visited and imaged to show the difference in photobleaching of vacuolar sorted Mup1-GFP. **c)** Levels of vacuolar processed GFP from cargo (Mup1-GFP, left and Can1-GFP, right) expressing cells were assessed in glucose and raffinose treated cells by immunoblotting lysates with GFP antibodies. Loading was assessed with anti-GAPDH antibodies. **d)** Wild-type cells expressing Yor1-GFP from the CUP1 promoter by addition of 50µM copper chloride were grown to mid-log phase in glucose containing media, processed for time-lapse microscope and imaged for indicated time course after exchange with raffinose media. **e)** Strains expressing GFP tagged Hxt6 and Hxt7 expressed from the NOP1 promoter were grown in glucose or raffinose media for indicated periods prior to fluorescence microscopy. **f)** Wild-type cells grown either in glucose media or exchanged with raffinose for 15 minutes were incubated with YPD containing 40 µM FM4-64 dye for 4 minutes at room temperature before ice cold washes were performed with minimal media to remove excess dye. Mean fluorescence of ~10,000 cells was then measured by flow cytometry, plotted with coeffecint of variation (cv) indicated. Scale bar, 5 µM.

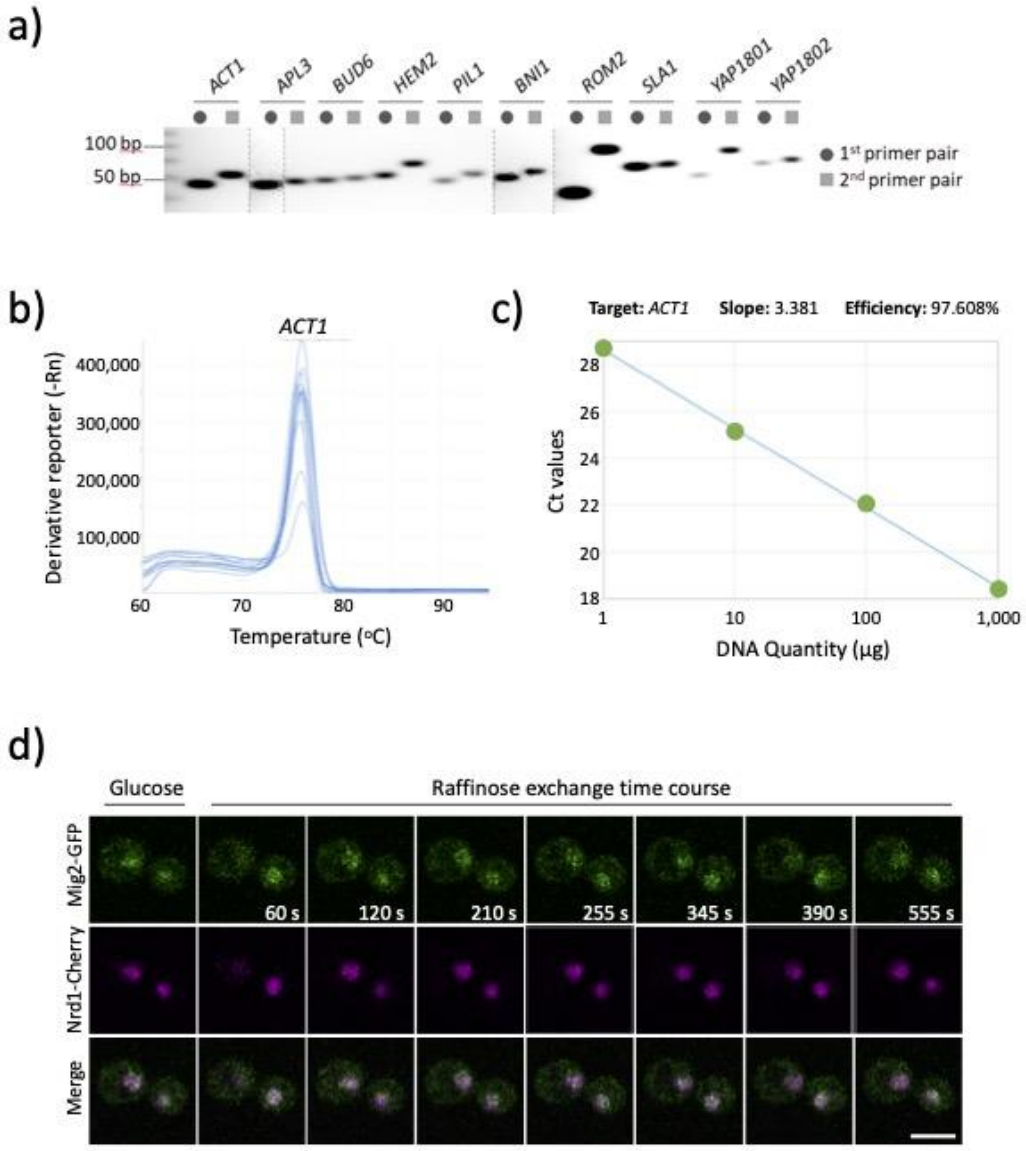

Supplemental Figure 3.2 qPCR optimisation and time-lapse microscopy of Mig2-GFP:

a) Indicated oligo pairs were used to generate PCR products from a gDNA template and analysed by agarose gel of primer pair validation of the qPCR using wild-type cells mRNA. **b)** Melt curve analyses for all qPCR primer pairs were carried out to ensure no primer dimer species were detected, read out shows example for ACT1. **c)** Primer pair efficiency was also performed for all primer pairs used in this study (shown for ACT1), with ΔCt values across a 10-fold serial dilution plotted (slope = -3.33 equivalent to 100% efficiency). Data for all primer pair analysis is recorded in Supplemental Table S2. **d)** Wild-type cells expressing Mig2-GFP and Nrd1-mCherry were grown to mid log phase in minimal media prior to processed for time-lapse microscopy. Images were captured every 5 seconds following raffinose exchange, with representative time-slices shown. Scale bar, 5 µM.

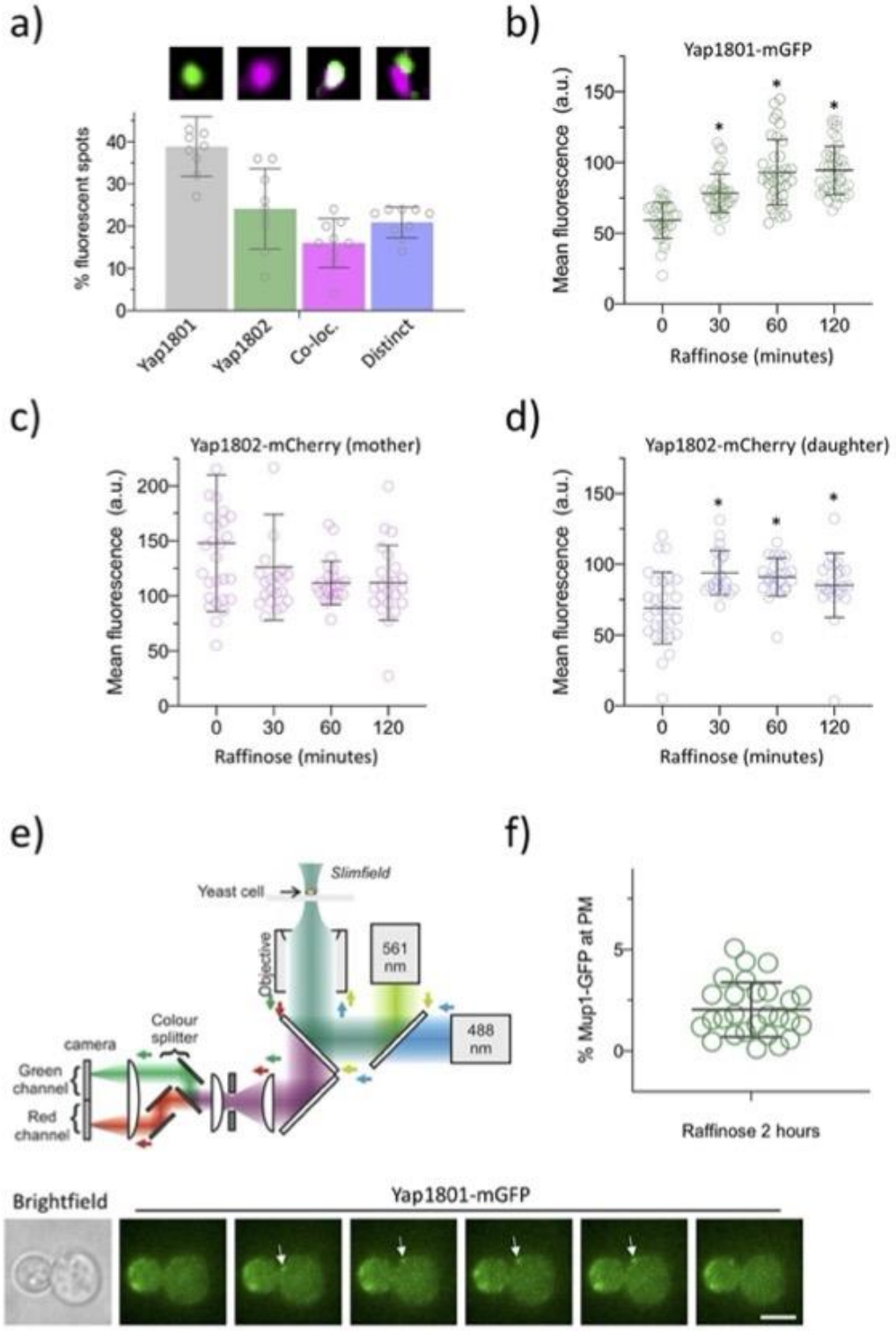
a)
% fluorescent spots
Yap1801
Yap1802
Co-loc.
Distinct
b)
Yap1801-mGFP
Mean fluorescence (a.u.)
Raffinose (minutes)
c)
Yap1802-mCherry (mother)
Mean fluorescence (a.u.)
Raffinose (minutes)
d)
Yap1802-mCherry (daughter)
Mean fluorescence (a.u.)
Raffinose (minutes)
e)
Yeast cell
Slimfield
Objective
561 nm
488 nm
Colour splitter
camera
Green channel
Red channel
f)
% Mup1-GFP at PM
Raffinose 2 hours
Brightfield
Yap1801-mGFP

Supplemental Figure 3.3 Localisation of Yap1801 and Yap1802:

a) Histogram showing the co-localisation analysis of Airyscan confocal images of Yap1801-mGFP and Yap1802-mCherry expressing wild-type cells grown to mid-log phase in SC selective media. Error bars showing standard deviation (n = 235 foci analysed). Examples of each localisation category is shown (upper). **b-d)** Histograms showing mean fluorscence from confocal images cells grown in indicated media condtions whlst expressing **b)** Yap1801-mGFP (total cell), **c)** Yap1802-mCherry (just mother cell), **d)** Yap1802-mCherry (just daughter cell). Intensity was averaged from n=>36 cells per condition over 3 biological replicates, with error bars showing standard deviation. **e)** Slimfield microscopy, schematic diagram showing set-up for dual-colour imaging of yeast cells. Lower panels show Yap1801-mGFP fluorescent spot (white arrow) tracking from images acquired every 5ms. **f)** Percentage plasma membrane localised Mup1-GFP was caculated from cells grown in raffinose for two hours. * indicates Student t-test p-values <0.05. Scale bar, 5 µM.

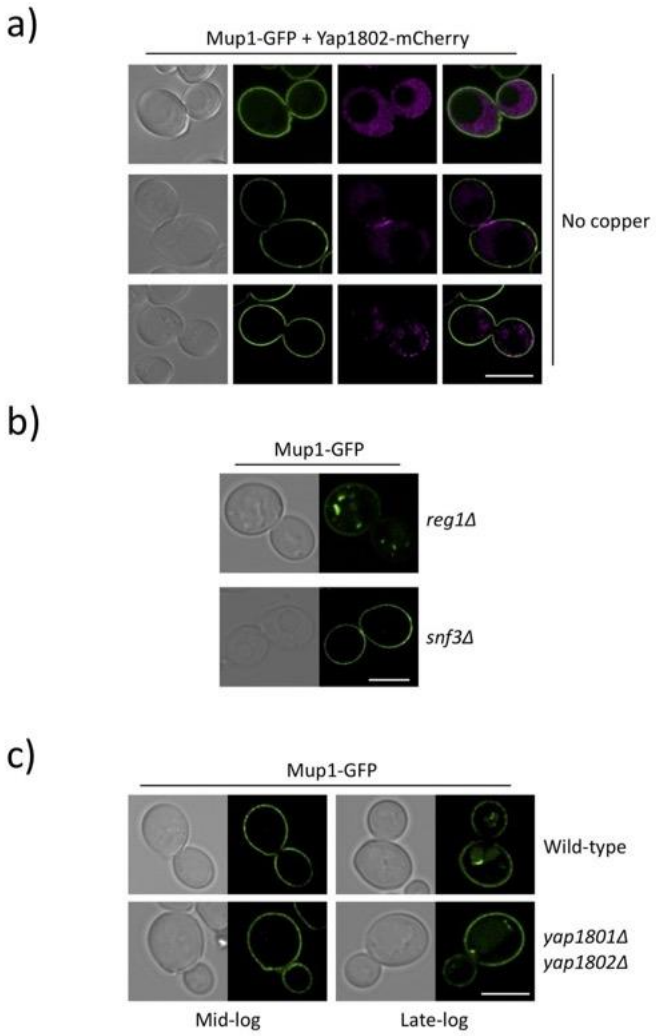

Supplemental Figure 3.4 Functional relationship between Mup1-GFP trafficking and yeast AP180s:

a) Representative examples of different Yap1802-mCherry localisations are shown from expression under the CUP1 promoter with no additional copper added to the media, in cells co-expressing Mup1-GFP. **b)** Indicated mutant null strains expression Mup1-GFP were imaged by confocal microscopy. **c)** Mup1-GFP localisation was imaged in wild-type and *yap1801*Δ *yap1802*Δ cells grown to mid-log (OD_{600} = 1.0) and late-log (OD_{600} = 2.0) phase.

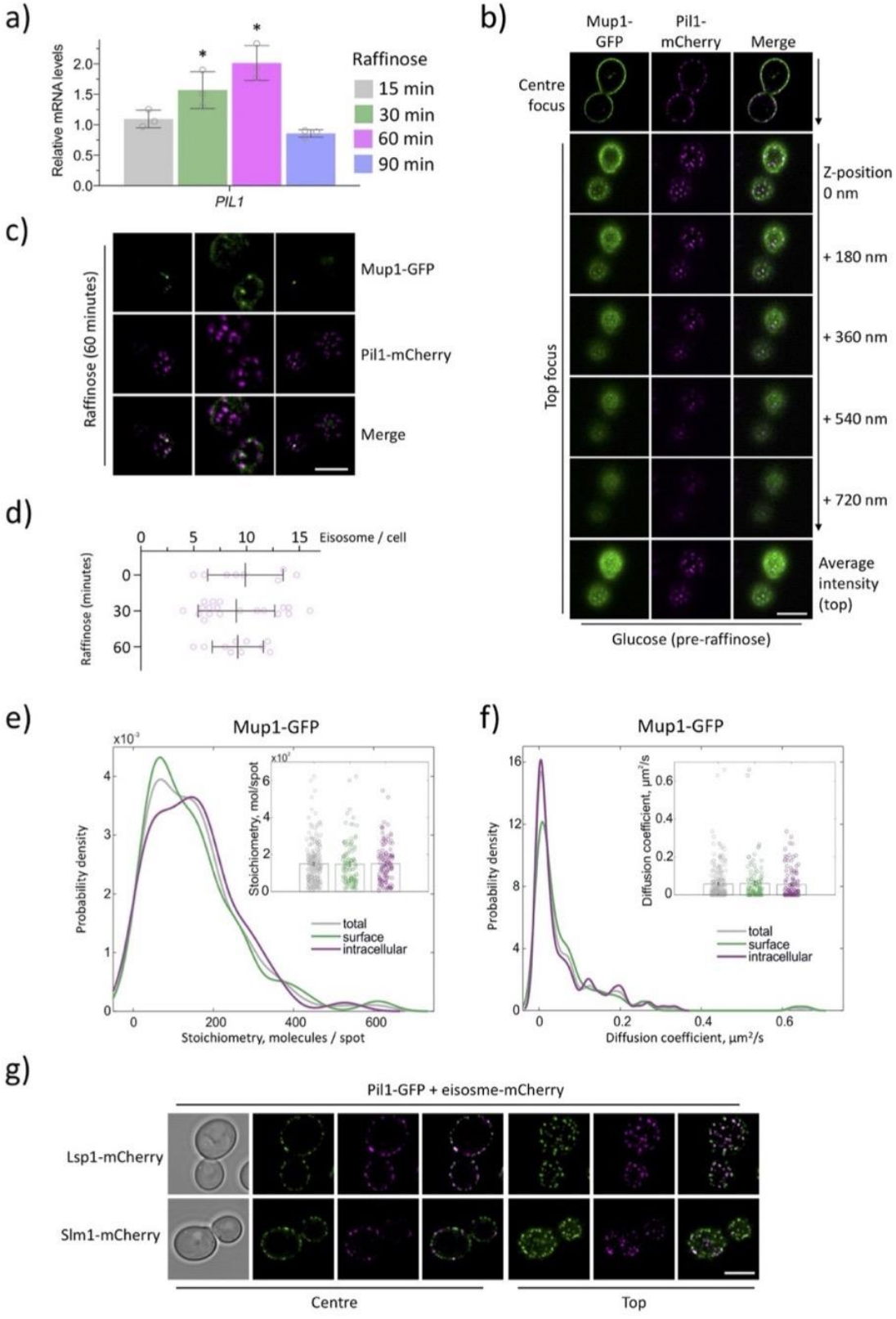
a)
Relative mRNA levels
2.0
1.5
1.0
0.5
0.0
*
*
PIL1
Raffinose
15 min
30 min
60 min
90 min
b)
Mup1-GFP
Pil1-mCherry
Merge
Centre focus
Top focus
Z-position 0 nm
+ 180 nm
+ 360 nm
+ 540 nm
+ 720 nm
Average intensity (top)
Glucose (pre-raffinose)
c)
Raffinose (60 minutes)
Mup1-GFP
Pil1-mCherry
Merge
d)
0 5 10 15 Eisosome / cell
Raffinose (minutes)
0
30
60
e)
Mup1-GFP
x10⁻³
Probability density
Stoichiometry, molecules / spot
Stoichiometry, mol/spot
total
surface
intracellular
f)
Mup1-GFP
Probability density
Diffusion coefficient, µm²/s
total
surface
intracellular
g)
Pil1-GFP + eisosme-mCherry
Lsp1-mCherry
Slm1-mCherry
Centre
Top

Supplemental Figure 3.5 Analyses of eisosomes in response to changes in glucose levels:

a) Quantitative RT-PCR of PIL1 performed from RNA extracted from wild-type cells grown in glucose media and relative levels compared to cells grown in raffinose media for indicated time course. Error bars show the standard deviation from 3 biological replicates (each averaged from 3 technical replicates). **b)** Wild-type cells expressing Pil1-mCherry and Mup1-GFP were grown to mid-log phase in SC media and prepared for confocal imaging. Cells were focussed to the top of the cell and imaged at 0.18µm intervals in the z-axis. An average intensity projection from the indicated 5 slices is shown (lower panel). **c)** Top focus 3D confocal imaging of cells expressing Mup1-GFP and Pil1-mCherry after 60 minutes raffinose starvation. **d)** Number of Pil1-mCherry marked eisosomes per cell in glucose, 30-minutes or 60-minutes raffinose and depicted with standard deviation error bars. **e)** Kernel density plots of Mup1-GFP stoichiometry distribution of fluorescent foci in the whole cell (grey), on the surface (green) or inside the cell (purple). Inserts: jitter plots of stoichiometries of fluorescent foci detected in the whole cell, on the surface or inside the cell. Error bars represent standard error. **f)** Kernel density plots of Mup1-GFP diffusion coefficients, using same labelling as **(e)** for total, surface and intracellular signal. **g)** Cells co-expressing Pil1-GFP with either Lsp1-mCherry (upper) or Slm1-mCherry (lower) were imaged at centre and top focus by confocal microscopy. * indicates Student t-test p-values <0.05. Scale bar, 5 µm

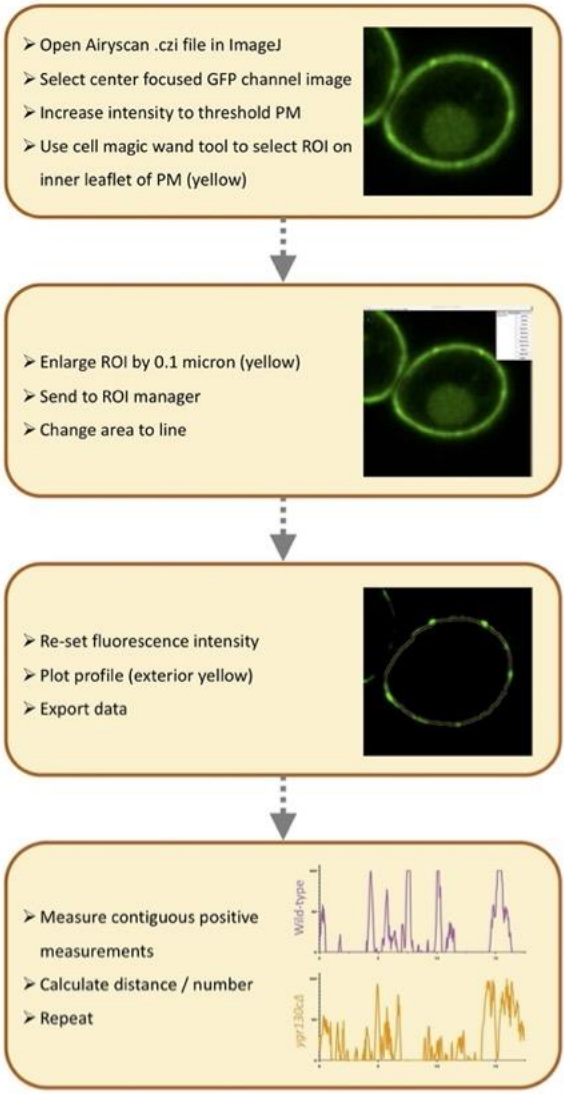

Supplemental Figure 3.6 Analyses of eisosomes in response to changes in glucose levels:

Workflow for systematic image processing used to measure the length of contiguous GFP signal at the plasma membrane in wild-type and *ygr130c*∆ yeast cells expressing Mup1-GFP.

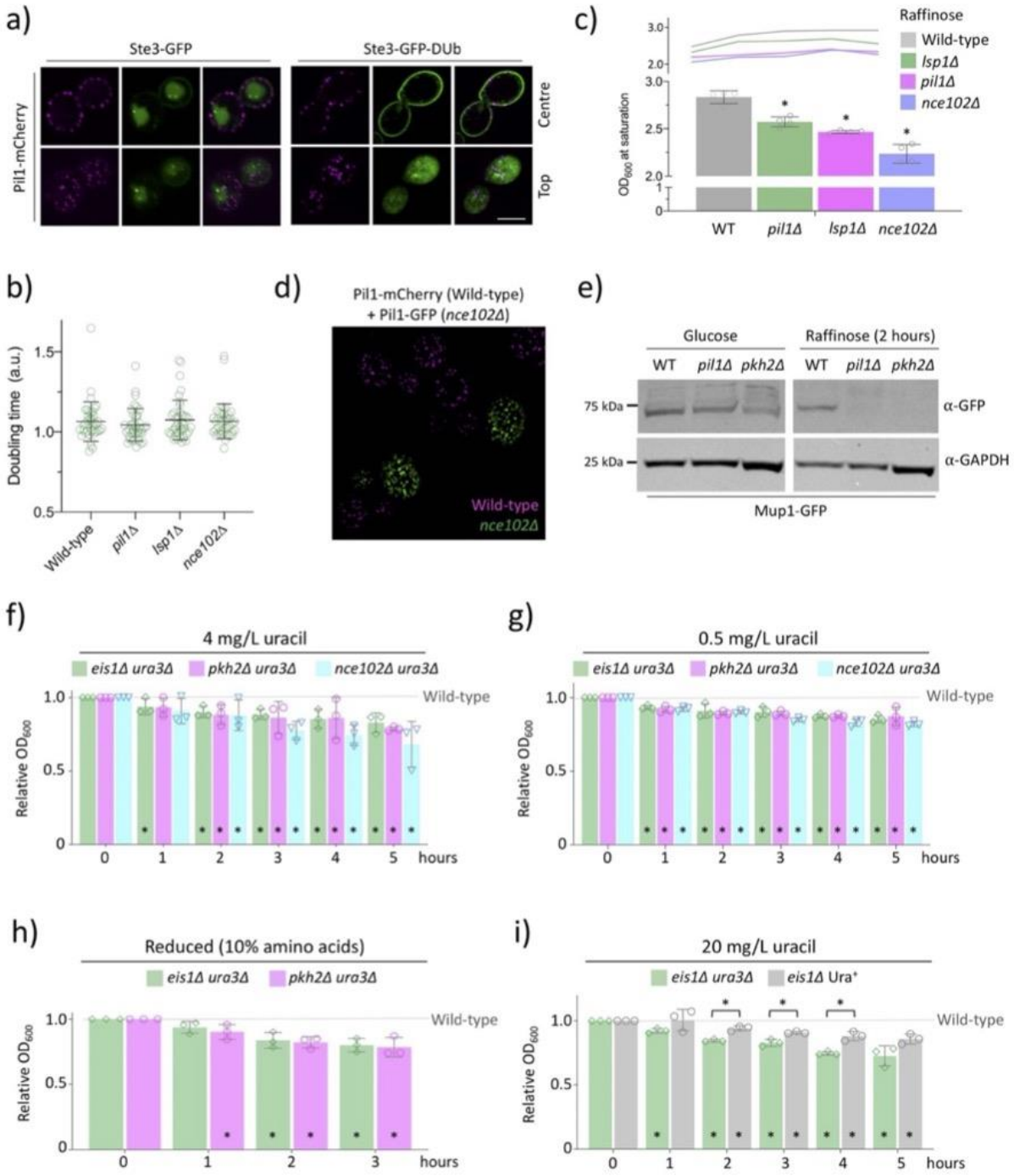
a)
Ste3-GFP
Ste3-GFP-DUb
Pil1-mCherry
Centre
Top
c)
Raffinose
Wild-type
lsp1Δ
pil1Δ
nce102Δ
OD600 at saturation
WT
pil1Δ
lsp1Δ
nce102Δ
b)
Doubling time (a.u.)
Wild-type
pil1Δ
lsp1Δ
nce102Δ
d)
Pil1-mCherry (Wild-type)
+ Pil1-GFP (nce102Δ)
Wild-type
nce102Δ
e)
Glucose
Raffinose (2 hours)
WT
pil1Δ
pkh2Δ
75 kDa
25 kDa
α-GFP
α-GAPDH
Mup1-GFP
f)
4 mg/L uracil
eis1Δ ura3Δ
pkh2Δ ura3Δ
nce102Δ ura3Δ
Wild-type
Relative OD600
hours
g)
0.5 mg/L uracil
h)
Reduced (10% amino acids)
i)
20 mg/L uracil
eis1Δ Ura+

Supplemental Figure 3.7 The role of eisosomes in cargo specific retention following starvation.

a) Wild-type cells co-expressing Pil1-mCherry and either Ste3-GFP (left) or Ste3-GFP-DUb (right) were imaged by 3D confocal Airyscan microscopy. **b)** Indicated strains were grown to mid-log phase overnight and allowed to reach saturation, with OD_{600} measurements captured every hour, depicted as a line graph (upper), or the maximum OD_{600} shown as a histogram (lower). **c)** Triplicate cultures were grown to mid-log phase overnight, diluted to low optical density and then grown in 5ml cultures. Samples were taken for OD_{600} measurements every hour over 8 – 10 hours and used to calculate average doubling times, with distribution displayed in scatter plot. **d)** Wild-type cells expressing Pil1-mCherry were co-cultured with *nce102*Δ cells expressing Pil1-GFP before Airyscan microscopy and merging colour channels. **e)** Indicated strains expressing Mup1-GFP were grown in either glucose (left) or 2 hours raffinose (right) media before denatured lysates generated and analysed by SDS-PAGE and immunoblot with antibodies against GFP and GAPDH. **f -i)** Indicated strains were grown to mid-log phase before incubation in raffinose media for two hours. Cells were then resuspended in SC media containing glucose and 4 mg/L Uracil **(f),** 0.5 mg/L Uracil, **(h)** SC-media supplemented with only 10% amino acids or **(i)** 20 mg/L Uracil before OD_{600} measurements recorded at 1-hour intervals during recovery period, depicted as histogram. Error bars show standard deviation from 3 biological replicates. * indicates Student t-test p-values <0.05. Scale bare, 5 μm.

4. Chapter IV: The phosphatase Glc7 controls eisosomal response to starvation via posttranslational modification of Pil1

Graphical abstract

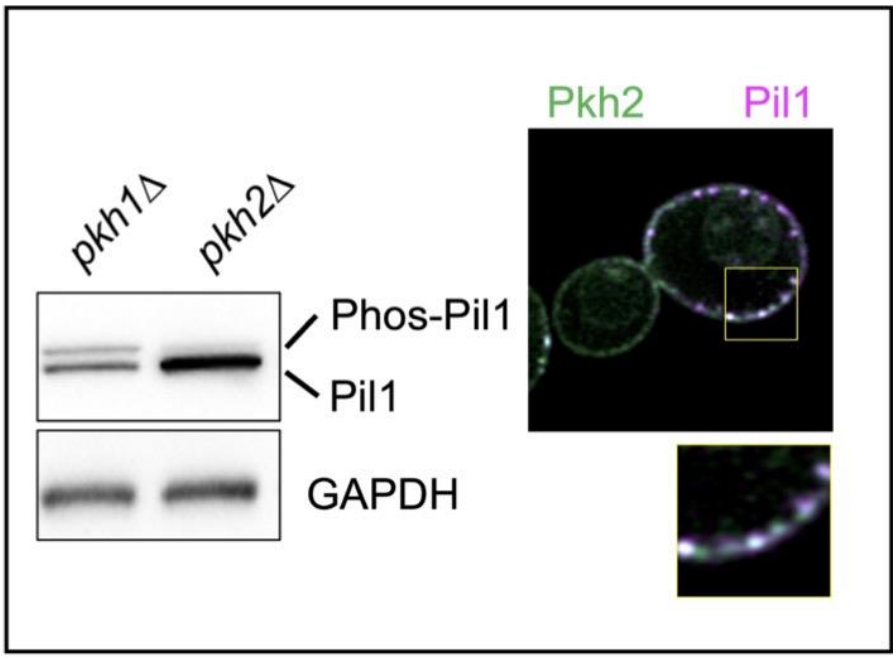

Eisosomes are subdomains of the yeast plasma membrane that play a role in the cellular response to glucose starvation. Core eisosomal component Pil1 is dephosphorylated in response to glucose starvation. We find Pkh2 is the main kinase responsible for this phosphorylation, with the levels of phosphorylated Pil1 in cells lacking Pkh2 (*pkh2*Δ) reduced significantly (left). Pkh2 is also observed to co-localise to eisosomes, marked by fluorescently labelled Pil1 (right). In this study we also performed a screen of all yeast phosphatases to reveal several that antagonises Pkh2 mediated phosphorylation. One phosphatase that appeared to have a major role in Pil1 dephosphorylation was Glc7, a conserved enzyme that has previously been associated with glucose-sensitive functions.

4.1. Introduction to project

Eisosomes are subdomains of the yeast plasma membrane enriched with ergosterol (Grossmann et al., 2007). Once formed *de novo* in daughter cells, eisosomes are static structures (Walther et al., 2006) that nutrient transporters can diffuse in and out of in a substrate dependent manner (Bianchi et al., 2018). The core component of eisosomes is the BAR domain protein Pil1 (Moreira et al., 2009) and phosphorylation of Pil1 has been established as being important for eisosome biogenesis (Karotki et al., 2011; Luo et al., 2008; Walther et al., 2007).

As mentioned in Chapter II, our work on the degradation of surface proteins in response to glucose starvation involved understanding the role of eisosomes during nutrient stress. In the lab at the time, Malaury Veillon, an undergraduate student from France, was performing immunoblots on cells expressing Pil1-GFP to test our hypothesis that the levels of Pil1 increase during glucose starvation. The effects on protein levels were significant, although modest. However, what we were all intrigued about was the repeated observation that Pil1-GFP blots showed a very different migration pattern following glucose starvation. Pil1 phosphorylation can be visualised by immunoblotting, with the protein in wild-type cells migrating as a fast moving unmodified species and a slower band representing phosphorylated protein species (Walther et al., 2007). Malaury's discovery that dephosphorylation of Pil1 occurred in response to glucose starvation was entirely novel, but there was not scope in that article to follow this up experimentally (**Chapter III, Figure 3.5.C**).

This curious observation was mentioned from time to time in lab meetings, with the suggestion that it should be followed up! Chris and Kamilla did write a proposal for the University's inclusive Summer Studentship Generation Research Programme to follow up on Pil1 dephosphorylation, but although this was selected for funding it never went ahead due to the lab being in lockdown. Around this time, I was developing an idea for a completely different project related to the transcriptional regulation of *PIL1*. My goal was to use a similar bioinformatic discovery approaches we employed to follow up transcriptional modifiers from my genetic screen (**Chapter II**) to identify regulators of *PIL1* expression that could be tested. My initial efforts using plasmid transformation of Pil1-GFP proved problematic. Although the GFP fusion protein was expressed from its endogenous promoter and we could blot levels well with antibodies against GFP, some cells exhibited aberrant localisation phenotypes. We suspected these effects were due to cells also expressing endogenous levels of Pil1, which is known to be a very abundant protein (Ho et al., 2018). With potentially equivocal results being generated from this expression plasmid in different transcriptional factor mutants I deemed this an inviable approach. However, during my reading of Pil1 phosphorylation at this time, I realised an antibody had been generated in the pioneering eisosomal work of the Walther lab. Having recently been followed on Twitter by Professor Walther (following tweets about my contribution to the eisosome story published in JCS), I felt sufficiently confident to email the Farese/Walther Lab and request an aliquot of Pil1 antibodies. The lab manager Kelly Higby kindly organised shipping. The antibody arrived in January 2021, which was an exciting day in the lab.

Although my plans were related to transcriptional mutants, my initial validation of the antibody I had procured clearly demonstrated this could be a powerful tool to explore the

dephosphorylation of Pil1. Yeast have 43 phosphatases (Offley and Schmidt, 2019), so I took null mutants from our deletion library for the 39 non-essential mutants (Winzeler et al., 1999). This left 4 essential phosphatases that, if I was attempting this earlier in my PhD, I would probably have just left untested. However, as our bioinformatics and genetic screening approaches had yielded essential gene candidates for testing (**Chapter II**, (Paine et al., 2021), I already had knowledge and experience of the "DaMP" library where the expression of essential genes is reduced in a library of viable strains (Breslow et al., 2008). I therefore included the DAmP strains for yeast essential phosphatase in my analysis.

Fortuitously, as the Pil1 antibody arrived from Harvard at the same time as I had pulled the DAmP strains with reduced expression of essential phosphatases - I ended up making lysates from those strains and wild-type cells to test if the antibody worked. The very first blot I performed with the Pil1 antibodies from the Walther lab revealed that *glc7* mutants have defective dephosphorylation of Pil1! I have validated this result many times, but this very first immunoblot has been included in the manuscript (**Figure 4.4, bottom right**). Surprisingly this turned out to be one of the critical discoveries of this paper and I have a distinct memory of visualising that first blot and seeing the phenotype that *glc7-DaMP* yielded. I was then eager to work my way through the non-essential mutants to see what other factors I might identify. I set about performing a screen of all phosphatase mutants alongside my original screen idea looking at transcriptional mutants. With the help of Chris and a Bluetooth speaker we managed to perform the screen in triplicate under glucose replete and glucose starvation conditions. We immediately found some interesting hits and so this project took off quickly.

As the results discussed in this chapter grew, we scrutinised the literature to frame our work in a broader context. On inspection, we realised neither activity or localisation of the individual Pkh1 and Pkh2 enzymes had been convincingly tested. As phosphorylation of Pil1 is so obviously important for its regulation, we thought it important that a study revealing discoveries about Pil1 dephosphorylation should also examine the contribution of kinases to the project. Pkh1 and Pkh2 are homologs to the mammalian Pdk1 (Casamayor et al., 1999), and Pkh3 was identified as a third homolog (Inagaki et al., 1999) but was never included in previous work relating to Pil1 and the Pkh family of kinases. I explored these kinases both through blotting and microscopy (**Figure 4.1., Supplemental Figure S4.1.**). I thought it would be worthwhile screening other potential kinases, as although these candidates had been at least loosely associated to eisosomes, other kinases were possible regulators. Dr. Gareth Evans joined the project to assist with this effort by performing a bioinformatic analysis to identify potential kinases - based on phosphosite signatures - that may act on Pil1. I tested the hits from this screen experimentally, assessing the phosphorylation profile of Pil1 in kinase null mutants (**Figure 4.2.**).

We submitted this paper to the Journal of Cell Science in August 2022 and received reviewer comments September 2022 which I am currently addressing. Reviews were encouraging and positive but have also highlighted some additional experiments that would bolster the model.

4.1.1. Aims of chapter

This chapter presents a screen that assesses the phosphorylation status of core eisosomal component Pil1 in phosphatase mutants with the aim to identify potential phosphatases previously not implicated in eisosomal regulation. Additionally, the work aims to clarify aspects of the literature surrounding the kinases responsible for Pil1 phosphorylation.

4.1.2. Declaration of authorship

4.1.2.1. Author contributions

Conceptualization: K.M.E.L., C.M.; Methodology: **K.M.P.**, C.M.; Validation: **K.M.P.**, G.J.O.E., C.M.; Formal analysis: **K.M.P.**, G.J.O.E., C.M.; Investigation: **K.M.P.**, C.M.; Data curation: C.M.; Writing - original draft: **K.M.P.**, C.M.; Writing - review & editing: **K.M.P.**, G.J.O.E., K.M.E.L., C.M.; Visualization: **K.M.P.**, C.M.; Supervision: C.M.; Project administration: C.M.; Funding acquisition: C.M.;

4.1.2.2. History of manuscript

Uploaded to bioRxiv: 11th August 2022
Submitted to Journal of Cell Science: 10th August 2022
Reviewers comments received: 6th September 2022

4.2. The phosphatase Glc7 controls eisosomal response to starvation via posttranslational modification of Pil1

Katherine M. Paine[1], Gareth J. O. Evans[1], Kamilla M. E. Laidlaw[1] and Chris MacDonald[1 2]

[1] *York Biomedical Research Institute and Department of Biology, University of York, York, UK*

[2] *Correspondence: Email: chris.macdonald@york.ac.uk Tel: +44 (0) 1904 328 609*

ABSTRACT

The yeast plasma membrane (PM) is organised into specific subdomains that can regulate the activity of surface membrane proteins localised within them. Nutrient transporters actively uptake substrates in particular regions of the PM where they are also susceptible to the endocytic machinery for substrate induced degradation. However, transporters also diffuse into distinct subdomains termed eisosomes, where they are inactive for substrate uptake and are protected from endocytosis. Although most nutrient transporter populations are sorted to the vacuole for degradation during glucose starvation, a small pool are retained in eisosomes. Sequestering this small pool of transporters during nutrient stress is essential for efficient recovery from starvation following a return to replete conditions. However, the mechanisms controlling this process at a biochemical level are poorly defined. We find the core eisosome subunit Pil1, a Bin, Amphiphysin and Rvs. (BAR) domain protein involved in membrane dynamics required for eisosome biogenesis, is primarily phosphorylated by Pkh2 but that Pil1 dephosphorylation occurs during acute glucose starvation. We screened for enzyme localisation and activity to implicate the essential phosphatase Glc7 as the primary enzyme responsible for Pil1 dephosphorylation. Manipulation of *GLC7* expression correlates with Pil1 hypo/hyper phosphorylation. Furthermore, *glc7* mutants and Pil1-phosphomutants are defective in recovering from glucose starvation. We propose precise posttranslational control of Pil1 modulates nutrient transporter retention within eisosomes depending on cellular nutritional status, to maximise recovery from starvation.

INTRODUCTION

The plasma membrane (PM) of eukaryotic cells is organised into distinct domains of specific lipids and proteins (Kraft, 2013). In the budding yeast *Saccharomyces cerevisiae*, microdomains of the PM have been characterised by fluorescence microscopy and shown to house distinct protein populations (Léon and Teis, 2018). Original localisation studies distinguished between the hexose transporter Hxt1, that is uniformly dispersed across the surface and other proteins that were found in discrete, non-overlapping regions (Malínská et al., 2003). The 2-type H^+-ATPase Pma1 is distinct from punctate subdomains marked by the amino acid transporters Can1 and Fur4 (Grossmann et al., 2007; Malinska et al., 2004). The subdomains containing these nutrient transporters are also termed eisosomes (Walther et al., 2006). Since then, many distinct regions and spatiotemporal patterns have been observed for different proteins localised to the yeast PM (Berchtold and Walther, 2009; Grossmann et al., 2007; Heinisch et al., 2010; Murley et al., 2017; Spira et al., 2012). The punctate eisosome regions with concentrated Can1 signal were originally estimated to be membrane furrows approximately 300nm long and enriched in sterols and sphingolipids (Grossmann et al., 2007; Malínská et al., 2003; StráDalová et al., 2009). Eisosomes are formed *de novo* randomly across the PM, where they are immobilised (Moreira et al., 2009). Beyond the original proteins localised to eisosomes, many additional factors have been identified, such as core structural proteins, posttranslational modifiers, tetraspan membrane proteins and uncharacterised proteins (Foderaro et al., 2017). Eisosomes have been identified in other fungal species, such as *Aspergillus nidulans* and *Ashbya gossypii* (Seger et al., 2011; Vangelatos et al., 2010), as well as various species of lichens and algae (Lee et al., 2015).

Eisosome structure and function is known to be regulated by some of these factors. Examples include the Bin, Amphiphysin and Rvs (BAR) domain proteins Pil1 and Lsp1 required for eisosome biogenesis, which are involved in binding to the PM and organising lipids during the sculpting of eisosomes (Moreira et al., 2009; Walther et al., 2006; Zhao et al., 2013a; Ziółkowska et al., 2011). The eisosomal kinases Pkh1 and Pkh2 function by phosphorylating both Pil1 and Lsp1, which is required for eisosome assembly (Luo et al., 2008; Walther et al., 2007). A screen for $PI(4,5)P_2$ regulators revealed eisosome factors Slm1 and Slm2 also bind lipids, which are required for proper eisosomal organisation and integrate with TORC2 signalling and lipid synthesis (Audhya et al., 2004; Berchtold et al., 2012; Kamble et al., 2011; Riggi et al., 2018). Other examples of proteins required for proper eisosome assembly include Nce102, a sphingolipid sensor (Fröhlich et al., 2009; Vaskovicova et al., 2020; Zahumenský et al., 2022), and Seg1, a stability factor that operates upstream of Pil1 (Moreira et al., 2012; Seger et al., 2011).

Many nutrient transporters diffuse in and out of eisosomes (Babst, 2019; Grossmann et al., 2008). Yeast cells uptake nutrients from their external environment through specific transporters that localise to the PM (Jack et al., 2000). Regulation of these transporters at the PM allows for nutrient acquisition to be tightly controlled in response to cellular requirements. When nutrient transporters are in eisosomes they are protected from endocytosis (Grossmann et al., 2008) and nutrient uptake activity is inhibited. For uptake of arginine, the Can1 transporter undergoes a conformational shift and moves from eisosomes to distinct regions of the PM, where it can subsequently be endocytosed

(Gournas et al., 2018). A similar PM relocation mechanism is observed for the Mup1 transporter in response to methionine addition (Busto et al., 2018; Moharir et al., 2018).

Active transporters localised to the PM, like Fur4, Can1 and Mup1, undergo conformational changes in response to nutrients and are more efficiently serviced by the endocytic machinery (Gournas et al., 2017; Guiney et al., 2016; Keener and Babst, 2013). Nutrient transporter ubiquitination is the signal for trafficking through the multivesicular body pathway, where ubiquitinated proteins are recognised and packaged into intralumenal vesicles of the MVB by the endosomal sorting complex required for transport (ESCRT) apparatus (Migliano et al., 2022). Upon MVB-vacuole fusion, intraluminal vesicles containing surface proteins are deposited in the degradative environment of the vacuolar lumen. These feedback mechanisms allow degradation to avoid excessive nutrient uptake, which can be detrimental (Kaur and Bachhawat, 2007; Séron et al., 1999; Watanabe et al., 2014). This pathway is coordinated in response to nutritional cues, for example in response to nitrogen starvation, surface proteins are degraded more readily by the elevation in vacuolar sorting triggered via Rsp5 and its adaptors (MacGurn et al., 2011; Müller et al., 2015). Rsp5 mediated degradation is also upregulated in response to growth past log-phase when niacin becomes limited (MacDonald et al., 2015a). Surface proteins are also degraded faster and recycled less efficiently in response to leucine starvation (Jones et al., 2012; MacDonald and Piper, 2017). A similar dual control of trafficking pathways in response to glucose starvation, which triggers surface protein degradation (Lang et al., 2014), occurs through an increase in AP180 mediated endocytosis and a decrease in Gpa1-PI3-kinase mediated recycling (Laidlaw et al., 2021; Laidlaw et al., 2022b).

Some of these stress condition experiments have shown that the entire nutrient transporter population is not degraded, with at least some of the cellular pool being sequestrated in eisosomes. This has only been shown for nutrient transporters, suggesting other cargoes are degraded in response to starvation but specifically retaining a reserve pool of nutrient transporters allows efficient recovery from starvation. Unlike the response to substrate, where transporters like Can1, Fur4 and Mup1 move from eisosomes and undergo endocytosis, starvation conditions like poor nitrogen source or growth to stationary phase results in increased transporter concentration in eisosomes (Gournas et al., 2018; Moharir et al., 2018). Stress conditions trigger restructuring of eisosomes, with changes in PM tension and deepening of these structures, to better retain this reserve pool of nutrient transporters (Appadurai et al., 2020; Moharir et al., 2018; Riggi et al., 2018). Our single molecule work has shown that biophysical changes in Pil1 are observed at this time, including an increase in molecular stoichiometry and diffusion coefficients (Laidlaw et al., 2021), which might contribute to such structural alterations during stress. Furthermore, there is a physiological benefit to harbouring these nutrient transporters in eisosomes: to allow efficient recovery following a return to replete conditions. For example, the uracil transporter Fur4 that is required at the surface for efficient growth in limited uracil conditions contributes to efficient recovery following glucose starvation, in a uracil-dependent manner (Laidlaw et al., 2021; Paine et al., 2021).

The retention of nutrient transporters in response to stress is not well understood at a mechanistic level. As mentioned, phosphorylation of the core factor Pil1 by Pkh-kinases is required for eisosome biogenesis (Karotki et al., 2011; Luo et al., 2008; Walther et al., 2007). We show Pkh2 is the main kinase that regulates Pil1 phosphorylation but also

that Pil1 is dephosphorylated in response to the glucose starvation conditions that trigger transporter retention. We identify Glc7 as a critical enzyme that regulates Pil1 dephosphorylation and show Glc7 activity is required for efficient recovery from starvation. Furthermore, phosphoablative and phosphomimetic Pil1 mutants are both defective in starvation recovery. We propose that the alteration of Pil1 phosphorylation modulates lipid binding to alter eisosomes, not only during biogenesis but in response to changes in nutritional conditions, allowing better retention of nutrient transporters.

RESULTS

Pkh2 is the predominant kinase that phosphorylates Pil1

It has been previously shown that Pil1 phosphorylation is ablated in a double *pkh1^{ts} pkh2*Δ mutant (Walther et al., 2007). To determine the contribution of Pkh1 and Pkh2 to Pil1 phosphorylation, we assessed individual deletion mutants. As Pkh3 was identified as a multicopy suppressor *pkh ^{ts}pkh2* mutants (Inagaki et al., 1999) but has not been tested for a role in Pil1 phosphorylation, we included *pkh3*Δ mutants in this analysis. Pil1 phosphorylation status affects its migration during electrophoresis and can be visualised by immunoblot (Walther et al., 2007). Pil1 phosphorylation was assessed in all three *pkh* mutants to reveal *pkh2*Δ mutants were most defective in Pil1 phosphorylation and that *pkh1*Δ and *pkh2*Δ mutants have a small but significant defect (**Figure 4.1.A**). We next performed localisation studies for these kinases. Although previous studies have demonstrated that over-expression of Pkh1/2 with the galactose inducible promoter *GAL1* is required for sufficient levels to localise these proteins (Roelants et al., 2002; Walther et al., 2007), we avoided this glucose-repression strategy, due to its effect on eisosome biology (Laidlaw et al., 2021). GFP-tagged kinases were instead over-expressed from the constitutive *NOP1* promoter (Weill et al., 2018) in cells co-expressing the eisosomal marker Nce102 tagged with mCherry. Only GFP-Pkh2 predominantly colocalised with Nce102-mCherry (**Figure 4.1.B**). This small apparent contribution of Pkh1 and Pkh3 to Pil1 phosphorylation observed by immunoblot might be explained by the fact that although most cells do not localise Pkh1/3 to eisosomes, a small number of cells do (**Supplemental Figure S4.1.A – S4.1.B**). In further support of Pkh2 being a regulator of Pil1 phosphorylation, overexpressing Pkh2 in wild-type cells leads to a significant increase in Pil1 phosphorylation and Pkh2 plasmid expression in *pkh2*Δ cells increases Pil1 phosphorylation (**Figure 4.1.C**). These data demonstrate that Pkh2 is the primary Pkh-family member responsible for Pil1 phosphorylation, but that Pkh1 and Pkh3 also exhibit subsidiary regulatory roles for Pil1.

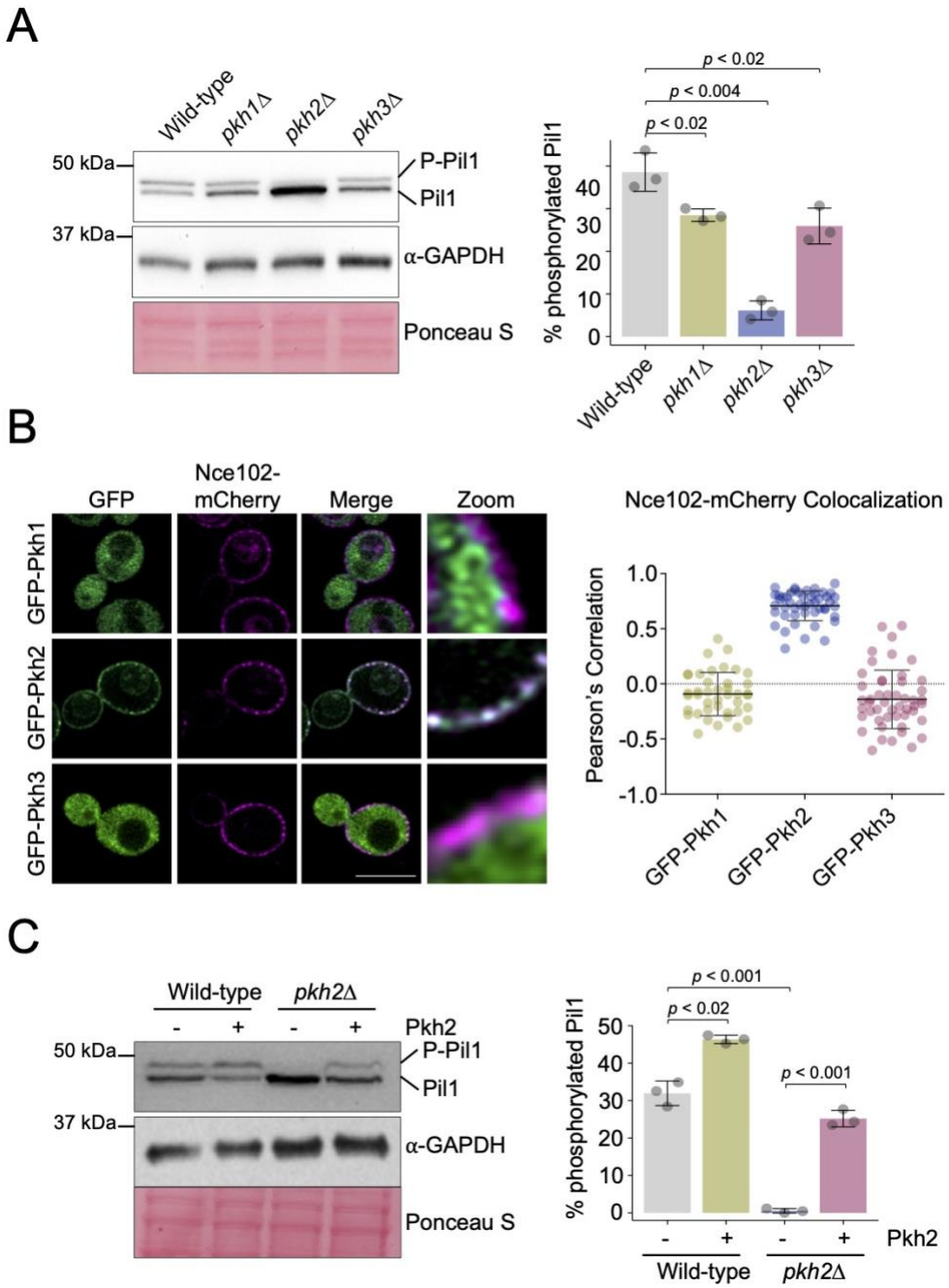

Figure 4. 1 Pkh2 predominately regulates phosphorylation of Pil1.

A) Whole cell lysates of wild-type, *pkh1Δ*, *pkh2Δ* and *pkh3Δ* cells were analysed by immunoblot using α-Pil1 and α-GAPDH antibodies, with Ponceau S stained membrane included. The percentage phosphorylated Pil1 from each yeast strain was quantified (n=3). **B)** Cells co-expressing Nce102-mCherry and indicated GFP tagged Pkh-kinases were grown to mid-log phase and imaged using confocal microscopy (Airyscan 2). The Pearson's Correlation Coefficient was measured of colocalisation between Nce102-mCherry with the respective GFP-tagged kinases (n > 40). **C)** Wild-type and *pkh2Δ* cells were transformed with either an empty vector control (-) or a 2μ Pkh2 over-expression plasmid (+). Whole cell lysates were generated from transformants and Pil1 phosphorylation assessed by immunoblot. Levels of GAPDH and Ponceau S are shown as loading controls (left). The percentage of phosphorylated Pil1 was quantified (n=3) and shown (right). Statistical significance was determined using Student's t-test. Scale bar = 5μm

Phosphorylated peptides of Pil1 have previously been identified by mass spectrometry (Albuquerque et al., 2008; Luo et al., 2008; Swaney et al., 2013; Walther et al., 2007), suggesting multiple levels of potential phosphorylation. This is also implied by the various species observed by immunoblot using an inverted step-gradient electrophoresis strategy (Laidlaw et al., 2021). Experimental work has determined several key phosphosites (Luo et al., 2008; Walther et al., 2007), which map to distinct regions of the Pil1 structure (**Figure 4.2.A**). To ascertain if any additional kinases beyond the Pkh-family were responsible for Pil1 phosphorylation, NetPhorest analysis (Horn et al., 2014) was used to predict potential kinases for known Pil1 phosphosites (**Figure 4.2.B**). Mutants of any high scoring kinases were tested for a role in phosphorylating Pil1 by immunoblot (**Supplemental Figure S4.2.**). Only eight mutants showed any indication of a potential role, which was followed up quantitatively. This revealed *hog1*Δ cells lacking the yeast homologue of the mammalian MAPK p38, Hog1 (Han et al., 1994), had reduced levels of Pil1 phosphorylation. Also, depletion mutants with reduced levels of the Hippo-like kinase Cdc15 (Rock et al., 2013; Steensma et al., 1987), by virtue of a DAmP cassette (Breslow et al., 2008), showed higher levels of Pil1 phosphorylation (**Figure 4.2.C**). This additional analysis again supports the notion that Pkh2 is the primary enzyme responsible for Pil1 phosphorylation, but that phosphorylation via other kinases may also have an impact, potentially through indirect mechanisms such as transcriptional or stress-induced control.

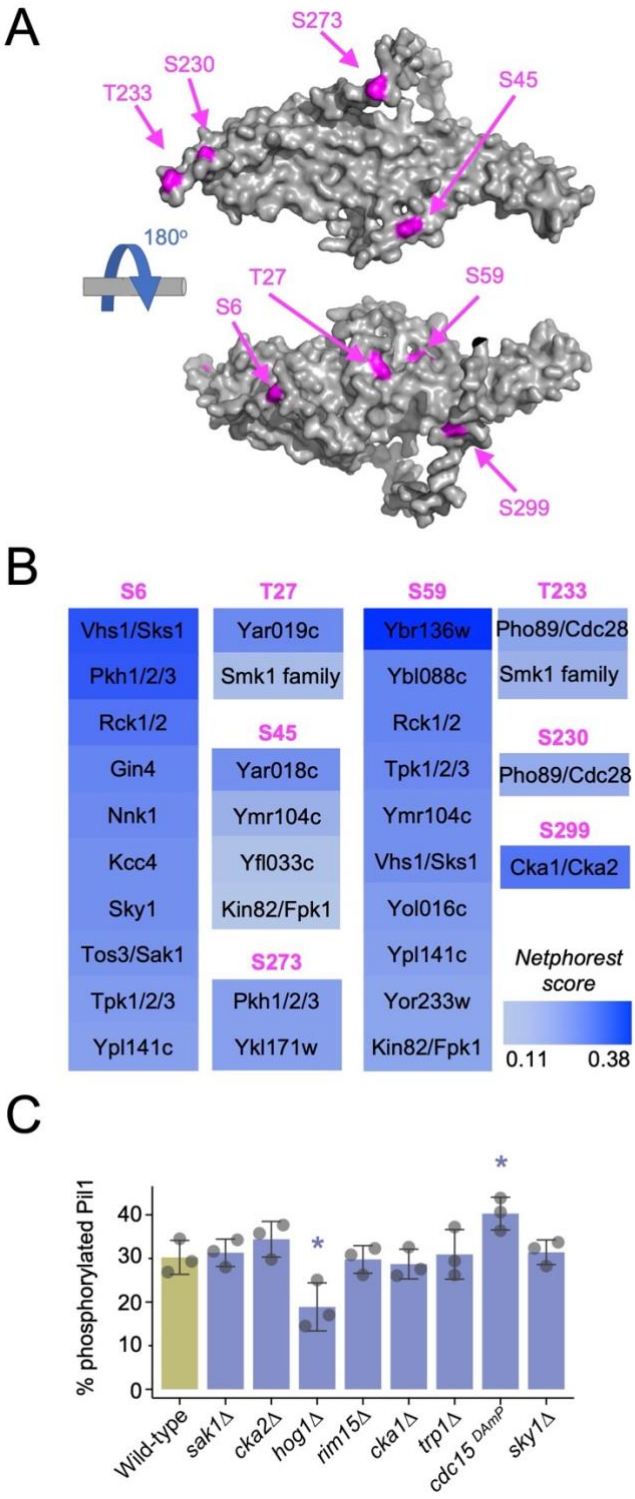

Figure 4. 2 Bioinformatic screen for additional kinases that service Pil1.

A) Alphafold structural model of Pil1 residues 1-307 (grey) shown with eight previously verified phosphorylation sites indicated (magenta). **B)** The Pil1 protein sequerce was surveyed using NetPhorest searching against a reference kinase database for Saccharomyces cerevisiae. Kinases that scored above threshold (0.1) are presented as a heat map (blue) with the indicated potential phosphorylated residue (magenta). **C)** Whole cell lysates of wild-type and kinase mutant cells were generated and percentage Pil1 phosphorylation assessed by immunoblot and presented as a histogram (n=3).

Pil1 is dephopshorylated in response to glucose starvation

In response to acute glucose starvation, nutrient transporters localise to eisosomes (Laidlaw et al., 2021) and are hypothesised to relocate to PM regions for nutrient uptake upon return to replete conditions (**Figure 4.3.A**). For glucose starvation, media lacking glucose but containing the trisaccharide raffinose, which cannot be quickly metabolised (de la Fuente and Sols, 1962), is used. Upon raffinose exchange, nutrient transporters such as Mup1 concentrate to eisosomes within 10 minutes (**Figure 4.3.B**). During the initial period of glucose starvation when nutrient transporters accumulate in eisosomes, we observe rapid Pil1 dephosphorylation (**Figure 4.3.C**). We also observe significant glucose induced dephosphorylation in *pkh1*∆, again suggesting it is not a key regulator of Pil1 phosphorylation (**Supplemental Figure S4.3.**).

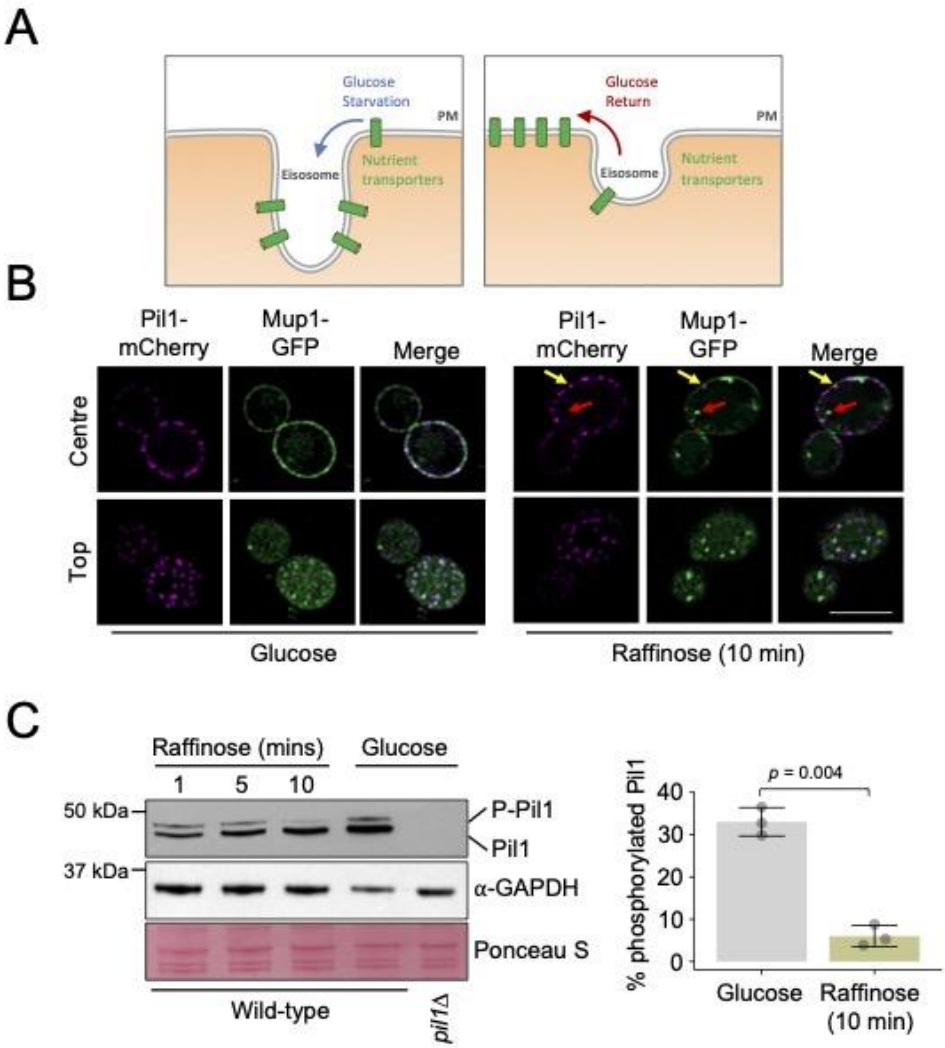

Figure 4. 3 Pil1 is dephosphorylated in response to glucose starvation.

A) Schematic showing the increased diffusion of nutrient transporters into eisosomes in response to glucose starvation, and their potential exit upon a return to replete nutrient conditions to aid recovery. **B)** Cells co-expressing Pil1-mCherry and Mup1-GFP were imaged using confocal microscopy (Airyscan 2) with centre and top focus under glucose conditions and following 10 minutes of exchange with raffinose media. Mup1 localised to endosomes (red arrow) and Pil1 marked eisosomes (yellow arrow) after raffinose treatment are indicated. **C)** Wild-type cells exposed to raffinose media for 1, 5 and 10 minutes prior to lysate generation were immunoblotted using α-Pil1 antibodies and compared to wild-type and *pil1Δ* cells grown in glucose replete conditions. GAPDH blot and Ponceau S stained membrane is included as a loading control. Percentage of phosphorylated Pil1 was generated for WT vs 10 minutes of raffinose treatment for wild-type cells was quantified (right).

We hypothesise that Pil1 dephosphorylation in response to glucose starvation plays a role in the ability of eisosomes to sequester nutrient transporters in response to glucose starvation. In *Saccharomyces cerevisiae* 43 phosphatases have been identified (Offley and Schmidt, 2019), of which 39 are non-essential and 4 are essential. To identify the phosphatase(s) responsible for Pil1 dephosphorylation, we screened mutants of all phosphatase enzymes for their activity in glucose and raffinose conditions (**Figure 4.4.A**). Pil1 phosphorylation status was assessed in null mutants (Δ) lacking non-essential phosphatases or with reduced expression of essential phosphatases, by virtue of a DaMP cassette (Breslow et al., 2008). Mutants were scored based on defects in Pil1 dephosphorylation (**Figure 4.4.B**). This screen revealed 7 top scoring phosphatase mutants selected for further quantitative analysis (**Figure 4.5.A – 4.5.B**). Next, we assessed the localisation of GFP tagged phosphatases at mid-log phase and stationary phase (**Figure 4.5.C, Supplemental Figure S4.4.**). We included stationary phase as a nutritional stress associated with eisosome transporter retention (Gournas et al., 2018). This confirmed a range of localisations, many to the nucleus and cytoplasm but also Ppn2 at the vacuole and Ptc5 at the mitochondria (Breker et al., 2013). Interestingly, we also observed several GFP tagged phosphatases that had changes in localisation following growth to stationary phase, including Sdp1, Ptc5, and Nem1. Although GFP-Msg5 and GFP-Siw14 fusions localised to the periphery upon growth to stationary phase, deletion of these mutants had no impact on Pil1 phosphorylation, so we assume this peripheral localisation is not related to eisosome regulation. However, GFP-Glc7 showed significant peripheral punctate localisation in both growth conditions, in addition to localisation to the mid-body, the cytoplasm and the nucleus (Bloecher and Tatchell, 2000; Breker et al., 2013). The only phosphatase that showed significant localisation to the cell periphery and that exhibited defects in phosphorylation upon mutation, was Glc7.

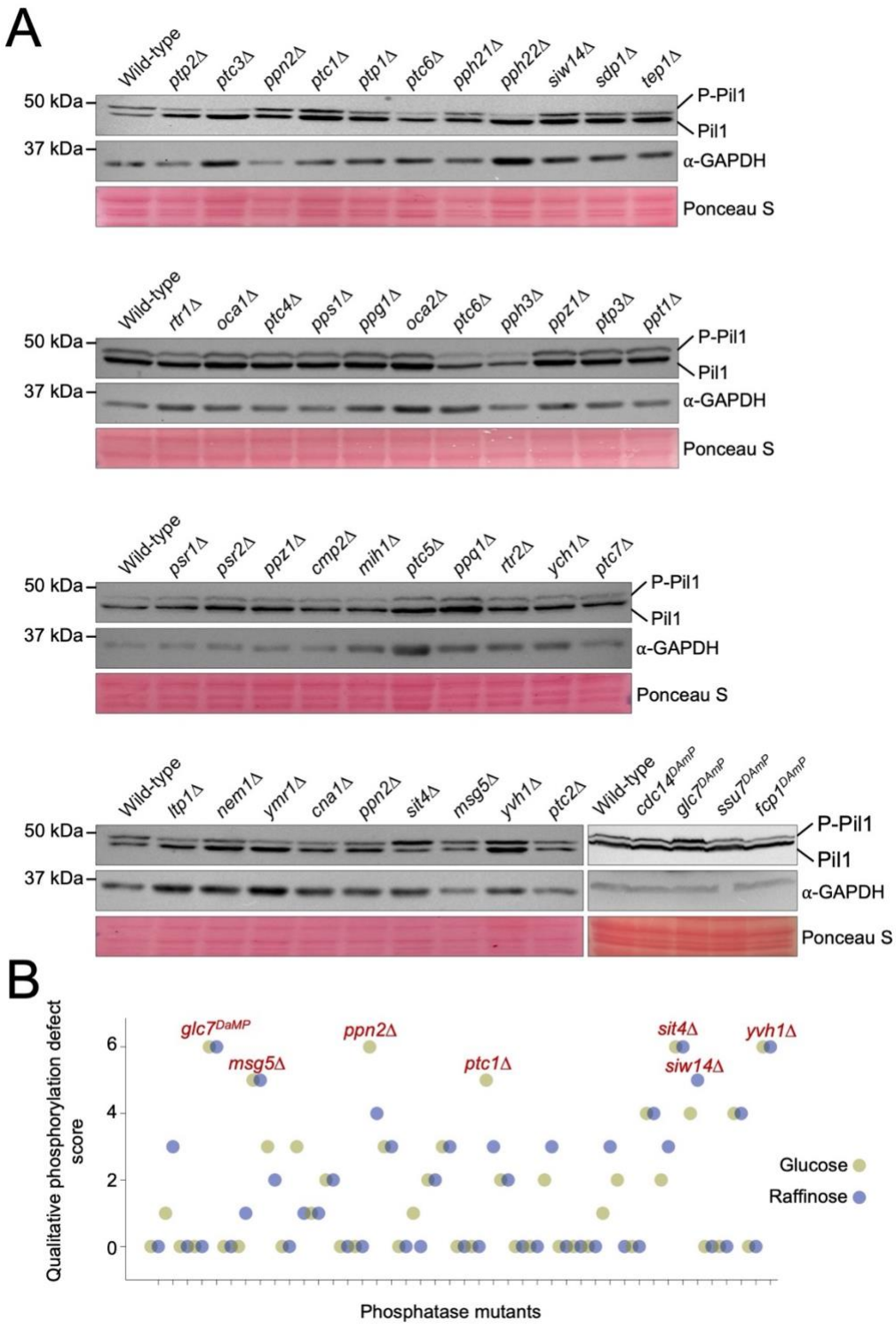

Figure 4. 4 Screen for regulators of Pil1 dephosphorylation

A)Wild-type cells and indicated phosphatase mutants were grown to log-phase in glucose replete conditions prior to lysate generation and immunoblotting with α-Pil1 and α-GAPDH antibodies. Representative blots for at least one mutant are shown, alongside Ponceau S stained membrane. **B)** Immunoblots for all phosphatase mutants were qualitatively scored based on their Pil1 phosphorylation phenotype in both glucose (green) and raffinose (purple) conditions compared with wild-type controls. The highest scoring mutants are labelled in red.

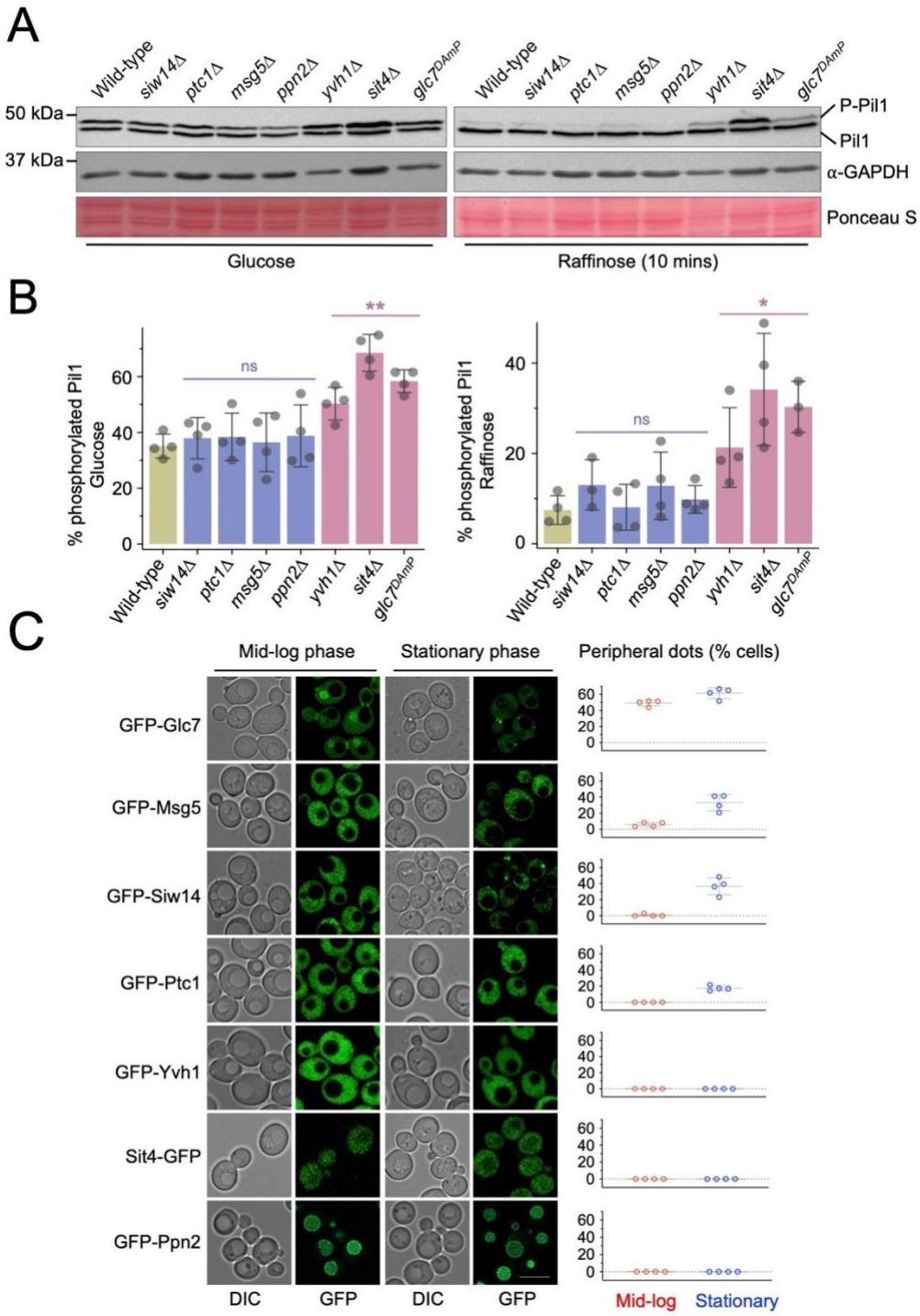

Figure 4. 5 Activity and localisation screens implicate Glc7 in Pil1 regulation.

A) Whole cell lysates of wild-type and phosphatase mutant candidates from glucose replete media (left) or following 10 minutes exchange with raffinose media were generated and analysed by immunoblotting using α-Pil1and α-GAPDH antibodies. **B)** Quantification of percentage of Pil1 phosphorylated in indicated mutants was calculated. Statistical significance was determined using Student's t-test. **C)** Yeast expressing GFP tagged phosphatases were cultured to mid-log and stationary phase prior to confocal microscopy (Airyscan). The number of peripheral dots per cell (n > 30) from separate experiments (n = 4) were quantified in each condition (right). Scale bar = 5 μm.

Glc7 functions in regulation of Pil1

Glc7 is an essential phosphatase (Clotet et al., 1991; Feng et al., 1991) that has been previously show to function in glucose related pathways, where it acts with its regulatory subunit Reg1 (Tu and Carlson, 1995) and bud neck formation (Larson et al., 2008), amongst other roles in the cell. We confirmed that *glc7*^{DAmP} results in reduced dephosphorylation of Pil1 in both glucose replete and glucose starvation conditions (**Figure 4.6.A**). Intriguingly, these effects are independent of Reg1, as *reg1*∆ cells exhibit slightly increased levels of Pil1 dephosphorylation (**Figure 4.6.B – 4.6.C**). As a complementary approach to test the role of Glc7 in Pil1 phosphorylation we altered *GLC7* expression levels using a YETI (Yeast Estradiol with Titratable Induction) strain (Arita et al., 2021b) which allows modulation using ß-estradiol concentrations (**Figure 4.6.D**). We reveal *GLC7* expression correlates with Pil1 phosphorylation, with 100 mM ß-estradiol induced over-expression of *GLC7* reducing Pil1 phosphorylation and removing ß-estradiol entirely increasing phosphorylated species (**Figure 4.6.E – 4.6.F**). This analysis demonstrates the YETI system in media lacking ß-estradiol for 6-hours has a more pronounced decrease in *GLC7* expression than *glc7*^{DAmP}. Collectively, this suggests the role of Glc7 in Pil1 phosphorylation might be direct, so we sought to test if Glc7 colocalises to eisosomes marked with Nce102-mCherry. However, neither steady state or time lapse imaging in glucose and raffinose media revealed large amounts of Glc7 localisation to eisosomes, but there were often small regions of colocalisation in a restricted number of eisosomes (**Figure 4.6.G – 4.6.H**).

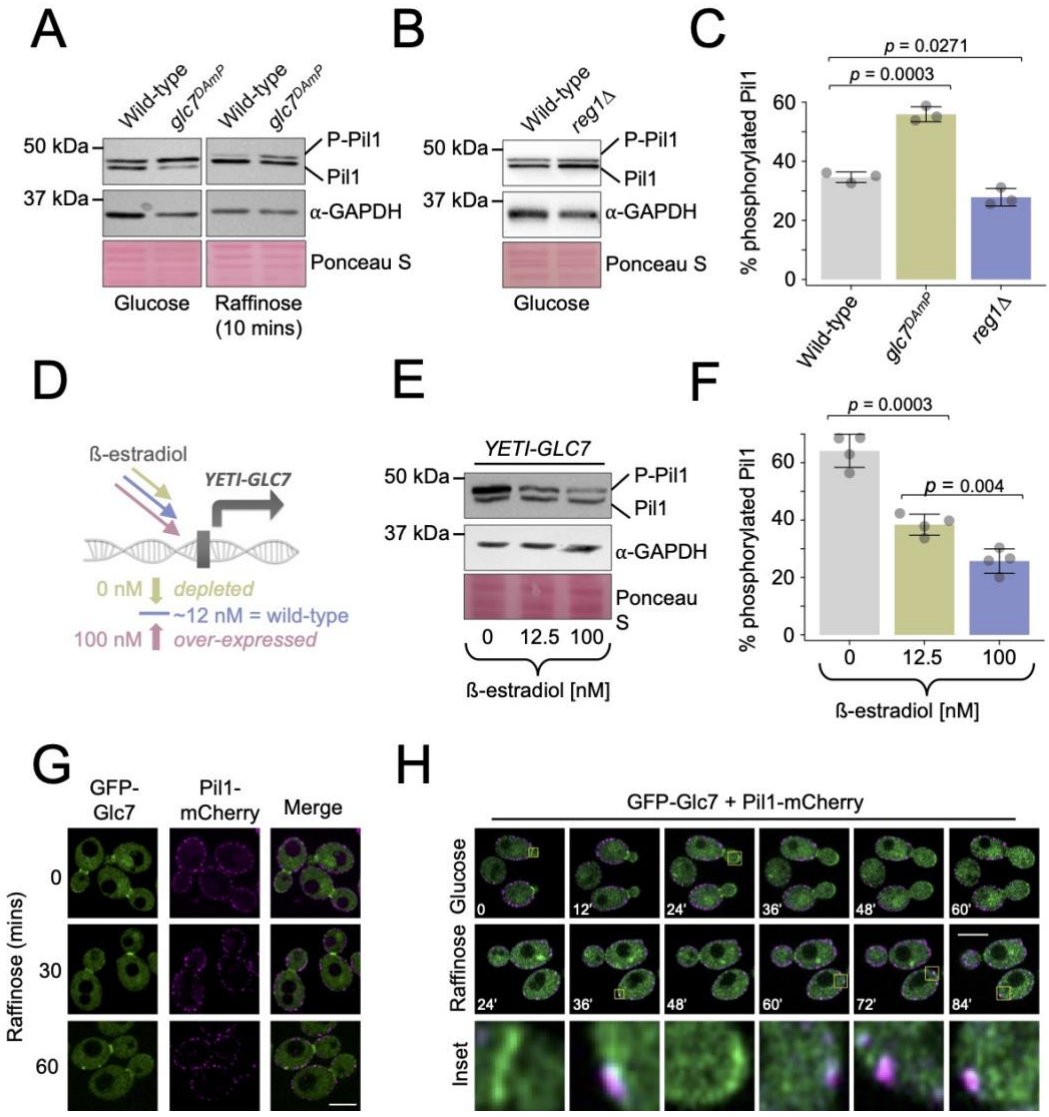

Figure 4. 6 Glc7 regulates Pil1 dephosphorylation in a Reg1 independent manner

A) Wild-type and *glc7DAmP* cells were cultured in glucose media and following 10 minutes of raffinose treatment prior to the generation of whole cell lysates and immunoblotting with α-Pil1 and α-GAPDH antibodies. **B)** Whole cell lysates of wild-type and *reg1Δ* cells were generated for α-Pil1 and α-GAPDH immunoblot. **C)** The percentage of phosphorylated Pil1 from experiments in **A** and **B** was quantified (n=3) and p values from Student's f-tests indicated. **D)** Schematic outlining the principle of the YETI expression system for titratable expression of GLC7 to mimic severely depleted (green) and over-expressed (pink) levels. **E)** YETI-GLC7 cells were grown overnight in 12.5 nM β-estradiol before washing x3 in YPD media and dilution in fresh media containing 0, 12.5 nM and 100 nM β-estradiol. Cells were then grown for 6 hours prior to the generation of whole-cell lysates and immunoblots using α-Pil1and α-GAPDH antibodies. **F)** Pil1 phosphorylation was quantified (n=3) from β-estradiol titrations shown in **E** with p values from Student's t-tests shown. **G)** Cells coexpressing GFP-Glc7 and Pil1-mCherry were grown to mid-log phase and imaged using confocal microscopy at 0, 30 and 60 minutes of raffinose treatment. **H)** Time-lapse microscopy of GFP-Glc7 and Pil1-mCherry expressing cells was performed in glucose and 25 minutes raffinose conditions. Scale bar = 5μm.

Phosphorylation of Pil1 is important for recovery after glucose starvation

Having implicated Glc7 in Pil1 dephosphorylation that occurs during glucose starvation, we next wanted to test if this regulation controls Pil1 function in starvation recovery. Previous studies have assessed the phosphorylation profile of various Pil1 mutants with mutation of 8 verified phosphosites (Luo et al., 2008; Walther et al., 2007). We generated phosphoablative (changed to alanine, 8A) and phosphomimetic (changed to aspartate, 8D) versions of Pil1 at these phosphosites (**Figure 4.7.A**). Western blotting confirmed that the 8A and 8D mutations resulted in Pil1 migrating not as a doublet, but as a single band, with faster migration of the phosphoablative Pil1-8A-mGFP and slower migration of the phosphomimetic Pil1-8D-mGFP fusion (**Figure 4.7.B**). Fluorescence microscopy of GFP tagged Pil1 versions showed both 8A and 8D expressing strains exhibited an altered localisation phenotype compared to wild-type cells (**Figure 4.7.C**), as previously documented for phosphomutants of Pil1. This confirms what was previously shown for phosphomimetic and ablative mutants (Luo et al., 2008; Walther et al., 2007). We quantified these differences (**Supplemental Figure S4.5.**) revealing both mutants have fewer eisosomes per cell compared to wild type (**Figure 4.7.D**). Furthermore, both ablative and mimetic mutants exhibit more cytoplasmic signal (**Figure 4.7.E**). This analysis showed a more pronounced defect in eisosome number and levels for Pil1-8D-mGFP than Pil1-8A-mGFP.

To test if Pil1 phosphomutants were functional in starvation recovery, we used an assay that tracks recovery growth following 2 hours glucose starvation (Laidlaw et al., 2021). This assay cultures cells in minimal media, which shows no growth differences between wild-type and phosphomutants of Pil1 (**Figure 4.7.F**). We do note that in rich YPD media, the Pil1-8A and Pil1-8D mutants have defects in growth at early time points, potentially explained by a connection between nutritional status and Pil1 phosphorylation. However, unlike comparable growth under non-stress conditions, we find that both Pil1-8A and Pil1-8D mutations are defective in recovery growth (**Figure 4.7.G – 4.7.H**). This suggests phosphoregulation of Pil1 is required to modify eisosomes that sequester nutrient transporters during nutritional challenges.

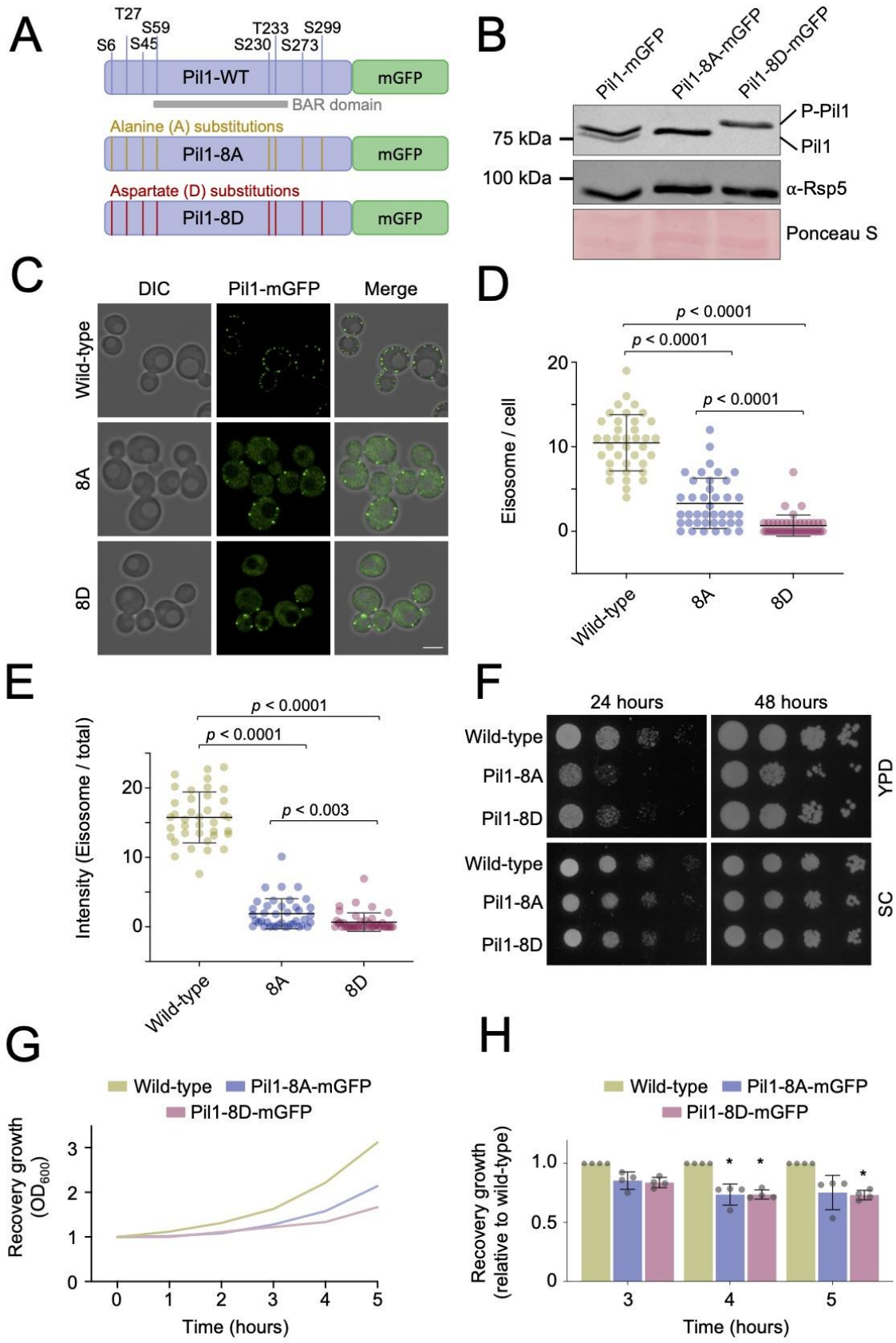
A
T27
S59
S6
S45
T233
S299
S230
S273
Pil1-WT
mGFP
BAR domain
Alanine (A) substitutions
Pil1-8A
mGFP
Aspartate (D) substitutions
Pil1-8D
mGFP
B
Pil1-mGFP
Pil1-8A-mGFP
Pil1-8D-mGFP
75 kDa
100 kDa
P-Pil1
Pil1
α-Rsp5
Ponceau S
C
DIC
Pil1-mGFP
Merge
Wild-type
8A
8D
D
p < 0.0001
p < 0.0001
p < 0.0001
Eisosome / cell
20
10
0
Wild-type
8A
8D
E
p < 0.0001
p < 0.0001
p < 0.003
Intensity (Eisosome / total)
20
10
0
Wild-type
8A
8D
F
24 hours
48 hours
Wild-type
Pil1-8A
Pil1-8D
YPD
Wild-type
Pil1-8A
Pil1-8D
SC
G
Wild-type
Pil1-8A-mGFP
Pil1-8D-mGFP
Recovery growth (OD600)
3
2
1
0
0
1
2
3
4
5
Time (hours)
H
Wild-type
Pil1-8A-mGFP
Pil1-8D-mGFP
Recovery growth (relative to wild-type)
1.0
0.5
0
*
*
*
3
4
5
Time (hours)

Figure 4. 7 Phosphomutants of Pil1 are defective in starvation recovery

A) Cartoon showing Pil1 fusion to mGFP, including its verified phosphosites and BAR domain. Pil1 cassettes that have been mutated to alanine (yellow) or aspartate (red) that were stably integrated at the *PIL1* locus are also shown. **B)** Pil1 or indicated 8A and 8D mutants were expressed from the endogenous locus as mGFP fusions in strains grown to mid-log phase, harvesting and lysate generation for immunoblotting with α-Pil1 and α-GAPDH antibodies. **C)** Versions of mGFP tagged Pil1 were expressed as the sole chromosomal copy and localised by confocal microscopy coupled to Airyscan 2 detector. **D)** Pil1 labelled eisosomes were identified by otsu segmentation and number per cell quantified (n = > 37) with p values generated from Student's t-test comparisons. **E)** Integrated density for all GFP tagged Pil1 versions localised to eisosomes identified from segmentation performed in D was calculated as a percentage of the total signal, with Student's t-test comparison generated p values shown. **F)** Indicated yeast strains were grown to log phase in either YPD rich media or SC minimal media, equivalent cell numbers were estimated by optical density measurements and harvested. 10-fold serial dilutions were generated, and yeast spotted out on YPD and SC plates. Growth was recorded at 24 and 48 hours. **G)** Cells at mid-log phase were subjected to 2 hours of glucose starvation (raffinose treatment), returned to glucose replete conditions and growth measured over time. **H)** The growth assay in **G** was repeated (n = 4) and the growth relative to wild-type was quantified for each indicated timepoint. Statistical significance was determined using a Student's t-test.

Pil1 mutants that cannot modulate phosphorylation status are impaired in their ability to recover from starvation, and Pkh2 and Glc7 are required for these post translational modifications. Therefore, our model would predict that these enzymes are also required to efficiently sequester nutrient transporters in eisosomes, and for full recovery following starvation. We have previously shown that *pkh2*Δ mutants have reduced retention of nutrient transporters and an attenuated recovery following glucose starvation (Laidlaw et al., 2021). Similarly, *glc7*^{DAmP} cells with reduced levels of *GLC7* have reduced eisosomal localisation of the methionine permease Mup1 tagged with GFP, in both glucose replete conditions and following a brief incubation with raffinose (**Figure 4.8.A**). Growth assays on both rich and minimal media show that *glc7*^{DAmP} cell growth is comparable to wild-type cells that are not exposed to starvation conditions (**Figure 4.8.B**). However, recovery growth of *glc7*^{DAmP} mutants following 2 hours of glucose starvation is significantly hampered (**Figure 4.8.C and D**).

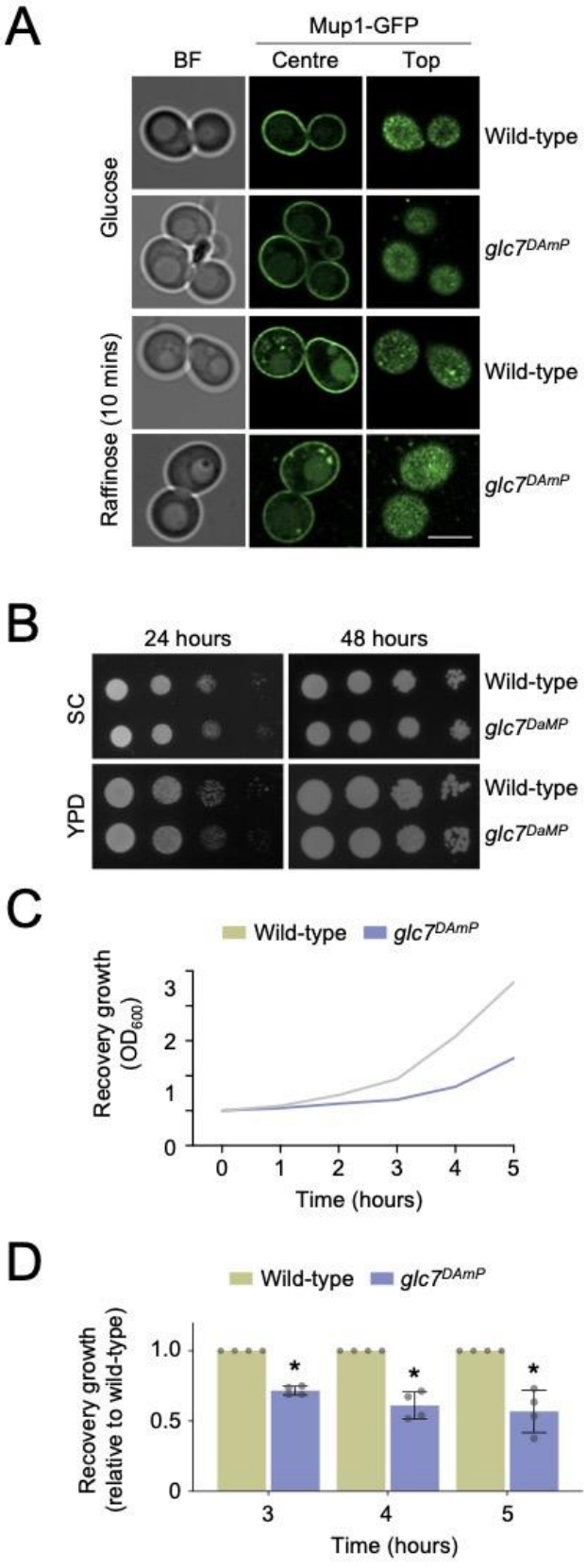
A
Mup1-GFP
BF
Centre
Top
Glucose
Raffinose (10 mins)
Wild-type
glc7DAmP
Wild-type
glc7DAmP
B
24 hours
48 hours
SC
YPD
Wild-type
glc7DaMP
Wild-type
glc7DaMP
C
Wild-type
glc7DAmP
Recovery growth (OD600)
0
1
2
3
0
1
2
3
4
5
Time (hours)
D
Wild-type
glc7DAmP
Recovery growth (relative to wild-type)
0
0.5
1.0
*
*
*
3
4
5
Time (hours)

Figure 4. 8 Glc7 is required for efficient recovery from glucose starvation

A) Wild-type and *glc7DAmP* cells expressing Mup1-GFP were imaged under glucose replete and after 10 minutes Raffinose treatment. Representative images for centre and top focus are shown. Scale bar = 5μm. **B)** Indicated yeast strains were grown to log phase in either YPD rich media or SC minimal media, equivalent cell numbers were estimated by optical density measurements and harvested. 10-fold serial dilutions were generated, and yeast spotted on YPD and SC plates followed by recording growth at 24 and 48 hours. **C)** Cells at mid-log phase were subjected to 2 hours of glucose starvation (raffinose treatment) and then returned to glucose replete conditions where growth was tracked through OD600 measurements every hour for 5 hours. **D)** The growth assay in **C** was repeated (n = 4) and the growth relative to wild-type was quantified for each time-point. Statistical significance was determined using a Student's t-test.

DISCUSSION

The organisation of the yeast PM is very complex with a multitude of possible surface localisation patterns known for both integral membrane proteins and surface associated factors (Spira et al., 2012). Since the discovery of the eisosome subdomain, progress has been made in understanding the formation and biological function of these structures, particularly in response to cellular stress (Babst, 2019; Moseley, 2018). The discovery that Pil1 and Lsp1, and their phosphorylation by the Pkh-family kinases, are required for proper eisosome biogenesis (Walther et al., 2007; Walther et al., 2006) suggests post-translational modification of core components could regulate the eisosome environment. Pkh1 and Pkh2 were originally identified as homologues of human and *Drosophila* 3-phosphoinositide-dependent protein kinase-1 (PDK1) that are essential for viability (Casamayor et al., 1999). As this work showed the double *pkh1Δ pkh2Δ* yeast mutant was inviable, a double mutant with a temperature sensitive allele of *PKH1* (D398G) and deletion of *PKH2,* termed *pkh1^{ts} pkh2Δ*, was used to study kinase signalling pathways (Inagaki et al., 1999). This double *pkh1^{ts} pkh2Δ* mutant also revealed an early association of Pkh-kinases with endocytosis, with this strain impaired for internalization from the PM (Friant et al., 2001). Due to the shared essential function of Pkh1 and Pkh2, the double mutant was the most logical strain to test effects on biogenesis of eisosomes upon their discovery (Walther et al., 2007; Walther et al., 2006). However, we find Pkh2 is predominantly responsible for phosphorylating Pil1 with only minor roles for Pkh1 or indeed the related kinase Pkh3 (**Figure 4.1.A**). We also did not observe substantial amounts of Pkh1 or Pkh3 at eisosomes. One key difference to our work and previous localisation of Pkh1 to eisosomes (Walther et al., 2007) is that we did not use the *GAL1* promoter for over-expression, so it may be that the glucose starvation stress of galactose induction media alters Pkh1 localisation or the eisosome environment. Further exploring other potential kinase and phosphosites did suggest the Hog1 and Cdc15 kinases might also exhibit small roles regulating Pil1, but these effects were also relatively modest compared with Pkh2 (**Figure 4.2.**). Of note, the phosphoshift seen for Pil1 is mainly caused by phosphorylation at S273 (Walther et al., 2007), as the focus of this work was not kinase regulation future work using alternative approaches may better clarify the role of alternative kinases in Pil1 regulation.

The finding that extracellular stress results in the accumulation of nutrient transporters in eisosome compartments, which deepen to facilitate this process, suggests a key role of eisosomes is related to nutritional uptake following stress (Appadurai et al., 2020; Gournas et al., 2018). We have previously shown the specific stress of acute glucose starvation (0-2 hours) results in concentration of the nutrient transporter Mup1 to eisosomes. As eisosomal mutants fail to properly retain nutrient transporters and fail to recover efficiently from starvation (Laidlaw et al., 2021), we propose acute glucose starvation modulates eisosomes to better harbour transporters for recovery. We find the core eisosomal Pil1 is rapidly dephosphorylated during the same acute glucose starvation period (**Figure 4.3.**). This led to the model that the phosphorylation status of Pil1 is important for reorganisation of existing eisosomes during cargo retention, in addition to its established role in eisosome biogenesis. These functions could be one and the same at the molecular level, with changes in phosphorylation and charge of Pil1 having the potential to affect its lipid binding/sculping capacity. As membrane bending effects of other BAR domain proteins are known to be affected by disordered regions (Busch et al., 2015; Zeno et al., 2018), it is conceivable that phosphorylation can alter the biophysical properties of eisosomes.

To identify possible regulators of Pil1 dephosphorylation that might regulate eisosomes during stress, we systematically screened mutants of all encoded yeast phosphatases, in both glucose replete and starved conditions. This effort implicated a role for Glc7, an essential Type 1 Serine/Threonine protein phosphatase (Cannon et al., 1994; Peng et al., 1990). We confirmed Glc7 regulates Pil1 by decreasing Glc7 levels using a Decreased Abundance by mRNA Perturbation (DAmP) method (Breslow et al., 2008) and a Yeast Estradiol with Titratable Induction (YETI) strategy (Arita et al., 2021b), both of which showed elevated levels of Pil1 phosphorylation (**Figure 4.6.**). This latter approach also allowed over-expression of *GLC7*, which resulted in further Pil1 dephosphorylation. Although Glc7 was the only phosphatase to regulate Pil1 phosphorylation in addition to localising to the cell periphery (**Figure 4.5.**), we only observed small levels of colocalisation of Glc7 with Pil1. Glc7 has several roles in the cell including, growth, mitosis, transcription, stabilisation of emerging buds, glycogen metabolism and ion homeostasis (Feng et al., 1991; Hisamoto et al., 1995; Kozubowski et al., 2003; Peggie et al., 2002; Sanz et al., 2004; Williams-Hart et al., 2002), which we corroborate with expected localisations at the bud-neck, nucleus and cytoplasm. It may be that at steady state very little Glc7 is required for eisosome maintenance, and this may be achieved via a transient interaction, either direct or indirect via accessory proteins.

Glc7 having a role in eisosomal modulation during glucose starvation is conceptually consistent with many studies demonstrating that Glc7 integrates with transcriptional repression in response to glucose availability, via Snf1 and downstream factors (Sanz et al., 2000; Tu and Carlson, 1994). However, as the changes we observe in both Pil1 dephosphorylation and transporter retention are very rapid, we assume these effects are not mediated at the transcriptional level. In further support of this idea, the regulatory subunit Reg1, which is required for many transcriptional related Glc7-activities (Alms et al., 1999; Cui et al., 2004; Dombek et al., 1999), showed no increase in phosphorylated Pil1 species upon its deletion (**Figure 4.6.B – 4.6.C**). We did note a small but significant decrease in Pil1 phosphorylation in *reg1*Δ mutants, which could be explained by Glc7 being liberated from Reg1-mediated commitments, and more available to further dephosphorylate Pil1. Nonetheless, the fact that Glc7 is robustly associated with glucose metabolism via distinct mechanisms suggests there may be more complexity to the cellular response to carbon source availability.

The findings that *glc7* mutants are defective for transporter retention and recovery from starvation (**Figure 4.8.**) is consistent with dephosphorylation of Pil1 during glucose starvation being the responsible biochemical driver of this response. Cells lacking the primary Pil1 kinase Pkh2 (*pkh2*Δ) are defective in recovery from glucose starvation (Laidlaw et al., 2021), as are both phosphomimetic and phosphoablative mutants of Pil1 (**Figure 4.7.**). Collectively this implies that hyper- or hypo-phosphorylated Pil1 are not locked in a biochemical state that maximises eisosomal retention of transporters, but rather the fine-tuning of Pil1 phosphorylation is required to better harbour transporters acutely in response to nutritional stress. This mechanism could be important for understanding metabolic response of yeast to varying nutrient conditions, including pathogenic fungi (Rutherford et al., 2019). Beyond this, the role of post-translational modifications to membrane interacting proteins from other structures and compartments throughout eukaryotic cells could inform future biochemical and biophysical experimentation and understanding.

METHODS

Reagents
Supplemental Table T2 documents yeast strains used in this study.

Cell culture
Yeast cells were routinely grown in YPD (1% yeast extract, 2% peptone, 2% dextrose) or synthetic complete (SC) minimal media (2% glucose, 0.675% yeast nitrogen base without amino acids, plus appropriate amino acid dropouts for plasmid selection) (Formedium, Norfolk, UK). 2% Glucose was routinely used, where stated 4% glucose was used. Cells were subjected to glucose starvation using 2% raffinose rather than glucose as described previously (Laidlaw et al., 2021). Plasmid pCM1054 is a 2µ over-expression plasmid for Pkh2 (Jones et al., 2008) used in **Figure 4.1.C** and plasmid pCM264 is *CEN* based pPR315 expression vector containing Mup1-GFP under control of its endogenous promoter (Stringer and Piper, 2011) used in **Figure 4.3.B** and **Figure 4.8.A**.

Mating of yeast strains
Haploid BY4741 mat**a** yeast strains encoding *URA3*-GFP-tagged Pkh-family kinases (Weill et al., 2018) were mated with BY4742 Matα modified at the *NCE102* locus (*nce102-mCherry-his5*$^{+}$) on YPD rich media overnight. Single diploid colonies were isolated on media lacking uracil and histidine and confirmed by fluorescence microscopy.

Immunoblotting
Strains were grown to mid-log phase and equivalent volumes were harvested or starved for glucose with raffinose treatment prior to harvesting. Cells were treated to 0.2 N NaOH for 5 minutes prior to resuspension in lysis buffer (8 M urea, 10% glycerol, 50 mM Tris-HCl pH 6.8, 5% SDS, 0.1 % bromophenol blue and 10% 2-mercaptoethanol). SDS-PAGE was used to resolve proteins which were then transferred to a nitrocellulose membrane using the iBlot dry transfer system (Invitrogen). Ponceau S strain was used to confirm successful transfer and equal loading. Membranes were probed with antibodies stated and visualised using enhanced chemiluminescence (ECL) Super Signal Pico Plus (Thermo) and captured using a ChemiDoc Imager (Bio-Rad).

Confocal microscopy
Yeast cells expressing fluorescently tagged proteins were grown to mid-log phase (unless stated) and then visualised in minimal media at room temperature on Zeiss laser scanning confocal instruments (Zeiss LSM880 or Zeiss 980) using a 63x/1.4 objective lens. GFP was excited using a 488nm laser and emission collected from 495 to 500 nm and mCherry was excited using the 561nm laser and emission collected from 570 – 620 nm using an Airyscan (LSM880) or Airyscan 2 (LSM980) detector. Images were captured sequentially to minimise any potential bleedthrough and processed using Zeiss Zen software standard airyscan algorithm and modified for publication using ImageJ software (NIH).

Recovery Growth Assays
Equivalent volumes of cells were harvested from mid-log cultures and washed three times with raffinose media before being resuspended in raffinose media and incubated in a shaking incubator at 30°C for 2 hours. Equivalent volumes of the raffinose starved cells were harvested and washed three times with glucose media before being resuspended in 100 µl of glucose media. This was added to 3 ml of glucose media and absorbance at OD_{600} was measured to obtain time point 0. Subsequent OD_{600} measurements were taken every hour using a plate reader (Thermo Scientific) and normalised to wild-type.

Spot Growth Assays

Equivalent volumes of cells at mid-log phase were harvested and a 10-fold serial dilution was created and spotted onto indicated plates. Plates were incubated at 30 °C and images were captured at indicated time-points using a scanner (Epson).

Bioinformatic and Statistical analyses

Prediction of kinase consensus motifs in Pil1 was undertaken by submitting the Pil1 amino acid sequence to the yeast database in Netphorest (Horn et al., 2014) and experimentally determined phosphosites (Luo et al., 2008; Walther et al., 2007) were selected for analysis. The results were filtered with a minimum phosphorylation probability score of 0.1. Unpaired Student's *t*-tests were performed using GraphPad Prism v8.3.1. to compare the statistical significance between experimental conditions, with p values in **Supplemental Table T3**. An asterisk (*) is used to denote significance.

ACKNOWLEDGMENTS

We would like to thank staff at the York Bioscience Technology Facility for technical assistance. We are very grateful to Robert Farese and Tobi Walther (Harvard Medical School) for providing us with antibodies raised against Pil1, to Scott McIsaac (Calico Life Sciences, LLC) for sending the YETI yeast library used to modulate *GLC7* expression, and to Paul Pryor for access to the over-expression plasmid library used to over-express Pkh2. This research was supported by a Sir Henry Dale Research Fellowship from the Wellcome Trust and the Royal Society 204636/Z/16/Z (CM).

DECLARATION OF INTERESTS

The authors declare no competing interests.

4.3. Supplemental material

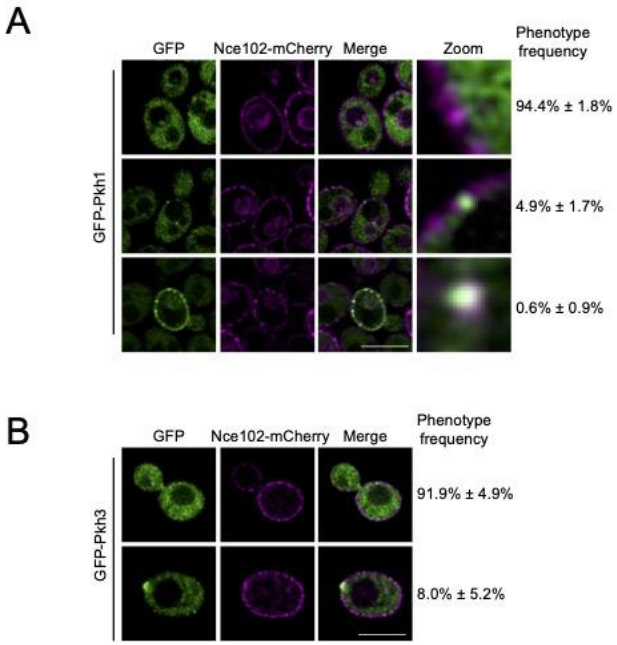

Supplemental Figure 4.1 Localisation phenotypes of Pkh kinases

A - B: Wild-type cells co-expressing Nce102-mCherry with either GFP-Pkh1 (**A**) or GFP-Pkh3 (**B**) were imaged using confocal Airyscan 2 microscopy and the frequency of each phenotype observed was quantified. Scale bar = 5µm.

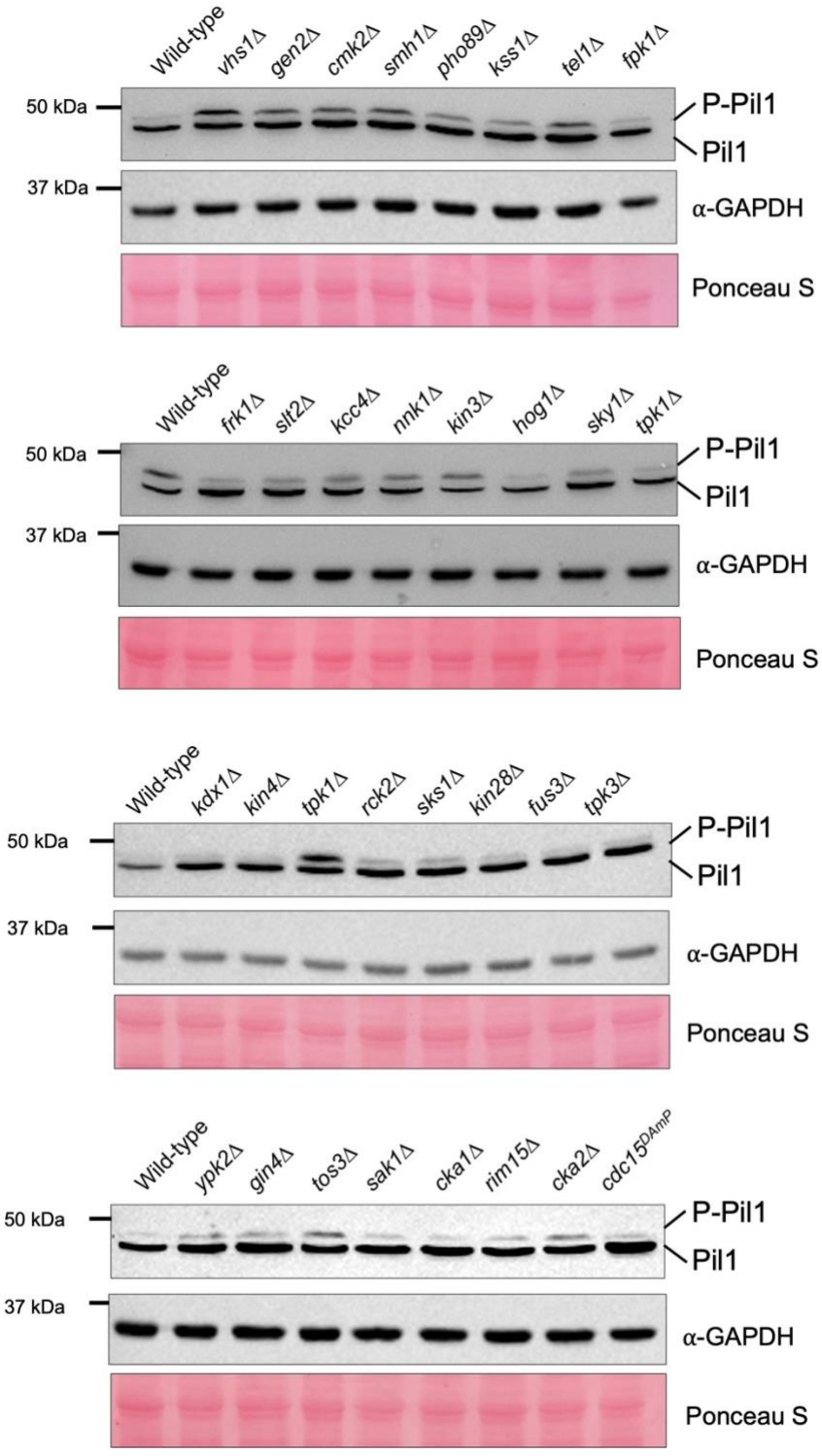

Supplemental Figure 4.2 Pil1 phosphorylation profiles in implicated kinase mutants.

Wild-type and mutant cells either lacking non-essential kinases (Δ) or with reduced expression of essential kinases (*DAmP*) were grown to mid-log phase and lysates were generated for immunoblot using α-Pil1and α-GAPDH antibodies. Ponceau S stained membranes are also provided as loading controls.

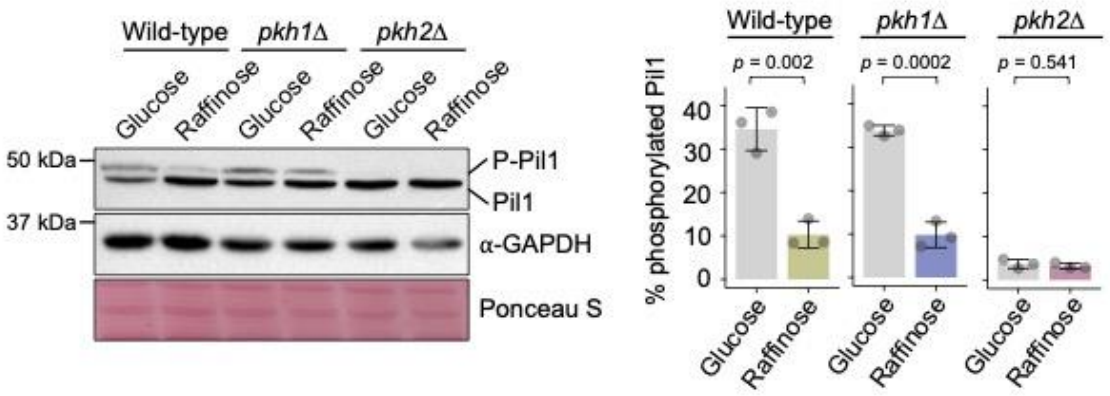

Supplemental Figure 4.3 Pil1 dephosphorylation in response to glucose starvation.

Whole cell lysates of wild-type, *pkh1*Δ and *pkh2*Δ cells in glucose media and after 10 minutes of raffinose treatment were analysed by immunoblotting using α-Pil1 and α-GAPDH antibodies; Ponceau-S stained membrane is also shown (left). The percentage of phosphorylated Pil1 from each strain was quantified (right).

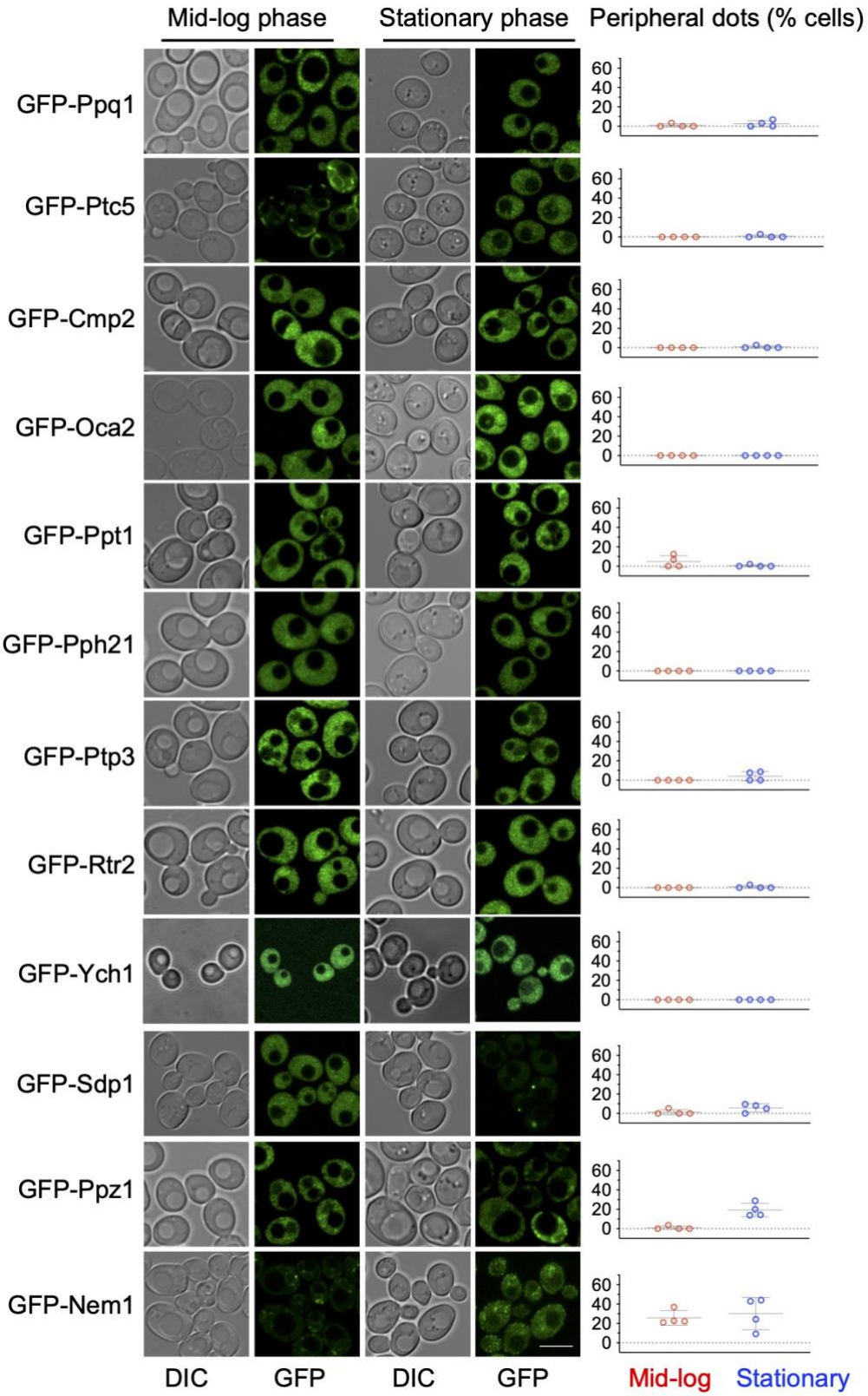

Supplemental Figure 4.4 Localisation of phosphatases at mid-log and stationary phase.

Indicated GFP tagged phosphatases were imaged using confocal Airyscan microscopy at mid-log and stationary phase. The number of peripheral dots per cell (n > 50) was quantified and the average for each experiment plotted (n = 4). Scale bar = 5µm.

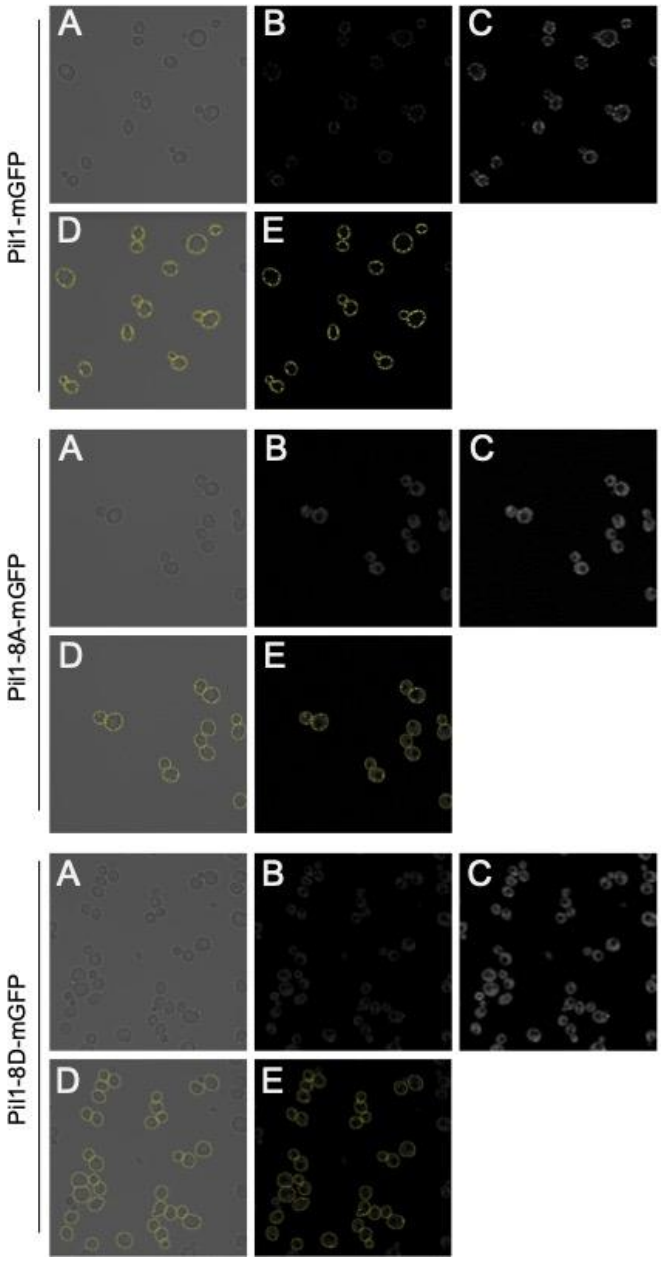

Supplemental Figure 4.5 Quantification method for Pil1 eisosome phenotypes.

Versions of Pil1 tagged with mGFP were imaged using Airyscan 2 microscopy, brightfield (A) and fluorescence channels (B) are shown. A brighter version of GFP signal is included (C) to better demonstrate localisation distribution between eisosomes and the cytoplasm but not used for quantifications. Whole cell segmentation (A) was performed using Cell Magic Wand tool and combined with eisosome-only segmentation (D) using *ostu* thresholding using ImageJ. The number of eisosomes per cell were counted and the percentage of eisosome signal compared to total cellular signal was calculated from these regions of interest from each cell.

5. Chapter V: Endosomal cargo recycling mediated by Gpa1 and Phosphatidylinositol-3-Kinase is inhibited by glucose starvation

Graphical abstract

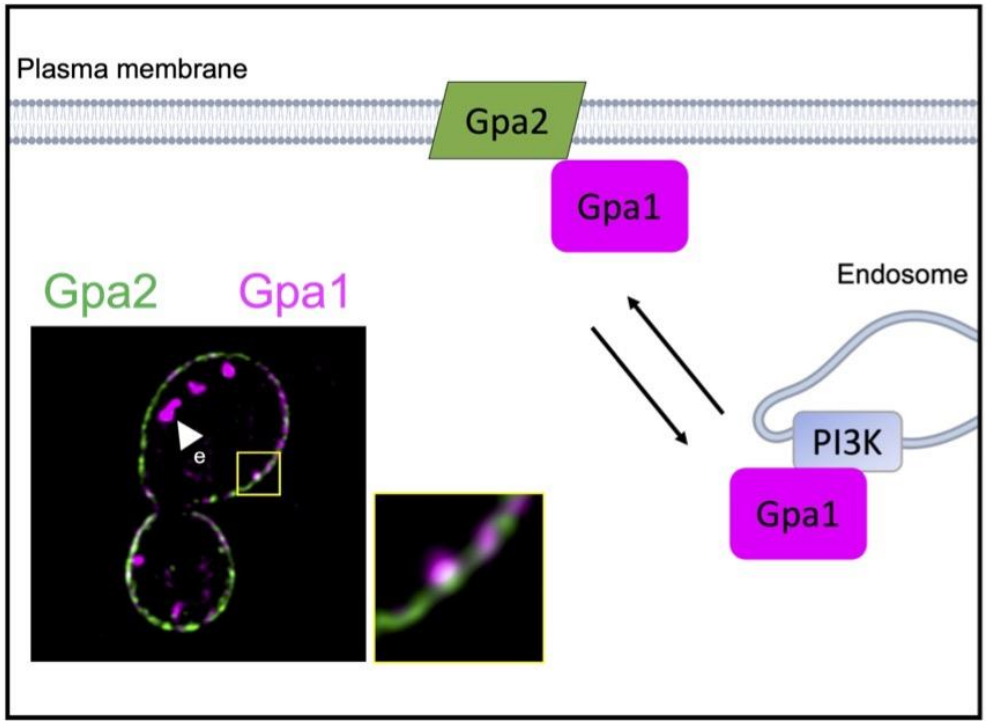

In this work we find that recycling of surface proteins from endosomes back to the plasma membrane is controlled by PI3-kinase (PI3K) and its effector protein Gpa1. In response to glucose starvation, transcript and protein levels of the recycling inhibitor Gpa2 are elevated. We demonstrate that Gpa1 localises to an endosomal population (white arrow e) in addition to a pool at the cell surface (inset, yellow box) and further show Gpa1 physically interacts with Gpa2. We propose a model whereby higher levels of Gpa2 during starvation sequesters Gpa1 at the surface, and the reduced endosomal levels effectively inhibit recycling. This serves as a protective response to starvation by downregulating surface proteins.

5.1. Introduction to project

The work presented in this chapter is conceptually related to the work discussed in Chapter III that investigated how the glucose sensitive transcription factors Mig1 and Mig2 regulate endocytosis through their regulation of clathrin adaptors *YAP1801* and *YAP1802* (Laidlaw et al., 2021). The initial work demonstrated an increase in endocytosis following overexpression of yeast AP180s from a plasmid. I worked with Chris MacDonald to repeat these observations for the surface cargo Mup1-GFP in experiments that also showed that over-expression of AP180s had no noticeable effect on the steady state levels of a recycling reporter that was dedicated to endosome to surface recycling (**Figure 5.1. and 5.1. B**). This was initially surprising, as work from Chris and Dr. Kamilla Laidlaw in the lab had clearly demonstrated that endosomal recycling was inhibited in response to glucose starvation. As increased endocytosis could not explain these effects, we sought an alternative mechanism that reduces recycling back to the surface.

A previous genetic screen for recycling machinery had implicated Gpa1 in recycling back to the surface (MacDonald and Piper, 2017). Chris and Daniel Bisinski, with the help of Dr. Sveta Shaskova, had previously performed a bioinformatic approach to identify target genes likely to be repressed by Mig1 (including the discovery of AP180s). This work identified *GPA2* as a candidate, which Daniel confirmed is repressed by Mig1 in response to glucose. As other work had shown Gpa1 and Gpa2 might physically interact, we pursued the hypothesis that higher levels of Gpa2 following glucose starvation served to inhibit recycling via Gpa1.

G proteins (G alpha, G beta and G gamma) interact with membrane spanning G protein coupled receptors (GPCRs) and their interaction with GDP and GTP causes conformational changes and transduces signals through the cell (McCudden et al., 2005). Both Gpa1 and Gpa2 were both identified through being homologs to mammalian G-proteins (Miyajima et al., 1987; Nakafuku et al., 1988). Gpa1 was established to interact with G proteins Ste4 and Ste18 to mediate the mating response (Blumer and Thorner, 1990) and cells lacking GPA2 were found to have defects in glucose-induced cAMP signalling (Colombo et al., 1998). As well as its role with Ste4-Ste18, the G alpha subunit Gpa1 interacts with PI3K subunits Vps34-Vps15 at the endosome and this interaction was found to mediate pheromone signalling (Slessareva et al., 2006). Studies have used a GTPase-deficient mutant of Gpa1 ($Gpa1^{Q323L}$) have been used to understand the functionality of Gpa1 (Apanovitch et al., 1998; Guo et al., 2003). Vps34 is a 95 kDa protein first identified to function in the vacuolar system (Herman and Emr, 1990), that is a PI3-Kinase that phosphorylates PIs at the D-3 position (Auger et al., 1989). In these early studies Vps34 was found to require Vps15 to form a Vps15-Vps34 complex to allow delivery of proteins to the vacuole (Budovskaya et al., 2002; Stack et al., 1995). Both Vps15 and Vps34 were first identified in the screen looking for mutants the mislocalised the vacuolar protein CPY (Robinson et al., 1988).

We submitted this paper to Molecular Biology of the Cell and received constructive reviews, but there were a lot of reviewer requested experiments to bolster the model. As the co-first author was on furlough and long-term sick leave at this time, I took on the bulk of these experiments.

It was suggested that our cells interpretation of experiments using yeast lacking Gpa1 (*gpa1*∆) were flawed as Gpa1 is an essential gene, the strain should not be viable as it has

previously been found to be essential for cell growth, with its deletion leading to mating-factor-mediated cell-cycle arrest (Miyajima et al., 1987). As this early work also demonstrated that *gpa1* null mutants are prone to suppressors that allow growth we assumed our observations could be attributed to the lack of *GPA1* but admittedly couldn't prove that. Initially I genotyped wild-type cells and *gpa1*∆ mutants from different backgrounds. I then set about learning how to prepare genomic DNA from these cells for genome sequencing, with the help of Dr Sally James. When we received the raw data files back from the sequencing reactions, I collaborated with Dr Sophia Ahmed who trained me in using IGV viewer to analyse the sequencing data. The work with Sophia allowed me to identify and prioritise mutations specific to our *gpa1*∆ cells, whilst also confirming the entire *GPA1* locus was absent. Initial analysis showed there were a lot of mutations between strains, but when I refined the search to only include mutations that were in Open Reading Frames (ORFs) including 1000bp up/down stream there was much fewer. Furthermore, the vast majority of these were either silent mutations or encoded very subtle amino acid changes (**Figure 5.3.**). The only significantly severe mutation was a premature stop codon introduced to a Gpa1 regulator termed Ste11, of which, mutations in Ste11 had previously been shown to supress the lethality of loss of Gpa1 (Nakayama et al., 1988). Whilst this effort did not really alter our model, it did allow us to fully back up all the observations in *gpa1*∆ cells, whilst providing a great training opportunity for me, which could be used in many other scenarios going forward.

Our model predicted that in glucose replete conditions, Gpa1 functions at the endosome with the PI3K subunits Vps34/Vps15 to generate phosphatidylinositol-3-phosphate and thus promoting the recycling of cargo to the plasma membrane. Under glucose starvation conditions, where recycling is reduced, Gpa1 is sequestered away from the endosome through its interaction with Gpa2 at the plasma membrane. Although we showed Gpa1-Gpa2 colocalization by microscopy and Gpa1 and Gpa2 had been found to interact from high-throughput mass spectrometry data (Ho et al., 2002) one weakness in our study that reviewers pointed out was that we do not formally show an interaction. I began optimising a protocol for a co-immunoprecipitation where my aim was to use GFP nanobodies bound to beads to pull out Gpa2-GFP and then use a mCherry antibody to identify Gpa1-mCherry. The co-immunoprecipitation was unsuccessful because we were unable to lyse cells, despite attempting a large number of conditions, with a large amount of stable Gpa1 or Gpa2 under native conditions. Lysing yeast cells is difficult due to their cell walls, amending my protocol and using techniques such as cryogrinding might have helped (Phillips et al., 2021).

We had visualised Gpa1-mCherry and Gpa2-GFP by microscopy. One reviewer had made a good point about testing the fluorescently tagged proteins for functionality. Gpa1 is part of the yeast pheromone response pathway (Bardwell, 2005). I was familiar with yeast mating assays after optimising and performing a mating assay on hits from my genetic screen (**Chapter II**, (Paine et al., 2021)). I performed a halo-mating assay, demonstrating that the Gpa1-mCherry construct could rescue the phenotype seen in the *gpa1*∆ cells (**Supplemental Figure S5.1.**), further supporting the notion that these mutants are defective in Gpa1-related processes whilst being viable. Whilst Chris confirmed the functionality of Gpa2 fluorescently tagged protein through the small cell size phenotype seen in *gpa2*∆ cells (**Supplemental Figure S5.4.**).

With the added reassurance that our fluorescently tagged proteins were functional as well as confirming their localisation (**Figure 5.10.A**) we set about exploring microscopical ways of identifying interactions. In collaboration with staff at the technology facility we developed

an acceptor-bleach Förster resonance energy transfer (FRET) protocol and were able to demonstrate an interaction between these proteins (**Figure 5.10.F- G**).

This was a collaborative project with various people bringing their expertise. We received reviewers' comments at a time when due to the ongoing pandemic I was the only lab member able to work in the lab. Therefore, my experimental contribution is scattered throughout the paper as well as being concentrated in the superresolution microscopy and FRET data. We began writing up this paper February 2021 and this gave me an opportunity to be involved with the writing process from the initial draft to the accepted article. This increased my confidence whilst preparing me to play bigger roles in writing for my sole first author paper that was published later that year (Paine et al., 2021) and my first author paper that is currently under review (**Chapter IV**). The Gpa1 paper was accepted for publication by MBoC in March 2022. Having demonstrated that glucose starvation specifically inhibits recycling, this nicely complements the story from Chapter III, that showed endocytosis is upregulated in glucose starvation conditions. These complementary mechanisms combine to maximise endosomal retention and degradation of surface proteins in response to starvation conditions.

5.1.1. Aims of chapter

This chapter presents a model as to how recycling of surface proteins are regulated in glucose replete and glucose starvation conditions. The model presents both evidence of the role Gpa1 plays at endosomes with Vps34-Vps15 and evidence of its interaction with Gpa2 at the plasma membrane.

5.1.2. Declaration of authorship

The work presented in this chapter was a collaborative project.
Experimental work carried out by K. M. Paine:
Figure 5.1.A and B
Figure 5.3.
Figure 5.4.B, 5.4.E and 5.4.F
Figure 5.10.
Supplemental Figure S5.1.
Supplemental Figure S5.8.

5.1.2.1. Author contributions

Conceptualization: C.M.; Methodology: C.M., G.C., K.H., S.A., P.J.O.; Validation: K.M.E.L., **K.M.P.**, D.D.B., C.M.; Formal analysis: K.M.E.L., D.D.B., **K.M.P.**, C.M.; Investigation: K.M.E.L., **K.M.P.**, D.D.B., G.C., S.J., C.M.; Data curation: C.M.; Writing - original draft: C.M.; Writing - review & editing: K.M.E.L., **K.M.P.**, C.M.; Visualization: K.M.E.L., D.D.B., **K.M.P.**, C.M.; Supervision: C.M.; Project administration: C.M.; Funding acquisition: P.J.O., C.M.;

5.1.2.2. History of manuscript

Uploaded to bioRxiv: 2nd April 2021
Submitted to Molecular Biology of the Cell: 5th April 2021
Published at Molecular Biology of the Cell: 17th March 2022
DOI: 10.1091/mbc.E21-04-0163
PMID: 35080991

5.2. Endosomal cargo recycling mediated by Gpa1 and Phosphatidylinositol-3-Kinase is inhibited by glucose starvation

Kamilla ME. Laidlaw*[1], Katherine M. Paine*[1], Daniel D. Bisinski[1,2], Grant Calder[3], Karen Hogg[3], Sophia Ahmed[3], Sally James[3], Peter J. O'Toole[3], Chris MacDonald[1,4]

* Equal contribution

[1] York Biomedical Research Institute and Department of Biology, University of York, York, UK

[2] Present address: Department of Biology & Chemistry, University of Osnabrück, Osnabrück, Germany

[3] Bioscience Technology Facility, Department of Biology, University of York, UK

[4] Correspondence: Email: chris.macdonald@york.ac.uk Tel: +44 (0) 1904 328 609

ABSTRACT

Cell surface protein trafficking is regulated in response to nutrient availability, with multiple pathways directing surface membrane proteins to the lysosome for degradation in response to suboptimal extracellular nutrients. Internalised protein and lipid cargoes recycle back to the surface efficiently in glucose replete conditions, but this trafficking is attenuated following glucose starvation. We find cells with either reduced or hyperactive phosphatidylinositol 3-kinase (PI3K) activity are defective for recycling. Furthermore, we find the yeast Gα subunit Gpa1, an endosomal PI3K effector, is required for surface recycling of cargoes. Following glucose starvation, mRNA and protein levels of a distinct Gα subunit Gpa2 are elevated following nuclear translocation of Mig1, which inhibits recycling of various cargoes. As Gpa1 and Gpa2 interact at the surface where Gpa2 concentrates during glucose starvation, we propose this disrupts PI3K activity required for recycling, potentially diverting Gpa1 to the surface and interfering with its endosomal role in recycling. In support of this model, glucose starvation and over-expression of Gpa2 alters PI3K endosomal phosphoinositide production. Glucose deprivation therefore triggers a survival mechanism to increase retention of surface cargoes in endosomes and promote their lysosomal degradation.

INTRODUCTION

The surface localisation and activity of plasma membrane (PM) proteins can be regulated by the balance of action between endocytic trafficking pathways. Clathrin dependent and independent mechanisms internalise proteins from the PM, which then transit through different compartments *en route* to the lysosome for degradation. Various recycling mechanisms transport cargoes back to the surface, providing multiple regulatable steps to fine tune the surface protein environment in response to external conditions. Yeast has been a useful model organism to uncover conserved trafficking mechanisms of surface proteins. Upon internalisation from the yeast PM, surface cargoes can be sorted to the lysosome-like vacuole, in a process that involves cargo ubiquitination, mediated by E1-E2-E3 enzyme cascade in collaboration with competing trafficking adaptors (MacDonald et al., 2020; Sardana and Emr, 2021). Ubiquitinated cargoes are recognised at multivesicular bodies (MVBs) by the Endosomal Sorting Complex Required for Transport (ESCRT) apparatus, which also package cargo destined for degradation into intraluminal vesicles (Laidlaw and MacDonald, 2018). Proteins that are not targeted for degradation can recycle back to the surface, including a retrograde route that traffics material to the surface via the *trans*-Golgi network (TGN) using dedicated machineries that interact with recycled cargoes(Chen et al., 2019). Recycling in animal cells can also occur directly from early endosomes or indirectly, first traversing defined recycling endosomes (MacDonald and Piper, 2016). Endosomal organisation and recycling mechanisms in yeast are less clear (Ma and Burd, 2020), but work using the yeast exocytic v-SNARE protein Snc1 revealed multiple endosomal transport steps regulate Snc1 trafficking back to the PM (Best et al., 2020; Ma and Burd, 2019; Ma et al., 2017). Although retrograde recycling is perturbed by deubiquitination (Xu et al., 2017), recycling of some nutrient transporters is triggered by deubiquitination (Laidlaw et al., 2021; MacDonald and Piper, 2017). Genetic dissection of this latter pathway implies recycling is controlled at transcriptional and metabolic levels (Amoiradaki et al., 2021; MacDonald and Piper, 2017), suggesting early endocytic trafficking decisions contribute to the eventual downregulation of surface cargoes in response to nutritional cues.

During periods of nutritional stress, multiple mechanisms involving surface cargoes and endocytic pathways are modulated to promote proliferation, particularly in cancer cells (Finicle et al., 2018; Selwan et al., 2016). Recycling internalised cargoes back to the surface can promote anabolic processes. During starvation, when some such processes are not required, reduced recycling can route surface cargoes to the lysosomal (vacuolar in yeast) degradation pathway instead, to promote catabolism. Conceptually, these pathways can be modulated to drive growth/proliferation appropriate to extracellular nutrient availability. One such example has been elucidated in yeast responding to nitrogen starvation, where increased trafficking to the vacuole is achieved through the amino acid sensing TORC1 complex, which activates Rsp5-adaptors via the Npr1 kinase and promotes cargo ubiquitination and degradation (MacGurn et al., 2011). The Rag GTPases integrate with nutrient sensing and TORC1 activity via the EGO complex (Binda et al., 2009; Bonfils et al., 2012; Péli-Gulli et al., 2015), but in addition regulate recycling via endosomally-localised Ltv1 in response to extracellular Leucine (MacDonald and Piper, 2017). Glucose starvation may also trigger a similar dual regulation of recycling and degradation pathways in yeast, where many metabolic pathways are evolutionarily conserved (Santangelo, 2006). Although most transcriptional changes elucidated in response to suboptimal glucose availability involve

alternative carbon pathways, we recently revealed a response that increases trafficking from the surface to the lysosome in response to glucose starvation (Laidlaw et al., 2021). Furthermore, recycling back to the surface is reduced when cells are exposed to media lacking sugar (Lang et al., 2014), but the molecular players involved in this response are not fully established.

In high glucose levels, Snf1 (yeast AMP-activated protein kinase, AMPK (Hong et al., 2003)) is inactivated primarily through its dephosphorylation by Reg1-Glc7(Sanz et al., 2000; Tu and Carlson, 1994). Whilst Snf1 can influence endosomal trafficking during glucose changes in yeast independently (O'Donnell et al., 2015), one key downstream consequence of glucose starvation involves Snf1 activation and regulation of the Mig1 transcriptional repressor(Johnston et al., 1994; Treitel et al., 1998). Mig1 is a zinc finger transcription factor that mediates glucose repression in yeast cells(Lundin et al., 1994; Nehlin and Ronne, 1990) and in response activates alternative metabolic pathways (Schüller, 2003). In addition to this, Mig1 influences membrane trafficking machinery through its repression of clathrin adaptor genes *YAP1801* and *YAP1802* under glucose replete conditions that stabilise endocytosis levels (Laidlaw et al., 2021). Furthermore, the reduced recycling following glucose starvation (Lang et al., 2014) can be bypassed by enforcing cargo ubiquitination in the endomembrane system upstream of MVB sorting (Buelto et al., 2020). This suggests that both the ubiquitin-mediated degradation pathway (MacDonald and Piper, 2016), and the counteracting recycling pathway induced following cargo deubiquitination (MacDonald et al., 2012a; MacDonald et al., 2015a) are both regulated in response to glucose starvation to collectively reduce surface activity and increased vacuolar degradation.

A genetic screen for recycling machinery identified several candidates for glucose-mediated control, including the G-protein coupled receptor (GPCR) Gpr1 and downstream GTPase Ras2 (MacDonald and Piper, 2017). The Gα subunit Gpa2, which is activated Gpr1, initiates cAMP signalling in response to glucose through recruiting Ras-GTP to the PM (Broggi et al., 2013; Colombo et al., 1998). This cAMP signalling cascade in response to glucose leads to changes in a variety of different targets through protein kinase A (PKA) (Kraakman et al., 1999; Thevelein, 1994). The screen for recycling machinery also implicated a distinct Gα subunit, Gpa1 in recycling (MacDonald and Piper, 2017). Gpa1 is the Gα subunit of a heterotrimeric G protein complex also comprised of Gβ and Gγ subunits Ste4p and Ste18p, that functions in the pheromone response pathway (Dietzel and Kurjan, 1987; Miyajima et al., 1987; Whiteway et al., 1989). Just as Gpa2 cannot functionally couple with distinct mating GPCRs (Blumer and Thorner, 1990) it is thought that the distinct the Gα subunit Gpa1 does not regulate Gpr1 directly. In addition to playing a role in pheromone response at the PM, Gpa1 interacts with the yeast phosphatidylinositol 3-kinase (Vps15 and Vps34) at endosomes (Heenan et al., 2009; Slessareva et al., 2006). The phosphorylation status of a variety of different phosphoinositide (PI) species regulates membrane trafficking pathways (De Camilli et al., 1996). Phosphoinositide 3-kinases (PI3Ks) are therefore key regulatory proteins known to control a variety of different membrane trafficking steps (Lindmo and Stenmark, 2006). Vps34, in complex with Vps15, was first identified in yeast as being required for the post-Golgi trafficking of biosynthetic enzymes to the vacuole (Herman and Emr, 1990; Schu et al., 1993; Stack et al., 1993) and generation of phosphatidylinositol 3-phosphates (PtdIns3P) through Vps34 activity is required for efficient retrograde recycling from the endosome to the late-Golgi (Burda et al., 2002).

In this study, we use both lipid and protein recycling reporters to show that glucose starvation inhibits endosomal recycling of cargo back to the surface. We show the Gα subunit Gpa1 and PI3K, and their functional association, are required for efficient

recycling in glucose replete conditions. During glucose starvation, we document Mig1-dependent elevation of Gpa2, which concentrates at the PM where it physically interacts with Gpa1. Increased levels of Gpa2 observed in glucose starved cells impairs production of PtdIns3P and results in recycling defects of a wide range of cargoes. We propose a role for Gpa2 as a glucose responsive recycling inhibitor, potentially by commandeering Gpa1 from endosomal PI3K, and ultimately serving to increases endosomal retention and vacuolar degradation of surface cargoes, as a survival response to glucose starvation.

RESULTS

Glucose starvation inhibits surface recycling

Previous work has shown that in response to glucose starvation, the yeast AP180 clathrin adaptors are transcriptionally upregulated with a concurrent increase in endocytosis (Laidlaw et al., 2021). Under basal conditions in media lacking methionine, the methionine transporter Mup1 tagged with GFP localises to the plasma membrane (PM), but much of this signal is redistributed to endosomes and the vacuole upon plasmid over-expression of mCherry-tagged AP180s: Yap1801-Cherry or Yap1802-mCherry (**Figure 5.1.A**). In contrast, a recycling reporter based on the fusion of the G-protein couple receptor (GPCR) Ste3 tagged with GFP and the catalytic domain of a deubiquitinating enzyme (MacDonald and Piper, 2017; Stringer and Piper, 2011), showed no increase in endosomal localisation following over-expression of yeast AP180s (**Figure 5.1.B**). This correlates with observations that Ste3-GFP-DUb does not accumulate when endocytosis rates are elevated by the addition of **a**-factor or at elevated temperature (MacDonald and Piper, 2017). We conclude that although different manipulations increase the rate of endocytosis, the deubiquitination-driven recycling of Ste3-GFP-DUb predominates to maintain an exclusive steady state localisation at the PM. Having established that Ste3-GFP-DUb primarily reports on cell surface recycling, we used this reporter to test whether glucose starvation impacts recycling specifically. Treating the cells in media completely lacking sugar, or by substituting glucose for the alternative carbon course raffinose, results in an accumulation of Ste3-GFP-DUb in intracellular endosomes (**Figure 5.1.C**). A distinct recycling assay, which measures recycling by efflux of endocytosed fluorescent FM4-64 (Wiederkehr et al., 2000), has previously shown carbon source removal inhibits recycling (Lang et al., 2014). Similarly, we find shifting cells to media lacking sugar or supplemented with raffinose also results in robust inhibition of recycling (**Figure 5.1.D**). Therefore, although internalisation from the PM increases following glucose starvation (Laidlaw et al., 2021), two dedicated recycling reporters show glucose starvation also triggers a reduction in protein and lipid traffic from endosomes back to the PM. We propose increased internalisation and decreased recycling during glucose starvation cooperate to drive vacuolar degradation of cargoes *en masse* in response to nutritional stress. We set out to explain this recycling response at a molecular level. As both glucose removal and raffinose exhibit defects in recycling, we use raffinose substitution to deprive cells of glucose in downstream experiments, as it cannot be readily metabolised (de la Fuente and Sols, 1962) and therefore in the time-frame we perform experiments provides a glucose starvation condition.

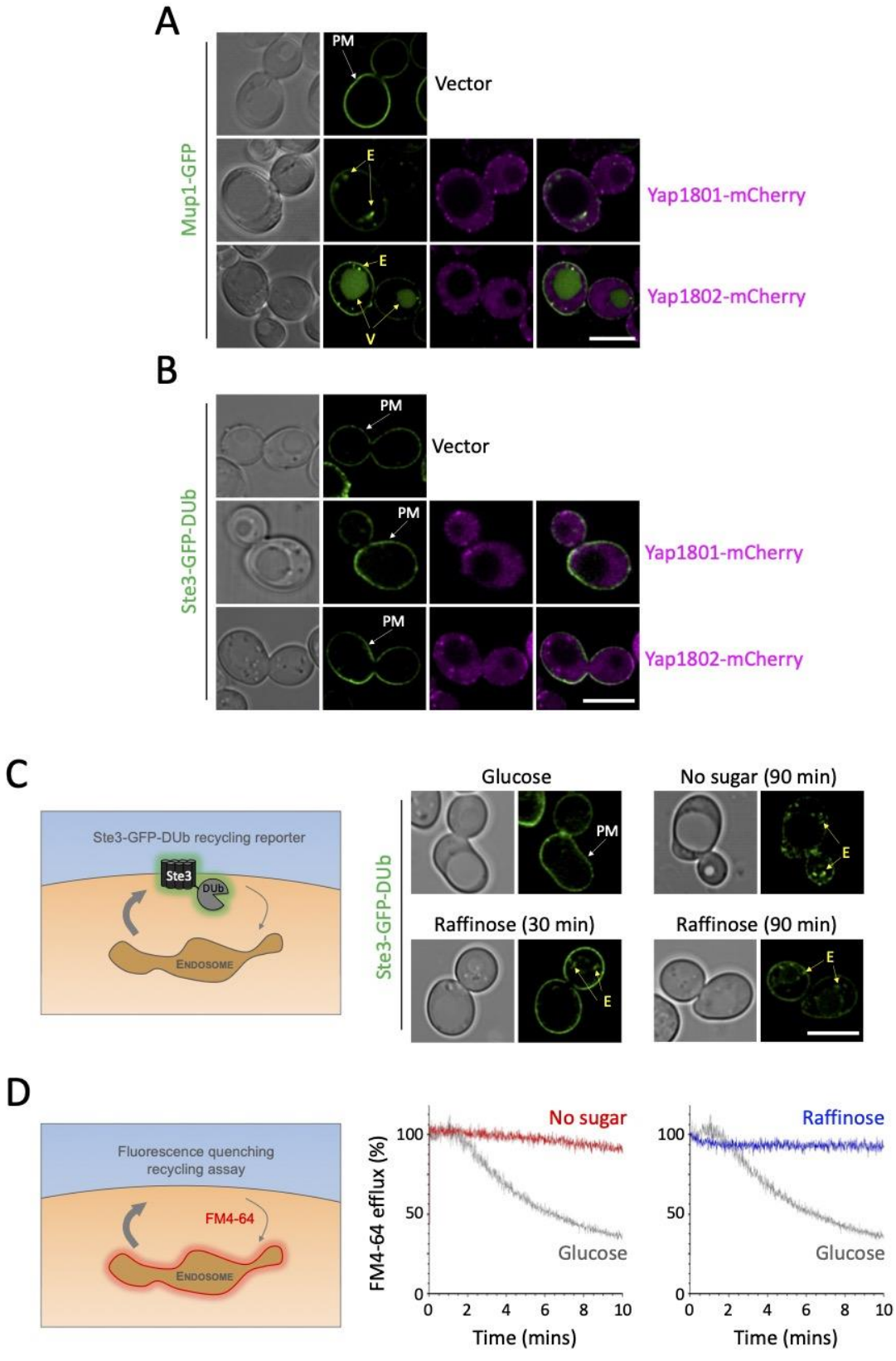
A
Mup1-GFP
PM
Vector
E
Yap1801-mCherry
E
V
Yap1802-mCherry
B
Ste3-GFP-DUb
PM
Vector
PM
Yap1801-mCherry
PM
Yap1802-mCherry
C
Ste3-GFP-DUb recycling reporter
Ste3
DUb
ENDOSOME
Ste3-GFP-DUb
Glucose
PM
No sugar (90 min)
E
Raffinose (30 min)
E
Raffinose (90 min)
E
D
Fluorescence quenching recycling assay
FM4-64
ENDOSOME
FM4-64 efflux (%)
No sugar
Glucose
Time (mins)
Raffinose
Glucose
Time (mins)

Figure 5. 1 Glucose starvation specifically inhibits recycling

A) Confocal imaging of cells expressing Mup1-GFP under control of its endogenous promoter co-expressed with Yap1801-mCherry or Yap1802-mCherry expressed from the *CUP1* promoter through addition of 50 µM copper chloride for 2 hours. A vector control exposed to copper was also included. **B)** Cells stably integrated with Ste3-GFP-DUb were exposed to 2 hours copper chloride to induce expression of mCherry tagged versions of Yap1801 and Yap1802, before confocal microscopy. **C)** Cells expressing Ste3-GFP-DUb from the *STE3* promoter were grown under indicated media conditions prior to confocal microscopy. **D)** Wild-type cells loaded with rich media containing 40 µM FM4-64 for 8-minutes before washing and dye efflux measured over time by flow cytometry. Control cells grown in glucose media were compared with 30-minute prior incubation with media lacking any carbon source (red) or media supplemented with raffinose (blue). White arrows indicate exclusive plasma membrane (PM) signal and yellow arrows indicate endosome (E) or vacuole (V) localisations. Scale bar, 5 µm.

Gpa1-PI3K is required for surface recycling

A previous genetic screen for novel recycling machinery, based on the mis-localisation of Ste3-GFP-DUb, (MacDonald et al., 2017) identified 89 candidate factors as required for recycling (**Figure 5.2.A**). To identify any proteins from this list that might inhibit recycling during glucose starvation (**Figure 5.1.**), a network analysis of all 89 proteins was performed based on both physical and functional associations to reveal a small cluster, containing the glucose regulated receptor Gpr1, and associated factors Ras2 and Gpa1 (**Figure 5.2.B**). We stably integrated the Ste3-GFP-DUb reporter into strains lacking each factor (*gpa1*Δ, *ras2*Δ, and *gpr1*Δ) and confirmed they exhibit defects in recycling (**Figure 5.2.C, 5.2.D**). Although deletion of these genes results in a pronounced mis-localisation phenotype, we also performed flow cytometry experiments to confirm that total levels of Ste3-GFP-DUb were not elevated to account for additional signal in intracellular compartments (**Figure 5.2.E**). Although all three candidates are known to localise and function at the PM, we focussed on the Gα subunit Gpa1 for this study, as it has also been shown to localise to endosomes and activate PI3K (Slessareva et al., 2006), which is involved in various endomembrane trafficking events (Lindmo and Stenmark, 2006; Reidick et al., 2017). We first considered the G-protein subunit Gpa1 might specifically perturb the Ste-GFP-DUb reporter, as it's based on the G-protein coupled receptor Ste3. However, we found general recycling of lipids, as assessed by FM4-64 efflux, was also defective in *gpa1*Δ mutants (**Figure 5.2.F**). Furthermore, trafficking of endogenous cargoes to the PM was also perturbed in *gpa1*Δ cells. We found the methionine transporter Mup1 tagged with GFP, which localises exclusively to the PM in wild-type cells, is shifted to endosomes and the vacuole in *gpa1*Δ mutants (**Figure 5.2.G**). Similarly, the PM signal of the uracil transporter Fur4, tagged with mNeonGreen (mNG) (Paine et al., 2021), or Ste3 tagged with GFP (but lacking a deubiquitinating enzyme fusion), was sorted to the vacuole in *gpa1*Δ cells. These defects in lipid and protein trafficking are consistent with a role for Gpa1 in surface recycling.

Constitutive signalling in haploid *gpa1*Δ mutants is lethal (Miyajima et al., 1987) so we first confirmed *GPA1* deletion in both our Mat**a** and Matα backgrounds by genotyping (**Figure 5.3.A**) and genome sequencing (**Figure 5.3.B**). We surveyed all genetic mutations identified from both *gpa1*Δ mutants and wild-type cells and found most variants were far from ORFs, so unlikely to affect expression, or missense variants unlikely to alter function. Gene ontology of mutated genes revealed a premature stop codon in the *STE11* gene of Mat**a** *gpa1*Δ cells (**Figure 5.3.C, 5.3.D**), which would perturb downstream signalling and suppress lethality (Nakayama et al., 1988). Explanation of suppression in Matα mutants is less clear but might be due to a substitution in the downstream mitogen activated protein (MAP) kinase kinase (MAPKK) *MKK1*. This alone, or in combination with a parental strain point mutation in *SST2*, which encodes a negative regulator of Gpa1-signalling (Apanovitch et al., 1998; Dohlman et al., 1996), might explain viability of *gpa1*Δ mutants.

To test if these Gpa1 effects are mediated through PI3K, we analysed recycling in cells lacking PI3K subunits (*vps15*Δ and *vps34*Δ), which both exhibit morphological defects of the vacuolar / endolysosomal system (**Figure 5.4.A**). Vacuole morphology following FM4-64 staining was difficult to resolve by conventional confocal microscopy but Airyscan microscopy revealed layers of small vacuolar-like structures in both *vps15*Δ and *vps34*Δ cells. Both *vps15*Δ and *vps34*Δ mutants were confirmed to have a growth defect at 30ºC (**Figure 5.4.B**) before we revealed that *vps15*Δ and *vps34*Δ cells are severely defective in their ability to recycle internalised FM4-64 dye (**Figure 5.4.C**). To further corroborate this model, we employed a hyperactive version of Vps34, termed $Vps34^{EDC}$ (harbouring R283E, A287D, Y501C point mutations) that was recently used to

show PtdIns3P production is rate limiting for some, but not all, membrane trafficking pathways (Steinfeld et al., 2021). We found that unlike deletion of PI3K, increased expression of $Vps34^{WT}$ or $Vps34^{EDC}$ had no effect on growth at 30ºC (**Figure 5.4.B**). However, expressing hyperactive $Vps34^{EDC}$ was sufficient to perturb efficient recycling of FM4-64 (**Figure 5.4.D**) and Ste3-GFP-DUb (**Figure 5.4.E**), suggesting elevated PtdIns3P production deregulates recycling, but to a lesser degree than in cells lacking PI3K activity. To test if a functional connection between Gpa1 and PI3K is required for efficient recycling, we created an R1261A mutation in endogenous Vps15 (**Figure 5.4.F, 5.4.G**), which disrupts interaction with Gpa1 (Heenan et al., 2009), and found this was sufficient to inhibit efficient FM4-64 recycling (**Figure 5.4.H**) .This supports the notion that yeast PI3K in collaboration with Gpa1 is responsible for recycling from endosomes to the surface.

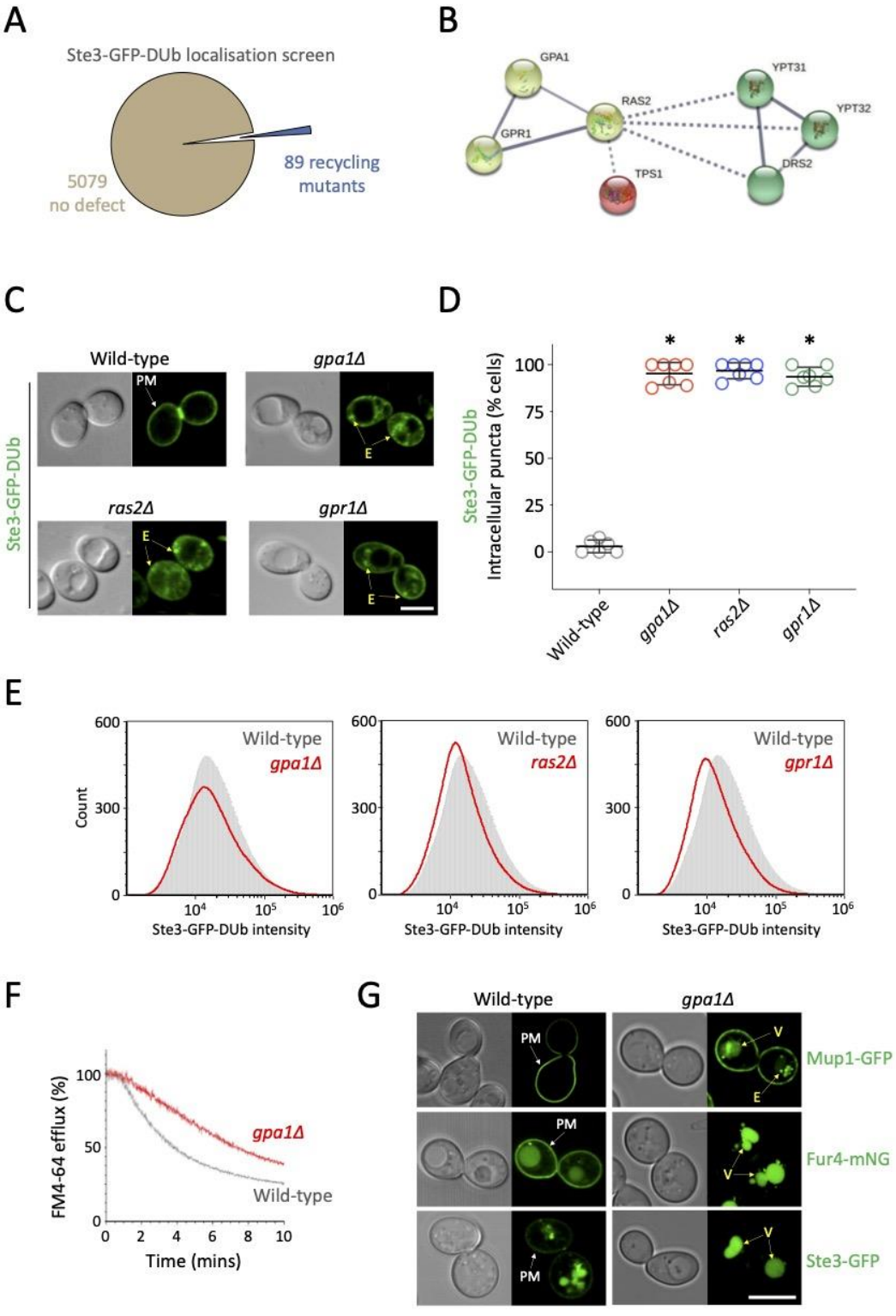
A
Ste3-GFP-DUb localisation screen
5079
no defect
89 recycling
mutants
B
GPA1
YPT31
RAS2
YPT32
GPR1
DRS2
TPS1
C
Wild-type
gpa1Δ
ras2Δ
gpr1Δ
Ste3-GFP-DUb
PM
E
D
Ste3-GFP-DUb
Intracellular puncta (% cells)
100
75
50
25
0
*
Wild-type
gpa1Δ
ras2Δ
gpr1Δ
E
Wild-type
gpa1Δ
ras2Δ
gpr1Δ
Count
600
300
0
10^4
10^5
10^6
Ste3-GFP-DUb intensity
F
FM4-64 efflux (%)
100
50
0
gpa1Δ
Wild-type
0
2
4
6
8
10
Time (mins)
G
Wild-type
gpa1Δ
PM
V
E
Mup1-GFP
Fur4-mNG
Ste3-GFP

Figure 5. 2 Gpa1 is required for protein and lipid recycling to the surface

A) Pie chart representing gene deletions that have no impact on Ste3-GFP-DUb recycling (brown), or those that accumulate the reporter in endosomes (blue). **B)** String pathway analysis was performed on all 89 recycling factor candidates (minimum interaction score = high confidence, 0.700) before application of a k-means clustering algorithm to define 9 groups. A small cluster connected by solid lines, representing strongly supported functional and physical associations (yellow) is shown alongside associations with distinct clusters (red and green) shown by broken lines. **C)** Quantification of Ste3-GFP-DUb intracellular localisations calculated as an average of population (n=3) from WT = 90; *gpa1*Δ = 75; *ras2*Δ = 94; and *gpr1*Δ = 70 cells. **D)** Ste3-GFP-DUb localisation recorded in indicated cells by confocal microscopy. **E)** Flow cytometry was used to measure Ste3-GFP-DUb fluorescence from approximately 75,000 cells of each indicated mutant (red) and compared with expression in wild-type cells (grey overlay). **F)** Wild-type (grey) or *gpa1*Δ (red) cells were loaded with FM4-64 for 8-minutes before dye efflux was assessed by flow cytometry over 10-minutes. **G)** Wild-type and *gpa1*Δ cells expressing Mup1-GFP, Fur4-mNG or Ste3-GFP were grown to log phase before confocal microscopy to determine localisation. White arrows (exclusive PM) and yellow arrows (vacuole; V) are indicated. Scale bar, 5 µm.

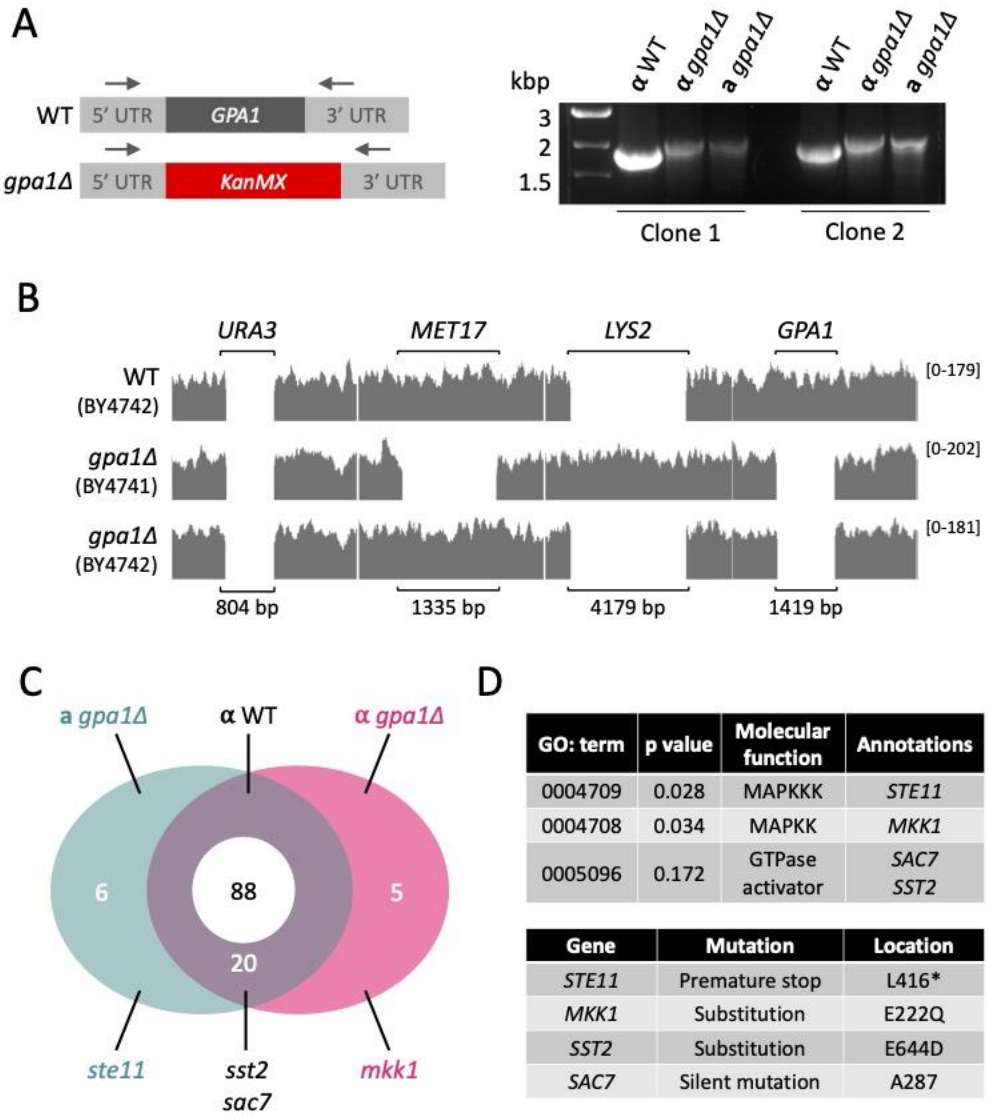

GO: term	p value	Molecular function	Annotations
0004709	0.028	MAPKKK	*STE11*
0004708	0.034	MAPKK	*MKK1*
0005096	0.172	GTPase activator	*SAC7* *SST2*

Gene	Mutation	Location
STE11	Premature stop	L416*
MKK1	Substitution	E222Q
SST2	Substitution	E644D
SAC7	Silent mutation	A287

Figure 5. 3 Genetic validation of viable *gpa1*Δ mutant yeast strains

A) Schematic depicting region of the genome that was PCR amplified using oligos in 5' and 3' UTRs of *GPA1* (Left). gDNA was isolated from Mat**α** (wild-type and *gpa1*Δ) and Mat**a** *gpa1*Δ cells and used for PCR confirmation of the *KanMX* deletion cassette in *gpa1*Δ mutants (right). **B)** Genome sequencing was performed on cells described in **(A)** with read-depth visualised in Integrative Genomics Viewer (IGV) software for specific loci shown: *URA3*, deleted in both BY-parental strains; *MET17* deleted in BY4741; *LYS2* deleted in BY4742; and *GPA1*, deleted in *gpa1*Δ cells in both mating type. **C)** Venn diagram depicting the overlapping gene mutations related to Gpa1 found in sequenced strains. **D)** List of enriched annotations from gene ontology (GO) analysis related to mating and Gpa1-signalling (upper) and specific mutation details of identified mutations (lower).

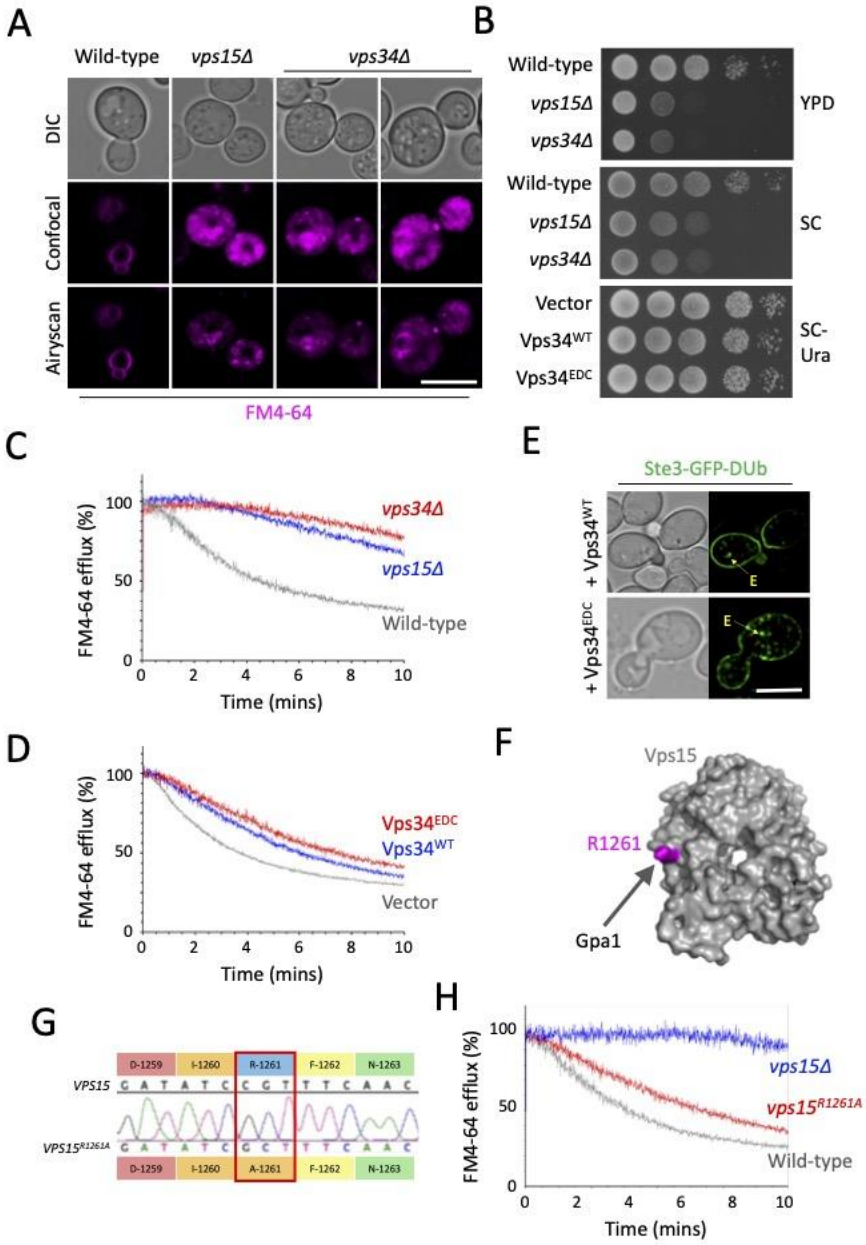

Figure 5. 4 Defined PI3-Kinase activity is required for efficient surface recycling

A) Confocal and Airyscan imaging of wild-type, *vps15*Δ and *vps34*Δ cells first labelled with 10 µM FM4-64 for 30 minutes, followed by washing and a 1-hour chase in SC minimal media. **B)** Indicated cells were grown to log phase, equivalent volumes harvested and a 1 in 10 serial dilution spotted onto YPD and synthetic complete (SC) media and incubated at 30°C. **C & D)** Indicated strains and transformants were loaded with 40 µM FM4-64 in rich media for 8-minutes, before 3x 5 minute washes and FM4-64 dye efflux measured over time by flow cytometry and plotted by the % of the initial 10 s fluorescence. **E)** Wild-type cells co-expressing Ste3-GFP-DUb with either Vps34^{WT} or Vps34^{EDC} were imaged using confocal microscopy. **F)** Surface model of Vps15 WD-repeat domain (grey) with R1261 shown (magenta). **G)** Sequencing results of the *vps15*^{R1261A} allele confirmed by Sanger sequencing of PCR product generate by PCR. **H)** FM4-64 efflux was assessed following protocol in (C) for indicated strains. Scale bar, 5 µm.

Reg1 regulates recycling at transcriptional level

Gpa1 localises to the PM and endomembrane compartments (Dixit et al., 2014; Slessareva et al., 2006). Fluorescently tagged Gpa1, which functionally complements *gpa1*Δ cells (**Figure S1**), colocalises with the late endosome marker Vps4, and to a lesser degree, the TGN marker Sec7 (**Figure 5A**). We found there was a subtle defect in Ste3-GFP-DUb recycling upon over-expression of Gpa1-mCherry (**Figure 5B**), suggesting both PI3K and Gpa1 levels need to be finely tuned for efficient recycling back to the surface. Intracellular Ste3-GFP-DUb colocalised with Gpa1-mCherry, in both wild-type and recycling defective *rcy1*Δ mutants, suggesting a trafficking block in endosomes from which recycling occurs. Expressing a constitutively active version (Gpa1^{Q323L}-mCherry) caused more severe defects in Ste3-GFP-DUb (**Figure 5C, 5F**), again with endosomal recycling reporter colocalise Gpa1. Intriguingly, the Gpa1^{Q323L} screen that revealed Gpa1 couples with PI3K during PtdIns3P production (Slessareva et al., 2006) also demonstrated the glucose-related phosphatase *REG1* is functionally associated Gpa1 (**Figure 5D**). To explore whether the recycling defects associated with Gpa1-PI3K are related to glucose mediated recycling, we tested recycling in *reg1*Δ mutants and found both Ste3-GFP-DUb (**Figure 5E, 5F**) and FM4-64 (**Figure 5F**) do not efficiently recycle. No obvious recycling defects were observed in cells lacking the distinct *SNF3* glucose sensing component. We hypothesised the connection between Glucose / Reg1 and Gpa1 / PI3K allowed cargo recycling from endosomes to the surface to be regulated in response to available glucose.

Reg1, alongside the essential phosphatase Glc7 and the yeast AMPK family member Snf1, participate in a signal transduction pathway that controls transcription in response to glucose (Ludin et al., 1998; Sanz et al., 2000; Tu and Carlson, 1994; Tu and Carlson, 1995). Snf1 regulates the Mig1 transcriptional repressor in response to glucose levels to repress various metabolic genes (Johnston et al., 1994; Treitel et al., 1998; Vallier and Carlson, 1994). We considered a model whereby this signalling mechanism maintained high levels of surface cargoes in glucose replete conditions by repression of a recycling inhibitor that acts on Gpa1-PI3K (**Figure 6A**). We went on to identify one candidate inhibitor (discussed below): the Gα subunit Gpa2, which physically and genetically interacts with Gpa1 (Ho et al., 2002; Xue et al., 1998) that we propose fulfils the function of Gpa1-recycling inhibitor. This model would predict that deletion of *MIG1* and *MIG2* repressors (Lutfiyya et al., 1998; Westholm et al., 2008), would phenocopy the defective recycling observed followed by glucose starvation or in either *reg1*Δ or *gpa1*Δ cells. As a glucose responsive inhibitor, transcript levels of *GPA2* would increase Gpa2 protein levels following glucose starvation, which would consequently inhibit Gpa1-recycling (**Figure 6B**). This model would predict that elevated levels of PM localised Gpa2 interacting with Gpa1 would hamper the finely tuned production of PtdIns3P via Gpa1-PI3K required for efficient surface recycling.

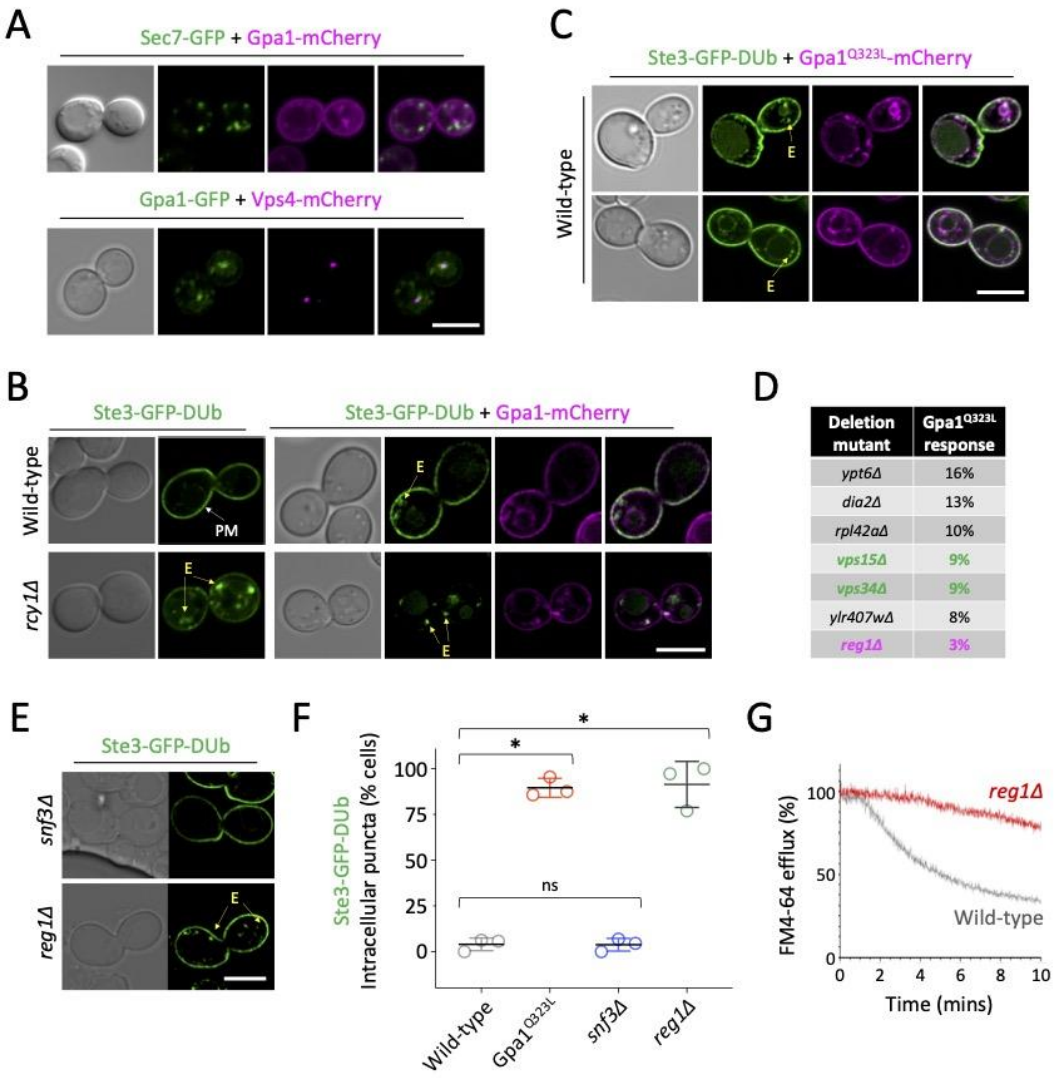

Figure 5. 5 Reg1 is a proposed upstream Gpa1 regulator in recycling

A) Confocal microscopy of wild-type cells co-expressing Sec7-GFP and Gpa1-mCherry (top) and Gpa1-GFP and Vps4-mCherry (bottom). **B)** Wild-type and *rcy1*Δ cells expressing Ste3-GFP-DUb with and without Gpa1-mCherry were imaged by confocal microscopy. **C)** Ste3-GFP-DUb localisation in wild-type cells co-expressing Gpa1^{Q323L}-mCherry was assessed by fluorescence microscopy. **D)** Top scoring mutants from a Gpa1^{Q323L} mating response screen (Slessareva *et al.*, 2006) are shown, with PI3K mutants (green) and *reg1*Δ (magenta) highlighted. **E)** Confocal microscopy of *snf3*Δ and *reg1*Δ cells stably expressing Ste3-GFP-DUb. **F)** Quantification of Ste3-GFP-DUb intracellular localisations calculated as an average of population (n=3) from WT = 68; Gpa1^{Q323L} = 51; *snf3*Δ = 83; and *reg1*Δ = 73 cells. **G)** Wild-type (grey) and *reg1*Δ (red) cells were incubated with rich media containing 40 µM FM4-64 for 8-minutes before washing and FM4-64 dye efflux measured over time by flow cytometry and plotted by the % of the initial 10 s fluorescence. Scale bar, 5 µm.

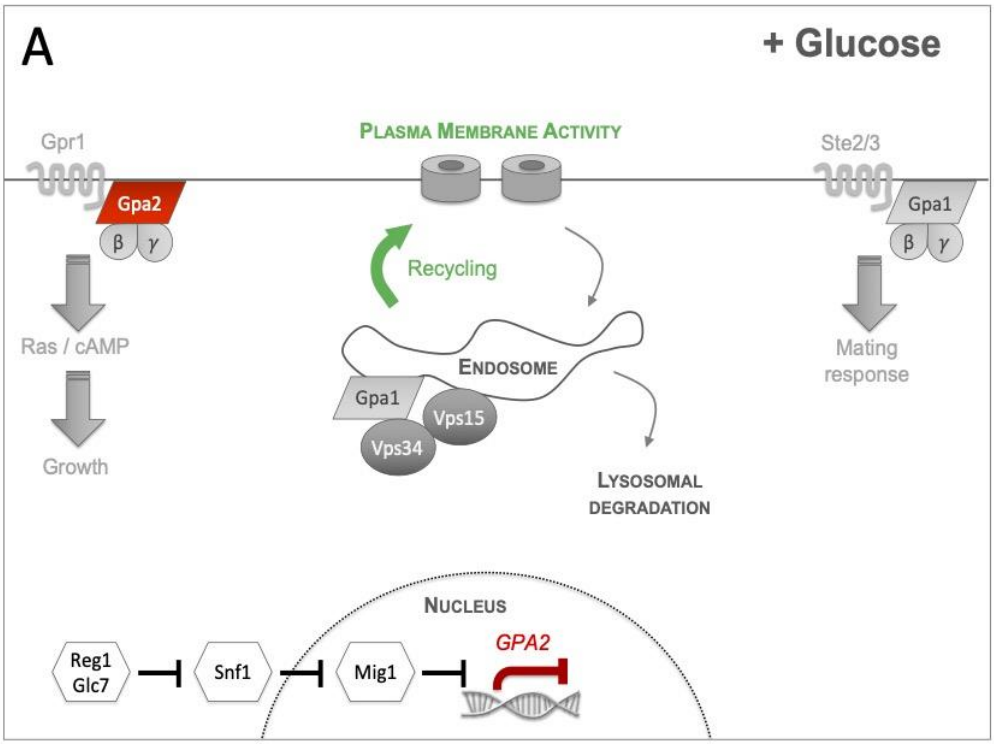
A
+ Glucose
Gpr1
PLASMA MEMBRANE ACTIVITY
Ste2/3
Gpa2
β
γ
Gpa1
Recycling
Ras / cAMP
ENDOSOME
Mating response
Gpa1
Vps15
Vps34
Growth
LYSOSOMAL DEGRADATION
NUCLEUS
GPA2
Reg1 Glc7
Snf1
Mig1

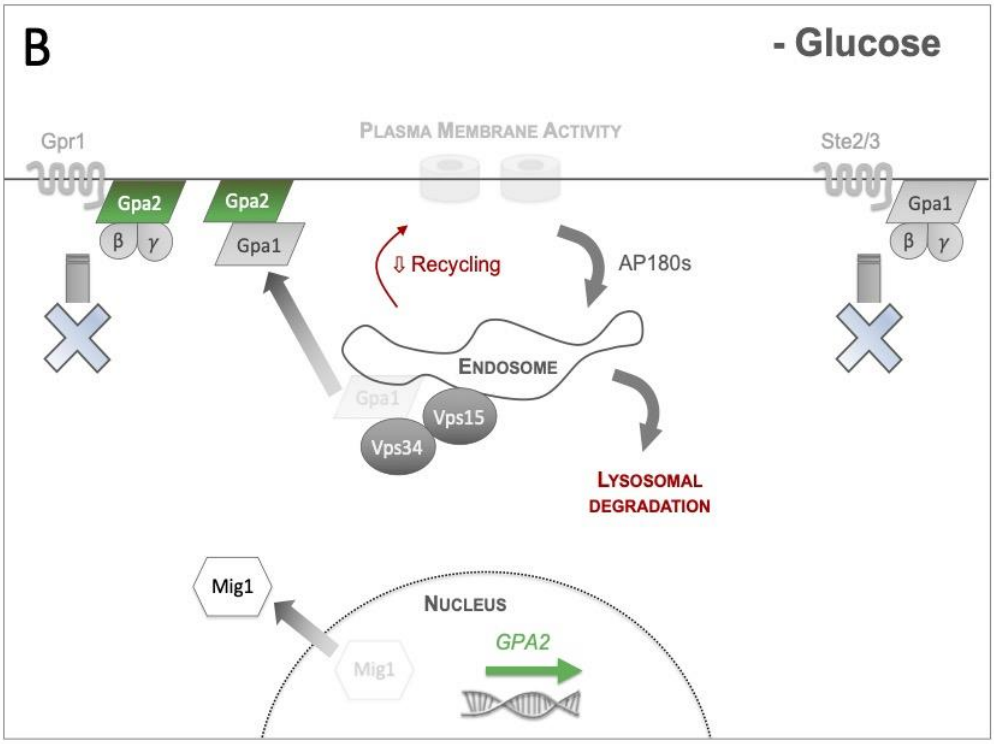
B
- Glucose
Gpr1
PLASMA MEMBRANE ACTIVITY
Ste2/3
Gpa2
Gpa2
Gpa1
Gpa1
β
γ
⇩ Recycling
AP180s
ENDOSOME
Gpa1
Vps15
Vps34
LYSOSOMAL DEGRADATION
Mig1
NUCLEUS
GPA2
Mig1

Figure 5. 6 Model for glucose mediated control of cargo recycling

A) In glucose rich conditions, metabolism of the cell is maintained to promote growth, in part through the cAMP synthesis pathway sensed through the GPCR Gpr1 and heterotrimeric G protein alpha subunit, Gpa2. In glucose conditions, we propose *GPA2* expression is suppressed via the established glucose repression pathway involving Glc7/Reg1 > Snf1 > Mig1. The pheromone signalling and mating pathway, controlled through haploid specific GPCRs Ste2/Ste3 also function at the PM via the G protein alpha subunit, Gpa1. Gpa1 also has a function at endosomes, with PI3Kinase subunits Vps15/Vps34 producing PtdIns3P. Surface recycling of PM cargoes is efficient in glucose replete conditions, via an active and efficient recycling pathway from endosomes back to the surface. **B)** Glucose starvation triggers several metabolic changes, including growth arrest sensed via Gpr1. This is accompanied by a reduction in mating response, as the Ste2/3 receptors are downregulated. The Glc7 > Snf1 pathway results in dephosphorylation and translocation of nuclear repressor Mig1. In consequence to this, the yeastAP180 clathrin adaptors are transcriptionally upregulated and induce higher levels of internalisation from the PM. Concomitantly, levels of *GPA2* are increased, which we propose acts as an inhibitor of Gpa1-mediated recycling, potentially through sequestering more Gpa1 at the PM and therefore decamping from PI3kinase at the endosome and disrupting the lipid organisation required to efficiently promote recycling.

Gpa2 inhibits surface recycling

We find recycling defects of *gpa1*Δ cells are phenocopied in *reg1*Δ mutants (**Figure 5.2.C, 5.2.E, 5.5.E, 5.5.F**). We reasoned if the functional role of Reg1 in recycling is through its capacity to modulate transcription via the Reg1/Glc7 > Snf1 > Mig1/2 pathway, then recycling defects of *reg1*Δ cells would also be phenocopied in *mig1*Δ *mig2*Δ mutant cells. Alternatively, if recycling is efficient in *mig1*Δ *mig2*Δ cells, a direct role between Reg1, and its substrate Gpa1 (Clement et al., 2013), might best explain the data. Mig1 is a glucose sensitive transcriptional repressor that rapidly translocate from the nucleus when cells are shifted to raffinose media (**Figure 5.7.A, 5.7.B, S5.2.**). Many glucose repressed genes are transcriptionally upregulated upon glucose starvation or in *mig1*Δ *mig2*Δ cells lacking the repressors (Westholm et al., 2008). As *mig1*Δ *mig2*Δ mutants exhibit perturbed Ste3-GFP-DUb recycling (**Figure 5.7.C**), we assume recycling defects in *reg1*Δ mutants are explained via a transcriptional response, as discussed (**Figure 5.6.**). To identify genes transcriptionally controlled by Reg1>Mig1 that inhibit Gpa1-mediated recycling, we cross-referenced a list of genes predicted to be repressed by Mig1 (Wollman et al., 2017) with the physical interactome of Gpa1 to reveal only one candidate, Gpa2 (**Figure 5.7.D**). To test whether *GPA2* was a *bona fide* target gene for Mig1 repression controlled by glucose we performed qPCR experiments. Firstly, we revealed that *GPA1* transcript levels are unchanged in response to Mig1-repression or available glucose. In contrast, the proposed Gpa1-inhibitor *GPA2* is transcriptionally upregulated ~2.0 ± 0.3 fold in *mig1*Δ*mig2*Δ cells and ~6.4 ± 0.7 fold upon a shift to raffinose for 1-hour (**Figure 5.7.E**). This transcriptional profile is consistent with over-expression of a Gpa1-recycling-inhibitor. Similarly, deletion of the proposed inhibitor exhibits no defects in Ste3-GFP-DUb recycling (**Figure 5.7.F**), suggesting only increasing levels of Gpa2 inhibits recycling. We did find *gpa1*Δ *gpa2*Δ cells are defective for Ste3-GFP-DUb recycling, supporting the idea that whilst Gpa1-PI3K is required for recycling, Gpa2 is a downstream regulator. The Ste3-GFP-DUb recycling defects triggered by deletion of *MIG1* and *MIG2* can be attributed to the induced levels of Gpa2 in these cells, as additionally deleting *GPA2* in a *mig1*Δ *mig2*Δ background suppresses recycling defects (**Figure 5.7.G**). We found cells expressing Gpa2-GFP localised almost exclusively to the PM, where Gpa1-mCherry partially co-localises, in addition to its endosomal localisation. However, this endosomal population shifts to primarily PM in *rcy1*Δ recycling mutants (**Figure S5.3.**).

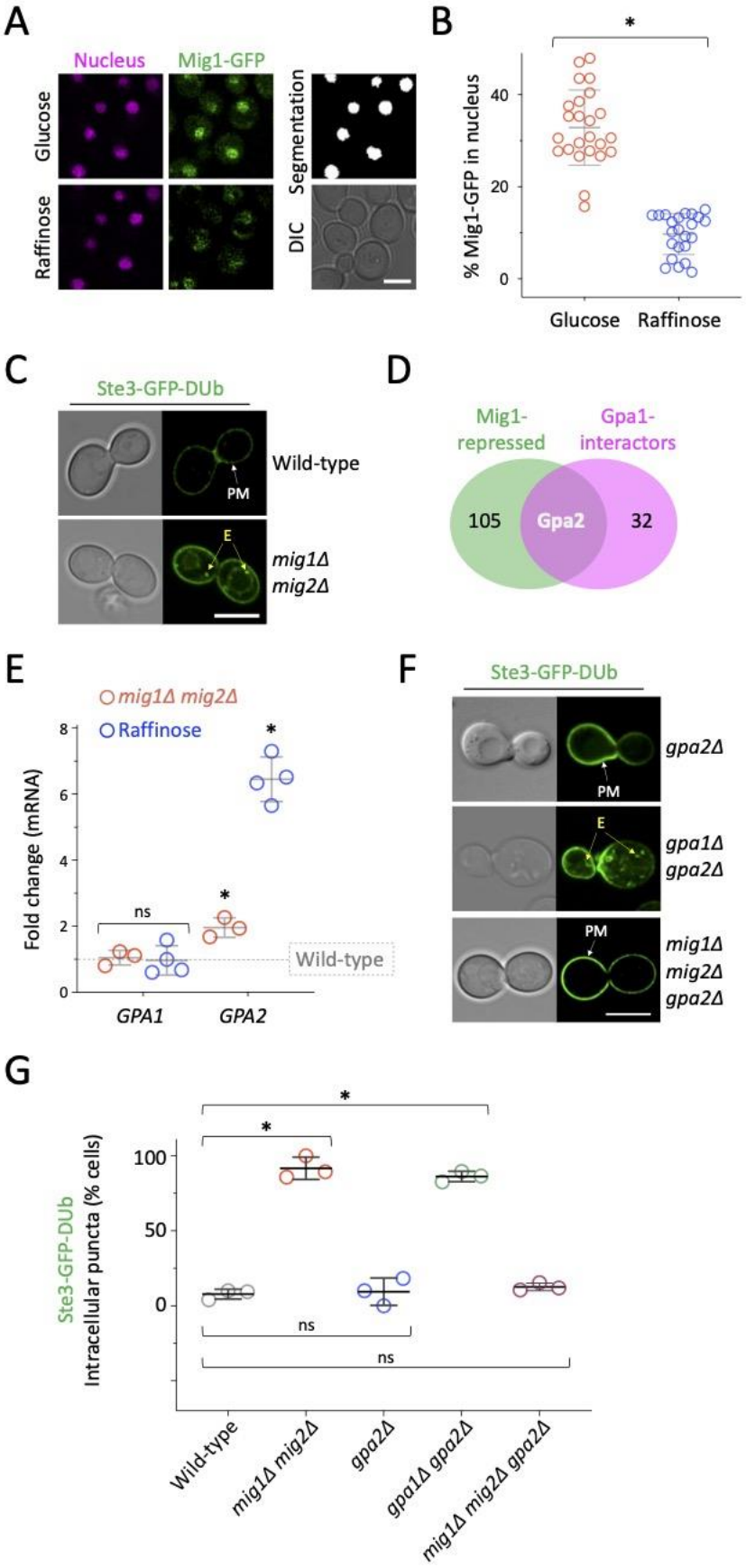
A
Nucleus
Mig1-GFP
Glucose
Raffinose
Segmentation
DIC
B
*
% Mig1-GFP in nucleus
40
20
0
Glucose
Raffinose
C
Ste3-GFP-DUb
Wild-type
PM
E
mig1Δ
mig2Δ
D
Mig1-repressed
Gpa1-interactors
105
Gpa2
32
E
mig1Δ mig2Δ
Raffinose
Fold change (mRNA)
8
6
4
2
0
*
*
ns
Wild-type
GPA1
GPA2
F
Ste3-GFP-DUb
gpa2Δ
PM
E
gpa1Δ
gpa2Δ
PM
mig1Δ
mig2Δ
gpa2Δ
G
*
*
Ste3-GFP-DUb
Intracellular puncta (% cells)
100
50
0
ns
ns
Wild-type
mig1Δ mig2Δ
gpa2Δ
gpa1Δ gpa2Δ
mig1Δ mig2Δ gpa2Δ

Figure 5. 7 Glucose and Mig1-controlled expression of recycling inhibitor *GPA2*

A) Confocal microscopy of wild-type cells co-expressing Mig1-GFP (green) and Nrd1-mCherry as a nuclear marker (magenta) under glucose replete conditions. The same cells were imaged 5-minutes later following a raffinose exchange performed with microfluidics. **B)** The percentage of nuclear Mig1-GFP signal under glucose and raffinose conditions was quantified (see methods). * indicates unpaired Holm–Sidak *t*-test ($p < 0.0001$). **C)** Confocal microscopy of wild-type and *mig1*Δ*mig2*Δ cells expressing Ste3-GFP-DUb. **D)** Venn diagram of Mig1-repressed candidates (green) and proteins that physically interact with Gpa1 (magenta). **E)** RT-qPCR was used to measure transcript levels of indicated genes, compared to *ACT1*, in wild-type versus *mig1*Δ *mig2*Δ (red) and wild-type cells grown in glucose versus 60-minutes raffinose media (blue). Unpaired Holm–Sidak *t*-tests showed *GPA1* levels were not significantly (ns) altered in either experiment ($p = 0.748$ and 0.907, respectively) but levels of *GPA2* increased in both *mig1*Δ *mig2*Δ ($p = <0.001$) and raffinose ($p = < 0.00001$). **F)** Confocal microscopy of indicated mutants expressing Ste3-GFP-DUb. **G)** Quantification of Ste3-GFP-DUb intracellular localisations calculated as an average of population (n=3) from WT = 77; *mig1*Δ *mig2*Δ = 64; *gpa2*Δ = 69; *gpa1*Δ *gpa2*Δ = 79; and *mig1*Δ *mig2*Δ *gpa2*Δ = 87 cells. Scale bar, 5 µm.

We next confirmed this Mig1-based transcriptional response results in an increase in Gpa2-GFP protein levels by immunoblot following 2-hours raffinose treatment (**Figure 5.8.A, 5.8.B**). By assessing maximum intensity projects from 3D Airyscan imaging of cells expressing Gpa2-GFP, we also found a pool of cytosolic Gpa2-GFP in glucose grown cells redistributes to the PM following raffinose treatment (**Figure 5.8.C, 5.8.D**). Similar analysis of 3D images focussing only on the top or bottom of cells also revealed punctate PM accumulations of Gpa2-GFP in raffinose grown cells (**Figure 5.8.E, 5.8.F**), but it is unclear if these have functional significance or are indirectly due to the influx of higher protein levels and greater surface/cytoplasm ratios. Our model predicts that elevated levels of Gpa2 would inhibit recycling, which was confirmed by over-expressing plasmid borne fluorescently tagged versions of Gpa2, which we confirmed are functional (**Figure S5.4.**). We find over-expressed Gpa2-mCherry triggered accumulation of Ste3-GFP-DUb in intracellular compartments (**Figure 5.9.A, 5.9.B**). Similarly, cells over-expressing Gpa2-GFP have reduced efflux of FM4-64 from the recycling pathway, when compared to control cells expressing the methionine transporter Mup1-GFP (**Figure 5.9.C, S5.5.**). In addition to these recycling specific cargoes, we also used the Gpa2-mCherry over-expression system to reveal prominent defects in recycling of the PM localised GFP tagged transporters Mup1 and Can1, which shift to endosomes and the vacuole (**Figure 5.9.D**). Gpa2 over-expression induced a reduction of Ste3-GFP from the PM, however we also note that vacuolar sorting, which is typically evident in wild-type cells at steady state, is blocked following Gpa2-mCherry overexpression, and cargo accumulates in prevacuolar structures. We assume overexpression of the Gα subunit Gpa2 perturbs trafficking of Ste3 in a manner distinct from general Gpa1-PI3K lipid-mediated trafficking. As Ste3 is a GPCR, excess Gpa2 might force it to adopt a conformation at the PM that is not conducive to MVB sorting.

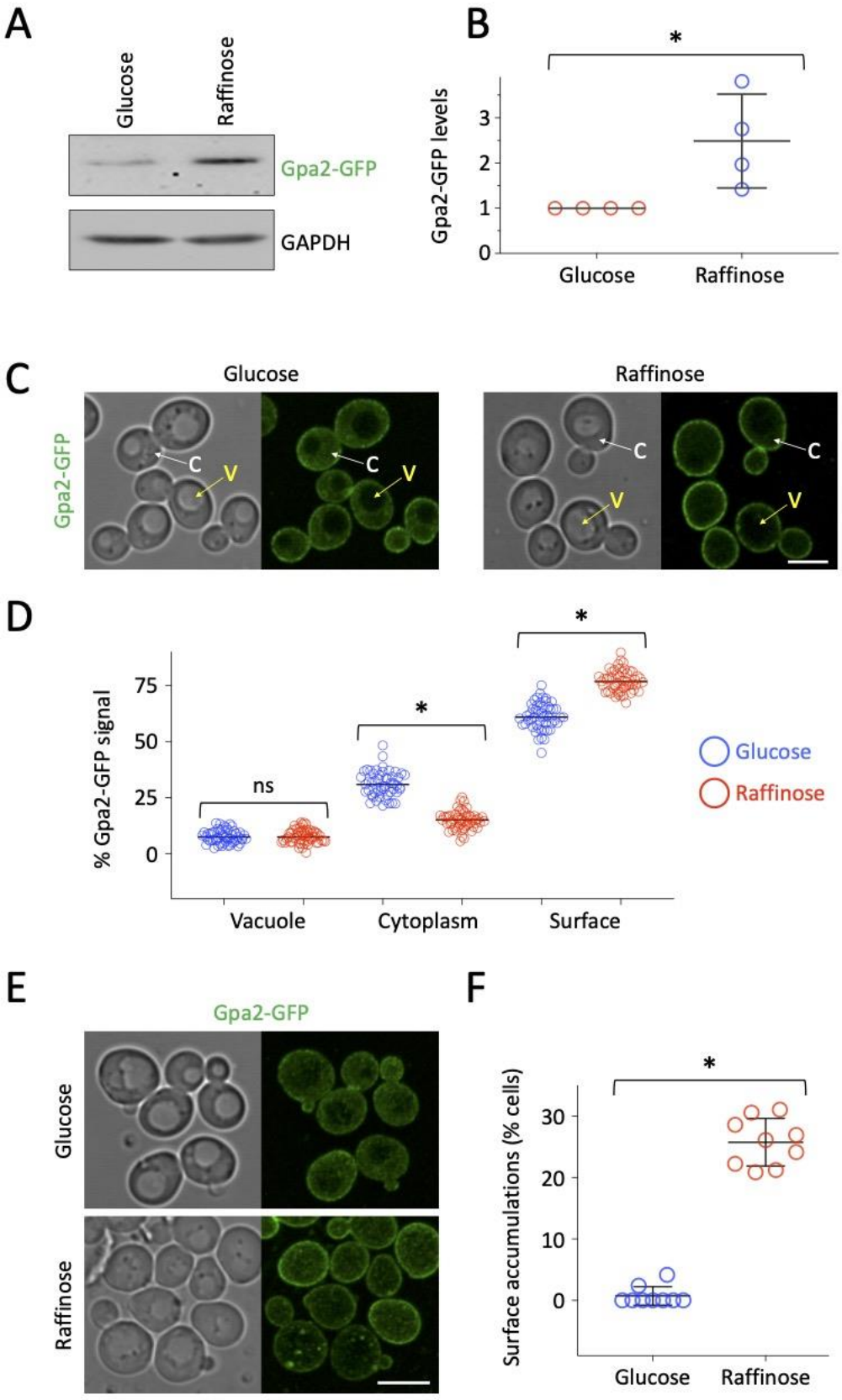
A
Glucose
Raffinose
Gpa2-GFP
GAPDH
B
Gpa2-GFP levels
0
1
2
3
*
Glucose
Raffinose
C
Glucose
Raffinose
Gpa2-GFP
C
V
D
% Gpa2-GFP signal
0
25
50
75
ns
*
*
Vacuole
Cytoplasm
Surface
Glucose
Raffinose
E
Gpa2-GFP
Glucose
Raffinose
F
Surface accumulations (% cells)
0
10
20
30
*
Glucose
Raffinose

Figure 5. 8 Glucose starvation induced expression and surface concentration of Gpa2-GFP

A) Wild-type cells expressing GFP tagged Gpa2 were grown in glucose and 90 minutes raffinose conditions before lysates were made for immunoblot analysis probing with **α**-GFP and **α**-GAPDH antibodies. **B)** Gpa2-GFP expression levels in glucose and 90 minutes raffinose treatment were quantified from immunoblots (A) using imageJ and normalised to GAPDH signal. * indicates unpaired *t*-test ($p = 0.0287$). **C)** Wild-type cells expressing endogenously expressed Gpa2-GFP were imaged by Airyscan in glucose (left) and following 2 hours raffinose treatment (right) were presented as max-intensity projections from 4 z-stack slices from centre focussed cells Arrows showing vacuole (V; yellow) and cytoplasm (C; white) are shown. Mean intensity measurements for vacuole, cytoplasm and surface from cells in **(C)** were performed. **E)** Max-intensity projections of 3D confocal images of 4 z-stack slices covering the top-focussed area of the cell. **F)** Cells exhibiting surface puncta of Gpa2-GFP were quantified as a percentage of total population. * indicates unpaired *t*-test ($p < 0.0001$). Scale bar, 5 µm.

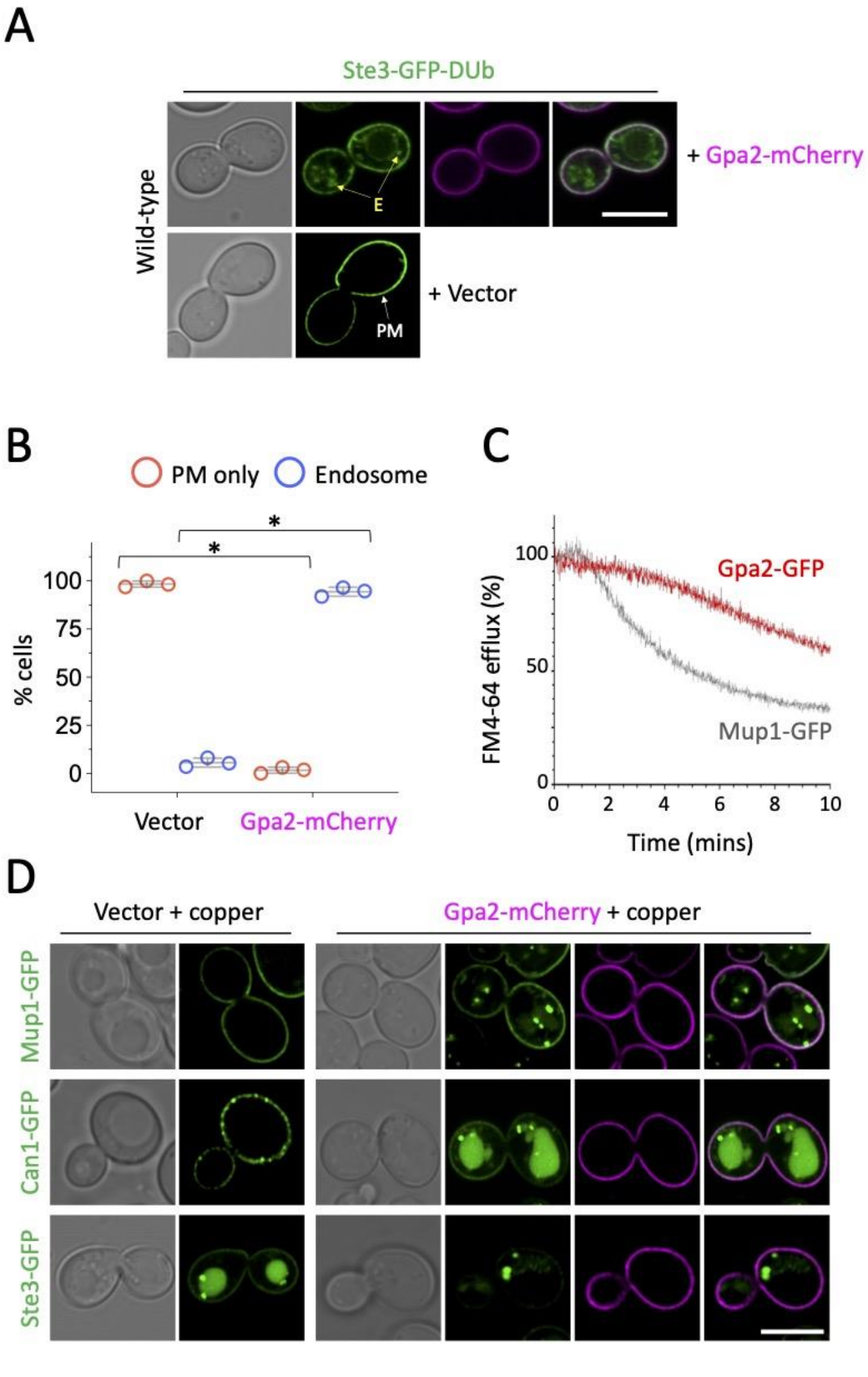
A
Ste3-GFP-DUb
Wild-type
E
+ Gpa2-mCherry
+ Vector
PM
B
PM only
Endosome
*
*
% cells
100
75
50
25
0
Vector
Gpa2-mCherry
C
FM4-64 efflux (%)
100
50
0
Gpa2-GFP
Mup1-GFP
0
2
4
6
8
10
Time (mins)
D
Vector + copper
Gpa2-mCherry + copper
Mup1-GFP
Can1-GFP
Ste3-GFP

Figure 5. 9 Over-expression of Gpa1 perturbs surface recycling

A) Confocal microscopy of wild-type cells expressing Ste3-GFP-DUb with and without Gpa2-mCherry. **B)** Localisation of Ste3-GFP-DUb in wild-type cells transformed with vector or Gpa2-mCherry at mid-log phase was quantified from >35 cells (n = 3). Unpaired Students *t*-tests were performed, with asterisk (*) indicating $p < 0.000001$. **C)** FM4-64 efflux assay was measured from wild-type cells expressing either Gpa2-GFP or Mup1-GFP. Cells were loaded with rich media containing 40 µM FM4-64 for 8-minutes before washing and dye efflux measured over time by flow cytometry and expressed a % of the initial 10 s fluorescence. **D)** Wild-type cells expressing the copper inducible Gpa2-mCherry construct, using 50 µM copper chloride, and co-expressing either Mup1-GFP, Can1-GFP or Ste3-GFP were imaged using confocal microscopy. Scale bar, 5 µm.

To explore whether Gpa2 could function at endosomes directly we performed time-lapse microscopy of cells expressing Gpa2-GFP and only very rarely observed intracellular puncta, however these did not colocalise with Gpa1-mCherry (**Figure 5.10.A**). We did find strong accumulations of Gpa2-GFP within subdomains of the PM, which are distinct from Mup1-GFP localisation and partially colocalise with brief pulses of the endocytic dye FM4-64 (**Figure 5.10.B**). In order to assess Gpa2-GFP localisation across the entire cell, we optimised fast yet gentle Apotome Structured Illumination Microscopy (SIM) imaging to capture fluorescence across the entire cell volume, with 42 distinct z-stack slices in both colour channels, captured in only 4.3 seconds. Initial experiments were calibrated using the vacuolar cargo Cos5 (MacDonald et al., 2015a). Cos5-GFP accumulates in the vacuole of wild-type cells but concentrates in class E endosomes in *vps25*Δ mutant cells (**Figure S5.6.**), so we used a dual tagged Cos5-GFP-mCherry to optimise processing and noise correction (**Figure 5.10.C**). 4D Apotome SIM microscopy experiments show Gpa2-GFP displays a continuous network distribution pattern across the PM (**Figure 5.10.D**) reminiscent of the localisation of the Gpa2 associated protein Ras2 (Spira et al., 2012) but no co-localisation with mCherry tagged markers for the trans-Golgi network (TGN) and the multivesicular body (MVB) (**Figures 5.10.E, S5.7.**). As these efforts did not provide strong evidence for Gpa2 localising anywhere other than the surface, we propose the function of higher levels of Gpa2 at the PM during glucose starvation could simply be to appropriate more Gpa1, thereby depriving PI3K of Gpa1 and reducing its capacity to mediate efficient recycling. In support of this idea, we reveal a significant Förster Resonance Energy Transfer (FRET) signal between Gpa2-GFP and Gpa1-mCherry at the surface (**Figure 5.10.F, 5.10.G, S5.8.**), but no indication of FRET between Gpa1 and Sec7 or in unbleached controls. Finally, we show that PI3K production of PtdIns3P is impaired in raffinose treated cells, indicated by the mis-localisation of the PX-domain protein Snx41 and the FYVE-domain protein Pib1(**Figure 5.11.A, 5.11.B**), which both bind endosomal membranes rich in PtdIns3P produced by PI3K (Burd and Emr, 1998; Hettema et al., 2003; Shin et al., 2001; Yu and Lemmon, 2001). These mis-localisation effects were phenocopied in glucose grown cells over-expressing Gpa2 from a plasmid.

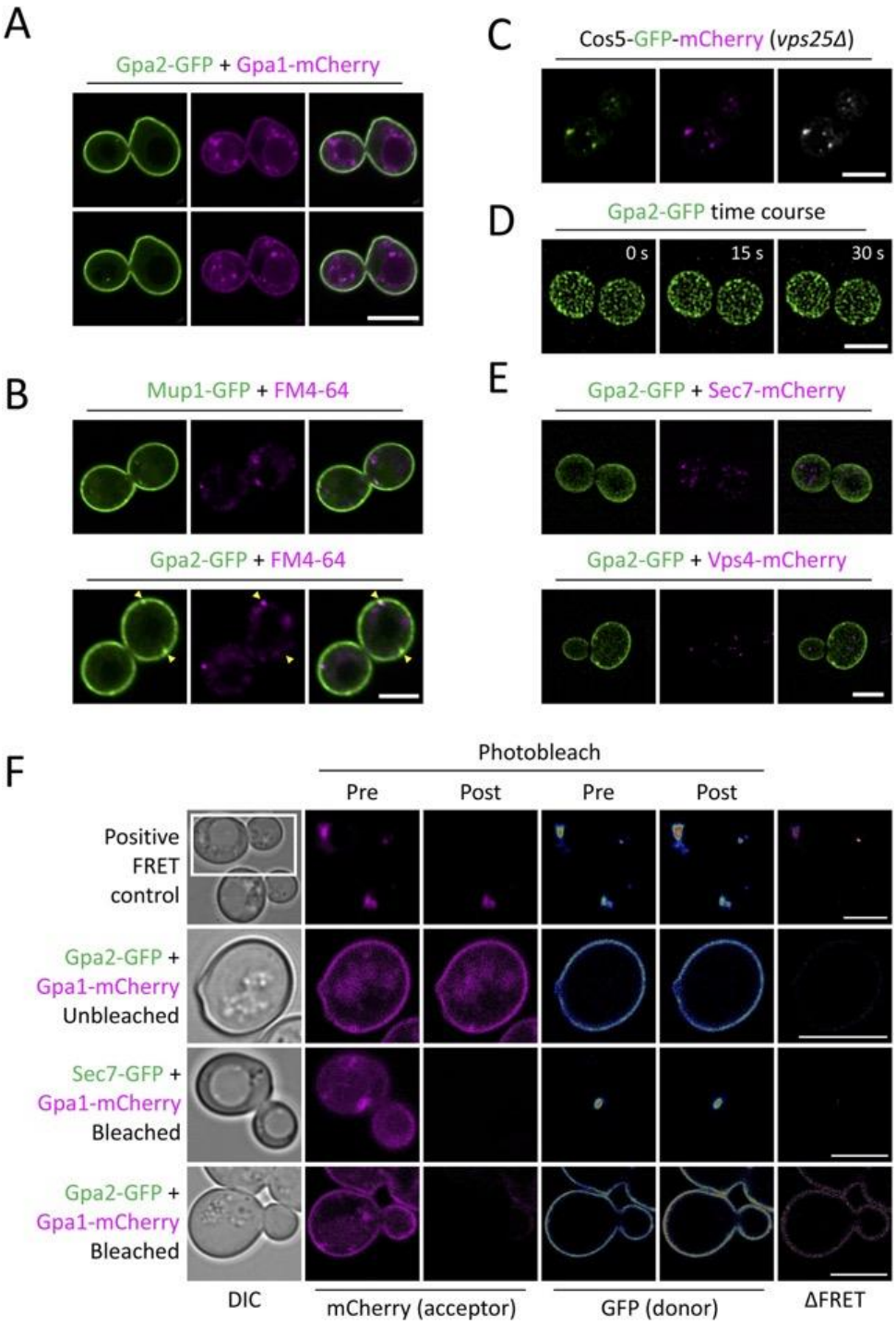
A
Gpa2-GFP + Gpa1-mCherry
B
Mup1-GFP + FM4-64
Gpa2-GFP + FM4-64
C
Cos5-GFP-mCherry (vps25Δ)
D
Gpa2-GFP time course
0 s
15 s
30 s
E
Gpa2-GFP + Sec7-mCherry
Gpa2-GFP + Vps4-mCherry
F
Photobleach
Pre
Post
Pre
Post
Positive FRET control
Gpa2-GFP + Gpa1-mCherry Unbleached
Sec7-GFP + Gpa1-mCherry Bleached
Gpa2-GFP + Gpa1-mCherry Bleached
DIC
mCherry (acceptor)
GFP (donor)
ΔFRET
G
Gpa1-Gpa2 Unbleached
Sec7 (Negative)
Cos5 (Positive)
Gpa1-Gpa2 Bleached
Normalized fluorescence
0.5
0.0
-0.5
-1.0
GFP
mCherry
*
*

Figure 5. 10 Gpa2 chiefly localises to the PM where it interacts with Gpa1

A) Wild-type cells co-expressing Gpa2-GFP and Gpa1-mCherry were imaged by confocal microscopy. **B)** Cells expressing either Mup1-GFP or Gpa2-GFP were labelled with 40 µM FM4-64 for 3 minutes followed by quenching of extracellular dye with 2.4 µM SCAS and confocal imaging **C)** 4D Apotome SIM experiments were performed for *vps25*Δ cells expressing a dual GFP- mCherry tagged Cos5. **D)** 3D time lapse Apotome SIM microscopy was used to image wild-type cells expressing Gpa2-GFP with 42 z-stack slices to cover fluorescence across depth of cells. Maximum projections of the top 10 z-slices are shown for top-focussed, surface labelled signal. **E)** Imaging was performed as described in (**D**) for wild-type cells co-expressing Gpa2-GFP with either Sec7-mCherry (upper) or Vps4-mCherry (lower), with maximum intensity projections generated across all 42 z-stack slices for each sample shown. **F)** Acceptor bleaching experiments using the 561nm laser at 100% were performed with expressed fluorescent proteins indicated. Conditions were optimised using a positive control: *vps25*Δ cells expressing Cos5-mCherry-GFP with a 7 amino acid linker between mCherry and GFP designed to give maximal FRET signal (upper). Gpa2-GFP and Gpa1-mCherry experiment was controlled by assessing fluorescence from an unbleached sample and from colocalised Gpa1-mCherry and Sec7-GFP. GFP fluorescence pre- and post-bleach are shown in RGB LUT format, The GFP fluorescence of pre-bleach was subtracted from post-bleach image (ΔFRET) and the Fire LUT applied. **G)** Normalised fluorescence for GFP and mCherry pre- and post-post-bleach datasets from (F) were quantified from n=3 experiments. Scale bar, 5 µm.

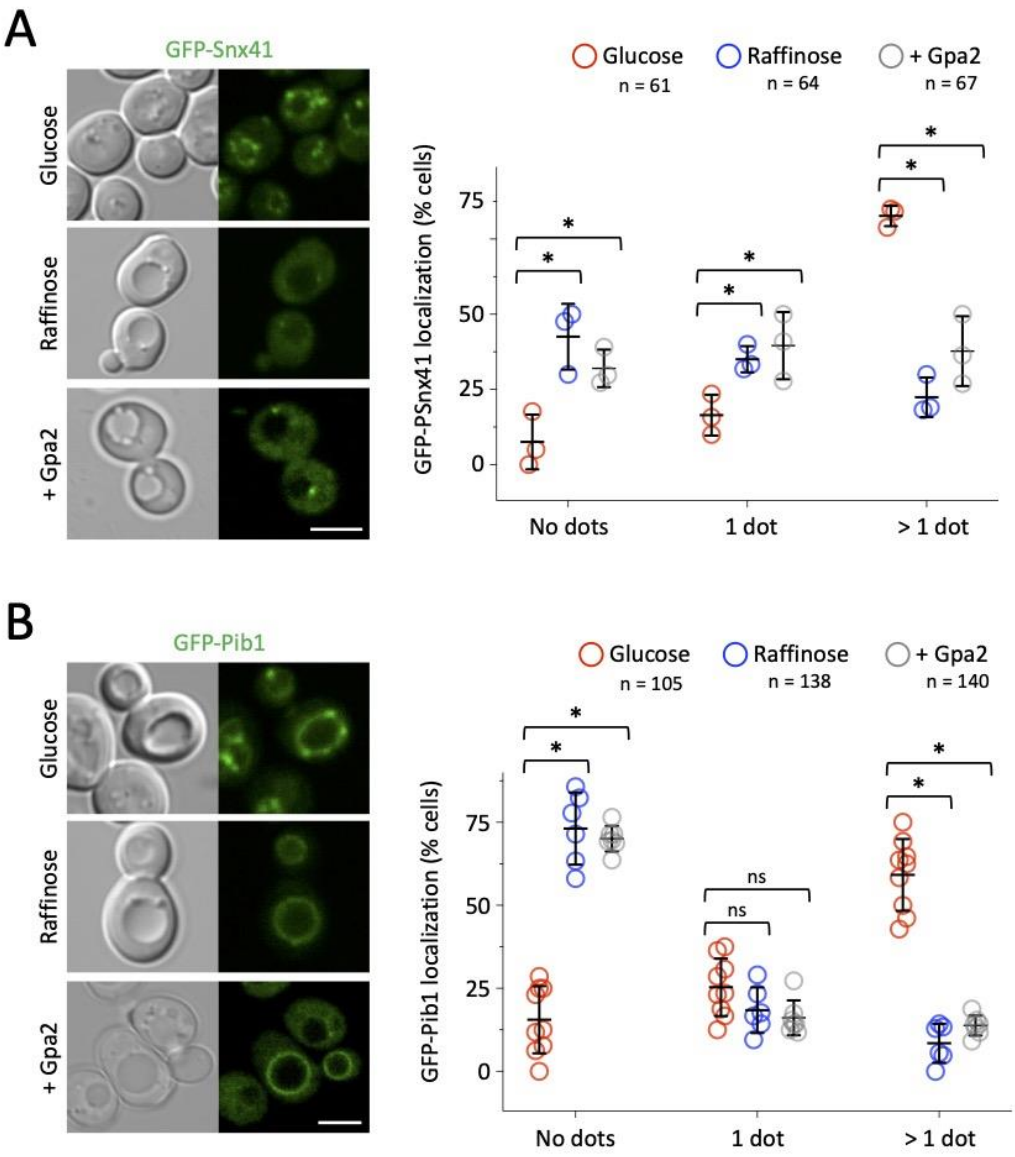

Figure 5. 11 Glucose starvation and Gpa2 overexpression

A-B) Wild-type cells expressing GFP-Snx41 (**A**) and GFP-Pib1 (**B**) were imaged in glucose replete media, following 2 hours raffinose exchange, and in cells over-expressing Gpa2. Quantifications for each experiment were performed (right) by measuring how many dots of GFP-Snx41 were observed in each cell or by comparing the distribution of GFP-Pib1 dots as a percentage. Scale bar, 5 µm.

DISCUSSION

Many protein and lipid trafficking itineraries are overhauled following acute nutrient depletion to equilibrate the energy balance of the cell and adjust metabolism appropriately for the change in extracellular conditions. Reduced recycling of material from endosomal compartments back to the PM benefits the cell by reducing anabolic load. Furthermore, surface proteins that are not recycled can be directed to the vacuolar degradation pathway instead and promote survival via catabolic processes. The division of labour between recycling and degradation pathways is not fully understood. Many surface proteins in yeast routinely accumulate in the vacuole, where fluorescent tags are stable, potentially overinflating the predominance of the well characterised degradation pathway. Ubiquitination of surface cargoes is sufficient to mediate their sorting via the ESCRT-driven multivesicular body pathway (Babst et al., 2002a; Babst et al., 2002b; Katzmann et al., 2001; Urbanowski and Piper, 2001). Most vacuolar cargoes are ubiquitinated by the Rsp5 E3-ligase and its cargo specific adaptors (O'Donnell and Schmidt, 2019; Sardana and Emr, 2021), but other ligases, such as Tul1 and Pib1, also contribute (Li et al., 2015; MacDonald and Piper, 2017; Reggiori and Pelham, 2002; Yang et al., 2020). Employing a ubiquitination reversal strategy, achieved by fusion of cargo, E3-ligases, or ESCRT-subunits to the catalytic domain of a deubiquitinating enzyme blocks cargo trafficking through the degradation pathway and allows focus on other endosomal trafficking events (MacDonald and Piper, 2015; MacDonald et al., 2012c; Stringer and Piper, 2011). Here, we show that the GPCR Ste3, tagged with GFP and a DUb domain (Ste3-GFP-DUb) recycling is specifically inhibited following glucose starvation, with Ste3-GFP-DUb accumulating in endosomes. We assume efficient recycling of Ste3-GFP-DUb in wild-type cells maintains steady state signal at the PM, as increased internalisation through over-expression of the yeast AP180 adaptors (**Figure 5.1.A**) or pheromone or temperature is insufficient to accumulate Ste3-GFP-DUb in endosomes (MacDonald and Piper, 2017). Additionally, irrespective of the internalisation rates of FM4-64 to endosomes (Vida and Emr, 1995), we find glucose starvation inhibits FM4-64 recycling back to the PM, measured as a percentage of internalised dye that subsequently effluxes (Wiederkehr et al., 2000). Therefore, we conclude that the Ste3-GFP-DUb reporter is a highly specific recycling reporter and that recycling of both protein and lipids is reduced in response to acute glucose starvation. A genetic screen for defects in Ste3-GFP-DUb recycling implicated the Gα subunit Gpa1 as required for recycling (MacDonald and Piper, 2017), which we confirmed by stably expressing Ste3-GFP-DUb in *gpa1*Δ cells, to show recycling is perturbed. Furthermore, *gpa1*Δ mutants cannot recycle FM4-64 as efficiently as wild-type cells and display either reduced PM signal or enhanced vacuolar sorting of various fluorescently tagged cargoes (**Figure 5.2.**), the latter phenotype could be explained as an indirect consequence of reduced recycling.

Gpa1 has a role outside of surface GPCR signalling and can functionally connect with the yeast PI3K, comprised of Vps34 and Vps15, to simulate phosphatidylinositol 3-phosphate (PtdIns3P) synthesis at endosomes (Slessareva et al., 2006). Like *gpa1*Δ mutants, we find PI3K mutants are also defective in recycling (**Figure 5.4.**). In addition to the role of PI3K in vacuolar trafficking of proteins through the biosynthetic (Robinson et al., 1988; Schu et al., 1993) and autophagy (Kihara et al., 2001; Wurmser and Emr, 2002) pathways, Vps34 generation of PtdIns3P is required for retrograde transport (Burda et al., 2002) and for the trafficking of proteins internalised from the PM and trafficked through the multivesicular body (MVB) pathway (Katzmann et al., 2003; Munn and Riezman, 1994). Our attempts to recover *vps15*Δ and *vps34*Δ cells from the Matα

collection, or to generate the mutants by homologous recombination, were unsuccessful. Localisation of the endogenously expressed Ste3-GFP-DUb reporter, which is mating-type specific, was therefore not possible. Instead, we performed experiments with Mat**a** *vps15*Δ and *vps34*Δ mutants, that are both extremely defective in FM4-64 recycling (**Figure 5.4.A**), which one might reasonably expect following such dramatic abrogation of the endolysosomal system. However, our additional work suggest that the recycling pathway is modulated in response to more subtle PI3K regulatory effects. For example, we took advantage of an optimised hyperactive Vps34 allele ($Vps34^{EDC}$) that stimulates over-production of PtdIns3P, which had previously been shown to upregulate retrograde trafficking, perturb late stages of autophagy and have no effect of MVB sorting (Steinfeld et al., 2021). Expression of hyperactive Vps34 resulted in defects in FM4-64 recycling (**Figure 5.4.D**) suggesting, like the late stages of autophagy, recycling to the surface requires specific PtdIns3P regulation. This result also implies Gpa1-PI3K mediated recycling is distinct from retrograde trafficking routes via the Golgi (Best et al., 2020; Ma et al., 2017). The finding that a single point mutation in Vps15, which disrupts the interaction of the Gpa1 effector with PI3K (Heenan et al., 2009) was sufficient to attenuate recycling to a similar degree as *GPA1* deletion (**Figure 5.4.F-H**) suggests that the recycling defects of *gpa1*Δ cells could be explained by improper PtdIns3P production. We note disruption of these regulators do not exhibit the extreme FM4-64 recycling defects found in glucose starved (**Figure 5.1.D**) or PI3K-null cells **Figure 5.4.C**), but they are similar to deletion of other factors previously shown to perturb recycling, such as Rcy1, the Rag GTPases, and the Rpd3 complex (Amoiradaki et al., 2021; MacDonald and Piper, 2017; Wiederkehr et al., 2000). A potential connection between recycling defects observed during glucose starvation and PI3K-Gpa1 regulation was noted due to a constitutively active $Gpa1^{Q323L}$ mutant also being defective in recycling (**Figure 5.5.**). The screen that discovered signalling of $Gpa1^{Q323L}$ requires PI3K also revealed *reg1*Δ cells, which lack the phosphatase subunit Reg1(Sanz et al., 2000; Tu and Carlson, 1995), the largest defect in signalling across all ~5000 mutants tested (Slessareva et al., 2006). Although Gpa1 phosphorylation status is controlled by glucose associated enzymes (Elm1, Sak1, Tos3 and Glc7-Reg1), this has little impact on GDP or GTP binding (Clement et al., 2013), the latter being required for PI3K mediated production of PtdIns3P (Slessareva et al., 2006). Therefore, we hypothesised the reason *reg1*Δ cells suppress constitutively active Gpa1 was through a glucose sensitive transcriptional response mediated via Glc7 and the downstream transcriptional repressor Mig1 (DeVit and Johnston, 1999; Shashkova et al., 2017).

In support of this hypothesis, we observe recycling defects in both *reg1*Δ mutants (**Figure 5.5.E, 5.5.F**) but also in *mig1*Δ *mig2*Δ cells (**Figure 5.7.C**) lacking downstream transcriptional repressor activity (Schüller, 2003). This suggested expression of an unknown inhibitor of Gpa1-mediated recycling would be de-repressed following glucose starvation or in *mig1*Δ *mig2*Δ mutants. The other yeast Gα subunit Gpa2 was the only candidate recycling inhibitor that both physically interacts with Gpa1 (Ho et al., 2002) but has also been proposed as a gene product repressed by Mig1 (Wollman et al., 2017). We confirmed *GPA2* meet these criteria by being transcriptionally upregulated ~6.4 ± 0.7 fold following 1-hour raffinose exchange compared with glucose grown cells, and increasing ~2.0 ± 0.3 fold in *mig1*Δ *mig2*Δ cells compared to wild-type (**Figure 5.7.E**). We went on to show that Gpa2 over-expression is sufficient to reduce recycling efficiency of Ste3-GFP-DUb, FM4-64 and various fluorescently tagged surface cargoes (**Figure 5.9.**). The finding that Ste3-GFP-DUb recycling defects in *mig1*Δ *mig2*Δ can be supressed by further deletion of *GPA2* supports the notion that Gpa2 is a recycling inhibitor controlled at the transcriptional level via Mig1 in response to glucose starvation

(**Figure 5.7.G**). The exact mechanisms of recycling inhibition via Gpa2 are not known, but we found little evidence of Gpa2 localising to endosomal structures that might suggest a direct role with Gpa1-PI3K (**Figure 5.10.A – 5.10.E**). Instead, based on the increased protein levels that concentrate at the surface during glucose starvation (**Figure 5.8.**) and physical interaction of Gpa1 and Gpa2 (**Figure 5.10.F, 5.10.G**), we propose elevated levels of surface localised Gpa2 following glucose starvation divert Gpa1 from endosomes, thereby attenuating PI3K activity and recycling (**Figure 5.6.B**). Although our steady state evidence is not sufficient to conclude that Gpa1 is sequestered by Gpa2 at the surface, we did find an increase of surface localised Gpa1 in the recycling mutant *rcy1*∆, suggesting at least the distribution between surface and endosomal Gpa1 can be modulated in response to recycling efficiency (**Figure S5.3.**). Alternatively, as Gpa1 is both palymitoylated and myristoylated (Song and Dohlman, 1996; Song et al., 1996), its ability to regulate endosomal lipids with PI3K may be required for its correct localisation. To test our model that elevated surface levels of Gpa2 inhibits recycling by reducing PI3K production of PtdIns3P, we examined the localisation of two proteins that bind endosomal membranes enriched in PtdIns3P. We found localisation of both the PX-domain protein Snx41(Hettema et al., 2003) and the FYVE-domain protein Pib1 (Shin *et al.*, 2001) were disrupted following glucose starvation, with marked reduction in membrane association (**Figure 5.11.**). Support for our model that Gpa1 mediated PI3K activity is inhibited by the Gpa2 inhibitor comes from our discovery that simply over-expressing Gpa2 on a plasmid mimics glucose starvation and mis-localises Snx41 and Pib1.

We believe the mechanism described here serves as a medium-term transcriptional based solution in the initial hours of starvation. As surface proteome effects are also observed more rapidly, this response presumably integrates with faster acting regulation, potentially involving posttranslational modification of Rsp5 adaptors (Kahlhofer et al., 2021), and contributes to sustained accumulation in the vacuole over longer periods (Lang et al., 2014; Müller et al., 2015). Beyond the exact mechanism of Gpa2 inhibition, other important questions remain, such as the molecular function of Gpr1 and Ras2, which we confirmed are required for recycling (**Figure 5.2.C**) whilst also being functionally associated with Gpa2 and glucose metabolism(Colombo et al., 1998; Colombo et al., 2004). We speculate recycling inhibition via increased *GPA2* expression is distinct from its role with Gpr1-Ras to induce cAMP signalling (Kraakman et al., 1999; Xue et al., 1998), as over-expression of Gpa2 does not inhibit Gpr1 function, instead it triggers increased Ras signalling and cAMP accumulation (Nakafuku et al., 1988). Our model would suggest clathrin mediated endocytosis of surface cargoes is counter-balanced by efficient Gpa1-PI3K recycling in glucose replete conditions. In glucose, the tuneable inhibitor of recycling Gpa2 is transcriptionally repressed, collectively maintaining high levels of surface proteins at the PM for optimal growth (**Figure 5.6.A**). Upon glucose depletion, the Mig1-dependent increase in endocytosis via yeast AP180 adaptors (Laidlaw et al., 2021), would complement decreased recycling via the Glc7-Reg1 > Mig1 > *GPA2* pathway to modulate the surface proteome to suit nutritional availability, increase lysosomal / vacuolar degradation and calibrate metabolic processes for cellular survival. G-protein regulators and PI3K orthologues are evolutionarily conserved (Engelman et al., 2006; Pierce et al., 2002), and although G-protein signalling is much more complex in animal cells, $G\alpha_s$ have been shown to regulate endosomal trafficking and surface protein function (Beas et al., 2012; Berón et al., 1995; Colombo et al., 1992; Colombo et al., 1994; Zheng et al., 2004). Therefore, this mode of surface protein regulation in response to nutrition may be conserved in mammalian cells.

METHODS

Reagents

Supplemental tables are included to document use of yeast strains (**Table S1**), plasmids (**Table S2**) and statistical tests (**Table S3**).

Cell culture

Yeast cells were cultured in either rich media (yeast extract peptone dextrose (YPD); 2% glucose, 2% peptone, 1% yeast extract) or synthetic complete minimal medium (SC; 2% glucose, yeast nitrogen base supplemented with amino acid / base dropout mixtures. Cultures were routinely prepared in serial dilution overnight so that cells were harvested for downstream experiments from early / mid-log phase log phase (OD_{600} = <1.0). For glucose starvation experiments, 2% glucose media was washed 3x and exchanged with either identical media lacking any carbon source (no sugar) or media of the same recipe but instead containing 2% raffinose instead of glucose. KanMX and ClonNAT strain selections were performed in rich media containing 250 µg/ml geneticin/G418 (Formedium) or 150 µg/ml Nourseothricin (Jena Bioscience), respectively. GFP and mCherry fusions of *SEC7* were created with a methotrexate cassette selected on 20 mM methotrexate (Alfa Aesar) supplemented with 5 mg/ml sulphanilamide. The *loxP* flanked cassette was then excised by *TEF1*-Cre expression and plasmid removal, as described (MacDonald and Piper, 2015). Expression of plasmids from the *CUP1* promoter in appropriate selective media was induced by the addition of Copper chloride (typically 20 - 100 µM).

Confocal microscopy and Förster resonance energy transfer (FRET)

Cells were typically harvested from mid-log phase SC minimal media cultures and prepared for confocal microscopy on Zeiss laser scanning confocal instruments (LSM710 or LSM880 equipped with an Airyscan) using a Plan-Apochromat 63x/1.4 Differential Interference Contrast (DIC) objective lens. The fluorescent proteins GFP, mGFP and mNeonGreen were excited using the 488nm line from an Argon laser their emission collected from 495 – 550 nm. Fluorescent protein mCherry and dye FM4-64 were excited using 561nm line from a yellow DPSS laser and the emission collected 570 – 620 nm. Acceptor bleaching was used to determine the occurrence of FRET. The targeted bleaching of the mCherry (acceptor) using 561nm laser was used to de-quench any FRET GFP (donor). Bleach acquisition was controlled by Zeiss Zen FRAP module where a short time-lapse series was taken before and after the bleaching of mCherry. The change in GFP intensity was measured and the data exported for visual representation in Fiji or plotted as graphs in GraphPad Prism (v9.0.2).

Apotome Structured Illumination Microscopy

Cells were imaged on a Zeiss Elyra 7 system using Plan-Apochromat 40x/1.4 oil objective lens. Multi-coloured acquisition was performed sequentially to minimise cross talk between channels. The fluorescent images were capture on 2 PCO Edge sCMOS cameras attached to a DuoLink motorised dual camera adapter and the colour split using the secondary beam splitter BP420-480 + BP470-640 + LP740. The fluorescent protein mCherry was excited using 561nm laser line and emission collected from 570 to 640nm. The fluorescent protein GFP was excited using 488nm laser line and emission collected from 490 to 570nm. Apotome acquisition was set to collect 5 phase images with 25ms

camera exposure time. Yeast cells were optical Z sections using step size optimised for "Leap" acquisition. For time lapse experiments z stacks were collected with an interval of 4.3 seconds. Apotome phase images were processed using Zeiss Zen Black software set to 3D SIM Leap. The alignment between the colour channels was further improved by taking a Z stack of multi-colour TetraSpec microspheres (ThermoFisher) that was used to generate an alignment matrix using the "Channel alignment" tool in Zen Black and applied to the time lapse data.

Image analysis

Micrographs were processed by Zeiss Zen and Fiji software. Images were processed using Zen software (Zeiss) and were further modified (e.g. coloured, merged) using Fiji.

Halo mating assay

Mat**a** wild-type cells and *gpa1*Δ mutants transformed with either empty vector or Gpa1-mCherry cells were grown to saturation overnight, diluted in fresh SC media and grown for ~6 hours. Equal amounts of cells were estimated by measuring the OD_{600} of the culture, harvested and resuspended in 50 µl sterile water before spotting onto lawns of Matα *bar1-1* mutant cells. Lawns were created from mid-log phase cultures spread on YPD solid agar and left to dry for several hours. Plates were incubated at 30 degrees for 2 days before the area of growth inhibition was measured using ImageJ (NIH) for each spot of Mat**a** cells. These area measurements were normalised to wild-type cells from the same plate and the average plotted for 4 biological replicates.

Yeast RNA extraction

For gene expression analysis following glucose starvation wild-type cells were grown to mid-log phase in YPD before being split and incubated in 10 ml YPD (dextrose) or 10 ml YPR (raffinose) media for 1 hour prior to harvesting. For experiments to test the role of Mig1 / Mig2, wild-type and *mig1*Δ *mig2*Δ cells were grown to mid-log phase in 10 ml YPD before harvesting. Spheroplasting of harvested yeast cells was performed for 2 minutes in lysis buffer (1 M sorbitol 100 mM EDTA, 0.1% β-mercaptoethanol) containing 25 units of zymolyase (Zymo Research). RNA extraction was performed with an RNeasy kit (QIAGEN) including additional DNaseI treatment using a TURBO DNA-free kit (Invitrogen).

Quantitative reverse transcription PCR (RT-qPCR)

cDNA was synthesised from 5µg extracted RNA with SuperScript IV reverse transcriptase (Invitrogen) using 50ng/µ random hexamers and 10mM dNTPs. 5-minute incubations at 65°C were carried out before 100mM DTT and Ribonuclease inhibitor added and the Superscript IV reverse transcriptase to initiate the qPCR reaction (10 mins 23°C; 10 mins 55°C; 10 mins 80°C) immediately. In order to amplify *GPA1*, oligonucleotides 361 (5' ACATCGGCTCGTCCAAATTC) and 362 (5' TCTGGTCGTATTCACTCATTGC) were used. To amplify *GPA2* oligonucleotides 365 (5' CAATGGGCCTAACGCATCG) and 366 (5' GGGTCTGTAATTGGGCGAAG) were used. All experiments were compared to *ACT1* reference gene amplified by oligonucleotides 207 (5' CTCCACCACTGCTGAAAGAG) and 208 (5' GCAGCGGTTTGCATTTCTTG). Single product amplification was confirmed by PCR using genomic DNA as a template, and near-100% amplification efficiencies were confirmed (102.2±0.12% for *GPA1,* 101.5±0.03% for *GPA2*, and 100.6±0.08% for *ACT1*) by duplicate qPCR reactions on a standard curve of known input quantity. qPCR reactions were performed on 20 ng cDNA, including relevant negative controls, in 20 µl reactions containing 350 nM of each primer,

and 10 µl Fast SYBR™ Green Master Mix (ThermoFisher Scientific). The QuantStudio 3 system (Thermofisher) was used for reactions under the following conditions: 40 cycles of 95°C for 1 second, 20 seconds 60°C, before a continuous ramp from 60°C to 95°C at a rate of 0.1 °C/S for melt curve analysis. Expression of *GPA1* and *GPA2* under indicated conditions were quantified using the comparative Ct (ΔΔCt) method, relative to the expression of the housekeeping gene *ACT1* and normalised to control sample (glucose for raffinose comparisons and wild-type cells for comparison with *mig1*Δ *mig2*Δ mutants).

Yeast genomic DNA extractions

Yeast for genotyping and genome sequencing was grown to mid-log phase in YPD, before being harvested and resuspended in 50 mM Tris.HCl 20 mM Ethylenediaminetetraacetic acid (EDTA) and then 3 µl β-mercaptoethanol, 10 µl zymolyase and 1 mg/ul RNase (QIAGEN). This was incubated in a 37 °C shaker for 1 hour before the addition of Proteinase K (10 µl, QIAGEN, >600 mAU / ml) and left at 55 °C for 1 hour. 500 µl of Phenol:Chloroform:Isoamyl alcohol was added and the solution was vortexed for 5 minutes before being spun at 15 000 rpm for 5 minutes. The aqueous layer was transferred to a fresh Eppendorf and this was repeated two more times. The final aqueous layer was transferred to a fresh Eppendorf and 50 µl 3M Sodium Acetate was added. DNA was precipitated by the addition of 1 ml 100% ethanol and spinning (10 °C 15000rpm) for 10 minutes. The pellet was then washed with 70% ethanol before residual ethanol was removed. The pellet was then dissolved in 100 µl TE Lite and left to resuspend overnight at room temperature.

Yeast genome sequencing

Prior to sequencing library generation, genomic DNA samples extracted as above were subject to an additional clean up step, by binding samples with a 1.5 X volume of AMPure XP beads (Beckman Coulter), washing twice with 70 % ethanol, and eluting into fresh TE. Libraries were then prepared from 500 ng genomic DNA using the NEBNext Ultra II FS DNA library prep kit for Illumina (New England Biolabs), according to the manufacturer's instructions, and using a 14 minute, 37 °C incubation for DNA fragmentation, and 3 cycles of PCR for incorporation of unique dual indices (NEBNext multiplex oligos for Illumina) to the final libraries. Following library quantitation and quality assessment using the Agilent Tapestation, libraries were pooled at equimolar ratios, and subject to 150 base paired end sequencing on an Illumina NovaSeq at Novogene, Europe.

Genome Alignment and Variant Detection

Illumina paired end reads were quality trimmed and verified using Cutadapt v3.4 (Martin, 2011) and FastQC (Andrews, 2021) respectively, before alignment to the *Saccharomyces cerevisiae* reference strain S288C using BWAmem (Li, 2013). Any mistakes in mate pairing and duplicates were detected and removed, and read sorting was performed using samtools v1.11 (Danecek et al., 2021). Resultant bam files were visually inspected in IGV viewer (Robinson et al., 2011) for verification of the modifications to the *GPA1* locus (*gpa1*Δ*::kan*^{r}) in both the BY4741 Mat**a** and BY4742 Mat**α** strain backgrounds. The three bam files were arranged into genomic positions using samtools and variants were identified using VarScan v2.9.3 (Koboldt et al., 2009). Variants were analysed with SnpEff (Cingolani et al., 2012) for annotation of variants as well as Variant Effect Predictor (McLaren et al., 2016) for confirmation.

Flow cytometry

Fluorescence intensity of different strains stably expressing Ste3-GFP-DUb was measured using a CytoFLEX flow cytometer (Beckman Coulter) with 488 nm laser excitation, 525 / 40 nm emission filter and avalanche photo diode detector. Approximately 75,000 cells in culture medium per sample were analysed with logical gating (forward/side scatter: single cells) used to quantify GFP fluorescence-positive yeast cells. Sample analysis was performed using the software FCS Express v7.04 (DeNovo software).

FM4-64 recycling assay

Cells were grown to mid-log phase in YPD, or SC-Ura minimal media when plasmid selection was necessary, before 1ml of cells (OD = 1.0) was harvested and incubated in 100 µl YPD containing 40 µM FM4-64 dye (*N*-(3-Triethylammoniumpropyl)-4-(6-(4-(Diethylamino) Phenyl) Hexatrienyl) Pyridinium Dibromide) dye for 8 minutes at room temperature. Cells were then washed 3x in cold SC media, with each wash left for 3 minutes on ice, before final wash was concentrated in 100 µl SC media in preparation for flow cytometry. For raffinose and glucose starvation media, the same rich and SC media was used with glucose exchanged with either no sugar or 2% raffinose. 20 µl of concentrated cells were brought up in 3 mls room temperature SC medium, and approximately analysed by flow cytometry at 1000 – 2500 cells per second using an LSR Fortessa X20 instrument (BD Biosciences). FM4-64 intensity was measured over a 10-minute period with 561nm laser excitation and emission filter 710 / 50. Measurements from 488 nm laser excitation with 530 / 50 nm emission filter were also recorded for monitoring background autofluorescence. Any comparisons are performed from cells labelled at the same time in the same media, with empty vector controls included when effects from plasmids assessed.

Image quantification for Mig1-GFP

The nuclear signal of Mig1-GFP was calculated as a percentage of nuclear / total signal in the green channel, as shown in (**Figure S2**). Briefly, whole cells were segmented based on DIC image using the Cell Magic Wand Plugin (Min = 8, Max = 300, roughness = 2.0) and used to calculate the total (nuclear plus cytoplasmic) signal for each cell in the Mig1-GFP / Green channel. The Nrd1-mCherry signal was used with *otsu* threshold to segment the nucleus based on the red channel and these regions of interest were applied to measure nuclear Mig1-GFP from the green channel.

Statistical analyses

Unpaired Student's *t*-tests were performed using GraphPad Prism v8.3.1. to compare the statistical significance between experimental conditions, with an asterisk (*) used to denote p-values of <0.05 or less, as mentioned in specific figure legends, or (ns) used to define differences that are not significant.

ACKNOWLEDGMENTS

We would like to thank staff at the York Bioscience Technology Facility for technical assistance. We are grateful to Lois Weismann and Noah Steinfeld (University of Michigan) for reagents to manipulate yeast PI3-kinase activity and Chris Stefan (UCL) for fruitful discussions. This research was supported by a Sir Henry Dale Research Fellowship from the Wellcome Trust and the Royal Society 204636/Z/16/Z (CM), and a BBSRC award BB/T017589/1 (POT, CM).

DECLARATION OF INTERESTS

The authors declare no competing interests.

5.3. SUPPLEMENTAL MATERIAL

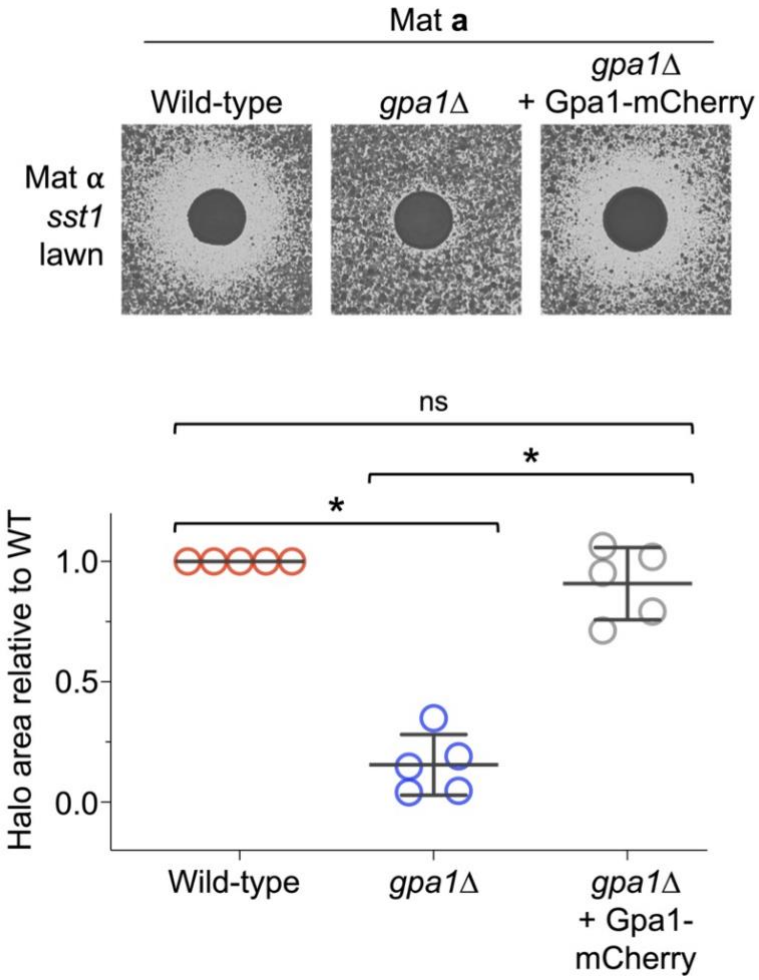

Supplemental Figure 5.1 Fluorescently tagged Gpa1 complements the mating defect of *gpa1*Δ mutants

Matα cells harbouring the *bar1-1* allele were grown to mid-log phase then plated as a lawn on rich media agar plates and left to dry. Mata cells grown to exponential phase were spotted onto the dried lawns and grown for 2 days (upper). The 'halo' area of growth inhibition was measured using ImageJ and normalised to a wild-type control on the same plate (lower). n = 5, Student's *t*-test was used to determine significance (* denotes $p < 0.0001$).

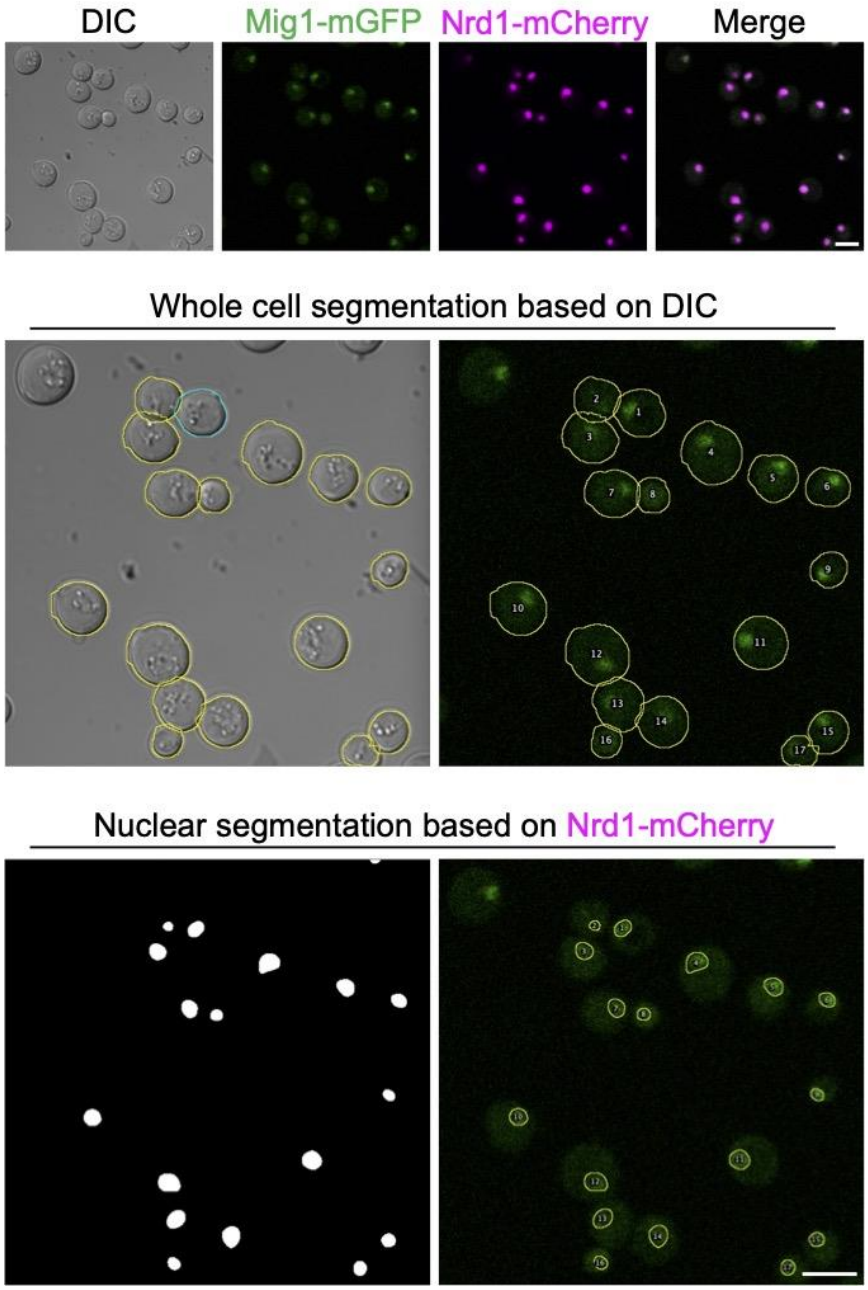

Supplemental Figure 5.2 Segmentation and quantification of nuclear Mig1-GFP

Wild-type cells stably expressing Mig1-mGFP and Nrd1-mCherry were grown to mid-log phase in SC media containing 2% glucose (upper). Using the Cell Magic Wand Plugin (Fiji) set to roughness = 2.0 whole cells were identified from the DIC image, and these segmented regions of interest (ROIs) were applied to the green channel image to calculate the overall Mig1-mGFP fluorescence (middle). For nuclear specific localisations, Ostu segmentation was applied to the red Nrd1-mCherry channel to create nuclear ROIs that were then applied to the same Mig1-mGFP fluorescence cannel. Percentage Mig1-mGFP nuclear / total fluorescence was calculated for individual cells across multiple imaging experiments (n = 3). The same process was also performed for cells grown in SC media containing raffinose instead of glucose. Scale bar, 5 μM.

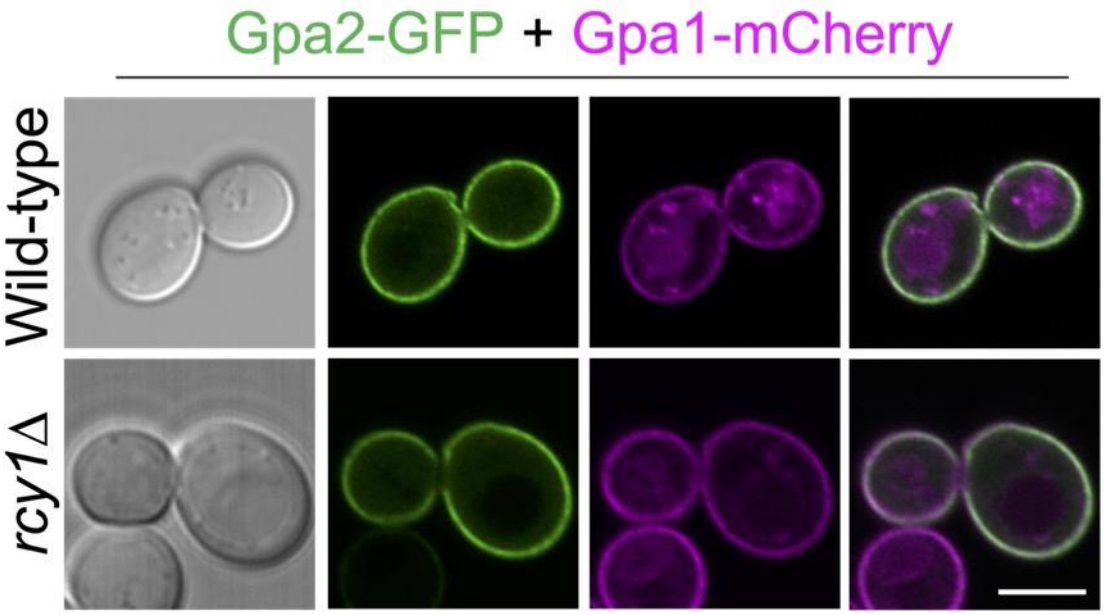

Supplemental Figure 5.3 Gpa1 and Gpa2 colocalisation in wild-type and recycling mutant cells

Wild-type and *rcy1*Δ cells co-expressing Gpa2-GFP and Gpa1-mCherry expressed from the *CUP1* promoter induced by addition of 50 µM copper chloride to the media were imaged using confocal microscopy. Scale bar, 5 µm.

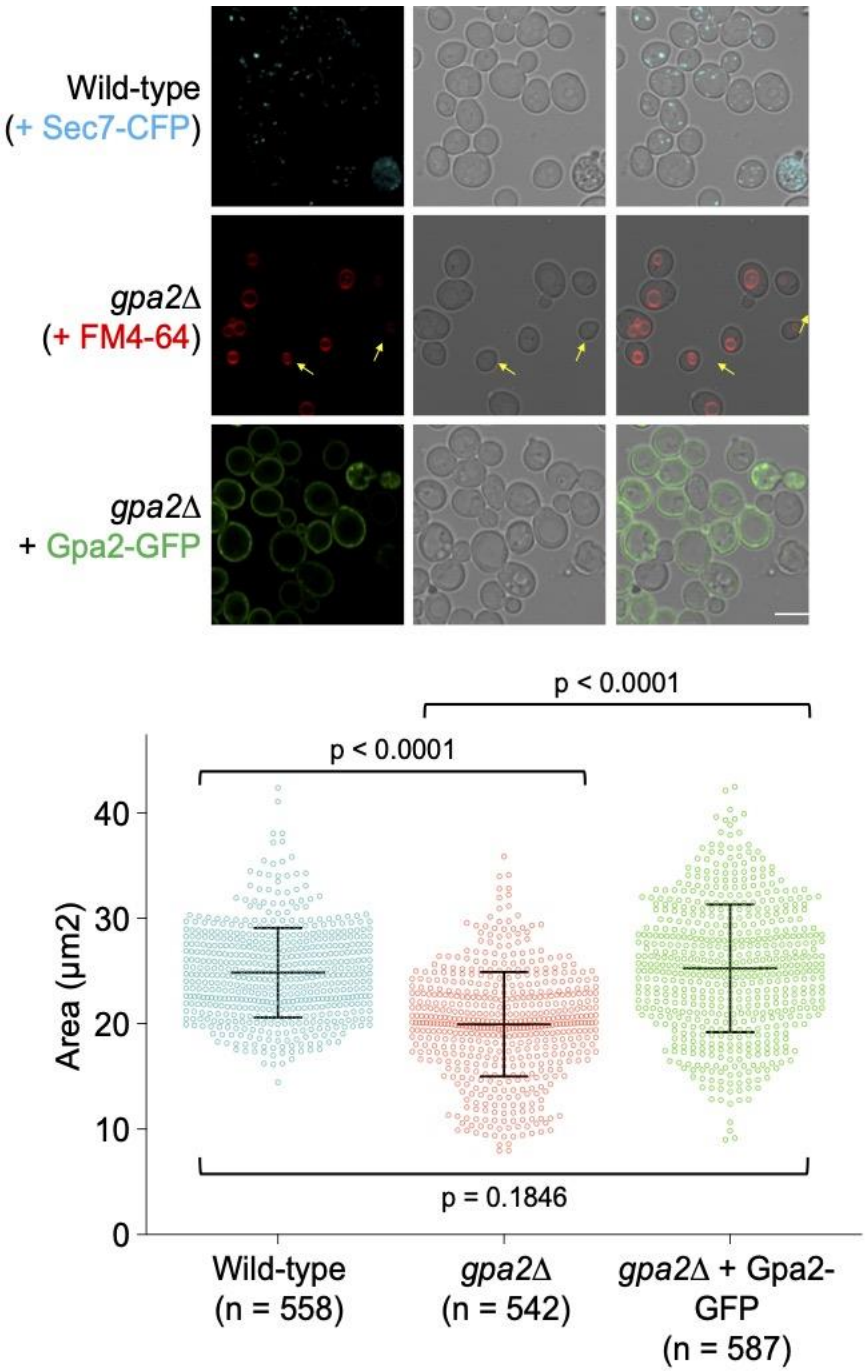
Wild-type
(+ Sec7-CFP)
gpa2Δ
(+ FM4-64)
gpa2Δ
+ Gpa2-GFP
p < 0.0001
p < 0.0001
Area (µm2)
40
30
20
10
0
p = 0.1846
Wild-type
(n = 558)
gpa2Δ
(n = 542)
gpa2Δ + Gpa2-
GFP
(n = 587)

Supplemental Figure 5.4 Fluorescently tagged Gpa2 complements the small cell size defect of *gpa2*Δ mutants

Wild-type indicated cells were grown to mid-log phase and prepared for fluorescence microscopy. To distinguish cell populations, wild-type cells expressed Sec7-CFP, the vacuoles of *gpa2*Δ nulls transformed with a vector were labelled with FM4-64 for 1 hour followed by a 30 minute dye-free chase period, and *gpa2*Δ nulls were expressing Gpa2-GFP (upper). Following segmentation using Cell Magic Wand tool in ImageJ, cellular area was measured and plotted (lower). As the cell size varies throughout cell cycle, a large number of cells (n > 500) were quantified for each condition. Scale bar, 5 μm. *p* value from Student's *t*-test comparisons indicated.

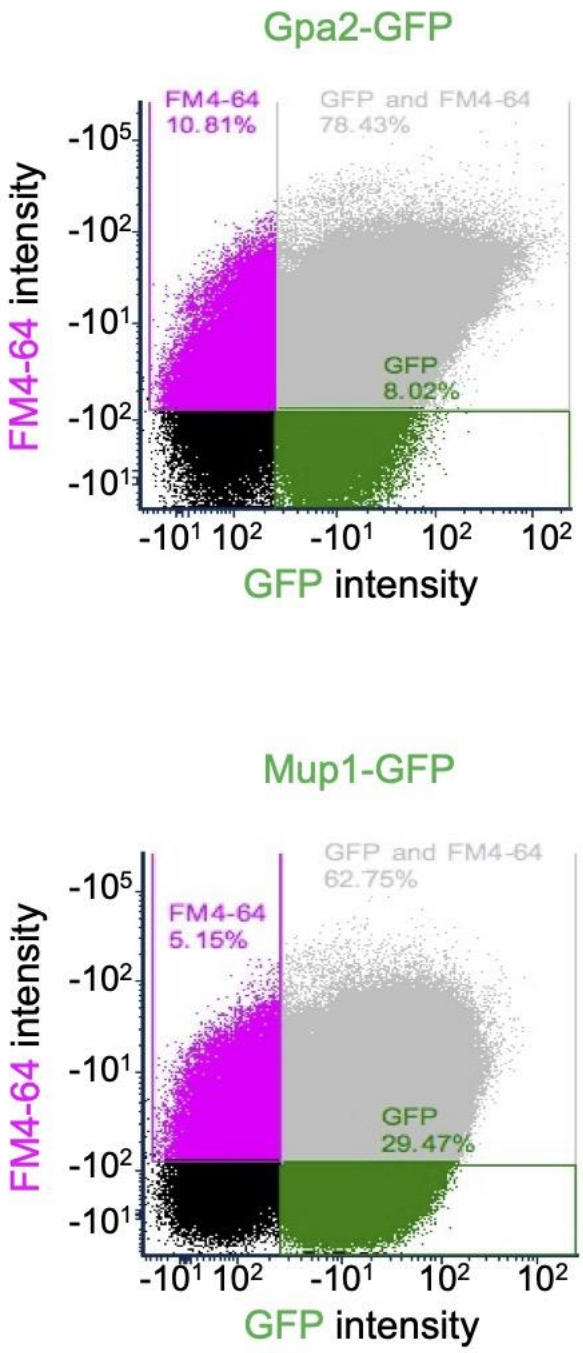

Supplemental Figure 5.5 Flow cytometry analysis focussed specifically on transformed cells

Wild-type cells expressing either Gpa2-GFP (lower) or Mup1-GFP (lower) were grown to mid-log phase before preparation for FM4-64 efflux assays (see methods). Briefly, cells were loaded with FM4-64 dye before excess dye was washed with ice cold media. Flow cytometry measurements of cells upon a return to room temperature media was recorded and gates set to only calculate FM4-64 fluorescence from cells also co-expressing either Gpa2-GFP or Mup1-GFP. A decrease in fluorescence is plotted in Figure 9C, calculated from the mean fluorescence from the first 10 seconds of recording, considered 100%, and then applied to all subsequent measurements over the 10- minute period of continuous flow / measurements.

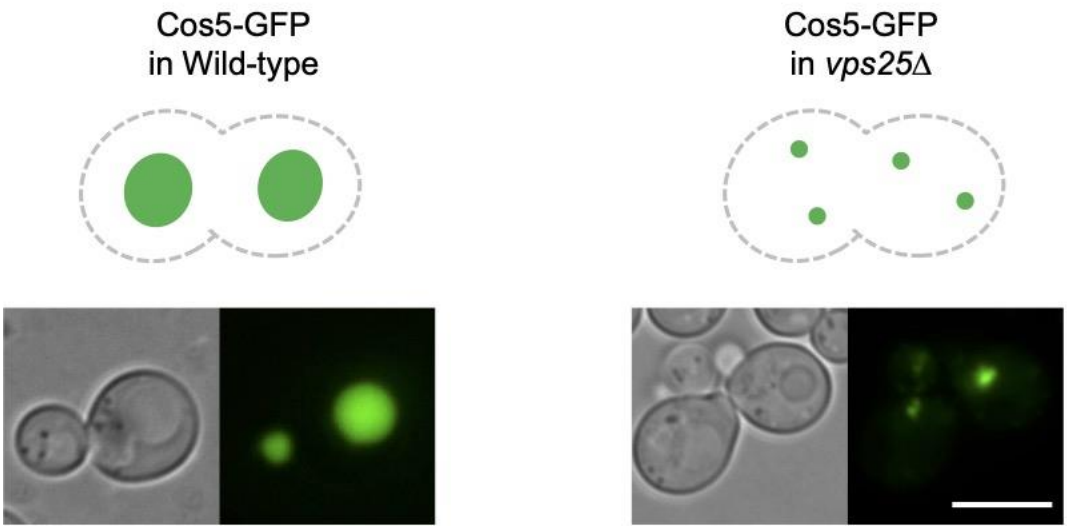

Supplemental Figure 5.6 Localisation of Cos5-GFP in wild-type and MVB sorting mutants

Cos5-GFP was expressed from the *TDH3* promoter in either wild-type cells (left) or in *vps25*Δ mutants, that are defective in multivesicular body sorting and accumulate cargoes in aberrant endosomes (right). Scale bar, 5 µM.

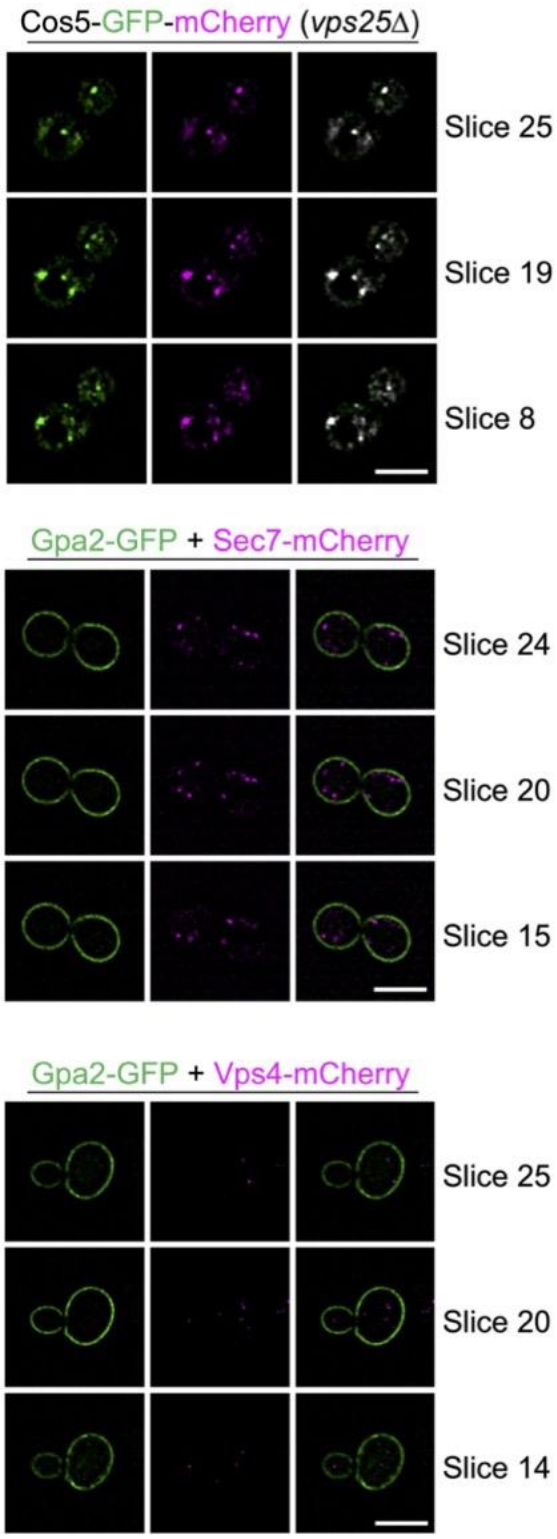

Supplemental Figure 5.7 Apotome SIM localisation experiments

4D Apotome SIM was achieved across 42 z-stacks (distance 0.126µm) repeated over 100 time slices, each of 4.3 seconds with no interval period. This approach was used to image: a dual tagged version of Cos5, carrying both GFP and mCherry at the C-terminus was expressed in *vps25*Δ (upper), and wild-type cells co-expressing Gpa2-GFP with either Sec7-mCherry (middle) or Vps4-mCherry (lower). Scale bar, 5 µM.

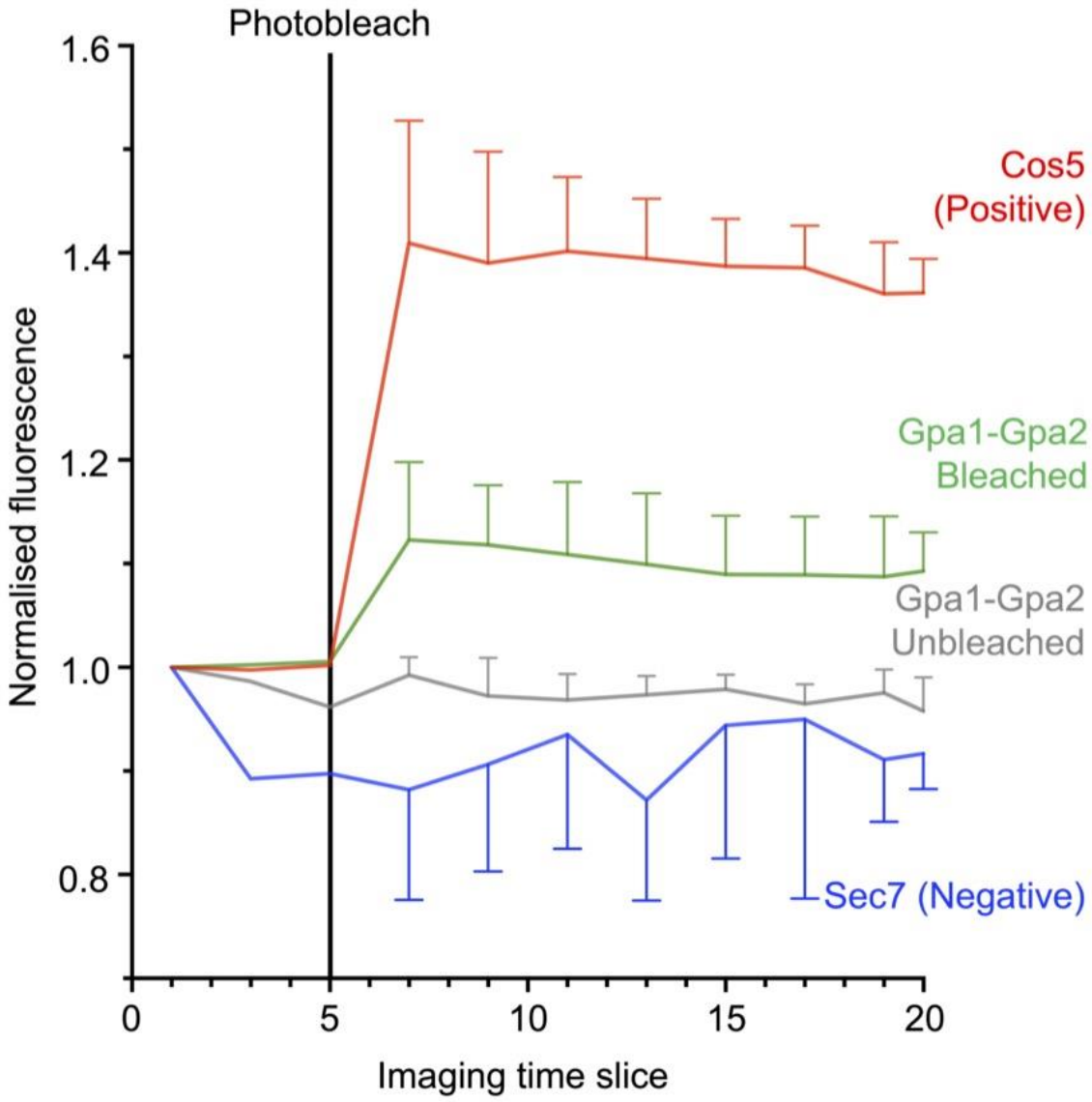

Supplemental Figure 5.8 FRET measurements to document surface interaction between Gpa1 and Gpa2

Acceptor photobleaching experiments were performed as described in methods and shown in Figure 10F, 10G. To ensure stable measurements were observed, before and after bleaching was recorded in both red and green channels. The average change in GFP fluorescence is shown with error bars representing standard deviation from 3 replicates. As a positive control, Cos5 labelled with mCherry and GFP on the same molecule separated by a 7 residue linker was imaged (red). Gpa1-Cherry bleaching showed a positive FRET signal when colocalised with Gpa2-GFP (green) but not when colocalised with the *trans*-Golgi marker Sec7-GFP (blue). As a further control, Gpa2-GFP did not show any FRET signal in cells co- expressing Gpa1-mCherry but that were not subjected to bleaching.

6. Discussion

6.1. General summary

The work in this thesis focused on the regulation of cell surface membrane proteins, using yeast as a model system. Much of the work features molecular factors, membrane trafficking pathways and biological processes that are evolutionarily conserved. This suggests the mechanisms uncovered herein may also be conserved in human cells and could be used in a biomedical context to understand diseases associated with surface protein regulation. Beyond this, my work on eisosomes may transcend yeast as it details the molecular drivers that segregate plasma membrane proteins into specific domains, a feature of all cells. Furthermore, as eisosomes are found in yeast and algae but not higher eukaryotes, and are known to be required for virulence of pathogenic fungi, the fungal-specific mechanisms I have discovered that regulate biogenesis and stress response could make for attractive drug targets for human pathogens like *Candida albicans* (Wang et al., 2016).

The uracil-scavenging growth assay that reports of surface localisation of the Fur4 transporter provided the basis of the genetic screen I carried out, which uncovered a number of conserved factors, with a range of biological functions that are required for surface protein trafficking (**Chapter II**). This was a useful assay throughout my PhD to understand cell-surface trafficking mechanisms. Using the principles of the assay allowed me to develop a glucose starvation recovery assay that demonstrated the physiological benefit to sequestering nutrient transporters in eisosomes (**Chapter III**). My involvement in this project sparked an interest in the regulation of eisosomes which led to the work presented in **Chapter IV**, where I assessed the phosphorylation dynamics of the core eisosomal component Pil1.

The cellular response to external factors was a running theme throughout my PhD. From exploiting uracil-scavenging in **Chapter II** to understanding the cellular response to glucose availability in **Chapters III**, **IV** and **V**. Yeast are widely used for genetic screens due to their genetic tractability and their fast growth. I exploited this throughout my projects, doing a screen for all ~5200 non-essential genes to identify around 150 candidates for regulation of surface protein trafficking, which I then further explored through other screening mechanisms such as a mating assay I optimised. The mating assay used the secretion of the mating factor by MATalpha cells to try and dissect whether the factors identified from the screen were chiefly involved in the secretory or endosomal pathways (**Chapter II**). Beyond this, I did a comprehensive analysis of the phosphorylation status of core eisosomal component Pil1 in mutant strains representing all yeast phosphatases, in triplicate for both glucose replete and acute glucose starvation conditions (**Chapter IV**).

The discovery based genetic screen has obvious potential for downstream analysis and follow up experiments for the candidates identified. Collectively my additional projects can be summarised by detailing the molecular mechanisms that modify: 1) clathrin mediated endocytosis 2) endosomal recycling, and 3) eisosomal retention of surface proteins in response to glucose starvation.

6.1.1. The cellular response to glucose

How eukaryotic cells respond to glucose starvation is an important area of research as understanding these actions can inform on pathologies such as cancer. The Warburg effect describes how in mammalian systems, cancerous cells metabolise glucose in a different way to healthy cells. Yeast cells suppress respiration in the presence of high glucose levels, this resembles the metabolism of cancer cells described as the Warburg effect. Whereby healthy cells will obtain more energy from respiration than fermentation, but cancerous cells will obtain the same amount of energy from each (Warburg, 1956). It has not been established why this occurs; why these aberrant cells use a less efficient metabolism but are more proliferative. Work understanding how yeast cells respond to high levels of glucose has provided evidence for certain theories as to why this might occur in mammalian cells (Diaz-Ruiz et al., 2011). Whilst my work has focussed on the yeast cellular response to acute glucose starvation, there are some studies that demonstrate how cancerous cells can be more susceptible to glucose starvation (Goji et al., 2017; Koppula et al., 2017).

Glucose is the primary carbon source for yeast (Gancedo, 1998) and therefore glucose acquisition and response to extracellular glucose is complex. In response to glucose starvation there is an increase in surface protein endocytosis and degradation, which is at least in part explained by the upregulation of the yeast AP180 proteins (**Chapter III**). In addition to this, we find a concomitant decrease in cell surface recycling from endosomes in response to glucose starvation, which is distinct from any AP180 mediated effects on endolysosomal trafficking (**Chapter III**). For this latter mechanism, we propose a model for Gpa2 to be involved in this response as a glucose sensitive inhibitor of recycling. We demonstrated that *GPA2* expression increases in response to glucose starvation, with an elevation in Gpa2 protein levels and an increase in surface localisation from the cytosolic pool. We show that Gpa2 localises close enough to Gpa1 at the surface to give a FRET signal, supporting the notion from a previous study that Gpa2 physically interacts with Gpa1 at the plasma membrane (**Chapter V**, (Ho et al., 2002; Laidlaw et al., 2022b)).

Gpa1 and Gpa2 are both G alpha subunits and so interact with membrane spanning GPCRs (Versele et al., 2001). Membrane proteins are notoriously difficult to isolate (Ivanusic et al., 2014) and so potentially membrane associated proteins might have similar issues. This process would require a lot of optimisation but once successful would support the FRET data in the paper (**Figure 5.10**). To demonstrate that the Vps15-Gpa1 interaction is required for recycling, I generated a Vps15 mutant that was unable to interact with Gpa1. As hypothesised, this mutant displayed defects in recycling (**Figure 5.4**). After biochemically showing the Gpa1-Gpa2 interaction, the next step would be to identify the region through which these proteins interact. Upon identifying this region and generating strains where these two proteins cannot interact, the use of the Ste3-GFP-DUb recycling reporter would allow for recycling defects to be observed. It would be expected that if the interaction between Gpa1 and Gpa2 at the plasma membrane sequesters Gpa1 from its role in facilitating recycling endosomes then preventing this interaction would mean that in glucose starvation conditions would not result in a downregulation of recycling in these strains (**Figure 5.2**).

In response to glucose starvation endocytosis is upregulated and a small proportion of surface cargo is sequestered in eisosomes providing a physiological benefit to the cells when recovering in replete conditions (**Chapter III**). Not all cargo localises to eisosomes but nutrient transporters of the APC family do (Moharir et al., 2018). One big question needing to be addressed is the mechanism by which nutrient transporters localise to eisosomes.

Nutrient transporters diffuse in and out of eisosomes and this is thought to be substrate dependent, where binding of substrate causes a conformational change in the transporter and thus altering its localisation (Bianchi et al., 2018). The lipids that make up eisosomes stabilise these transporters in an inactive state (Moharir et al., 2018), but how these lipids interact with nutrient transporters is not fully understood and there are various hypothesis. The conformation of the arginine transporter Can1 has been shown to direct its surface localisation. With its open conformation causing it to preferentially localise to eisosomes and then upon substrate transport its inward-conformation causing Can1 to diffuse out of eisosomes and be susceptible to ubiquitination and internalisation (Gournas et al., 2018). Another study did not observe a decrease in Can1 localisation to eisosomes in response to the addition of substrate but did with the tryptophan transporter Tat2 (Brach et al., 2011).

Fur4 localises to eisosomes (Malinska et al., 2004) and like Can1 its endocytosis is seen to be faster in cells unable to form eisosomes (Grossmann et al., 2008). Fur4 lacking its first 60 amino acids (Fur4$^{\Delta N60}$) is unable to be endocytosed due to the removal of the site of ubiquitination from the protein (Keener and Babst, 2013). This mutant acted as a reporter cargo to study trafficking mutants which I could then compare the ability of my genetic screen to identify trafficking mutants with (**Figure 2.7.**). This mutant may provide insight into how Fur4 localises to eisosomes and inform studies using other nutrient transporters. It would be intriguing to perform the recovery growth assay (**Figure 3.7. I-M**) on cells containing modified nutrient transporters that are locked in certain conformations to observe how well these cells recover compared to wild-type cells. A dependence on surface localisation for growth would be required to carry out this assay which differs between transporters.

6.1.2. The organisation of the eukaryotic plasma membrane

The yeast plasma membrane is divided into subdomains. The use of microscopy to visualise fluorescently tagged surface cargos has provided information about the regions that they occupy. One study used total internal reflection (TIRF) microscopy to visualise the localisation and dynamics of the plasma membrane in yeast (Spira et al., 2012). TIRF microscopy involves exciting fluorophores in a small region (Fish, 2009), which is especially useful when wanting to image just the plasma membrane and avoid signal from fluorophores within the cell. Spira *et al.* used 46 fluorescently tagged proteins and scored the pattern based on how network or patch-like it was, creating a gradient of different phenotypes. Their work was able to be carried out in yeast cells due to the stability of these domains, something not seen in mammalian systems (Spira *et al.*, 2012).

Having gained training on the Elyra7 microscope as soon as it was installed at our technology facility, I was keen to apply the Apotome SIM mode to mimic the wonderful TIRF analyses of the surface of yeast expressing Gpa2-GFP but allowing the entire surface (~60 z-slices) to also be imaged. York was the test centre for the Zeiss processing software SIM^2 and my data showing Gpa2 occupies a continuous network across the plasma membrane was the first to use and publish with this technique (**Chapter V, Figure 5.10. D**).

Pil1 is a BAR domain protein (Ziółkowska et al., 2011). BAR domains allow for curvature of membranes and are found to fulfil a variety of different functions (Frost et al., 2009; Peter et al., 2004). The endocytic Amphiphysin protein family contain BAR domains to allow them to fulfil their function in assisting with the formation of a vesicle (Takei et al., 1999). BAR domain containing proteins form either homo- or hetero-dimers and as well as functioning to induce membrane curvature they also regulate a small GTPase (Habermann, 2004). BAR proteins regulate the activity of Rho GTPases and these GTPases regulate their function

(Aspenström, 2014). Pil1 has not yet been implicated in regulating the activity of a GTPase, it was used in a study with the Rho GTPase Cdc42 but as a control for a slow diffusing plasma membrane protein (Sartorel et al., 2018). We did consider this as a possibility and using the techniques described in this paper are exploring potential Glc7 subunits that may be required for the dephosphorylation of Pil1. It will be intriguing to see if any of these are GTPases.

BAR domain proteins have been demonstrated to be regulated by phosphorylation. For example, phosphorylation of the N-terminal region of the mammalian ACAP4 BAR domain protein allows the curvature of the protein and thus leads to membrane remodelling (Zhao et al., 2013b). We hypothesised that eisosomes deepen in response to glucose starvation (**Chapter III**) and demonstrate that core eisosomal component Pil1 is dephosphorylate in response to glucose starvation (**Chapter IV**). It seems likely that the phosphorylation/dephosphorylation dynamics of Pil1 must be influencing its membrane bending activity. In mammalian cells, families of BAR domain proteins have been demonstrated to facilitate membrane curvature through different regulatory mechanisms (Saarikangas et al., 2009). Pil1 contains an N-BAR domain (Olivera-Couto et al., 2011) and so perhaps uncovering how phosphorylation regulates this N-BAR domain protein might be consistent with the regulation of other N-BAR domain proteins.

One aim in **Chapter IV** was to clarify the role of the Pkh kinases. Previous work had used the *GAL1* promoter to induce expression of Pkh1 and Pkh2 (Walther et al., 2007). Previous work had been done using constructs that were under the control of the *GAL* promoter. The *GAL1* promoter has previously been demonstrated to mediate glucose repression (Flick and Johnston, 1990). The work in **Chapter III** demonstrates that glucose -repression alters eisosomes and so we wanted to explore the localisation of previously implicated kinases under an alternative promoter to avoid any downstream effects from the *GAL1* promoter. After we uploaded this to the bioRxiv preprint server, one of the authors from this 2007 paper contacted us to point out they had included microscopy for the localisation of Pkh2 under its endogenous promoter in the supplemental information of a later paper (Fröhlich et al., 2009), validating our findings for Pkh2.

The phosphorylation of Pil1 is important for eisosome biogenesis (Moreira et al., 2009; Walther *et al.*, 2007). Discovering that phosphorylation is reversed in response to glucose starvation, led to our hypothesis that eisosomes are modulated via Pil1 to harbour the nutrient transporters that allow recovery growth. From my phosphatase screen, the PP1 phosphatase Glc7 was a strong hit (Offley and Schmidt, 2019). There are hundreds of targets for the mammalian PP1 and the specificity to these targets is thought to be conferred through PP1-interacting proteins (PIPs) (Heroes et al., 2013). As the catalytic subunit of PP1 proteins works in complex, Glc7 has many proposed regulatory proteins, there have been around 44 potential regulators suggested (Cannon, 2010). As this list is not exhaustive there is a high likelihood that there will be more. As part of our resubmission of Chapter IV I have explored this idea through literature searches to identify the most likely Glc7 adaptors in the regulation of Pil1.

Although our paper focussed on Glc7, we also identified Sit4 and Yvh1 as verified phosphatases that modify Pil1 (**Figure 5, Chapter IV**). It is unclear if these effects are direct or indirect, which is also true for Glc7, as it does not localise intensely to Pil1-labelled eisosomes (for example compared to Pkh2). Intriguingly, Glc7 and Sit4 have been shown to act to dephosphorylate Snf1 in high-glucose conditions (Ruiz et al., 2011) so perhaps multiple phosphatases might be acting on Pil1 in response to glucose starvation. Generating

a double mutant lacking Sit4 (*sit4*Δ) and this Glc7 regulatory subunit (Δ*regulatory subunit*) would allow Pil1 immunoblots to visualise the phosphorylation status of Pil1 in this strain under glucose starvation conditions and contribute to understanding the interplay of these factors.

6.1.3. Screening in yeast to identify novel factors

I successfully optimised and generated a high-throughput screening protocol to identify mutant strains that are defective in trafficking surface proteins. Nhx1, which is a Na^+/H^+ exchanger that functions to control the trafficking of vesicles out of the endosome (Brett et al., 2005) and Rcy1 which has been implicated in recycling from endosomes to the plasma membrane (MacDonald and Piper, 2017; Wiederkehr et al., 2000), were both identified in this screen. These were just two examples of known trafficking factors that the screen identified, confirming its validity (**Chapter II**). The screen revealed 150 hits, as well as known trafficking factors, many unknown trafficking factors were implicated. Bioinformatic analysis provided a great framework for assessing how these 150 factors interlinked. We explored how these factors might be associated with essential gene functions, that were implied from our screen but were difficult to test. Exploring some of these candidates using strains with reduced expression, achieved by integration of a DaMP cassette (Breslow et al., 2008), to perform the uracil growth assay and visualise fluorescently tagged trafficking cargos implicated them in membrane trafficking and confirmed the bioinformatic findings. The DaMP library was generated by the insertion of a kanamycin-resistance (Kan^R) cassette after the open reading frame of each gene to destabilize the transcript and reduce expression by around two- to tenfold (Schuldiner et al., 2005).

This screen provides a wealth of information, and the next steps would involve studying the clusters of hits to identify related mechanisms. The mating assay performed on these hits aimed to classify them as either functioning in the secretory or endosomal system. This is not a definitive classification as fundamental trafficking factors do play roles in both processes and there is overlap. For example, clathrin functions at the Golgi when associated with AP1 proteins (Ahle et al., 1988) and in endocytosis when associated with AP180s (Wendland and Emr, 1998). However, it does provide an insight into where more specific factors might be acting.

6.1.4. Conservation across species

Factors and trafficking pathways are highly conserved across evolution, from *Saccharomyces cerevisiae* and mammalian cells. From my genetic screen I identified 150 potential trafficking factor hits, of which 93 had homologous human genes (**Chapter II**) (Paine et al., 2021). This sets the scene for future exploratory work into what these genes do in yeast cells which may inform the orthologous function in humans. In this study we did explore the human diseases associated with these factors but understanding specific roles in yeast could shed light on the importance of these genes in humans.

Many of the gene products I studied more closely share homology with higher eukaryotes. For example, as well as Gpa1 and Gpa2 having homology to each other, they both has homology to mammalian G proteins (Miyajima et al., 1987; Nakafuku et al., 1987; Nakafuku et al., 1988). Gpa2 binds to its GPCR Gpr1 in yeast cells and mediates response to excess glucose through PKA signalling and cAMP production (Peeters et al., 2006). This has been compared to the mammalian cellular response to epinephrine which also involves a GPCR and G protein triggering PKA signalling and cAMP production (Levitzki, 1988). Highlighting

the importance of understanding how single celled organisms like yeast respond to extracellular cues. More broadly, aspects of the regulation of G proteins is shared across evolution such as the phosphorylation of G proteins (Chakravorty and Assmann, 2018). The kinase responsible for Gpa1 phosphorylation in response to changes in the cell cycle has been identified (Torres et al., 2011). Gpa2 has predicted phospho-sites (Ficarro et al., 2002; Holt et al., 2009; Lanz et al., 2021). The kinase responsible has not yet been identified but Gpa2 phosphorylation has been demonstrated to regulate its localisation to the plasma membrane in response to external nutritional demands, in particular up regulating PKA signalling (Huang et al., 2019). Understanding this regulation of Gpa2 could provide insight into how other G proteins are regulated and might assist understanding the different functions Gpa2 has, such as its role in recycling (**Chapter V**) (Laidlaw et al., 2022b).

Whilst planning experiments to screen the yeast phosphatases for a Pil1 phosphorylation phenotype I did not want to exclude essential phosphatases from my protocol. Around 38% of yeast essential genes are conserved in humans compared to 20% of nonessential genes (Mnaimneh et al., 2004) demonstrating the importance of not excluding essential genes from screening protocols. Despite Pil1 not being conserved in mammalian cells, I reasoned that the enzyme or enzymes responsible for its regulation might be. It turned out that one of our highest scoring hits was the essential gene *GLC7* which is part of a highly conserved phosphatase family (Ramaswamy et al., 1998). Intriguingly, yeast cells expressing the Glc7 human homologue PP1 are viable. Their ability to function in glucose derepression does not differ from wild-type cells (Gibbons et al., 2007) demonstrating that homology shared through sequence to function. Although mammalian cells do not contain eisosomes or Pil1 there could be alternative targets that Glc7 dephosphorylates through similar mechanisms in response to glucose starvation.

6.2. Concluding remarks

The work in this thesis provides novel findings in the field of membrane trafficking. I have used *Saccharomyces cerevisiae* as a model organism to understand cell surface trafficking mechanisms. For this I have used yeast genetics, high-throughput screening approaches, biochemical analyses, various imaging approaches, including super resolution techniques and FRET, and a series of customised functional assays to investigate a series of regulatory mechanisms that control the membrane trafficking features of surface membrane proteins.

7. Appendix

7.1. Appendix Chapter II: Fur4 mediated uracil-scavenging to screen

Table S1: Uracil growth screen results and statistics

	Phenotype Vs WT	Systematic name	Standard name	Mutant strain	4 mg/L / 0.1 mg/L	4 mg/L / 0.05 mg/L	p value 4 mg/L / 0.1 mg/L	Significant?	p value 4 mg/L / 0.05 mg/L	Significant?
1	Defective growth	YHR047C	aap1	*aap1Δ*	0.313671853	0.503870646	<0.000001	Yes	<0.000001	Yes
2	No difference	YMR300C	ade4	*ade4Δ*	0.92137818	0.96880538	0.352196	No	0.774221	No
3	Defective growth	YDR226W	adk1	*adk1Δ*	0.70799974	0.691164692	0.000003	Yes	0.000133	Yes
4	No difference	YML050W	aim32	*aim32Δ*	1.05625946	1.06747037	0.505766	No	0.535227	No
5	Growth advantage	YKL135C	apl2	*apl2Δ*	1.536367663	2.344736467	0.00043	Yes	<0.000001	Yes
6	Defective growth	YML022W	apt1	*apt1Δ*	0.650610853	0.578477892	0.000046	Yes	0.000133	Yes
7	Defective growth	YNL059C	arp5	*arp5Δ*	0.357589967	0.557185931	<0.000001	Yes	0.00009	Yes
8	Defective growth	YLR085C	arp6	*arp6Δ*	0.006171685	0.077716304	<0.000001	Yes	<0.000001	Yes
9	No difference	YOR141C	arp8	*arp8Δ*	1.02462566	1.04842068	0.825888	No	0.736834	No
10	Defective growth	YGR097W	ask10	*ask10Δ*	0.779114894	0.761250155	0.003786	Yes	0.01496	Yes
11	Defective growth	YLR114C	avl9	*avl9Δ*	0.55876137	0.762625828	<0.000001	Yes	0.019954	Yes
12	No difference	YJL095W	bck1	*bck1Δ*	1.00716842	0.94008992	0.930425	No	0.570801	No
13	Defective growth	YBR200W	bem1	*bem1Δ*	0.471107561	0.800434683	<0.000001	Yes	0.139497	No
14	Defective growth	YER155C	bem2	*bem2Δ*	0.334514358	0.6881844	<0.000001	Yes	0.017131	Yes
15	Defective growth	YPL161C	bem4	*bem4Δ*	0.82464966	1.040738978	0.016342	Yes	0.664176	No
16	Defective growth	YBL098W	bna4	*bna4Δ*	0.476447136	0.774541281	0.000003	Yes	0.118405	No
17	Growth advantage	YDL074C	bre1	*bre1Δ*	1.858834905	2.225171594	<0.000001	Yes	<0.000001	Yes
18	Defective growth	YNR051C	bre5	*bre5Δ*	0.703468575	0.754940045	0.00099	Yes	0.034121	Yes
19	Defective growth	YEL029C	bud16	*bud16Δ*	0.686320465	0.625472583	0.000058	Yes	0.000191	Yes
20	Defective growth	YOR078W	bud21	*bud21Δ*	0.649437902	0.837756956	0.00018	Yes	0.176527	No
21	Defective growth	YMR014W	bud22	*bud22Δ*	0.638375048	0.755498301	0.000005	Yes	0.015941	Yes
22	Defective growth	YCR094W	cdc50	*cdc50Δ*	0.64374825	0.674290046	0.000277	Yes	0.009665	Yes
23	Defective growth	YGL190C	cdc55	*cdc55Δ*	0.48338964	0.734766585	<0.000001	Yes	0.046693	Yes
24	Defective growth	YML036W	cgi121	*cgi121Δ*	0.742387859	0.599919818	0.002109	Yes	0.000211	Yes
25	Defective growth	YHR142W	chs7	*chs7Δ*	0.465602395	0.804163392	0.000005	Yes	0.189713	No
26	No difference	YMR198W	cik1	*cik1Δ*	1.0287786	0.88821777	0.849889	No	0.567932	No
27	No difference	YOR349W	cin1	*cin1Δ*	1.08431462	1.33080169	0.335295	No	0.003387	Yes
28	Defective growth	YPL241C	cin2	*cin2Δ*	0.449593307	0.716886253	<0.000001	Yes	0.021811	Yes
29	No difference	YPL014W	cip1	*cip1Δ*	0.99486171	0.84026947	0.951562	No	0.142595	No
30	No difference	YJL158C	cis3	*cis3Δ*	0.85525189	0.8013094	0.056884	No	0.042309	Yes
31	No difference	YOR039W	ckb2	*ckb2Δ*	0.8575331	0.9604825	0.101653	No	0.724063	No
32	No difference	YNL298W	cla4	*cla4Δ*	1.03052866	1.0670834	0.682194	No	0.484554	No
33	Defective growth	YGL215W	clg1	*clg1Δ*	0.627129817	0.781118353	0.000026	Yes	0.054248	No
34	Defective growth	YAL040C	cln3	*cln3Δ*	0.384100618	0.315802575	0.000079	Yes	0.000648	Yes
35	No difference	YHR146W	crp1	*crp1Δ*	1.0902684	1.63549941	0.321548	No	<0.000001	Yes
36	No difference	YBR036C	csg2	*csg2Δ*	0.92465811	0.93861199	0.249633	No	0.466026	No
37	No difference	YKL096W-A	cwp2	*cwp2Δ*	1.04663059	0.76636856	0.534085	No	0.015674	Yes
38	Growth advantage	YGR092W	dbf2	*dbf2Δ*	2.059707227	1.920082991	<0.000001	Yes	<0.000001	Yes
39	No difference	YOR030W	dfg16	*dfg16Δ*	0.88651976	0.8735601	0.200014	No	0.267215	No
40	Growth advantage	YOR311C	dgk1	*dgk1Δ*	1.293835122	1.401867052	0.001313	Yes	0.000643	Yes
41	Defective growth	YNL001W	dom34	*dom34Δ*	0.706418437	0.793857903	0.000183	Yes	0.040627	Yes
42	No difference	YAL026C	drs2	*drs2Δ*	1.02624363	1.35839738	0.788008	No	0.004425	Yes
43	No difference	YHR143W	dse2	*dse2Δ*	1.04928634	1.05487014	0.491706	No	0.551999	No
44	Defective growth	YOL087C	duf1	*duf1Δ*	0.747050801	0.952590025	0.021499	Yes	0.737385	No
45	No difference	YBR078W	ecm33	*ecm33Δ*	0.90585051	0.89857334	0.339776	No	0.424253	No
46	Defective growth	YKL160W	elf1	*elf1Δ*	0.700380421	0.638155882	0.000608	Yes	0.001292	Yes
47	Defective growth	YNL280C	erg24	*erg24Δ*	0.77108097	1.032610757	0.023466	Yes	0.801693	No
48	Defective growth	YMR015C	erg5	*erg5Δ*	0.213062256	0.447204295	<0.000001	Yes	<0.000001	Yes
49	Defective growth	YIL009C-A	est3	*est3Δ*	0.685157519	0.666452577	0.000852	Yes	0.005994	Yes
50	Defective growth	YFR019W	fab1	*fab1Δ*	0.48139109	0.590562815	<0.000001	Yes	0.000141	Yes
51	Defective growth	YCL058C	fyv5	*fyv5Δ*	0.777708674	0.75480477	0.018893	Yes	0.044138	Yes
52	Growth advantage	YMR307W	gas1	*gas1Δ*	1.19770928	1.419815809	0.029553	Yes	0.000342	Yes
53	Defective growth	YJR040W	gef1	*gef1Δ*	0.438493826	0.499266127	<0.000001	Yes	<0.000001	Yes
54	Defective growth	YGL020C	get1	*get1Δ*	0.815544408	0.623304828	0.006847	Yes	0.000019	Yes
55	Defective growth	YER083C	get2	*get2Δ*	0.607920252	0.717999311	0.000016	Yes	0.015602	Yes
56	Defective growth	YDL100C	get3	*get3Δ*	0.438961998	0.543184734	<0.000001	Yes	0.000005	Yes
57	Defective growth	YEL003W	gim4	*gim4Δ*	0.62704945	0.791685828	0.000091	Yes	0.088256	No
58	Growth advantage	YML094W	gim5	*gim5Δ*	31.14602295	40.99525129	0.017744	Yes	0.43685	No
59	Defective growth	YER122C	glo3	*glo3Δ*	0.137073072	0.116315073	<0.000001	Yes	<0.000001	Yes
60	No difference	YHR183W	gnd1	*gnd1Δ*	0.99395221	1.03291995	0.93845	No	0.744004	No
61	Defective growth	YHL031C	gos1	*gos1Δ*	0.611798742	0.64602956	0.000003	Yes	0.000906	Yes
62	Defective growth	YML121W	gtr1	*gtr1Δ*	0.512439827	0.454944289	<0.000001	Yes	<0.000001	Yes
63	Defective growth	YDL234C	gyp7	*gyp7Δ*	0.786521063	0.80722267	0.005364	Yes	0.050489	No
64	Defective growth	YDR317W	him1	*him1Δ*	0.430795414	0.635294727	<0.000001	Yes	0.001218	Yes
65	Growth advantage	YOR038C	hir2	*hir2Δ*	1.205672642	1.278126917	0.014292	Yes	0.01007	Yes
66	Defective growth	YJR140C	hir3	*hir3Δ*	0.714797472	0.666508758	0.000331	Yes	0.001101	Yes
67	No difference	YOR258W	hnt3	*hnt3Δ*	0.96434854	1.06283526	0.683284	No	0.5764	No
68	Growth advantage	YMR032W	hof1	*hof1Δ*	1.274858214	1.249849583	0.005947	Yes	0.051789	No
69	Growth advantage	YLR113W	hog1	*hog1Δ*	1.339545166	1.5852562	0.000133	Yes	<0.000001	Yes
70	Defective growth	YDR158W	hom2	*hom2Δ*	0.707580069	0.696433977	0.000002	Yes	0.000125	Yes
71	No difference	YER052C	hom3	*hom3Δ*	0.87121978	0.84760415	0.137448	No	0.172002	No
72	Growth advantage	YOL068C	hst1	*hst1Δ*	1.422587642	1.46102513	0.000021	Yes	0.000303	Yes
73	Growth advantage	YNL215W	ies2	*ies2Δ*	1.894089899	1.989399535	<0.000001	Yes	<0.000001	Yes
74	Defective growth	YOL108C	ino4	*ino4Δ*	0.624171543	0.69663779	0.000009	Yes	0.005291	Yes
75	Growth advantage	YDR315C	ipk1	*ipk1Δ*	1.816139235	2.575916722	<0.000001	Yes	<0.000001	Yes
76	Defective growth	YOL081W	ira2	*ira2Δ*	0.730581004	0.892272456	0.000267	Yes	0.255704	No
77	Defective growth	YPL017C	irc15	*irc15Δ*	0.682370024	0.773165813	0.000105	Yes	0.030896	Yes
78	Defective growth	YMR073C	irc21	*irc21Δ*	0.572546763	0.692034744	0.000004	Yes	0.009693	Yes
79	Growth advantage	YLR021W	irc25	*irc25Δ*	1.352689629	2.302887258	0.020689	Yes	<0.000001	Yes
80	No difference	YPL053C	ktr6	*ktr6Δ*	1.11285936	1.12412634	0.175747	No	0.247215	No

81	Growth advantage	YOR123C	leo1	*leo1Δ*	1.187991352	1.105288766	0.011177	Yes	0.26884	No
82	No difference	YOR196C	lip5	*lip5Δ*	0.99918177	1.01651908	0.992896	No	0.888924	No
83	No difference	YLL007C	lmo1	*lmo1Δ*	0.97691327	0.97204941	0.769683	No	0.783004	No
84	No difference	YNL147W	lsm7	*lsm7Δ*	0.87694511	0.60848428	0.128445	No	0.000181	Yes
85	No difference	YJL199C	mbb1	*mbb1Δ*	1.01075442	0.96555788	0.900129	No	0.754843	No
86	Defective growth	YOR298C-A	mbf1	*mbf1Δ*	0.433127686	0.502239861	<0.000001	Yes	0.000004	Yes
87	Defective growth	YGL197W	mds3	*mds3Δ*	0.472281769	1.397292015	0.000962	Yes	0.052962	No
88	No difference	YKR069W	met1	*met1Δ*	0.78462355	1.18688351	0.088179	No	0.250128	No
89	Defective growth	YFR030W	met10	*met10Δ*	0.44968385	0.520339762	<0.000001	Yes	<0.000001	Yes
90	Defective growth	YLR303W	met17	*met17Δ*	0.412200689	0.736144612	<0.000001	Yes	0.028421	Yes
91	Defective growth	YIL128W	met18	*met18Δ*	0.754737987	0.841316431	0.004107	Yes	0.148387	No
92	No difference	YER091C	met6	*met6Δ*	1.04562697	0.92672231	0.582911	No	0.493239	No
93	Defective growth	YEL007W	mit1	*mit1Δ*	0.829430685	0.849547172	0.032971	Yes	0.143621	No
94	Defective growth	YNL076W	mks1	*mks1Δ*	0.658421146	0.793903905	0.000303	Yes	0.089349	No
95	Defective growth	YJL183W	mnn11	*mnn11Δ*	0.711641051	0.780766052	0.000661	Yes	0.043792	Yes
96	No difference	YGL257C	mnt2	*mnt2Δ*	1.16295915	1.87077655	0.087866	No	<0.000001	Yes
97	No difference	YIL014W	mnt3	*mnt3Δ*	1.08309131	1.06792256	0.347483	No	0.550664	No
98	Defective growth	YJR074W	mog1	*mog1Δ*	0.736189208	0.753850033	0.00326	Yes	0.032725	Yes
99	Defective growth	YER077C	mrx1	*mrx1Δ*	0.458872403	0.651810159	<0.000001	Yes	0.001236	Yes
100	Defective growth	YEL033W	mtc7	*mtc7Δ*	0.452970719	0.709103121	<0.000001	Yes	0.025931	Yes
101	No difference	YPL226W	new1	*new1Δ*	1.04898224	1.0153223	0.51517	No	0.874307	No
102	Defective growth	YDR456W	nhx1	*nhx1Δ*	0.15661421	0.133637981	<0.000001	Yes	<0.000001	Yes
103	No difference	YLR315W	nkp2	*nkp2Δ*	0.97496197	0.88730784	0.768209	No	0.302872	No
104	Defective growth	YLR328W	nma1	*nma1Δ*	0.619656412	0.603287705	0.000001	Yes	0.000091	Yes
105	Growth advantage	YOL041C	nop12	*nop12Δ*	1.184332766	1.311543262	0.033747	Yes	0.005351	Yes
106	Growth advantage	YDR043C	nrg1	*nrg1Δ*	1.300933635	1.171054734	0.003972	Yes	0.202455	No
107	Defective growth	YML060W	ogg1	*ogg1Δ*	0.595972989	0.911586199	0.000013	Yes	0.45589	No
108	No difference	YLR054C	osw2	*osw2Δ*	1.22671945	1.42877405	0.161886	No	0.039989	Yes
109	Defective growth	YGR078C	pac10	*pac10Δ*	0.500012351	0.69562765	<0.000001	Yes	0.004591	Yes
110	Defective growth	YJL210W	pex2	*pex2Δ*	0.597050124	0.721759675	0.000005	Yes	0.013983	Yes
111	Defective growth	YNL326C	pfa3	*pfa3Δ*	0.560170044	0.739770186	<0.000001	Yes	0.002972	Yes
112	No difference	YOL003C	pfa4	*pfa4Δ*	0.94888657	0.96741999	0.445198	No	0.705336	No
113	Defective growth	YJL179W	pfd1	*pfd1Δ*	0.511402808	0.697884377	<0.000001	Yes	0.001373	Yes
114	No difference	YOL001W	pho80	*pho80Δ*	1.04300293	1.16541316	0.608723	No	0.126297	No
115	Defective growth	YBR106W	pho88	*pho88Δ*	0.407478542	0.169756437	0.000004	Yes	<0.000001	Yes
116	Defective growth	YGL023C	pib2	*pib2Δ*	0.274206627	0.523313371	<0.000001	Yes	0.000016	Yes
117	Defective growth	YEL017C-A	pmp2	*pmp2Δ*	0.371383897	0.593384694	<0.000001	Yes	0.000379	Yes
118	Defective growth	YAL023C	pmt2	*pmt2Δ*	0.165593466	0.187344223	<0.000001	Yes	0.000002	Yes
119	Defective growth	YNR052C	pop2	*pop2Δ*	0.39617448	0.190869896	<0.000001	Yes	<0.000001	Yes
120	No difference	YDR300C	pro1	*pro1Δ*	0.97196234	0.94143137	0.669647	No	0.488717	No
121	No difference	YOR265W	rbl2	*rbl2Δ*	0.9349418	1.00737856	0.420065	No	0.943348	No
122	Defective growth	YOR220W	rcn2	*rcn2Δ*	0.783197637	0.803609346	0.011552	Yes	0.075211	No
123	Defective growth	YJL204C	rcy1	*rcy1Δ*	0.649017323	0.87687182	0.000146	Yes	0.298639	No
124	Growth advantage	YPL066W	rgl1	*rgl1Δ*	1.715410117	1.822821089	<0.000001	Yes	<0.000001	Yes
125	Defective growth	YDR137W	rgp1	*rgp1Δ*	0.771469221	0.755864807	0.013639	Yes	0.040518	Yes
126	Defective growth	YMR283C	rit1	*rit1Δ*	0.795833624	0.89628456	0.020527	Yes	0.359901	No
127	Defective growth	YOR018W	rod1	*rod1Δ*	0.495572992	0.851460362	0.000002	Yes	0.276883	No
128	Defective growth	YLR371W	rom2	*rom2Δ*	0.706831293	0.802640361	0.001562	Yes	0.09733	No
129	Defective growth	YCR045C	rrt12	*rrt12Δ*	0.653972299	0.701552658	0.000068	Yes	0.007437	Yes
130	Defective growth	YGL252C	rtg2	*rtg2Δ*	0.609215062	1.013530884	0.000243	Yes	0.921044	No
131	No difference	YOR216C	rud3	*rud3Δ*	1.02342391	1.01161132	0.795592	No	0.920525	No
132	Defective growth	YCR009C	rvs161	*rvs161Δ*	0.630702986	0.768771485	0.000053	Yes	0.048518	Yes
133	Defective growth	YKL212W	sac1	*sac1Δ*	0.474495632	0.678693982	<0.000001	Yes	0.001198	Yes
134	Defective growth	YDR129C	sac6	*sac6Δ*	0.349049984	0.613753253	<0.000001	Yes	0.000865	Yes
135	Defective growth	YCR008W	sat4	*sat4Δ*	0.606653558	0.870444472	0.000024	Yes	0.277511	No
136	No difference	YHR205W	sch9	*sch9Δ*	0.92287326	0.95975161	0.404173	No	0.735154	No
137	Defective growth	YJL080C	scp160	*scp160Δ*	0.574422894	0.506996435	<0.000001	Yes	<0.000001	Yes
138	No difference	YMR272C	scs7	*scs7Δ*	1.01816944	1.08823064	0.820383	No	0.39175	No
139	Defective growth	YDR469W	sdc1	*sdc1Δ*	0.05951792	0.016958209	<0.000001	Yes	<0.000001	Yes
140	No difference	YLR268W	sec22	*sec22Δ*	1.00692541	1.03055472	0.944	No	0.809726	No
141	No difference	YDR363W-A	sem1	*sem1Δ*	1.03666473	1.00296741	0.630525	No	0.97587	No
142	Defective growth	YOR184W	ser1	*ser1Δ*	0.816231532	0.869728008	0.039064	Yes	0.255319	No
143	No difference	YOR140W	sfl1	*sfl1Δ*	0.99288681	1.03534162	0.934987	No	0.752858	No
144	Defective growth	YOL110W	shr5	*shr5Δ*	0.82013776	0.747941071	0.027683	Yes	0.016548	Yes
145	Defective growth	YMR175W	sip18	*sip18Δ*	0.454268157	0.799495771	<0.000001	Yes	0.083363	No
146	No difference	YKR072C	sis2	*sis2Δ*	1.01015847	0.94683791	0.903459	No	0.621915	No
147	Defective growth	YBR266C	slm6	*slm6Δ*	0.330680072	0.609421563	<0.000001	Yes	0.000138	Yes
148	Defective growth	YHR030C	slt2	*slt2Δ*	0.726233202	0.984026115	0.004079	Yes	0.896156	No
149	Defective growth	YBR289W	snf5	*snf5Δ*	0.779040045	0.734546251	0.00145	Yes	0.002943	Yes
150	Defective growth	YGL127C	soh1	*soh1Δ*	0.485293083	0.257636885	<0.000001	Yes	<0.000001	Yes
151	No difference	YJL192C	sop4	*sop4Δ*	0.99047969	1.04418911	0.915262	No	0.701201	No
152	No difference	YEL031W	spf1	*spf1Δ*	1.14634554	1.11388186	0.083349	No	0.294871	No
153	Defective growth	YDR392W	spt3	*spt3Δ*	0.797590838	0.929739549	0.048724	Yes	0.59463	No
154	Growth advantage	YLR055C	spt8	*spt8Δ*	1.245515467	1.622854921	0.008823	Yes	<0.000001	Yes
155	Defective growth	YMR125W	sto1	*sto1Δ*	0.47918656	0.451903131	<0.000001	Yes	<0.000001	Yes
156	No difference	YDR297W	sur2	*sur2Δ*	0.92786499	1.0611728	0.544707	No	0.689813	No
157	No difference	YAL011W	swc3	*swc3Δ*	1.12608424	1.80524683	0.304321	No	<0.000001	Yes
158	Defective growth	YAR003W	swd1	*swd1Δ*	0.711936436	0.36391785	0.000593	Yes	<0.000001	Yes
159	Defective growth	YBR175W	swd3	*swd3Δ*	0.808485441	0.862130383	0.044069	Yes	0.259708	No
160	Growth advantage	YDR126W	swf1	*swf1Δ*	1.177410378	1.275084365	0.047199	Yes	0.016875	Yes
161	Defective growth	YJL176C	swi3	*swi3Δ*	0.588114786	0.539241339	<0.000001	Yes	0.000007	Yes

162	Defective growth	YLR182W	swi6	*swi6Δ*	0.639001162	0.856771754	0.000025	Yes	0.191286	No
163	Defective growth	YPL180W	tco89	*tco89Δ*	0.788801297	0.8000552	0.002528	Yes	0.026144	Yes
164	No difference	YPL214C	thi6	*thi6Δ*	1.02328981	1.00514021	0.757951	No	0.957855	No
165	Defective growth	YJL164C	tpk1	*tpk1Δ*	0.645841278	0.665680308	0.002118	Yes	0.011658	Yes
166	Defective growth	YDR074W	tps2	*tps2Δ*	0.567490335	0.793953735	0.000972	Yes	0.220835	No
167	Defective growth	YOL093W	trm10	*trm10Δ*	0.523451541	0.825564644	<0.000001	Yes	0.153361	No
168	Growth advantage	YOL125W	trm13	*trm13Δ*	1.264985449	1.154297367	0.000053	Yes	0.066345	No
169	Defective growth	YDR007W	trp1	*trp1Δ*	0.771041138	0.929272659	0.021499	Yes	0.580525	No
170	Defective growth	YPR066W	uba3	*uba3Δ*	0.366672836	0.487210809	<0.000001	Yes	0.000002	Yes
171	Growth advantage	YHR111W	uba4	*uba4Δ*	1.186738652	1.182222204	0.021485	Yes	0.081086	No
172	No difference	YLR306W	ubc12	*ubc12Δ*	0.93766577	1.09069777	0.540904	No	0.489441	No
173	Defective growth	YBL067C	ubp13	*ubp13Δ*	0.440321386	0.670608143	<0.000001	Yes	0.002279	Yes
174	Defective growth	YER151C	ubp3	*ubp3Δ*	0.52782037	0.30573327	0.000076	Yes	0.000006	Yes
175	Defective growth	YLR024C	ubr2	*ubr2Δ*	0.259494451	0.122803261	<0.000001	Yes	<0.000001	Yes
176	Defective growth	YLR420W	ura4	*ura4Δ*	0.672328954	0.548994679	0.00004	Yes	0.000011	Yes
177	Defective growth	YNL229C	ure2	*ure2Δ*	0.613904204	1.021079707	0.000206	Yes	0.874368	No
178	No difference	YIL008W	urm1	*urm1Δ*	0.9708406	0.83779267	0.690706	No	0.085753	No
179	No difference	YEL013W	vac8	*vac8Δ*	0.90327332	0.89188365	0.198544	No	0.264132	No
180	Defective growth	YNL212W	vid27	*vid27Δ*	0.574220235	0.730830632	0.000003	Yes	0.020906	Yes
181	Defective growth	YJR102C	vps25	*vps25Δ*	0.324543156	0.410851109	<0.000001	Yes	<0.000001	Yes
182	Defective growth	YDR495C	vps3	*vps3Δ*	0.00435199	0.022590338	<0.000001	Yes	<0.000001	Yes
183	Defective growth	YDR027C	vps54	*vps54Δ*	0.548110657	0.506140409	<0.000001	Yes	<0.000001	Yes
184	Growth advantage	YDR200C	vps64	*vps64Δ*	4.858343419	3.995334936	<0.000001	Yes	0.000055	Yes
185	Defective growth	YDR372C	vps74	*vps74Δ*	0.78262852	0.847676779	0.025286	Yes	0.222766	No
186	Growth advantage	YPL239W	yar1	*yar1Δ*	1.171858355	1.068914252	0.029586	Yes	0.497344	No
187	No difference	ybr292c	ybr292c	*ybr292cΔ*	0.98752297	0.92841251	0.878514	No	0.629965	No
188	Defective growth	ycr050c	ycr050c	*ycr050cΔ*	0.605055287	0.636521645	<0.000001	Yes	0.000119	Yes
189	Defective growth	ydl118w	ydl118w	*ydl118wΔ*	0.508486716	0.479618206	<0.000001	Yes	<0.000001	Yes
190	No difference	ydr048c	ydr048c	*ydr048cΔ*	1.0263837	1.06287507	0.702227	No	0.479073	No
191	Defective growth	ydr222w	ydr222w	*ydr222wΔ*	0.577165159	0.502662907	<0.000001	Yes	<0.000001	Yes
192	Defective growth	ydr525w	ydr525w	*ydr525wΔ*	0.397312494	0.207925011	0.000013	Yes	0.000009	Yes
193	No difference	yel004w	yea4	*yea4Δ*	0.91754464	0.81948108	0.445965	No	0.194988	No
194	Defective growth	ygl214w	ygl214w	*ygl214wΔ*	0.432692765	0.591712737	<0.000001	Yes	0.000005	Yes
195	No difference	yhr029c	yhi9	*yhi9Δ*	1.14458015	1.20076712	0.188261	No	0.155783	No
196	Defective growth	ycr059c	yih1	*yih1Δ*	0.367247615	0.564417346	<0.000001	Yes	0.00002	Yes
197	Defective growth	yjl132w	yjl132w	*yjl132wΔ*	0.729270964	0.778884688	0.001464	Yes	0.043112	Yes
198	Defective growth	yjr018w	yjr018w	*yjr018wΔ*	0.667477499	0.698960976	0.000023	Yes	0.002804	Yes
199	Defective growth	ylr200w	yke2	*yke2Δ*	0.616453349	0.712078106	<0.000001	Yes	0.000983	Yes
200	Defective growth	ymr001c-a	ymr001c-a	*ymr001c-aΔ*	0.665719937	0.578951185	0.000044	Yes	0.000064	Yes
201	Defective growth	ynl089c	ynl089c	*ynl089cΔ*	0.450687297	0.784008962	0.000004	Yes	0.155047	No
202	No difference	ynl140c	ynl140c	*ynl140cΔ*	1.01132794	1.00206934	0.887377	No	0.983963	No
203	Defective growth	ynr068c	ynr068c	*ynr068cΔ*	0.607515142	0.669878668	<0.000001	Yes	0.001254	Yes
204	Defective growth	yor139c	yor139c	*yor139cΔ*	0.558883992	0.655186174	<0.000001	Yes	0.000212	Yes
205	No difference	ypl150w	ypl150w	*ypl150wΔ*	0.98281997	1.26652602	0.809018	No	0.003663	Yes
206	No difference	ypl205c	ypl205c	*ypl205cΔ*	1.05924464	1.00900802	0.437485	No	0.926905	No
207	Growth advantage	yol109w	zeo1	*zeo1Δ*	1.752214168	2.241048557	<0.000001	Yes	<0.000001	Yes
208	Defective growth	ynl241c	zwf1	*zwf1Δ*	0.673124372	0.639566886	0.000029	Yes	0.000337	Yes

Table S2: Orthologues of screen candidates and associated human diseases

	GENE STANDARD NAME	GENE SYSTEMATIC NAME	GENE NAME	HOMOLOGUE STANDARD NAME	HOMOLOGUE NAME	HOMOLOGUE GENE IDENTIFIER	CROSS REFERENCES IDENTIFIER	DISEASE IDENTIFIER	HOMOLOGUE DISEASES
1	*AAP1*	*YHR047C*	Arginine/alanine AminoPeptidase	ANPEP	alanyl (membrane) aminopeptidase	290	151530		
2	*AAP1*	*YHR047C*	Arginine/alanine AminoPeptidase	ENPEP	glutamyl aminopeptidase (aminopeptidase A)	2028	138297		
3	*AAP1*	*YHR047C*	Arginine/alanine AminoPeptidase	ERAP1	endoplasmic reticulum aminopeptidase 1	51752	606832		
4	*AAP1*	*YHR047C*	Arginine/alanine AminoPeptidase	ERAP2	endoplasmic reticulum aminopeptidase 2	64167	609497		
5	*AAP1*	*YHR047C*	Arginine/alanine AminoPeptidase	LNPEP	leucyl/cystinyl aminopeptidase	4012	151300		
6	*AAP1*	*YHR047C*	Arginine/alanine AminoPeptidase	LVRN	laeverin	206338	610046		
7	*AAP1*	*YHR047C*	Arginine/alanine AminoPeptidase	NPEPPS	aminopeptidase puromycin sensitive	9520	606793		
8	*AAP1*	*YHR047C*	Arginine/alanine AminoPeptidase	TRHDE	thyrotropin-releasing hormone degrading enzyme	29953	606950		
9	*ADK1*	*YDR226W*	ADenylate Kinase	AK2	adenylate kinase 2	204	103020	267500	RETICULAR DYSGENESIS
10	*APL2*	*YKL135C*	clathrin Adaptor Protein complex Large chain	AP1B1	adaptor-related protein complex 1, beta 1 subunit	162	600157		
11	*APL2*	*YKL135C*	clathrin Adaptor Protein complex Large chain	AP2B1	adaptor-related protein complex 2, beta 1 subunit	163	601025		
12	*APL2*	*YKL135C*	clathrin Adaptor Protein complex Large chain	AP4B1	adaptor-related protein complex 4, beta 1 subunit	10717	607245	614066	SPASTIC PARAPLEGIA 47, AUTOSOMAL RECESSIVE; SPG47
13	*APT1*	*YML022W*	Adenine PhosphoribosylTransferase	APRT	adenine phosphoribosyltransferase	353	102600	614723	ADENINE PHOSPHORIBOSYLTRANSFERASE DEFICIENCY; APRTD
14	*AVL9*	*YLR114C*	Apl2 Vps1 Lethal	AVL9	AVL9 homolog (S. cerevisiase)	23080	612927		
15	*BEM2*	*YER155C*	Bud EMergence	ARHGAP10	Rho GTPase activating protein 10	79658	609746		
16	*BEM2*	*YER155C*	Bud EMergence	ARHGAP12	Rho GTPase activating protein 12	94134	610577		
17	*BEM2*	*YER155C*	Bud EMergence	ARHGAP15	Rho GTPase activating protein 15	55843	610578		
18	*BEM2*	*YER155C*	Bud EMergence	ARHGAP21	Rho GTPase activating protein 21	57584	609870		
19	*BEM2*	*YER155C*	Bud EMergence	ARHGAP23	Rho GTPase activating protein 23	57636	610590		
20	*BEM2*	*YER155C*	Bud EMergence	ARHGAP26	Rho GTPase activating protein 26	23092	605370	607785	JUVENILE MYELOMONOCYTIC LEUKEMIA; JMML
21	*BEM2*	*YER155C*	Bud EMergence	ARHGAP27	Rho GTPase activating protein 27	201176	610591		
22	*BEM2*	*YER155C*	Bud EMergence	ARHGAP35	Rho GTPase activating protein 35	2909	605277		
23	*BEM2*	*YER155C*	Bud EMergence	ARHGAP42	Rho GTPase activating protein 42	143872	615936		
24	*BEM2*	*YER155C*	Bud EMergence	ARHGAP9	Rho GTPase activating protein 9	64333	610576		
25	*BEM2*	*YER155C*	Bud EMergence	CHN1	chimerin 1	1123	118423	604356	DUANE RETRACTION SYNDROME 2; DURS2
26	*BEM2*	*YER155C*	Bud EMergence	CHN2	chimerin 2	1124	602857		
27	*BEM2*	*YER155C*	Bud EMergence	GMIP	GEM interacting protein	51291	609694		
28	*BEM2*	*YER155C*	Bud EMergence	HMHA1	histocompatibility (minor) HA-1	23526	601155		
29	*BEM2*	*YER155C*	Bud EMergence	OPHN1	oligophrenin 1	4983	300127	300486	MENTAL RETARDATION, X-LINKED, WITH CEREBELLAR HYPOPLASIA AND DISTINCTIVE FACIAL
30	*BEM2*	*YER155C*	Bud EMergence	RACGAP1	Rac GTPase activating protein 1	29127	604980		
31	*BEM4*	*YPL161C*	Bud EMergence	RAP1GDS1	RAP1, GTP-GDP dissociation stimulator 1	5910	179502		
32	*BNA4*	*YBL098W*	Biosynthesis of Nicotinic Acid	COQ6	coenzyme Q6 monooxygenase	51004	614647	614650	COENZYME Q10 DEFICIENCY, PRIMARY, 6; COQ10D6
33	*BNA4*	*YBL098W*	Biosynthesis of Nicotinic Acid	KMO	kynurenine 3-monooxygenase (kynurenine 3-hydroxylase)	8564	603538		
34	*BRE1*	*YDL074C*	BREfeldin A sensitivity	RNF20	ring finger protein 20, E3 ubiquitin protein ligase	56254	607699		
35	*BRE1*	*YDL074C*	BREfeldin A sensitivity	RNF40	ring finger protein 40, E3 ubiquitin protein ligase	9810	607700		
36	*BRE5*	*YNR051C*	BREfeldin A sensitivity	G3BP1	GTPase activating protein (SH3 domain) binding protein 1	10146	608431		
37	*BUD16*	*YEL029C*	BUD site selection	PDXK	pyridoxal (pyridoxine, vitamin B6) kinase	8566	179020		
38	*BUD22*	*YMR014W*	BUD site selection	SRFBP1	serum response factor binding protein 1	153443	610479		
39	*CDC50*	*YCR094W*	Cell Division Cycle	TMEM30A	transmembrane protein 30A	55754	611028		
40	*CDC50*	*YCR094W*	Cell Division Cycle	TMEM30B	transmembrane protein 30B	161291	611029		
41	*CDC50*	*YCR094W*	Cell Division Cycle	TMEM30C	transmembrane protein 30C	644444	611030		
42	*CDC55*	*YGL190C*	Cell Division Cycle	PPP2R2A	protein phosphatase 2, regulatory subunit B, alpha	5520	604941		
43	*CDC55*	*YGL190C*	Cell Division Cycle	PPP2R2B	protein phosphatase 2, regulatory subunit B, beta	5521	604325	604326	SPINOCEREBELLAR ATAXIA 12; SCA12
44	*CDC55*	*YGL190C*	Cell Division Cycle	PPP2R2C	protein phosphatase 2, regulatory subunit B, gamma	5522	605997		
45	*CDC55*	*YGL190C*	Cell Division Cycle	PPP2R2D	protein phosphatase 2, regulatory subunit B, delta	55844	613992		
46	*CGI121*	*YML036W*	homolog of human CGI-121	TPRKB	TP53RK binding protein	51002	608680		
47	*CIN2*	*YPL241C*	Chromosome INstability	TBCC	tubulin folding cofactor C	6903	602971		
48	*CLN3*	*YAL040C*	CycLiN	CCNA2	cyclin A2	890	123835		
49	*CLN3*	*YAL040C*	CycLiN	CCNB1	cyclin B1	891	123836		
50	*CLN3*	*YAL040C*	CycLiN	CCNB2	cyclin B2	9133	602755		
51	*CLN3*	*YAL040C*	CycLiN	CCNB3	cyclin B3	85417	300456		
52	*CLN3*	*YAL040C*	CycLiN	CCNE1	cyclin E1	898	123837		
53	*CLN3*	*YAL040C*	CycLiN	CCNE2	cyclin E2	9134	603775		
54	*CLN3*	*YAL040C*	CycLiN	CCNF	cyclin F	899	600227		
55	*CLN3*	*YAL040C*	CycLiN	CCNO	cyclin O	10309	607752	615872	CILIARY DYSKINESIA, PRIMARY, 29; CILD29
56	*DBF2*	*YGR092W*	DumbBell Former	DMPK	dystrophia myotonica-protein kinase	1760	605377	160900	MYOTONIC DYSTROPHY 1; DM1
57	*DOM34*	*YNL001W*	Duplication Of Multilocus region	PELO	pelota homolog (Drosophila)	53918	605757		
58	*DUF1*	*YOL087C*	DUB-associated Factor 1	WDR48	WD repeat domain 48	57599	612167		
59	*ERG24*	*YNL280C*	ERGosterol biosynthesis	DHCR7	7-dehydrocholesterol reductase	1717	602858	270400	SMITH-LEMLI-OPITZ SYNDROME; SLOS
60	*ERG24*	*YNL280C*	ERGosterol biosynthesis	LBR	lamin B receptor	3930	600024	169400	PELGER-HUET ANOMALY; PHA
61	*ERG24*	*YNL280C*	ERGosterol biosynthesis	LBR	lamin B receptor	3930	600024	613471	REYNOLDS SYNDROME
62	*ERG24*	*YNL280C*	ERGosterol biosynthesis	LBR	lamin B receptor	3930	600024	215140	GREENBERG DYSPLASIA; GRBGD
63	*ERG24*	*YNL280C*	ERGosterol biosynthesis	TM7SF2	transmembrane 7 superfamily member 2	7108	603414		
64	*ERG5*	*YMR015C*	ERGosterol biosynthesis	CYP26A1	cytochrome P450, family 26, subfamily A, polypeptide 1	1592	602239		
65	*ERG5*	*YMR015C*	ERGosterol biosynthesis	CYP26B1	cytochrome P450, family 26, subfamily B, polypeptide 1	56603	605207	614416	RADIOHUMERAL FUSIONS WITH OTHER SKELETAL AND CRANIOFACIAL ANOMALIES; RHFCA
66	*ERG5*	*YMR015C*	ERGosterol biosynthesis	CYP26C1	cytochrome P450, family 26, subfamily C, polypeptide 1	340665	608428	614974	FOCAL FACIAL DERMAL DYSPLASIA 4; FFDD4
67	*FAB1*	*YFR019W*	Forms Aploid and Binucleate cells	PIKFYVE	phosphoinositide kinase, FYVE finger containing	200576	609414	121850	CORNEAL DYSTROPHY, FLECK
68	*FAB1*	*YFR019W*	Forms Aploid and Binucleate cells	ZFYVE16	zinc finger, FYVE domain containing 16	9765	608880		
69	*FAB1*	*YFR019W*	Forms Aploid and Binucleate cells	ZFYVE21	zinc finger, FYVE domain containing 21	79038	613504		
70	*FAB1*	*YFR019W*	Forms Aploid and Binucleate cells	ZFYVE28	zinc finger, FYVE domain containing 28	57732	614176		
71	*FAB1*	*YFR019W*	Forms Aploid and Binucleate cells	ZFYVE9	zinc finger, FYVE domain containing 9	9372	603755		
72	*GEF1*	*YJR040W*	Glycerol Ethanol, Ferric requiring	CLCN1	chloride channel, voltage-sensitive 1	1180	118425	255700	MYOTONIA CONGENITA, AUTOSOMAL RECESSIVE
73	*GEF1*	*YJR040W*	Glycerol Ethanol, Ferric requiring	CLCN1	chloride channel, voltage-sensitive 1	1180	118425	160800	MYOTONIA CONGENITA, AUTOSOMAL DOMINANT
74	*GEF1*	*YJR040W*	Glycerol Ethanol, Ferric requiring	CLCN2	chloride channel, voltage-sensitive 2	1181	600570	615651	LEUKOENCEPHALOPATHY WITH ATAXIA; LKPAT
75	*GEF1*	*YJR040W*	Glycerol Ethanol, Ferric requiring	CLCN2	chloride channel, voltage-sensitive 2	1181	600570	607628	EPILEPSY, IDIOPATHIC GENERALIZED, SUSCEPTIBILITY TO, 11; EIG11 EPILEPSY, JUVENILE MYOCLONIC, SUSCEPTIBILITY TO, 8, INCLUDED; EJM8, INCLUDED
76	*GEF1*	*YJR040W*	Glycerol Ethanol, Ferric requiring	CLCN3	chloride channel, voltage-sensitive 3	1182	600580		
77	*GEF1*	*YJR040W*	Glycerol Ethanol, Ferric requiring	CLCN4	chloride channel, voltage-sensitive 4	1183	302910		
78	*GEF1*	*YJR040W*	Glycerol Ethanol, Ferric requiring	CLCN5	chloride channel, voltage-sensitive 5	1184	300008	300009	DENT DISEASE 1
79	*GEF1*	*YJR040W*	Glycerol Ethanol, Ferric requiring	CLCN5	chloride channel, voltage-sensitive 5	1184	300008	300554	HYPOPHOSPHATEMIC RICKETS, X-LINKED RECESSIVE
80	*GEF1*	*YJR040W*	Glycerol Ethanol, Ferric requiring	CLCN5	chloride channel, voltage-sensitive 5	1184	300008	308990	PROTEINURIA, LOW MOLECULAR WEIGHT, WITH HYPERCALCIURIA AND NEPHROCALCINOSIS
81	*GEF1*	*YJR040W*	Glycerol Ethanol, Ferric requiring	CLCN5	chloride channel, voltage-sensitive 5	1184	300008	310468	NEPHROLITHIASIS, X-LINKED RECESSIVE, WITH RENAL FAILURE; XRN
82	*GEF1*	*YJR040W*	Glycerol Ethanol, Ferric requiring	CLCN6	chloride channel, voltage-sensitive 6	1185	602726		
83	*GEF1*	*YJR040W*	Glycerol Ethanol, Ferric requiring	CLCN7	chloride channel, voltage-sensitive 7	1186	602727	166600	OSTEOPETROSIS, AUTOSOMAL DOMINANT 2; OPTA2
84	*GEF1*	*YJR040W*	Glycerol Ethanol, Ferric requiring	CLCN7	chloride channel, voltage-sensitive 7	1186	602727	611490	OSTEOPETROSIS, AUTOSOMAL RECESSIVE 4; OPTB4
85	*GEF1*	*YJR040W*	Glycerol Ethanol, Ferric requiring	CLCNKA	chloride channel, voltage-sensitive Ka	1187	602024	613090	BARTTER SYNDROME, TYPE 4B
86	*GEF1*	*YJR040W*	Glycerol Ethanol, Ferric requiring	CLCNKB	chloride channel, voltage-sensitive Kb	1188	602023	613090	BARTTER SYNDROME, TYPE 4B
87	*GEF1*	*YJR040W*	Glycerol Ethanol, Ferric requiring	CLCNKB	chloride channel, voltage-sensitive Kb	1188	602023	607364	BARTTER SYNDROME, TYPE 3
88	*GET1*	*YGL020C*	Guided Entry of Tail-anchored proteins	WRB	tryptophan rich basic protein	7485	602915		
89	*GET3*	*YDL100C*	Guided Entry of Tail-anchored proteins	ASNA1	arsA arsenite transporter, ATP-binding, homolog 1 (bacterial)	439	601913		
90	*GIM4*	*YEL003W*	Gene Involved in Microtubule biogenesis	PFDN2	prefoldin subunit 2	5202	613466		
91	*GIM5*	*YML094W*	Gene Involved in Microtubule biogenesis	PFDN5	prefoldin subunit 5	5204	604899		
92	*GLO3*	*YER122C*	GLyOxalase	ADAP1	ArfGAP with dual PH domains 1	11033	608114		
93	*GLO3*	*YER122C*	GLyOxalase	ADAP2	ArfGAP with dual PH domains 2	55803	608635		
94	*GLO3*	*YER122C*	GLyOxalase	AGAP1	ArfGAP with GTPase domain, ankyrin repeat and PH domain 1	116987	608651		
95	*GLO3*	*YER122C*	GLyOxalase	AGAP2	ArfGAP with GTPase domain, ankyrin repeat and PH domain 2	116986	605476		
96	*GLO3*	*YER122C*	GLyOxalase	ARAP1	ArfGAP with RhoGAP domain, ankyrin repeat and PH domain 1	116985	606646		
97	*GLO3*	*YER122C*	GLyOxalase	ARAP2	ArfGAP with RhoGAP domain, ankyrin repeat and PH domain 2	116984	606645		
98	*GLO3*	*YER122C*	GLyOxalase	ARFGAP2	ADP-ribosylation factor GTPase activating protein 2	84364	606908		
99	*GLO3*	*YER122C*	GLyOxalase	ARFGAP3	ADP-ribosylation factor GTPase activating protein 3	26286	612439		
100	*GLO3*	*YER122C*	GLyOxalase	GIT1	G protein-coupled receptor kinase interacting ArfGAP 1	28964	608434		
101	*GLO3*	*YER122C*	GLyOxalase	GIT2	G protein-coupled receptor kinase interacting ArfGAP 2	9815	608564		
102	*GLO3*	*YER122C*	GLyOxalase	SMAP1	small ArfGAP 1	60682	611372		
103	*GOS1*	*YHL031C*	GOlgi Snare	GOSR1	golgi SNAP receptor complex member 1	9527	604026		
104	*GTR1*	*YML121W*	GTp binding protein Resemblance	RRAGA	Ras-related GTP binding A	10670	612194		
105	*GTR1*	*YML121W*	GTp binding protein Resemblance	RRAGB	Ras-related GTP binding B	10325	300725		
106	*GYP7*	*YDL234C*	Gtpase-activating protein for Ypt7 Protein	SGSM1	small G protein signaling modulator 1	129049	611417		
107	*GYP7*	*YDL234C*	Gtpase-activating protein for Ypt7 Protein	SGSM2	small G protein signaling modulator 2	9905	611418		
108	*GYP7*	*YDL234C*	Gtpase-activating protein for Ypt7 Protein	TBC1D15	TBC1 domain family, member 15	64786	612662		
109	*GYP7*	*YDL234C*	Gtpase-activating protein for Ypt7 Protein	TBC1D25	TBC1 domain family, member 25	4943	311240		
110	*HIR2*	*YOR038C*	Histone Regulation	HIRA	histone cell cycle regulator	7290	600237		
111	*HIR3*	*YJR140C*	Histone Regulation	CABIN1	calcineurin binding protein 1	23523	604251		
112	*HOF1*	*YMR032W*	Homolog Of cdc Fifteen	PACSIN1	protein kinase C and casein kinase substrate in neurons 1	29993	606512		
113	*HOF1*	*YMR032W*	Homolog Of cdc Fifteen	PACSIN2	protein kinase C and casein kinase substrate in neurons 2	11252	604960		
114	*HOF1*	*YMR032W*	Homolog Of cdc Fifteen	PACSIN3	protein kinase C and casein kinase substrate in neurons 3	29763	606513		
115	*HOF1*	*YMR032W*	Homolog Of cdc Fifteen	PSTPIP1	proline-serine-threonine phosphatase interacting protein 1	9051	606347	604416	PYOGENIC STERILE ARTHRITIS, PYODERMA GANGRENOSUM, AND ACNE
116	*HOF1*	*YMR032W*	Homolog Of cdc Fifteen	PSTPIP2	proline-serine-threonine phosphatase interacting protein 2	9050	616046		
117	*HOG1*	*YLR113W*	High Osmolarity Glycerol response	MAPK10	mitogen-activated protein kinase 10	5602	602897		
118	*HOG1*	*YLR113W*	High Osmolarity Glycerol response	MAPK11	mitogen-activated protein kinase 11	5600	602898		
119	*HOG1*	*YLR113W*	High Osmolarity Glycerol response	MAPK12	mitogen-activated protein kinase 12	6300	602399		
120	*HOG1*	*YLR113W*	High Osmolarity Glycerol response	MAPK13	mitogen-activated protein kinase 13	5603	602899		
121	*HOG1*	*YLR113W*	High Osmolarity Glycerol response	MAPK14	mitogen-activated protein kinase 14	1432	600289		
122	*HOG1*	*YLR113W*	High Osmolarity Glycerol response	MAPK8	mitogen-activated protein kinase 8	5599	601158		
123	*HOG1*	*YLR113W*	High Osmolarity Glycerol response	MAPK9	mitogen-activated protein kinase 9	5601	602896		
124	*HST1*	*YOL068C*	Homolog of SIR Two (SIR2)	SIRT1	sirtuin 1	23411	604479		
125	*HST1*	*YOL068C*	Homolog of SIR Two (SIR2)	SIRT4	sirtuin 4	23409	604482		
126	*HST1*	*YOL068C*	Homolog of SIR Two (SIR2)	SIRT5	sirtuin 5	23408	604483		
127	*IES2*	*YNL215W*	Ino Eighty Subunit	INO80B	INO80 complex subunit B	83444	616456		
128	*INO4*	*YOL108C*	INOsitol requiring	MITF	microphthalmia-associated transcription factor	4286	156845	614456	MELANOMA, CUTANEOUS MALIGNANT, SUSCEPTIBILITY TO, 8; CMM8
129	*INO4*	*YOL108C*	INOsitol requiring	MITF	microphthalmia-associated transcription factor	4286	156845	103470	ALBINISM, OCULAR, WITH SENSORINEURAL DEAFNESS
130	*INO4*	*YOL108C*	INOsitol requiring	MITF	microphthalmia-associated transcription factor	4286	156845	103500	TIETZ SYNDROME
131	*INO4*	*YOL108C*	INOsitol requiring	MITF	microphthalmia-associated transcription factor	4286	156845	193510	WAARDENBURG SYNDROME, TYPE 2A; WS2A
132	*INO4*	*YOL108C*	INOsitol requiring	TFE3	transcription factor binding to IGHM enhancer 3	7030	314310	300854	RENAL CELL CARCINOMA, Xp11-ASSOCIATED; RCCX1
133	*INO4*	*YOL108C*	INOsitol requiring	TFEB	transcription factor EB	7942	600744		
134	*INO4*	*YOL108C*	INOsitol requiring	TFEC	transcription factor EC	22797	604732		
135	*INO4*	*YOL108C*	INOsitol requiring	USF1	upstream transcription factor 1	7391	191523	602491	HYPERLIPIDEMIA, COMBINED, 1
136	*INO4*	*YOL108C*	INOsitol requiring	USF2	upstream transcription factor 2, c-fos interacting	7392	600390		
137	*IRA2*	*YOL081W*	Inhibitory Regulator of the RAS-cAMP pathway	DAB2IP	DAB2 interacting protein	153090	609205		
138	*IRA2*	*YOL081W*	Inhibitory Regulator of the RAS-cAMP pathway	NF1	neurofibromin 1	4763	613113	162200	NEUROFIBROMATOSIS, TYPE I; NF1

139	*IRA2*	*YOL081W*	Inhibitory Regulator of the RAS-cAMP pathway	NF1	neurofibromin 1	4763	613113	607785	JUVENILE MYELOMONOCYTIC LEUKEMIA; JMML
140	*IRA2*	*YOL081W*	Inhibitory Regulator of the RAS-cAMP pathway	NF1	neurofibromin 1	4763	613113	193520	WATSON SYNDROME; WTSN
141	*IRA2*	*YOL081W*	Inhibitory Regulator of the RAS-cAMP pathway	NF1	neurofibromin 1	4763	613113	601321	NEUROFIBROMATOSIS-NOONAN SYNDROME; NFNS
142	*IRA2*	*YOL081W*	Inhibitory Regulator of the RAS-cAMP pathway	NF1	neurofibromin 1	4763	613113	162210	NEUROFIBROMATOSIS, FAMILIAL SPINAL
143	*IRA2*	*YOL081W*	Inhibitory Regulator of the RAS-cAMP pathway	RASA1	RAS p21 protein activator (GTPase activating protein) 1	5921	139150	605462	BASAL CELL CARCINOMA, SUSCEPTIBILITY TO, 1; BCC1 BASAL CELL CARCINOMA, NONSYNDROMIC, INCLUDED
144	*IRA2*	*YOL081W*	Inhibitory Regulator of the RAS-cAMP pathway	RASA1	RAS p21 protein activator (GTPase activating protein) 1	5921	139150	608354	CAPILLARY MALFORMATION-ARTERIOVENOUS MALFORMATION; CMAVM CAPILLARY MALFORMATION WITHOUT ARTERIOVENOUS MALFORMATION, INCLUDED
145	*IRA2*	*YOL081W*	Inhibitory Regulator of the RAS-cAMP pathway	RASA1	RAS p21 protein activator (GTPase activating protein) 1	5921	139150	608355	PARKES WEBER SYNDROME
146	*IRA2*	*YOL081W*	Inhibitory Regulator of the RAS-cAMP pathway	RASA2	RAS p21 protein activator 2	5922	601589		
147	*IRA2*	*YOL081W*	Inhibitory Regulator of the RAS-cAMP pathway	RASA3	RAS p21 protein activator 3	22821	605182		
148	*IRA2*	*YOL081W*	Inhibitory Regulator of the RAS-cAMP pathway	RASA4	RAS p21 protein activator 4	10156	607943		
149	*IRA2*	*YOL081W*	Inhibitory Regulator of the RAS-cAMP pathway	RASAL1	RAS protein activator like 1 (GAP1 like)	8437	604118		
150	*IRA2*	*YOL081W*	Inhibitory Regulator of the RAS-cAMP pathway	RASAL2	RAS protein activator like 2	9462	606136		
151	*IRA2*	*YOL081W*	Inhibitory Regulator of the RAS-cAMP pathway	RASAL3	RAS protein activator like 3	64926	616561		
152	*IRA2*	*YOL081W*	Inhibitory Regulator of the RAS-cAMP pathway	SYNGAP1	synaptic Ras GTPase activating protein 1	8831	603384	612621	MENTAL RETARDATION, AUTOSOMAL DOMINANT 5; MRD5
153	*IRC15*	*YPL017C*	Increased Recombination Centers	AIFM1	apoptosis-inducing factor, mitochondrion-associated, 1	9131	300169	300816	COMBINED OXIDATIVE PHOSPHORYLATION DEFICIENCY 6; COXPD6
154	*IRC15*	*YPL017C*	Increased Recombination Centers	AIFM1	apoptosis-inducing factor, mitochondrion-associated, 1	9131	300169	310490	COWCHOCK SYNDROME; COWCK
155	*IRC15*	*YPL017C*	Increased Recombination Centers	AIFM1	apoptosis-inducing factor, mitochondrion-associated, 1	9131	310490	300816	COMBINED OXIDATIVE PHOSPHORYLATION DEFICIENCY 6; COXPD6
156	*IRC15*	*YPL017C*	Increased Recombination Centers	AIFM1	apoptosis-inducing factor, mitochondrion-associated, 1	9131	310490	310490	COWCHOCK SYNDROME; COWCK
157	*IRC15*	*YPL017C*	Increased Recombination Centers	DLD	dihydrolipoamide dehydrogenase	1738	238331	246900	DIHYDROLIPOAMIDE DEHYDROGENASE DEFICIENCY; DLDD
158	*IRC15*	*YPL017C*	Increased Recombination Centers	GSR	glutathione reductase	2936	138300		
159	*IRC15*	*YPL017C*	Increased Recombination Centers	TXNRD1	thioredoxin reductase 1	7296	601112		
160	*IRC15*	*YPL017C*	Increased Recombination Centers	TXNRD2	thioredoxin reductase 2	10587	606448		
161	*IRC15*	*YPL017C*	Increased Recombination Centers	TXNRD3	thioredoxin reductase 3	114112	606235		
162	*LEO1*	*YOR123C*	LEft Open reading frame	LEO1	LEO1 homolog, Paf1/RNA polymerase II complex component	123169	610507		
163	*MBF1*	*YOR298C-A*	Multiprotein Bridging Factor	EDF1	endothelial differentiation-related factor 1	8721	605107		
164	*MDS3*	*YGL197W*	Mck1 Dosage Suppressor	FBXO42	F-box protein 42	54455	609109		
165	*MDS3*	*YGL197W*	Mck1 Dosage Suppressor	HCFC1	host cell factor C1	3054	300019	309541	METHYLMALONIC ACIDEMIA AND HOMOCYSTEINEMIA, cblX TYPE
166	*MDS3*	*YGL197W*	Mck1 Dosage Suppressor	KLHDC2	kelch domain containing 2	23588	611280		
167	*MET10*	*YFR030W*	METhionine requiring	MTRR	5-methyltetrahydrofolate-homocysteine methyltransferase reductase	4552	602568	601634	NEURAL TUBE DEFECTS, FOLATE-SENSITIVE; NTDFS
168	*MET10*	*YFR030W*	METhionine requiring	MTRR	5-methyltetrahydrofolate-homocysteine methyltransferase reductase	4552	602568	236270	HOMOCYSTINURIA-MEGALOBLASTIC ANEMIA, cblE COMPLEMENTATION TYPE; HMAE
169	*MET18*	*YIL128W*	METhionine requiring	MMS19	MMS19 homolog, cytosolic iron-sulfur assembly component	64210	614777		
170	*MOG1*	*YJR074W*	Multicopy suppressor Of ts Gsp1	RANGRF	RAN guanine nucleotide release factor	29098	607954		
171	*MRX1*	*YER077C*	Mitochondrial oRganization of gene eXpression (MIOREX)	LRPPRC	leucine-rich pentatricopeptide repeat containing	10128	607544	220111	LEIGH SYNDROME, FRENCH CANADIAN TYPE; LSFC
172	*NHX1*	*YDR456W*	Na+/H+ eXchanger	SLC9A1	solute carrier family 9, subfamily A (NHE1, cation proton antiporter 1), member 1	6548	107310	616291	LICHTENSTEIN-KNORR SYNDROME; LIKNS
173	*NHX1*	*YDR456W*	Na+/H+ eXchanger	SLC9A2	solute carrier family 9, subfamily A (NHE2, cation proton antiporter 2), member 2	6549	600530		
174	*NHX1*	*YDR456W*	Na+/H+ eXchanger	SLC9A3	solute carrier family 9, subfamily A (NHE3, cation proton antiporter 3), member 3	6550	182307		
175	*NHX1*	*YDR456W*	Na+/H+ eXchanger	SLC9A4	solute carrier family 9, subfamily A (NHE4, cation proton antiporter 4), member 4	389015	600531		
176	*NHX1*	*YDR456W*	Na+/H+ eXchanger	SLC9A5	solute carrier family 9, subfamily A (NHE5, cation proton antiporter 5), member 5	6553	600477		
177	*NHX1*	*YDR456W*	Na+/H+ eXchanger	SLC9A6	solute carrier family 9, subfamily A (NHE6, cation proton antiporter 6), member 6	10479	300231	300243	MENTAL RETARDATION, X-LINKED, SYNDROMIC, CHRISTIANSON TYPE; MRXSCH
178	*NHX1*	*YDR456W*	Na+/H+ eXchanger	SLC9A7	solute carrier family 9, subfamily A (NHE7, cation proton antiporter 7), member 7	84679	300368		
179	*NHX1*	*YDR456W*	Na+/H+ eXchanger	SLC9A8	solute carrier family 9, subfamily A (NHE8, cation proton antiporter 8), member 8	23315	612730		
180	*NHX1*	*YDR456W*	Na+/H+ eXchanger	SLC9A9	solute carrier family 9, subfamily A (NHE9, cation proton antiporter 9), member 9	285195	608396	613410	AUTISM, SUSCEPTIBILITY TO, 16; AUTS16
181	*NMA1*	*YLR328W*	Nicotinamide Mononudeotide Adenylyltransferase	NMNAT1	nicotinamide nudeotide adenylyltransferase 1	64802	608700	608553	LEBER CONGENITAL AMAUROSIS 9; LCA9
182	*NMA1*	*YLR328W*	Nicotinamide Mononudeotide Adenylyltransferase	NMNAT2	nicotinamide nudeotide adenylyltransferase 2	23057	608701		
183	*NMA1*	*YLR328W*	Nicotinamide Mononudeotide Adenylyltransferase	NMNAT3	nicotinamide nudeotide adenylyltransferase 3	349565	608702		
184	*NOP12*	*YOL041C*	NucleOlar Protein	HNRNPA0	heterogeneous nudear ribonudeoprotein A0	10949	609409		
185	*NOP12*	*YOL041C*	NucleOlar Protein	HNRNPAB	heterogeneous nudear ribonudeoprotein A/B	3182	602688		
186	*NOP12*	*YOL041C*	NucleOlar Protein	HNRNPD	heterogeneous nudear ribonudeoprotein D (AU-rich element RNA binding protein 1, 37kDa)	3184	601324		
187	*NOP12*	*YOL041C*	NucleOlar Protein	HNRNPDL	heterogeneous nudear ribonudeoprotein D-like	9987	607137	609115	LIMB-GIRDLE MUSCULAR DYSTROPHY, TYPE 1G; LGMD1G
188	*NRG1*	*YDR043C*	Negative Regulator of Glucose-repressed genes	YY1	YY1 transcription factor	7528	600013		
189	*NRG1*	*YDR043C*	Negative Regulator of Glucose-repressed genes	YY2	YY2 transcription factor	404281	300570		
190	*NRG1*	*YDR043C*	Negative Regulator of Glucose-repressed genes	ZFP42	ZFP42 zinc finger protein	132625	614572		
191	*OGG1*	*YML060W*	8-OxoGuanine Glycosylase/lyase	OGG1	8-oxoguanine DNA glycosylase	4968	601982	144700	RENAL CELL CARCINOMA, NONPAPILLARY; RCC
192	*PAC10*	*YGR078C*	Perish in the Absence of Cin8p	VBP1	von Hippel-Lindau binding protein 1	7411	300133		
193	*PFA3*	*YNL326C*	Protein Fatty Acyltransferase	ZDHHC15	zinc finger, DHHC-type containing 15	158866	300576	300577	MENTAL RETARDATION, X-LINKED 91; MRX91
194	*PFA3*	*YNL326C*	Protein Fatty Acyltransferase	ZDHHC21	zinc finger, DHHC-type containing 21	340481	614605		
195	*PFA3*	*YNL326C*	Protein Fatty Acyltransferase	ZDHHC7	zinc finger, DHHC-type containing 7	55625	614604		
196	*PFD1*	*YJL179W*	PreFoldin	PFDN1	prefoldin subunit 1	5201	604897		
197	*PIB2*	*YGL023C*	PhosphatidylInositol(3)-phosphate Binding	RBSN	rabenosyn, RAB effector	64145	609511		
198	*PMT2*	*YAL023C*	Protein O-MannosylTransferase	POMT1	protein-O-mannosyltransferase 1	10585	607423	613155	MUSCULAR DYSTROPHY-DYSTROGLYCANOPATHY (CONGENITAL WITH MENTAL RETARDATION), TYPE B, 1; MDDGB1
199	*PMT2*	*YAL023C*	Protein O-MannosylTransferase	POMT1	protein-O-mannosyltransferase 1	10585	607423	236670	MUSCULAR DYSTROPHY-DYSTROGLYCANOPATHY (CONGENITAL WITH BRAIN AND EYE ANOMALIES), TYPE A, 1; MDDGA1
200	*PMT2*	*YAL023C*	Protein O-MannosylTransferase	POMT1	protein-O-mannosyltransferase 1	10585	607423	609308	MUSCULAR DYSTROPHY-DYSTROGLYCANOPATHY (LIMB-GIRDLE), TYPE C, 1; MDDGC1
201	*PMT2*	*YAL023C*	Protein O-MannosylTransferase	POMT2	protein-O-mannosyltransferase 2	29954	607439	613150	MUSCULAR DYSTROPHY-DYSTROGLYCANOPATHY (CONGENITAL WITH BRAIN AND EYE ANOMALIES), TYPE A, 2; MDDGA2
202	*PMT2*	*YAL023C*	Protein O-MannosylTransferase	POMT2	protein-O-mannosyltransferase 2	29954	607439	613156	MUSCULAR DYSTROPHY-DYSTROGLYCANOPATHY (CONGENITAL WITH MENTAL RETARDATION), TYPE B, 2; MDDGB2
203	*PMT2*	*YAL023C*	Protein O-MannosylTransferase	POMT2	protein-O-mannosyltransferase 2	29954	607439	613158	MUSCULAR DYSTROPHY-DYSTROGLYCANOPATHY (LIMB-GIRDLE), TYPE C, 2; MDDGC2
204	*POP2*	*YNR052C*	PGK promoter directed OverProduction	CNOT7	CCR4-NOT transcription complex, subunit 7	29883	604913		
205	*POP2*	*YNR052C*	PGK promoter directed OverProduction	CNOT8	CCR4-NOT transcription complex, subunit 8	9337	603731		
206	*RCY1*	*YJL204C*	ReCYding	EXOC5	exocyst complex component 5	10640	604469		
207	*RGP1*	*YDR137W*	Reduced Growth Phenotype	RGP1	RGP1 homolog, RAB6A GEF complex partner 1	9827	615742		
208	*ROD1*	*YOR018W*	Resistance to O-Dinitrobenzene	ARRDC3	arrestin domain containing 3	57561	612464		
209	*ROD1*	*YOR018W*	Resistance to O-Dinitrobenzene	TXNIP	thioredoxin interacting protein	10628	606599		
210	*ROM2*	*YLR371W*	RhO1 Multicopy suppressor	AKAP13	A kinase (PRKA) anchor protein 13	11214	604686		
211	*ROM2*	*YLR371W*	RhO1 Multicopy suppressor	ARHGEF11	Rho guanine nucleotide exchange factor (GEF) 11	9826	605708		
212	*ROM2*	*YLR371W*	RhO1 Multicopy suppressor	ARHGEF12	Rho guanine nucleotide exchange factor (GEF) 12	23365	604763		
213	*ROM2*	*YLR371W*	RhO1 Multicopy suppressor	ARHGEF18	Rho/Rac guanine nucleotide exchange factor (GEF) 18	23370	616432		
214	*ROM2*	*YLR371W*	RhO1 Multicopy suppressor	ARHGEF2	Rho/Rac guanine nucleotide exchange factor (GEF) 2	9181	607560		
215	*ROM2*	*YLR371W*	RhO1 Multicopy suppressor	ARHGEF28	Rho guanine nucleotide exchange factor (GEF) 28	64283	612790		
216	*ROM2*	*YLR371W*	RhO1 Multicopy suppressor	ARHGEF3	Rho guanine nucleotide exchange factor (GEF) 3	50650	612115		
217	*ROM2*	*YLR371W*	RhO1 Multicopy suppressor	NET1	neuroepithelial cell transforming 1	10276	606450		
218	*RRT12*	*YCR045C*	Regulator of rDNA Transcription	MBTPS1	membrane-bound transcription factor peptidase, site 1	8720	603355		
219	*RRT12*	*YCR045C*	Regulator of rDNA Transcription	PCSK9	proprotein convertase subtilisin/kexin type 9	255738	607786	603776	HYPERCHOLESTEROLEMIA, AUTOSOMAL DOMINANT, 3; HCHOLA3
220	*RVS161*	*YCR009C*	Reduced Viability on Starvation	BIN3	bridging integrator 3	55909	606396		
221	*SAC1*	*YKL212W*	Suppressor of ACtin	INPP5F	inositol polyphosphate-5-phosphatase F	22876	609389		
222	*SAC1*	*YKL212W*	Suppressor of ACtin	SACM1L	SAC1 suppressor of actin mutations 1-like (yeast)	22908	606569		
223	*SAC6*	*YDR129C*	Suppressor of ACtin	LCP1	lymphocyte cytosolic protein 1 (L-plastin)	3936	153430		
224	*SAC6*	*YDR129C*	Suppressor of ACtin	PLS1	plastin 1	5357	602734		
225	*SAC6*	*YDR129C*	Suppressor of ACtin	PLS3	plastin 3	5358	300131	300910	BONE MINERAL DENSITY QUANTITATIVE TRAIT LOCUS 18; BMND18
226	*SAT4*	*YCR008W*		HUNK	hormonally up-regulated Neu-associated kinase	30811	606532		
227	*SAT4*	*YCR008W*		PRKAA2	protein kinase, AMP-activated, alpha 2 catalytic subunit	5563	600497		
228	*SCP160*	*YJL080C*	S. cerevisiae protein involved in the Control of Ploidy	BICC1	BicC family RNA binding protein 1	80114	614295	601331	RENAL DYSPLASIA, CYSTIC, SUSCEPTIBILITY TO; CYSRD
229	*SCP160*	*YJL080C*	S. cerevisiae protein involved in the Control of Ploidy	HDLBP	high density lipoprotein binding protein	3069	142695		
230	*SER1*	*YOR184W*	SERine requiring	PSAT1	phosphoserine aminotransferase 1	29968	610936	616038	NEU-LAXOVA SYNDROME 2; NLS2
231	*SER1*	*YOR184W*	SERine requiring	PSAT1	phosphoserine aminotransferase 1	29968	610936	610992	PHOSPHOSERINE AMINOTRANSFERASE DEFICIENCY; PSATD
232	*SHR5*	*YOL110W*	Suppressor of Hyperactive Ras	GOLGA7	golgin A7	51125	609453		
233	*SHR5*	*YOL110W*	Suppressor of Hyperactive Ras	GOLGA7B	golgin A7 family, member B	401647	614189		
234	*SLT2*	*YHR030C*	Suppressor of the LyTic phenotype	MAPK7	mitogen-activated protein kinase 7	5598	602521		
235	*SNF5*	*YBR289W*	Sucrose NonFermenting	SMARCB1	SWI/SNF related, matrix associated, actin dependent regulator of chromatin, subfamily b, member 1	6598	601607	609322	RHABDOID TUMOR PREDISPOSITION SYNDROME 1; RTPS1
236	*SNF5*	*YBR289W*	Sucrose NonFermenting	SMARCB1	SWI/SNF related, matrix associated, actin dependent regulator of chromatin, subfamily b, member 1	6598	601607	162091	SCHWANNOMATOSIS 1; SWNTS1
237	*SNF5*	*YBR289W*	Sucrose NonFermenting	SMARCB1	SWI/SNF related, matrix associated, actin dependent regulator of chromatin, subfamily b, member 1	6598	601607	614608	MENTAL RETARDATION, AUTOSOMAL DOMINANT 15; MRD15
238	*SPT3*	*YDR392W*	SuPpressor of Ty's	SUPT3H	SPT3 homolog, SAGA and STAGA complex component	8464	602947		
239	*STO1*	*YMR125W*	Suppressor of TOp1	NCBP1	nuclear cap binding protein subunit 1, 80kDa	4686	600469		
240	*SWD1*	*YAR003W*	Set1c, WD40 repeat protein	RBBP5	retinoblastoma binding protein 5	5929	600697		
241	*SWI3*	*YJL176C*	SWItching deficient	SMARCC1	SWI/SNF related, matrix associated, actin dependent regulator of chromatin, subfamily c, member 1	6599	601732		
242	*SWI3*	*YJL176C*	SWItching deficient	SMARCC2	SWI/SNF related, matrix associated, actin dependent regulator of chromatin, subfamily c, member 2	6601	601734		
243	*TPK1*	*YJL164C*	Takashi's Protein Kinase	PRKACA	protein kinase, cAMP-dependent, catalytic, alpha	5566	601639	615830	PIGMENTED NODULAR ADRENOCORTICAL DISEASE, PRIMARY, 4; PPNAD4
244	*TPK1*	*YJL164C*	Takashi's Protein Kinase	PRKACB	protein kinase, cAMP-dependent, catalytic, beta	5567	176892		
245	*TPK1*	*YJL164C*	Takashi's Protein Kinase	PRKACG	protein kinase, cAMP-dependent, catalytic, gamma	5568	176893	616176	BLEEDING DISORDER, PLATELET-TYPE, 19; BDPLT19
246	*TPK1*	*YJL164C*	Takashi's Protein Kinase	PRKG1	protein kinase, cGMP-dependent, type I	5592	176894	615436	AORTIC ANEURYSM, FAMILIAL THORACIC 8; AAT8

247	*TPK1*	*YJL164C*	Takashi's Protein Kinase	PRKG2	protein kinase, cGMP-dependent, type II	5593	601591		
248	*TPK1*	*YJL164C*	Takashi's Protein Kinase	PRKX	protein kinase, X-linked	5613	300083		
249	*TPK1*	*YJL164C*	Takashi's Protein Kinase	PRKY	protein kinase, Y-linked, pseudogene	5616	400008		
250	*TPK1*	*YJL164C*	Takashi's Protein Kinase	RPS6KA1	ribosomal protein S6 kinase, 90kDa, polypeptide 1	6195	601684		
251	*TPK1*	*YJL164C*	Takashi's Protein Kinase	RPS6KA2	ribosomal protein S6 kinase, 90kDa, polypeptide 2	6196	601685		
252	*TPK1*	*YJL164C*	Takashi's Protein Kinase	RPS6KA3	ribosomal protein S6 kinase, 90kDa, polypeptide 3	6197	300075	300844	MENTAL RETARDATION, X-LINKED 19; MRX19
253	*TPK1*	*YJL164C*	Takashi's Protein Kinase	RPS6KA3	ribosomal protein S6 kinase, 90kDa, polypeptide 3	6197	300075	303600	COFFIN-LOWRY SYNDROME; CLS
254	*TPK1*	*YJL164C*	Takashi's Protein Kinase	RPS6KA4	ribosomal protein S6 kinase, 90kDa, polypeptide 4	8986	603606		
255	*TPK1*	*YJL164C*	Takashi's Protein Kinase	RPS6KA5	ribosomal protein S6 kinase, 90kDa, polypeptide 5	9252	603607		
256	*TPK1*	*YJL164C*	Takashi's Protein Kinase	RPS6KA6	ribosomal protein S6 kinase, 90kDa, polypeptide 6	27330	300303		
257	*TRM10*	*YOL093W*	Transfer RNA Methyltransferase	TRMT10A	tRNA methyltransferase 10A	93587	616013	616033	MICROCEPHALY, SHORT STATURE, AND IMPAIRED GLUCOSE METABOLISM; MSSGM
258	*TRM10*	*YOL093W*	Transfer RNA Methyltransferase	TRMT10C	tRNA methyltransferase 10C, mitochondrial RNase P subunit	54931	615423		
259	*UBA3*	*YPR066W*	UBiquitin-like protein-Activating enzyme	UBA3	ubiquitin-like modifier activating enzyme 3	9039	603172		
260	*UBA4*	*YHR111W*	UBiquitin-Activating	MOCS3	molybdenum cofactor synthesis 3	27304	609277		
261	*UBA4*	*YHR111W*	UBiquitin-Activating	UBA5	ubiquitin-like modifier activating enzyme 5	79876	610552		
262	*UBP13*	*YBL067C*	UBiquitin-specific Protease	USP1	ubiquitin specific peptidase 1	7398	603478		
263	*UBP13*	*YBL067C*	UBiquitin-specific Protease	USP46	ubiquitin specific peptidase 46	64854	612849		
264	*UBP3*	*YER151C*	UBiquitin-specific Protease	USP10	ubiquitin specific peptidase 10	9100	609818		
265	*UBR2*	*YLR024C*		UBR1	ubiquitin protein ligase E3 component n-recognin 1	197131	605981	243800	JOHANSON-BLIZZARD SYNDROME; JBS
266	*UBR2*	*YLR024C*		UBR2	ubiquitin protein ligase E3 component n-recognin 2	23304	609134		
267	*URE2*	*YNL229C*	UREidosuccinate transport	GDAP1	ganglioside induced differentiation associated protein 1	54332	606598	214400	CHARCOT-MARIE-TOOTH DISEASE, TYPE 4A; CMT4A
268	*URE2*	*YNL229C*	UREidosuccinate transport	GDAP1	ganglioside induced differentiation associated protein 1	54332	606598	608340	CHARCOT-MARIE-TOOTH DISEASE, RECESSIVE INTERMEDIATE A; CMTRIA
269	*URE2*	*YNL229C*	UREidosuccinate transport	GDAP1	ganglioside induced differentiation associated protein 1	54332	606598	607831	CHARCOT-MARIE-TOOTH DISEASE, AXONAL, TYPE 2K; CMT2K
270	*URE2*	*YNL229C*	UREidosuccinate transport	GDAP1	ganglioside induced differentiation associated protein 1	54332	606598	607706	CHARCOT-MARIE-TOOTH DISEASE, AXONAL, WITH VOCAL CORD PARESIS, AUTOSOMAL RECESSIVE
271	*URE2*	*YNL229C*	UREidosuccinate transport	GSTZ1	glutathione S-transferase zeta 1	2954	603758		
272	*VPS25*	*YJR102C*	Vacuolar Protein Sorting	VPS25	vacuolar protein sorting 25 homolog (S. cerevisiae)	84313	610907		
273	*VPS3*	*YDR495C*	Vacuolar Protein Sorting	TGFBRAP1	transforming growth factor beta receptor associated protein 1	9392	606237		
274	*VPS54*	*YDR027C*	Vacuolar Protein Sorting	VPS54	vacuolar protein sorting 54 homolog (S. cerevisiae)	51542	614633		
275	*VPS64*	*YDR200C*	Vacuolar Protein Sorting	CCDC136	coiled-coil domain containing 136	64753	611902		
276	*VPS64*	*YDR200C*	Vacuolar Protein Sorting	CEP170	centrosomal protein 170kDa	9859	613023		
277	*VPS64*	*YDR200C*	Vacuolar Protein Sorting	SLMAP	sarcolemma associated protein	7871	602701		
278	*VPS64*	*YDR200C*	Vacuolar Protein Sorting	TRAF3IP3	TRAF3 interacting protein 3	80342	608255		
279	*VPS74*	*YDR372C*	Vacuolar Protein Sorting	GOLPH3	golgi phosphoprotein 3 (coat-protein)	64083	612207		
280	*VPS74*	*YDR372C*	Vacuolar Protein Sorting	GOLPH3L	golgi phosphoprotein 3-like	55204	612208		
281	*YIH1*	*YCR059C*	Yeast Impact Homolog	IMPACT	impact RWD domain protein	55364	615319		
282	*YKE2*	*YLR200W*	Yeast ortholog of mouse KE2	PFDN6	prefoldin subunit 6	10471	605660		
283	*ZWF1*	*YNL241C*	ZWischenFerment	G6PD	glucose-6-phosphate dehydrogenase	2539	305900	300908	ANEMIA, NONSPHEROCYTIC HEMOLYTIC, DUE TO G6PD DEFICIENCY
284	*ZWF1*	*YNL241C*	ZWischenFerment	G6PD	glucose-6-phosphate dehydrogenase	2539	305900	611162	MALARIA, SUSCEPTIBILITY TO MALARIA, RESISTANCE TO, INCLUDED
285	*ZWF1*	*YNL241C*	ZWischenFerment	G6PD	glucose-6-phosphate dehydrogenase	2539	305900	134700	FAVISM, SUSCEPTIBILITY TO
286	*ZWF1*	*YNL241C*	ZWischenFerment	H6PD	hexose-6-phosphate dehydrogenase (glucose 1-dehydrogenase)	9563	138090	604931	CORTISONE REDUCTASE DEFICIENCY 1; CORTRD1
287		*YDR222W*		HIST1H4A	histone cluster 1, H4a	8359	602822		
288		*YDR222W*		HIST1H4B	histone cluster 1, H4b	8365	602829		
289		*YDR222W*		HIST1H4C	histone cluster 1, H4c	8364	602827		
290		*YDR222W*		HIST1H4D	histone cluster 1, H4d	8360	602823		
291		*YDR222W*		HIST1H4E	histone cluster 1, H4e	8367	602830		
292		*YDR222W*		HIST1H4F	histone cluster 1, H4f	8361	602824		
293		*YDR222W*		HIST1H4G	histone cluster 1, H4g	8369	602832		
294		*YDR222W*		HIST1H4H	histone cluster 1, H4h	8365	602828		
295		*YDR222W*		HIST1H4I	histone cluster 1, H4i	8294	602833		
296		*YDR222W*		HIST1H4J	histone cluster 1, H4j	8363	602826		
297		*YDR222W*		HIST1H4K	histone cluster 1, H4k	8362	602825		
298		*YDR222W*		HIST1H4L	histone cluster 1, H4l	8368	602831		
299		*YDR222W*		HIST2H4A	histone cluster 2, H4a	8370	142750		
300		*YDR222W*		HIST4H4	histone cluster 4, H4	121504	615069		
301		*YJL132W*		GPLD1	glycosylphosphatidylinositol specific phospholipase D1	2822	602515		

S6: Mating factor induced growth arrest screen results and statistics

Systematic name	Mutant	Average size of halo	Significant	p value
YHR047C	*aap1Δ*	*0.944192637*	No	0.545809
YDR226W	*adk1Δ*	0.849018327	No	0.102544
YKL135C	*apl2Δ*	0.018851863	Yes	<0.000001
YML022W	*apt1Δ*	0.99795759	No	0.98236
YNL059C	*arp5Δ*	0.01460632	Yes	<0.000001
YLR085C	*arp6Δ*	*0.764471393*	Yes	0.010995
YGR097W	*ask10Δ*	0.75784026	Yes	0.008948
YLR114C	*avl9Δ*	0.833350753	No	0.071604
YBR200W	*bem1Δ*	*0.523276713*	Yes	<0.000001
YER155C	*bem2Δ*	1.07255707	No	0.432297
YPL161C	*bem4Δ*	0.36763164	Yes	<0.000001
YBL098W	*bna4Δ*	1.099833257	No	0.280043
YDL074C	*bre1Δ*	0.616297613	Yes	0.000037
YNR051C	*bre5Δ*	0.972984493	No	0.769945
YEL029C	*bud16Δ*	0.006093847	Yes	<0.000001
YOR078W	*bud21Δ*	0.90637302	No	0.310999
YMR014W	*bud22Δ*	0.75515919	Yes	0.008222
YCR094W	*cdc50Δ*	0.59578838	Yes	0.000014
YGL190C	*cdc55Δ*	0.58397623	Yes	0.000008
YML036W	*cgi121Δ*	0.48660026	Yes	<0.000001
YHR142W	*chs7Δ*	*0.915022583*	No	0.357781
YPL241C	*cin2Δ*	0.710058757	Yes	0.001772
YGL215W	*clg1Δ*	0.82120747	No	0.053296
YAL040C	*cln3Δ*	0.68194929	Yes	0.000612
YGR092W	*dbf2Δ*	0.33841902	Yes	<0.000001
YOR311C	*dgk1Δ*	1.018422723	No	0.841924
YNL001W	*dom34Δ*	0.96361327	No	0.693669
YOL087C	*duf1Δ*	0.851021863	No	0.107175
YKL160W	*elf1Δ*	0.704597393	Yes	0.001451
YNL280C	*erg24Δ*	0.749514683	Yes	0.006864
YMR015C	*erg5Δ*	0.876153103	No	0.180341
YIL009C-A	*est3Δ*	0.454914547	Yes	<0.000001
YFR019W	*fab1Δ*	*0.783657063*	Yes	0.019455
YCL058C	*fyv5Δ*	1.047776493	No	0.605053
YMR307W	*gas1Δ*	0.658168097	Yes	0.000234
YJR040W	*gef1Δ*	0.789208007	Yes	0.022786
YGL020C	*get1Δ*	0.533998487	Yes	<0.000001
YER083C	*get2Δ*	*0.8060707*	Yes	0.036122
YDL100C	*get3Δ*	0.75671898	Yes	0.008637
YEL003W	*gim4Δ*	*0.649106957*	Yes	0.000159
YML094W	*gim5Δ*	0.337429807	Yes	<0.000001
YER122C	*glo3Δ*	0.736974593	Yes	0.004542
YHL031C	*gos1Δ*	*1.006939077*	No	0.94012
YML121W	*gtr1Δ*	0.641827	Yes	0.000116
YDL234C	*gyp7Δ*	0.894565733	No	0.253968
YDR317W	*him1Δ*	0.899140703	No	0.275135
YOR038C	*hir2Δ*	0.793078387	Yes	0.025393
YJR140C	*hir3Δ*	1.024161163	No	0.793668
YMR032W	*hof1Δ*	1.00505357	No	0.956371
YLR113W	*hog1Δ*	0.902430217	No	0.29108
YDR158W	*hom2Δ*	*0.647839333*	Yes	0.000151
YOL068C	*hst1Δ*	0.879672787	No	0.193024
YNL215W	*ies2Δ*	0.659754587	Yes	0.00025
YOL108C	*ino4Δ*	0.237014783	Yes	<0.000001
YDR315C	*ipk1Δ*	0.744648827	Yes	0.005859
YOL081W	*ira2Δ*	1.043023407	No	0.641424
YPL017C	*irc15Δ*	*0.10184192*	Yes	<0.000001
YMR073C	*irc21Δ*	0.858637153	No	0.126305
YLR021W	*irc25Δ*	0.65662328	Yes	0.000219
YOR123C	*leo1Δ*	0.65488782	Yes	0.000204
YOR298C-A	*mbf1Δ*	*1.00846372*	No	0.926997
YGL197W	*mds3Δ*	0.736738477	Yes	0.004506
YFR030W	*met10Δ*	1.024337567	No	0.792196
YLR303W	*met17Δ*	0.860797953	No	0.132192
YIL128W	*met18Δ*	0.636212493	Yes	0.000091
YEL007W	*mit1Δ*	*1.166281097*	No	0.072231
YNL076W	*mks1Δ*	0.904501527	No	0.301435
YJL183W	*mnn11Δ*	0.561573113	Yes	0.000003
YJR074W	*mog1Δ*	0.81465944	Yes	0.045171
YER077C	*mrx1Δ*	0.92762935	No	0.43348
YEL033W	*mtc7Δ*	*0.846891233*	No	0.097805
YDR456W	*nhx1Δ*	0.922168643	No	0.399611
YLR328W	*nma1Δ*	0.913720683	No	0.350469
YOL041C	*nop12Δ*	0.7186635	Yes	0.002414
YDR043C	*nrg1Δ*	1.044572293	No	0.629471

YML060W	*ogg1Δ*	0.79770818	Yes	0.028848
YGR078C	*pac10Δ*	0.692496443	Yes	0.000921
YJL210W	*pex2Δ*	0.867217497	No	0.150944
YNL326C	*pfa3Δ*	0.929197947	No	0.443508
YJL179W	*pfd1Δ*	1.024719153	No	0.789015
YBR106W	*pho88Δ*	0.897214587	No	0.266081
YGL023C	*pib2Δ*	0.851847423	No	0.10913
YEL017C-A	*pmp2Δ*	*1.071086347*	No	0.441681
YAL023C	*pmt2Δ*	0.651484673	Yes	0.000176
YNR052C	*pop2Δ*	1.139410413	No	0.131615
YOR220W	*rcn2Δ*	0.80208964	Yes	0.032484
YJL204C	*rcy1Δ*	0.972469637	No	0.765688
YPL066W	*rgl1Δ*	0.95865446	No	0.654478
YDR137W	*rgp1Δ*	*0.99301717*	No	0.939743
YMR283C	*rit1Δ*	0.846079577	No	0.096043
YOR018W	*rod1Δ*	*0.889609263*	No	0.23235
YLR371W	*rom2Δ*	0.94805394	No	0.573932
YCR045C	*rrt12Δ*	0.709690897	Yes	0.001749
YGL252C	*rtg2Δ*	0.97205224	No	0.762242
YCR009C	*rvs161Δ*	0.93923724	No	0.51075
YKL212W	*sac1Δ*	0.55473672	Yes	0.000002
YDR129C	*sac6Δ*	*0.78095454*	Yes	0.017993
YCR008W	*sat4Δ*	*0.944317977*	No	0.546711
YJL080C	*scp160Δ*	1.047057177	No	0.610497
YDR469W	*sdc1Δ*	1.02051411	No	0.824258
YOR184W	*ser1Δ*	0.239626973	Yes	<0.000001
YOL110W	*shr5Δ*	0.819324987	No	0.050844
YMR175W	*sip18Δ*	0.927834597	No	0.434785
YBR266C	*slm6Δ*	*0.7769024*	Yes	0.015983
YHR030C	*slt2Δ*	*0.822077687*	No	0.054463
YBR289W	*snf5Δ*	0.632917877	Yes	0.000079
YGL127C	*soh1Δ*	0.511464193	Yes	<0.000001
YDR392W	*spt3Δ*	*0.554775987*	Yes	0.000002
YLR055C	*spt8Δ*	0.615394923	Yes	0.000036
YMR125W	*sto1Δ*	0.13336057	Yes	<0.000001
YAR003W	*swd1Δ*	0.725959923	Yes	0.003118
YBR175W	*swd3Δ*	*0.833342763*	No	0.071591
YDR126W	*swf1Δ*	*0.80805789*	Yes	0.038065
YJL176C	*swi3Δ*	0.657833037	Yes	0.00023
YLR182W	*swi6Δ*	0.54033086	Yes	<0.000001
YPL180W	*tco89Δ*	0.968690863	No	0.734669
YJL164C	*tpk1Δ*	0.868000247	No	0.153363
YDR074W	*tps2Δ*	0.836873427	No	0.077792
YOL093W	*trm10Δ*	0.813463913	Yes	0.043807
YOL125W	*trm13Δ*	0.005354753	Yes	<0.000001
YDR007W	*trp1Δ*	0.81237064	Yes	0.04259
YPR066W	*uba3Δ*	1.025535013	No	0.782224
YHR111W	*uba4Δ*	*0.635385617*	Yes	0.000088
YBL067C	*ubp13Δ*	0.878617217	No	0.189153
YER151C	*ubp3Δ*	1.061392487	No	0.50638
YLR024C	*ubr2Δ*	0.791552567	Yes	0.024336
YLR420W	*ura4Δ*	0.926097627	No	0.423815
YNL229C	*ure2Δ*	0.720609017	Yes	0.002586
YNL212W	*vid27Δ*	0.747609067	Yes	0.006453
YJR102C	*vps25Δ*	0.542337093	Yes	<0.000001
YDR495C	*vps3Δ*	0.458433033	Yes	<0.000001
YDR027C	*vps54Δ*	0.685561267	Yes	0.000705
YDR200C	*vps64Δ*	*0.644358267*	Yes	0.00013
YDR372C	*vps74Δ*	*0.885716663*	No	0.216314
YPL239W	*yar1Δ*	0.821234157	No	0.053332
ycr050c	*ycr050cΔ*	0.76495621	Yes	0.01116
ydl118w	*ydl118wΔ*	0.83170356	No	0.068853
ydr222w	*ydr222wΔ*	*0.91189856*	No	0.340396
ydr535w	*ydr535wΔ*	0.999739653	No	0.997751
ygl214w	*ygl214wΔ*	0.65499555	Yes	0.000204
yih1	*yih1Δ*	0.578285787	Yes	0.000006
yjl132w	*yjl132wΔ*	0.980718953	No	0.834664
yjr018w	*yjr018wΔ*	0.419176673	Yes	<0.000001
YLR200W	*yke2Δ*	1.107071703	No	0.246676
ymr001c-a	*ymr001c-aΔ*	0.583939677	Yes	0.000008
ynl089c	*ynl089cΔ*	1.100342667	No	0.277599
ynr068c	*ynr068cΔ*	0.16740833	Yes	<0.000001
yor139c	*yor139cΔ*	0.72875805	Yes	0.003435
YOL109W	*zeo1Δ*	0.88030066	No	0.195353
YNL241C	*zwf1Δ*	0.85754984	No	0.123421

S7: Yeast strains used in this study

Freezer Strain	Parental strain	Genotype	Reference	Figure Used
CMY56	BY4742	MAT**α**, *his3Δ leu2Δ lys2Δ ura3Δ*	Brachmann *et al*., 1998	Throughout as wild-type and parental strain
CMY211	BY4741	MAT**A**, *his3Δ leu2Δ met15Δ ura3Δ*	Brachmann *et al*., 1999	Throughout as wild-type and parental strain
CMY1482	BY4742	MAT**α**, *his3Δ leu2Δ lys2Δ ura3Δ::URA3*	Laidlaw *et al*., 2021	1B, 1C
CMY820	BY4742	*fur4Δ::G418*	Winzeler *et al*., 1999	1B, 1C
CMY12	SEY5076	*leu2-3,112, ura3-52 sec7-1*	Novick and Schekman, 1979, 1980	2A
CMY926	BY4742	*vps2Δ::G418*	Winzeler *et al*., 1999	2A
CMY635	BY4742	*rcy1Δ::G418*	Winzeler *et al*., 1999	2A, 2B, 2C, 3B, 3D, 6F
CMY638	BY4742	*nhx1Δ::G418*	Winzeler *et al*., 1999	2A, 2B, 2C, 3B, 3D, 6F
CMY1091	BY4742	*cln3Δ::G418*	Winzeler *et al*., 1999	3D, 5C, 6B, S3
CMY1092	BY4742	*drs2Δ::G418*	Winzeler *et al*., 1999	3D
CMY1093	BY4742	*pmt2Δ::G418*	Winzeler *et al*., 1999	3D
CMY1094	BY4742	*swc3Δ::G418*	Winzeler *et al*., 1999	3D
CMY1095	BY4742	*swd1Δ::G418*	Winzeler *et al*., 1999	3D, 5B, 5C, 6B, 6C, S3
CMY1096	BY4742	*irc25Δ::G418*	Winzeler *et al*., 1999	3D
CMY1097	BY4742	*ubr2Δ::G418*	Winzeler *et al*., 1999	3D
CMY1098	BY4742	*osw2Δ::G418*	Winzeler *et al*., 1999	3D
CMY1099	BY4742	*spt8Δ::G418*	Winzeler *et al*., 1999	3D, 5C, 6B, S3
CMY1100	BY4742	*arp6Δ::G418*	Winzeler *et al*., 1999	3D, 5C, 6B, S3
CMY1101	BY4742	*hog1Δ::G418*	Winzeler *et al*., 1999	3D
CMY1102	BY4742	*avl9Δ::G418*	Winzeler *et al*., 1999	3D
CMY1103	BY4742	*ogg1Δ::G418*	Winzeler *et al*., 1999	3D
CMY1104	BY4742	*aim32Δ::G418*	Winzeler *et al*., 1999	3D
CMY1105	BY4742	*bud22Δ::G418*	Winzeler *et al*., 1999	3D
CMY1106	BY4742	*hof1Δ::G418*	Winzeler *et al*., 1999	3D
CMY1107	BY4742	*sip18Δ::G418*	Winzeler *et al*., 1999	3D
CMY1108	BY4742	*scs7Δ::G418*	Winzeler *et al*., 1999	3D
CMY1109	BY4742	*rit1Δ::G418*	Winzeler *et al*., 1999	3D
CMY1110	BY4742	*ade4Δ::G418*	Winzeler *et al*., 1999	3D
CMY1111	BY4742	*gas1Δ::G418*	Winzeler *et al*., 1999	3D
CMY1112	BY4742	*pfa3Δ::G418*	Winzeler *et al*., 1999	3D
CMY1113	BY4742	*cla4Δ::G418*	Winzeler *et al*., 1999	3C, 3D
CMY1114	BY4742	*erg24Δ::G418*	Winzeler *et al*., 1999	3D
CMY1115	BY4742	*rod1Δ::G418*	Winzeler *et al*., 1999	3D, 6F
CMY1116	BY4742	*dfg16Δ::G418*	Winzeler *et al*., 1999	3D
CMY1117	BY4742	*hir2Δ::G418*	Winzeler *et al*., 1999	3D, 5C, 6B, S3
CMY1118	BY4742	*ckb2Δ::G418*	Winzeler *et al*., 1999	3D
CMY1119	BY4742	*bud21Δ::G418*	Winzeler *et al*., 1999	3D
CMY1120	BY4742	*dgk1Δ::G418*	Winzeler *et al*., 1999	3D
CMY1121	BY4742	*cin1Δ::G418*	Winzeler *et al*., 1999	3D
CMY1122	BY4742	*pho80Δ::G418*	Winzeler *et al*., 1999	3D
CMY1123	BY4742	*pfa4Δ::G418*	Winzeler *et al*., 1999	3D
CMY1124	BY4742	*nop12Δ::G418*	Winzeler *et al*., 1999	3D
CMY1125	BY4742	*hst1Δ::G418*	Winzeler *et al*., 1999	3D, 5C, 6B, S3
CMY1126	BY4742	*ira2Δ::G418*	Winzeler *et al*., 1999	3D
CMY1127	BY4742	*cin2Δ::G418*	Winzeler *et al*., 1999	3D
CMY1128	BY4742	*yar1Δ::G418*	Winzeler *et al*., 1999	3D
CMY1129	BY4742	*new1Δ::G418*	Winzeler *et al*., 1999	3D
CMY1130	BY4742	*thi6Δ::G418*	Winzeler *et al*., 1999	3D
CMY1131	BY4742	*ypl205cΔ::G418*	Winzeler *et al*., 1999	3D
CMY1132	BY4742	*tco89Δ::G418*	Winzeler *et al*., 1999	3D, 6F
CMY1133	BY4742	*bem4Δ::G418*	Winzeler *et al*., 1999	3D
CMY1134	BY4742	*ypl150wΔ::G418*	Winzeler *et al*., 1999	3D
CMY1135	BY4742	*swd3Δ::G418*	Winzeler *et al*., 1999	3D, 5B, 5C, 6B, S3
CMY1136	BY4742	*bem1Δ::G418*	Winzeler *et al*., 1999	3D
CMY1137	BY4742	*slm6Δ::G418*	Winzeler *et al*., 1999	3D
CMY1138	BY4742	*swf1Δ::G418*	Winzeler *et al*., 1999	3D
CMY1139	BY4742	*sac6Δ::G418*	Winzeler *et al*., 1999	3D
CMY1140	BY4742	*rgp1Δ::G418*	Winzeler *et al*., 1999	3D
CMY1141	BY4742	*vps74Δ::G418*	Winzeler *et al*., 1999	3D
CMY1142	BY4742	*spt3Δ::G418*	Winzeler *et al*., 1999	3D, 5C, 6B, 6F, S3
CMY1143	BY4742	*gim4Δ::G418*	Winzeler *et al*., 1999	3D, 4D
CMY1144	BY4742	*mit1Δ::G418*	Winzeler *et al*., 1999	3D

CMY1145	BY4742	*vac8Δ::G418*	Winzeler *et al.*, 1999	3D
CMY1146	BY4742	*pmp2Δ::G418*	Winzeler *et al.*, 1999	3C, 3D
CMY1147	BY4742	*spf1Δ::G418*	Winzeler *et al.*, 1999	3D
CMY1148	BY4742	*mtc7Δ::G418*	Winzeler *et al.*, 1999	3D
CMY1149	BY4742	*get2Δ::G418*	Winzeler *et al.*, 1999	3D, 4B, 4C
CMY1150	BY4742	*gos1Δ::G418*	Winzeler *et al.*, 1999	3D
CMY1151	BY4742	*yhi9Δ::G418*	Winzeler *et al.*, 1999	3D
CMY1152	BY4742	*slt2Δ::G418*	Winzeler *et al.*, 1999	3D
CMY1153	BY4742	*aap1Δ::G418*	Winzeler *et al.*, 1999	3D
CMY1154	BY4742	*uba4Δ::G418*	Winzeler *et al.*, 1999	3D, 5C, 6B, S3
CMY1155	BY4742	*chs7Δ::G418*	Winzeler *et al.*, 1999	3D
CMY1156	BY4742	*dse2Δ::G418*	Winzeler *et al.*, 1999	3D
CMY1157	BY4742	*gnd1Δ::G418*	Winzeler *et al.*, 1999	3D
CMY1158	BY4742	*sat4Δ::G418*	Winzeler *et al.*, 1999	3D
CMY1159	BY4742	*rvs161Δ::G418*	Winzeler *et al.*, 1999	3D, 6F
CMY1160	BY4742	*ura4Δ::G418*	Winzeler *et al.*, 1999	3D
CMY1161	BY4742	*swi6Δ::G418*	Winzeler *et al.*, 1999	3D, 5C, 6B, S3
CMY1162	BY4742	*yke2Δ::G418*	Winzeler *et al.*, 1999	3D, 4D
CMY1163	BY4742	*elf1Δ::G418*	Winzeler *et al.*, 1999	3D, 5B, 5C, 6B, S3
CMY1164	BY4742	*pac10Δ::G418*	Winzeler *et al.*, 1999	3D, 4D, 4E
CMY1165	BY4742	*ask10Δ::G418*	Winzeler *et al.*, 1999	3D
CMY1166	BY4742	*leo1Δ::G418*	Winzeler *et al.*, 1999	3D, 5C, 6B, S3
CMY1167	BY4742	*yor139cΔ::G418*	Winzeler *et al.*, 1999	3D, 6A
CMY1168	BY4742	*sfl1Δ::G418*	Winzeler *et al.*, 1999	3D
CMY1169	BY4742	*ser1Δ::G418*	Winzeler *et al.*, 1999	3D
CMY1170	BY4742	*lip5Δ::G418*	Winzeler *et al.*, 1999	3D
CMY1171	BY4742	*rud3Δ::G418*	Winzeler *et al.*, 1999	3D
CMY1172	BY4742	*rcn2Δ::G418*	Winzeler *et al.*, 1999	3D
CMY1173	BY4742	*hnt3Δ::G418*	Winzeler *et al.*, 1999	3D
CMY1174	BY4742	*pex2Δ::G418*	Winzeler *et al.*, 1999	3D
CMY1175	BY4742	*mbb1Δ::G418*	Winzeler *et al.*, 1999	3D
CMY1176	BY4742	*sop4Δ::G418*	Winzeler *et al.*, 1999	3D
CMY1177	BY4742	*mnn11Δ::G418*	Winzeler *et al.*, 1999	3D
CMY1178	BY4742	*pfd1Δ::G418*	Winzeler *et al.*, 1999	3D, 4D, 4E
CMY1179	BY4742	*swi3Δ::G418*	Winzeler *et al.*, 1999	3D, 5B, 5C, 6B, S3
CMY1180	BY4742	*tpk1Δ::G418*	Winzeler *et al.*, 1999	3D
CMY1181	BY4742	*cis3Δ::G418*	Winzeler *et al.*, 1999	3D
CMY1182	BY4742	*nma1Δ::G418*	Winzeler *et al.*, 1999	3D
CMY1183	BY4742	*hom2Δ::G418*	Winzeler *et al.*, 1999	3D
CMY1184	BY4742	*vps64Δ::G418*	Winzeler *et al.*, 1999	3D
CMY1185	BY4742	*ydr222wΔ::G418*	Winzeler *et al.*, 1999	3D, 6A, 6D, 6F
CMY1186	BY4742	*adk1Δ::G418*	Winzeler *et al.*, 1999	3D, 6E
CMY1187	BY4742	*yea4Δ::G418*	Winzeler *et al.*, 1999	3D
CMY1188	BY4742	*bud16Δ::G418*	Winzeler *et al.*, 1999	3D, 6E
CMY1189	BY4742	*hom3Δ::G418*	Winzeler *et al.*, 1999	3D
CMY1190	BY4742	*apl2Δ::G418*	Winzeler *et al.*, 1999	3D, 6F
CMY1192	BY4742	*sec22Δ::G418*	Winzeler *et al.*, 1999	3D
CMY1193	BY4742	*met17Δ::G418*	Winzeler *et al.*, 1999	3D
CMY1194	BY4742	*ubc12Δ::G418*	Winzeler *et al.*, 1999	3D
CMY1195	BY4742	*nkp2Δ::G418*	Winzeler *et al.*, 1999	3D
CMY1196	BY4742	*mds3Δ::G418*	Winzeler *et al.*, 1999	3D
CMY1197	BY4742	*clg1Δ::G418*	Winzeler *et al.*, 1999	3D
CMY1198	BY4742	*rtg2Δ::G418*	Winzeler *et al.*, 1999	3D, 5C, 6B, S3
CMY1199	BY4742	*mnt2Δ::G418*	Winzeler *et al.*, 1999	3D
CMY1200	BY4742	*rgl1Δ::G418*	Winzeler *et al.*, 1999	3D
CMY1201	BY4742	*ktr6Δ::G418*	Winzeler *et al.*, 1999	3D
CMY1202	BY4742	*cip1Δ::G418*	Winzeler *et al.*, 1999	3D
CMY1203	BY4742	*sem1Δ::G418*	Winzeler *et al.*, 1999	3D
CMY1204	BY4742	*ubp13Δ::G418*	Winzeler *et al.*, 1999	3D
CMY1205	BY4742	*zwf1Δ::G418*	Winzeler *et al.*, 1999	3D
CMY1206	BY4742	*ure2Δ::G418*	Winzeler *et al.*, 1999	3D, 5C, 6B, S3
CMY1207	BY4742	*ies2Δ::G418*	Winzeler *et al.*, 1999	3D, 5B, 5C, 6B, S3
CMY1208	BY4742	*vid27Δ::G418*	Winzeler *et al.*, 1999	3D
CMY1209	BY4742	*sac1Δ::G418*	Winzeler *et al.*, 1999	3D, 6F

CMY1210	BY4742	*sur2Δ::G418*	Winzeler *et al.*, 1999	3D
CMY1211	BY4742	*pro1Δ::G418*	Winzeler *et al.*, 1999	3D
CMY1212	BY4742	*ipk1Δ::G418*	Winzeler *et al.*, 1999	3C, 3D
CMY1213	BY4742	*him1Δ::G418*	Winzeler *et al.*, 1999	3D
CMY1214	BY4742	*mnt3Δ::G418*	Winzeler *et al.*, 1999	3D
CMY1215	BY4742	*est3Δ::G418*	Winzeler *et al.*, 1999	3D
CMY1216	BY4742	*met1Δ::G418*	Winzeler *et al.*, 1999	3D
CMY1217	BY4742	*sis2Δ::G418*	Winzeler *et al.*, 1999	3D
CMY1218	BY4742	*irc21Δ::G418*	Winzeler *et al.*, 1999	3D
CMY1219	BY4742	*duf1Δ::G418*	Winzeler *et al.*, 1999	3D
CMY1220	BY4742	*trm10Δ::G418*	Winzeler *et al.*, 1999	3D, 5C, 6B, S3
CMY1221	BY4742	*ino4Δ::G418*	Winzeler *et al.*, 1999	3D, 5B, 5C, 6B, S3
CMY1222	BY4742	*zeo1Δ::G418*	Winzeler *et al.*, 1999	3D
CMY1223	BY4742	*shr5Δ::G418*	Winzeler *et al.*, 1999	3D
CMY1224	BY4742	*mrx1Δ::G418*	Winzeler *et al.*, 1999	3D
CMY1225	BY4742	*met6Δ::G418*	Winzeler *et al.*, 1999	3D
CMY1226	BY4742	*gim5Δ::G418*	Winzeler *et al.*, 1999	3D
CMY1227	BY4742	*gtr1Δ::G418*	Winzeler *et al.*, 1999	3D, 5C, 6B, S3
CMY1228	BY4742	*sto1Δ::G418*	Winzeler *et al.*, 1999	3D
CMY1229	BY4742	*uba3Δ::G418*	Winzeler *et al.*, 1999	3D
CMY1230	BY4742	*bck1Δ::G418*	Winzeler *et al.*, 1999	3D
CMY1231	BY4742	*scp160Δ::G418*	Winzeler *et al.*, 1999	3D, 5C, 6B, S3
CMY1232	BY4742	*vps25Δ::G418*	Winzeler *et al.*, 1999	3D, 5C, 6B, S3
CMY1233	BY4742	*lmo1Δ::G418*	Winzeler *et al.*, 1999	3D
CMY1234	BY4742	*bre5Δ::G418*	Winzeler *et al.*, 1999	3D
CMY1235	BY4742	*ynr068cΔ::G418*	Winzeler *et al.*, 1999	3D, 6A
CMY1236	BY4742	*fyv5Δ::G418*	Winzeler *et al.*, 1999	3D
CMY1237	BY4742	*mog1Δ::G418*	Winzeler *et al.*, 1999	3D
CMY1238	BY4742	*hir3Δ::G418*	Winzeler *et al.*, 1999	3D
CMY1239	BY4742	*gyp7Δ::G418*	Winzeler *et al.*, 1999	3D, 6F
CMY1240	BY4742	*vps54Δ::G418*	Winzeler *et al.*, 1999	3D
CMY1241	BY4742	*nrg1Δ::G418*	Winzeler *et al.*, 1999	3D, 5C, 6B, S3
CMY1242	BY4742	*ybr292cΔ::G418*	Winzeler *et al.*, 1999	3D
CMY1243	BY4742	*rrt12Δ::G418*	Winzeler *et al.*, 1999	3D
CMY1244	BY4742	*ycr050cΔ::G418*	Winzeler *et al.*, 1999	3D, 6A
CMY1245	BY4742	*yih1Δ::G418*	Winzeler *et al.*, 1999	3D
CMY1246	BY4742	*yjr018wΔ::G418*	Winzeler *et al.*, 1999	3D, 6A
CMY1247	BY4742	*gef1Δ::G418*	Winzeler *et al.*, 1999	3D
CMY1248	BY4742	*get3Δ::G418*	Winzeler *et al.*, 1999	3D, 4B, 4C, 6F
CMY1249	BY4742	*ydl118wΔ::G418*	Winzeler *et al.*, 1999	3D
CMY1250	BY4742	*get1Δ::G418*	Winzeler *et al.*, 1999	3D, 4B, 4C, 6F
CMY1251	BY4742	*pib2Δ::G418*	Winzeler *et al.*, 1999	3D
CMY1252	BY4742	*ygl214wΔ::G418*	Winzeler *et al.*, 1999	3D, 6A
CMY1253	BY4742	*urm1Δ::G418*	Winzeler *et al.*, 1999	3D
CMY1254	BY4742	*bna4Δ::G418*	Winzeler *et al.*, 1999	3D
CMY1255	BY4742	*csg2Δ::G418*	Winzeler *et al.*, 1999	3D
CMY1256	BY4742	*ecm33Δ::G418*	Winzeler *et al.*, 1999	3D
CMY1257	BY4742	*dom34Δ::G418*	Winzeler *et al.*, 1999	3D
CMY1258	BY4742	*met18Δ::G418*	Winzeler *et al.*, 1999	3D, 5C, 6B, S3
CMY1259	BY4742	*arp8Δ::G418*	Winzeler *et al.*, 1999	3D
CMY1260	BY4742	*trp1Δ::G418*	Winzeler *et al.*, 1999	3D
CMY1261	BY4742	*ydr048cΔ::G418*	Winzeler *et al.*, 1999	3D
CMY1262	BY4742	*mks1Δ::G418*	Winzeler *et al.*, 1999	3D, 5C, 6B, S3
CMY1263	BY4742	*dbf2Δ::G418*	Winzeler *et al.*, 1999	3D
CMY1264	BY4742	*yjl132wΔ::G418*	Winzeler *et al.*, 1999	3D, 6A
CMY1265	BY4742	*cwp2Δ::G418*	Winzeler *et al.*, 1999	3D
CMY1266	BY4742	*snf5Δ::G418*	Winzeler *et al.*, 1999	3D, 5B, 5C, 6B, S3
CMY1267	BY4742	*tps2Δ::G418*	Winzeler *et al.*, 1999	3D
CMY1268	BY4742	*apt1Δ::G418*	Winzeler *et al.*, 1999	3D
CMY1269	BY4742	*cgi121Δ::G418*	Winzeler *et al.*, 1999	3D, 5C, 6B, S3
CMY1270	BY4742	*cik1Δ::G418*	Winzeler *et al.*, 1999	3D
CMY1271	BY4742	*mbf1Δ::G418*	Winzeler *et al.*, 1999	3D
CMY1272	BY4742	*ynl140cΔ::G418*	Winzeler *et al.*, 1999	3D, 6A
CMY1273	BY4742	*rbl2Δ::G418*	Winzeler *et al.*, 1999	3D

CMY1274	BY4742	*irc15Δ::G418*	Winzeler *et al.*, 1999	3D
CMY1275	BY4742	*fab1Δ::G418*	Winzeler *et al.*, 1999	3D
CMY1276	BY4742	*met10Δ::G418*	Winzeler *et al.*, 1999	3D
CMY1277	BY4742	*crp1Δ::G418*	Winzeler *et al.*, 1999	3D
CMY1278	BY4742	*pop2Δ::G418*	Winzeler *et al.*, 1999	3D
CMY1279	BY4742	*trm13Δ::G418*	Winzeler *et al.*, 1999	3D
CMY1280	BY4742	*pho88Δ::G418*	Winzeler *et al.*, 1999	3D
CMY1281	BY4742	*bre1Δ::G418*	Winzeler *et al.*, 1999	3D, 5B, 5C, 6B, S3
CMY1283	BY4742	*sdc1Δ::G418*	Winzeler *et al.*, 1999	3D, 5B, 5C, 6B, 6C, S3
CMY1284	BY4742	*vps3Δ::G418*	Winzeler *et al.*, 1999	3D
CMY1285	BY4742	*ydr525wΔ::G418*	Winzeler *et al.*, 1999	3D, 6A
CMY1286	BY4742	*soh1Δ::G418*	Winzeler *et al.*, 1999	3D
CMY1287	BY4742	*glo3Δ::G418*	Winzeler *et al.*, 1999	3D, 6F
CMY1288	BY4742	*ubp3Δ::G418*	Winzeler *et al.*, 1999	3D
CMY1289	BY4742	*bem2Δ::G418*	Winzeler *et al.*, 1999	3D
CMY1290	BY4742	*arp5Δ::G418*	Winzeler *et al.*, 1999	3D
CMY1291	BY4742	*ynl089cΔ::G418*	Winzeler *et al.*, 1999	3D
CMY1292	BY4742	*lsm7Δ::G418*	Winzeler *et al.*, 1999	3D
CMY1293	BY4742	*erg5Δ::G418*	Winzeler *et al.*, 1999	3D
CMY1294	BY4742	*cdc50Δ::G418*	Winzeler *et al.*, 1999	3D
CMY1295	BY4742	*cdc55Δ::G418*	Winzeler *et al.*, 1999	3D
CMY1296	BY4742	*ymr001c-aΔ::G418*	Winzeler *et al.*, 1999	3D, 6A
CMY1297	BY4742	*rom2Δ::G418*	Winzeler *et al.*, 1999	3D
CMY1298	BY4742	*sch9Δ::G418*	Winzeler *et al.*, 1999	3D
CMY1873	BY4741	*sec62-DAmP*	Breslow *et al.*, 2008	5D, 5F
CMY1870	BY4741	*pma1-DAmP*	Breslow *et al.*, 2008	5D
CMY1871	BY4741	*gpi8-DAmP*	Breslow *et al.*, 2008	5D
CMY1874	BY4741	*mrs6-DAmP*	Breslow *et al.*, 2008	5D
CMY1872	BY4741	*gpi12-DAmP*	Breslow *et al.*, 2008	5D
CMY55	RC634	*MATa sst1-3 rme ade2-1 ura1 his6 met1 can1 cyh2 GAL*	Breslow, 1977	6E, 6F
CMY1069	BY4741	*rcy1Δ::G418*	Winzeler *et al.*, 1999	S2
CMY1070	BY4741	*nhx1Δ::G418*	Winzeler *et al.*, 1999	S2

Table S8: Plasmids used in this study

Plasmid	Genotype	Reference	Figure Used
pCM988	pRS315 expressing Fur4-mNeonGreen from *FUR4* promoter	Laidlaw *et al.*, 2021	Fig 1D, 2A, 5F, S7a
pCM1021	pRS315 expressing Fur4-GFP from a *CUP1* promoter	This study	Fig 7B, 7D
pCM1022	pRS315 expressing Fur4-ΔN60-GFP from *CUP1* promoter	This study	Fig 7C, 7D, 7E, 7F, 7H, 7I
pCM264	pRS315 expressing Mup1-GFP from *MUP1* promoter	Laidlaw *et al.*, 2021	Fig 5F, 6D, S7c
pCM191	pRS316 expressing Ste3-mCherry from *STE3* promoter	MacDonald *et al.*, 2015	S7c
pCM420	pRS316 expressing Tna1-GFP from *TNA1* promoter.	This study	7F, S6
pCM476	pRS315 expressing Sec63-RFP from *SEC63* promoter.	This study	7F, 7H, 7I
pCM266	pRS315 expressing Fur4-Cherry from *FUR4* promoter.	This study	7F

Table S9: Statistical significance tests

Experiemnt	Notes	Significant	p value	Figure Used
*ura3*Δ vs WT growth	*ura3*Δ YPD	No	0.020281	1C
*ura3*Δ vs WT growth	*ura3*Δ 4 mg/L uracil	No	0.02126	1C
*ura3*Δ vs WT growth	*ura3*Δ 0.1 mg/L uracil	Yes	<0.000001	1C
*ura3*Δ *fur4*Δ vs WT growth	*ura3*Δ *fur4*Δ YPD	No	0.038119	1C
*ura3*Δ *fur4*Δ vs WT growth	*ura3*Δ *fur4*Δ 4 mg/L uracil	Yes	<0.000001	1C
*ura3*Δ *fur4*Δ vs WT growth	*ura3*Δ *fur4*Δ 0.1 mg/L uracil	Yes	<0.000001	1C
*rcy1*Δ vs WT growth	32 mg/L uracil	No	0.042047	2C
*rcy1*Δ vs WT growth	16 mg/L uracil	No	0.215419	2C
*rcy1*Δ vs WT growth	8 mg/L uracil	No	0.345309	2C
*rcy1*Δ vs WT growth	4 mg/L uracil	No	0.006666	2C
*rcy1*Δ vs WT growth	2 mg/L uracil	No	0.329933	2C
*rcy1*Δ vs WT growth	1 mg/L uracil	No	0.453213	2C
*rcy1*Δ vs WT growth	0.5 mg/L uracil	Yes	0.000006	2C
*rcy1*Δ vs WT growth	0.25 mg/L uracil	Yes	0.002131	2C
*rcy1*Δ vs WT growth	0.1 mg/L uracil	Yes	0.000143	2C
*rcy1*Δ vs WT growth	0.05 mg/L uracil	Yes	0.000002	2C
*nhx1*Δ vs WT growth	32 mg/L uracil	No	0.339929	2C
*nhx1*Δ vs WT growth	16 mg/L uracil	No	0.475067	2C
*nhx1*Δ vs WT growth	8 mg/L uracil	No	0.074915	2C
*nhx1*Δ vs WT growth	4 mg/L uracil	No	0.916033	2C
*nhx1*Δ vs WT growth	2 mg/L uracil	No	0.741979	2C
*nhx1*Δ vs WT growth	1 mg/L uracil	No	0.564531	2C
*nhx1*Δ vs WT growth	0.5 mg/L uracil	Yes	0.0009	2C
*nhx1*Δ vs WT growth	0.25 mg/L uracil	Yes	0.001946	2C
*nhx1*Δ vs WT growth	0.1 mg/L uracil	Yes	0.000028	2C
*nhx1*Δ vs WT growth	0.05 mg/L uracil	Yes	0.000005	2C
*get1*Δ vs WT	4 mg/L uracil	No	>0.999999	4B
*get2*Δ vs WT	4 mg/L uracil	No	>0.999999	4B
*get3*Δ vs WT	4 mg/L uracil	No	>0.999999	4B
*get1*Δ vs WT	0.1 mg/L uracil	Yes	0.000549	4B
*get2*Δ vs WT	0.1 mg/L uracil	Yes	<0.000001	4B
*get3*Δ vs WT	0.1 mg/L uracil	Yes	<0.000001	4B
*get1*Δ vs WT	0.05 mg/L uracil	Yes	0.000002	4B
*get2*Δ vs WT	0.05 mg/L uracil	Yes	0.000043	4B
*get3*Δ vs WT	0.05 mg/L uracil	Yes	<0.000001	4B
*gim4*Δ vs WT	4 mg/L uracil	No	>0.999999	4D
*pac10*Δ vs WT	4 mg/L uracil	No	>0.999999	4D
*pfd1*Δ vs WT	4 mg/L uracil	No	>0.999999	4D
*yke1*Δ vs WT	4 mg/L uracil	No	>0.999999	4D
*gim4*Δ vs WT	0.1 mg/L uracil	Yes	0.000017	4D
*pac10*Δ vs WT	0.1 mg/L uracil	Yes	<0.000001	4D
*pfd1*Δ vs WT	0.1 mg/L uracil	Yes	<0.000001	4D
*yke1*Δ vs WT	0.1 mg/L uracil	Yes	0.000012	4D
*gim4*Δ vs WT	0.05 mg/L uracil	Yes	0.009	4D
*pac10*Δ vs WT	0.05 mg/L uracil	Yes	0.000505	4D
*pfd1*Δ vs WT	0.05 mg/L uracil	Yes	0.00054	4D
*yke1*Δ vs WT	0.05 mg/L uracil	Yes	0.000824	4D
*ies2*Δ vs WT	4 mg/L uracil	No	>0.999999	5B
*bre1*Δ vs WT	4 mg/L uracil	No	>0.999999	5B
*elf1*Δ vs WT	4 mg/L uracil	No	>0.999999	5B
*ino4*Δ vs WT	4 mg/L uracil	No	>0.999999	5B
*swd1*Δ vs WT	4 mg/L uracil	No	>0.999999	5B
*swd3*Δ vs WT	4 mg/L uracil	No	>0.999999	5B
*sdc1*Δ vs WT	4 mg/L uracil	No	>0.999999	5B
*swi3*Δ vs WT	4 mg/L uracil	No	>0.999999	5B
*snf5*Δ vs WT	4 mg/L uracil	No	>0.999999	5B
*ies2*Δ vs WT	0.1 mg/L uracil	Yes	<0.000001	5B
*bre1*Δ vs WT	0.1 mg/L uracil	Yes	<0.000001	5B
*elf1*Δ vs WT	0.1 mg/L uracil	Yes	0.0002	5B
*ino4*Δ vs WT	0.1 mg/L uracil	Yes	0.000008	5B
*swd1*Δ vs WT	0.1 mg/L uracil	Yes	0.00032	5B
*swd3*Δ vs WT	0.1 mg/L uracil	Yes	0.012009	5B
*sdc1*Δ vs WT	0.1 mg/L uracil	Yes	<0.000001	5B
*swi3*Δ vs WT	0.1 mg/L uracil	Yes	0.00032	5B
*snf5*Δ vs WT	0.1 mg/L uracil	Yes	0.012009	5B
*ies2*Δ vs WT	0.05 mg/L uracil	Yes	<0.000001	5B

*bre1*Δ vs WT	0.05 mg/L uracil	Yes	<0.000001	5B
*elf1*Δ vs WT	0.05 mg/L uracil	Yes	0.012272	5B
*ino4*Δ vs WT	0.05 mg/L uracil	Yes	0.033492	5B
*swd1*Δ vs WT	0.05 mg/L uracil	Yes	0.000046	5B
*swd3*Δ vs WT	0.05 mg/L uracil	No	0.321733	5B
*sdc1*Δ vs WT	0.05 mg/L uracil	Yes	<0.000001	5B
*swi3*Δ vs WT	0.05 mg/L uracil	Yes	0.000046	5B
*snf5*Δ vs WT	0.05 mg/L uracil	No	0.321733	5B
pma1-DAmP vs WT growth	4 mg/L uracil	No	>0.999999	5E
gpi8-DAmP vs WT growth	4 mg/L uracil	No	>0.999999	5E
mrs6-DAmP vs WT growth	4 mg/L uracil	No	0.775271	5E
gpi12-DAmP vs WT growth	4 mg/L uracil	No	>0.999999	5E
sec62-DAmP vs WT growth	4 mg/L uracil	No	>0.999999	5E
pma1-DAmP vs WT growth	0.1 mg/L uracil	No	0.916689	5E
gpi8-DAmP vs WT growth	0.1 mg/L uracil	No	0.969782	5E
mrs6-DAmP vs WT growth	0.1 mg/L uracil	No	0.883157	5E
gpi12-DAmP vs WT growth	0.1 mg/L uracil	No	0.02774	5E
sec62-DAmP vs WT growth	0.1 mg/L uracil	Yes	0.000388	5E
pma1-DAmP vs WT growth	0.05 mg/L uracil	No	0.516661	5E
gpi8-DAmP vs WT growth	0.05 mg/L uracil	No	0.323593	5E
mrs6-DAmP vs WT growth	0.05 mg/L uracil	No	0.381219	5E
gpi12-DAmP vs WT growth	0.05 mg/L uracil	No	0.496057	5E
sec62-DAmP vs WT growth	0.05 mg/L uracil	Yes	0.00004	5E
*ydr525w*Δ vs WT	4 mg/L uracil	No	>0.999999	6A
*ygl214w*Δ vs WT	4 mg/L uracil	No	>0.999999	6A
*ynl089c*Δ vs WT	4 mg/L uracil	No	>0.999999	6A
*yor139c*Δ vs WT	4 mg/L uracil	No	0.999996	6A
*ydr222w*Δ vs WT	4 mg/L uracil	No	>0.999999	6A
*ycr050c*Δ vs WT	4 mg/L uracil	No	>0.999999	6A
*ynr068c*Δ vs WT	4 mg/L uracil	No	>0.999999	6A
*ymr001c-a*Δ vs WT	4 mg/L uracil	No	0.999996	6A
*yjr018w*Δ vs WT	4 mg/L uracil	No	0.999996	6A
*yjl132w*Δ vs WT	4 mg/L uracil	No	>0.999999	6A
*ydr525w*Δ vs WT	0.1 mg/L uracil	Yes	<0.000001	6A
*ygl214w*Δ vs WT	0.1 mg/L uracil	Yes	<0.000001	6A
*ynl089c*Δ vs WT	0.1 mg/L uracil	Yes	<0.000001	6A
*yor139c*Δ vs WT	0.1 mg/L uracil	Yes	<0.000001	6A
*ydr222w*Δ vs WT	0.1 mg/L uracil	Yes	<0.000001	6A
*ycr050c*Δ vs WT	0.1 mg/L uracil	Yes	<0.000001	6A
*ynr068c*Δ vs WT	0.1 mg/L uracil	Yes	<0.000001	6A
*ymr001c-a*Δ vs WT	0.1 mg/L uracil	Yes	0.000011	6A
*yjr018w*Δ vs WT	0.1 mg/L uracil	Yes	0.000011	6A
*yjl132w*Δ vs WT	0.1 mg/L uracil	Yes	0.00021	6A
*ydr525w*Δ vs WT	0.05 mg/L uracil	Yes	<0.000001	6A
*ygl214w*Δ vs WT	0.05 mg/L uracil	Yes	<0.000001	6A
*ynl089c*Δ vs WT	0.05 mg/L uracil	Yes	0.000432	6A
*yor139c*Δ vs WT	0.05 mg/L uracil	Yes	<0.000001	6A
*ydr222w*Δ vs WT	0.05 mg/L uracil	Yes	<0.000001	6A
*ycr050c*Δ vs WT	0.05 mg/L uracil	Yes	<0.000001	6A
*ynr068c*Δ vs WT	0.05 mg/L uracil	Yes	<0.000001	6A
*ymr001c-a*Δ vs WT	0.05 mg/L uracil	Yes	<0.000001	6A
*yjr018w*Δ vs WT	0.05 mg/L uracil	Yes	0.000004	6A
*yjl132w*Δ vs WT	0.05 mg/L uracil	Yes	0.000329	6A
*get3*Δ vs WT	Halo assay	Yes	0.01237	6E
*glo3*Δ vs WT	Halo assay	Yes	0.007118	6E
*spt3*Δ vs WT	Halo assay	Yes	0.000017	6E
*sac1*Δ vs WT	Halo assay	Yes	0.000017	6E
*get1*Δ vs WT	Halo assay	Yes	0.000008	6E
*apl2*Δ vs WT	Halo assay	Yes	<0.000001	6E
*ydr222w*Δ vs WT	Halo assay	No	0.352308	6E
*rcy1*Δ vs WT	Halo assay	No	0.770477	6E
*tco89*Δ vs WT	Halo assay	No	0.740073	6E
*rvs161*Δ vs WT	Halo assay	No	0.520285	6E
*nhx1*Δ vs WT	Halo assay	No	0.41082	6E
*gyp7*Δ vs WT	Halo assay	No	0.266519	6E
*rod1*Δ vs WT	Halo assay	No	0.244958	6E
*rcy1*Δ vs WT methionine	10 mg/L methionine	No	0.012818	S1
*rcy1*Δ vs WT methionine	4 mg/L methionine	No	0.489553	S1
*rcy1*Δ vs WT methionine	0.05 mg/L methionine	No	0.007233	S1
*rcy1*Δ vs WT methionine	0.025 mg/L methionine	No	0.020532	S1
*rcy1*Δ vs WT methionine	0.012 mg/L methionine	No	0.019221	S1

7.2. Appendix chapter III: A glucose starvation response governs endocytic trafficking and eisosomal retention of surface cargoes

Table S4: Yeast strains used in this study

Strain	Parental strain	Genotype	Reference	Figure Used
CMY56	BY4742	MAT**α**, *his3Δ leu2Δ lys2Δ ura3Δ*	Brachmann *et al*., 1998	Throughout as wild-type and parental strain
CMY211	BY4741	MAT**a**, *his3Δ leu2Δ met15Δ ura3Δ*	Brachmann *et al*., 1998	Parental strain
CMY41	SEY6210	MAT**α**, *leu2-3,112 ura3-52 his3-Δ200 trp1-Δ901 lys2-801 suc2-Δ9*	Robinson *et al*., 1988	Parental strain
CM1424	BY4741	*NOP1-sfGFP-HXT6::URA3*	Weill *et al*., 2018	S1e
CM1425	BY4741	*NOP1-sfGFP-HXT7::URA3*	Weill *et al*., 2018	S1e
CMY844	BY4741	*MIG1-mGFP::HIS3 NRD1-mCherry::Hyg^r*	Wollman *et al*., 2017	2A
CM768	BY4742	*mig1Δ::Kan^r*	Winzeler *et al*., 1999	2F, 4C, 4D
CMY997	BY4742	*mig1Δ::Kan^r mig2Δ::his5+*	This study	2F, 4C, 4D, 4E, 4F, 5B
CMY821	BY4742	*msn2Δ::Kan^r*	Winzeler *et al*., 1999	2G
CMY950	BY4741	*MIG2-mGFP::his5$^+$ NRD1-mCherry::Hyg^r*	This study	S2d
CMY903	BY4742	*YAP1801-mGFP::Mtx^r*	This study	3A, 3B, S3b, S3e
CMY905	BY4742	*YAP1802-mGFP::Mtx^r*	This study	3A, 3B
CMY949	BY4742	*YAP1801-mGFP:Mtx^r YAP1802-mCherry::his5+*	This study	3C, 3D, S3a, S3b
CMY1008	BY4742	*YAP1801-mCherry::his5+*	This study	3E
CMY1010	BY4742	*YAP1802-mCherry::his5+*	This study	3E, S3c, S3d
CMY1543	BY4742	*yap1801Δ::Kanr yap1802Δ::his5$^+$*	This study	4G, 4H, S4c
CMY789	BY4742	*Sec7-mCherry::loxP*	This study	4H
CMY1626	BY4742	*yap1801Δ::loxP yap1801Δ::loxP mig1Δ::his5+ mig2Δ::loxP*	This study	4I
CMY1555	BY4742	*reg1Δ::Kan^r*	Winzeler *et al*., 1999	S4b
CMY1554	BY4742	*snf3Δ::Kan^r*	Winzeler *et al*., 1999	S4b
CMY944	BY4742	*YAP1801-mGFP::Mtx^r PIL1-mCherry::his5+yap1802Δ::his5+*	This study	5A
CMY1309	BY4742	*PIL1-mGFP::his5$^+$*	This study	5A, 5C, 5D
CMY952	BY4742	*PIL1-mCherry::his5$^+$*	This study	5E, 5F, 5G, 5H, 5I, 5J, 5K, 5L, 5M, S5b, S5c, S5d, 6D,
CMY1623	BY4742	*LSP1-mCherry::his5$^+$*	This study	5O, 5P, S5g
CMY1467	BY4742	*NCE102-mCherry::his5$^+$*	This study	5P
CMY1625	BY4742	*SLM1-mCherry::his5$^+$*	This study	5P, S5g
CMY1607	BY4742	*YGR130c-mCherry::his5$^+$*	This study	6B, 6C
CMY1367	BY4742	*pil1Δ::Kan^r*	Winzeler *et al*., 1999	7A, S7b, S7c, S7e
CMY1371	BY4742	*lsp1Δ::Kan^r*	Winzeler *et al*., 1999	7A, S7b, S7c
CMY1374	BY4742	*slm2Δ::Kan^r*	Winzeler *et al*., 1999	7A
CMY1370	BY4742	*sur7Δ::Kan^r*	Winzeler *et al*., 1999	7A
CMY1369	BY4742	*eis1Δ::Kan^r*	Winzeler *et al*., 1999	7A, 7D, 7E, 7F, 7G, 7I, 7J, 7K, S7f, S7g
CMY1368	BY4742	*nce102Δ::Kan^r*	Winzeler *et al*., 1999	7A, 7D, 7E, 7F, 7G, 7I, 7J, 7K, S7b, S7c, S7d, S7f, S7
CMY1372	BY4742	*pkh2Δ::Kan^r*	Winzeler *et al*., 1999	7A, 7D, 7E, 7F, 7G, 7H, 7I, 7J, 7K, S7e, S7f, S7g
CMY1373	BY4742	*slm1Δ::Kan^r*	Winzeler *et al*., 1999	7A
CMY820	BY4742	*fur4Δ::Kan^r*	Winzeler *et al*., 1999	7C
CMY1588	BY4742	*ura3Δ::URA3*	This study	7L, 7M, S7h, S7i
CMY1589	BY4742	*ura3Δ::URA3 eis1Δ::Kan^r*	This study	7L, 7M, S7h, S7i
CMY1590	BY4742	*ura3Δ::URA3 pkh2Δ::Kan^r*	This study	7L, 7M, S7h, S7i
CMY1591	BY4742	*ura3Δ::URA3 nce102Δ::Kan^r*	This study	7L, 7M, S7h, S7i

Table S5: Plasmids used in this study

Plasmid	Genotype	Reference	Figure Used
pRS315	Low copy centromeric yeast expression plasmid containing *LEU2* marker	Sikorski and Hieter, 1989	Parent / control vector
pRS316	Low copy centromeric yeast expression plasmid containing *URA3* marker	Sikorski and Hieter, 1989	Parent / control vector
pRS303	Integration / shuttle plasmid containing *URA3* marker	Sikorski and Hieter, 1989	Parent vector
pCM264	pRS315 expressing Mup1-GFP from *MUP1* promoter	Stringer and Piper, 2011	1A, 1B, 1C, 1D, S1a, S1b, S1c, 3E, 4A, 4C, 4D, 4E, 4G, 4H, 4I, S4a, S4b, S4c, 5E, 5H, 5I, 5J, 5P, S5b, S5c, S5e, S5f, 6C, 6D, 6E, 6F, S6
pCM387	pRS315 expressing Ste3-GFP from *STE3* promoter	Urbanowski and Piper, 2001	1A, 4F, 4I, S7a
pCM988	pRS315 expressing Fur4-mNG from *FUR4* promoter	This study	1A, 4F, 4I, 6B, 6F, 6G
pCM859	pRS416 expressing GFP-Snc1^{PM} (contains L96V mutation) from *SNC1* promoter	Xu et al., 2017	1E
pCM386	pRS415 expressing Can1-GFP from *CAN1* promoter	This study	S1c, 4B, 4F, 4I
pCM503	pRS316 expressing Yor1-GFP from *CUP1* promoter	MacDonald et al., 2015	S1d
pCM995	pRS316 expressing Yap1801-mCherry from *CUP1* promoter	This study	4A, 4B
pCM996	pRS316 expressing Yap1802-mCherry from *CUP1* promoter	This study	4A, 4B, 5A
pCM691	pRS315 expressing Ste3-GFP-UL36 from *STE3* promoter	Stringer and Piper, 2011	S7a
pCM994	pRS316 expressing Pil1-mCherry from *CUP1* promoter	This study	5A
pCM1006	pRS316 expressing Pil1-GFP from *PIL1* promoter	This study	7D, 7E, S7g

Table S8: Statistical analysis

Experiemnt	Notes	Significant	p value	Figure Used
30 min raffinose	*YAP1801*	Yes	<0.000001	2D
30 min raffinose	*YAP1802*	Yes	0.014765	2D
30 min raffinose	*APL3*	No	0.999996	2D
30 min raffinose	*BNI1*	No	0.999996	2D
30 min raffinose	*BUD6*	No	0.999996	2D
30 min raffinose	*SLA1*	No	0.999996	2D
30 min raffinose	*ROM2*	No	0.999981	2D
60 min raffinose	*YAP1801*	Yes	<0.000001	2D
60 min raffinose	*YAP1802*	Yes	<0.000001	2D
60 min raffinose	*APL3*	No	0.999971	2D
60 min raffinose	*BNI1*	No	0.999996	2D
60 min raffinose	*BUD6*	No	0.999996	2D
60 min raffinose	*SLA1*	No	0.99998	2D
60 min raffinose	*ROM2*	No	0.999996	2D
15 min raffinose	*YAP1801*	Yes	<0.000001	2E
15 min raffinose	*YAP1802*	No	0.923942	2E
30 min raffinose	*YAP1801*	Yes	<0.000001	2E
30 min raffinose	*YAP1802*	Yes	<0.000001	2E
60 min raffinose	*YAP1801*	Yes	<0.000001	2E
60 min raffinose	*YAP1802*	Yes	<0.000001	2E
90 min raffinose	*YAP1801*	Yes	0.000003	2E
90 min raffinose	*YAP1802*	No	0.417664	2E
mig1Δ	*YAP1801*	No	0.998571	2F
mig1Δ	*YAP1802*	No	0.998571	2F
mig1Δ mig2Δ	*YAP1801*	Yes	<0.000001	2F
mig1Δ mig2Δ	*YAP1802*	Yes	0.000258	2F
msn2Δ	*YAP1801*	Yes	0.035138	2G
msn2Δ	*YAP1802*	No	0.081538	2G
msn2Δ	*APL3*	No	0.36662	2G
msn2Δ	*BNI1*	No	0.492061	2G
msn2Δ	*BUD6*	No	0.7751	2G
msn2Δ	*SLA1*	No	0.730214	2G
msn2Δ	*ROM2*	No	0.234561	2G
60 min raffinose	*PIL1*	Yes	<0.000001	5B
60 min raffinose	*SUR7*	No	0.834054	5B
60 min raffinose	*NCE102*	Yes	<0.000001	5B
60 min raffinose	*PKH2*	Yes	<0.000001	5B
60 min raffinose	*SLM1*	Yes	<0.000001	5B
60 min raffinose	*SLM2*	No	0.456706	5B
60 min raffinose	*LSP1*	Yes	<0.000001	5B
60 min raffinose	*EIS1*	Yes	<0.000001	5B
60 min raffinose	*SEG1*	Yes	<0.000001	5B
mig1Δ mig2Δ	*PIL1*	No	0.997483	5B
15 min raffinose	*PIL1*	No	0.997483	S5a
30 min raffinose	*PIL1*	Yes	0.01328	S5a
60 min raffinose	*PIL1*	Yes	<0.000001	S5a
90 min raffinose	*PIL1*	No	0.989609	S5a
Slimfield abundance raffinose	Yap1801	Yes	0.0046	3D
Slimfield abundance raffinose	Yap1802	Yes	<0.0001	3D
Confocal abundance 30 min raffinose	Yap1801	Yes	<0.0001	S3b
Confocal abundance 60 min raffinose	Yap1801	Yes	<0.0001	S3b
Confocal abundance 120 min raffinose	Yap1801	Yes	<0.0001	S3b
Confocal abundance 30 min raffinose	Yap1802 (mother)	No	0.1742	S3c
Confocal abundance 60 min raffinose	Yap1802 (mother)	Yes	0.0085	S3c
Confocal abundance 120 min raffinose	Yap1802 (mother)	Yes	0.0158	S3c
Confocal abundance 30 min raffinose	Yap1802 (daughter)	Yes	0.0002	S3d
Confocal abundance 60 min raffinose	Yap1802 (daughter)	Yes	0.0004	S3d
Confocal abundance 120 min raffinose	Yap1802 (daughter)	Yes	0.021	S3d
Eisosome number 30 min raffinose	Pil1-mCherry puncta	No	0.5847	S5d
Eisosome number 30 min raffinose	Pil1-mCherry puncta	No	0.6187	S5d

Immunoblot abundance 60 min raffinose	Yap1801	Yes	0.000338	3B
Immunoblot abundance 60 min raffinose	Yap1801	Yes	0.002452	3B
Immunoblot abundance 120 min raffinose	Yap1802	No	0.914469	3B
Immunoblot abundance 60 min raffinose	Yap1802	No	0.381398	3B
No of eisosomes	*eis1Δ*	Yes	<0.0001	8G
No of eisosomes	*pkh2Δ*	Yes	<0.0001	8G
No of eisosomes	*nce102Δ*	Yes	<0.0001	8G
20 mg/L uracil *eis1Δura3Δ*	1 hour	Yes	0.00227	7J
20 mg/L uracil *eis1Δura3Δ*	2 hours	Yes	0.000011	7J
20 mg/L uracil *eis1Δura3Δ*	3 hours	Yes	0.000379	7J
20 mg/L uracil *eis1Δura3Δ*	4 hours	Yes	0.000005	7J
20 mg/L uracil *eis1Δura3Δ*	5 hours	Yes	0.003579	7J
20 mg/L uracil *pkh2Δura3Δ*	1 hour	Yes	0.00082	7J
20 mg/L uracil *pkh2Δura3Δ*	2 hours	Yes	0.01455	7J
20 mg/L uracil *pkh2Δura3Δ*	3 hours	Yes	0.008838	7J
20 mg/L uracil *pkh2Δura3Δ*	4 hours	Yes	0.003654	7J
20 mg/L uracil *pkh2Δura3Δ*	5 hours	Yes	0.000604	7J
20 mg/L uracil *nce102Δura3Δ*	1 hour	Yes	0.047034	7J
20 mg/L uracil *nce102Δura3Δ*	2 hours	Yes	0.007179	7J
20 mg/L uracil *nce102Δura3Δ*	3 hours	Yes	0.000005	7J
20 mg/L uracil *nce102Δura3Δ*	4 hours	Yes	0.000852	7J
20 mg/L uracil *nce102Δura3Δ*	5 hours	Yes	0.001979	7J
2 mg/L uracil *eis1Δura3Δ*	1 hour	Yes	0.044581	7K
2 mg/L uracil *eis1Δura3Δ*	2 hours	Yes	0.019016	7K
2 mg/L uracil *eis1Δura3Δ*	3 hours	Yes	0.001129	7K
2 mg/L uracil *eis1Δura3Δ*	4 hours	Yes	0.025949	7K
2 mg/L uracil *eis1Δura3Δ*	5 hours	Yes	0.020623	7K
2 mg/L uracil *pkh2Δura3Δ*	1 hour	Yes	0.014549	7K
2 mg/L uracil *pkh2Δura3Δ*	2 hours	No	0.054356	7K
2 mg/L uracil *pkh2Δura3Δ*	3 hours	Yes	0.001431	7K
2 mg/L uracil *pkh2Δura3Δ*	4 hours	No	0.126574	7K
2 mg/L uracil *pkh2Δura3Δ*	5 hours	Yes	0.000498	7K
2 mg/L uracil *nce102Δura3Δ*	1 hour	No	0.069487	7K
2 mg/L uracil *nce102Δura3Δ*	2 hours	Yes	0.009382	7K
2 mg/L uracil *nce102Δura3Δ*	3 hours	Yes	0.0012	7K
2 mg/L uracil *nce102Δura3Δ*	4 hours	Yes	0.000006	7K
2 mg/L uracil *nce102Δura3Δ*	5 hours	No	0.078305	7K
20mg/L uracil *pkh2Δura3Δ* compared to *pkh2Δ*	1 hour	No	0.121715	7L
20mg/L uracil *pkh2Δura3Δ* compared to *pkh2Δ*	2 hours	No	0.252002	7L
20mg/L uracil *pkh2Δura3Δ* compared to *pkh2Δ*	3 hours	No	0.052244	7L
20mg/L uracil *pkh2Δura3Δ* compared to *pkh2Δ*	4 hours	Yes	0.030158	7L
20mg/L uracil *pkh2Δura3Δ* compared to *pkh2Δ*	5 hours	Yes	0.004866	7L
20mg/L uracil *pkh2Δura3Δ* compared to WT	1 hour	Yes	0.00082	7L
20mg/L uracil *pkh2Δura3Δ* compared to WT	2 hours	Yes	0.01455	7L
20mg/L uracil *pkh2Δura3Δ* compared to WT	3 hours	Yes	0.008838	7L
20mg/L uracil *pkh2Δura3Δ* compared to WT	4 hours	Yes	0.003654	7L
20mg/L uracil *pkh2Δura3Δ* compared to WT	5 hours	Yes	0.000604	7L
20mg/L uracil *pkh2Δ* compared to WT	1 hour	No	0.945499	7L
20mg/L uracil *pkh2Δ* compared to WT	2 hours	No	0.051822	7L
20mg/L uracil *pkh2Δ* compared to WT	3 hours	Yes	0.000393	7L
20mg/L uracil *pkh2Δ* compared to WT	4 hours	Yes	0.00047	7L
20mg/L uracil *pkh2Δ* compared to WT	5 hours	Yes	0.000415	7L
20mg/L uracil *nce102Δura3Δ* compared to *nce102Δ*	1 hour	No	0.12083	7M
20mg/L uracil *nce102Δura3Δ* compared to *nce102Δ*	2 hours	Yes	0.022449	7M
20mg/L uracil *nce102Δura3Δ* compared to *nce102Δ*	3 hours	Yes	0.000351	7M
20mg/L uracil *nce102Δura3Δ* compared to *nce102Δ*	4 hours	Yes	0.011903	7M
20mg/L uracil *nce102Δura3Δ* compared to *nce102Δ*	5 hours	Yes	0.005691	7M
20mg/L uracil *nce102Δura3Δ* compared to WT	1 hour	Yes	0.047034	7M
20mg/L uracil *nce102Δura3Δ* compared to WT	2 hours	Yes	0.007179	7M
20mg/L uracil *nce102Δura3Δ* compared to WT	3 hours	Yes	0.000005	7M
20mg/L uracil *nce102Δura3Δ* compared to WT	4 hours	Yes	0.000852	7M

20mg/L uracil *nce102Δura3Δ* compared to WT	5 hours	Yes	0.001979	7M
20mg/L uracil *nce102Δ* compared to WT	1 hour	No	0.962957	7M
20mg/L uracil *nce102Δ* compared to WT	2 hours	Yes	0.006227	7M
20mg/L uracil *nce102Δ* compared to WT	3 hours	Yes	0.016253	7M
20mg/L uracil *nce102Δ* compared to WT	4 hours	Yes	0.047776	7M
20mg/L uracil *nce102Δ* compared to WT	5 hours	Yes	0.00236	7M
OD_{600} at saturation mutant compared to WT	*lsp1Δ*	Yes	0.000907	S7c
OD_{600} at saturation mutant compared to WT	*pil1Δ*	Yes	0.000044	S7c
OD_{600} at saturation mutant compared to WT	*nce102Δ*	Yes	0.000059	S7c
4 mg/L uracil *eis1Δura3Δ*	1 hour	No	0.128459	S7f
4 mg/L uracil *eis1Δura3Δ*	2 hours	Yes	0.011841	S7f
4 mg/L uracil *eis1Δura3Δ*	3 hours	Yes	0.004634	S7f
4 mg/L uracil *eis1Δura3Δ*	4 hours	Yes	0.017735	S7f
4 mg/L uracil *eis1Δura3Δ*	5 hours	Yes	0.011625	S7f
4 mg/L uracil *pkh2Δura3Δ*	1 hour	No	0.14216	S7f
4 mg/L uracil *pkh2Δura3Δ*	2 hours	Yes	0.041153	S7f
4 mg/L uracil *pkh2Δura3Δ*	3 hours	No	0.097597	S7f
4 mg/L uracil *pkh2Δura3Δ*	4 hours	No	0.160603	S7f
4 mg/L uracil *pkh2Δura3Δ*	5 hours	Yes	0.000009	S7f
4 mg/L uracil *nce102Δura3Δ*	1 hour	No	0.14412	S7f
4 mg/L uracil *nce102Δura3Δ*	2 hours	No	0.117626	S7f
4 mg/L uracil *nce102Δura3Δ*	3 hours	Yes	0.003456	S7f
4 mg/L uracil *nce102Δura3Δ*	4 hours	Yes	0.003245	S7f
4 mg/L uracil *nce102Δura3Δ*	5 hours	Yes	0.023808	S7f
0.5 mg/L uracil *eis1Δura3Δ*	1 hour	Yes	0.00113	S7g
0.5 mg/L uracil *eis1Δura3Δ*	2 hours	Yes	0.03096	S7g
0.5 mg/L uracil *eis1Δura3Δ*	3 hours	Yes	0.008464	S7g
0.5 mg/L uracil *eis1Δura3Δ*	4 hours	Yes	0.000104	S7g
0.5 mg/L uracil *eis1Δura3Δ*	5 hours	Yes	0.000575	S7g
0.5 mg/L uracil *pkh2Δura3Δ*	1 hour	Yes	0.002126	S7g
0.5 mg/L uracil *pkh2Δura3Δ*	2 hours	Yes	0.000125	S7g
0.5 mg/L uracil *pkh2Δura3Δ*	3 hours	Yes	0.000354	S7g
0.5 mg/L uracil *pkh2Δura3Δ*	4 hours	Yes	0.000014	S7g
0.5 mg/L uracil *pkh2Δura3Δ*	5 hours	Yes	0.024552	S7g
0.5 mg/L uracil *nce102Δura3Δ*	1 hour	Yes	0.001146	S7g
0.5 mg/L uracil *nce102Δura3Δ*	2 hours	Yes	0.00009	S7g
0.5 mg/L uracil *nce102Δura3Δ*	3 hours	Yes	0.000049	S7g
0.5 mg/L uracil *nce102Δura3Δ*	4 hours	Yes	0.000269	S7g
0.5 mg/L uracil *nce102Δura3Δ*	5 hours	Yes	0.000064	S7g
10% amino acids *eis1Δ*	1 hour	No	0.079633	S7h
10% amino acids *eis1Δ*	2 hours	Yes	0.008999	S7h
10% amino acids *eis1Δ*	3 hours	Yes	0.002477	S7h
10% amino acids *pkh2Δ*	1 hour	Yes	0.043162	S7h
10% amino acids *pkh2Δ*	2 hours	Yes	0.001908	S7h
10% amino acids *pkh2Δ*	3 hours	Yes	0.007449	S7h
20mg/L uracil *eis1Δura3Δ* compared to *eis1Δ*	1 hour	No	0.165941	S7i
20mg/L uracil *eis1Δura3Δ* compared to *eis1Δ*	2 hours	Yes	0.001654	S7i
20mg/L uracil *eis1Δura3Δ* compared to *eis1Δ*	3 hours	Yes	0.008675	S7i
20mg/L uracil *eis1Δura3Δ* compared to *eis1Δ*	4 hours	Yes	0.003773	S7i
20mg/L uracil *eis1Δura3Δ* compared to *eis1Δ*	5 hours	No	0.059399	S7i
20mg/L uracil *eis1Δura3Δ* compared to WT	1 hour	Yes	0.00227	S7i
20mg/L uracil *eis1Δura3Δ* compared to WT	2 hours	Yes	0.000011	S7i
20mg/L uracil *eis1Δura3Δ* compared to WT	3 hours	Yes	0.000379	S7i
20mg/L uracil *eis1Δura3Δ* compared to WT	4 hours	Yes	0.000005	S7i
20mg/L uracil *eis1Δura3Δ* compared to WT	5 hours	Yes	0.003579	S7i
20mg/L uracil *eis1Δ* compared to WT	1 hour	No	0.905461	S7i
20mg/L uracil *eis1Δ* compared to WT	2 hours	Yes	0.006818	S7i
20mg/L uracil *eis1Δ* compared to WT	3 hours	Yes	0.000082	S7i
20mg/L uracil *eis1Δ* compared to WT	4 hours	Yes	0.004413	S7i
20mg/L uracil *eis1Δ* compared to WT	5 hours	Yes	0.00325	S7i

7.3. Appendix Chapter IV: The phosphatase Glc7 controls eisosomal response to starvation via posttranslational modification of Pil1

NetPhorest Hits

Systematic Name	Standard Name	Prediction Score	Sequence	Pil1 Phosphosite	Kinase family
YDR247W	Vhs1	0.32	MHRTYSLRNSR	S6	Vhs1/Sks1
YPL026C	Sks1	0.32	MHRTYSLRNSR	S6	Vhs1/Sks1
YDR490C	Pkh1	0.31	MHRTYSLRNSR	S6	Pkh1/2/3
YOL100W	Pkh2	0.31	MHRTYSLRNSR	S6	Pkh1/2/3
YDR466W	Pkh3	0.31	MHRTYSLRNSR	S6	Pkh1/2/3
YGL158W	Rck1	0.26	MHRTYSLRNSR	S6	Rck1/2
YLR248W	Rck2	0.26	MHRTYSLRNSR	S6	Rck1/2
YDR507C	Gin4	0.23	MHRTYSLRNSR	S6	Ydr507c
YKL171W	Nnk1	0.22	MHRTYSLRNSR	S6	Ykl171w
YCL024W	Kcc4	0.21	MHRTYSLRNSR	S6	Ycl024w
YMR216C	Sky1	0.21	MHRTYSLRNSR	S6	Ymr216c
YGL179C	Tos3	0.2	MHRTYSLRNSR	S6	Tos3/Sak1
YER129W	Sak1	0.2	MHRTYSLRNSR	S6	Tos3/Sak1
YJL164C	Tpk1	0.19	MHRTYSLRNSR	S6	Tpk1/2/3
YPL203W	Tpk2	0.19	MHRTYSLRNSR	S6	Tpk1/2/3
YKL166C	Tpk3	0.19	MHRTYSLRNSR	S6	Tpk1/2/3
YPL141C	Frk1	0.18	MHRTYSLRNSR	S6	Ypl141c
YAR019C	Cdc15	0.22	PPPPSTTKGRF	T27	Yar019c
YPR054W	Smk1	0.13	PPPPSTTKGRF	T27	Smk1/Kdx1/Slt2/Hog1/Kss1/Fus3
YKL161C	Kdx1	0.13	PPPPSTTKGRF	T27	Smk1/Kdx1/Slt2/Hog1/Kss1/Fus3
YHR030C	Slt2	0.13	PPPPSTTKGRF	T27	Smk1/Kdx1/Slt2/Hog1/Kss1/Fus3
YLR113W	Hog1	0.13	PPPPSTTKGRF	T27	Smk1/Kdx1/Slt2/Hog1/Kss1/Fus3
YGR040W	Kss1	0.13	PPPPSTTKGRF	T27	Smk1/Kdx1/Slt2/Hog1/Kss1/Fus3
YBL016W	Fus3	0.13	PPPPSTTKGRF	T27	Smk1/Kdx1/Slt2/Hog1/Kss1/Fus3
YDR490C	Pkh1	0.22	GGLAYSFRRSA	S41	Pkh1/2/3
YOL100W	Pkh2	0.22	GGLAYSFRRSA	S41	Pkh1/2/3
YDR466W	Pkh3	0.22	GGLAYSFRRSA	S41	Pkh1/2/3
YAR018C	Kin3	0.19	GGLAYSFRRSA	S41	Yar018c
YCR091W	Kin82	0.19	GGLAYSFRRSA	S41	Kin82/Fpk1
YNR047W	Fpk1	0.19	GGLAYSFRRSA	S41	Kin82/Fpk1
YKL171W	Nnk1	0.13	GGLAYSFRRSA	S41	Ykl171w
YDR283C	Gcn2	0.11	GGLAYSFRRSA	S41	Ydr283c
YAR018C	Kin3	0.21	YSFRRSAAGAF	S45	Yar018c
YMR104C	Ypk2	0.15	YSFRRSAAGAF	S45	Ymr104c
YFL033C	Rim15	0.12	YSFRRSAAGAF	S45	Yfl033c
YCR091W	Kin82	0.11	YSFRRSAAGAF	S45	Kin82/Fpk1
YNR047W	Fpk1	0.11	YSFRRSAAGAF	S45	Kin82/Fpk1
YBR136W	Mec1	0.38	LSRKLSQLVKI	S59	Ybr136w
YBL088C	Tel1	0.23	LSRKLSQLVKI	S59	Ybl088c
YGL158W	Rck1	0.23	LSRKLSQLVKI	S59	Rck1/2
YLR248W	Rck2	0.23	LSRKLSQLVKI	S59	Rck1/2
YJL164C	Tpk1	0.22	LSRKLSQLVKI	S59	Tpk1/2/3
YPL203W	Tpk2	0.22	LSRKLSQLVKI	S59	Tpk1/2/3
YKL166C	Tpk3	0.22	LSRKLSQLVKI	S59	Tpk1/2/3
YMR104C	Ypk2	0.21	LSRKLSQLVKI	S59	Ymr104c
YDR247W	Vhs1	0.21	LSRKLSQLVKI	S59	Vhs1/Sks1
YPL026C	Sks1	0.21	LSRKLSQLVKI	S59	Vhs1/Sks1
YOL016C	Cmk2	0.19	LSRKLSQLVKI	S59	Yol016c
YPL141C	Frk1	0.18	LSRKLSQLVKI	S59	Ypl141c
YOR233W	Kin4	0.17	LSRKLSQLVKI	S59	Yor233w
YCR091W	Kin82	0.17	LSRKLSQLVKI	S59	Kin82/Fpk1
YNR047W	Fpk1	0.17	LSRKLSQLVKI	S59	Kin82/Fpk1
YBR296C	Pho89	0.16	ELLDDSPVTPG	S230	Pho89/Cdc28
YBR160W	Cdc28	0.16	ELLDDSPVTPG	S230	Pho89/Cdc28

Yeast strains used in this study

Freezer Strain	Parental strain	Genotype	Reference	Figure Used
CMY56	BY4742	MAT**α**, *his3Δ leu2Δ lys2Δ ura3Δ*	Brachmann *et al.*, 1998	Throughout as wild-type and parental strain
CMY211	BY4741	MAT**A**, *his3Δ leu2Δ met15Δ ura3Δ*	Brachmann *et al.*, 1999	Throughout as wild-type and parental strain
CMY1467	BY4742	*Nce102-mCherry-his5+ his3Δ1 leu2Δ0 lys2Δ0 ura3Δ0*	This study	1B, S1a, S1b
CMY2026	BY4741/BY4742 diploid	*Nce102-mCherry-his5+ ; Ura3-NOP1-GFP-Pkh1*	This study	1B, S1a
CMY2027	BY4741/BY4742 diploid	*Nce102-mCherry-his5+ ; Ura3-NOP1-GFP-Pkh2*	This study	1B
CMY2361	BY4741/BY4742 diploid	*Nce102-mCherry-his5+ ; Ura3-NOP1-GFP-Pkh2*	This study	1B, S1b
CMY1784	BY4742	*pkh1Δ::KanMX4*	Winzeler *et al.*, 1999	1A
CMY1764	BY4742	pkh2Δ::KanMX4	Winzeler *et al.*, 1999	1A, 1C
CMY1783	BY4742	*pkh3Δ::KanMX4*	Winzeler *et al.*, 1999	1A
CMY2279	BY4742	*sak1Δ::KanMX4*	Winzeler *et al.*, 1999	2C, S2
CMY72282	BY4742	*cka2Δ::KanMX4*	Winzeler *et al.*, 1999	2C, S2
CMY2273	BY4742	*hog1Δ::KanMX4*	Winzeler *et al.*, 1999	2C, S2
CMY2280	BY4742	*rim15Δ::KanMX4*	Winzeler *et al.*, 1999	2C, S2
CMY2281	BY4742	*cka1Δ::KanMX4*	Winzeler *et al.*, 1999	2C, S2
CMY2275	BY4742	*tpk1Δ::KanMX4*	Winzeler *et al.*, 1999	2C, S2
CMY2283	BY4742	*CDC15::KanMX4*	Breslow *et al.*, 2008	2C, S2
CMY2274	BY4742	*sky1Δ::KanMX4*	Winzeler *et al.*, 1999	2C, S2
CMY2252	BY4742	*vhs1Δ::KanMX4*	Winzeler *et al.*, 1999	S2
CMY2253	BY4742	*gen2Δ::KanMX4*	Winzeler *et al.*, 1999	S2
CMY2254	BY4742	*cmk2Δ::KanMX4*	Winzeler *et al.*, 1999	S2
CMY2255	BY4742	*smh1Δ::KanMX4*	Winzeler *et al.*, 1999	S2
CMY2256	BY4742	*pho89Δ::KanMX4*	Winzeler *et al.*, 1999	S2
CMY2257	BY4742	*kss1Δ::KanMX4*	Winzeler *et al.*, 1999	S2
CMY2258	BY4742	*fpk1Δ::KanMX4*	Winzeler *et al.*, 1999	S2
CMY2259	BY4742	*tel1Δ::KanMX4*	Winzeler *et al.*, 1999	S2
CMY2260	BY4742	*rdx1Δ::KanMX4*	Winzeler *et al.*, 1999	S2
CMY2261	BY4742	*kin4Δ::KanMX4*	Winzeler *et al.*, 1999	S2
CMY2263	BY4742	*rck2Δ::KanMX4*	Winzeler *et al.*, 1999	S2
CMY2264	BY4742	*sks1Δ::KanMX4*	Winzeler *et al.*, 1999	S2
CMY2265	BY4742	*kin28Δ::KanMX4*	Winzeler *et al.*, 1999	S2
CMY2266	BY4742	*fus3Δ::KanMX4*	Winzeler *et al.*, 1999	S2
CMY2267	BY4742	*tpk3Δ::KanMX4*	Winzeler *et al.*, 1999	S2
CMY2268	BY4742	*frk1Δ::KanMX4*	Winzeler *et al.*, 1999	S2
CMY2269	BY4742	*slt2Δ::KanMX4*	Winzeler *et al.*, 1999	S2
CMY2270	BY4742	*rcc4Δ::KanMX4*	Winzeler *et al.*, 1999	S2
CMY2271	BY4742	*nnk1Δ::KanMX4*	Winzeler *et al.*, 1999	S2
CMY2272	BY4742	*kin3Δ::KanMX4*	Winzeler *et al.*, 1999	S2
CMY2276	BY4742	*ypk2Δ::KanMX4*	Winzeler *et al.*, 1999	S2
CMY2277	BY4742	*gin4Δ::KanMX4*	Winzeler *et al.*, 1999	S2
CMY2278	BY4742	*tos3Δ::KanMX4*	Winzeler *et al.*, 1999	S2
CMY1367	BY4742	*pil1Δ::KanMX4*	Winzeler *et al.*, 1999	3C
CMY1760	BY4742	*ptp2Δ::KanMX4*	Winzeler *et al.*, 1999	4A
CMY1761	BY4742	*ptc3Δ::KanMX4*	Winzeler *et al.*, 1999	4A
CMY1762	BY4742	*ppn2Δ::KanMX4*	Winzeler *et al.*, 1999	4A, 5A
CMY1782	BY4742	*ptc1Δ::KanMX4*	Winzeler *et al.*, 1999	4A, 5A
CMY1769	BY4742	*ptp1Δ::KanMX4*	Winzeler *et al.*, 1999	4A
CMY1770	BY4742	*ptc6Δ::KanMX4*	Winzeler *et al.*, 1999	4A
CMY1771	BY4742	*pph21Δ::KanMX4*	Winzeler *et al.*, 1999	4A
CMY1772	BY4742	*pph22Δ::KanMX4*	Winzeler *et al.*, 1999	4A
CMY1773	BY4742	*siw14Δ::KanMX4*	Winzeler *et al.*, 1999	4A, 5A
CMY1774	BY4742	*sdp1Δ::KanMX4*	Winzeler *et al.*, 1999	4A
CMY1775	BY4742	*tep1Δ::KanMX4*	Winzeler *et al.*, 1999	4A
CMY1785	BY4742	*rtr1Δ::KanMX4*	Winzeler *et al.*, 1999	4A
CMY1778	BY4742	*oca1Δ::KanMX4*	Winzeler *et al.*, 1999	4A
CMY1779	BY4742	*ptc4Δ::KanMX4*	Winzeler *et al.*, 1999	4A
CMY1780	BY4742	*pps1Δ::KanMX4*	Winzeler *et al.*, 1999	4A
CMY1776	BY4742	*ppg1Δ::KanMX4*	Winzeler *et al.*, 1999	4A
CMY1777	BY4742	*oca2Δ::KanMX4*	Winzeler *et al.*, 1999	4A
CMY1754	BY4742	*pph3Δ::KanMX4*	Winzeler *et al.*, 1999	4A
CMY1748	BY4742	*ppz1Δ::KanMX4*	Winzeler *et al.*, 1999	4A
CMY1756	BY4742	*ptp3Δ::KanMX4*	Winzeler *et al.*, 1999	4A
CMY1757	BY4742	*ppt1Δ::KanMX4*	Winzeler *et al.*, 1999	4A
CMY1746	BY4742	*psr1Δ::KanMX4*	Winzeler *et al.*, 1999	4A
CMY1747	BY4742	*psr2Δ::KanMX4*	Winzeler *et al.*, 1999	4A
CMY1749	BY4742	*cmp2Δ::KanMX4*	Winzeler *et al.*, 1999	4A
CMY1750	BY4742	*mih1Δ::KanMX4*	Winzeler *et al.*, 1999	4A
CMY1751	BY4742	*ptc5Δ::KanMX4*	Winzeler *et al.*, 1999	4A
CMY1752	BY4742	*ppq1Δ::KanMX4*	Winzeler *et al.*, 1999	4A

CMY1758	BY4742	*ych1Δ::KanMX4*	Winzeler *et al*., 1999	4A
CMY1759	BY4742	*ptc7Δ::KanMX4*	Winzeler *et al*., 1999	4A
CMY1765	BY4742	*ltp1Δ::KanMX4*	Winzeler *et al*., 1999	4A
CMY1766	BY4742	*nem1Δ::KanMX4*	Winzeler *et al*., 1999	4A
CMY1767	BY4742	*ymr1Δ::KanMX4*	Winzeler *et al*., 1999	4A
CMY1768	BY4742	*cna1Δ::KanMX4*	Winzeler *et al*., 1999	4A
CMY1786	BY4742	*sit4Δ::KanMX4*	Winzeler *et al*., 1999	4A, 5A
CMY1788	BY4742	*msg5Δ::KanMX4*	Winzeler *et al*., 1999	4A, 5A
CMY1763	BY4742	*yvh1Δ::KanMX4*	Winzeler *et al*., 1999	4A, 5A
CMY1787	BY4742	*ptc2Δ::KanMX4*	Winzeler *et al*., 1999	4A
CMY1789	BY4742	*CDC14::KanMX4*	Breslow *et al*., 2008	4A
CMY1790	BY4742	*GLC7::KanMX4*	Breslow *et al*., 2008	4A, 5A, 6A, 8A, 8B, 8C, 8D
CMY1791	BY4742	*SSU72::KanMX4*	Breslow *et al*., 2008	4A
CMY1792	BY4742	*FCP1::KanMX4*	Breslow *et al*., 2008	4A
CMY1847	BY4741	*URA3-NOP1-GFP-GLC7*	Weill *et al*., 2018	5C, 6G, 6H
CMY1849	BY4741	*URA3-NOP1-GFP-MSG5*	Weill *et al*., 2018	5C
CMY1851	BY4741	*URA3-NOP1-GFP-SIW14*	Weill *et al*., 2018	5C
CMY1860	BY4741	*URA3-NOP1-GFP-PTC1*	Weill *et al*., 2018	5C
CMY1861	BY4741	*URA3-NOP1-GFP-YVH1*	Weill *et al*., 2018	5C
CMY1896	BY4741	*Sit4-GFP His+ Met+*	This study	5C
CMY2123	BY4741	*URA3-NOP1-GFP-PPN2*	Weill *et al*., 2018	5C
CMY1877	BY4741/BY4742	*URA3-NOP1-GFP-GLC7 ; Pil1-mCherry-his5+*	This study	6G and 6H
CMY1850	BY4741	*URA3-NOP1-GFP-PPQ1*	Weill *et al*., 2018	S4
CMY1848	BY4741	*URA3-NOP1-GFP-PTC5*	Weill *et al*., 2018	S4
CMY1853	BY4741	*URA3-NOP1-GFP-CMP2*	Weill *et al*., 2018	S4
CMY1854	BY4741	*URA3-NOP1-GFP-OCA2*	Weill *et al*., 2018	S4
CMY1856	BY4741	*URA3-NOP1-GFP-PPT1*	Weill *et al*., 2018	S4
CMY1855	BY4741	*URA3-NOP1-GFP-PPH21*	Weill *et al*., 2018	S4
CMY1859	BY4741	*URA3-NOP1-GFP-PTP3*	Weill *et al*., 2018	S4
CMY1858	BY4741	*URA3-NOP1-GFP-RTR2*	Weill *et al*., 2018	S4
CMY1862	BY4741	*URA3-NOP1-GFP-YCH1*	Weill *et al*., 2018	S4
CMY1865	BY4741	*URA3-NOP1-GFP-SDP1*	Weill *et al*., 2018	S4
CMY1852	BY4741	*URA3-NOP1-GFP-PPZ1*	Weill *et al*., 2018	S4
CMY1864	BY4741	*URA3-NOP1-GFP-NEM1*	Weill *et al*., 2018	S4
CMY2219	BY4742	*YETI-GLC7*	Arita *et al*., 2021	6D, 6E, 6F
CMY1555	BY4742	*reg1Δ::KanMX4*	Winzeler *et al*., 1999	6B, 6C
CMY952	BY4742	*Pil1-mCherry*	Laidlaw *et al*., 2021	3B, 6G, 6H
CMY2227	BY4742	*Pil1-8D-GFP S6D, S27D, S45D, S59D, S230D, S233D, S273D, S299*	This study.	7B, 7C, 7D, 7E, 7F, 7G, 7H, S5
CMY2229	BY4742	*Pil1-8A-GFP S6D, S27D, S45D, S59D, S230D, S233D, S273D, S299*	This study.	7B, 7C, 7D, 7E, 7F, 7G, 7H, S5
CMY1460	BY4742	*Pil1-mGFP::His5*	This study.	7B, 7C, 7D, 7E, 7F, 7G, 7H, S5

Statistical tests

Experiemnt	Notes	Significant	p value	Figure Used
pkh1Δ vs WT	Pil1 phosphorylated	Yes	0.0209	1A
pkh2Δ vs WT	Pil1 phosphorylated	Yes	0.0004	1A
pkh3Δ vs WT	Pil1 phosphorylated	Yes	0.0236	1A
WT plus vector vs WT plus Pkh2	Pil1 phosphorylated	Yes	0.002	1C
pkh2Δ plus vector vs WT plus vector	Pil1 phosphorylated	Yes	<0.0001	1C
pkh2Δ plus Pkh2 vs WT plus vector	Pil1 phosphorylated	Yes	0.0412	1C
sak1Δ vs WT	Pil1 phosphorylated	No	0.7307	2C
cka2Δ vs WT	Pil1 phosphorylated	No	0.271	2C
hog1Δ vs WT	Pil1 phosphorylated	Yes	0.0435	2C
rim15Δ vs WT	Pil1 phosphorylated	No	0.8813	2C
cka1Δ vs WT	Pil1 phosphorylated	No	0.639	2C
trp1Δ vs WT	Pil1 phosphorylated	No	0.87	2C
cdc15-DaMP vs WT	Pil1 phosphorylated	Yes	0.0325	2C
sky1Δ vs WT	Pil1 phosphorylated	No	0.6919	2C
Glucose vs Raffinose (10 mins)	Pil1 phosphorylated	Yes	0.002	3C
siw14Δ vs WT	Glucose	No	0.5334	5B
ptc1Δ vs WT	Glucose	No	0.5132	5B
msg5Δ vs WT	Glucose	No	0.8185	5B
ppn2Δ vs WT	Glucose	No	0.559	5B
ywh1Δ vs WT	Glucose	Yes	0.0059	5B
sit4Δ vs WT	Glucose	Yes	0.0001	5B
glc7-DaMP vs WT	Glucose	Yes	0.0002	5B
siw14Δ vs WT	Raffinose	No	0.1505	5B
ptc1Δ vs WT	Raffinose	No	0.8419	5B
msg5Δ vs WT	Raffinose	No	0.2318	5B
ppn2Δ vs WT	Raffinose	No	0.3234	5B
ywh1Δ vs WT	Raffinose	Yes	0.0255	5B
sit4Δ vs WT	Raffinose	Yes	0.0059	5B
glc7-DaMP vs WT	Raffinose	Yes	0.001	5B
WT vs Glc7-DAmP	Phosphorylated Pil1	Yes	0.0003	6C
WT vs *reg1Δ*	Phosphorylated Pil1	Yes	0.0271	6C
12.5 nM β-estradiol	Phosphorylated Pil1	Yes	0.0003	6F
100 nM β-estradiol	Phosphorylated Pil1	Yes	0.004	6F
Wild-type vs 8A	Eisosome/cell	Yes	<0.0001	7D
Wild-type vs 8D	Eisosome/cell	Yes	<0.0001	7D
8A vs 8D	Eisosome/cell	Yes	<0.0001	7D
Wild-type vs 8A	Spot intensity	Yes	<0.0001	7E
Wild-type vs 8D	Spot intensity	Yes	<0.0001	7E
8A vs 8D	Spot intensity	Yes	0.0027	7E
Pil1-8D-mGFP vs WT	1 hour	No	0.14863	7H
Pil1-8D-mGFP vs WT	2 hours	Yes	0.006288	7H
Pil1-8D-mGFP vs WT	3 hours	Yes	0.007398	7H
Pil1-8D-mGFP vs WT	4 hours	Yes	0.001023	7H
Pil1-8D-mGFP vs WT	5 hours	No	0.014527	7H
Pil1-8A-mGFP vs WT	1 hour	Yes	0.018924	7H
Pil1-8A-mGFP vs WT	2 hours	Yes	0.0032	7H
Pil1-8A-mGFP vs WT	3 hours	Yes	0.000305	7H
Pil1-8A-mGFP vs WT	4 hours	Yes	0.00001	7H
Pil1-8A-mGFP vs WT	5 hours	Yes	0.000011	7H
Glc7-DAmP vs WT	1 hour	Yes	0.009257	8D
Glc7-DAmP vs WT	2 hours	Yes	0.000509	8D
Glc7-DAmP vs WT	3 hours	Yes	0.000002	8D
Glc7-DAmP vs WT	4 hours	Yes	0.000193	8D
Glc7-DAmP vs WT	5 hours	Yes	0.001268	8D
Glc7-DAmP vs WT	6 hours	Yes	0.004007	8D
Glucose vs Raffinose	Wild-type	Yes	0.002	S3
Glucose vs Raffinose	*pkh1Δ*	Yes	0.0002	S3
Glucose vs Raffinose	*pkh2Δ*	No	0.5412	S3

7.4. Appendix chapter V: Endosomal cargo recycling mediated by Gpa1 and Phosphatidylinositol-3-Kinase is inhibited by glucose starvation

Yeast strains used in this study

Freezer Strain	Parental strain	Genotype	Reference	Figure Used
CMY56	BY4742	MAT**α**, *his3Δ leu2Δ lys2Δ ura3Δ*	Brachmann *et al.*, 1998	Throughout as wild-type and parental strain
CMY211	BY4741	MAT**a**, *his3Δ leu2Δ met15Δ ura3Δ*	Brachmann *et al.*, 1999	
CMY703	BY4742	*his3Δ::HIS3-pRS303-Ste3-GFP-UL36*	This study	1B, 1C, 4E, 5B, 5C, 7C, 9A
CMY741	BY4742	*gpr1Δ::Kan^r his3Δ::HIS3-pRS303-Ste3-GFP-UL36*	This study	2C, 2D, 2E
CMY747	BY4742	*ras2Δ::Kan^r his3Δ::HIS3-pRS303-Ste3-GFP-UL36*	This study	2C, 2D, 2E
CMY743	BY4742	*gpa1Δ::Kan^r his3Δ::HIS3-pRS303-Ste3-GFP-UL36*	This study	2C, 2D, 2E, 2F, 2G
CMY1919	BY4741	*gpa1Δ::G418* MAT**a**, *his3Δ1 leu2Δ0 met15Δ0 ura3Δ0* Clone 1	Giaever, *et al.*, 2002	3A, 3B, S1
CMY1920	BY4741	*gpa1Δ::G418* MAT**a**, *his3Δ1 leu2Δ0 met15Δ0 ura3Δ0* Clone 2	Giaever, *et al.*, 2002	3B
CMY1921	BY4741	*gpa1Δ::G418* MAT**a**, *his3Δ1 leu2Δ0 met15Δ0 ura3Δ0* Clone 3	Giaever, *et al.*, 2002	3B
CMY1923	BY4742	*gpa1Δ::G418* MAT**α**, his3Δ1 leu2Δ0 lys2Δ0 ura3Δ0 Clone 1	Giaever, *et al.*, 2002	3A, 3B
CMY1924	BY4742	*gpa1Δ::G418* MAT**α**, his3Δ1 leu2Δ0 lys2Δ0 ura3Δ0 Clone 2	Giaever, *et al.*, 2002	3B
CMY1925	BY4742	*gpa1Δ::G418* MAT**α**, his3Δ1 leu2Δ0 lys2Δ0 ura3Δ0 Clone 3	Giaever, *et al.*, 2002	3B
CMY1718	LWY7235	MAT**a**, *leu2-3,112 ura3-52 his3-Δ200 trp1-Δ901 lys2-801 suc2-Δ9*	Bonangelino *et al.* 1997	4A, 4B, 4C, 4D, 4H
CMY1719	LWY13700	MAT**a**, leu2-3,112 ura3-52 his3-Δ200 trp1-Δ901 lys2-801 suc2-Δ9 *vps15Δ::Kan^r*		4A, 4B, 4C, 4H
CMY1720	LWY13693	MAT**a**, leu2-3,112 ura3-52 his3-Δ200 trp1-Δ901 lys2-801 suc2-Δ9 *vps34Δ::Kan^r*	Steinfeld *et al.* 2021	4A, 4B, 4C
CMY1977	BY4742	*vps15-Damp R1261A Clone 1*	This study	4H
CMY786	BY4742	*SEC7-mGFP::loxP*	This study	5A, 10F, 10G, S8
CMY828	SEY6210	*VPS4-mCherry::His5+*	Adell *et al.*, 2017	5A, 10E, S7
CMY704	BY4742	*rcy1Δ::Kan^r his3Δ::HIS3-pRS303-Ste3-GFP-UL36*	This study	5B
CMY1573	BY4742	*snf3Δ::Kan^r his3Δ::HIS3-pRS303-Ste3-GFP-UL36*	This study	5E
CMY1571	BY4742	*reg1Δ::Kan^r his3Δ::HIS3-pRS303-Ste3-GFP-UL36*	This study	5E, 5F
CMY1555	BY4742	*reg1Δ::Kan^r*	Giaever, *et al.*, 2002	5G
CMY844	BY4741	*MIG1-mGFP::HIS3 NRD1-mCherry::Hyg^r*	Wollman *et al.*, 2017	7A, 7B, S2
CMY997	BY4742	*mig1Δ::Kan^r mig2Δ::His5$^+$*	Laidlaw *et al.*, 2021	7C
CMY745	BY4742	*gpa2Δ::Kan^r his3Δ::HIS3-pRS303-Ste3-GFP-UL36*	This study	7F, 7G
CMY1592	BY4742	*gpa1Δ::Kan^r gpa2Δ::Nrs^r his3Δ::HIS3-pRS303-Ste3-GFP-UL36*	This study	7F, 7G
CMY1644	BY4742	*gpa2Δ::Kan^r mig2Δ::loxP mig1Δ::His5$^+$*	This study	7F, 7G
CMY1555	BY4742	*rcy1Δ::Kan^r*	Giaever, *et al.*, 2002	7H, S3
CMY738	BY4742	*gpa2Δ::Kan^r*	Giaever, *et al.*, 2002	7G, S4
CMY1555	BY4742	*vps25Δ::Kan^r*	Giaever, *et al.*, 2002	10C, S6, S7
CMY789	BY4742	*SEC7-mCherry::loxP*	This study	10E, S7
CMY1996	BY4742	*vps4Δ::Kanr*	Giaever, *et al.*, 2002	10F, 10G, S8
CMY2001	BY4741	*NOP1-GFP-Pib1*	Weill, et al., 2018	11A
CMY2002	BY4741	*NOP1-GFP-Snx41*	Weill, et al., 2018	11B
CMY54	RC634	MAT*α sst1-3 rme ade2-1 ura1 his6 met1 can1 cyh2 GAL*	Breslow, 1977	S1
CMY886	BY4742	YIplac211-SEC7-msCFPx6 plasmid was linearised with SpeI and integrated weith -Ura selection	This study	S4

Plasmids used in this study

Plasmid	Genotype	Reference	Figure Used
pRS315	Low copy centromeric yeast expression plasmid containing *LEU2* marker	Sikorski and Hieter, 1989	Parent / control vector
pRS316	Low copy centromeric yeast expression plasmid containing *URA3* marker	Sikorski and Hieter, 1989	Parent / control vector
pRS303	Integration / shuttle plasmid containing *URA3* marker	Sikorski and Hieter, 1989	Parent vector
pCM264	pRS315 expressing Mup1-GFP from *MUP1* promoter	Stringer and Piper, 2011	1A, 2G, 9C, 9D, S5
pCM995	pRS316 expressing Yap1801-mCherry from *CUP1* promoter	Laidlaw *et al*., 2021	1A, 1B
pCM996	pRS316 expressing Yap1802-mCherry from *CUP1* promoter	Laidlaw *et al*., 2021	1A, 1B
pCM988	pRS315 expressing Fur4-mNG from *FUR4* promoter	This study	2G
pCM387	pRS315 expressing Ste3-GFP from *STE3* promoter	Urbanowski and Piper, 2001	2G, 9D
pCM1049	pRS416 expressing wild-type Vps34^{WT}	Steinfeld *et al.* 2021	4B, 4D, 4E
pCM1050	pRS416 expressing wild-type Vps34^{EDC} (R283E, A287D, Y501C)	Steinfeld *et al.* 2021	4B, 4D, 4E
pCM1016	pRS316 expressing Gpa1-mGFP from *CUP1* promoter	This study	5A
pCM1004	pRS316 expressing Gpa1-mCherry from *CUP1* promoter	This study	5A, 5B, 10A, 10F, 10G, S1, S3, S8
pCM1011	pRS315 expressing Gpa2-GFP from *CUP1* promoter	This study	8A, 8B, 8C, 8D, 8E, 9C, 10A, 10B, 10D, 10E, 10F, 10G, S3, S4, S5, S7, S8
pCM1044	pRS316 expressing Gpa1 (Q323L) -mCherry from *CUP1* promoter	This study	5C, 5F
pCM691	pRS315 expressing Ste3-GFP-UL36 from *STE3* promoter	Stringer and Piper, 2011	7C, 7F
pCM1015	pRS316 expressing Gpa2-mCherry from *CUP1* promoter	This study	9A, 9B, 9D
pCM386	pRS415 expressing Can1-GFP from *CAN1* promoter	Laidlaw *et al*., 2021	9D
pCM1002	pRS316 expressing Gpa2-GFP from *CUP1* promoter	This study	10A, 10B
pCM438	pRS316 expressing Cos5-mCherry-GFP from *CUP1* promoter	MacDonald *et al*., 2015	10C, 10F, 10G, S6, S7, S8
pCM1126	YGPM2o15 *LEU2* based 2µ plasmid that contains *GPA2*	Jones *et al*., 2008	11A, 11B
pCM946	YIplac211-SEC7-msCFPx6	Day *et al*., 2018	S4

8. References

Aspenström, P. (2014). BAR domain proteins regulate Rho GTPase signaling. Small GTPases *5*, 7. 10.4161/sgtp.28580.

Bianchi, F., Syga, L., Moiset, G., Spakman, D., Schavemaker, P.E., Punter, C.M., Seinen, A.B., Van Oijen, A.M., Robinson, A., and Poolman, B. (2018). Steric exclusion and protein conformation determine the localization of plasma membrane transporters. Nature Communications *9*. 10.1038/s41467-018-02864-2.

Breslow, D.K., Cameron, D.M., Collins, S.R., Schuldiner, M., Stewart-Ornstein, J., Newman, H.W., Braun, S., Madhani, H.D., Krogan, N.J., and Weissman, J.S. (2008). A comprehensive strategy enabling high-resolution functional analysis of the yeast genome. Nature Methods *5*, 711-718. 10.1038/nmeth.1234.

Brett, C.L., Tukaye, D.N., Mukherjee, S., and Rao, R. (2005). The yeast endosomal Na+K+/H+ exchanger Nhx1 regulates cellular pH to control vesicle trafficking. Mol Biol Cell *16*, 1396-1405. 10.1091/mbc.e04-11-0999.

Cannon, J.F. (2010). Function of protein phosphatase-1, Glc7, in Saccharomyces cerevisiae. Adv Appl Microbiol *73*, 27-59. 10.1016/s0065-2164(10)73002-1.

Colombo, S., Ma, P., Cauwenberg, L., Winderickx, J., Crauwels, M., Teunissen, A., Nauwelaers, D., De Winde, J.H., Oise Gorwa, M.-F., Colavizza, D., et al. (1998). Involvement of distinct G-proteins, Gpa2 and Ras, in glucose-and intracellular acidification-induced cAMP signalling in the yeast Saccharomyces cerevisiae.

Diaz-Ruiz, R., Rigoulet, M., and Devin, A. (2011). The Warburg and Crabtree effects: On the origin of cancer cell energy metabolism and of yeast glucose repression. Biochimica et Biophysica Acta (BBA) - Bioenergetics *1807*, 568-576. https://doi.org/10.1016/j.bbabio.2010.08.010.

Fish, K.N. (2009). Total internal reflection fluorescence (TIRF) microscopy. Curr Protoc Cytom *Chapter 12*, Unit12.18. 10.1002/0471142956.cy1218s50.

Flick, J.S., and Johnston, M. (1990). Two systems of glucose repression of the GAL1 promoter in Saccharomyces cerevisiae. Mol Cell Biol *10*, 4757-4769. 10.1128/mcb.10.9.4757-4769.1990.

Frost, A., Unger, V.M., and De Camilli, P. (2009). The BAR domain superfamily: membrane-molding macromolecules. Cell *137*, 191-196. 10.1016/j.cell.2009.04.010.

Gancedo, J.M. (1998). Yeast carbon catabolite repression. Microbiol Mol Biol Rev *62*, 334-361. 10.1128/mmbr.62.2.334-361.1998.

Goji, T., Takahara, K., Negishi, M., and Katoh, H. (2017). Cystine uptake through the cystine/glutamate antiporter xCT triggers glioblastoma cell death under glucose deprivation. J Biol Chem *292*, 19721-19732. 10.1074/jbc.M117.814392.

Habermann, B. (2004). The BAR-domain family of proteins: a case of bending and binding? EMBO Rep *5*, 250-255. 10.1038/sj.embor.7400105.

Harashima, T., and Heitman, J. (2005). Galpha subunit Gpa2 recruits kelch repeat subunits that inhibit receptor-G protein coupling during cAMP-induced dimorphic transitions in Saccharomyces cerevisiae. Mol Biol Cell *16*, 4557-4571. 10.1091/mbc.e05-05-0403.

Heroes, E., Lesage, B., Görnemann, J., Beullens, M., Van Meervelt, L., and Bollen, M. (2013). The PP1 binding code: a molecular-lego strategy that governs specificity. Febs j *280*, 584-595. 10.1111/j.1742-4658.2012.08547.x.

Koppula, P., Zhang, Y., Shi, J., Li, W., and Gan, B. (2017). The glutamate/cystine antiporter SLC7A11/xCT enhances cancer cell dependency on glucose by exporting glutamate. J Biol Chem *292*, 14240-14249. 10.1074/jbc.M117.798405.

Laidlaw, K.M.E., Paine, K.M., Bisinski, D.D., Calder, G., Hogg, K., Ahmed, S., James, S., O'Toole, P.J., and MacDonald, C. (2022). Endosomal cargo recycling mediated by Gpa1

and phosphatidylinositol 3-kinase is inhibited by glucose starvation. Molecular biology of the cell *33*. 10.1091/MBC.E21-04-0163.
Lorenz, M.C., Pan, X., Harashima, T., Cardenas, M.E., Xue, Y., Hirsch, J.P., and Heitman, J. (2000). The G protein-coupled receptor gpr1 is a nutrient sensor that regulates pseudohyphal differentiation in Saccharomyces cerevisiae. Genetics *154*, 609-622. 10.1093/genetics/154.2.609.
MacDonald, C., and Piper, R.C. (2017). Genetic dissection of early endosomal recycling highlights a TORC1-independent role for Rag GTPases. Journal of Cell Biology *216*, 3275-3290. 10.1083/jcb.201702177.
McGuire, C.M., and Forgac, M. (2018). Glucose starvation increases V-ATPase assembly and activity in mammalian cells through AMP kinase and phosphatidylinositide 3-kinase/Akt signaling. J Biol Chem *293*, 9113-9123. 10.1074/jbc.RA117.001327.
Mnaimneh, S., Davierwala, A.P., Haynes, J., Moffat, J., Peng, W.-T., Zhang, W., Yang, X., Pootoolal, J., Chua, G., Lopez, A., et al. (2004). Exploration of Essential Gene Functions via Titratable Promoter Alleles. Cell *118*, 31-44. https://doi.org/10.1016/j.cell.2004.06.013.
Moreira, K.E., Walther, T.C., Aguilar, P.S., and Walter, P. (2009). Pil1 Controls Eisosome Biogenesis. Molecular Biology of the Cell *20*, 809-818. 10.1091/mbc.e08-03-0313.
Offley, S.R., and Schmidt, M.C. (2019). Protein phosphatases of Saccharomyces cerevisiae. Curr Genet *65*, 41-55. 10.1007/s00294-018-0884-y.
Ramaswamy, N.T., Li, L., Khalil, M., and Cannon, J.F. (1998). Regulation of yeast glycogen metabolism and sporulation by Glc7p protein phosphatase. Genetics *149*, 57-72. 10.1093/genetics/149.1.57.
Rolland, F., De Winde, J.H., Lemaire, K., Boles, E., Thevelein, J.M., and Winderickx, J. (2000). Glucose-induced cAMP signalling in yeast requires both a G-protein coupled receptor system for extracellular glucose detection and a separable hexose kinase-dependent sensing process. Mol Microbiol *38*, 348-358. 10.1046/j.1365-2958.2000.02125.x.
Sartorel, E., Ünlü, C., Jose, M., Massoni-Laporte, A., Meca, J., Sibarita, J.B., and McCusker, D. (2018). Phosphatidylserine and GTPase activation control Cdc42 nanoclustering to counter dissipative diffusion. Mol Biol Cell *29*, 1299-1310. 10.1091/mbc.E18-01-0051.
Schuldiner, M., Collins, S.R., Thompson, N.J., Denic, V., Bhamidipati, A., Punna, T., Ihmels, J., Andrews, B., Boone, C., Greenblatt, J.F., et al. (2005). Exploration of the function and organization of the yeast early secretory pathway through an epistatic miniarray profile. Cell *123*, 507-519. 10.1016/j.cell.2005.08.031.
Spira, F., Mueller, N.S., Beck, G., Von Olshausen, P., Beig, J., and Wedlich-Söldner, R. (2012). Patchwork organization of the yeast plasma membrane into numerous coexisting domains. Nature Cell Biology *14*, 640-648. 10.1038/ncb2487.
Takei, K., Slepnev, V.I., Haucke, V., and De Camilli, P. (1999). Functional partnership between amphiphysin and dynamin in clathrin-mediated endocytosis. Nature Cell Biology *1*, 33-39. 10.1038/9004.
Walther, T.C., Aguilar, P.S., Fröhlich, F., Chu, F., Moreira, K., Burlingame, A.L., and Walter, P. (2007). Pkh-kinases control eisosome assembly and organization. EMBO Journal *26*, 4946-4955. 10.1038/sj.emboj.7601933.
Warburg, O. (1956). On the origin of cancer cells. Science *123*, 309-314. 10.1126/science.123.3191.309.
Wiederkehr, A., Avaro, S., Prescianotto-Baschong, C., Haguenauer-Tsapis, R., and Riezman, H. (2000). The F-box protein Rcy1p is involved in endocytic membrane traffic and recycling out of an early endosome in Saccharomyces cerevisiae. Journal of Cell Biology *149*, 397-410. 10.1083/jcb.149.2.397.
Ziółkowska, N.E., Karotki, L., Rehman, M., Huiskonen, J.T., and Walther, T.C. (2011). Eisosome-driven plasma membrane organization is mediated by BAR domains. Nature Structural and Molecular Biology *18*, 854-856. 10.1038/nsmb.2080.

Abeliovich, H., T. Darsow, and S.D. Emr. 1999. Cytoplasm to vacuole trafficking of aminopeptidase I requires a t-SNARE-Sec1p complex composed of Tlg2p and Vps45p. *Embo j*. 18:6005-6016.

Aguilar, P.S., F. Fröhlich, M. Rehman, M. Shales, I. Ulitsky, A. Olivera-Couto, H. Braberg, R. Shamir, P. Walter, M. Mann, C.S. Ejsing, N.J. Krogan, and T.C. Walther. 2010. A plasma-membrane E-MAP reveals links of the eisosome with sphingolipid metabolism and endosomal trafficking. *Nature Publishing Group*. 17.

Ahle, S., A. Mann, U. Eichelsbacher, and E. Ungewickell. 1988. Structural relationships between clathrin assembly proteins from the Golgi and the plasma membrane. *The EMBO Journal*. 7:919-919.

Ahmad, M., and H. Bussey. 1986. Yeast arginine permease: nucleotide sequence of the CAN1 gene. *Current genetics*. 10:587-592.

Alboukadel, K., and M. Fabian. 2019. factoextra: Extract and Visualize the Results of Multivariate Data Analyses. R package.

Albuquerque, C.P., M.B. Smolka, S.H. Payne, V. Bafna, J. Eng, and H. Zhou. 2008. A multidimensional chromatography technology for in-depth phosphoproteome analysis. *Mol Cell Proteomics*. 7:1389-1396.

Aldhous, P. 1993. Breaking the code for the tuberculosis invasion. *Science*. 261:1390.

Alexander, A.G., V. Marfil, and C. Li. 2014. Use of Caenorhabditis elegans as a model to study Alzheimer's disease and other neurodegenerative diseases. *Front Genet*. 5:279.

Alms, G.R., P. Sanz, M. Carlson, and T.A. Haystead. 1999. Reg1p targets protein phosphatase 1 to dephosphorylate hexokinase II in Saccharomyces cerevisiae: characterizing the effects of a phosphatase subunit on the yeast proteome. *Embo j*. 18:4157-4168.

Amerik, A.Y., S.J. Li, and M. Hochstrasser. 2000a. Analysis of the deubiquitinating enzymes of the yeast Saccharomyces cerevisiae. *Biol Chem*. 381:981-992.

Amerik, A.Y., J. Nowak, S. Swaminathan, and M. Hochstrasser. 2000b. The Doa4 deubiquitinating enzyme is functionally linked to the vacuolar protein-sorting and endocytic pathways. *Mol Biol Cell*. 11:3365-3380.

Amoiradaki, K., K.R. Bunting, K.M. Paine, J.E. Ayre, K. Hogg, K.M.E. Laidlaw, and C. Macdonald. 2021. The Rpd3-Complex Regulates Expression of Multiple Cell Surface Recycling Factors in Yeast. *International Journal of Molecular Sciences 2021, Vol. 22, Page 12477*. 22:12477-12477.

Andrews, S. 2021. FastQC: A quality control tool for high throughput sequence data., https://www.bioinformatics.babraham.ac.uk/projects/fastqc/.

Apanovitch, D.M., K.C. Slep, P.B. Sigler, and H.G. Dohlman. 1998. Sst2 is a GTPase-activating protein for Gpa1: purification and characterization of a cognate RGS-Galpha protein pair in yeast. *Biochemistry*. 37:4815-4822.

Appadurai, D., L. Gay, A. Moharir, M.J. Lang, M.C. Duncan, O. Schmidt, D. Teis, T.N. Vu, M. Silva, E.M. Jorgensen, and M. Babst. 2019. Plasma membrane tension regulates eisosome structure and function. *Molecular Biology of the Cell*. 31:mbc.E19-0218.

Appadurai, D., L. Gay, A. Moharir, M.J. Lang, M.C. Duncan, O. Schmidt, D. Teis, T.N. Vu, M. Silva, E.M. Jorgensen, and M. Babst. 2020. Plasma membrane tension regulates eisosome structure and function. *Mol Biol Cell*. 31:287-303.

Arita, Y., G. Kim, Z. Li, H. Friesen, G. Turco, R.Y. Wang, D. Climie, M. Usaj, M. Hotz, E. Stoops, A. Baryshnikova, C. Boone, D. Botstein, B.J. Andrews, and R. Scott McIsaac. 2021a. A genome-scale yeast library with inducible expression of individual genes. *bioRxiv*:2020.2012.2030.424776-422020.424712.424730.424776.

Arita, Y., G. Kim, Z. Li, H. Friesen, G. Turco, R.Y. Wang, D. Climie, M. Usaj, M. Hotz, E.H. Stoops, A. Baryshnikova, C. Boone, D. Botstein, B.J. Andrews, and R.S. McIsaac.

2021b. A genome-scale yeast library with inducible expression of individual genes. *Mol Syst Biol*. 17:e10207.

Audhya, A., R. Loewith, A.B. Parsons, L. Gao, M. Tabuchi, H. Zhou, C. Boone, M.N. Hall, and S.D. Emr. 2004. Genome-wide lethality screen identifies new PI4,5P2 effectors that regulate the actin cytoskeleton. *Embo j*. 23:3747-3757.

Auger, K.R., C.L. Carpenter, L.C. Cantley, and L. Varticovski. 1989. Phosphatidylinositol 3-kinase and its novel product, phosphatidylinositol 3-phosphate, are present in Saccharomyces cerevisiae. *J Biol Chem*. 264:20181-20184.

Babst, M. 2011. MVB vesicle formation: ESCRT-dependent, ESCRT-independent and everything in between. *Curr Opin Cell Biol*. 23:452-457.

Babst, M. 2019. Eisosomes at the intersection of TORC1 and TORC2 regulation. *In* Traffic. Vol. 20. Blackwell Munksgaard. 543-551.

Babst, M., D.J. Katzmann, E.J. Estepa-Sabal, T. Meerloo, and S.D. Emr. 2002a. ESCRT-III: An endosome-associated heterooligomeric protein complex required for MVB sorting. *Developmental Cell*. 3:271-282.

Babst, M., D.J. Katzmann, W.B. Snyder, B. Wendland, and S.D. Emr. 2002b. Endosome-associated complex, ESCRT-II, recruits transport machinery for protein sorting at the multivesicular body. *Developmental Cell*. 3:283-289.

Babst, M., T.K. Sato, L.M. Banta, and S.D. Emr. 1997. Endosomal transport function in yeast requires a novel AAA-type ATPase, Vps4p. *The EMBO journal*. 16:1820-1831.

Babst, M., B. Wendland, E.J. Estepa, and S.D. Emr. 1998. The Vps4p AAA ATPase regulates membrane association of a Vps protein complex required for normal endosome function. *The EMBO journal*. 17:2982-2993.

Backer, J.M., M.G. Myers, Jr., S.E. Shoelson, D.J. Chin, X.J. Sun, M. Miralpeix, P. Hu, B. Margolis, E.Y. Skolnik, J. Schlessinger, and et al. 1992. Phosphatidylinositol 3'-kinase is activated by association with IRS-1 during insulin stimulation. *Embo j*. 11:3469-3479.

Badrinarayanan, A., R. Reyes-Lamothe, S. Uphoff, M.C. Leake, and D.J. Sherratt. 2012. In vivo architecture and action of bacterial structural maintenance of chromosome proteins. *Science*. 338:528-531.

Balakrishnan, R., J. Park, K. Karra, B.C. Hitz, G. Binkley, E.L. Hong, J. Sullivan, G. Micklem, and J.M. Cherry. 2012. YeastMine-An integrated data warehouse for Saccharomyces cerevisiae data as a multipurpose tool-kit. *Database*. 2012.

Banerjee, A., V.A. Barry, B.R. DasGupta, and T.F. Martin. 1996. N-Ethylmaleimide-sensitive factor acts at a prefusion ATP-dependent step in Ca2+-activated exocytosis. *J Biol Chem*. 271:20223-20226.

Bankaitis, V.A., L.M. Johnson, and S.D. Emr. 1986. Isolation of yeast mutants defective in protein targeting to the vacuole. *Proceedings of the National Academy of Sciences of the United States of America*. 83:9075-9079.

Banta, L.M., J.S. Robinson, D.J. Klionsky, and S.D. Emr. 1988. Organelle Assembly in Yeast: Characterization of Yeast Mutants Defective in Vacuolar Biogenesis and Protein Sorting. *The Journal of Cell Biology*.

Bardwell, L. 2005. A walk-through of the yeast mating pheromone response pathway. *Peptides*. 26:339-350.

Barlowe, C., L. Orci, T. Yeung, M. Hosobuchi, S. Hamamoto, N. Salama, M.F. Rexach, M. Ravazzola, M. Amherdt, and R. Schekman. 1994. COPII: A membrane coat formed by Sec proteins that drive vesicle budding from the endoplasmic reticulum. *Cell*. 77:895-907.

Beas, A.O., V. Taupin, C. Teodorof, L.T. Nguyen, M. Garcia-Marcos, and M.G. Farquhar. 2012. Gαs promotes EEA1 endosome maturation and shuts down proliferative signaling through interaction with GIV (Girdin). *Mol Biol Cell*. 23:4623-4634.

Becuwe, M., and S. Léon. 2014. Integrated control of transporter endocytosis and recycling by the arrestin-related protein Rod1 and the ubiquitin ligase Rsp5. *eLife*. 3:e03307.

Becuwe, M., N. Vieira, D. Lara, J. Gomes-Rezende, C. Soares-Cunha, M. Casal, R. Haguenauer-Tsapis, O. Vincent, S. Paiva, and S. Léon. 2012. A molecular switch on an arrestin-like protein relays glucose signaling to transporter endocytosis. *The Journal of cell biology*. 196:247-259.

Beeler, T., D. Bacikova, K. Gable, L. Hopkins, C. Johnson, H. Slife, and T. Dunn. 1998. The Saccharomyces cerevisiae TSC10/YBR265W gene encoding 3- ketosphinganine reductase is identified in a screen for temperature-sensitive suppressors of the Ca2+-sensitive csg2Δ mutant. *Journal of Biological Chemistry*. 273:30688-30694.

Belgareh-Touzé, N., S. Léon, Z. Erpapazoglou, M. Stawiecka-Mirota, D. Urban-Grimal, and R. Haguenauer-Tsapis. 2008. Versatile role of the yeast ubiquitin ligase Rsp5p in intracellular trafficking. *Biochem Soc Trans*. 36:791-796.

Bellen, H.J., C. Tong, and H. Tsuda. 2010. 100 years of Drosophila research and its impact on vertebrate neuroscience: a history lesson for the future. *Nat Rev Neurosci*. 11:514-522.

Bennett, M.K., N. Calakos, and R.H. Scheller. 1992. Syntaxin: A Synaptic Protein Implicated in Docking of Synaptic Vesicles at Presynaptic Active Zones. *Science*. 257:255-259.

Bennett, M.K., J.E. Garcia-Arrarás, L.A. Elferink, K. Peterson, A.M. Fleming, C.D. Hazuka, and R.H. Scheller. 1993. The syntaxin family of vesicular transport receptors. *Cell*. 74:863-873.

Berchtold, D., M. Piccolis, N. Chiaruttini, I. Riezman, H. Riezman, A. Roux, T.C. Walther, and R. Loewith. 2012. Plasma membrane stress induces relocalization of Slm proteins and activation of TORC2 to promote sphingolipid synthesis. *Nat Cell Biol*. 14:542-547.

Berchtold, D., and T.C. Walther. 2009. TORC2 plasma membrane localization is essential for cell viability and restricted to a distinct domain. *Molecular biology of the cell*. 20:1565-1575.

Berón, W., M.I. Colombo, L.S. Mayorga, and P.D. Stahl. 1995. In vitro reconstitution of phagosome-endosome fusion: evidence for regulation by heterotrimeric GTPases. *Arch Biochem Biophys*. 317:337-342.

Best, J.T., P. Xu, J.G. McGuire, S.N. Leahy, and T.R. Graham. 2020. Yeast synaptobrevin, Snc1, engages distinct routes of postendocytic recycling mediated by a sorting nexin, Rcy1-COPI, and retromer. *Molecular Biology of the Cell*. 31:944-962.

Bianchi, F., L. Syga, G. Moiset, D. Spakman, P.E. Schavemaker, C.M. Punter, A.B. Seinen, A.M. Van Oijen, A. Robinson, and B. Poolman. 2018. Steric exclusion and protein conformation determine the localization of plasma membrane transporters. *Nature Communications*. 9.

Bianchi, F., J.S. van't Klooster, S.J. Ruiz, and B. Poolman. 2019. Regulation of Amino Acid Transport in Saccharomyces cerevisiae. *Microbiology and Molecular Biology Reviews*. 83.

Bilodeau, P.S., J.L. Urbanowski, S.C. Winistorfer, and R.C. Piper. 2002. The Vps27p Hse1p complex binds ubiquitin and mediates endosomal protein sorting. *Nature cell biology*. 4:534-539.

Bilodeau, P.S., S.C. Winistorfer, W.R. Kearney, A.D. Robertson, and R.C. Piper. 2003. Vps27-Hse1 and ESCRT-I complexes cooperate to increase efficiency of sorting ubiquitinated proteins at the endosome. *The Journal of cell biology*. 163:237-243.

Binda, M., M.-P. Peli-Gulli, G. Bonfils, N. Panchaud, J. Urban, T.W. Sturgill, R. Loewith, and C. De Virgilio. 2009. The Vam6 GEF Controls TORC1 by Activating the EGO Complex. *Molecular Cell*. 35:563-573.

Block, M.R., B.S. Glick, C.A. Wilcox, F.T. Wieland, and J.E. Rothman. 1988. Purification of an N-ethylmaleimide-sensitive protein catalyzing vesicular transport. *Proceedings of the National Academy of Sciences of the United States of America*. 85:7852-7852.

Bloecher, A., and K. Tatchell. 2000. Dynamic localization of protein phosphatase type 1 in the mitotic cell cycle of Saccharomyces cerevisiae. *J Cell Biol*. 149:125-140.

Blondel, M.-O., J. Morvan, S. Dupré, D. Le Urban-Grimal, R. Haguenauer-Tsapis, and C. Volland. 2004. Direct Sorting of the Yeast Uracil Permease to the Endosomal System Is Controlled by Uracil Binding and Rsp5p-dependent Ubiquitylation. *Molecular Biology of the Cell*. 15:883-895.

Blumer, K.J., and J. Thorner. 1990. Beta and gamma subunits of a yeast guanine nucleotide-binding protein are not essential for membrane association of the alpha subunit but are required for receptor coupling. *Proc Natl Acad Sci U S A*. 87:4363-4367.

Boeke, J.D., F. La Croute, and G.R. Fink. 1984. A positive selection for mutants lacking orotidine-5'-phosphate decarboxylase activity in yeast: 5-fluoro-orotic acid resistance. *MGG Molecular & General Genetics*. 197:345-346.

Bonangelino, C.J., E.M. Chavez, and J.S. Bonifacino. 2002. Genomic screen for vacuolar protein sorting genes in Saccharomyces cerevisiae. *Molecular Biology of the Cell*. 13:2486-2501.

Bonfils, G., M. Jaquenoud, S. Bontron, C. Ostrowicz, C. Ungermann, and Claudio. 2012. Leucyl-tRNA Synthetase Controls TORC1 via the EGO Complex. *Molecular Cell*. 46:105-110.

Bonifacino, J.S., and B.S. Glick. 2004. The Mechanisms of Vesicle Budding and Fusion. *In* Cell. Vol. 116. Cell Press. 153-166.

Bonifacino, J.S., and J. Lippincott-Schwartz. 2003. Coat proteins: Shaping membrane transport. *In* Nature Reviews Molecular Cell Biology. Vol. 4. Nature Publishing Group. 409-414.

Borklu Yucel, E., and K.O. Ulgen. 2011. A network-based approach on elucidating the multi-faceted nature of chronological aging in S. cerevisiae. *PLoS One*. 6:e29284.

Botstein, D., and G.R. Fink. 1988. Yeast: An experimental organism for modern biology. *Science*. 240:1439-1443.

Brach, T., T. Specht, and M. Kaksonen. 2011. Reassessment of the role of plasma membrane domains in the regulation of vesicular traffic in yeast. *Journal of Cell Science*. 124:328-337.

Brachmann, C.B., A. Davies, G.J. Cost, E. Caputo, J. Li, P. Hieter, and J.D. Boeke. 1998. Designer deletion strains derived from Saccharomyces cerevisiae S288C: A useful set of strains and plasmids for PCR-mediated gene disruption and other applications. *In* Yeast. Vol. 14. 115-132.

Breker, M., M. Gymrek, and M. Schuldiner. 2013. A novel single-cell screening platform reveals proteome plasticity during yeast stress responses. *J Cell Biol*. 200:839-850.

Brenner, S. 1974. The genetics of Caenorhabditis elegans. *Genetics*. 77:71-94.

Breslow, D.K., D.M. Cameron, S.R. Collins, M. Schuldiner, J. Stewart-Ornstein, H.W. Newman, S. Braun, H.D. Madhani, N.J. Krogan, and J.S. Weissman. 2008. A comprehensive strategy enabling high-resolution functional analysis of the yeast genome. *Nature Methods*. 5:711-718.

Brett, C.L., D.N. Tukaye, S. Mukherjee, and R. Rao. 2005. The Yeast Endosomal Na (K)/H Exchanger Nhx1 Regulates Cellular pH to Control Vesicle Trafficking. *Molecular Biology of the Cell*. 16:1396-1405.

Broach, J.R. 2012. Nutritional control of growth and development in yeast. *Genetics*. 192:73-105.

Broggi, S., E. Martegani, and S. Colombo. 2013. Live-cell imaging of endogenous Ras-GTP shows predominant Ras activation at the plasma membrane and in the nucleus in

Saccharomyces cerevisiae. *International Journal of Biochemistry and Cell Biology*. 45:384-394.

Brown, D.A., and J.K. Rose. 1992. Sorting of GPI-anchored proteins to glycolipid-enriched membrane subdomains during transport to the apical cell surface. *Cell*. 68:533-544.

Brown, R.W., and J.H. Henderson. 1983. The mass production and distribution of HeLa cells at Tuskegee Institute, 1953-55. *J Hist Med Allied Sci*. 38:415-431.

Bryant, N.J., and D.E. James. 2001. Vps45p stabilizes the syntaxin homologue Tlg2p and positively regulates SNARE complex formation. *Embo j*. 20:3380-3388.

Bryant, N.J., and T.H. Stevens. 1998. Vacuole biogenesis in Saccharomyces cerevisiae: protein transport pathways to the yeast vacuole. *Microbiol Mol Biol Rev*. 62:230-247.

Budovskaya, Y.V., H. Hama, D.B. DeWald, and P.K. Herman. 2002. The C terminus of the Vps34p phosphoinositide 3-kinase is necessary and sufficient for the interaction with the Vps15p protein kinase. *J Biol Chem*. 277:287-294.

Buelto, D., C.W. Hung, Q.L. Aoh, S. Lahiri, and M.C. Duncan. 2020. Plasma membrane to vacuole traffic induced by glucose starvation requires Gga2-dependent sorting at thetrans-Golgi network. *Biology of the Cell*. 112:349-367.

Bulbarelli, A., T. Sprocati, M. Barberi, E. Pedrazzini, and N. Borgese. 2002. Trafficking of tail-anchored proteins: transport from the endoplasmic reticulum to the plasma membrane and sorting between surface domains in polarised epithelial cells. *Journal of Cell Science*. 115:1689-1702.

Burd, C.G., and S.D. Emr. 1998. Phosphatidylinositol(3)-Phosphate Signaling Mediated by Specific Binding to RING FYVE Domains. *Molecular Cell*. 2:157-162.

Burda, P., S.M. Padilla, S. Sarkar, and S.D. Emr. 2002. Retromer function in endosome-to-Golgi retrograde transport is regulated by the yeast Vps34 Ptdlns 3-kinase. *Journal of Cell Science*. 115:3889-3900.

Burroughs, A.M., L.M. Iyer, and L. Aravind. 2012. Structure and Evolution of Ubiquitin and Ubiquitin-Related Domains. *In* Ubiquitin Family Modifiers and the Proteasome: Reviews and Protocols. R.J. Dohmen and M. Scheffner, editors. Humana Press, Totowa, NJ. 15-63.

Burston, H.E., L. Maldonado-Báez, M. Davey, B. Montpetit, C. Schluter, B. Wendland, and E. Conibear. 2009. Regulators of yeast endocytosis identified by systematic quantitative analysis. *Journal of Cell Biology*. 185:1097-1110.

Busch, D.J., J.R. Houser, C.C. Hayden, M.B. Sherman, E.M. Lafer, and J.C. Stachowiak. 2015. Intrinsically disordered proteins drive membrane curvature. *Nature Communications*. 6:7875.

Busto, J.V., A. Elting, D. Haase, F. Spira, J. Kuhlman, M. Schäfer-Herte, and R. Wedlich-Söldner. 2018. Lateral plasma membrane compartmentalization links protein function and turnover. *The EMBO Journal*. 37.

Busto, J.V., and R. Wedlich-Söldner. 2019. Integration Through Separation - The Role of Lateral Membrane Segregation in Nutrient Uptake. *Front Cell Dev Biol*. 7:97.

Caballe, A., and J. Martin-Serrano. 2011. ESCRT machinery and cytokinesis: the road to daughter cell separation. *Traffic*. 12:1318-1326.

Cannon, J.F., J.R. Pringle, A. Fiechter, and M. Khalil. 1994. Characterization of glycogen-deficient glc mutants of Saccharomyces cerevisiae. *Genetics*. 136:485-503.

Caro, L.G., and G.E. Palade. 1964. PROTEIN SYNTHESIS, STORAGE, AND DISCHARGE IN THE PANCREATIC EXOCRINE CELL : An Autoradiographic Study. *The Journal of Cell Biology*. 20:473-473.

Carr, C.M., E. Grote, M. Munson, F.M. Hughson, and P.J. Novick. 1999. Sec1p binds to SNARE complexes and concentrates at sites of secretion. *J Cell Biol*. 146:333-344.

Carrel, A. 1912. ON THE PERMANENT LIFE OF TISSUES OUTSIDE OF THE ORGANISM. *J Exp Med*. 15:516-528.

Carrel, A. 1923. A METHOD FOR THE PHYSIOLOGICAL STUDY OF TISSUES IN VITRO. *J Exp Med*. 38:407-418.

Carrel, A., and M.T. Burrows. 1911. CULTIVATION OF TISSUES IN VITRO AND ITS TECHNIQUE. *J Exp Med*. 13:387-396.

Carroll, S.Y., H.E. Stimpson, J. Weinberg, C.P. Toret, Y. Sun, and D.G. Drubin. 2012. Analysis of yeast endocytic site formation and maturation through a regulatory transition point. *Mol Biol Cell*. 23:657-668.

Casamayor, A., P.D. Torrance, T. Kobayashi, J. Thorner, and D.R. Alessi. 1999. Functional counterparts of mammalian protein kinases PDK1 and SGK in budding yeast. *Current Biology*. 9:186-197.

Caulfield, T., and A.L. McGuire. 2013. Policy uncertainty, sequencing, and cell lines. *G3 (Bethesda)*. 3:1205-1207.

Chakravorty, D., and S.M. Assmann. 2018. G protein subunit phosphorylation as a regulatory mechanism in heterotrimeric G protein signaling in mammals, yeast, and plants. *Biochem J*. 475:3331-3357.

Chavrier, P., J.P. Gorvel, E. Stelzer, K. Simons, J. Gruenberg, and M. Zerial. 1991. Hypervariable C-terminal domain of rab proteins acts as a targeting signal. *Nature*. 353:769-772.

Chen, B.C., W.R. Legant, K. Wang, L. Shao, D.E. Milkie, M.W. Davidson, C. Janetopoulos, X.S. Wu, J.A. Hammer, 3rd, Z. Liu, B.P. English, Y. Mimori-Kiyosue, D.P. Romero, A.T. Ritter, J. Lippincott-Schwartz, L. Fritz-Laylin, R.D. Mullins, D.M. Mitchell, J.N. Bembenek, A.C. Reymann, R. Böhme, S.W. Grill, J.T. Wang, G. Seydoux, U.S. Tulu, D.P. Kiehart, and E. Betzig. 2014. Lattice light-sheet microscopy: imaging molecules to embryos at high spatiotemporal resolution. *Science*. 346:1257998.

Chen, K.E., M.D. Healy, and B.M. Collins. 2019. Towards a molecular understanding of endosomal trafficking by Retromer and Retriever. *Traffic*. 20:465-478.

Chen, Y.A., and R.H. Scheller. 2001. SNARE-mediated membrane fusion. *Nature Reviews Molecular Cell Biology*. 2:98-106.

Chernomordik, L.V., G.B. Melikyan, and Y.A. Chizmadzhev. 1987. Biomembrane fusion: a new concept derived from model studies using two interacting planar lipid bilayers. *Biochimica et Biophysica Acta (BBA) - Reviews on Biomembranes*. 906:309-352.

Cherry, J.M., E.L. Hong, C. Amundsen, R. Balakrishnan, G. Binkley, E.T. Chan, K.R. Christie, M.C. Costanzo, S.S. Dwight, S.R. Engel, D.G. Fisk, J.E. Hirschman, B.C. Hitz, K. Karra, C.J. Krieger, S.R. Miyasato, R.S. Nash, J. Park, M.S. Skrzypek, M. Simison, S. Weng, and E.D. Wong. 2012. Saccharomyces Genome Database: The genomics resource of budding yeast. *Nucleic Acids Research*. 40.

Chothia, C. 1976. The nature of the accessible and buried surfaces in proteins. *J Mol Biol*. 105:1-12.

Cingolani, P., A. Platts, L.L. Wang, M. Coon, T. Nguyen, L. Wang, S.J. Land, X. Lu, and D.M. Ruden. 2012. A program for annotating and predicting the effects of single nucleotide polymorphisms, SnpEff: SNPs in the genome of Drosophila melanogaster strain w1118; iso-2; iso-3. *Fly (Austin)*. 6:80-92.

Clary, D.O., I.C. Griff, and J.E. Rothman. 1990. SNAPs, a family of NSF attachment proteins involved in intracellular membrane fusion in animals and yeast. *Cell*. 61:709-721.

Clement, S.T., G. Dixit, and H.G. Dohlman. 2013. Regulation of yeast G protein signaling by the kinases that activate the AMPK homolog Snf1. *Sci Signal*. 6:ra78.

Clotet, J., F. Posas, A. Casamayor, I. Schaaff-Gerstenschläger, and J. Ariño. 1991. The gene DIS2S1 is essential in Saccharomyces cerevisiae and is involved in glycogen phosphorylase activation. *Curr Genet*. 19:339-342.

Cocucci, E., F. Aguet, S. Boulant, and T. Kirchhausen. 2012. The first five seconds in the life of a clathrin-coated pit. *Cell*. 150:495-507.

Colombo, M.I., L.S. Mayorga, P.J. Casey, and P.D. Stahl. 1992. Evidence of a role for heterotrimeric GTP-binding proteins in endosome fusion. *Science*. 255:1695-1697.

Colombo, M.I., L.S. Mayorga, I. Nishimoto, E.M. Ross, and P.D. Stahl. 1994. Gs regulation of endosome fusion suggests a role for signal transduction pathways in endocytosis. *Journal of Biological Chemistry*. 269:14919-14923.

Colombo, S., P. Ma, L. Cauwenberg, J. Winderickx, M. Crauwels, A. Teunissen, D. Nauwelaers, J.H. De Winde, M.-F. Oise Gorwa, D. Colavizza, J.M. Thevelein, S. Colombo, and P. Ma. 1998. Involvement of distinct G-proteins, Gpa2 and Ras, in glucose-and intracellular acidification-induced cAMP signalling in the yeast Saccharomyces cerevisiae. *In* The EMBO Journal. Vol. 17. 3326-3341.

Colombo, S., D. Ronchetti, J.M. Thevelein, J. Winderickx, and E. Martegani. 2004. Activation State of the Ras2 Protein and Glucose-induced Signaling in Saccharomyces cerevisiae. *Journal of Biological Chemistry*. 279:46715-46722.

Conibear, E., J.N. Cleck, and T.H. Stevens. 2003. Vps51p mediates the association of the GARP (Vps52/53/54) complex with the late Golgi t-SNARE Tlg1p. *Molecular biology of the cell*. 14:1610-1623.

Conibear, E., and T.H. Stevens. 2000. Vps52p, Vps53p, and Vps54p form a novel multisubunit complex required for protein sorting at the yeast late Golgi. *Molecular biology of the cell*. 11:305-323.

Connolly, T., P.J. Rapiejko, and R. Gilmore. 1991. Requirement of GTP hydrolysis for dissociation of the signal recognition particle from its receptor. *Science (New York, N.Y.)*. 252:1171-1173.

Cooke, F.T., S.K. Dove, R.K. McEwen, G. Painter, A.B. Holmes, M.N. Hall, R.H. Michell, and P.J. Parker. 1998. The stress-activated phosphatidylinositol 3-phosphate 5-kinase Fab1p is essential for vacuole function in S. cerevisiae. *Curr Biol*. 8:1219-1222.

Cooper, G.M. 2000. The Cell: A Molecular Approach. Sinauer Associates, Sunderland (MA).

Cosson, P., and F. Letourneur. 1994. Coatomer interaction with di-lysine endoplasmic reticulum retention motifs. *Science (New York, N.Y.)*. 263:1629-1631.

Costa, E.A., K. Subramanian, J. Nunnari, and J.S. Weissman. 2018. Defining the physiological role of SRP in protein-targeting efficiency and specificity. *Science*. 359:689-692.

Costa, E.C., A.F. Moreira, D. de Melo-Diogo, V.M. Gaspar, M.P. Carvalho, and I.J. Correia. 2016. 3D tumor spheroids: an overview on the tools and techniques used for their analysis. *Biotechnol Adv*. 34:1427-1441.

Cowles, C.R., W.B. Snyder, C.G. Burd, and S.D. Emr. 1997. Novel Golgi to vacuole delivery pathway in yeast: identification of a sorting determinant and required transport component. *The EMBO journal*. 16:2769-2782.

Cremona, O., G. Di Paolo, M.R. Wenk, A. Lüthi, W.T. Kim, K. Takei, L. Daniell, Y. Nemoto, S.B. Shears, R.A. Flavell, D.A. McCormick, and P. De Camilli. 1999. Essential role of phosphoinositide metabolism in synaptic vesicle recycling. *Cell*. 99:179-188.

Cueva, R., N. García-Alvarez, and P. Suárez-Rendueles. 1989. Yeast vacuolar aminopeptidase yscI. Isolation and regulation of the APE1 (LAP4) structural gene. *FEBS Lett*. 259:125-129.

Cui, D.Y., C.R. Brown, and H.L. Chiang. 2004. The type 1 phosphatase Reg1p-Glc7p is required for the glucose-induced degradation of fructose-1,6-bisphosphatase in the vacuole. *J Biol Chem*. 279:9713-9724.

Danecek, P., J.K. Bonfield, J. Liddle, J. Marshall, V. Ohan, M.O. Pollard, A. Whitwham, T. Keane, S.A. McCarthy, R.M. Davies, and H. Li. 2021. Twelve years of SAMtools and BCFtools. *GigaScience*. 10:giab008.

Daum, G., N.D. Lees, M. Bard, and R. Dickson. 1998. Biochemistry, cell biology and molecular biology of lipids of Saccharomyces cerevisiae. *Yeast*. 14:1471-1510.

Davenport, C.B. 1941. The Early History of Research with Drosophila. *Science*. 93:305-306.

Day, K.J., J.C. Casler, and B.S. Glick. 2018. Budding Yeast Has a Minimal Endomembrane System. *Dev Cell*. 44:56-72.e54.

De Camilli, P., S.D. Emr, P.S. McPherson, and P. Novick. 1996. Phosphoinositides as regulators in membrane traffic. *Science*. 271:1533-1539.

de la Fuente, G., and A. Sols. 1962. Transport of sugars in yeasts. II. Mechanisms of utilization of disaccharides and related glycosides. *Biochimica et biophysica acta*. 56:49-62.

De Vit, M.J., J.A. Waddle, and M. Johnston. 1997. Regulated nuclear translocation of the Mig1 glucose repressor. *Mol Biol Cell*. 8:1603-1618.

Deshaies, R.J., and C.A.P. Joazeiro. 2009. RING Domain E3 Ubiquitin Ligases. *Annual Review of Biochemistry*. 78:399-434.

Deshaies, R.J., S.L. Sanders, D.A. Feldheim, and R. Schekman. 1991. Assembly of yeast Sec proteins involved in translocation into the endoplasmic reticulum into a membrane-bound multisubunit complex. *Nature*. 349:806-808.

Deshaies, R.J., and R. Schekman. 1989. SEC62 encodes a putative membrane protein required for protein translocation into the yeast endoplasmic reticulum. *Journal of Cell Biology*. 109:2653-2664.

DeVit, M.J., and M. Johnston. 1999. The nuclear exportin Msn5 is required for nuclear export of the Mig1 glucose repressor of Saccharomyces cerevisiae. *Current biology : CB*. 9:1231-1241.

Diaz-Ruiz, R., M. Rigoulet, and A. Devin. 2011. The Warburg and Crabtree effects: On the origin of cancer cell energy metabolism and of yeast glucose repression. *Biochimica et Biophysica Acta (BBA) - Bioenergetics*. 1807:568-576.

Dickson, R.C. 1998. SPHINGOLIPID FUNCTIONS IN SACCHAROMYCES CEREVISIAE: Comparison to Mammals. *Annual Review of Biochemistry*. 67:27-48.

Dickson, R.C., and R.L. Lester. 1999. Yeast sphingolipids. *In* Biochimica et Biophysica Acta - General Subjects. Vol. 1426. Biochim Biophys Acta. 347-357.

Dickson, R.C., and R.L. Lester. 2002. Sphingolipid functions in Saccharomyces cerevisiae. *In* Biochimica et Biophysica Acta - Molecular and Cell Biology of Lipids. Vol. 1583. Biochim Biophys Acta. 13-25.

Dietzel, C., and J. Kurjan. 1987. The yeast SCG1 gene: a G alpha-like protein implicated in the a- and alpha-factor response pathway. *Cell*. 50:1001-1010.

Dixit, G., R. Baker, C.M. Sacks, M.P. Torres, and H.G. Dohlman. 2014. Guanine Nucleotide-binding Protein (Gα) Endocytosis by a Cascade of Ubiquitin Binding Domain Proteins Is Required for Sustained Morphogenesis and Proper Mating in Yeast. *Journal of Biological Chemistry*. 289:15052-15063.

Dohlman, H.G., J. Song, D. Ma, W.E. Courchesne, and J. Thorner. 1996. Sst2, a negative regulator of pheromone signaling in the yeast Saccharomyces cerevisiae: expression, localization, and genetic interaction and physical association with Gpa1 (the G-protein alpha subunit). *Mol Cell Biol*. 16:5194-5209.

Dombek, K.M., V. Voronkova, A. Raney, and E.T. Young. 1999. Functional analysis of the yeast Glc7-binding protein Reg1 identifies a protein phosphatase type 1-binding motif as essential for repression of ADH2 expression. *Mol Cell Biol*. 19:6029-6040.

Drexler, H.G., and C.C. Uphoff. 2002. Mycoplasma contamination of cell cultures: Incidence, sources, effects, detection, elimination, prevention. *Cytotechnology*. 39:75-90.

Duden, R., G. Griffiths, R. Frank, P. Argos, and T.E. Kreis. 1991. Beta-COP, a 110 kd protein associated with non-clathrin-coated vesicles and the Golgi complex, shows homology to beta-adaptin. *Cell*. 64:649-665.

Duden, R., and R. Schekman. 1997. Insights into Golgi function through mutants in yeast and animal cells. *In* The Golgi Apparatus. E.G. Berger and J. Roth, editors. Birkhäuser Basel, Basel. 219-246.

Duncan, M.C., M.J. Cope, B.L. Goode, B. Wendland, and D.G. Drubin. 2001. Yeast Eps15-like endocytic protein, Pan1p, activates the Arp2/3 complex. *Nat Cell Biol*. 3:687-690.

Ehrenreich, J.H., J.J.M. Bergeron, P. Siekevitz, and G.E. Palade. 1973. GOLGI FRACTIONS PREPARED FROM RAT LIVER HOMOGENATES I. Isolation Procedure and Morphological Characterization. *Journal of Cell Biology*. 59:45-72.

Engelman, J.A., J. Luo, and L.C. Cantley. 2006. The evolution of phosphatidylinositol 3-kinases as regulators of growth and metabolism. *Nature Reviews Genetics*. 7:606-619.

Fadri, M., A. Daquinag, S. Wang, T. Xue, and J. Kunz. 2005. The pleckstrin homology domain proteins Slm1 and Slm2 are required for actin cytoskeleton organization in yeast and bind phosphatidylinositol-4,5-bisphosphate and TORC2. *Mol Biol Cell*. 16:1883-1900.

Fahy, E., D. Cotter, M. Sud, and S. Subramaniam. 2011. Lipid classification, structures and tools. *Biochim Biophys Acta*. 1811:637-647.

Fasshauer, D., R.B. Sutton, A.T. Brunger, and R. Jahn. 1998. Conserved structural features of the synaptic fusion complex: SNARE proteins reclassified as Q- and R-SNAREs. *Proceedings of the National Academy of Sciences*. 95:15781-15786.

Feigenson, G.W. 2006. Phase behavior of lipid mixtures. *Nat Chem Biol*. 2:560-563.

Feldheim, D., K. Yoshimura, A. Admon, and R. Schekman. 1993. Structural and functional characterization of Sec66p, a new subunit of the polypeptide translocation apparatus in the yeast endoplasmic reticulum. *Molecular biology of the cell*. 4:931-939.

Feng, Z.H., S.E. Wilson, Z.Y. Peng, K.K. Schlender, E.M. Reimann, and R.J. Trumbly. 1991. The yeast GLC7 gene required for glycogen accumulation encodes a type 1 protein phosphatase. *J Biol Chem*. 266:23796-23801.

Ferguson, M.A., S.W. Homans, R.A. Dwek, and T.W. Rademacher. 1988. Glycosyl-phosphatidylinositol moiety that anchors Trypanosoma brucei variant surface glycoprotein to the membrane. *Science*. 239:753-759.

Ferguson, M.A.J., T. Kinoshita, and G.W. Hart. 2009. Glycosylphosphatidylinositol Anchors. *In* Essentials of Glycobiology. A. Varki, R.D. Cummings, J.D. Esko, H.H. Freeze, P. Stanley, C.R. Bertozzi, G.W. Hart, and M.E. Etzler, editors. Cold Spring Harbor Laboratory Press

Copyright © 2009, The Consortium of Glycobiology Editors, La Jolla, California., Cold Spring Harbor (NY).

Feyder, S., J.-O. De Craene, S. Bär, D. Bertazzi, S. Friant, S. Feyder, J.-O. De Craene, S. Bär, D.L. Bertazzi, and S. Friant. 2015. Membrane Trafficking in the Yeast Saccharomyces cerevisiae Model. *International Journal of Molecular Sciences*. 16:1509-1525.

Ficarro, S.B., M.L. McCleland, P.T. Stukenberg, D.J. Burke, M.M. Ross, J. Shabanowitz, D.F. Hunt, and F.M. White. 2002. Phosphoproteome analysis by mass spectrometry and its application to Saccharomyces cerevisiae. *Nat Biotechnol*. 20:301-305.

Finicle, B.T., V. Jayashankar, and A.L. Edinger. 2018. Nutrient scavenging in cancer. *Nature Reviews Cancer*. 18:619-633.

Firke, S. 2021. Simple Tools for Examining and Cleaning Dirty Data [R package janitor version 2.1.0].

Foderaro, J.E., L.M. Douglas, and J.B. Konopka. 2017. MCC/Eisosomes Regulate Cell Wall Synthesis and Stress Responses in Fungi. *J Fungi (Basel)*. 3.

Ford, M.G., B.M. Pearse, M.K. Higgins, Y. Vallis, D.J. Owen, A. Gibson, C.R. Hopkins, P.R. Evans, and H.T. McMahon. 2001. Simultaneous binding of PtdIns(4,5)P2 and

clathrin by AP180 in the nucleation of clathrin lattices on membranes. *Science*. 291:1051-1055.

Fox, J.A., M. Duszenkog, M.A.J. Fergusonq, M.G. Low, and G.A. Cross. 1986. Purification and Characterization of a Novel Glycan-Phosphatidylinositol-specific Phospholipase C from Trypanosoma brucei. *Journal of Biological Chemistry*. 261:15767-15771.

Franzusoff, A., K. Redding, J. Crosby, R.S. Fuller, and R. Schekman. 1991. Localization of components involved in protein transport and processing through the yeast Golgi apparatus. *Journal of Cell Biology*. 112:27-37.

Friant, S., R. Lombardi, T. Schmelzle, M.N. Hall, and H. Riezman. 2001. Sphingoid base signaling via Pkh kinases is required for endocytosis in yeast. *The EMBO journal*. 20:6783-6792.

Fröhlich, F., R. Christiano, D.K. Olson, A. Alcazar-Roman, P. DeCamilli, and T.C. Walther. 2014. A role for eisosomes in maintenance of plasma membrane phosphoinositide levels. *Mol Biol Cell*. 25:2797-2806.

Fröhlich, F., K. Moreira, P.S. Aguilar, N.C. Hubner, M. Mann, P. Walter, and T.C. Walther. 2009. A genome-wide screen for genes affecting eisosomes reveals Nce102 function in sphingolipid signaling. *Journal of Cell Biology*. 185:1227-1242.

Fröhlich, F., C. Petit, N. Kory, R. Christiano, H.-K. Hannibal-Bach, M. Graham, X. Liu, C.S. Ejsing, R.V. Farese, Jr., and T.C. Walther. 2015. The GARP complex is required for cellular sphingolipid homeostasis. *eLife*. 4:e08712.

Fröhlich, K.U., and F. Madeo. 2001. Apoptosis in yeast: a new model for aging research. *Exp Gerontol*. 37:27-31.

Frost, A., V.M. Unger, and P. De Camilli. 2009. The BAR domain superfamily: membrane-molding macromolecules. *Cell*. 137:191-196.

Fruman, D.A., R.E. Meyers, and L.C. Cantley. 1998. Phosphoinositide kinases. *Annu Rev Biochem*. 67:481-507.

Funato, K., and H. Riezman. 2001. Vesicular and nonvesicular transport of ceramide from ER to the Golgi apparatus in yeast. *Journal of Cell Biology*. 155:949-959.

Gaidarov, I., Q. Chen, J.R. Falck, K.K. Reddy, and J.H. Keen. 1996. A functional phosphatidylinositol 3,4,5-trisphosphate/phosphoinositide binding domain in the clathrin adaptor AP-2 alpha subunit. Implications for the endocytic pathway. *J Biol Chem*. 271:20922-20929.

Galan, J.M., V. Moreau, B. Andre, C. Volland, and R. Haguenauer-Tsapis. 1996. Ubiquitination mediated by the Npi1p/Rsp5p ubiquitin-protein ligase is required for endocytosis of the yeast uracil permease. *Journal of Biological Chemistry*. 271:10946-10952.

Gancedo, J.M. 1998. Yeast carbon catabolite repression. *Microbiol Mol Biol Rev*. 62:334-361.

Geissler, S., K. Siegers, and E. Schiebel. 1998. A novel protein complex promoting formation of functional alpha- and gamma-tubulin. *The EMBO journal*. 17:952-966.

Gerber, M., and A. Shilatifard. 2003. Transcriptional elongation by RNA polymerase II and histone methylation. *In* Journal of Biological Chemistry. Vol. 278. American Society for Biochemistry and Molecular Biology. 26303-26306.

Ghaemmaghami, S., W.K. Huh, K. Bower, R.W. Howson, A. Belle, N. Dephoure, E.K. O'Shea, and J.S. Weissman. 2003. Global analysis of protein expression in yeast. *Nature*. 425:737-741.

Giaever, G., A.M. Chu, L. Ni, C. Connelly, L. Riles, S. Véronneau, S. Dow, A. Lucau-Danila, K. Anderson, B. André, A.P. Arkin, A. Astromoff, M. El Bakkoury, R. Bangham, R. Benito, S. Brachat, S. Campanaro, M. Curtiss, K. Davis, A. Deutschbauer, K.D. Entian, P. Flaherty, F. Foury, D.J. Garfinkel, M. Gerstein, D. Gotte, U. Güldener, J.H. Hegemann, S. Hempel, Z. Herman, D.F. Jaramillo, D.E. Kelly, S.L. Kelly, P. Kötter, D. LaBonte, D.C.

Lamb, N. Lan, H. Liang, H. Liao, L. Liu, C. Luo, M. Lussier, R. Mao, P. Menard, S.L. Ooi, J.L. Revuelta, C.J. Roberts, M. Rose, P. Ross-Macdonald, B. Scherens, G. Schimmack, B. Shafer, D.D. Shoemaker, S. Sookhai-Mahadeo, R.K. Storms, J.N. Strathern, G. Valle, M. Voet, G. Volckaert, C.Y. Wang, T.R. Ward, J. Wilhelmy, E.A. Winzeler, Y. Yang, G. Yen, E. Youngman, K. Yu, H. Bussey, J.D. Boeke, M. Snyder, P. Philippsen, R.W. Davis, and M. Johnston. 2002. Functional profiling of the Saccharomyces cerevisiae genome. *Nature*. 418:387-391.

Gibbons, J.A., L. Kozubowski, K. Tatchell, and S. Shenolikar. 2007. Expression of Human Protein Phosphatase-1 in Saccharomyces cerevisiae Highlights the Role of Phosphatase Isoforms in Regulating Eukaryotic Functions*. *Journal of Biological Chemistry*. 282:21838-21847.

Glick, B.S., and J.E. Rothman. 1987. Possible role for fatty acyl-coenzyme A in intracellular protein transport. *Nature 1987 326:6110*. 326:309-312.

Goffeau, A., G. Barrell, H. Bussey, R.W. Davis, B. Dujon, H. Feldmann, F. Galibert, J.D. Hoheisel, C. Jacq, M. Johnston, E.J. Louis, H.W. Mewes, Y. Murakami, P. Philippsen, H. Tettelin, and S.G. Oliver. 1996. Life with 6000 genes. *Science (New York, N.Y.)*. 274:546-567.

Goldstein, G., M. Scheid, U. Hammerling, D.H. Schlesinger, H.D. Niall, and E.A. Boyse. 1975. Isolation of a polypeptide that has lymphocyte-differentiating properties and is probably represented universally in living cells. *Proceedings of the National Academy of Sciences of the United States of America*. 72:11-15.

Goode, B.L., J.A. Eskin, and B. Wendland. 2015. Actin and endocytosis in budding yeast. *Genetics*. 199:315-358.

Görlich, D., S. Prehn, E. Hartmann, K.U. Kalies, and T.A. Rapoport. 1992. A mammalian homolog of SEC61p and SECYp is associated with ribosomes and nascent polypeptides during translocation. *Cell*. 71:489-503.

Goud, B., A. Salminen, N.C. Walworth, and P.J. Novick. 1988. A GTP-binding protein required for secretion rapidly associates with secretory vesicles and the plasma membrane in yeast. *Cell*. 53:753-768.

Gournas, C., S. Gkionis, M. Carquin, L. Twyffels, D. Tyteca, and B. André. 2018. Conformation-dependent partitioning of yeast nutrient transporters into starvation-protective membrane domains. *Proceedings of the National Academy of Sciences of the United States of America*. 115:E3145-E3154.

Gournas, C., E. Saliba, E.-M. Krammer, C. Barthelemy, M. Prévost, and B. André. 2017. Transition of yeast Can1 transporter to the inward-facing state unveils an α-arrestin target sequence promoting its ubiquitylation and endocytosis. *Molecular Biology of the Cell*. 28:2819-2832.

Graham, F.L., J. Smiley, W.C. Russell, and R. Nairn. 1977. Characteristics of a Human Cell Line Transformed by DNA from Human Adenovirus Type 5. *Journal of General Virology*. 36:59-72.

Green, N., H. Fang, and P. Walter. 1992. Mutants in three novel complementation groups inhibit membrane protein insertion into and soluble protein translocation across the endoplasmic reticulum membrane of Saccharomyces cerevisiae. *The Journal of cell biology*. 116:597-604.

Grenson, M., C. Hou, and M. Crabeel. 1970. Multiplicity of the amino acid permeases in Saccharomyces cerevisiae. IV. Evidence for a general amino acid permease. *Journal of bacteriology*. 103:770-777.

Griggs, D.W., and M. Johnston. 1991. Regulated expression of the GAL4 activator gene in yeast provides a sensitive genetic switch for glucose repression. *Proceedings of the National Academy of Sciences of the United States of America*. 88:8597-8601.

Grilley, M.M., S.D. Stock, R.C. Dickson, R.L. Lester, and J.Y. Takemoto. 1998. Syringomycin Action Gene SYR2 Is Essential for Sphingolipid 4-Hydroxylation in Saccharomyces cerevisiae *.

Grossmann, G., J. Malinsky, W. Stahlschmidt, M. Loibl, I. Weig-Meckl, W.B. Frommer, M. Opekarová, and W. Tanner. 2008. Plasma membrane microdomains regulate turnover of transport proteins in yeast. *Journal of Cell Biology*. 183:1075-1088.

Grossmann, G., M. Opekarová, J. Malinsky, I. Weig-Meckl, and W. Tanner. 2007. Membrane potential governs lateral segregation of plasma membrane proteins and lipids in yeast. *EMBO Journal*. 26:1-8.

Guiney, E.L., T. Klecker, and S.D. Emr. 2016. Identification of the endocytic sorting signal recognized by the Art1-Rsp5 ubiquitin ligase complex. *Mol Biol Cell*. 27:4043-4054.

Guo, M., C. Aston, S.A. Burchett, C. Dyke, S. Fields, S.J.R. Rajarao, P. Uetz, Y. Wang, K. Young, and H.G. Dohlman. 2003. The Yeast G Protein α Subunit Gpa1 Transmits a Signal through an RNA Binding Effector Protein Scp160. *Molecular Cell*. 12:517-524.

Guo, W., A. Grant, and P. Novick. 1999. Exo84p Is an Exocyst Protein Essential for Secretion *. *Journal of Biological Chemistry*. 274:23558-23564.

Gurunathan, S., D. Chapman-Shimshoni, S. Trajkovic, and J.E. Gerst. 2000. Yeast exocytic v-SNAREs confer endocytosis. *Mol Biol Cell*. 11:3629-3643.

Gustin, M.C., B. Martinac, Y. Saimi, M.R. Culbertson, and C. Kung. 1986. Ion channels in yeast. *Science*. 233:1195-1197.

Haak, D., K. Gable, T. Beeler, and T. Dunn. 1997. Hydroxylation of Saccharomyces cerevisiae ceramides requires Sur2p and Scs7p. *Journal of Biological Chemistry*. 272:29704-29710.

Haft, C.R., M. de la Luz Sierra, V.A. Barr, D.H. Haft, and S.I. Taylor. 1998. Identification of a family of sorting nexin molecules and characterization of their association with receptors. *Molecular and cellular biology*. 18:7278-7287.

Hammond, G.R.V., M.P. Machner, and T. Balla. 2014. A novel probe for phosphatidylinositol 4-phosphate reveals multiple pools beyond the Golgi. *Journal of Cell Biology*. 205:113-126.

Han, J., J.D. Lee, L. Bibbs, and R.J. Ulevitch. 1994. A MAP kinase targeted by endotoxin and hyperosmolarity in mammalian cells. *Science*. 265:808-811.

Hanada, K. 2003. Serine palmitoyltransferase, a key enzyme of sphingolipid metabolism. *In* Biochimica et Biophysica Acta - Molecular and Cell Biology of Lipids. Vol. 1632. Elsevier. 16-30.

Hann, B.C., and P. Walter. 1991. The signal recognition particle in S. cerevisiae. *Cell*. 67:131-144.

Hannun, Y.A., and L.M. Obeid. 2018. Sphingolipids and their metabolism in physiology and disease. *Nature Reviews Molecular Cell Biology*. 19:175-191.

Hartwell, L.H., R.K. Mortimer, J. Culotti, and M. Culotti. 1973. Genetic Control of the Cell Division Cycle in Yeast: V. Genetic Analysis of cdc Mutants. *Genetics*. 74:267-286.

Hata, Y., C.A. Slaughter, and T.C. Südhof. 1993. Synaptic vesicle fusion complex contains unc-18 homologue bound to syntaxin. *Nature*. 366:347-351.

Hecht, K.A., A.F. O'Donnell, and J.L. Brodsky. 2014. The proteolytic landscape of the yeast vacuole. *Cell Logist*. 4:e28023.

Heenan, E.J., J.L. Vanhooke, B.R. Temple, L. Betts, J.E. Sondek, and H.G. Dohlman. 2009. Structure and Function of Vps15 in the Endosomal G Protein Signaling Pathway †. *Biochemistry*. 48:6390-6401.

Hein, C., J.Y.Y. Springael, C. Volland, R. Haguenauer-Tsapis, and B. André. 1995. NPI1, an essential yeast gene involved in induced degradation of Gap1 and Fur4 permeases, encodes the Rsp5 ubiquitin—protein ligase. *Molecular Microbiology*. 18:77-87.

Heiniger, H.J., A.A. Kandutsch, and H.W. Chen. 1976. Depletion of L-cell sterol depresses endocytosis. *Nature*. 263:515-517.

Heinisch, J.J., V. Dupres, S. Wilk, A. Jendretzki, and Y.F. Dufrêne. 2010. Single-molecule atomic force microscopy reveals clustering of the yeast plasma-membrane sensor Wsc1. *PLoS One*. 5:e11104.

Hemmings, B.A., G.S. Zubenko, A. Hasilik, and E.W. Jones. 1981. Mutant defective in processing of an enzyme located in the lysosome-like vacuole of Saccharomyces cerevisiae. *Proc Natl Acad Sci U S A*. 78:435-439.

Herman, P.K., and S.D. Emr. 1990. Characterization of VPS34, a gene required for vacuolar protein sorting and vacuole segregation in Saccharomyces cerevisiae. *Molecular and Cellular Biology*. 10:6742-6754.

Hershko, A., A. Ciechanover, H. Heller, A.L. Haas, and I.A. Rose. 1980. Proposed role of ATP in protein breakdown: conjugation of protein with multiple chains of the polypeptide of ATP-dependent proteolysis. *Proc Natl Acad Sci U S A*. 77:1783-1786.

Hettema, E.H., M.J. Lewis, M.W. Black, and H.R.B. Pelham. 2003. Retromer and the sorting nexins Snx4/41/42 mediate distinct retrieval pathways from yeast endosomes. *The EMBO Journal*. 22:548-557.

Hicke, L., and R. Schekman. 1989. Yeast Sec23p acts in the cytoplasm to promote protein transport from the endoplasmic reticulum to the Golgi complex in vivo and in vitro. *Embo j*. 8:1677-1684.

Hicke, L., H.L. Schubert, and C.P. Hill. 2005. Ubiquitin-binding domains. *Nature Reviews Molecular Cell Biology*. 6:610-621.

Hisamoto, N., D.L. Frederick, K. Sugimoto, K. Tatchell, and K. Matsumoto. 1995. The EGP1 gene may be a positive regulator of protein phosphatase type 1 in the growth control of Saccharomyces cerevisiae. *Mol Cell Biol*. 15:3767-3776.

Ho, B., A. Baryshnikova, and G.W. Brown. 2018. Unification of Protein Abundance Datasets Yields a Quantitative Saccharomyces cerevisiae Proteome. *Cell Syst*. 6:192-205.e193.

Ho, Y., A. Gruhler, A. Heilbut, G.D. Bader, L. Moore, S.L. Adams, A. Millar, P. Taylor, K. Bennett, K. Boutilier, L. Yang, C. Wolting, I. Donaldson, S. Schandorff, J. Shewnarane, M. Vo, J. Taggart, M. Goudreault, B. Muskat, C. Alfarano, D. Dewar, Z. Lin, K. Michalickova, A.R. Willems, H. Sassi, P.A. Nielsen, K.J. Rasmussen, J.R. Andersen, L.E. Johansen, L.H. Hansen, H. Jespersen, A. Podtelejnikov, E. Nielsen, J. Crawford, V. Poulsen, B.D. Sørensen, J. Matthiesen, R.C. Hendrickson, F. Gleeson, T. Pawson, M.F. Moran, D. Durocher, M. Mann, C.W.V. Hogue, D. Figeys, and M. Tyers. 2002. Systematic identification of protein complexes in Saccharomyces cerevisiae by mass spectrometry. *In* Nature. Vol. 415. Nature Publishing Group. 180-183.

Holt, L.J., B.B. Tuch, J. Villén, A.D. Johnson, S.P. Gygi, and D.O. Morgan. 2009. Global analysis of Cdk1 substrate phosphorylation sites provides insights into evolution. *Science*. 325:1682-1686.

Hong, S.-P., F.C. Leiper, A. Woods, D. Carling, and M. Carlson. 2003. Activation of yeast Snf1 and mammalian AMP-activated protein kinase by upstream kinases. *Proceedings of the National Academy of Sciences*. 100:8839-8843.

Horn, H., E.M. Schoof, J. Kim, X. Robin, M.L. Miller, F. Diella, A. Palma, G. Cesareni, L.J. Jensen, and R. Linding. 2014. KinomeXplorer: an integrated platform for kinome biology studies. *Nature Methods*. 11:603-604.

Hovsepian, J., V. Albanèse, M. Becuwe, V. Ivashov, D. Teis, and S. Léon. 2018. The yeast arrestin-related protein Bul1 is a novel actor of glucose-induced endocytosis. *Mol Biol Cell*. 29:1012-1020.

Hovsepian, J., Q. Defenouillère, V. Albanèse, L. Váchová, C. Garcia, Z. Palková, and S. Léon. 2017. Multilevel regulation of an α-arrestin by glucose depletion controls hexose transporter endocytosis. *Journal of Cell Biology*. 216:1811-1831.

Hsu, S.C., A.E. Ting, C.D. Hazuka, S. Davanger, J.W. Kenny, Y. Kee, and R.H. Scheller. 1996. The mammalian brain rsec6/8 complex. *Neuron*. 17:1209-1219.

Hu, Z., J.O. Nehlin, H. Ronne, and C.A. Michels. 1995. MIG1-dependent and MIG1-independent glucose regulation of MAL gene expression in Saccharomyces cerevisiae. *Current Genetics*. 28:258-266.

Huang, K.M., K. D'Hondt, H. Riezman, and S.K. Lemmon. 1999. Clathrin functions in the absence of heterotetrameric adaptors and AP180-related proteins in yeast. *Embo j*. 18:3897-3908.

Huang, S., A. Benben, R. Green, N. Cheranda, G. Lee, B. Joseph, S. Keaveney, and Y. Wang. 2019. Phosphorylation of the Gα protein Gpa2 promotes protein kinase A signaling in yeast. *J Biol Chem*. 294:18836-18845.

Huh, W.K., J.V. Falvo, L.C. Gerke, A.S. Carroll, R.W. Howson, J.S. Weissman, and E.K. O'Shea. 2003. Global analysis of protein localization in budding yeast. *Nature*. 425:686-691.

Huibregtse, J.M., J.C. Yang, and S.L. Beaudenon. 1997. The large subunit of RNA polymerase II is a substrate of the Rsp5 ubiquitin-protein ligase. *Proc Natl Acad Sci U S A*. 94:3656-3661.

Husnjak, K., and I. Dikic. 2012. Ubiquitin-binding proteins: decoders of ubiquitin-mediated cellular functions. *Annu Rev Biochem*. 81:291-322.

Inagaki, M., T. Schmelzle, K. Yamaguchi, K. Irie, M.N. Hall, and K. Matsumoto. 1999. PDK1 homologs activate the Pkc1-mitogen-activated protein kinase pathway in yeast. *Mol Cell Biol*. 19:8344-8352.

Isnard, A.D., D. Thomas, and Y. Surdin-Kerjan. 1996. The study of methionine uptake in Saccharomyces cerevisiae reveals a new family of amino acid permeases. *Journal of Molecular Biology*. 262:473-484.

Ito, T., H. Ando, T. Suzuki, T. Ogura, K. Hotta, Y. Imamura, Y. Yamaguchi, and H. Handa. 2010. Identification of a primary target of thalidomide teratogenicity. *Science*. 327:1345-1350.

Itoh, T., S. Koshiba, T. Kigawa, A. Kikuchi, S. Yokoyama, and T. Takenawa. 2001. Role of the ENTH domain in phosphatidylinositol-4,5-bisphosphate binding and endocytosis. *Science*. 291:1047-1051.

Ivanusic, D., M. Eschricht, and J. Denner. 2014. Investigation of membrane protein-protein interactions using correlative FRET-PLA. *Biotechniques*. 57:188-191, 193-188.

Jaber, N., Z. Dou, J.S. Chen, J. Catanzaro, Y.P. Jiang, L.M. Ballou, E. Selinger, X. Ouyang, R.Z. Lin, J. Zhang, and W.X. Zong. 2012. Class III PI3K Vps34 plays an essential role in autophagy and in heart and liver function. *Proc Natl Acad Sci U S A*. 109:2003-2008.

Jack, D.L., I.T. Paulsen, and Saier, Jr. 2000. The amino acid/polyamine/organocation (APC) superfamily of transporters specific for amino acids, polyamines and organocations. *Microbiology*. 146:1797-1814.

Jacobson, K., O.G. Mouritsen, and R.G. Anderson. 2007. Lipid rafts: at a crossroad between cell biology and physics. *Nat Cell Biol*. 9:7-14.

Jahn, R., T. Lang, and T.C. Südhof. 2003. Membrane Fusion. *Cell*. 112:519-533.

Jahn, R., and T.C. Südhof. 1999. Membrane fusion and exocytosis. *Annu Rev Biochem*. 68:863-911.

Jensen, C., and Y. Teng. 2020. Is It Time to Start Transitioning From 2D to 3D Cell Culture? *Front Mol Biosci*. 7:33.

Johnson, L.M., V.A. Bankaitis, and S.D. Emr. 1987. Distinct sequence determinants direct intracellular sorting and modification of a yeast vacuolar protease. *Cell*. 48:875-885.

Johnston, M., J.S. Flick, and T. Pexton. 1994. Multiple mechanisms provide rapid and stringent glucose repression of GAL gene expression in Saccharomyces cerevisiae. *Molecular and cellular biology*. 14:3834-3841.

Jones, C.B., E.M. Ott, J.M. Keener, M. Curtiss, V. Sandrin, and M. Babst. 2012. Regulation of membrane protein degradation by starvation-response pathways. *Traffic (Copenhagen, Denmark)*. 13:468-482.

Jones, G.M., J. Stalker, S. Humphray, A. West, T. Cox, J. Rogers, I. Dunham, and G. Prelich. 2008. A systematic library for comprehensive overexpression screens in Saccharomyces cerevisiae. *Nat Methods*. 5:239-241.

Jund, R., and F. Lacroute. 1970. Genetic and Physiological Aspects of Resistance to 5-Fluoropyrimidines in Saccharomyces cerevisiae "C-labeled pyrimidines and 32p were supplied by. 607-615.

Kabcenell, A.K., B. Gouds, Northup, J. K., and P.J. Novickn. 1990. Binding and Hydrolysis of Guanine Nucleotides by Sec4p, a Yeast Protein Involved in the Regulation of Vesicular Traffic. *The Journal of Biological Chemistry*. 265:9366-9372.

Kabeche, R., L. Howard, and J.B. Moseley. 2015. Eisosomes provide membrane reservoirs for rapid expansion of the yeast plasma membrane. *Journal of Cell Science*. 128:4057-4062.

Kachroo, A.H., J.M. Laurent, C.M. Yellman, A.G. Meyer, C.O. Wilke, and E.M. Marcotte. 2015. Evolution. Systematic humanization of yeast genes reveals conserved functions and genetic modularity. *Science*. 348:921-925.

Kahlhofer, J., S. Leon, D. Teis, and O. Schmidt. 2021. The α-arrestin family of ubiquitin ligase adaptors links metabolism with selective endocytosis. *Biol Cell*. 113:183-219.

Kaksonen, M., and A. Roux. 2018. Mechanisms of clathrin-mediated endocytosis. *Nature Reviews Molecular Cell Biology*. 19:313-326.

Kaksonen, M., Y. Sun, and D.G. Drubin. 2003. A pathway for association of receptors, adaptors, and actin during endocytic internalization. *Cell*. 115:475-487.

Kamble, C., S. Jain, E. Murphy, and K. Kim. 2011. Requirements of Slm proteins for proper eisosome organization, endocytic trafficking and recycling in the yeast Saccharomyces cerevisiae. *J Biosci*. 36:79-96.

Kanaar, R., C. Troelstra, S.M. Swagemakers, J. Essers, B. Smit, J.H. Franssen, A. Pastink, O.Y. Bezzubova, J.M. Buerstedde, B. Clever, W.D. Heyer, and J.H. Hoeijmakers. 1996. Human and mouse homologs of the Saccharomyces cerevisiae RAD54 DNA repair gene: evidence for functional conservation. *Curr Biol*. 6:828-838.

Kanai, F., H. Liu, S.J. Field, H. Akbary, T. Matsuo, G.E. Brown, L.C. Cantley, and M.B. Yaffe. 2001. The PX domains of p47phox and p40phox bind to lipid products of PI(3)K. *Nature cell biology*. 3:675-678.

Kanaseki, T., and K. Kadota. 1969. The "vesicle in a basket". A morphological study of the coated vesicle isolated from the nerve endings of the guinea pig brain, with special reference to the mechanism of membrane movements. *The Journal of cell biology*. 42:202-220.

Kappler, J., N. Roehm, P. Marrack, U. Staerz, J. White, and H.R. Macdonald. 1991. 'Coatomer': a cytosolic protein complex containing subunits of non-clathrin-coated Golgi transport vesicles. *Nature 1991 349:6306*. 349:248-251.

Karnovsky, M.J., A.M. Kleinfeld, R.L. Hoover, and R.D. Klausner. 1982. The concept of lipid domains in membranes. *J Cell Biol*. 94:1-6.

Karotki, L., J.T. Huiskonen, C.J. Stefan, N.E. Ziółkowska, R. Roth, M.A. Surma, N.J. Krogan, S.D. Emr, J. Heuser, K. Grünewald, and T.C. Walther. 2011. Eisosome proteins assemble into a membrane scaffold. *J Cell Biol*. 195:889-902.

Katzmann, D.J., M. Babst, and S.D. Emr. 2001. Ubiquitin-dependent sorting into the multivesicular body pathway requires the function of a conserved endosomal protein sorting complex, ESCRT-I. *Cell*. 106:145-155.

Katzmann, D.J., G. Odorizzi, and S.D. Emr. 2002. Receptor downregulation and multivesicular-body sorting. *In* Nature Reviews Molecular Cell Biology. Vol. 3. 893-905.

Katzmann, D.J., C.J. Stefan, M. Babst, and S.D. Emr. 2003. Vps27 recruits ESCRT machinery to endosomes during MVB sorting. *The Journal of Cell Biology*. 162:413-413.

Kaur, J., and A.K. Bachhawat. 2007. Yct1p, a novel, high-affinity, cysteine-specific transporter from the yeast Saccharomyces cerevisiae. *Genetics*. 176:877-890.

Keen, J.H. 1987. Clathrin assembly proteins: affinity purification and a model for coat assembly. *The Journal of cell biology*. 105:1989-1998.

Keener, J.M., and M. Babst. 2013. Quality Control and Substrate-Dependent Downregulation of the Nutrient Transporter Fur4. *Traffic*. 14:412-427.

Kelly, B.T., S.C. Graham, N. Liska, P.N. Dannhauser, S. Höning, E.J. Ungewickell, and D.J. Owen. 2014. Clathrin adaptors. AP2 controls clathrin polymerization with a membrane-activated switch. *Science (New York, N.Y.)*. 345:459-463.

Kemmeren, P., K. Sameith, L.A.L. Van De Pasch, J.J. Benschop, T.L. Lenstra, T. Margaritis, E. O'Duibhir, E. Apweiler, S. Van Wageningen, C.W. Ko, S. Van Heesch, M.M. Kashani, G. Ampatziadis-Michailidis, M.O. Brok, N.A.C.H. Brabers, A.J. Miles, D. Bouwmeester, S.R. Van Hooff, H. Van Bakel, E. Sluiters, L.V. Bakker, B. Snel, P. Lijnzaad, D. Van Leenen, M.J.A. Groot Koerkamp, and F.C.P. Holstege. 2014. Large-scale genetic perturbations reveal regulatory networks and an abundance of gene-specific repressors. *Cell*. 157:740-752.

Kihara, A., T. Noda, N. Ishihara, and Y. Ohsumi. 2001. Two distinct Vps34 phosphatidylinositol 3-kinase complexes function in autophagy and carboxypeptidase y sorting in Saccharomyces cerevisiae. *Journal of Cell Biology*. 153:519-530.

Kirchhausen, T., and S.C. Harrison. 1981. Protein organization in clathrin trimers. *Cell*. 23:755-761.

Kiss, A.L., and E. Botos. 2009. Endocytosis via caveolae: alternative pathway with distinct cellular compartments to avoid lysosomal degradation? *J Cell Mol Med*. 13:1228-1237.

Klausner, R.D., A.M. Kleinfeld, R.L. Hoover, and M.J. Karnovsky. 1980. Lipid domains in membranes. Evidence derived from structural perturbations induced by free fatty acids and lifetime heterogeneity analysis - PubMed. *The Journal of Biological Chemistry*.

Klionsky, D.J., R. Cueva, and D.S. Yaver. 1992. Aminopeptidase I of Saccharomyces cerevisiae is localized to the vacuole independent of the secretory pathway. *J Cell Biol*. 119:287-299.

Klionsky, D.J., and S.D. Emr. 1990. A new class of lysosomal/vacuolar protein sorting signals. *J Biol Chem*. 265:5349-5352.

Kloepper, T.H., C.N. Kienle, and D. Fasshauer. 2007. An elaborate classification of SNARE proteins sheds light on the conservation of the eukaryotic endomembrane system. *Mol Biol Cell*. 18:3463-3471.

Koboldt, D.C., K. Chen, T. Wylie, D.E. Larson, M.D. McLellan, E.R. Mardis, G.M. Weinstock, R.K. Wilson, and L. Ding. 2009. VarScan: variant detection in massively parallel sequencing of individual and pooled samples. *Bioinformatics*. 25:2283-2285.

Kolde, R. 2019. CRAN - Package pheatmap. *In* Cran.R-Project.Org.

Komander, D., and M. Rape. 2012. The Ubiquitin Code. *Annual Review of Biochemistry*. 81:203-229.

Kozlov, M.M., and V.S. Markin. 1983. Possible mechanism of membrane fusion. *Biofizika*.

Kozubowski, L., H. Panek, A. Rosenthal, A. Bloecher, D.J. DeMarini, and K. Tatchell. 2003. A Bni4-Glc7 phosphatase complex that recruits chitin synthase to the site of bud emergence. *Mol Biol Cell*. 14:26-39.

Kraakman, L., K. Lemaire, P. Ma, A.W.R.H. Teunlssen, M.C.V. Donaton, P. Van Dijck, J. Winderickx, J.H. De Winde, and J.M. Thevelein. 1999. A Saccharomyces cerevisiae G-protein coupled receptor, Gpr1, is specifically required for glucose activation of the cAMP pathway during the transition to growth on glucose. *Molecular Microbiology*. 32:1002-1012.

Kraft, M.L. 2013. Plasma membrane organization and function: moving past lipid rafts. *Mol Biol Cell*. 24:2765-2768.

Krogh, B.O., and L.S. Symington. 2004. Recombination proteins in yeast. *Annu Rev Genet*. 38:233-271.

Kübler, E., and H. Riezman. 1993. Actin and fimbrin are required for the internalization step of endocytosis in yeast. *Embo j*. 12:2855-2862.

Kurzchalia, T.V., E. Hartmann, and P. Dupree. 1995. Guilty by insolubility--does a protein's detergent insolubility reflect a caveolar location? *Trends Cell Biol*. 5:187-189.

Lagunas, R. 1993. Sugar transport in Saccharomyces cerevisiae. *FEMS Microbiology Letters*. 104:229-242.

Lahtvee, P.J., B.J. Sánchez, A. Smialowska, S. Kasvandik, I.E. Elsemman, F. Gatto, and J. Nielsen. 2017. Absolute Quantification of Protein and mRNA Abundances Demonstrate Variability in Gene-Specific Translation Efficiency in Yeast. *Cell Syst*. 4:495-504.e495.

Laidlaw, K.M.E., D.D. Bisinski, S. Shashkova, K.M. Paine, M.A. Veillon, M.C. Leake, and C. MacDonald. 2021. A glucose-starvation response governs endocytic trafficking and eisosomal retention of surface cargoes in budding yeast. *Journal of Cell Science*. 134:jcs.257733-jcs.257733.

Laidlaw, K.M.E., G. Calder, and C. MacDonald. 2022a. Recycling of cell surface membrane proteins from yeast endosomes is regulated by ubiquitinated Ist1. *J Cell Biol*. 221.

Laidlaw, K.M.E., and C. MacDonald. 2018. Endosomal trafficking of yeast membrane proteins. *In* Biochemical Society Transactions. Vol. 46. Portland Press Ltd. 1551-1558.

Laidlaw, K.M.E., K.M. Paine, D.D. Bisinski, G. Calder, K. Hogg, S. Ahmed, S. James, P.J. O'Toole, and C. MacDonald. 2022b. Endosomal cargo recycling mediated by Gpa1 and phosphatidylinositol 3-kinase is inhibited by glucose starvation. *Molecular biology of the cell*. 33.

Lalonde, M.-E., and Y. Durocher. 2017. Therapeutic glycoprotein production in mammalian cells. *Journal of Biotechnology*. 251:128-140.

Lamaze, C., A. Dujeancourt, T. Baba, C.G. Lo, A. Benmerah, and A. Dautry-Varsat. 2001. Interleukin 2 receptors and detergent-resistant membrane domains define a clathrin-independent endocytic pathway. *Mol Cell*. 7:661-671.

Lander, E.S., L.M. Linton, B. Birren, C. Nusbaum, M.C. Zody, J. Baldwin, K. Devon, K. Dewar, M. Doyle, W. Fitzhugh, R. Funke, D. Gage, K. Harris, A. Heaford, J. Howland, L. Kann, J. Lehoczky, R. Levine, P. McEwan, K. McKernan, J. Meldrim, J.P. Mesirov, C. Miranda, W. Morris, J. Naylor, C. Raymond, M. Rosetti, R. Santos, A. Sheridan, C. Sougnez, N. Stange-Thomann, N. Stojanovic, A. Subramanian, D. Wyman, J. Rogers, J. Sulston, R. Ainscough, S. Beck, D. Bentley, J. Burton, C. Clee, N. Carter, A. Coulson, R. Deadman, P. Deloukas, A. Dunham, I. Dunham, R. Durbin, L. French, D. Grafham, S. Gregory, T. Hubbard, S. Humphray, A. Hunt, M. Jones, C. Lloyd, A. McMurray, L. Matthews, S. Mercer, S. Milne, J.C. Mullikin, A. Mungall, R. Plumb, M. Ross, R. Shownkeen, S. Sims, R.H. Waterston, R.K. Wilson, L.W. Hillier, J.D. McPherson, M.A.

Marra, E.R. Mardis, L.A. Fulton, A.T. Chinwalla, K.H. Pepin, W.R. Gish, S.L. Chissoe, M.C. Wendl, K.D. Delehaunty, T.L. Miner, A. Delehaunty, J.B. Kramer, L.L. Cook, R.S. Fulton, D.L. Johnson, P.J. Minx, S.W. Clifton, T. Hawkins, E. Branscomb, P. Predki, P. Richardson, S. Wenning, T. Slezak, N. Doggett, J.F. Cheng, A. Olsen, S. Lucas, C. Elkin, E. Uberbacher, M. Frazier, et al. 2001. Initial sequencing and analysis of the human genome. *Nature 2001 409:6822*. 409:860-921.

Landry, J.J., P.T. Pyl, T. Rausch, T. Zichner, M.M. Tekkedil, A.M. Stütz, A. Jauch, R.S. Aiyar, G. Pau, N. Delhomme, J. Gagneur, J.O. Korbel, W. Huber, and L.M. Steinmetz. 2013. The genomic and transcriptomic landscape of a HeLa cell line. *G3 (Bethesda)*. 3:1213-1224.

Lane, N., and W. Martin. 2010. The energetics of genome complexity. *Nature*. 467:929-934.

Lang, M.J., J.Y. Martinez-Marquez, D.C. Prosser, L.R. Ganser, D. Buelto, B. Wendland, and M.C. Duncan. 2014. Glucose starvation inhibits autophagy via vacuolar hydrolysis and induces plasma membrane internalization by down-regulating recycling. *Journal of Biological Chemistry*. 289:16736-16747.

Lanz, M.C., K. Yugandhar, S. Gupta, E.J. Sanford, V.M. Faça, S. Vega, A.M.N. Joiner, J.C. Fromme, H. Yu, and M.B. Smolka. 2021. In-depth and 3-dimensional exploration of the budding yeast phosphoproteome. *EMBO Rep*. 22:e51121.

Larson, J.R., J.P. Bharucha, S. Ceaser, J. Salamon, C.J. Richardson, S.M. Rivera, and K. Tatchell. 2008. Protein phosphatase type 1 directs chitin synthesis at the bud neck in Saccharomyces cerevisiae. *Mol Biol Cell*. 19:3040-3051.

Le Borgne, R. 2006. Regulation of Notch signalling by endocytosis and endosomal sorting. *Curr Opin Cell Biol*. 18:213-222.

Leake, M.C., J.H. Chandler, G.H. Wadhams, F. Bai, R.M. Berry, and J.P. Armitage. 2006. Stoichiometry and turnover in single, functioning membrane protein complexes. *Nature*. 443:355-358.

Lee, J.H., J.E. Heuser, R. Roth, and U. Goodenough. 2015. Eisosome ultrastructure and evolution in fungi, microalgae, and lichens. *Eukaryotic Cell*. 14:1017-1042.

Lee, M.G., and P. Nurse. 1987. Complementation used to clone a human homologue of the fission yeast cell cycle control gene cdc2. *Nature*. 327:31-35.

Leikin, S.L., M.M. Kozlov, L.V. Chernomordik, V.S. Markin, and Y.A. Chizmadzhev. 1987. Membrane fusion: overcoming of the hydration barrier and local restructuring. *Journal of theoretical biology*. 129:411-425.

Lemmon, S.K., and E.W. Jones. 1987. Clathrin requirement for normal growth of yeast. *Science*. 238:504-509.

Léon, S., and D. Teis. 2018. Functional patchworking at the plasma membrane. *Embo j*. 37.

Letourneur, F., E.C. Gaynor, S. Hennecke, C. Démollière, R. Duden, S.D. Emr, H. Riezman, and P. Cosson. 1994. Coatomer is essential for retrieval of dilysine-tagged proteins to the endoplasmic reticulum. *Cell*. 79:1199-1207.

Leung, K.F., J.B. Dacks, and M.C. Field. 2008. Evolution of the multivesicular body ESCRT machinery; retention across the eukaryotic lineage. *Traffic*. 9:1698-1716.

Levental, I., K.R. Levental, and F.A. Heberle. 2020. Lipid Rafts: Controversies Resolved, Mysteries Remain. *Trends Cell Biol*. 30:341-353.

Levitzki, A. 1988. From epinephrine to cyclic AMP. *Science*. 241:800-806.

Lewis, M.J., B.J. Nichols, C. Prescianotto-Baschong, H. Riezman, and H.R. Pelham. 2000. Specific retrieval of the exocytic SNARE Snc1p from early yeast endosomes. *Mol Biol Cell*. 11:23-38.

Li, F., L. Yi, L. Zhao, A. Itzen, R.S. Goody, and Y.W. Wu. 2014. The role of the hypervariable C-terminal domain in Rab GTPases membrane targeting. *Proc Natl Acad Sci U S A*. 111:2572-2577.

Li, H. 2013. Aligning sequence reads, clone sequences and assembly contigs with BWA-MEM, https://arxiv.org/abs/1303.3997.
Li, M., T. Koshi, and S.D. Emr. 2015. Membrane-anchored ubiquitin ligase complex is required for the turnover of lysosomal membrane proteins. *J Cell Biol*. 211:639-652.
Li, S.C., and P.M. Kane. 2009. The yeast lysosome-like vacuole: endpoint and crossroads. *Biochim Biophys Acta*. 1793:650-663.
Lin, Y., C.H. Sohn, C.K. Dalal, L. Cai, and M.B. Elowitz. 2015. Combinatorial gene regulation by modulation of relative pulse timing. *Nature*. 527:54-58.
Lin, Y.-C., M. Boone, L. Meuris, I. Lemmens, N. Van Roy, A. Soete, J. Reumers, M. Moisse, S. Plaisance, R. Drmanac, J. Chen, F. Speleman, D. Lambrechts, Y. Van de Peer, J. Tavernier, and N. Callewaert. 2014. Genome dynamics of the human embryonic kidney 293 lineage in response to cell biology manipulations. *Nature Communications*. 5:4767.
Lindmo, K., and H. Stenmark. 2006. Regulation of membrane traffic by phosphoinositide 3-kinases. *In* Journal of Cell Science. Vol. 119. The Company of Biologists Ltd. 605-614.
Ljungdahl, P.O., and B. Daignan-Fornier. 2012. Regulation of amino acid, nucleotide, and phosphate metabolism in Saccharomyces cerevisiae. *In* Genetics. Vol. 190. Genetics. 885-929.
Loibl, M., G. Grossmann, V. Stradalova, A. Klingl, R. Rachel, W. Tanner, J. Malinsky, and M. Opekarová. 2010. C terminus of Nce102 determines the structure and function of microdomains in the Saccharomyces cerevisiae plasma membrane. *Eukaryot Cell*. 9:1184-1192.
Low, M.G., M.A.J. Ferguson, A.H. Futerman, and I. Silman. 1986. Covalently attached phosphatidylinositol as a hydrophobic anchor for membrane proteins. *Trends in Biochemical Sciences*. 11:212-215.
Ludin, K., R. Jiang, and M. Carlson. 1998. Glucose-regulated interaction of a regulatory subunit of protein phosphatase 1 with the Snf1 protein kinase in Saccharomyces cerevisiae. *Proc Natl Acad Sci U S A*. 95:6245-6250.
Luhtala, N., and G. Odorizzi. 2004. Bro1 coordinates deubiquitination in the multivesicular body pathway by recruiting Doa4 to endosomes. *J Cell Biol*. 166:717-729.
Lundin, M., J.O. Nehlin, and H. Ronne. 1994. Importance of a flanking AT-rich region in target site recognition by the GC box-binding zinc finger protein MIG1. *Molecular and Cellular Biology*. 14:1979-1985.
Luo, G., A. Gruhler, Y. Liu, O.N. Jensen, and R.C. Dickson. 2008. The sphingolipid long-chain base-Pkh1/2-Ypk1/2 signaling pathway regulates eisosome assembly and turnover. *Journal of Biological Chemistry*. 283:10433-10444.
Luo, G., J. Zhang, and W. Guo. 2014. The role of Sec3p in secretory vesicle targeting and exocyst complex assembly. *Mol Biol Cell*. 25:3813-3822.
Lutfiyya, L.L., V.R. Iyer, J. DeRisi, M.J. DeVit, P.O. Brown, and M. Johnston. 1998. Characterization of three related glucose repressors and genes they regulate in Saccharomyces cerevisiae. *Genetics*. 150:1377-1391.
Ma, M., and C.G. Burd. 2019. Retrograde trafficking and quality control of yeast synaptobrevin, Snc1, are conferred by its transmembrane domain. *Molecular Biology of the Cell*. 30:1729-1742.
Ma, M., and C.G. Burd. 2020. Retrograde trafficking and plasma membrane recycling pathways of the budding yeastSaccharomyces cerevisiae. *Traffic*. 21:45-59.
Ma, M., C.G. Burd, and R.J. Chi. 2017. Distinct complexes of yeast Snx4 family SNX-BARs mediate retrograde trafficking of Snc1 and Atg27. *Traffic*. 18:134-144.
MacDonald, C., N.J. Buchkovich, D.K. Stringer, S.D. Emr, and R.C. Piper. 2012a. Cargo ubiquitination is essential for multivesicular body intralumenal vesicle formation. *EMBO reports*. 13:331-338.

MacDonald, C., J.A. Payne, M. Aboian, W. Smith, D.J. Katzmann, and R.C. Piper. 2015a. A Family of Tetraspans Organizes Cargo for Sorting into Multivesicular Bodies. *Developmental Cell*. 33:328-342.

MacDonald, C., and R.C. Piper. 2015. Puromycin- and methotrexate-resistance cassettes and optimized Cre-recombinase expression plasmids for use in yeast. *Yeast*. 32:423-438.

MacDonald, C., and R.C. Piper. 2016. Cell surface recycling in yeast: Mechanisms and machineries. *Biochemical Society Transactions*. 44:474-478.

MacDonald, C., and R.C. Piper. 2017. Genetic dissection of early endosomal recycling highlights a TORC1-independent role for Rag GTPases. *Journal of Cell Biology*. 216:3275-3290.

MacDonald, C., S.B. Shields, C.A. Williams, S. Winistorfer, and R.C. Piper. 2020. A Cycle of Ubiquitination Regulates Adaptor Function of the Nedd4-Family Ubiquitin Ligase Rsp5. *Current biology : CB*. 30:465-479.e465.

MacDonald, C., M.A. Stamnes, D.J. Katzmann, and R.C. Piper. 2015b. Tetraspan cargo adaptors usher GPI-anchored proteins into multivesicular bodies. *Cell Cycle*. 14:3673-3673.

Macdonald, C., D.K. Stringer, and R.C. Piper. 2012b. Sna3 Is an Rsp5 Adaptor Protein that Relies on Ubiquitination for Its MVB Sorting. *Traffic*. 13:586-598.

MacDonald, C., D.K. Stringer, and R.C. Piper. 2012c. Sna3 is an Rsp5 adaptor protein that relies on ubiquitination for its MVB sorting. *Traffic*. 13:586-598.

MacDonald, C., S. Winistorfer, R.M. Pope, M.E. Wright, and R.C. Piper. 2017. Enzyme reversal to explore the function of yeast E3 ubiquitin-ligases. *Traffic*. 18:465-484.

MacGurn, J.A., P.C. Hsu, M.B. Smolka, and S.D. Emr. 2011. TORC1 regulates endocytosis via Npr1-mediated phosphoinhibition of a ubiquitin ligase adaptor. *Cell*. 147:1104-1117.

Maldonado-Báez, L., M.R. Dores, E.M. Perkins, T.G. Drivas, L. Hicke, and B. Wendland. 2008. Interaction between Epsin/Yap180 adaptors and the scaffolds Ede1/Pan1 is required for endocytosis. *Mol Biol Cell*. 19:2936-2948.

Maldonado-Báez, L., and B. Wendland. 2006. Endocytic adaptors: recruiters, coordinators and regulators. *Trends Cell Biol*. 16:505-513.

Malinska, K., J. Malinsky, M. Opekarova, and W. Tanner. 2004. Distribution of Can1p into stable domains reflects lateral protein segregation within the plasma membrane of living S. cerevisiae cells. *Journal of Cell Science*. 117:6031-6041.

Malínská, K., J. Malínský, M. Opekarová, and W. Tanner. 2003. Visualization of Protein Compartmentation within the Plasma Membrane of Living Yeast Cells. *Molecular Biology of the Cell*. 14:4427-4436.

Manford, A.G., C.J. Stefan, H.L. Yuan, J.A. Macgurn, and S.D. Emr. 2012. ER-to-plasma membrane tethering proteins regulate cell signaling and ER morphology. *Dev Cell*. 23:1129-1140.

Marchal, C., R. Haguenauer-Tsapis, and D. Urban-Grimal. 1998. A PEST-Like Sequence Mediates Phosphorylation and Efficient Ubiquitination of Yeast Uracil Permease. *In* MOLECULAR AND CELLULAR BIOLOGY. Vol. 18. 314-321.

Markin, V.S., M.M. Kozlov, and V.L. Borovjagin. 1984. On the theory of membrane fusion. The stalk mechanism - PubMed. *General Physiology and Biophysics*.

Martin, M. 2011. Cutadapt removes adapter sequences from high-throughput sequencing reads. *EMBnet.journal*. 17:10.

Martin, W.F., S. Garg, and V. Zimorski. 2015. Endosymbiotic theories for eukaryote origin. *Philos Trans R Soc Lond B Biol Sci*. 370:20140330.

Martin-Serrano, J., T. Zang, and P.D. Bieniasz. 2001. HIV-1 and Ebola virus encode small peptide motifs that recruit Tsg101 to sites of particle assembly to facilitate egress. *Nat Med*. 7:1313-1319.

Matsuoka, K., L. Orci, M. Amherdt, S.Y. Bednarek, S. Hamamoto, R. Schekman, and T. Yeung. 1998. COPII-coated vesicle formation reconstituted with purified coat proteins and chemically defined liposomes. *Cell*. 93:263-275.

Mayor, S., and R.E. Pagano. 2007. Pathways of clathrin-independent endocytosis. *Nature Reviews Molecular Cell Biology*. 8:603-612.

McCudden, C.R., M.D. Hains, R.J. Kimple, D.P. Siderovski, and F.S. Willard. 2005. G-protein signaling: back to the future. *Cell Mol Life Sci*. 62:551-577.

McLaren, W., L. Gil, S.E. Hunt, H.S. Riat, G.R.S. Ritchie, A. Thormann, P. Flicek, and F. Cunningham. 2016. The Ensembl Variant Effect Predictor. *Genome Biology*. 17.

McMahon, H.T., and E. Boucrot. 2011. Molecular mechanism and physiological functions of clathrin-mediated endocytosis. *In* Nature Reviews Molecular Cell Biology. Vol. 12. Nature Publishing Group. 517-533.

Merten, O.W. 2002. Virus contaminations of cell cultures - A biotechnological view. *Cytotechnology*. 39:91-116.

Meyer, H.A., H. Grau, R. Kraft, S. Kostka, S. Prehn, K.U. Kalies, and E. Hartmann. 2000. Mammalian Sec61 is associated with Sec62 and Sec63. *The Journal of biological chemistry*. 275:14550-14557.

Migliano, S.M., E.M. Wenzel, and H. Stenmark. 2022. Biophysical and molecular mechanisms of ESCRT functions, and their implications for disease. *Current Opinion in Cell Biology*. 75:102062.

Millán-Zambrano, G., A. Rodríguez-Gil, X. Peñate, L. de Miguel-Jiménez, M. Morillo-Huesca, N. Krogan, and S. Chávez. 2013. The Prefoldin Complex Regulates Chromatin Dynamics during Transcription Elongation. *PLoS Genetics*. 9.

Miller, E.A., T.H. Beilharz, P.N. Malkus, M.C. Lee, S. Hamamoto, L. Orci, and R. Schekman. 2003. Multiple cargo binding sites on the COPII subunit Sec24p ensure capture of diverse membrane proteins into transport vesicles. *Cell*. 114:497-509.

Miller, H., Z. Zhou, A.J. Wollman, and M.C. Leake. 2015a. Superresolution imaging of single DNA molecules using stochastic photoblinking of minor groove and intercalating dyes. *Methods*. 88:81-88.

Miller, S.E., S. Mathiasen, N.A. Bright, F. Pierre, B.T. Kelly, N. Kladt, A. Schauss, C.J. Merrifield, D. Stamou, S. Höning, and D.J. Owen. 2015b. CALM regulates clathrin-coated vesicle size and maturation by directly sensing and driving membrane curvature. *Dev Cell*. 33:163-175.

Misra, S., and J.H. Hurley. 1999. Crystal structure of a phosphatidylinositol 3-phosphate-specific membrane-targeting motif, the FYVE domain of Vps27p. *Cell*. 97:657-666.

Miyajima, I., M. Nakafuku, N. Nakayama, C. Brenner, A. Miyajima, K. Kaibuchi, K.i. Arai, Y. Kaziro, and K. Matsumoto. 1987. GPA1, a haploid-specific essential gene, encodes a yeast homolog of mammalian G protein which may be involved in mating factor signal transduction. *Cell*. 50:1011-1019.

Moharir, A., L. Gay, D. Appadurai, J. Keener, and M. Babst. 2018. Eisosomes are metabolically regulated storage compartments for APC-type nutrient transporters. *Molecular Biology of the Cell*. 29:2113-2127.

Moorthy, B.T., A. Sharma, D.R. Boettner, T.E. Wilson, and S.K. Lemmon. 2019. Identification of Suppressor of Clathrin Deficiency-1 (SCD1) and Its Connection to Clathrin-Mediated Endocytosis in Saccharomyces cerevisiae. *G3 (Bethesda)*. 9:867-877.

Moran, C.J., A. Ramesh, P.A. Brama, J.M. O'Byrne, F.J. O'Brien, and T.J. Levingstone. 2016. The benefits and limitations of animal models for translational research in cartilage repair. *J Exp Orthop*. 3:1.

More, K., C.M. Klinger, L.D. Barlow, and J.B. Dacks. 2020. Evolution and Natural History of Membrane Trafficking in Eukaryotes. *Current Biology*. 30:R553-R564.

Moreira, K.E., S. Schuck, B. Schrul, F. Fröhlich, J.B. Moseley, T.C. Walther, and P. Walter. 2012. Seg1 controls eisosome assembly and shape. *J Cell Biol*. 198:405-420.

Moreira, K.E., T.C. Walther, P.S. Aguilar, and P. Walter. 2009. Pil1 Controls Eisosome Biogenesis. *Molecular Biology of the Cell*. 20:809-818.

Morgera, F., M.R. Sallah, M.L. Dubuke, P. Gandhi, D.N. Brewer, C.M. Carr, and M. Munson. 2012. Regulation of exocytosis by the exocyst subunit Sec6 and the SM protein Sec1. *Mol Biol Cell*. 23:337-346.

Morris, S.A., S. Schröder, U. Plessmann, K. Weber, and E. Ungewickell. 1993. Clathrin assembly protein AP180: primary structure, domain organization and identification of a clathrin binding site. *Embo j*. 12:667-675.

Mortimer, R.K., and J.R. Johnston. 1986. Genealogy of principal strains of the yeast genetic stock center. *Genetics*. 113:35-43.

Moseley, J.B. 2018. Eisosomes. *Curr Biol*. 28:R376-r378.

Mouritsen, O.G., and M. Bloom. 1984. Mattress model of lipid-protein interactions in membranes. *Biophys J*. 46:141-153.

Müller, M., O. Schmidt, M. Angelova, K. Faserl, S. Weys, L. Kremser, T. Pfaffenwimmer, T. Dalik, C. Kraft, Z. Trajanoski, H. Lindner, and D. Teis. 2015. The coordinated action of the MVB pathway and autophagy ensures cell survival during starvation. *eLife*. 4:e07736.

Mund, M., J.A. van der Beek, J. Deschamps, S. Dmitrieff, P. Hoess, J.L. Monster, A. Picco, F. Nédélec, M. Kaksonen, and J. Ries. 2018. Systematic Nanoscale Analysis of Endocytosis Links Efficient Vesicle Formation to Patterned Actin Nucleation. *Cell*. 174:884-896.e817.

Munn, A.L., and H. Riezman. 1994. Endocytosis is required for the growth of vacuolar H(+)-ATPase-defective yeast: identification of six new END genes. *J Cell Biol*. 127:373-386.

Murley, A., J. Yamada, B.J. Niles, A. Toulmay, W.A. Prinz, T. Powers, and J. Nunnari. 2017. Sterol transporters at membrane contact sites regulate TORC1 and TORC2 signaling. *J Cell Biol*. 216:2679-2689.

Murray, A. 2016. Paul Nurse and Pierre Thuriaux on wee Mutants and Cell Cycle Control. *Genetics*. 204:1325-1326.

Nakafuku, M., H. Itoh, S. Nakamura, and Y. Kaziro. 1987. Occurrence in Saccharomyces cerevisiae of a gene homologous to the cDNA coding for the alpha subunit of mammalian G proteins. *Proc Natl Acad Sci U S A*. 84:2140-2144.

Nakafuku, M., T. Obara, K. Kaibuchi, I. Miyajima, A. Miyajima, H. Itoh, S. Nakamura, K. Arai, K. Matsumoto, and Y. Kaziro. 1988. Isolation of a second yeast Saccharomyces cerevisiae gene (GPA2) coding for guanine nucleotide-binding regulatory protein: studies on its structure and possible functions. *Proceedings of the National Academy of Sciences of the United States of America*. 85:1374-1378.

Nakańo, A., and M. Muramatsu. 1989. A novel GTP-binding protein, Sar1p, is involved in transport from the endoplasmic reticulum to the Golgi apparatus. *J Cell Biol*. 109:2677-2691.

Nakayama, N., Y. Kaziro, K. Arai, and K. Matsumoto. 1988. Role of STE genes in the mating factor signaling pathway mediated by GPA1 in Saccharomyces cerevisiae. *Mol Cell Biol*. 8:3777-3783.

Nehlin, J.O., M. Carlberg, and H. Ronne. 1991. Control of yeast GAL genes by MIG1 repressor: a transcriptional cascade in the glucose response. *The EMBO Journal*. 10:3373-3377.

Nehlin, J.O., and H. Ronne. 1990. Yeast MIG1 repressor is related to the mammalian early growth response and Wilms' tumour finger proteins. *Embo j*. 9:2891-2898.
Nelson, N. 1999. Metal ion transporters and homeostasis. *In* EMBO Journal. Vol. 18. John Wiley & Sons, Ltd. 4361-4371.
Nelson, W.J. 2003. Adaptation of core mechanisms to generate cell polarity. *Nature*. 422:766-774.
Newpher, T.M., R.P. Smith, V. Lemmon, and S.K. Lemmon. 2005. In vivo dynamics of clathrin and its adaptor-dependent recruitment to the actin-based endocytic machinery in yeast. *Dev Cell*. 9:87-98.
Ng, D.T.W., J.D. Brown, and P. Walter. 1996. Signal sequences specify the targeting route to the endoplasmic reticulum membrane. *The Journal of cell biology*. 134:269-278.
Nguyen, T.H., D.T.S. Law, and D.B. Williams. 1991. Binding protein BiP is required for translocation of secretory proteins into the endoplasmic reticulum in Saccharomyces cerevisiae. *Proceedings of the National Academy of Sciences of the United States of America*. 88:1565-1565.
Nickas, M.E., and M.P. Yaffe. 1996. BRO1, a novel gene that interacts with components of the Pkc1p-mitogen-activated protein kinase pathway in Saccharomyces cerevisiae. *Mol Cell Biol*. 16:2585-2593.
NIH. 2013. NIH, Lacks family reach understanding to share genomic data of HeLa cells.
Nothwehr, S.F., and A.E. Hindes. 1997. The yeast VPS5/GRD2 gene encodes a sorting nexin-1-like protein required for localizing membrane proteins to the late Golgi. *Journal of Cell Science*. 110:1063-1072.
Novick, P., S. Ferro, and R. Schekman. 1981. Order of events in the yeast secretory pathway. *Cell*. 25:461-469.
Novick, P., C. Field, and R. Schekman. 1980. Identification of 23 complementation groups required for post-translational events in the yeast secretory pathway. *Cell*. 21:205-215.
Novick, P., M.D. Garrett, P. Brennwald, A. Lauring, F.P. Finger, R. Collins, and D.R. TerBush. 1995. Control of exocytosis in yeast. *Cold Spring Harb Symp Quant Biol*. 60:171-177.
Nurse, P. 1975. Genetic control of cell size at cell division in yeast. *Nature*. 256:547-551.
Nurse, P., and P. Thuriaux. 1980. Regulatory genes controlling mitosis in the fission yeast Schizosaccharomyces pombe. *Genetics*. 96:627-637.
O'Donnell, A.F., R.R. McCartney, D.G. Chandrashekarappa, B.B. Zhang, J. Thorner, and M.C. Schmidt. 2015. 2-Deoxyglucose impairs Saccharomyces cerevisiae growth by stimulating Snf1-regulated and α-arrestin-mediated trafficking of hexose transporters 1 and 3. *Mol Cell Biol*. 35:939-955.
O'Donnell, A.F., and M.C. Schmidt. 2019. AMPK-Mediated Regulation of Alpha-Arrestins and Protein Trafficking. *Int J Mol Sci*. 20.
Odorizzi, G. 2006. The multiple personalities of Alix. *J Cell Sci*. 119:3025-3032.
Odorizzi, G., M. Babst, and S.D. Emr. 2000. Phosphoinositide signaling and the regulation of membrane trafficking in yeast. *Trends Biochem Sci*. 25:229-235.
Offley, S.R., and M.C. Schmidt. 2019. Protein phosphatases of Saccharomyces cerevisiae. *Curr Genet*. 65:41-55.
Olivera-Couto, A., M. Graña, L. Harispe, and P.S. Aguilar. 2011. The eisosome core is composed of BAR domain proteins. *Molecular Biology of the Cell*. 22:2360-2372.
Onishi, H.R., J.S. Tkacz, and J.O. Lampen. 1979. Glycoprotein nature of yeast alkaline phosphatase. Formation of active enzyme in the presence of tunicamycin. *Journal of Biological Chemistry*. 254:11943-11952.
Orci, L., D.J. Palmer, M. Amherdt, and J.E. Rothman. 1993. Coated vesicle assembly in the Golgi requires only coatomer and ARF proteins from the cytosol. *Nature*. 364:732-734.

Orr-Weaver, T.L., J.W. Szostak, and R.J. Rothstein. 1981. Yeast transformation: a model system for the study of recombination. *Proceedings of the National Academy of Sciences*. 78:6354-6358.

Paine, K.M., G.B. Ecclestone, and C. MacDonald. 2021. Fur4-mediated uracil-scavenging to screen for surface protein regulators. *Traffic*. 22:397-408.

Paine, K.M., G.J.O. Evans, K.M.E. Laidlaw, and C. MacDonald. 2022. The phosphatase Glc7 controls eisosomal response to starvation via posttranslational modification of Pil1. *bioRxiv*:2022.2008.2009.503340.

Palade, G. 1975. Intracellular aspects of the process of protein synthesis. *Science*. 189:347-358.

Panzner, S., L. Dreier, E. Hartmann, S. Kostka, and T.A. Rapoport. 1995. Posttranslational protein transport in yeast reconstituted with a purified complex of Sec proteins and Kar2p. *Cell*. 81:561-570.

Papa, F.R., and M. Hochstrasser. 1993. The yeast DOA4 gene encodes a deubiquitinating enzyme related to a product of the human tre-2 oncogene. *Nature*. 366:313-319.

Pashkova, N., L. Gakhar, S.C. Winistorfer, A.B. Sunshine, M. Rich, M.J. Dunham, L. Yu, and R.C. Piper. 2013. The yeast Alix homolog Bro1 functions as a ubiquitin receptor for protein sorting into multivesicular endosomes. *Dev Cell*. 25:520-533.

Payne, G.S., and R. Schekman. 1985. A test of clathrin function in protein secretion and cell growth. *Science*. 230:1009-1014.

Pearse, B.M. 1975. Coated vesicles from pig brain: purification and biochemical characterization. *Journal of molecular biology*. 97:93-98.

Pederson, T. 2011. The nucleus introduced. *Cold Spring Harb Perspect Biol*. 3.

Peeters, T., W. Louwet, R. Geladé, D. Nauwelaers, J.M. Thevelein, and M. Versele. 2006. Kelch-repeat proteins interacting with the Galpha protein Gpa2 bypass adenylate cyclase for direct regulation of protein kinase A in yeast. *Proc Natl Acad Sci U S A*. 103:13034-13039.

Peggie, M.W., S.H. MacKelvie, A. Bloecher, E.V. Knatko, K. Tatchell, and M.J. Stark. 2002. Essential functions of Sds22p in chromosome stability and nuclear localization of PP1. *J Cell Sci*. 115:195-206.

Péli-Gulli, M.-P., A. Sardu, N. Panchaud, S. Raucci, and Claudio. 2015. Amino Acids Stimulate TORC1 through Lst4-Lst7, a GTPase-Activating Protein Complex for the Rag Family GTPase Gtr2. *Cell Reports*. 13:1-7.

Peng, Z.Y., R.J. Trumbly, and E.M. Reimann. 1990. Purification and characterization of glycogen synthase from a glycogen-deficient strain of Saccharomyces cerevisiae. *J Biol Chem*. 265:13871-13877.

Perli, T., A.K. Wronska, R.A. Ortiz-Merino, J.T. Pronk, and J.M. Daran. 2020. Vitamin requirements and biosynthesis in Saccharomyces cerevisiae. *Yeast*. 37:283-304.

Peter, B.J., H.M. Kent, I.G. Mills, Y. Vallis, P.J. Butler, P.R. Evans, and H.T. McMahon. 2004. BAR domains as sensors of membrane curvature: the amphiphysin BAR structure. *Science*. 303:495-499.

Phillips, E.O.N., S. Giovinazzi, S.L. Menz, Y. Son, and A. Gunjan. 2021. Preparation of Cell Extracts by Cryogrinding in an Automated Freezer Mill. *J Vis Exp*.

Pickart, C.M. 2001. Mechanisms Underlying Ubiquitination. *Annual Review of Biochemistry*. 70:503-533.

Pierce, K.L., R.T. Premont, and R.J. Lefkowitz. 2002. Seven-transmembrane receptors. *Nature Reviews Molecular Cell Biology*. 3:639-650.

Pike, L.J. 2006. Rafts defined: a report on the Keystone Symposium on Lipid Rafts and Cell Function. *J Lipid Res*. 47:1597-1598.

Piper, R.C., N.J. Bryant, and T.H. Stevens. 1997. The Membrane Protein Alkaline Phosphatase Is Delivered to the Vacuole by a Route That Is Distinct from the VPS-dependent Pathway. *Journal of Cell Biology*. 138:531-545.

Piper, R.C., and D.J. Katzmann. 2007. Biogenesis and Function of Multivesicular Bodies. *Annual Review of Cell and Developmental Biology*. 23:519-547.

Plath, K., B.M. Wilkinson, C.J. Stirling, and T.A. Rapoport. 2004. Interactions between Sec Complex and Prepro-Factor during Posttranslational Protein Transport into the Endoplasmic Reticulum. *Molecular Biology of the Cell*. 15:1-10.

Polaina, J., and J. Conde. 1982. Genes involved in the control of nuclear fusion during the sexual cycle of Saccharomyces cerevisiae. *Molecular and General Genetics MGG 1982 186:2*. 186:253-258.

Ponting, C.P. 1996. Novel domains in NADPH oxidase subunits, sorting nexins, and PtdIns 3-kinases: binding partners of SH3 domains? *Protein science : a publication of the Protein Society*. 5:2353-2357.

Preuss, D., J. Mulholland, A. Franzusoff, N. Segev, and D. Botstein. 1992. Characterization of the Saccharomyces Golgi complex through the cell cycle by immunoelectron microscopy. *Mol Biol Cell*. 3:789-803.

Pronk, J.T. 2002. Auxotrophic yeast strains in fundamental and applied research. *Appl Environ Microbiol*. 68:2095-2100.

Prosser, D.C., T.G. Drivas, L. Maldonado-Báez, and B. Wendland. 2011. Existence of a novel clathrin-independent endocytic pathway in yeast that depends on Rho1 and formin. *J Cell Biol*. 195:657-671.

Protopopov, V., B. Govindan, P. Novick, and J.E. Gerst. 1993. Homologs of the synaptobrevin/VAMP family of synaptic vesicle proteins function on the late secretory pathway in S. cerevisiae. *Cell*. 74:855-861.

Rad, M.R., H.L. Phan, L. Kirchrath, P.K. Tan, T. Kirchhausen, C.P. Hollenberg, and G.S. Payne. 1995. Saccharomyces cerevisiae Apl2p, a homologue of the mammalian clathrin AP β subunit, plays a role in clathrin-dependent Golgi functions. *Journal of Cell Science*. 108:1605-1615.

Ramgopal, M., and K. Bloch. 1983. Sterol synergism in yeast. *Proc Natl Acad Sci U S A*. 80:712-715.

Rand, R.P., T.S. Reese, and R.G. Miller. 1981. Phospholipid bilayer deformations associated with interbilayer contact and fusion. *Nature*. 293:237-238.

Raymond, C.K., I. Howald-Stevenson, C.A. Vater, and T.H. Stevens. 1992. Morphological classification of the yeast vacuolar protein sorting mutants: Evidence for a prevacuolar compartment in class E vps mutants. *Molecular Biology of the Cell*. 3:1389-1402.

Reggiori, F., and D.J. Klionsky. 2002. Autophagy in the eukaryotic cell. *Eukaryot Cell*. 1:11-21.

Reggiori, F., and H.R.B. Pelham. 2002. A transmembrane ubiquitin ligase required to sort membrane proteins into multivesicular bodies. *Nature Cell Biology*. 4:117-123.

Reggiori, F., C.W. Wang, P.E. Stromhaug, T. Shintani, and D.J. Klionsky. 2003. Vps51 is part of the yeast Vps fifty-three tethering complex essential for retrograde traffic from the early endosome and Cvt vesicle completion. *The Journal of biological chemistry*. 278:5009-5020.

Reidick, C., F. Boutouja, and H.W. Platta. 2017. The class III phosphatidylinositol 3-kinase Vps34 in Saccharomyces cerevisiae. *Biological Chemistry*. 398:677-685.

Reizer, J., A. Reizer, M.H. Saier, K. Finley, D. Kakuda, and C.L. Macleod. 1993. Mammalian integral membrane receptors are homologous to facilitators and antiporters of yeast, fungi, and eubacteria. *Protein Science*. 2:20-30.

Ren, J., Y. Kee, J.M. Huibregtse, and R.C. Piper. 2007. Hse1, a component of the yeast Hrs-STAM ubiquitin-sorting complex, associates with ubiquitin peptidases and a ligase to control sorting efficiency into multivesicular bodies. *Mol Biol Cell*. 18:324-335.

Reyes-Lamothe, R., D.J. Sherratt, and M.C. Leake. 2010. Stoichiometry and architecture of active DNA replication machinery in Escherichia coli. *Science*. 328:498-501.

Riggi, M., K. Niewola-Staszkowska, N. Chiaruttini, A. Colom, B. Kusmider, V. Mercier, S. Soleimanpour, M. Stahl, S. Matile, A. Roux, and R. Loewith. 2018. Decrease in plasma membrane tension triggers PtdIns(4,5)P(2) phase separation to inactivate TORC2. *Nat Cell Biol*. 20:1043-1051.

Ringer, S. 1882. Concerning the Influence exerted by each of the Constituents of the Blood on the Contraction of the Ventricle. *J Physiol*. 3:380-393.

Rivier, A.S., G.A. Castillon, L. Michon, M. Fukasawa, M. Romanova-Michaelides, N. Jaensch, K. Hanada, and R. Watanabe. 2010. Exit of GPI-anchored proteins from the ER differs in yeast and mammalian cells. *Traffic*. 11:1017-1033.

Robinson, J.S., D.J. Klionsky, L.M. Banta, and S.D. Emr. 1988. Protein sorting in Saccharomyces cerevisiae: isolation of mutants defective in the delivery and processing of multiple vacuolar hydrolases. *Molecular and Cellular Biology*. 8:4936-4936.

Robinson, J.T., H. Thorvaldsdóttir, W. Winckler, M. Guttman, E.S. Lander, G. Getz, and J.P. Mesirov. 2011. Integrative genomics viewer. *Nature biotechnology*. 29:24-26.

Robinson, M.S. 1987. 100-kD coated vesicle proteins: molecular heterogeneity and intracellular distribution studied with monoclonal antibodies. *J Cell Biol*. 104:887-895.

Rock, J.M., D. Lim, L. Stach, R.W. Ogrodowicz, J.M. Keck, M.H. Jones, C.C. Wong, J.R. Yates, 3rd, M. Winey, S.J. Smerdon, M.B. Yaffe, and A. Amon. 2013. Activation of the yeast Hippo pathway by phosphorylation-dependent assembly of signaling complexes. *Science*. 340:871-875.

Rodriguez, R.J., and L.W. Parks. 1983. Structural and physiological features of sterols necessary to satisfy bulk membrane and sparking requirements in yeast sterol auxotrophs. *Arch Biochem Biophys*. 225:861-871.

Roelants, F.M., P.D. Torrance, N. Bezman, and J. Thorner. 2002. Pkh1 and Pkh2 Differentially Phosphorylate and Activate Ypk1 and Ykr2 and Define Protein Kinase Modules Required for Maintenance of Cell Wall Integrity. *Molecular Biology of the Cell*. 13:3005-3028.

Rose, M.D., L.M. Misra, and J.P. Vogel. 1989. KAR2, a Karyogamy Gene, Is the Yeast Homolog of the Mammalian BiP/GRP78 Gene. *Cell*. 57:1211-1221.

Roth, T.F., and K.R. Porter. 1964. Yolk protein uptake in the oocyte of the mosquito Aedes aegypti . L. *The Journal of cell biology*. 20:313-332.

Rothe, C., and L. Lehle. 1998. Sorting of invertase signal peptide mutants in yeast dependent and independent on the signal-recognition particle. *European journal of biochemistry*. 252:16-24.

Rothman, J.E. 1981. The Golgi apparatus: Two organelles in tandem. *In* Science. Vol. 213. American Association for the Advancement of Science. 1212-1219.

Rothman, J.H., and T.H. Stevens. 1986. Protein sorting in yeast: Mutants defective in vacuole biogenesis mislocalize vacuolar proteins into the late secretory pathway. *Cell*. 47:1041-1051.

Ruiz, A., X. Xu, and M. Carlson. 2011. Roles of two protein phosphatases, Reg1-Glc7 and Sit4, and glycogen synthesis in regulation of SNF1 protein kinase. *Proceedings of the National Academy of Sciences*. 108:6349-6354.

Rutherford, J.C., Y.S. Bahn, B. van den Berg, J. Heitman, and C. Xue. 2019. Nutrient and Stress Sensing in Pathogenic Yeasts. *Front Microbiol*. 10:442.

Rybin, V., O. Ullrich, M. Rubino, K. Alexandrov, I. Simon, M.C. Seabra, R. Goody, and M. Zerial. 1996. GTPase activity of Rab5 acts as a timer for endocytic membrane fusion. *Nature*. 383:266-269.

Saarikangas, J., H. Zhao, A. Pykäläinen, P. Laurinmäki, P.K. Mattila, P.K.J. Kinnunen, S.J. Butcher, and P. Lappalainen. 2009. Molecular Mechanisms of Membrane Deformation by I-BAR Domain Proteins. *Current Biology*. 19:95-107.

Saksena, S., J. Wahlman, D. Teis, A.E. Johnson, and S.D. Emr. 2009. Functional reconstitution of ESCRT-III assembly and disassembly. *Cell*. 136:97-109.

Santangelo, G.M. 2006. Glucose Signaling in Saccharomyces cerevisiae. *Microbiology and Molecular Biology Reviews*. 70:253-282.

Sanz, M., F. Castrejón, A. Durán, and C. Roncero. 2004. Saccharomyces cerevisiae Bni4p directs the formation of the chitin ring and also participates in the correct assembly of the septum structure. *Microbiology (Reading)*. 150:3229-3241.

Sanz, P., G.R. Alms, T.A. Haystead, and M. Carlson. 2000. Regulatory interactions between the Reg1-Glc7 protein phosphatase and the Snf1 protein kinase. *Mol Cell Biol*. 20:1321-1328.

Sapp, J. 2005. The prokaryote-eukaryote dichotomy: meanings and mythology. *Microbiol Mol Biol Rev*. 69:292-305.

Saraogi, I., and S.o. Shan. 2011. Molecular Mechanism of Co-translational Protein Targeting by the Signal Recognition Particle. *Traffic (Copenhagen, Denmark)*. 12:535-535.

Sardana, R., and S.D. Emr. 2021. Membrane Protein Quality Control Mechanisms in the Endo-Lysosome System. *In* Trends in Cell Biology. Vol. 31. Elsevier Ltd. 269-283.

Scales, S.J., B.Y. Yoo, and R.H. Scheller. 2001. The ionic layer is required for efficient dissociation of the SNARE complex by alpha-SNAP and NSF. *Proc Natl Acad Sci U S A*. 98:14262-14267.

Schaffitzel, E., and M. Hertweck. 2006. Recent aging research in Caenorhabditis elegans. *Exp Gerontol*. 41:557-563.

Scherer, W.F., J.T. Syverton, and G.O. Gey. 1953. Studies on the propagation in vitro of poliomyelitis viruses. IV. Viral multiplication in a stable strain of human malignant epithelial cells (strain HeLa) derived from an epidermoid carcinoma of the cervix. *J Exp Med*. 97:695-710.

Schlacht, A., E.K. Herman, M.J. Klute, M.C. Field, and J.B. Dacks. 2014. Missing pieces of an ancient puzzle: evolution of the eukaryotic membrane-trafficking system. *Cold Spring Harb Perspect Biol*. 6:a016048.

Schu, P. 2008. Aminopeptidase I enzymatic activity. *Methods Enzymol*. 451:67-78.

Schu, P.V., K. Takegawa, M.J. Fry, J.H. Stack, M.D. Waterfield, and S.D. Emr. 1993. Phosphatidylinositol 3-kinase encoded by yeast VPS34 gene essential for protein sorting. *Science*. 260:88-91.

Schuldiner, M., S.R. Collins, N.J. Thompson, V. Denic, A. Bhamidipati, T. Punna, J. Ihmels, B. Andrews, C. Boone, J.F. Greenblatt, J.S. Weissman, and N.J. Krogan. 2005. Exploration of the function and organization of the yeast early secretory pathway through an epistatic miniarray profile. *Cell*. 123:507-519.

Schuldiner, M., J. Metz, V. Schmid, V. Denic, M. Rakwalska, H.D. Schmitt, B. Schwappach, and J.S. Weissman. 2008. The GET Complex Mediates Insertion of Tail-Anchored Proteins into the ER Membrane. *Cell*. 134:634-645.

Schüller, H.J. 2003. Transcriptional control of nonfermentative metabolism in the yeast Saccharomyces cerevisiae. *In* Current Genetics. Vol. 43. Springer Verlag. 139-160.

Schulman, B.A., and J. Wade Harper. 2009. Ubiquitin-like protein activation by E1 enzymes: The apex for downstream signalling pathways. *In* Nature Reviews Molecular Cell Biology. Vol. 10. 319-331.

Schwarz, D.S., and M.D. Blower. 2016. The endoplasmic reticulum: structure, function and response to cellular signaling. *Cell Mol Life Sci*. 73:79-94.

Scott, S.V., A. Hefner-Gravink, K.A. Morano, T. Noda, Y. Ohsumi, and D.J. Klionsky. 1996. Cytoplasm-to-vacuole targeting and autophagy employ the same machinery to deliver proteins to the yeast vacuole. *Proc Natl Acad Sci U S A*. 93:12304-12308.

Seaman, M.N.J. 2004. Cargo-selective endosomal sorting for retrieval to the Golgi requires retromer. *The Journal of cell biology*. 165:111-122.

Seaman, M.N.J., J.M. McCaffery, and S.D. Emr. 1998. A Membrane Coat Complex Essential for Endosome-to-Golgi Retrograde Transport in Yeast. *The Journal of Cell Biology*. 142:665-681.

Seger, S., R. Rischatsch, and P. Philippsen. 2011. Formation and stability of eisosomes in the filamentous fungus Ashbya gossypii. *J Cell Sci*. 124:1629-1634.

Selwan, E.M., B.T. Finicle, S.M. Kim, and A.L. Edinger. 2016. Attacking the supply wagons to starve cancer cells to death. *FEBS Letters*. 590:885-907.

Séron, K., M.O. Blondel, R. Haguenauer-Tsapis, and C. Volland. 1999. Uracil-induced down-regulation of the yeast uracil permease. *In* Journal of Bacteriology. Vol. 181. 1793-1800.

Serrano, R., M.C. Kielland-Brandt, and G.R. Fink. 1986. Yeast plasma membrane ATPase is essential for growth and has homology with (Na+ + K+), K+- and Ca2+-ATPases. *Nature*. 319:689-693.

Shashkova, S., M. Andersson, S. Hohmann, and M.C. Leake. 2021. Correlating single-molecule characteristics of the yeast aquaglyceroporin Fps1 with environmental perturbations directly in living cells. *Methods*. 193:46-53.

Shashkova, S., and M.C. Leake. 2017. Single-molecule fluorescence microscopy review: shedding new light on old problems. *Biosci Rep*. 37.

Shashkova, S., A.J. Wollman, S. Hohmann, and M.C. Leake. 2018. Characterising Maturation of GFP and mCherry of Genomically Integrated Fusions in Saccharomyces cerevisiae. *Bio Protoc*. 8:e2710.

Shashkova, S., A.J.M. Wollman, M.C. Leake, and S. Hohmann. 2017. The yeast Mig1 transcriptional repressor is dephosphorylated by glucose-dependent and -independent mechanisms. *FEMS Microbiol Lett*. 364.

Shen, D., H. Yuan, A. Hutagalung, A. Verma, D. Kümmel, X. Wu, K. Reinisch, J.A. McNew, and P. Novick. 2013. The synaptobrevin homologue Snc2p recruits the exocyst to secretory vesicles by binding to Sec6p. *J Cell Biol*. 202:509-526.

Sherman, F. 2002. Getting started with yeast. *Methods Enzymol*. 350:3-41.

Shin, M.E., K.D. Ogburn, O.A. Varban, P.M. Gilbert, and C.G. Burd. 2001. FYVE Domain Targets Pib1p Ubiquitin Ligase to Endosome and Vacuolar Membranes *. *Journal of Biological Chemistry*. 276:41388-41393.

Simon, S.M., and G. Blobel. 1991. A protein-conducting channel in the endoplasmic reticulum. *Cell*. 65:371-380.

Simons, K., and E. Ikonen. 1997. Functional rafts in cell membranes. *Nature*. 387:569-572.

Simpson, F., N.A. Bright, M.A. West, L.S. Newman, R.B. Darnell, and M.S. Robinson. 1996. A novel adaptor-related protein complex. *The Journal of cell biology*. 133:749-760.

Simpson, F., A.A. Peden, L. Christopoulou, and M.S. Robinson. 1997. Characterization of the adaptor-related protein complex, AP-3. *The Journal of cell biology*. 137:835-845.

Singer, S.J., and G.L. Nicolson. 1972. The fluid mosaic model of the structure of cell membranes. *Science (New York, N.Y.)*. 175:720-731.

Singer-Krüger, B., H. Stenmark, A. Düsterhöft, P. Philippsen, J.S. Yoo, D. Gallwitz, and M. Zerial. 1994. Role of three rab5-like GTPases, Ypt51p, Ypt52p, and Ypt53p, in the endocytic and vacuolar protein sorting pathways of yeast. *J Cell Biol*. 125:283-298.

Sivaram, M.V., J.A. Saporita, M.L. Furgason, A.J. Boettcher, and M. Munson. 2005. Dimerization of the exocyst protein Sec6p and its interaction with the t-SNARE Sec9p. *Biochemistry*. 44:6302-6311.

Slessareva, J.E., S.M. Routt, B. Temple, V.A. Bankaitis, and H.G. Dohlman. 2006. Activation of the Phosphatidylinositol 3-Kinase Vps34 by a G Protein α Subunit at the Endosome. *Cell*. 126:191-203.

Søgaard, M., K. Tani, R.R. Ye, S. Geromanos, P. Tempst, T. Kirchhausen, J.E. Rothman, and T. Söllner. 1994. A rab protein is required for the assembly of SNARE complexes in the docking of transport vesicles. *Cell*. 78:937-948.

Sogin, M.L. 1991. Early evolution and the origin of eukaryotes. *Current Opinion in Genetics and Development*. 1:457-463.

Söllner, T., M.K. Bennett, S.W. Whiteheart, R.H. Scheller, and J.E. Rothman. 1993a. A protein assembly-disassembly pathway in vitro that may correspond to sequential steps of synaptic vesicle docking, activation, and fusion. *Cell*. 75:409-418.

Söllner, T., S.W. Whiteheart, M. Brunner, H. Erdjument-Bromage, S. Geromanos, P. Tempst, and J.E. Rothman. 1993b. SNAP receptors implicated in vesicle targeting and fusion. *Nature*. 362:318-324.

Soltoff, S.P., S.L. Rabin, L.C. Cantley, and D.R. Kaplan. 1992. Nerve growth factor promotes the activation of phosphatidylinositol 3-kinase and its association with the trk tyrosine kinase. *J Biol Chem*. 267:17472-17477.

Song, J., and H.G. Dohlman. 1996. Partial Constitutive Activation of Pheromone Responses by a Palmitoylation-Site Mutant of a G Protein α Subunit in Yeast. *Biochemistry*. 35:14806-14817.

Song, J., J. Hirschman, K. Gunn, and H.G. Dohlman. 1996. Regulation of Membrane and Subunit Interactions by N-Myristoylation of a G Protein α Subunit in Yeast. *Journal of Biological Chemistry*. 271:20273-20283.

Song, W., D. Raden, E.C. Mandon, and R. Gilmore. 2000. Role of Sec61alpha in the regulated transfer of the ribosome-nascent chain complex from the signal recognition particle to the translocation channel. *Cell*. 100:333-343.

Spira, F., N.S. Mueller, G. Beck, P. Von Olshausen, J. Beig, and R. Wedlich-Söldner. 2012. Patchwork organization of the yeast plasma membrane into numerous coexisting domains. *Nature Cell Biology*. 14:640-648.

Stack, J.H., D.B. DeWald, K. Takegawa, and S.D. Emr. 1995. Vesicle-mediated protein transport: Regulatory interactions between the Vps15 protein kinase and the Vps34 PtdIns 3-kinase essential for protein sorting to the vacuole in yeast. *Journal of Cell Biology*. 129:321-334.

Stack, J.H., P.K. Herman, P.V. Schu, and S.D. Emr. 1993. A membrane-associated complex containing the Vps15 protein kinase and the Vps34 PI 3-kinase is essential for protein sorting to the yeast lysosome-like vacuole. *The EMBO journal*. 12:2195-2204.

Stalder, D., and D.C. Gershlick. 2020. Direct trafficking pathways from the Golgi apparatus to the plasma membrane. *In* Seminars in Cell and Developmental Biology. Vol. 107. Elsevier Ltd. 112-125.

Stamenova, S.D., R. Dunn, A.S. Adler, and L. Hicke. 2004. The Rsp5 ubiquitin ligase binds to and ubiquitinates members of the yeast CIN85-endophilin complex, Sla1-Rvs167. *J Biol Chem*. 279:16017-16025.

Stanley, P. 2011. Golgi glycosylation. *Cold Spring Harb Perspect Biol*. 3.

Steensma, H.Y., J.C. Crowley, and D.B. Kaback. 1987. Molecular cloning of chromosome I DNA from Saccharomyces cerevisiae: isolation and analysis of the CEN1-ADE1-CDC15 region. *Mol Cell Biol*. 7:410-419.

Steinfeld, N., V. Lahiri, A. Morrison, S.P. Metur, D.J. Klionsky, and L.S. Weisman. 2021. Elevating PI3P drives select downstream membrane trafficking pathways. *Mol Biol Cell*. 32:143-156.

Stenmark, H., R.G. Parton, O. Steele-Mortimer, A. Lütcke, J. Gruenberg, and M. Zerial. 1994. Inhibition of rab5 GTPase activity stimulates membrane fusion in endocytosis. *The EMBO Journal*. 13:1287-1287.

Stepp, J.D., K. Huang, and S.K. Lemmon. 1997. The yeast adaptor protein complex, AP-3, is essential for the efficient delivery of alkaline phosphatase by the alternate pathway to the vacuole. *The Journal of cell biology*. 139:1761-1774.

StráDalová, V., W. Stahlschmidt, G. Grossmann, M. BlažÍKová, R. Rachel, W. Tanner, and J. Malinsky. 2009. Furrow-like invaginations of the yeast plasma membrane correspond to membrane compartment of Can1. *Journal of Cell Science*. 122:2887-2894.

Stringer, D.K., and R.C. Piper. 2011. A single ubiquitin is sufficient for cargo protein entry into MVBs in the absence of ESCRT ubiquitination. *The Journal of cell biology*. 192:229-242.

Swaney, D.L., P. Beltrao, L. Starita, A. Guo, J. Rush, S. Fields, N.J. Krogan, and J. Villén. 2013. Global analysis of phosphorylation and ubiquitylation cross-talk in protein degradation. *Nat Methods*. 10:676-682.

Syeda, A.H., A.J.M. Wollman, A.L. Hargreaves, J.A.L. Howard, J.-G. Brüning, P. McGlynn, and M.C. Leake. 2019. Single-molecule live cell imaging of Rep reveals the dynamic interplay between an accessory replicative helicase and the replisome. *Nucleic Acids Research*. 47:6287-6298.

Szklarczyk, D., A.L. Gable, D. Lyon, A. Junge, S. Wyder, J. Huerta-Cepas, M. Simonovic, N.T. Doncheva, J.H. Morris, P. Bork, L.J. Jensen, and C. Von Mering. 2019. STRING v11: Protein-protein association networks with increased coverage, supporting functional discovery in genome-wide experimental datasets. *Nucleic Acids Research*. 47:D607-D613.

Tabuchi, M., A. Audhya, A.B. Parsons, C. Boone, and S.D. Emr. 2006. The phosphatidylinositol 4,5-biphosphate and TORC2 binding proteins Slm1 and Slm2 function in sphingolipid regulation. *Mol Cell Biol*. 26:5861-5875.

Tagaya, M., D.W. Wilson, M. Brunner, N. Arango, and J.E. Rothman. 1993. Domain structure of an N-ethylmaleimide-sensitive fusion protein involved in vesicular transport. *Journal of Biological Chemistry*. 268:2662-2666.

Takeshige, K., M. Baba, S. Tsuboi, T. Noda, and Y. Ohsumi. 1992. Autophagy in yeast demonstrated with proteinase-deficient mutants and conditions for its induction. *J Cell Biol*. 119:301-311.

Tanford, C. 1972. Micelle shape and size. *The Journal of Physical Chemistry*. 76:3020-3024.

Tanford, C. 1978. The hydrophobic effect and the organization of living matter. *Science*. 200:1012-1018.

Tebar, F., S.K. Bohlander, and A. Sorkin. 1999. Clathrin assembly lymphoid myeloid leukemia (CALM) protein: localization in endocytic-coated pits, interactions with clathrin, and the impact of overexpression on clathrin-mediated traffic. *Mol Biol Cell*. 10:2687-2702.

Teis, D., S. Saksena, and S.D. Emr. 2008. Ordered Assembly of the ESCRT-III Complex on Endosomes Is Required to Sequester Cargo during MVB Formation. *Developmental Cell*. 15:578-589.

Teng, X., M. Dayhoff-Brannigan, W.C. Cheng, C.E. Gilbert, C.N. Sing, N.L. Diny, S.J. Wheelan, M.J. Dunham, J.D. Boeke, F.J. Pineda, and J.M. Hardwick. 2013. Genome-wide consequences of deleting any single gene. *Mol Cell*. 52:485-494.

Terbush, D.R., T. Maurice, D. Roth, and P. Novick. 1996. The Exocyst is a multiprotein complex required for exocytosis in Saccharomyces cerevisiae. *In* The EMBO Journal. Vol. 15. 6483-6494.

Thevelein, J.M. 1994. Signal transduction in yeast. *Yeast*. 10:1753-1790.

Ting, A.E., C.D. Hazuka, S.C. Hsu, M.D. Kirk, A.J. Bean, and R.H. Scheller. 1995. rSec6 and rSec8, mammalian homologs of yeast proteins essential for secretion. *Proceedings of the National Academy of Sciences of the United States of America*. 92:9613-9617.

Tkach, J.M., A. Yimit, A.Y. Lee, M. Riffle, M. Costanzo, D. Jaschob, J.A. Hendry, J. Ou, J. Moffat, C. Boone, T.N. Davis, C. Nislow, and G.W. Brown. 2012. Dissecting DNA damage response pathways by analysing protein localization and abundance changes during DNA replication stress. *Nat Cell Biol*. 14:966-976.

Toke, D.A., and C.E. Martin. 1996. Isolation and characterization of a gene affecting fatty acid elongation in Saccharomyces cerevisiae. *Journal of Biological Chemistry*. 271:18413-18422.

Torres, M.P., S.T. Clement, S.D. Cappell, and H.G. Dohlman. 2011. Cell cycle-dependent phosphorylation and ubiquitination of a G protein alpha subunit. *J Biol Chem*. 286:20208-20216.

Traub, L.M. 2003. Sorting it out: AP-2 and alternate clathrin adaptors in endocytic cargo selection. *J Cell Biol*. 163:203-208.

Treitel, M.A., S. Kuchin, and M. Carlson. 1998. Snf1 protein kinase regulates phosphorylation of the Mig1 repressor in Saccharomyces cerevisiae. *Mol Cell Biol*. 18:6273-6280.

Tu, J., and M. Carlson. 1994. The GLC7 type 1 protein phosphatase is required for glucose repression in Saccharomyces cerevisiae. *Molecular and cellular biology*. 14:6789-6796.

Tu, J., and M. Carlson. 1995. REG1 binds to protein phosphatase type 1 and regulates glucose repression in Saccharomyces cerevisiae. *Embo j*. 14:5939-5946.

Tyedmers, J., M. Lerner, C. Bies, J. Dudek, M.H. Skowronek, I.G. Haas, N. Heim, W. Nastainczyk, J. Volkmer, and R. Zimmermann. 2000. Homologs of the yeast Sec complex subunits Sec62p and Sec63p are abundant proteins in dog pancreas microsomes. *Proceedings of the National Academy of Sciences of the United States of America*. 97:7214-7219.

Umebayashi, K., and A. Nakano. 2003. Ergosterol is required for targeting of tryptophan permease to the yeast plasma membrane. *J Cell Biol*. 161:1117-1131.

Ungewickell, E., and D. Branton. 1981. Assembly units of clathrin coats. *Nature*. 289:420-422.

Urbanowski, J.L., and R.C. Piper. 1999. The iron transporter Fth1p forms a complex with the Fet5 iron oxidase and resides on the vacuolar membrane. *J Biol Chem*. 274:38061-38070.

Urbanowski, J.L., and R.C. Piper. 2001. Ubiquitin sorts proteins into the intralumenal degradative compartment of the late-endosome/vacuole. *Traffic*. 2:622-630.

Vainberg, I.E., S.A. Lewis, H. Rommelaere, C. Ampe, J. Vandekerckhove, H.L. Klein, and N.J. Cowan. 1998. Prefoldin, a chaperone that delivers unfolded proteins to cytosolic chaperonin. *Cell*. 93:863-873.

Valdez-Taubas, J., and H.R. Pelham. 2003. Slow diffusion of proteins in the yeast plasma membrane allows polarity to be maintained by endocytic cycling. *Curr Biol*. 13:1636-1640.

Vallier, L.G., and M. Carlson. 1994. Synergistic release from glucose repression by mig1 and ssn mutations in Saccharomyces cerevisiae. *Genetics*. 137:49-54.

Valls, L.A., C.P. Hunter, J.H. Rothman, and T.H. Stevens. 1987. Protein sorting in yeast: the localization determinant of yeast vacuolar carboxypeptidase Y resides in the propeptide. *Cell*. 48:887-897.

van den Hazel, H.B., M.C. Kielland-Brandt, and J.R. Winther. 1992. Autoactivation of proteinase A initiates activation of yeast vacuolar zymogens. *Eur J Biochem*. 207:277-283.

van Meer, G., D.R. Voelker, and G.W. Feigenson. 2008. Membrane lipids: where they are and how they behave. *Nat Rev Mol Cell Biol*. 9:112-124.

Vander Heiden, M.G., J.S. Choy, D.J. VanderWeele, J.L. Brace, M.H. Harris, D.E. Bauer, B. Prange, S.J. Kron, C.B. Thompson, and C.M. Rudin. 2002. Bcl-x(L) complements Saccharomyces cerevisiae genes that facilitate the switch from glycolytic to oxidative metabolism. *The Journal of biological chemistry*. 277:44870-44876.

Vangelatos, I., K. Roumelioti, C. Gournas, T. Suarez, C. Scazzocchio, and V. Sophianopoulou. 2010. Eisosome organization in the filamentous ascomycete Aspergillus nidulans. *Eukaryot Cell*. 9:1441-1454.

Vaskovicova, K., P. Vesela, J. Zahumensky, D. Folkova, M. Balazova, and J. Malinsky. 2020. Plasma Membrane Protein Nce102 Modulates Morphology and Function of the Yeast Vacuole. *Biomolecules*. 10.

Versele, M., K. Lemaire, and J.M. Thevelein. 2001. Sex and sugar in yeast: two distinct GPCR systems. *EMBO Rep*. 2:574-579.

Vida, T.A., and S.D. Emr. 1995. A new vital stain for visualizing vacuolar membrane dynamics and endocytosis in yeast. *J Cell Biol*. 128:779-792.

Voeltz, G.K., M.M. Rolls, and T.A. Rapoport. 2002. Structural organization of the endoplasmic reticulum. *EMBO Rep*. 3:944-950.

Vogel, J.P., L.M. Misra, and M.D. Rose. 1990. Loss of BiP/GRP78 function blocks translocation of secretory proteins in yeast. *The Journal of Cell Biology*. 110:1885-1885.

Volland, C., C. Garnier, and R. Haguenauer-Tsapis. 1992. In vivo phosphorylation of the yeast uracil permease. *The Journal of biological chemistry*. 267:23767-23771.

Von Schwedler, U.K., M. Stuchell, B. Müller, D.M. Ward, H.Y. Chung, E. Morita, H.E. Wang, T. Davis, G.P. He, D.M. Cimbora, A. Scott, H.G. Kräusslich, J. Kaplan, S.G. Morham, and W.I. Sundquist. 2003. The protein network of HIV budding. *Cell*. 114:701-713.

Votteler, J., and W.I. Sundquist. 2013. Virus Budding and the ESCRT Pathway.

Walter, P., and G. Blobel. 1981. Translocation of proteins across the endoplasmic reticulum. II. Signal recognition protein (SRP) mediates the selective binding to microsomal membranes of in-vitro-assembled polysomes synthesizing secretory protein. *The Journal of cell biology*. 91:551-556.

Walther, T.C., P.S. Aguilar, F. Fröhlich, F. Chu, K. Moreira, A.L. Burlingame, and P. Walter. 2007. Pkh-kinases control eisosome assembly and organization. *EMBO Journal*. 26:4946-4955.

Walther, T.C., J.H. Brickner, P.S. Aguilar, S. Bernales, C. Pantoja, and P. Walter. 2006. Eisosomes mark static sites of endocytosis. *Nature*. 439:998-1003.

Wang, H.X., L.M. Douglas, P. Veselá, R. Rachel, J. Malinsky, and J.B. Konopka. 2016. Eisosomes promote the ability of Sur7 to regulate plasma membrane organization in Candida albicans. *Mol Biol Cell*. 27:1663-1675.

Watanabe, D., R. Kikushima, M. Aitoku, A. Nishimura, I. Ohtsu, R. Nasuno, and H. Takagi. 2014. Exogenous addition of histidine reduces copper availability in the yeast Saccharomyces cerevisiae. *Microb Cell*. 1:241-246.

Waters, M.G., and G. Blobel. 1986. Secretory protein translocation in a yeast cell-free system can occur posttranslationally and requires ATP hydrolysis. *The Journal of cell biology*. 102:1543-1550.

Waters, M.G., E.A. Evans, and G. Blobel. 1988. Prepro-alpha-factor has a cleavable signal sequence - PubMed. *Journal of Biological Chemistry*. 263:6209-6214.

Weber, T., B.V. Zemelman, J.A. McNew, B. Westermann, M. Gmachl, F. Parlati, T.H. Söllner, and J.E. Rothman. 1998. SNAREpins: Minimal Machinery for Membrane Fusion. *Cell*. 92:759-772.

Weill, U., I. Yofe, E. Sass, B. Stynen, D. Davidi, J. Natarajan, R. Ben-Menachem, Z. Avihou, O. Goldman, N. Harpaz, S. Chuartzman, K. Kniazev, B. Knoblach, J. Laborenz, F. Boos, J. Kowarzyk, S. Ben-Dor, E. Zalckvar, J.M. Herrmann, R.A. Rachubinski, O. Pines, D. Rapaport, S.W. Michnick, E.D. Levy, and M. Schuldiner. 2018. Genome-wide SWAp-Tag yeast libraries for proteome exploration. *Nature methods*. 15:617-622.

Weinberg, Z.Y., and M.A. Puthenveedu. 2019. Regulation of G protein-coupled receptor signaling by plasma membrane organization and endocytosis. *Traffic*. 20:121-129.

Wendland, B., and S.D. Emr. 1998. Pan1p, yeast eps15, functions as a multivalent adaptor that coordinates protein-protein interactions essential for endocytosis. *J Cell Biol*. 141:71-84.

Wendland, B., K.E. Steece, and S.D. Emr. 1999. Yeast epsins contain an essential N-terminal ENTH domain, bind clathrin and are required for endocytosis. *In* The EMBO Journal. Vol. 18. 4383-4393.

Westholm, J.O., N. Nordberg, E. Murén, A. Ameur, J. Komorowski, and H. Ronne. 2008. Combinatorial control of gene expression by the three yeast repressors Mig1, Mig2 and Mig3. *BMC Genomics*. 9:601.

Whiteway, M., L. Hougan, D. Dignard, D.Y. Thomas, L. Bell, G.C. Saari, F.J. Grant, P. O'Hara, and V.L. MacKay. 1989. The STE4 and STE18 genes of yeast encode potential β and γ subunits of the mating factor receptor-coupled G protein. *Cell*. 56:467-477.

Wickham, H., R. François, L. Henry, and K. Müller. 2020. A Grammar of Data Manipulation [R package dplyr version 1.0.0]. Comprehensive R Archive Network (CRAN).

Wiederkehr, A., S. Avaro, C. Prescianotto-Baschong, R. Haguenauer-Tsapis, and H. Riezman. 2000. The F-box protein Rcy1p is involved in endocytic membrane traffic and recycling out of an early endosome in Saccharomyces cerevisiae. *Journal of Cell Biology*. 149:397-410.

Wieland, F.T., M.L. Gleason, T.A. Serafini, and J.E. Rothman. 1987. The rate of bulk flow from the endoplasmic reticulum to the cell surface. *Cell*. 50:289-300.

Wiemken, A., M. Schellenberg, and K. Urech. 1979. Vacuoles: The Sole Compartments of Digestive Enzymes in Yeast (Saccharomyces cerevisiae) ? *Arch. Microbiol*. 123:3-3.

Wilkinson, K.D., M.K. Urban, and A.L. Haas. 1980. Ubiquitin is the ATP-dependent proteolysis factor I of rabbit reticulocytes. *Journal of Biological Chemistry*. 255:7529-7532.

Williams-Hart, T., X. Wu, and K. Tatchell. 2002. Protein phosphatase type 1 regulates ion homeostasis in Saccharomyces cerevisiae. *Genetics*. 160:1423-1437.

Wilson, D.W., C.A. Wilcox, G.C. Flynn, E. Chen, W.J. Kuang, W.J. Henzel, M.R. Block, A. Ullrich, and J.E. Rothman. 1989. A fusion protein required for vesicle-mediated transport in both mammalian cells and yeast. *Nature*. 339:355-359.

Winston, F., C. Dollard, and S.L. Ricupero-Hovasse. 1995. Construction of a set of convenient saccharomyces cerevisiae strains that are isogenic to S288C. *Yeast*. 11:53-55.

Winzeler, E.A., D.D. Shoemaker, A. Astromoff, H. Liang, K. Anderson, B. Andre, R. Bangham, R. Benito, J.D. Boeke, H. Bussey, A.M. Chu, C. Connelly, K. Davis, F. Dietrich, S.W. Dow, M. El Bakkoury, F. Foury, S.H. Friend, E. Gentalen, G. Giaever, J.H. Hegemann, T. Jones, M. Laub, H. Liao, N. Liebundguth, D.J. Lockhart, A. Lucau-Danila, M. Lussier, N. M'Rabet, P. Menard, M. Mittmann, C. Pai, C. Rebischung, J.L. Revuelta, L. Riles, C.J. Roberts, P. Ross-MacDonald, B. Scherens, M. Snyder, S. Sookhai-Mahadeo, R.K.

Storms, S. Véronneau, M. Voet, G. Volckaert, T.R. Ward, R. Wysocki, G.S. Yen, K. Yu, K. Zimmermann, P. Philippsen, M. Johnston, and R.W. Davis. 1999. Functional characterization of the S. cerevisiae genome by gene deletion and parallel analysis. *Science*. 285:901-906.

Woese, C.R., O. Kandler, and M.L. Wheelis. 1990. Towards a natural system of organisms: proposal for the domains Archaea, Bacteria, and Eucarya. *Proc Natl Acad Sci U S A*. 87:4576-4579.

Wollman, A.J., and M.C. Leake. 2015. Millisecond single-molecule localization microscopy combined with convolution analysis and automated image segmentation to determine protein concentrations in complexly structured, functional cells, one cell at a time. *Faraday Discuss*. 184:401-424.

Wollman, A.J.M., S. Shashkova, E.G. Hedlund, R. Friemann, S. Hohmann, and M.C. Leake. 2017. Transcription factor clusters regulate genes in eukaryotic cells. *eLife*. 6.

Wong, F.H., J.S. Chen, V. Reddy, J.L. Day, M.A. Shlykov, S.T. Wakabayashi, and M.H. Saier. 2012. The amino acid-polyamine-organocation superfamily. *Journal of molecular microbiology and biotechnology*. 22:105-113.

Wurmser, A.E., and S.D. Emr. 2002. Novel PtdIns(3)P-binding protein Etf1 functions as an effector of the Vps34 PtdIns 3-kinase in autophagy. *The Journal of cell biology*. 158:761-772.

Wymann, M.P., and R. Schneiter. 2008. Lipid signalling in disease. *Nat Rev Mol Cell Biol*. 9:162-176.

Xu, P., H.M. Hankins, C. Macdonald, S.J. Erlinger, M.N. Frazier, N.S. Diab, R.C. Piper, L.P. Jackson, J.A. Macgurn, and T.R. Graham. 2017. COPI mediates recycling of an exocytic SNARE by recognition of a ubiquitin sorting signal. *eLife*. 6.

Xu, Y., H. Hortsman, L. Seet, S.H. Wong, and W. Hong. 2001. SNX3 regulates endosomal function through its PX-domain-mediated interaction with PtdIns(3)P. *Nature cell biology*. 3:658-666.

Xue, Y., M. Batlle, and J.P. Hirsch. 1998. GPR1 encodes a putative G protein-coupled receptor that associates with the Gpa2p Galpha subunit and functions in a Ras-independent pathway. *Embo j*. 17:1996-2007.

Yamamoto, W., S. Wada, M. Nagano, K. Aoshima, D.E. Siekhaus, J.Y. Toshima, and J. Toshima. 2018. Distinct roles for plasma membrane PtdIns(4)P and PtdIns(4,5)P(2) during receptor-mediated endocytosis in yeast. *J Cell Sci*. 131.

Yang, X., W. Zhang, X. Wen, P.J. Bulinski, D.A. Chomchai, F.M. Arines, Y.-Y. Liu, S. Sprenger, D. Teis, D.J. Klionsky, and M. Li. 2020. TORC1 regulates vacuole membrane composition through ubiquitin- and ESCRT-dependent microautophagy. *Journal of Cell Biology*. 219.

Yarwood, R., J. Hellicar, P.G. Woodman, and M. Lowe. 2020. Membrane trafficking in health and disease. *Dis Model Mech*. 13.

Yofe, I., U. Weill, M. Meurer, S. Chuartzman, E. Zalckvar, O. Goldman, S. Ben-Dor, C. Schütze, N. Wiedemann, M. Knop, A. Khmelinskii, and M. Schuldiner. 2016. One library to make them all: Streamlining the creation of yeast libraries via a SWAp-Tag strategy. *Nature Methods*. 13:371-378.

Yorimitsu, T., and D.J. Klionsky. 2005. Autophagy: molecular machinery for self-eating. *Cell Death Differ*. 12 Suppl 2:1542-1552.

You, L., R. Tong, M. Li, Y. Liu, J. Xue, and Y. Lu. 2019. Advancements and Obstacles of CRISPR-Cas9 Technology in Translational Research. *Mol Ther Methods Clin Dev*. 13:359-370.

Young, B.P., R.A. Craven, P.J. Reid, M. Willer, and C.J. Stirling. 2001. Sec63p and Kar2p are required for the translocation of SRP-dependent precursors into the yeast endoplasmic reticulum in vivo. *The EMBO journal*. 20:262-271.

Young, M.E., T.S. Karpova, B. Brugger, D.M. Moschenross, G.K. Wang, R. Schneiter, F.T. Wieland, and J.A. Cooper. 2002. The Sur7p Family Defines Novel Cortical Domains in Saccharomyces cerevisiae, Affects Sphingolipid Metabolism, and Is Involved in Sporulation. *Molecular and Cellular Biology*. 22:927-934.

Yu, J.W., and M.A. Lemmon. 2001. All Phox Homology (PX) Domains from Saccharomyces cerevisiae Specifically Recognize Phosphatidylinositol 3-Phosphate *. *Journal of Biological Chemistry*. 276:44179-44184.

Zahumenský, J., C. Mota Fernandes, P. Veselá, M. Del Poeta, J.B. Konopka, and J. Malínský. 2022. Microdomain Protein Nce102 Is a Local Sensor of Plasma Membrane Sphingolipid Balance. *Microbiol Spectr*:e0196122.

Zaman, M.F., A. Nenadic, A. Radojičić, A. Rosado, and C.T. Beh. 2020. Sticking With It: ER-PM Membrane Contact Sites as a Coordinating Nexus for Regulating Lipids and Proteins at the Cell Cortex. *Frontiers in Cell and Developmental Biology*. 0:675-675.

Zeno, W.F., U. Baul, W.T. Snead, A.C.M. DeGroot, L. Wang, E.M. Lafer, D. Thirumalai, and J.C. Stachowiak. 2018. Synergy between intrinsically disordered domains and structured proteins amplifies membrane curvature sensing. *Nature Communications*. 9:4152.

Zhang, X., E. Bi, P. Novick, L. Du, K.G. Kozminski, J.H. Lipschutz, and W. Guo. 2001. Cdc42 interacts with the exocyst and regulates polarized secretion. *J Biol Chem*. 276:46745-46750.

Zhang, X., K. Orlando, B. He, F. Xi, J. Zhang, A. Zajac, and W. Guo. 2008. Membrane association and functional regulation of Sec3 by phospholipids and Cdc42. *J Cell Biol*. 180:145-158.

Zhang, Y.Q., and R. Rao. 2010. Beyond ergosterol: linking pH to antifungal mechanisms. *Virulence*. 1:551-554.

Zhao, H., A. Michelot, E.V. Koskela, V. Tkach, D. Stamou, D.G. Drubin, and P. Lappalainen. 2013a. Membrane-sculpting BAR domains generate stable lipid microdomains. *Cell Rep*. 4:1213-1223.

Zhao, X., D. Wang, X. Liu, L. Liu, Z. Song, T. Zhu, G. Adams, X. Gao, R. Tian, Y. Huang, R. Chen, F. Wang, D. Liu, X. Yu, Y. Chen, Z. Chen, M. Teng, X. Ding, and X. Yao. 2013b. Phosphorylation of the Bin, Amphiphysin, and RSV161/167 (BAR) domain of ACAP4 regulates membrane tubulation. *Proceedings of the National Academy of Sciences*. 110:11023-11028.

Zheng, B., C. Lavoie, T.-D. Tang, P. Ma, T. Meerloo, A. Beas, and M.G. Farquhar. 2004. Regulation of epidermal growth factor receptor degradation by heterotrimeric Galphas protein. *Molecular biology of the cell*. 15:5538-5550.

Zhou, H., G. Chen, C. Dong, X. Zhao, Z. Shen, F. Chen, B. Liu, and J. Long. 2020. Snf5 and Swi3 subcomplex formation is required for SWI/SNF complex function in yeast. *Biochemical and Biophysical Research Communications*. 526:934-940.

Ziółkowska, N.E., L. Karotki, M. Rehman, J.T. Huiskonen, and T.C. Walther. 2011. Eisosome-driven plasma membrane organization is mediated by BAR domains. *Nature Structural and Molecular Biology*. 18:854-856.